A Study of Brushless Doubly-Fed (Induction) Machines

CONTRIBUTIONS IN MACHINE ANALYSIS, DESIGN AND CONTROL

A DISSERTATION SUBMITTED FOR THE DEGREE OF DOCTOR OF PHILOSOPHY

Paul C. Roberts

September 2004
(revised January 2005)

Emmanuel College
University of Cambridge

To God, Ruth and my parents.

I will lift my eyes to the mountains;
From where shall my help come?
My help comes from the LORD,
Who made heaven and earth.
Psalm 121

Abstract

The Brushless Doubly-Fed Machine (BDFM) shows commercial promise as a variable speed drive or generator. However, for this promise to be realised the design of the machine must be improved beyond that proposed to date. This dissertation contributes towards this goal through machine analysis, design and control.

A generalised framework is developed for a coherent and rigorous derivation of models for a wide class of BDFMs, of which machines with 'nested-loop' design rotors are a subset. This framework is used to derive coupled circuit, d-q axis, sequence components and then equivalent circuit models for the class of machines. Proofs are given for all derivations, exploiting the circulant properties of the mutual inductance matrices. The coherence between the different models allows parameters calculated for the coupled circuit model to provide parameter values for the other models.

A method of model order reduction is proposed for the class of BDFMs with 'nested-loop' rotors, and examples given of the efficacy of the procedure. The reduction method allows parameter values to be computed for a simple equivalent circuit representation of the machine. These calculated parameter values, and those for other BDFM rotor designs are verified by experimental tests on a prototype BDFM.

The significance of particular equivalent circuit parameters is investigated from the model. Series rotor inductance terms are found to have a significant and direct effect on machine performance. These terms are shown to relate directly to the design of the rotor, and are quantified using the previously developed framework. Seven different rotor designs, including a new BDFM rotor design, are considered to show how the values of these parameters change.

An experimental method of parameter estimation is developed for the equivalent circuit model, and the relationship between these parameters and the parameters in other forms of the model derived. The experimental method is shown to be applicable both to standard induction machines and to BDFM machines, yielding accurate results in each case.

A synchronous reference frame model for the class of BDFMs is derived and is used to analyse the stability of the machine via a linearized model. Practical methods for the design of PID controllers are proposed to stabilise the machine using voltage source inverters. Results are presented from experimental implementations which show a significant improvement in performance over previously published results.

The non-linear control technique, feedback linearization, is applied to the BDFM and shown to have some robustness to modelling errors, in a realistic simulation. An initial attempt at implementation of the scheme is reported. Preliminary results are encouraging, and warrant further investigation.

Keywords: ac machines, BDFM, Brushless Doubly Fed Machines, control, coupled circuits, dq axis, equivalent circuits, feedback linearization, model reduction, parameter estimation, synchronous reference frame

Acknowledgements

First, and foremost, I would like to express my gratitude to my supervisors doctors Richard McMahon, Jan Maciejowski and Tim Flack whose insight and enthusiasm have greatly improved this dissertation.

I would like to thank colleagues past and present for making work much more enjoyable. Some pleasant memories include, the tea-time Bridge sessions, the Poker evenings, lunch with Dan and hitch-hiking to and from an international conference.

I would like to gratefully acknowledge the help of Ehsan Abdi-Jalebi and Xiaoyan Wang in the operation of the BDFM test rig. In particular their assistance in the collection of the experimental data used in figures 5.8, 5.9, 5.10, 5.11, 6.3 and 6.4. Thanks are also due to Ehsan for proof reading this dissertation.

I am most grateful for assistance of Mark Barrett, John Grundy, the electricians, carpenters, welders and other support staff in preparing and setting up the prototype BDFM test rig. Thanks are also due to Davor Dukic, Iskandar Samad and George Makrides for their assistance in the development of the instrumentation hardware for the test rig. I am very grateful for the assistance of computing support staff, particularly John Sloan and Patrick Gosling.

This work has been funded by the Engineering and Physical Sciences Research Council. A high-powered inverter was generously donated by Semikron UK Ltd. Cambridge Silicon Radio (CSR) Ltd. kindly supplied a number of Bluetooth models. FKI Energy Technology particularly its subsidiaries Laurence, Scott & Electromotors (LSE) Ltd. and Marelli Motori SpA provided the prototype machine frame and manufactured the prototype rotors described in chapter 5. I would like to thank these institutions for their support. In particular, thanks to Peter Tavner, formerly of FKI and Terry Gallant of LSE for their continued interest in the BDFM, and to David Hargreaves of CSR.

I would like to thank my parents for a lifetime of support and for continually fuelling my enthusiasm for tinkering with anything I could get my hands on.

Finally, I would like to thank my wife, Ruth, for her unflagging support throughout, and seemingly endless patience with me.

As required by the University Statute, I hereby declare that this dissertation is not substantially the same as any that I have submitted for a degree or diploma or other qualification at any other university. This dissertation is the result of my own work and includes nothing which is the outcome of work done in collaboration, except where specifically indicated. This dissertation is 64,277 words in length, and contains 83 figures.

Paul Roberts
Emmanuel College
September 2004

Contents

Notation & Terminology

Notation

Numbers

$\mathbb{R}$	field of real numbers
$\mathbb{C}$	field of complex numbers
$\mathbb{Z}$	set of integers
$\mathbb{Z}^*$	set of non-negative integers
$\mathbb{N}$	natural numbers (positive integers excluding zero)
j	the imaginary unit, i.e. $\sqrt{-1}$
$\Re\{X\}, \Im\{X\}$	denotes real, imaginary part of $X \in \mathbb{C}$
$\bar{X}$	denote the complex conjugate of $X \in \mathbb{C}$
$\mathbb{F}^{n\times m}$	denotes that a set comprised of matrices of dimension $n \times m$, the elements of which are in the set or field $\mathbb{F}$.

Vectors

$x \cdot y$	scalar (dot) product of x and y
$\nabla_x f$	Given a vector function, $f \in \mathbb{R}^n$, which is a function of the vector $x \in \mathbb{R}^m$, and possibly other vector or scalar variables, then $\nabla_x f = \begin{bmatrix} \frac{\partial f_1}{\partial x_1} & \frac{\partial f_1}{\partial x_2} & \cdots \\ \frac{\partial f_2}{\partial x_1} & \frac{\partial f_2}{\partial x_2} & \cdots \\ \vdots & \vdots & \ddots \end{bmatrix}$, which is known as the *Jacobian* of f when $n = m$.
$\|x\|_2$	2-norm of a vector or vector signal. For $x \in \mathbb{R}^n$, $\|x\|_2 \triangleq \sqrt{\sum_{i=1}^{n} x_i^2}$. Definition 3.1 defines the 2-norm of a continuous function x, which shares the same notation, however the reader should assume the standard definition unless otherwise indicated.
$\mathcal{L}_2$	The space of square integrable Lebesgue measurable functions, see definition 3.1.
$\|P\|_{i,2}$	The induced 2-norm of a system P, see definition 3.2

Matrices

X^{-1}, $X^{\dagger}$	indicating inverse, pseudo-inverse of matrix X
X^{T}, X^{*}	indicating transpose, complex-conjugate transpose of matrix X
X_{xy}	element of matrix X at x^{th} row, and y^{th} column
$\hat{X}$	estimated value of X
0	zero matrix of compatible dimension
I	the identity matrix of compatible dimension
I_n	the $n \times n$ identity matrix (also used to denote complex current)
$X^{\perp}$	$X^{\perp}$ is a matrix where the rows (or columns) of $X^{\perp}$ span the orthogonal complement of the subspace defined by the span of the rows (or columns) of X. Whether row space or column space is intended will be determined by the context.

Mathematical terminology

$\mathbb{B}$	$\left\{ x : \begin{bmatrix} I \\ -I \end{bmatrix} x \leq \begin{bmatrix} 1 \\ \vdots \\ 1 \end{bmatrix} \right\}$, a hypercube around the origin.
$\propto$	proportional to
$\emptyset$	the empty (null) set
$\cap$	intersection, e.g. $A \cap B$ denotes the set defined by the intersection of set A and set B
$\triangleq$	defined as
$\exists$	'there exists'
$\forall$	'for all'
:	'such that'
$\in$	'in', for example $\exists q \in \mathbb{R} : q^2 = q.$, reads 'there exists a q in the field of real numbers, such that $q^2 = q$'.
$\square$	end of proof.
$\heartsuit$	end of remark.
[0, 10]	closed interval from 0 to 10, that is a range from 0 to 10 including both 0 and 10.
(0, 10)	open interval from 0 to 10, as above but excluding 0 and 10. Hence $[0, \infty)$ is the interval from 0 to ∞ excluding ∞, but including 0.
$\Rightarrow$	'implies', from left to right, e.g. $A \Rightarrow B$ reads 'A implies B'.
$\Leftarrow$	'implies', from right to left, e.g. $A \Leftarrow B$ reads 'B implies A'.
$\Leftrightarrow$	'implies', from right to left and from left to right, e.g. $A \Leftrightarrow B$ reads 'B implies A and A implies B'.
iff	'if and only if'
$\gg$	'much greater than', for example $a \gg b \Rightarrow a > b + K$ for some ('large') $K > 0$.
$\ll$	the dual of $\gg$.

Electrical Machine Notation

X_{s1}, X_{s2}, X_r	indicating a stator 1, 2, or rotor quantity X
X_d, X_q, X_0	indicating *direct* (or d) axis component, *quadrature* (or q) axis component, *zero* (or 0) sequence X
X^e	indicating an equilibrium value of quantity X
X^s or X_{sync}	indicating the value of quantity X in the synchronous reference frame
R, M, L, Z	resistance, mutual inductance, self inductance, impedance
Q	an inductance-like term arising from the movement between stator and rotor
X_{cc}	indicates a coupled-coil inductance parameter
X'	indicates an apparent (referred) quantity
X_e	indicates an equivalent circuit inductance parameter
v, i, λ	instantaneous voltage, current, flux linked (λ is also used to denote eigenvalues).
ϕ	stator-rotor phase offset, or magnetic flux.
p_1, p_2	stator 1, stator 2 winding number of pole pairs
ω_1, ω_2	stator 1, stator 2 supply frequencies
ω_r	BDFM rotational shaft speed
ω_s	frequency of currents in the rotor reference frame in BDFM synchronous mode see (4.26).
θ_r	BDFM angular position
s_1, s_2	stator 1 and stator 2 slip, as defined in equations (4.32) and (4.33), not to be confused with s which denotes the complex variable of the Laplace transform.
J	current density, or moment of inertia
T_e, T_l	electrical torque, load torque
d	machine diameter, as shown in figure 2.1
w	machine stack length, as shown in figure 2.1
α_c	coil pitch, in radians (see figure 2.2)
α_s	slot pitch, in radians (see figure 2.2)
y_s	slot pitch, in metres
μ_0	permeability of free space, $\mu_0 = 4\pi \times 10^{-7}\text{H/m}$
B	magnetic flux density
g	air gap width (see figure 2.2)
H	magnetic field intensity, see definition 2.1

Terminology

absolute harmonic	see remark 2.6
A/D	analogue to digital converter
balanced three phase supply	three voltage or current sources supplying $K\cos(\omega t - \phi)$, $K\cos(\omega t - 2\pi/3 - \phi)$, and $K\cos(\omega t - 4\pi/3 - \phi)$ for some K, ϕ, ω.
cascade induction mode	operation of the BDFM when the second stator is short circuited, see section 1.2.1.
D/A	digital to analogue converter
FBL	feedback linearization, see chapter 8.
FFT	fast Fourier transform, a fast implementation of the discrete Fourier transform
I/O	input / output
inverter	a device which converts DC to AC, i.e. performs in *inverse* operation of a rectifier. In this dissertation the word always refers to an electronic device.
lamination stack length	length of the stack of laminations (typically made from electrical steel) used to make a machine stator or rotor. Figure 2.1 shows this dimension on a rotor.
LHP	left half-plane, the dual of RHP.
LMI	linear matrix inequality
LPV	linear, parameter-varying
LTI	linear, time-invariant
Matlab	'Matrix-Laboratory': computer software for numerical and symbolic computations from the Mathworks, Inc.; essentially a high level programming language design for mathematical computation.
MIMO	multiple input, multiple output
mmf	magneto-motive force, see definition 2.2
orthonormal completion	a set of mutually orthonormal vectors which span the orthogonal complement of a subspace.
ODE	ordinary differential equation.
orthogonal matrix	a unitary matrix with $X \in \mathbb{R}^{n\times n}$, hence its columns form an orthonormal basis for $\mathbb{R}^n$.
PI	Proportional-Integral, a controller with transfer function $K_p + \frac{K_i}{s}$.
PID	Proportional-Integral-Derivative, a controller with transfer function $K_p + \frac{K_i}{s} + K_d s$.
relative harmonic	see remark 2.6

RHP	right half-plane - refers to the position of (typically poles or zeros) in the complex plane, RHP means that $\Re\{X\} > 0$ where X is the complex number in question.
rms	root mean square - the square-root of the mean of the square of a quantity.
simple induction mode	operation of the BDFM when the second stator is open circuit, see section 1.2.1.
Simulink	A modelling environment within Matlab, allowing easy solution of ODEs.
SISO	single input, single output
stack length	abbreviation of lamination stack length.
unitary matrix	$X \in \mathbb{C}^{n\times n}$ is a unitary matrix if $X^*X = XX^* = I$, which means that the columns of X form an orthonormal basis for $\mathbb{C}^n$.

Chapter 1

Introduction

This dissertation is concerned with the analysis, design and control of the Brushless Doubly-Fed Machine (BDFM).

The BDFM, sometimes referred to as the Brushless Doubly-Fed *Induction* Machine, is an AC electrical machine which can operate as both a motor and a generator. As the name implies the machine requires two AC supplies, and has no direct electrical connection to the rotor, which removes the need for carbon brushes sometimes found in electrical machines.

This chapter reviews the development of the BDFM, then section 1.2 gives a basic description of the machine operation, and explains the modern interest in the machine. Readers unfamiliar with the machine may prefer to read this section first. We then outline the approach and structure of this dissertation in section 1.3

1.1 Evolution of the BDFM

The history of the modern BDFM can be originally traced back to a patent taken out by the Siemens Brothers and Mr. F. Lydall in 1902 for a self-cascaded machine [97].

At the time it had become clear that the supply distribution standard was changing from DC to AC. The adoption of AC brought the induction machine into industrial service. The induction machine offered a simple and robust construction, which was desirable, however industry required variable speed operation which led to a significant problem as the fundamental operating speed for an induction machine is fixed by the mains frequency. At the turn of the 20^{th} century the common method of controlling the speed of induction machines was the introduction of series resistance to the rotor, connected via slip rings, as the modern luxury of power electronic frequency converters (inverters) had not even been conceived.

The use of series resistance (rheostats) connected to the rotor is inherently lossy, and thus there was a strong desire to design machines which could be operated at different speeds without rheostatic loss [97].

It was well known at the time that connecting two induction machines together allowed one to achieve three different speeds of efficient operation [48, p. 648]. Such an arrangement was known as 'cascaded induction machines'. The Lydall patent covered the incorporation of two induction machines with air gap fields of different pole numbers in one frame. Lydall realised that the resulting machine would mimic the behaviour of two cascaded (but physically separate) machines because unlike pole number fields do not couple. His machine had two stator windings and two rotor windings each brought out on slip rings. Three different efficient speeds of operation could be achieved, the synchronous speed of winding 1, ω/p_1, the synchronous speed of winding 2, ω/p_2, and the cascade synchronous speed, $\frac{\omega}{p_1+p_2}$. Lydall's work was to achieve 'self-cascaded' operation by, in effect, putting two machines in the same frame.

At the same time as Lydall's work, others were attempting to create a 'self-cascaded' machine, but their attempts used suitable spacing of the stator windings to ensure non-linking of the stator fields, rather than different pole number fields. Prof. Silvanus P. Thompson took out a patent in 1901 [49, p.406] for such a machine, Steinmetz in the USA for a similar machine in 1903, and Meller in Germany in 1904 [48, p.651].

In 1907 Hunt [48] further developed Lydall's original idea, although it appears he was initially unaware of Lydall's work [49, p. 407]. Hunt realised that the slip rings were unnecessary, that is, if the cascade connection is made rotor to rotor, rather than rotor to stator, then no slip rings are needed, and three speeds of operation are still possible. Hunt also contributed to the development of the machine and showed that with suitably designed stator and rotor windings it was possible to reduce copper losses significantly. The single rotor winding was designed to couple to both air gap fields and needed significantly less cross-sectional area of copper than Lydall's design, leading to smaller slots and a more practical rotor design. Hunt developed the machine from 1907 to 1914, and he describes some refinements in his 1914 paper along with experiences gained from industrial applications, principally in the mining industry [49].

Further improvements were made to the rotor and stator designs by Creedy in 1920 [27]. Creedy also refined some of Hunt's rules for choosing suitable pole number combinations, thus providing greater choice of machine configurations. Most significantly Creedy's rules for choosing pole numbers led to the possibility of using a machine with 6 and 2 poles, which was 50% faster than the fastest machine available using Hunt's rules. However, in fact, Creedy's rules for choosing pole number combinations were still incomplete.

The self-cascaded machine met with some commercial success. Hunt reports a number of machines which found application in areas including an air compressor in a colliery, and as an air compressor for refrigeration [49, p. 426].

However, after Creedy's paper no further publications appeared until Smith published in 1966 [102]. Smith's machine was in the category of the Thompson/Steinmetz/Muller machines, that is, the non-linking of stator fields was achieved by spatial separation rather than different pole number

fields. Smith's initial motivation appears to have been for the cascade mode of operation, and he presents, for the first time, a model of the steady-state operation of the machine. The following year Smith published on the synchronous performance of his machine, and noted that a lower power frequency converter could be used to extract slip power from the rotor by induction, or if supplied from the second winding, the machine would behave as a synchronous machine [103]. This was a significant development as it was the first time that the full synchronous mode was noted, however the Smith machine was not a true BDFM, rather two magnetically separate machines in the same frame. Furthermore, in his 1967 paper Smith presents an equivalent circuit for his machine, and analyses its performance in the synchronous mode of operation. Cook and Smith went on to publish on stability of the synchronous mode of operation, [24, 25], however, as mentioned, his work concerns essentially two separate induction machines in cascade, which happen to be put in the same frame. Nevertheless Smith must be credited with first noting the synchronous mode of operation which is achieved by a double feed.

In 1970 an unquestionably significant contribution was made by Broadway and Burbridge [17]. Indeed, physically, the modern BDFM is essentially the same as that proposed by Broadway and Burbridge. It seems that they were unaware of the work of Smith, however. Broadway and Burbridge returned to the Hunt machine, and made significant contributions to the design of the rotor. They reasoned that a wound rotor, which the Hunt and Creedy designs required, would lead to higher losses and lower durability. They sought to design a cage-type rotor which could be made by the same means as a squirrel cage rotor, yet did not suffer from excessive leakage reactance. They have erroneously been credited with first realising that a cage rotor for a BDFM must have the number of bars given by the sum of the pole pairs of the stator windings; in fact Hunt noticed this [27, p. 534]. Nevertheless Broadway and Burbridge were the first to formalise this concept. Their main contribution was to propose the 'nested-loop' design rotor, which has been adopted in most subsequent work on the BDFM. Broadway and Burbridge presented an equivalent circuit for the BDFM, and some performance aspects were analysed in steady-state. They also noted that the second winding can, not only extract slip power, but also be used to run the machine in a synchronous mode. Yet unlike Smith, they only consider the synchronous mode in the case that the second stator supplies DC.

Broadway published again in 1971 on what is, in essence, the modern Brushless Doubly-Fed Reluctance Machine (BDFRM) [15]. In this paper it is noted that doubly-fed operation is possible with different supply frequencies, through the use of a variable frequency inverter. In 1974 a further publication by Broadway appeared, with a valuable discussion of the effects of two pole number fields sharing the same iron circuit, and the effects of saturation [16].

Four years later Kusko and Somuah [57] presented work on a BDFM with two 3 phase windings on the rotor, although they conceded that the Broadway/Burbridge design would have been an improvement. They are, perhaps, the first to have noticed that the BDFM equivalent circuit has similarities with that of the synchronous machine in synchronous operation, however they were principally

concerned with slip power recovery rather than true double feed - the latter requiring a fully controlled converter.

In 1983 and 1987 Shibata and Kohrin and Shibata and Taka published on the Broadway machine, firstly in the cascade mode of operation and then in the synchronous doubly-fed mode [94, 95].

In the mid-1980s as part of US Department of Energy contracts, interest developed in the BDFM at Oregon State Univserity [65]. Wallace, Spée, Li and others at Oregon studied BDFMs extensively, and indeed the name 'BDFM' originated in these publications. Their work used the Broadway/Burbridge rotor, and developed a coupled-circuit dynamic model for their prototype machine. They used this model to investigate performance [110, 104]. They then reconsidered the rotor design, and presented some analysis and proposals for refinement [109]. This work led towards a patent filed by Lauw in 1993 [59].

Hunt, Creedy and Broadway/Burbridge all proposed a single stator winding which allowed both pole number fields to be achieved without the need for separate stator windings. However Rochelle et. al investigated this winding configuration and concluded that it can lead to circulating currents [88]. Therefore, later work at Oregon used separate windings.

Li et. al. proposed a d-q (two axis) dynamic model for their prototype machine, and presented performance results [64, 63]. In these works the authors use separate three phase windings, although as they comment, under their modelling assumptions the multi-tap single winding is effectively the same. They used this d-q model to derive an equivalent circuit for their prototype BDFM, and considered steady state performance of the machine in the synchronous mode, [60]. This work was furthered by Gorti et. al [41]. Boger et. al. generalised the Li d-q model to any pole pair configuration, however their starting point was an assumed stator and rotor configuration [11, 12].

Also at Oregon, Ramchandran et. al. offered frequency-domain methods of extracting most parameters for the d-q model described in [64]. Their work was initially presented in simulation only, but then partially verified by experiment in a later paper [79, 80].

At this stage, work on the BDFM at Oregon concentrated on control aspects and applications of the machine, which will be discussed later. However further contributions were made on the modelling of the BDFM by Williamson et. al at Cambridge University. They presented a generalised harmonic analysis of the BDFM which is capable of predicting the steady-state performance of any BDFM with a nested loop rotor with any stator winding, allowing the harmonic contributions to be specifically analysed [115, 114, 33]. Williamson and Ferreira also used finite element analysis to verify their results and investigate the effect of iron loss and saturation [33, 34]. Williamson and Boger also used the harmonic analysis model as a starting point to investigate inter-bar currents in the BDFM. Significantly they found that, unlike in a conventional cage rotor induction machine, the performance of the BDFM is significantly impaired by inter-bar current, to the extent that they recommend insulation of the rotor bars [12, 117]. Nevertheless, this does not mean that it would be impossible to cast a rotor, as Koch et. al. present methods by which this can be achieved [55].

As previously discussed, Cook and Smith noted the presence of unstable operating modes in the doubly-fed single frame cascade induction machine [24, 25]. Similar lightly damped, and unstable regions were evidently of concern to the work at Oregon State University from the outset [104, p. 742].

The first attempt, and indeed the only to date, to analyse the open-loop (that is without any feedback, speed or otherwise) stability of the BDFM was undertaken by Li et. al. in 1991 [62], the same work was also published four years later [61].

Reference [61] (and [62]) used the d-q axis model developed in [64], and linearized this model about an operating point. The approach adopted used the first term of the Taylor series, as usual when performing a linearization. However the process is complicated by the choice of reference frame for the d-q axis model, which is synchronous with the rotor. In such a reference frame the equilibrium conditions are not constant, but sinusoidally varying. This rendered the linearised system periodic, and Li et. al. used Floquet theory (see [28]) to numerically analyse the stability, and present an algorithm for doing so.

In 1992 Brassfield et. al. published a 'direct torque control' algorithm for the BDFM [13] (also published as [14]). This is believed to be the first control algorithm proposed for the BDFM. The algorithm was developed from the d-q model developed in [64], but using a vector flux quantity instead of rotor current states. The algorithm seeks to regulate the torque and control winding flux derivatives, and then outer PI (proportional-integral) loops use these variables to drive the controlled outputs to their reference set points. However, the algorithm, in its most basic state, requires complete knowledge of the stator and rotor currents, speed and position in real time. To overcome this limitation an estimator was proposed to estimate the flux variables, leaving only measurement of the stator voltages and currents, and the speed and position. The results were presented in simulation only.

It is interesting to note that the development of the 'direct torque control' algorithm in [14] is, in fact, closely related to the application of *feedback linearization* to the BDFM, although the authors do not appear to have made this connection. Feedback linearization is a non-linear control design technique where full state feedback is used to remove non-linearities in a model. The application of feedback linearization to the BDFM will be discussed in chapter 8.

In reference [128] a variation of the 'direct torque control' algorithm of [14] was presented where the outer loop PI regulation is replaced with an adaptive control law. Simulation results were presented.

In 1993 Zhou et. al. presented experimental results from a so-called 'scalar' control algorithm for the BDFM. The algorithm comprised of two PI regulation loops, one for the shaft speed and the other for the grid-connected stator power factor, by varying the instantaneous magnitude and phase of the converter-fed stator. The proposed algorithm requires a current source inverter [127]. The 'scalar' control algorithm requires measurement of the grid-connected winding voltage, current and the rotor speed.

In reference [127] it was also noted that the 'direct torque control' algorithm was being implemented in hardware, however to date this is the last mention of the 'direct torque control' algorithm, suggesting that there were practical problems associated with its implementation. One problem mentioned was that of computational complexity and associated hardware limitations, but there may have been more fundamental problems with the algorithm.

A significant development took place in 1994 when Zhou and Spée noted that the d-q model of [64] could be rotated into a reference frame in synchronism with the machine d-q currents, rather than synchronous with the rotor itself [130]. While this reference frame lacks a concrete physical interpretation it is has the advantage that the d and q quantities become constant quantities in the steady state. In reference [130] version of the d-q model in the rotor reference frame supplied with a current source inverter (first presented in [42]) was converted into the synchronous reference frame.

From the synchronous reference frame model a rotor field orientated control scheme was developed, using the dynamic BDFM equations to decouple control winding flux and torque. The method assumes that the flux is a constant parameter, and then estimates the remaining quantities required to derive a demanded control winding current. The control input is the desired electrical torque, which is used to regulate the speed using a PI regulator. The effect of all stator resistance terms is neglected, as are leakage inductances. The control algorithm required measurement of the power winding voltages, position and speed. The control winding currents are the control outputs, which are fed into a current source inverter.

Reference [125] (also published as [129]) presents an experimental implementation of the control algorithm. Principally the implementation is as described in [130], with the same control inputs, however the internal calculations were manipulated for easier implementation, using a synchronous load angle as the internal variable.

Two simplifications of the proposed field orientated scheme were presented. The first, [126], removes the need for position measurement, by assuming a fixed value of the synchronous load angle during transients. This was reported as degrading the step response for a 100rpm step speed change from 0.4s to 1.2s. The second simplification proposed in [124] is conceptually similar to the original field orientated scheme. However, no attempt is made to estimate the electrical torque, instead the synchronous load angle is regulated. Although the new algorithm constitutes a conceptual simplification, the performance of the resulting control law was improved: 0.3s for a 100rpm step change. The authors attribute this improvement is due to an increase in controller bandwidth made possible by the reduced controller complexity.

An implementation of the original field orientated scheme ([125]) was reported in [96]. The results are for a much larger machine (30kW), and although the dynamic performance is not as good (100rpm step response of 1.3s), it is likely that the speed of response was limited by inverter rating, rather than the control algorithm.

More recent publications have appeared for the cascaded doubly-fed machine, which is electri-

cally similar to the machine of Lydall, but literally comprises of two machines, in two separate frames with the rotors coupled both mechanically and electrically. A stator flux orientated control scheme and 'combined magnetizing flux' control scheme were presented. It is claimed that these schemes would apply equally to the BDFM, although results are only presented for the cascaded machine [45, 46].

1.2 Description of the BDFM

The contemporary BDFM is single frame induction machine, without any brushes, which has two 3-phase stator supplies (hence 'doubly-fed'), of different pole numbers. Typically the two stator supplies are of different frequencies, one a fixed frequency supply connected to the grid, and the other a variable frequency supply derived from a power electronic frequency converter (inverter), as illustrated in figure 1.1.

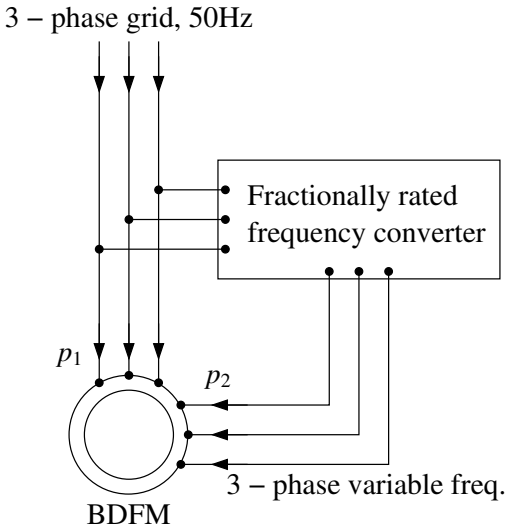

Figure 1.1: BDFM concept: a brushless, doubly-fed induction machine

1.2.1 Machine Concept

The machine may be thought of, conceptually, as two induction machines, of different pole numbers (and hence different synchronous speeds, for the same supply frequency) with their rotors connected together both physically and electrically. Physically the machine is very similar to the self-cascaded machine proposed by Hunt [48], the main distinction is that the BDFM is explicitly a doubly-fed machine.

This combination of induction machines is similar to the traditional *cascade* connection of induction machines. In a traditional cascade connection, the rotor of one machine was connected to the stator of the next (via slip rings). However it was Hunt who realised that if both machines were in the

same frame, then it was advantageous to connect the rotors together, rather than one machine's stator to another's rotor, as it removed the need for slip rings [48]. Hunt also showed that the rotor-rotor connections amounted to essentially the same system as stator-rotor connections.

If stator 1 has p_1 pole pairs, and stator 2 p_2 pole pairs, then the BDFM can be operated as an induction machine of either p_1 pole pairs or p_2 pole pairs, by connecting stator 1 or stator 2 respectively, and leaving the other supply unconnected in each case. In the sequel this mode of operation will be referred to as *simple induction* mode. The characteristics of the BDFM in this mode are the same as those of a standard induction machine, except that the performance will be poor. The reasons for this will be addressed in chapter 4.

However, if the non-supplied stator winding is short-circuited, then the behaviour of the machine is like that of a cascaded induction machine. A cascade induction machine formed from p_1 and p_2 pole pair induction machines has characteristics which resemble an induction machine with $p_1 + p_2$ pole pairs. This will be discussed in more detail in chapter 4, and in the sequel this mode will be referred to as *cascade induction mode*.

The previous two modes are both asynchronous modes of operation, that is, the shaft speed is dependent on the loading of the machine, as well as the supply frequency. However in doubly-fed mode the BDFM has a synchronous mode of operation which is the desirable operating mode, and the one for which the design of the machine is to be optimised.

1.2.2 Synchronous mode of operation

We shall now introduce the synchronous mode of operation of the BDFM. The synchronous mode of operation of the BDFM relies on *cross-coupling* between the stator and rotor [115], so does, in fact, the cascade induction mode of operation.

Cross-coupling means the coupling of the field produced by stator 1 to stator 2, and vice-versa. By design, this cross coupling cannot occur directly between stator 1 and 2 as they are chosen to be non-coupling - in the simple case this means that the pole number of each field must be different. A full discussion of this point is given in chapter 2.

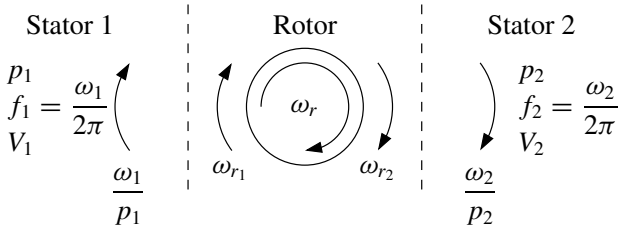

Figure 1.2: BDFM concept: speed of stator and rotor fundamental fields

If stator 1 has p_1 pole pairs and is supplied with a three phase supply at ω_1 rad/s, then the stator current wave, and hence air gap magnetic flux density will rotate at ω_1/p_1 rad/s. Similarly if stator 2 has p_2 pole pairs and rotates at ω_2 rad/s then the waveforms will rotate at ω_2/p_2 rad/s. Therefore the

fundamental magnetic flux density due to stators 1 and 2 may be expressed as follows (ignoring any fixed angular offsets):

$$b_1(\theta, t) = \hat{B}_1 \cos(\omega_1 t - p_1\theta)$$
$$b_2(\theta, t) = \hat{B}_2 \cos(\omega_2 t - p_2\theta)$$

where $\hat{B}_1$, $\hat{B}_2$ are the peak magnetic flux density and θ is the angular position around the circumference.

If the rotor is rotating at ω_r rad/s, then the fundamental flux density equations may be written in the rotor reference frame, $\theta' = \theta + \omega_r t$:

$$b_1'(\theta', t) = \hat{B}_1 \cos\left((\omega_1 - \omega_r p_1)t - \theta' p_1\right)$$
$$b_2'(\theta', t) = \hat{B}_2 \cos\left((\omega_2 - \omega_r p_2)t - \theta' p_2\right)$$

Therefore the magnetic flux densities, in the rotor reference frame, are travelling waves of frequency $(\omega_1 - \omega_r p_1)$ and $(\omega_2 - \omega_r p_2)$ respectively.

Cross coupling, then, requires currents induced by b_1' in the rotor to 'couple' with b_2' and vice-versa. By 'couple' we mean, in this context, that a constant torque be produced, i.e a torque with a non-zero mean. Torque can be expressed as the integral from 0 to 2π of the product of a current wave and magnetic field wave. The induced current wave due to a magnetic field will be of the same frequency in the steady state. Therefore if a constant torque is to be produced by cross coupling then $(\omega_1 - \omega_r p_1) = \pm(\omega_2 - \omega_r p_2)$. Taking the negative condition and rearranging gives:

$$\omega_r = \frac{\omega_1 + \omega_2}{p_1 + p_2} \tag{1.1}$$

Equation (1.1) gives the requirement on rotor speed for cross-coupling to occur in steady-state.

It is noteworthy that $\omega_2 = 0$ is a perfectly legitimate BDFM synchronous speed, that is, the second supply may be fed with DC. This operational condition was noted by Broadway and Burbridge [17].

The condition when $\omega_2 = 0$ will be referred to as *natural speed* in the sequel, and is given by:

$$\omega_n = \frac{\omega_1}{p_1 + p_2} \tag{1.2}$$

Furthermore there must be spatial compatibility for cross coupling to occur. That is, the current induced in the rotor by b_1' must produce a magnetic field containing a p_2 pole pair field harmonic component for cross coupling to occur; and of course, vice-versa. This requirement can be satisfied by a special design of rotor, one example of which is the 'nested-loop' rotor first proposed by Broadway and Burbridge [17]. Further consideration of rotor design is given in chapter 5.

When the synchronous conditions are satisfied then the machine produces torque, the value of which is controlled by a load angle, like that of a synchronous machine [115]. Also, the power supplied to the machine is approximately split between the two stator supplies in the ratio $\omega_2 : \omega_1$,

therefore if only a small speed deviation is required away from the natural speed, then it is likely that a variable speed drive installation could be designed with an inverter rating a fraction of the total drive power, perhaps as small as 30% of the total [104].

Furthermore, it can be shown that the power factor of the machine can be controlled in this synchronous mode, and, subject to inverter capacity, the grid-connected winding may run at leading power factor [115].

1.2.3 Potential Applications for the BDFM

The BDFM then has some very attractive features: it is brushless in operation, offers high power factor operation when operating as variable speed drive, and can achieve variable speed operation with a fractionally rated inverter. The fractional rating of the inverter will lead to significant economic benefits, as typically the cost of a variable speed drive is dominated by the cost of the inverter [127].

The most promising applications therefore are applications requiring variable speed operation, preferably over a limited speed range, and in environments where high power factor and lack of brushes are highly advantageous.

Wind power generation is a likely area of application at present, the advantages of fractional inverter and high power factor have already prompted the use of the doubly-fed induction machine [75]. The BDFM maintains these advantages but also achieves brushless operation, which particularly for off-shore installations, would be of considerable benefit; increasing the time between services [8, 19].

Other applications that have been considered, include pump drives [10]. Again the motivation is the reduced inverter rating, the typically low starting torque required for fluid loads means that this advantage can be maximised.

There is, however, likely to be a cost penalty for using a BDFM as compared to a conventional induction machine-based drive. The rotor is likely to be more complex, hence manufacturing costs will be slightly higher, and also it is likely that the machine itself may be slightly larger for the same output torque. However the benefits will certainly outweigh the costs in an appropriate number of application areas.

1.3 Approach of this work

The evidence of the previous discussions leads to a number of unresolved issues which prevent the commercial adoption of the BDFM. The BDFM is seen as a brushless replacement for certain electrical machines in particular applications, however to date no machines are in commercial service and there is no industrial experience of machine design or control. It is therefore desirable for the machines manufacturers to quantify the performance penalty incurred with the new technology (if any), as this decides the economic success, or otherwise. The performance of the machine is of commercial

concern in: its physical size, efficiency, the extent to which it draws harmonic currents, the required inverter rating for machine operation and the dynamic stability of the drive system.

Initially the focus of this work was on the dynamic stability of the machine, however it became clear that existing analysis of the machine was incomplete and provided only a partial solution. Therefore this dissertation addresses the following areas:

- The development of a coherent set of models for a general class of BDFM machines which accurately predict both steady state and dynamic performance (Chapters 2, 3, 4, and 7);
- The use of these models to investigate the steady-state performance of the machine and the stability of steady-state operating points, and to propose a method of quantifying machine performance in terms of machine equivalent circuit parameter values (Chapters 4 and 5);
- The estimation of machine parameter values by experiment (Chapter 6);
- The consideration of new rotor designs to improve the steady state performance (Chapter 5);
- The consideration of control strategies to stabilize and improve the damping of steady-state operating points (Chapters 7 and 8).

The specific context of these areas will now be discussed.

1.3.1 BDFM Model Development

A spectrum of modelling techniques has been successfully employed in the study of electrical machines, ranging from the elegant simplicity of the equivalent circuit model to the detail and precision of finite elements modelling. Both ends of this spectrum, and methods which fall in between, have their place in BDFM modelling and have been successfully used.

Finite elements modelling, from the users perspective, essentially allows 'experiments' to be performed on detailed numerical models of electrical machines which are defined by their physical dimensions and electrical connections. This approach allows dynamic and steady-state modelling and can include the effects of saturation. This technique has been applied to the BDFM in [34, 33], and gave very good predictions. However, the complexity of the model makes the computational burden significant, typically of the order of 1 hour of computation time to simulate 1 s, using a Pentium 4 class processor. Furthermore, the finite element approach is very much a computer-based method of experimentation rather than an analysis tool, that is, it provides little insight as to how designs may be improved, and machines must be investigated on a case by case basis. For these reasons finite elements modelling is not considered further in this dissertation.

While the finite elements technique leads to accurate results, it can be difficult to gain insight into machine operation. A generalised harmonic analysis for the BDFM with a 'nested-loop' design rotor

was presented in Williamson et. al. [115, 114]. Harmonic analysis performs a harmonic decomposition of the magnetic flux density, and couplings between constituent motor circuits, which can be vital in the optimization of machine design. The model presented in [115, 114], while not able to account for saturation, can model any configuration of nested-loop rotor BDFM (although not any other rotor design) in combination with any realistic stator winding. However, as is typical with harmonic analysis, it can only be used to model the steady-state operation of the machine, which means it cannot be used investigate stability of the machine.

Other modelling techniques applied to the BDFM include, dynamic coupled-circuit models, although these were applied to a specific example[110, 104]. d-q axis dynamic models have been presented [64, 63, 11, 12], however these models either apply to a specific machine, or to machines with 'nested-loop' design rotors, and furthermore the connection between these models and the coupled-circuit model is not made clear. Equivalent circuit models have been proposed by a number of authors [17, 60, 65, 59, 41]. However, these have generally been either given without derivation, or have been for a specific machine configuration. Again the connection between these equivalent circuit models and either the d-q axis models or coupled circuit model has not been made clear.

There is a need for a generalised dynamic and steady-state modelling framework which can be applied to a wide class of BDFM machines, including, but not limited to, those with a 'nested-loop' rotor. A rigorous derivation of other models is needed from this framework to give a d-q axis model, and equivalent circuit model which are consistent and for which parameter values may be calculated and their physical meaning made explicit. This dissertation provides such a framework and rigorous derivations.

1.3.2 Use of BDFM models to investigate performance, new rotor designs and the estimation of machine parameters

The majority of previous work on the BDFM has been analysis detached from any performance objectives. While some work has been done on the basic machine operation, [41, 60, 114, 10], it has not sought to identify key machine parameters which an ideal design would optimize. Therefore it is difficult to know what design compromises will lead to good machine performance without actually designing a machine and testing it.

This dissertation provides a partial solution by investigating which machine parameters in the derived equivalent circuit model have the greatest impact on machine performance.

Since the work of Broadway and Burbridge the rotor design has remained largely static for the BDFM [17]. Although some investigations into improving the performance of the 'nested-loop' design of rotor proposed by Broadway and Burbridge was undertaken [109], the design of the rotor has not been considered since. However the design of the rotor cannot be considered a closed area of research as Broadway and Burbridge themselves concede [17]. Therefore in this dissertation new rotor designs are considered and their performance evaluated using the derived equivalent circuit model

and by experimental means.

The issue of parameter estimation for the BDFM has received relatively little attention. Only two publications appear in the literature [80, 79]. These methods find parameter values for a d-q axis model. However little, or no, experimental evidence was presented supporting the efficacy of the approach. We therefore propose a new method of parameter estimation. The method gives parameters for the derived equivalent circuit model which are related back to parameter values for the d-q axis model, and for which considerable experimental evidence is presented for its effectiveness.

1.3.3 Analysis of stability of the BDFM and the development of control strategies

The only publication to address the stability of the BDFM in its synchronous mode of operation was presented by Li et. al. [61] (also published as [62]). However, because of the model used, Li et. al. were forced to analyse the stability of a periodic system, which therefore, did not admit the use of well-established controller design tools for LTI systems. Furthermore, the analysis was for a specific BDFM machine.

There is a need for a rigorous stability analysis which covers a wide class of BDFM machines. This dissertation develops a general linearized model which admits local stability analysis by standard eigenvalue techniques, and from which controllers may be designed. We also investigate the quadratic stability of the electrical dynamics of the class of BDFM machines considered.

Furthermore although a number of publications have appeared on control aspects of the BDFM [125, 129, 130, 126, 124], all of the publications containing experimental results were for control schemes which required a current source inverter. Therefore we propose two practical control strategies using a voltage source inverter.

Recognising the limitations of linear controller design techniques we consider the nonlinear controller design technique *feedback linearization*. We give two possible methods of application to the BDFM and outline initial attempts at implementation of such schemes on a prototype BDFM.

Chapter 2

BDFM Coupled Circuit Modelling and Parameter Calculation

2.1 Introduction

For the purposes of this work it is necessary for the adopted model to predict both dynamic and steady-state performance of a range of different machine designs. Furthermore, in order to make use of the model and to explore potential machine designs it is necessary to calculate parameter values for any such model.

As discussed, it has been decided to use a coupled-circuit model for this purpose.

Wallace et. al. and Spée et. al. [110, 104] used a coupled circuit technique to model a prototype BDFM, however no generalisation of this model was ever presented. Although Wallace et. al used the model to simulate their prototype machine, [104], the limitations of the model were never addressed, specifically, the inclusion of leakage inductance effects, allowance for finite conductor widths and the generalisation of the model to a wide class of machines. The work presented here is similar to their work, but generalised, to allow any realistic BDFM to be modelled, allow the inclusion of some leakage inductance effects and makes allowance for finite conductor widths.

The machine is modelled as a set of interconnected coils. This assumption is reasonable in practice, as will be argued, as it allows almost all industrial-type electrical machines to be modelled without further simplification. From this standpoint, relationships between stator and rotor of the machine are derived in terms of mutual inductance matrices.

Furthermore the parameter calculation technique adopted is particularly suited for implementation on computer, and when so done allows significant modification of the design of the machine to be performed with relative ease. This is achieved by calculating inductance parameters in a coil by coil basis, and then combining the results in a manner appropriate to the circuit being analysed.

In contrast to [110], two methods are proposed for the calculation of inductance parameters. Firstly the parameters are calculated by direct integration, and secondly by splitting into Fourier

series prior to integration.

The latter method is useful as it allows the harmonic content to be investigated. This is something that will be important in chapter 5.

Finally a dynamic model is derived for the BDFM using the calculated parameters.

Some of the results presented in this chapter will be of no surprise to readers familiar with electrical machine modelling. However the BDFM is an unusual machine, and great care must be taken in the analysis as not all results applicable to related machines, such as the induction machine, can be directly transfered. For this reason, and because it is anticipated that readers from a system-theory background will have had less exposure to electrical machine modelling, derivations are presented in detail.

An attempt has been made to state assumptions at the start of each section and in some cases references are provided to well-respected works which adopt the same assumptions.

2.2 Preliminaries

The following definitions are standard, for further information see, for example, [122].

Definition 2.1. Let there be N turns of wire with current $i \in \mathbb{R}$ A flowing in each. Let the magnetic field intensity vector be $H \in \mathbb{R}^3$, $dl \in \mathbb{R}^3$ a direction vector of infinitesimal magnitude, J be the current density, and $dA \in \mathbb{R}^3$ a direction vector normal to the surface S of infinitesimal magnitude. Ampere's Law states:

$$\oint_C H \cdot dl = \oint_S J \cdot dA = Ni$$

where S is any open surface bounded by a closed path C. In the case that the surface S contains N conductors each carrying current i, then the right hand side reduces to Ni, as shown. A right-hand coordinate system will be used, therefore an anti-clockwise closed path requires the positive direction of current flow to be out of the page. Ampere's Law is only valid if the rate of change of electric flux density is negligible. This fact will be assumed.

Definition 2.2. [35, p. 132] The magneto-motive force (mmf) of any closed path, C, is defined as the net ampere-turns, $Ni = \oint_S J \cdot dA$, enclosed by that path:

$$\mathcal{F}_C \triangleq \oint_S J \cdot dA = Ni$$

where N, i, S, and J are as given in definition 2.1

Definition 2.3. A magnetic material is said to be *linear* if:

$$\exists \mu : B = \mu H, \mu \text{ constant}$$

where μ is the magnetic permeability of the material, and B is the magnetic flux density.

Linearity of the magnetic material implies that there is no saturation, or skin effects.

Definition 2.4. The *magnetic flux*, ϕ, passing through a surface, A is defined as:

$$\phi \triangleq \oint_A B \cdot dA$$

Definition 2.5. *Gauss's Law* for magnetic fields states that total magnetic flux out of any closed surface, S, is zero:

$$\oint_S B \cdot dA = 0$$

Definition 2.6. The magnetic flux ϕ_l, linked by a circuit with conductor density, C, is defined as:

$$\phi_l \triangleq \oint_{A_2} \oint_{A_1(A_2)} B \cdot dA_1 C dA_2$$

where the surface A_1 is defined by the closed curve due to elemental conductor CdA_2 within which the magnetic flux density is B. In the simple case of N coincident conductors bounding a surface A the flux linked by the circuit reduces to:

$$\phi_l \triangleq N \oint_A B \cdot dA$$

Therefore from definitions 2.1, 2.3 and 2.4, in a network of k circuits, if a magnetic material is, or can be assumed to be, linear, the magnetic flux ϕ_l linked by circuit $n \leq k$ due to magnetic flux produced by circuit $m \leq k$ circuits is linearly dependent on the current flowing in circuit m.

Definition 2.7. For a network of n circuits with linear magnetic material the *Mutual inductance*, $M \in \mathbb{R}^{n \times n}$, can be defined in terms of the flux linked by each of the n circuits due to the current flowing in the n circuits:

$$\phi_l = Mi$$

where M is not a function of i. The flux linked by the j^{th} circuit due to current flowing in the k^{th} is M_{jk}.

Definition 2.8. *Self inductance*, L_k, is the flux linked in the k^{th} circuit ($k \leq n$) due to current flowing in the k^{th} circuit. Therefore:

$$L_k = M_{kk}$$

i.e. the *self inductance* terms are the diagonal elements of M.

Lemma 2.1. *[72] From energy conservation it can be shown that:*

$$\forall i, j \leq n : M_{ij} = M_{ji} \tag{2.1}$$

Lemma 2.2. *[72] For any mutually coupled coils of self inductance L_i and L_j and mutual inductance M_{ij}:*

$$M_{ij} \leq \sqrt{L_i L_j} \tag{2.2}$$

Definition 2.9. Faraday's law relates the voltage induced across the terminals of a circuit due to the flux linked by that circuit:

$$v = \frac{d\phi_l}{dt}$$

where the electro-motive force (emf) induced in the circuit is given by $-v$.

Definition 2.10. A matrix, $A \in \mathbb{R}^{n\times n}$ is said to *positive (semi) definite* if $x^{\mathrm{T}}Ax > (\geq)0\ \forall x \in \mathbb{R}^n \neq 0$. From this definition the following are immediate:

1. If A, B are positive definite then $A + B$ is positive definite.
2. If A is positive definite and $\gamma > 0$ where γ is scalar, then γA is positive definite.
3. $\begin{bmatrix} A & 0 \\ 0 & B \end{bmatrix}$ is positive definite if and only if A and B are positive definite.

Analogous results follow for positive semi-definite matrices and negative (semi) definite matrices.

Lemma 2.3. *[72] For any set of mutually coupled coils , $M \in \mathbb{R}^{n\times n}$, with constant inductance parameters, the work done in increasing the current from 0 to $i \in \mathbb{R}^n$, that is the energy stored, is $\frac{1}{2}i^{\mathrm{T}}Mi$. Furthermore from Lenz's law, with the chosen sign convention, this energy must be greater than or equal to zero. We may therefore conclude from def. 2.10 that M is positive definite.*

2.3 General Electrical Machine Coupled-Circuit Model

Given a network of n circuits, each with terminal voltage, $v \in \mathbb{R}^n$, current $i \in \mathbb{R}^n$ flowing in them, and $\phi \in \mathbb{R}^n$ being the flux linked by each circuit, combining Faraday's law and Ohm's law:

$$v = Ri + \frac{d\phi}{dt} \tag{2.3}$$

where $R \in \mathbb{R}^{n\times n}$ is the matrix of resistances.

This modelling approach is called a *coupled-circuit* or *coupled-coil* model.

It should be noted that for any physically realizable system the principle of reciprocity requires that R and M are symmetric, that is that $R = R^{\mathrm{T}}$ and $M = M^{\mathrm{T}}$. Further, it is usually the case that R is diagonal.

Assuming a linear magnetic circuit, from the definition of mutual inductance, def. 2.7, equation (2.3) may be expanded using the chain rule to give:

$$v = Ri + \frac{dM}{dt}i + M\frac{di}{dt} \tag{2.4}$$

In electrical machines the mutual inductance term, M, is assumed to vary only with the rotor position, $\theta_r \in \mathbb{R}$.

We define the rotor angular speed as:

$$\omega_r \triangleq \frac{d\theta_r}{dt} \tag{2.5}$$

It is then natural, to express (2.4) in terms of the rotor angular speed:

$$v = Ri + \omega_r\frac{dM}{d\theta_r}i + M\frac{di}{dt} \tag{2.6}$$

In systems theory terms an electrical machine can be thought of as a dynamic system with input voltage and output currents. In this case, the system admits a state-space representation where the currents are the system states. From (2.6):

$$M\frac{di}{dt} = -Ri - \omega_r\frac{dM}{d\theta_r}i + v \tag{2.7}$$

2.3.1 Torque Calculation

The electro-magnetic torque developed by the machine couples the electrical differential equations to the mechanical differential equations. The torque produced by an electrical machine can be determined by considering instantaneous power transfer in the system.

Firstly we recall that the energy stored in magnetic field in a coupled circuit network, or magnetic co-energy, is defined as:

$$W_{co} = \frac{1}{2}i^{\mathrm{T}}Mi \tag{2.8}$$

Therefore the instantaneous power transfer from the magnetic field is given by:

$$\begin{aligned}\frac{dW_{co}}{dt} &= \frac{1}{2}\frac{di^{\mathrm{T}}}{dt}Mi + \frac{1}{2}i^{\mathrm{T}}\frac{dM}{dt}i + \frac{1}{2}i^{\mathrm{T}}M\frac{di}{dt} \\ &= \frac{1}{2}i^{\mathrm{T}}\frac{dM}{dt}i + i^{\mathrm{T}}M\frac{di}{dt} \qquad \text{as } \frac{W_{co}}{dt} \text{ is scalar and } M = M^{\mathrm{T}}\end{aligned} \tag{2.9}$$

Multiplying (2.4) by i^{T} from the left:

$$i^{\mathrm{T}}v = i^{\mathrm{T}}Ri + i^{\mathrm{T}}\frac{dM}{dt}i + i^{\mathrm{T}}M\frac{di}{dt} \tag{2.10}$$

Therefore from (2.9) with (2.5), and expanding via the chain rule gives:

$$i^{\mathrm{T}}v = i^{\mathrm{T}}Ri + \frac{1}{2}i^{\mathrm{T}}\frac{dM}{dt}i + \frac{dW_{co}}{dt} = i^{\mathrm{T}}Ri + \omega_r\frac{1}{2}i^{\mathrm{T}}\frac{dM}{d\theta_r}i + \frac{dW_{co}}{dt} \tag{2.11}$$

Equation (2.11) is a balance of the instantaneous power transfer in the system. The input power, $i^{\mathrm{T}}v$ is balanced by the Ohmic loss term, $i^{\mathrm{T}}Ri$, the rate of change of stored energy in the magnetic field, $\frac{dW_{co}}{dt}$, and the remaining term corresponds to the mechanical power generated by the machine. Therefore the electrical torque generated by the machine is given by:

$$T_e = \frac{1}{2}i^{\mathrm{T}}\frac{dM}{d\theta_r}i \tag{2.12}$$

Notice that the torque may equivalently be defined as:

$$T_e = \frac{\partial W_{co}}{\partial \theta_r} \tag{2.13}$$

2.4 Calculation of Parameters for Electrical machines

In the previous section the general electrical machine equations have been derived. In order to proceed with simplifying transformations it is necessary to explore the structure of the inductance and resistance matrices in (2.4). The structure is most simply revealed by calculating values for these parameters, under the assumptions stated in section 2.3. The following additional assumptions will now be made:

- The permeability of iron can be considered to be infinite.
- The air gap width between the stator and rotor is small enough, relative to the machine length and diameter, that it may be assumed that:
  - The effects of finite machine length can be neglected.
  - The lines of magnetic flux in the air gap are parallel.
- The machine is assumed to consist of a cylindrical rotor inside a cylindrical stator, with conductors which may each be adequately modelled as a uniform conductor distribution on the surface of either the rotor or stator cylinder within the region containing those conductors (see figure 2.2). That is, the conductors are assumed to be of zero depth, but finite width.
- For the purposes of mutual inductance calculation the rotor and stator are separated by an *effective* air gap width, given by Carter's Factor. See section 2.8 for full details.
- All **conductors** in each slot of the stator (or rotor) are uniformly distributed over the same pitch, although the pitch may differ between stator and rotor. The pitch over which the conductors are distributed is assumed to be the slot mouth width.

- The effects of leakage (discussed in section 2.5.2) may be satisfactorily modelled by some suitable addition to the self-inductance terms only.

The assumptions stated above, combined with those used to derive (2.4), are known to yield a model with satisfactory accuracy in the modelling of induction machines and BDFMs: [115] and [110] present BDFM models derived using these assumptions. [114] and [104] verify these respective models against experimental results. Furthermore, [113] and [116] give examples of models for cage rotor induction machines derived with these assumptions, the results being verified against experimental data.

As calculation of parameters for a variety of different machines is required, the approach presented here is motivated by versatility. It is similar to that described in [110], but the assumption of point conductors relaxed, and generalised for any machine for which the stated assumptions are reasonable. We first calculate the flux density due to unit current flowing in a single coil. We then use this result to derive an expression for the mutual inductance between any two coils with a particular class of conductor distributions (to generalise to any conductor distribution is trivial, but of limited application). We then split the machine windings and rotor circuits into single coil elements and compute the mutual inductance between all single coil elements. We then sum the single coil elements taking care with the sign to yield the machine parameters. The calculation of flux density and inductance for a single coil is well-known, and can be found in, for example, [43, ch. 1], although it is usual to express the result as a Fourier series rather than a definite integral, as is required in this case. Furthermore point conductors are usually assumed, whereas, in common with [116] we allow for uniformly distributed finite width conductors. For these reasons, and for the benefit of the reader from a systems theory background, a full derivation is included.

2.4.1 Magnetic Flux Density due to Single Coil

We wish to determine the spatial magnetic flux density produced in the air gap due to current i flowing in a coil of N turns connected in series. The coil is the basic building block used to create machine windings. From Definition 2.1, we may relate the line integral of the magnetic field intensity around any closed path to the current flowing through the surface bounded by the closed path. Figure 2.1 shows a machine rotor in plan with a section through the rotor. As the air gap is assumed small, the rotor and stator diameter are taken to be the same. Figure 2.2 shows a cross-section through a rotor and stator of an electrical machine. For simplicity, the cylindrical rotor and stator surfaces have been flattened, thus the far left and right hand edges of the diagram are coincident. The figure shows two stator slots filled with conductors, and the remaining slots empty. $\otimes$ and $\odot$ indicate current flow into and out of the page respectively.

Consider the closed path, C_1: as we assume that the iron has infinite permeability the portion of the line integral of magnetic field intensity in the iron is zero regardless of the exact path. Therefore

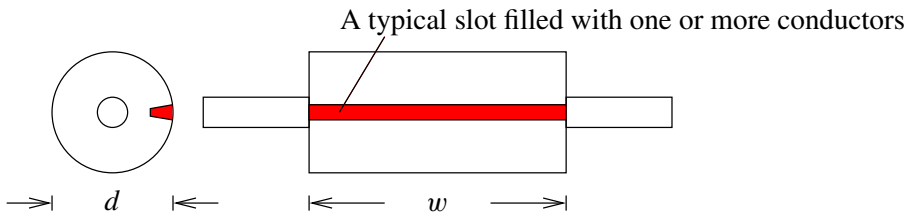

Figure 2.1: Cross-section and plan views of a typical machine rotor, showing the rotor diameter, d, and lamination stack length, w.

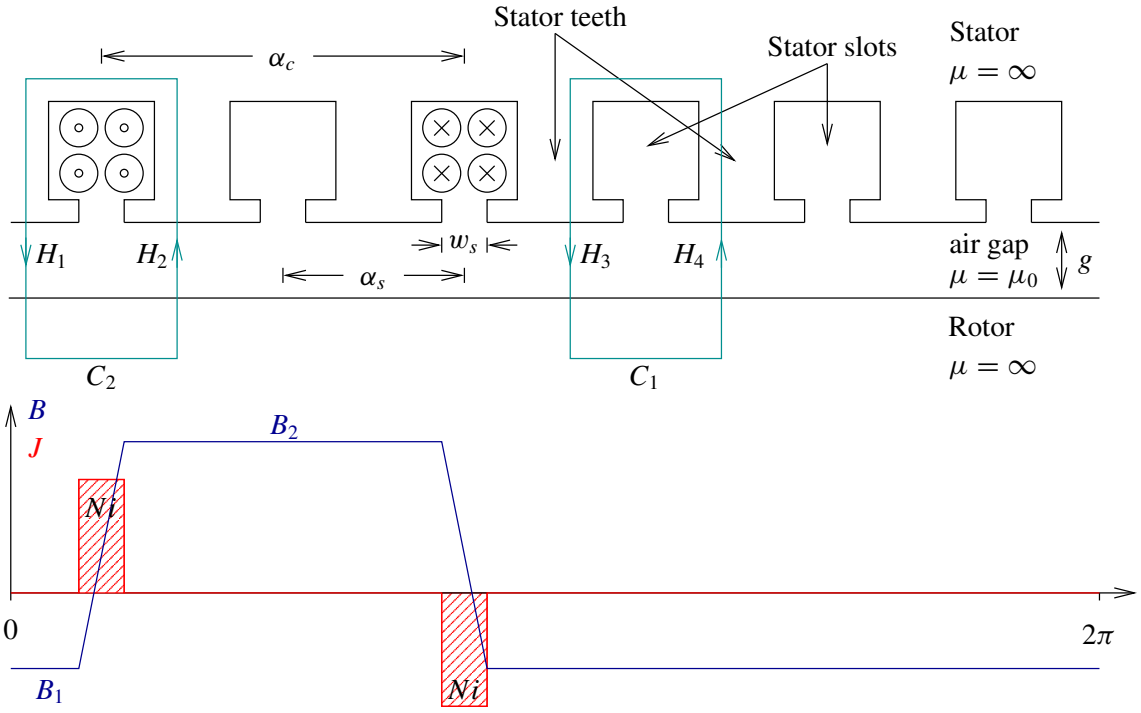

Figure 2.2: Magnetic flux and current density for a stator coil, all dimensions in radians except for g, the air gap width.

from Ampére's Law (def. 2.1), because $J = 0$ everywhere, around C_1:

$$H_3 g - H_4 g = 0 \tag{2.14}$$

$$\Rightarrow H_3 = H_4 \tag{2.15}$$

where g is the air gap length as shown in figure 2.2, and H_x are magnetic field intensities. Whereas, around path C_2 we get:

$$H_2 g - H_1 g = Ni$$

where N is the number of conductors each with current i flowing in them.

From def. 2.3 the total change in air gap magnetic flux density across a slot with N conductors with current i flowing in each is:

$$\Delta B = B_2 - B_1 = \frac{Ni\mu_0}{g} \tag{2.16}$$

Thus equations (2.16) and (2.14) show that changes in magnetic field in the air gap only occur between teeth, and that the value of this change is given by (2.16).

As in [116], it is assumed that the change in magnetic field is linear across the slot mouth, w_s, which therefore means that the current density, J for the two slots shown is as given in figure 2.2. The magnetic flux density, B is shown in blue.

In order to calculate B_1 and B_2 Gauss's Law (def (2.5)) may be applied to the cylindrical surface of the machine rotor. By considering the flux density waveform (see figure 2.2), it can easily be shown that:

$$B_2\alpha_c + B_1\,(2\pi - \alpha_c) = 0 \tag{2.17}$$

where α_c is the coil pitch in radians, as shown in figure 2.2.

From (2.17) and (2.16):

$$B_1 = \frac{-Ni\mu_0}{g}\frac{\alpha_c}{2\pi} \tag{2.18}$$

$$B_2 = \frac{Ni\mu_0}{g}\frac{(2\pi - \alpha_c)}{2\pi} \tag{2.19}$$

where w_s the slot mouth width in radians, as shown in figure 2.2.

We have now calculated the air gap magnetic field due to current i flowing in a coil, as shown in figure 2.2. We may now write down the equation of the air gap magnetic flux density, $B_k(\theta)$, due excitation of the k^{th} circuit as shown in blue in figure 2.3 (the green lines depicting the j^{th} circuit conductor distribution will be used in a later section):

$$B_k(\theta) = \begin{cases} B_{1_k} + (B_{2_k} - B_{1_k})\dfrac{\theta - \beta_k}{w_{s_k}} & \beta_k < \theta < \beta_k + w_{s_k} \\ B_{2_k} & \beta_k + w_{s_k} < \theta < \beta_k + \alpha_{c_k} \\ B_{2_k} + (B_{1_k} - B_{2_k})\dfrac{\theta - \beta_k - \alpha_{c_k}}{w_{s_k}} & \beta_k + \alpha_{c_k} < \theta < \beta_k + \alpha_{c_k} + w_{s_k} \\ B_{1_k} & \text{otherwise} \end{cases} \tag{2.20}$$

Using (2.18) and (2.19), equation (2.20) may be written in terms of the current, number of turns and slot and pitch geometries of the k^{th} circuit, shown in blue in figure 2.3:

$$B_k(\theta) = \frac{N_k i_k \mu_0}{g} \begin{cases} \dfrac{-\alpha_{c_k}}{2\pi} + \dfrac{\theta - \beta_k}{w_{s_k}} & \beta_k < \theta < \beta_k + w_{s_k} \\ \dfrac{2\pi - \alpha_{c_k}}{2\pi} & \beta_k + w_{s_k} < \theta < \beta_k + \alpha_{c_k} \\ \dfrac{2\pi - \alpha_{c_k}}{2\pi} - \dfrac{\theta - \beta_k - \alpha_{c_k}}{w_{s_k}} & \beta_k + \alpha_{c_k} < \theta < \beta_k + \alpha_{c_k} + w_{s_k} \\ \dfrac{-\alpha_{c_k}}{2\pi} & \text{otherwise} \end{cases} \tag{2.21}$$

2.4.2 Mutual (and self) Inductance of Single Coils

From the definition of mutual inductance 2.7 and flux linked 2.6, the mutual inductance between the j^{th} circuit and k^{th} circuit of an electrical machine, M_{jk}, is given by:

$$M_{jk} i_k = w \frac{d}{2} \int_0^{2\pi} B_k(\theta) \int_0^{\theta} C_j(\tau) d\tau d\theta$$

where i_k, B_k are the current and magnetic flux density in the air gap in the k^{th} circuit, C_j is the conductor density function for the j^{th} circuit ($\int_0^{\theta} C_j(\tau) d\tau$ will be referred to as the conductor distribution function for the j^{th} circuit). In particular, the conductor density function is related to the current density for the j^{th} circuit by the coil current, i_j:

$$J_j(\theta) = C_j(\theta) i_j$$

As self inductance is a special case of mutual inductance, *mutual* inductance will henceforth be used to refer to both mutual and self inductance.

We have assumed that the conductors in each coil are uniformly distributed across the slot mouth width (w_s in figure 2.2). Therefore, as each coil comprises of N series connected turns, the current in each turn is the same, and the current density function will always be of the form shown in figure 2.2, with each rectangle having area Ni, as depicted.

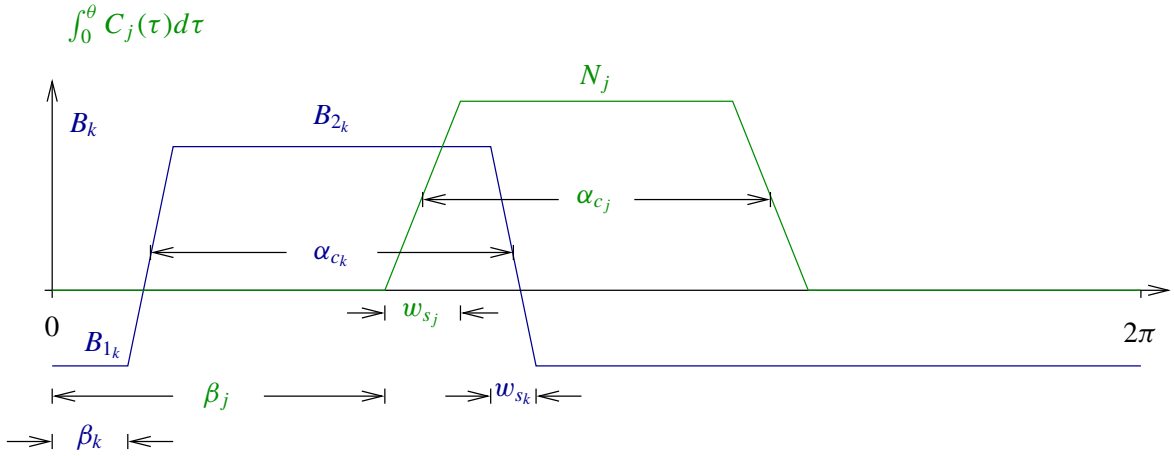

Figure 2.3: Air gap magnetic flux density due to excitation of the k^{th} coil and conductor distribution for the j^{th} coil

Figure 2.3 shows $B_k(\theta)$ and $\int_0^\theta C_j(\tau)d\tau$ for a typical jk pair. From this diagram we may write:

$$M_{jk}i_k = w\frac{d}{2}N_j\left[\int_{\beta_j}^{\beta_j+w_{s_j}} B_k(\theta)\frac{\theta-\beta_j}{w_{s_j}}d\theta + \int_{\beta_j+w_{s_j}}^{\beta_j+\alpha_{c_j}} B_k(\theta)d\theta + \int_{\beta_j+\alpha_{c_j}}^{\beta_j+w_{s_j}+\alpha_{c_j}} B_k(\theta)\frac{\beta_j+w_{s_j}+\alpha_{c_j}-\theta}{w_{s_j}}d\theta\right] \quad (2.22)$$

where $B_k(\theta)$, the magnetic field due to the k^{th} circuit is given by (2.21) and $\int_0^\theta C_j(\tau)d\tau$ is the conductor distribution function for the j^{th} circuit.

Therefore the mutual inductance between any two coils of differing pitches, and positions may be calculated by considering unit current flow in one coil, and computing Mi using (2.22), because the integral can be analytically solved for the magnetic field distribution assumed.

2.4.3 Calculation of spatial harmonic components of mutual inductance

Equation (2.22) can be used to calculate *space harmonic* components of the mutual inductance between two coils. The *space harmonic* components of the mutual inductance between two coils are the components of mutual inductance due to terms of the Fourier series representation of magnetic flux density. The method described is essentially the same as that used in [113, 116] although the presentation is rather different, and lends itself more directly to calculation by computer.

The Fourier series representation of the magnetic flux density for a single coil can be derived by finding the Fourier series of equation (2.21). It is straightforward to show that it is given by:

$$B_k(\theta) = \frac{2N_k i_k \mu_0}{\pi g}\sum_{n=1}^{\infty}\frac{\sin(n\alpha_{c_k}/2)}{n}\frac{\sin(nw_{s_k}/2)}{nw_{s_k}/2}\cos\left(n\left(\theta-\beta_k-\tfrac{\alpha_{c_k}}{2}-\tfrac{w_{s_k}}{2}\right)\right) \quad (2.23)$$

Thus the n^{th} spatial harmonic component of magnetic flux density for the k^{th} coil is:

$$B_{k_n}(\theta) = \frac{2N_k i_k \mu_0}{\pi g} \frac{\sin(n\alpha_{c_k}/2)}{n} \frac{\sin(nw_{s_k}/2)}{nw_{s_k}/2} \cos\left(n\left(\theta - \beta_k - \tfrac{\alpha_{c_k}}{2} - \tfrac{w_{s_k}}{2}\right)\right) \tag{2.24}$$

Hence the n^{th} spatial harmonic component of mutual inductance linking the j^{th} coil to the k^{th} coils is:

$$M_{jk_n} = w\frac{d}{2}N_j \left[\int_{\beta_j}^{\beta_j + w_{s_j}} B^1_{k_n}(\theta) \frac{\theta - \beta_j}{w_{s_j}} d\theta + \int_{\beta_j + w_{s_j}}^{\beta_j + \alpha_{c_j}} B^1_{k_n}(\theta) d\theta + \right.$$
$$\left. \int_{\beta_j + \alpha_{c_j}}^{\beta_j + w_{s_j} + \alpha_{c_j}} B^1_{k_n}(\theta) \frac{\beta_j + w_{s_j} + \alpha_{c_j} - \theta}{w_{s_j}} d\theta \right] \tag{2.25}$$

where $B^1_{k_n}$ is the B_{k_n} due to unit current flow.

Alternatively (2.25) can be derived directly from (2.4.2). The conductor distribution function, $\int_0^\theta C_j(\tau)d\tau$ from figure 2.3 may be written as a Fourier series:

$$\int_0^\theta C_j(\tau)d\tau = \frac{2N_j}{\pi} \sum_n^\infty \frac{\sin(n\alpha_{c_j}/2)}{n} \frac{\sin(nw_{s_j}/2)}{nw_{s_j}/2} \cos\left(n\left(\theta - \beta_j - \alpha_{s_j}/2 - w_{s_j}/2\right)\right) \tag{2.26}$$

Before proceeding it is necessary to recall the following trigonometric result:

Lemma 2.4. *Given $m, n \in \mathbb{N}$ and $\phi_1, \phi_2, \theta \in \mathbb{R}$ then:*

$$\int_0^{2\pi} \cos(n\theta + \phi_1)\cos(m\theta + \phi_2)d\theta = 0 \ \forall n \neq m$$

Proof. Apply trigonometric identity $2\cos(A)\cos(B) = \cos(A+B) + \cos(A-B)$, then integrate, and the result comes by inspection. □

Substituting (2.26) and (2.23) into (2.4.2), and using Lemma 2.4 gives:

$$M_{jk} = w\frac{d}{2}\frac{2N_k\mu_0}{\pi g}\frac{2N_j}{\pi} \sum_{n\in\mathbb{N}} \frac{\sin(n\alpha_{c_k}/2)}{n} \frac{\sin(nw_{s_k}/2)}{nw_{s_k}/2} \frac{\sin(n\alpha_{c_j}/2)}{n} \frac{\sin(nw_{s_j}/2)}{nw_{s_j}/2}$$
$$\int_0^{2\pi} \cos\left(n\left(\theta - \beta_k - \tfrac{\alpha_{c_k}}{2} - \tfrac{w_{s_k}}{2}\right)\right) \cos\left(n\left(\theta - \beta_j - \alpha_{s_j}/2 - w_{s_j}/2\right)\right) d\theta \tag{2.27}$$

Remark 2.5. The principle used to derive (2.27) applies more generally to the mutual inductance between any two circuits. From equation (2.4.2) and Lemma 2.4 it can be seen that the mutual inductance between two circuits can only consist of terms from the Fourier series representation of the magnetic flux density distribution, $B(\theta)$ and the conductor distribution function, $\int_0^\theta C(\tau)d\tau$ which corresponds to the same absolute harmonic. More precisely if Q_b, Q_c denote the set of absolute harmonics which have non-zero coefficients for the magnetic flux density and conductor distribution function respectively, then only harmonics in $Q_b \cap Q_c$ contribute to the mutual inductance. ♡

Remark 2.6. The terms *absolute* and *relative* harmonic are used to differentiate between the mathematical harmonics in a Fourier series (i.e. the value of n), and relative harmonics, that is integer multiples of some frequency (or pole number) field. In other words the fundamental absolute harmonic is $n = 1$, the second absolute harmonic $n = 2$ and so on. Whereas the first relative harmonic is $n = k$, for some integer k and the second relative harmonic is $n = 2k$ and so on. ♡

2.5 Mutual Inductance of Machine Windings

Using equation (2.22) the mutual inductance matrix for a machine winding may be calculated.

We are concerned with the calculation of mutual inductance parameters for any winding which can be made up of interconnected *groups* of coils. A *group* of coils is a number of coils, typically in different positions within the frame, connected in series.

In order to calculate the mutual inductance matrix for a machine winding, each group of coils can be represented by a single circuit as it is series connected. Therefore it can be represented by a single self-inductance term with mutual inductance terms for each coupling to other coil groups. Furthermore, these inductance terms are the summation of the inductance terms of the individual coils making up the group:

Suppose that there are a total of N coils, with mutual inductance matrix $\tilde{M} \in \mathbb{R}^{N\times N}$. Further suppose that there are m sets of series connected groups of coils. Hence there are m circuits in total, and the voltage induced at the terminals of each of the m circuits is given by:

$$v = T\tilde{M}\frac{d\tilde{i}}{dt} \tag{2.28}$$

where $\tilde{i} \in \mathbb{R}^N$ is the current vector and $T \in \mathbb{R}^{m\times N}$, T is a combination matrix made up of only 1s, -1s and 0s. Typically T will have only one non-zero element per column, because each coil is only connected to one series set. T can be found by considering the connections between the coils which form each group. When elements of T are -1 this corresponds to the coil being connected the opposite way around.

Furthermore, if the current flowing in each of the m series connected groups of coils is i, then, after some consideration, it can be seen that the current in each of the N coils is $T^{\mathrm{T}}i$. Therefore:

$$M = T\tilde{M}T^{\mathrm{T}} \tag{2.29}$$

where M is the mutual inductance matrix for the m sets of series coils.

The procedure outlined above can be used to calculate the mutual inductance matrices for any machine subject to the constraints described at the start of the section. The method has been implemented in Matlab, and has been used to calculate all inductance parameters used in this dissertation.

Functions were written which compute the mutual inductance between individual coils, returning the answer as a symmetric matrix, the fact that the matrix must be symmetric facilitates the elim-

ination of programming errors. Functions were written for the direct calculation method, equation (2.22), and for the calculation method using the Fourier series representation, equation (2.27).

As each coil must be placed in a slot, the functions were written to take a list of slots which house the 'out' and 'return' conductors for each coil, and from this compute the mutual inductances.

When one coil is on the stator of the machine, and the other on the rotor, then the functions take an angular offset parameter. The stator-rotor (and hence rotor-stator) mutual inductance terms will, of course, be parameterised by this angular offset.

2.5.1 Calculation of rotor and stator inductance matrices

When applying the previously outlined procedure to a machine, the transformation matrices can always be partitioned into a block diagonal matrix.

By choosing the coil order so that the stator coils appear before the rotor coils, the transformed mutual inductance matrix will be:

$$M = \begin{bmatrix} T_{ss} & 0 \\ 0 & T_{rr} \end{bmatrix} \begin{bmatrix} \tilde{M}_{ss} & \tilde{M}_{sr} \\ \tilde{M}_{sr}^{\mathrm{T}} & \tilde{M}_{rr} \end{bmatrix} \begin{bmatrix} T_{ss} & 0 \\ 0 & T_{rr} \end{bmatrix}^{\mathrm{T}} \tag{2.30}$$

where $\tilde{M}_{ss}$, $\tilde{M}_{sr}$, $\tilde{M}_{rr}$ are the coil mutual inductance matrices for the stator, stator to the rotor, and the rotor respectively. T_{ss}, T_{rr} are the combination matrices for the stator and rotor respectively.

Note that the $\tilde{M}_{sr}$ will be a function of the rotor position at any instant.

Appendix B.2 gives full details of the stator winding used on the prototype machine, including the coil order, and coil combination matrix used, and thus serves as an example application of this calculation procedure. Appendix B.2 also reviews standard 'winding factors' which are often used in the design of machine windings and can be used to verify inductance calculations for certain winding configurations.

2.5.2 Leakage inductance

Thus far, inductance arising from *leakage* effects have not been discussed. Inductance arising from leakage effects are inductances due to the magnetic flux not linking stator *and* rotor conductors. This definition is similar to that found in [31, sect. 5.2], except that for our purposes the harmonic mutual inductance terms are not considered part of the leakage terms, rather as a separate term (contrary to [43]).

There are various types of leakage effects, a summary of those used is found in appendix C.1.

Typically leakage inductances in a well designed machine are 1-2 orders of magnitude lower than the principal inductance terms. For simplicity it will be exclusively assumed that leakage inductance causes an increase in self inductance only. This assumption will typically lead to only very small errors, and simplifies the calculations which follow.

2.5.3 Resistance calculation

The calculation of resistance is rather more straightforward than inductance calculations. We assume that the resistivity is constant, and therefore the resistance of a coil is given by:

$$R = \frac{\rho l}{A} \tag{2.31}$$

where A is the wire cross-sectional area, l is the total length of wire in each coil, and ρ is the resistivity of the material at the operating temperature. The coil's length is approximately given by:

$$l = 2kN(\alpha_c \frac{d}{2} + w) \tag{2.32}$$

where α_c is the coil pitch, d the diameter of the centre-line of the slots, w the machine stack length, N the number of turns in the coil, and $k > 1$ a constant to allow for the space required to bend the conductors in the coil, typically $k < 1.1$.

Once the coil resistance has been calculated, the resistance of each group may be computed using the same combination matrices used to compute the group inductance parameters.

In this dissertation it is assumed that the resistance of each coil is constant throughout the machine operation. The major source of error introduced by this assumption is the increase in resistance due to temperature. However if resistance values are calculated at a normal running temperature, then the error will be minimised. There is also a small error due to the skin effect, however at the frequencies involved, with copper or aluminium conductors, this error is likely to be negligible.

2.6 Some properties of machine windings

Having described methods of computation for machine inductance parameters. It will be useful to derive analytic expressions for a class of stator windings. The general approach is well-known, however a complete derivation is included to ensure consistency with the previously used notation, and so that it can be used to draw some conclusions about suitable, and unsuitable, winding arrangements for the BDFM.

The ensuing approach shares much with that adopted in [43, chap. 1], although the presentation is different.

The following properties will now be assumed for stator windings. These assumptions cover concentrated, and distributed windings both fully pitched and short pitched when series connected:

- Each coil is of the same pitch.
- The machine slot pitch is constant for this winding.
- The coil is located inside the slots.

- The winding is comprised of groups of series connected coils. Each group comprises of N_g coils separated from one another by a constant angle α_1.
- There are $2p$ groups in each phase of the winding.

Before proceeding we will recall three trigonometric results which will be required later:

Lemma 2.7. *Given $\theta \in \mathbb{R}$, $N \in \mathbb{N}$:*

$$\sum_{n=0}^{N-1} e^{j(n\theta)} = \begin{cases} e^{j(N-1)\theta/2}\dfrac{\sin(N\theta/2)}{\sin(\theta/2)} & \theta \neq 2\pi k,\ k \in \mathbb{Z} \\ N & \textit{otherwise} \end{cases}$$

Proof. Notice that the left hand side is a geometric progression. Recalling that:

$$\sum_{t=0}^{N-1} x^t = \frac{1-x^N}{1-x},\ x \in \mathbb{C} \neq 1$$

then, for $\theta \neq 2\pi k,\ k \in \mathbb{Z}$:

$$\begin{aligned} \text{LHS} &= \frac{1-e^{j(N\theta)}}{1-e^{j(\theta)}} = \left(\frac{e^{j(N\theta)/2}}{e^{j(\theta)/2}}\right)\frac{e^{-j(N\theta)/2}-e^{j(N\theta)/2}}{e^{-j(\theta)/2}-e^{j(\theta)/2}} \\ &= e^{j(N-1)\theta/2}\frac{\sin(N\theta/2)}{\sin(\theta/2)} \end{aligned}$$

□

Lemma 2.8. *Given $p, n, k \in \mathbb{N}$ then:*

$$\frac{\sin(n\pi)}{p\sin(n\frac{\pi}{p})} = \begin{cases} 1 & n = kp,\ p\ odd \\ \cos(k\pi) & n = kp,\ p\ even \\ 0 & otherwise \end{cases}$$

Proof. When $n \neq kp$, $\sin(n\frac{\pi}{p}) \neq 0$, and clearly $\sin(n\pi) = 0$, hence the result.

When $n = kp$ we investigate what happens as n approaches kp. Let $q = n + \delta$ where $q, \delta \in \mathbb{R}$. Consider the limit as $q \to n$. By L'Hôpital's rule:

$$\lim_{q\to kp}\frac{\sin(q\pi)}{p\sin(q\frac{\pi}{p})} = \lim_{q\to kp}\frac{\cos(q\pi)\pi}{p\frac{\pi}{p}\cos(q\frac{\pi}{p})} = \frac{\cos(kp\pi)}{\cos(k\pi)} = \pm 1$$

□

Lemma 2.9. *Given $\theta, \phi \in \mathbb{R} \neq 2\pi k\ (k \in \mathbb{Z}),\ N \in \mathbb{N}$:*

$$\cos(\theta)+\cos(\theta-\phi)+\cos(\theta-2\phi)+\cdots+\cos(\theta-(N-1)\phi) = \frac{\sin(N\phi/2)}{\sin(\phi/2)}\cos\left(\theta-(N-1)\phi/2\right)$$

Proof.

Applying the trigonometric identity $\cos(A-B) = \cos(A)\cos(B) + \sin(A)\sin(B)$ gives:

$$\begin{aligned}\text{LHS} &= \cos(\theta)\left[1 + \cos(\phi) + \cos(2\phi) + \cdots + \cos((N-1)\phi)\right] + \\ &\qquad \sin(\theta)\left[\sin(\phi) + \sin(2\phi) + \cdots + \sin((N-1)\phi)\right] \\ &= \cos(\theta)\left[\sum_{n=0}^{N-1}\cos(n\phi)\right] + \sin(\theta)\left[\sum_{n=0}^{N-1}\sin(n\phi)\right]\end{aligned}$$

From Lemma 2.7, taking real and imaginary parts we may write:

$$\text{LHS} = \cos(\theta)\left[\cos((N-1)\phi/2)\frac{\sin(N\phi/2)}{\sin(\phi/2)}\right] + \sin(\theta)\left[\sin((N-1)\phi/2)\frac{\sin(N\phi/2)}{\sin(\phi/2)}\right]$$

recombining using $\cos(A-B) = \cos(A)\cos(B) + \sin(A)\sin(B)$ gives:

$$\text{LHS} = \frac{\sin(N\phi/2)}{\sin(\phi/2)}\cos\left(\theta - (N-1)\phi/2\right)$$

□

Magnetic flux density due to a coil group

We consider a group of N_g series connected coils of N_c turns each, with equal current i_g flowing and each displaced from the next by constant angle, α_g. Each coil has a magnetic flux density distribution given by (2.23) with $\beta_k = \{\beta_g, \beta_g + \alpha_g, \cdots, \beta_g + (N_g - 1)\alpha_g\}$ for the different coils in the group, $N_k = N_c$, $i_k = i_g$ To compute the resultant field distribution the contribution from each coil is summed. It can be shown using Lemma 2.9:

$$B_g(\theta) = \frac{2N_cN_gi_g\mu_0}{\pi g}\sum_{n\in\mathbb{N}}\frac{\sin(n\alpha_c/2)}{n}\frac{\sin(nw_s/2)}{nw_s/2}\frac{\sin(nN_g\alpha_g/2)}{N_g\sin(n\alpha_g/2)} \cos\left(n\left(\theta - \beta_g - \tfrac{\alpha_c}{2} - \tfrac{w_s}{2} - (N_g-1)\tfrac{\alpha_g}{2}\right)\right) \quad (2.33)$$

see [43, Sect. 1.4] for details.

Magnetic flux density due to a single series connected phase

It is assumed that a single phase comprises of either p or $2p$ groups of coils where $p \in \mathbb{N}$ is the number of pole-pairs. If the winding is a double layer winding (where coils are 'short-pitched'), then it is assumed that each phase comprises of $2p$ coil groups connected in series with alternating polarity. If the winding is single layer ('fully pitched') then it is assumed that each phase has p coil groups, connected in series, all of the same polarity.

In both cases the total magnetic flux density for a phase is the sum of its component groups. The flux density of each group is given by (2.33), but with different values of the group offset, β_g.

In the case of the single layer winding $\beta_g = \{\beta_k, \beta_k + \frac{2\pi}{p}, \cdots, \beta_k + \frac{2\pi(p-1)}{p}\}$, for the double layer winding $\beta_g = \{\beta_k, \beta_k + \frac{\pi}{p}, \cdots, \beta_k + \frac{2\pi(2p-1)}{2p}\}$, where β_k is the angular offset of the k^{th} phase. However in the case of the double layer winding the polarity of connection alternates.

Using Lemma 2.9 the magnetic flux density for the k^{th} phase, with current i_k, of a single layer winding can be written as:

$$B_{k_{\text{sing.}}}(\theta) = \frac{2N_c N_g i_k \mu_0 p}{\pi g} \sum_{n\in\mathbb{N}} \frac{\sin(n\alpha_c/2)}{n} \frac{\sin(nw_s/2)}{nw_s/2} \frac{\sin(nN_g\alpha_g/2)}{N_g \sin(n\alpha_g/2)} \frac{\sin(n\pi)}{p\sin(n\pi/p)} \left(\cos(n(\theta - \beta_k - \tfrac{\alpha_c}{2} - \tfrac{w_s}{2} - (N_g-1)\tfrac{\alpha_g}{2} - (p-1)\tfrac{\pi}{p}))\right)$$

from Lemma 2.8, assuming p even (modification trivial for p odd):

$$= \frac{2N_c N_g i_k \mu_0 p}{\pi g} \sum_{\substack{n=pt \\ t\in\mathbb{N}}} \frac{\sin(n\alpha_c/2)}{n} \frac{\sin(nw_s/2)}{nw_s/2} \frac{\sin(nN_g\alpha_g/2)}{N_g \sin(n\alpha_g/2)} \cos(n\pi/p) \left(\cos(n(\theta - \beta_k - \tfrac{\alpha_c}{2} - \tfrac{w_s}{2} - (N_g-1)\tfrac{\alpha_g}{2} - (p-1)\tfrac{\pi}{p}))\right) \tag{2.34}$$

For a single layer winding, the coil pitch, α_c will generally be $\alpha_c = \frac{\pi}{p}$ [99, sect. 10.7], therefore all even absolute harmonics vanish. The resulting magnetic flux density is:

$$= \frac{2N_c N_g i_k \mu_0 p}{\pi g} \sum_{\substack{n=p(2t-1) \\ t\in\mathbb{N}}} \frac{\sin(n\alpha_c/2)}{n} \frac{\sin(nw_s/2)}{nw_s/2} \frac{\sin(nN_g\alpha_g/2)}{N_g \sin(n\alpha_g/2)} \cos(n\pi/p) \cos(n(\theta - \beta_k - \tfrac{\alpha_c}{2} - \tfrac{w_s}{2} - (N_g-1)\tfrac{\alpha_g}{2} - (p-1)\tfrac{\pi}{p})) \tag{2.35}$$

A double layer winding consists of coil groups spaced by $\frac{\pi}{p}$. The polarity of connection of these coil groups alternates, thus a phase of a double layer winding can be thought of as two phases of a single layer winding connected in series, but with one set the opposite polarity to the other.

Therefore the magnetic flux density may be written as:

$$B_{k_{\text{doub.}}}(\theta) = \frac{2N_c N_g i_k \mu_0 p}{\pi g} \sum_{n}^{\infty} \frac{\sin(n\alpha_c/2)}{n} \frac{\sin(nw_s/2)}{nw_s/2} \frac{\sin(nN_g\alpha_g/2)}{N_g \sin(n\alpha_g/2)} \frac{\sin(n\pi)}{p\sin(n\pi/p)} \left(\cos(n(\theta - \beta_k - \tfrac{\alpha_c}{2} - \tfrac{w_s}{2} - (N_g-1)\tfrac{\alpha_g}{2} - (p-1)\tfrac{\pi}{p})) - \cos(n(\theta - \beta_k - \tfrac{\alpha_c}{2} - \tfrac{w_s}{2} - (N_g-1)\tfrac{\alpha_g}{2} - (p-1)\tfrac{\pi}{p} - \tfrac{\pi}{p}))\right) \tag{2.36}$$

from Lemma 2.8, assuming p even (modification trivial for p odd):

$$\begin{aligned}= \frac{2N_cN_gi_k\mu_0 p}{\pi g}\sum_{\substack{n=pt\\ t\in\mathbb{N}}}\frac{\sin(n\alpha_c/2)}{n}\frac{\sin(nw_{s_k}/2)}{nw_{s_k}/2}\frac{\sin(nN_g\alpha_1/2)}{N_g\sin(n\alpha_1/2)}\cos(n\pi/p)\\ \Big(\cos(n(\theta-\beta_k-\tfrac{\alpha_c}{2}-\tfrac{w_s}{2}-(N_g-1)\tfrac{\alpha_g}{2}-(p-1)\tfrac{\pi}{p}))-\\ \cos(n(\theta-\beta_k-\tfrac{\alpha_c}{2}-\tfrac{w_s}{2}-(N_g-1)\tfrac{\alpha_g}{2}-(p-1)\tfrac{\pi}{p}-\tfrac{\pi}{p}))\Big)\end{aligned} \tag{2.37}$$

applying the identity $\cos(B)-\cos(A)=2\sin(\frac{A+B}{2})\sin(\frac{A-B}{2})$:

$$\begin{aligned}= \frac{4N_gN_ci_k\mu_0 p}{\pi g}\sum_{\substack{n=pt\\ t\in\mathbb{N}}}\frac{\sin(n\alpha_c/2)}{n}\frac{\sin(nw_s/2)}{nw_s/2}\frac{\sin(nN_g\alpha_1/2)}{N_g\sin(n\alpha_1/2)}\cos(n\pi/p)\\ \Big(\sin(-n\tfrac{\pi}{2p})\sin(n(\theta-\beta_k-\tfrac{\alpha_c}{2}-\tfrac{w_s}{2}-(N_g-1)\tfrac{\alpha_g}{2}-(p-1)\tfrac{\pi}{p}-\tfrac{\pi}{2p}))\Big)\end{aligned} \tag{2.38}$$

notice that the $\sin(-n\frac{\pi}{2p})$ suppresses even multiples of the working harmonic, p. Hence the magnetic flux density for a phase from a double layer winding may be written as:

$$\begin{aligned}= \frac{4N_cN_gi_k\mu_0 p}{\pi g}\sum_{\substack{n=p(2t-1)\\ t\in\mathbb{N}}}\frac{\sin(n\alpha_c/2)}{n}\frac{\sin(nw_s/2)}{nw_s/2}\frac{\sin(nN_g\alpha_1/2)}{N_g\sin(n\alpha_1/2)}\cos(n\pi/p)\\ \Big(\sin(-n\tfrac{\pi}{2p})\sin(n(\theta-\beta_k-\tfrac{\alpha_c}{2}-\tfrac{w_s}{2}-(N_g-1)\tfrac{\alpha_g}{2}-(p-1)\tfrac{\pi}{p}-\tfrac{\pi}{2p}))\Big)\end{aligned} \tag{2.39}$$

2.6.1 Mutual inductance between two stator windings

Equation (2.39) gives the magnetic flux density for a single phase of any winding realisable under the assumptions stated.

Using a similar method to that used to derive (2.39) the conductor distribution function for each phase may be derived. Equation (2.26) gives the conductor distribution for a single coil, hence the conductor distribution for a phase of a double layer winding can be written as:

$$\begin{aligned}\int_0^\theta C_{jp}(\tau)d\tau = \frac{4N_cN_gp}{\pi}\sum_{\substack{n=p(2t-1)\\ t\in\mathbb{N}}}\frac{\sin(n\alpha_c/2)}{n}\frac{\sin(nw_s/2)}{nw_s/2}\frac{\sin(nN_g\alpha_1/2)}{N_g\sin(n\alpha_1/2)}\cos(n\pi/p)\\ \Big(\sin(-n\tfrac{\pi}{2p})\sin(n(\theta-\beta_j-\tfrac{\alpha_c}{2}-\tfrac{w_s}{2}-(N_g-1)\tfrac{\alpha_g}{2}-(p-1)\tfrac{\pi}{p}-\tfrac{\pi}{2p}))\Big)\end{aligned} \tag{2.40}$$

From equation (2.4.2) the mutual inductance between two phases is proportional to the integral of the product of (2.40) and (2.39) (if the winding is single layer a similar result ensues). This leads to the following results:

Remark 2.10. The mutual (and self) inductance between phases within any double or single layer three phase winding can only comprise of terms from the Fourier series representation of the magnetic flux density (or equivalently the conductor distribution function) which are odd harmonics of the

working harmonic (the number of pole pairs). Note that the mutual inductance will include 3rd harmonics of the working harmonic, however these terms can be shown to cancel out if the supply is a balanced three phase set, see for example [43]. ♡

Remark 2.11. The individual phases of a three phase winding will have the same self-inductance, and same mutual-inductance between phases. This is self-evident from considering (2.39) and (2.40): different phases differ only in the value of β_k and β_j, which correspond to a phase offset, which has no bearing on the value of the integral (Lemma 2.4). The self-inductance has $\beta_k = \beta_j$, and the mutual inductance $\beta_k = \beta_j + 2\pi/3$ (for $\beta_k > \beta_j$, which can be ensure for all phases). Therefore for a three phase winding the stator-stator mutual inductance matrix will be of the form:

$$M_{ss} = \begin{bmatrix} L_s & M_s & M_s \\ M_s & L_s & M_s \\ M_s & M_s & L_s \end{bmatrix}$$

which, from definition A.1 is a symmetric, *circulant* matrix. ♡

Rules for choosing pole numbers for BDFM stator windings

Kusko and Somuah [57] give general guidelines for choosing non-coupling pole pair combinations, however they offer no proof, or say for which windings their claims apply. From the preceding work a general statement may be made:

Theorem 2.12. *The mutual inductance between any two phases of any single layer three phase windings of $p_1 \in \mathbb{N}$ and $p_2 \in \mathbb{N}$ pole pairs respectively ($p_1 > p_2$) will be zero if and only if, p_1 is even and p_2 is odd, or p_1 and p_2 are both even providing that p_1/p_2 is not odd (p_1/p_2 may not be an integer) and $p_1 \neq p_2$. Furthermore the condition is sufficient for double layer windings.*

Proof. Sufficiency:

A three phase winding of p_1 pole pairs produces the set of absolute harmonic $Q_1 \triangleq p_1(2t-1), t \in \mathbb{N}$ and for p_2 pole pairs, $Q_2 \triangleq p_2(2t-1), t \in \mathbb{N}$.

If p_1 is even and p_2 odd then Q_1 therefore contains only even numbers, and Q_2 only odd numbers. Hence $Q_1 \cap Q_2 = \emptyset$, hence from Remark 2.5, the mutual inductance will be zero.

$Q_1 = p_1(2k-1), k \in \mathbb{N}$ and $Q_2 = p_2(2k-1), k \in \mathbb{N}$, hence $Q_1/p_2 = p_1(2k-1)/p_2$ and $Q_2/p_2 = (2k-1)$. As p_1/p_2 is not odd then $Q_1/p_2 \cap Q_2/p_2 = \emptyset$, as Q_2/p_2 is odd, hence $Q_1 \cap Q_2 = \emptyset$. □

Necessity:

From (2.35) none of the terms will be zero, hence:

If p_1 and p_2 are odd then $p_1 p_2$ is odd, and thus $p_1 p_2 \in Q_1$, hence the mutual inductance is non-zero.

If p_1 and p_2 is even and p_1/p_2 is odd, then Q_1/p_2 and Q_2/p_2 are both odd, and hence $\exists q \in Q_1/p_2 : q \in Q_2/p_2$, hence $Q_1 \cap Q_2 \neq \emptyset$ hence the mutual inductance is non-zero. □

Remark 2.13. For a double layer winding, the $\sin(n\alpha_c/2)$ term will typically be zero for certain harmonics, by design. It can be shown that this term is equivalent to $\pm\cos(\frac{n\pi q}{k})$ where k is the number of slots per pole, and q is the number of slots by which the winding is short-pitched. Therefore if, say, $p_1 = 1$, $p_2 = 15$, and if the 2 pole winding is wound with $q = 1, k = 5$ then no coupling will result as all odd 15^{th} harmonics are cancelled. However, practically speaking, because $k \gg q$ unless $p_2 \gg p_1$ too then there is little chance of being able to cancel out the coupling by careful choice of α_c, hence Theorem 2.12 is necessary and sufficient in most practical situations. ♡

Remark 2.14. Notice that Theorem 2.12 is derived from consideration of the mutual inductance between phases of different windings. It can be shown (see e.g. [43]) that when a p pole pair three phase winding of the types assumed, is supplied with a balanced set of three phase voltages, absolute harmonics of order $3np, n \in \mathbb{N}$ of the magnetic flux density and conduction distribution function are zero. Therefore the requirement of theorem 2.12 for zero coupling may be relaxed: any p_1 and p_2 such that $p_1/p_2 = 3k, k \in \mathbb{N}, p_1 > p_2$. This relaxed requirement allows the usage of 6/2 pole machines, such as [11]. However extra caution should be exercised, as there will be direct coupling between the two different pole number stator whenever the balanced condition is not met (e.g. due to differing end winding resistances in each phase). ♡

There is a further requirement which is imposed on candidate stator pole pair combinations, the requirement that there be no unbalanced magnetic pull on the rotor. If there were this would unduly stress the machine bearings. Creedy [27, p. 512] gives necessary and sufficient conditions for this to be so. He points out that the conditions given by Hunt [49, p.408], who first made this point, are sufficient but not necessary. Creedy states that to avoid unbalanced magnetic pull it must be ensured that, "...at every instant any value of the square of the magnetic [flux] density which appears at any point [around the circumference of the rotor] shall also appear at one or more other points equally distributed around the circumference with respect to the first." However Creedy's interpretation of this rule is still only sufficient. It is worth noting that some authors have cited Broadway and Burbridge [17, p. 1281] as stating that unbalanced magnetic pull can be avoided by ensuring that the pole pairs of the stator winding differ by at least 2, in fact Broadway and Burbridge states that this is a necessary, but *not sufficient* condition. However it turns out that the condition given in Broadway and Burbridge is both necessary and sufficient:

Theorem 2.15. *In order not to impose unbalanced magnetic pull on the rotor of a machine with two different pole pair fields in the airgap, p_1 and p_2, the pole pairs must be chosen so that $|p_1 - p_2| \neq 1$.*

Proof. Assume that the air gap field, at some time instant, t_i is given by:

$$B(\theta, t_i) = B_1 \cos(p_1\theta + \phi_1^i) + B_2 \cos(p_2\theta + \phi_2^i) \tag{2.41}$$

where B_1, $B_2 \in \mathbb{R}$ are the amplitudes of the flux density waves, and ϕ_1^i, $\phi_2^i \in \mathbb{R}$ are the phase offsets at time t_i. p_1, $p_2 \in \mathbb{N}$ are the number of pole pairs. Then from Creedy [27, p. 512], the square of this value, must be balanced. Squaring gives:

$$B(\theta, t_i)^2 = B_1^2 \cos^2(p_1\theta + \phi_1^i) + B_2^2 \cos^2(p_2\theta + \phi_2^i) + 2B_1B_2 \cos(p_1\theta + \phi_1^i)\cos(p_2\theta + \phi_2^i) \tag{2.42}$$

Applying the trigonometric identities: $\cos^2(A) = \frac{1}{2} + \frac{1}{2}\cos(2A)$ and $\cos(A+B) + \cos(A-B) = 2\cos(A)\cos(B)$ gives:

$$\begin{aligned} B(\theta, t_i)^2 = \frac{B_1^2}{2} + \frac{B_1^2}{2}\cos(2p_1\theta + 2\phi_1^i) + \frac{B_2^2}{2} + \frac{B_2^2}{2}\cos(2p_2\theta + 2\phi_2^i) + \\ B_1B_2 \cos((p_1+p_2)\theta + \phi_1^i + \phi_2^i) + B_1B_2 \cos((p_1-p_2)\theta + \phi_1^i - \phi_2^i) \end{aligned} \tag{2.43}$$

The only way unbalanced magnetic pull can occur is if $B(\theta, t_i)^2$ contains a point between 0 and 2π which is not balanced by another point or points. It is reasonably straightforward to see that $\cos(n\theta)$ (where $n \in \mathbb{Z}$) is only unbalanced if $n = \pm 1$. Therefore $B(\theta, t_i)^2$ is balanced iff $\pm 2p_1, \pm 2p_2, \pm(p_1 + p_2), \pm(p_1 - p_2) \neq 1$. As p_1, $p_2 \in \mathbb{N}$ then this condition reduces to $|p_1 - p_2| \neq 1$. □

2.6.2 Mutual inductance between two stator windings where coils groups are not in series

Early BDFM machines used a special tapping on their stator winding to avoid the need to have separate isolated 3 phase windings to produce the two pole number fields, see for example [48, 17]. However it was shown by experiment in Rochelle et. al. [88], and theoretically by Alexander [2], that connections of this nature can lead to windings where circulating currents are induced. Circulating currents lead to additional Ohmic losses, and may lead to poor iron utilisation and knock-on effects in the rest of the machine. Therefore separate 3 phase windings are now generally used.

In the preceding derivation of inductance parameters for single and double layer windings, we have assumed that each winding consists of only three distinct circuits. That is, the groups of coils making up a phase are connected only in series. However it is common practice when designing 3 phase electrical machine windings to choose to connect coils within a phase in either series, parallel or some combination of the two, as suits the particular situation (often parallel connections allow a narrower wire gauge to be used which is preferred by machine winders) [91, sect. 6.4].

It will be shown, however, that even when adhering to the criteria of theorem 2.12 it is possible to get coupling between two stator windings when the coil groups are connected in parallel. This fact has been inadvertently verified by experiment on the prototype machine.

Using the method outlined in section 2.5.1 the mutual inductance matrix for a series or parallel connected winding may be calculated. Appendix B.2.2 gives the details of the stator winding used in

the prototype machine. The windings are a 4 and 8 pole winding with all coil groups connected in series. After transformation by the combination matrix (B.8) the stator mutual inductance matrix is (without any leakage effects added):

$$M_{ss} = \begin{bmatrix} 0.210 & -0.0963 & -0.0963 & 0 & 0 & 0 \\ -0.0963 & 0.210 & -0.0963 & 0 & 0 & 0 \\ -0.0963 & -0.0963 & 0.210 & 0 & 0 & 0 \\ 0 & 0 & 0 & 0.217 & -0.0974 & -0.0974 \\ 0 & 0 & 0 & -0.0974 & 0.217 & -0.0974 \\ 0 & 0 & 0 & -0.0974 & -0.0974 & 0.217 \end{bmatrix} \tag{2.44}$$

Recall that:

$$\begin{bmatrix} V_{s_1} \\ V_{s_2} \end{bmatrix} = M_{ss} \frac{di_s}{dt} \tag{2.45}$$

$$\Rightarrow \frac{di_s}{dt} = M_{ss}^{-1} \begin{bmatrix} V_{s_1} \\ V_{s_2} \end{bmatrix} \tag{2.46}$$

where V_{s_1}, V_{s_2} are the stator 1 and 2 supply voltage vectors, i_s is the stator current vector. Furthermore from Lemma A.5 as M_{ss}^{-1} is block diagonal as M_{ss} is block diagonal. Therefore $\frac{di_s}{dt}$ may be expressed as:

$$\frac{di_s}{dt} = \begin{bmatrix} \tilde{M}_{ss_1} V_{s_1} \\ \tilde{M}_{ss_2} V_{s_2} \end{bmatrix} \tag{2.47}$$

where $\tilde{M}_{ss_1}$, $\tilde{M}_{ss_2}$ can be found from Lemma A.5.

Therefore we conclude that there is no direct coupling between the two stator supplies because the rate of change of current in the first winding is due *only* to stator 1 voltage supply.

An alternative winding was considered for the prototype machine, which comprised of the same coil groups, however connected such that four sets of groups were connected in parallel for each phase. Details can be found in appendix B.2.2. To analyse a winding with parallel paths it is necessary to treat each parallel path as a separate circuit. Therefore the stator mutual inductance matrix is 24×24, and as such too unwieldy to be printed here. However it can easily be shown that M_{ss} (and hence M_{ss}^{-1}) are not block diagonal. Performing the same analysis applied to the series connected winding we may write:

$$\frac{di_s}{dt} = M_{ss}^{-1} \begin{bmatrix} V_{s_{1p}} \\ V_{s_{2p}} \end{bmatrix} \tag{2.48}$$

where

$$V_{s_{1p}} = \begin{bmatrix} V_{s_{11}} \\ V_{s_{11}} \\ V_{s_{11}} \\ V_{s_{11}} \\ V_{s_{12}} \\ V_{s_{12}} \\ V_{s_{12}} \\ V_{s_{12}} \\ V_{s_{13}} \\ V_{s_{13}} \\ V_{s_{13}} \\ V_{s_{13}} \end{bmatrix} \qquad V_{s_{2p}} = \begin{bmatrix} V_{s_{21}} \\ V_{s_{21}} \\ V_{s_{21}} \\ V_{s_{21}} \\ V_{s_{22}} \\ V_{s_{22}} \\ V_{s_{22}} \\ V_{s_{22}} \\ V_{s_{23}} \\ V_{s_{23}} \\ V_{s_{23}} \\ V_{s_{23}} \end{bmatrix} \tag{2.49}$$

where $V_{s_{11}}$ is the first element of V_{s_1} etc.

Evaluation (2.48) for some balanced three phase voltage source of magnitudes V_1 and V_2 respectively give:

$$\frac{di_s}{dt} = \begin{bmatrix} 211.2\,V_1\cos(\omega t) - 87.0\,V_2\cos(\omega t) + 86.8\,V_2\sin(\omega t) \\ 211.2\,V_1\cos(\omega t) + 87.0\,V_2\cos(\omega t) - 86.8\,V_2\sin(\omega t) \\ 211.2\,V_1\cos(\omega t) - 87.0\,V_2\cos(\omega t) + 86.8\,V_2\sin(\omega t) \\ 211.2\,V_1\cos(\omega t) + 87.0\,V_2\cos(\omega t) - 86.8\,V_2\sin(\omega t) \\ -105.6\,V_1\cos(\omega t) + 182.9\,V_1\sin(\omega t) + 118.7\,V_2\cos(\omega t) + 31.9\,V_2\sin(\omega t) \\ -105.6\,V_1\cos(\omega t) + 182.9\,V_1\sin(\omega t) - 118.7\,V_2\cos(\omega t) - 31.9\,V_2\sin(\omega t) \\ -105.6\,V_1\cos(\omega t) + 182.9\,V_1\sin(\omega t) + 118.7\,V_2\cos(\omega t) + 31.9\,V_2\sin(\omega t) \\ -105.6\,V_1\cos(\omega t) + 182.9\,V_1\sin(\omega t) - 118.7\,V_2\cos(\omega t) - 31.9\,V_2\sin(\omega t) \\ -105.6\,V_1\cos(\omega t) - 182.9\,V_1\sin(\omega t) - 31.7\,V_2\cos(\omega t) - 118.8\,V_2\sin(\omega t) \\ -105.6\,V_1\cos(\omega t) - 182.9\,V_1\sin(\omega t) + 31.7\,V_2\cos(\omega t) + 118.8\,V_2\sin(\omega t) \\ -105.6\,V_1\cos(\omega t) - 182.9\,V_1\sin(\omega t) - 31.7\,V_2\cos(\omega t) - 118.8\,V_2\sin(\omega t) \\ -105.6\,V_1\cos(\omega t) - 182.9\,V_1\sin(\omega t) + 31.7\,V_2\cos(\omega t) + 118.8\,V_2\sin(\omega t) \\ 200.1\,V_1\cos(\omega t) - 83.1\,V_1\sin(\omega t) + 40.2\,V_2\cos(\omega t) \\ -200.1\,V_1\cos(\omega t) + 83.1\,V_1\sin(\omega t) + 40.2\,V_2\cos(\omega t) \\ 200.1\,V_1\cos(\omega t) - 83.1\,V_1\sin(\omega t) + 40.2\,V_2\cos(\omega t) \\ -200.1\,V_1\cos(\omega t) + 83.1\,V_1\sin(\omega t) + 40.2\,V_2\cos(\omega t) \\ 172.0\,V_1\cos(\omega t) + 131.8\,V_1\sin(\omega t) - 20.1\,V_2\cos(\omega t) + 34.8\,V_2\sin(\omega t) \\ -172.0\,V_1\cos(\omega t) - 131.8\,V_1\sin(\omega t) - 20.1\,V_2\cos(\omega t) + 34.8\,V_2\sin(\omega t) \\ 172.0\,V_1\cos(\omega t) + 131.8\,V_1\sin(\omega t) - 20.1\,V_2\cos(\omega t) + 34.8\,V_2\sin(\omega t) \\ -172.0\,V_1\cos(\omega t) - 131.8\,V_1\sin(\omega t) - 20.1\,V_2\cos(\omega t) + 34.8\,V_2\sin(\omega t) \\ -28.1\,V_1\cos(\omega t) + 214.9\,V_1\sin(\omega t) - 20.1\,V_2\cos(\omega t) - 34.8\,V_2\sin(\omega t) \\ 28.1\,V_1\cos(\omega t) - 214.9\,V_1\sin(\omega t) - 20.1\,V_2\cos(\omega t) - 34.8\,V_2\sin(\omega t) \\ -28.1\,V_1\cos(\omega t) + 214.9\,V_1\sin(\omega t) - 20.1\,V_2\cos(\omega t) - 34.8\,V_2\sin(\omega t) \\ 28.1\,V_1\cos(\omega t) - 214.9\,V_1\sin(\omega t) - 20.1\,V_2\cos(\omega t) - 34.8\,V_2\sin(\omega t) \end{bmatrix} \tag{2.50}$$

Therefore notice that all the coil groups are functions of both V_1 and V_2. Therefore there is significant direct coupling between the two windings. The effect of the cross coupling has been to introduce circulating currents in the other winding. This will lead to poor copper utilisation and efficiency. This winding was built and experiment confirmed the presence of circulating currents.

The machine was supplied from winding 1 (4 pole) with a balanced three phase supply derived from the 50Hz grid, with the rotor removed. The rotor was removed to eliminate any possibility of coupling via the rotor. The 4 pole winding was excited and allowed to reach thermal equilibrium while the 8 pole winding was left unconnected at the terminals. Once thermal equilibrium was attained then voltage, current and power were measured using a three phase digital power meter. Immediately after disconnecting the power supply the DC resistance was measured of each phase of the 4 pole winding. Table 2.1 summarises the results for both the parallel path winding and series connected winding. It can immediately be seen that an unaccounted extra loss of 29% appears in the parallel path winding whereas there is substantially no such extra loss in the series path winding, thus confirming that there

Phase	Voltage (V)	Current (A)	Power (W)	I^2R (W)	Diff. (W)
4 pole winding with parallel paths $R = 1.77\Omega$					
R	26.9	9	200	143	57
Y	26.9	9	200	143	57
B	25.8	8.67	186	133	53
4 pole winding with series paths $R = 3.4\Omega$ [1]					
R	47.1	8.95	270	272	2
Y	46.9	8.83	264	265	1
B	46.9	8.75	263	260	3

Table 2.1: Power dissipated as measured by a three phase power meter when the 4 pole winding of prototype machine described in appendix B.2 is excited with the 8 pole winding open circuit. The results compare the difference between series and parallel connection of the 4 pole winding.

are circulating currents induced in the 8 pole winding by the 4 pole winding when the windings are implemented with parallel coil groups.

Remark 2.16. The previous example leads to a general statement of caution: Theorem 2.12 gives rules for choosing non-coupling stator winding pole numbers. However non-coupling is only guaranteed when the coils groups are connected in series, furthermore it is easy to find examples of parallel connected coil groups which lead to circulating currents being directly induced. Therefore it cannot be assumed a priori that parallel connection of coils groups will lead to a satisfactory winding for the BDFM. ♡

2.7 BDFM Rotor Mutual Inductance terms

Having considered mutual inductance parameters for realistic stator windings it is pertinent to consider the mutual inductance parameter of potential BDFM rotors. Although section 2.5.1 provides a method of calculating rotor-rotor and rotor-stator mutual inductance matrices it will be of benefit to derive some analytical results.

As BDFMs are not used commercially, there is not a 'standard' BDFM rotor class, as there is for conventional induction machines. The most commonly adopted rotor design for the recent prototypes described in the literature (see table D.1) is the nested-loop rotor design, conceived by Broadway/Burbridge [17].

It is generally accepted that, at the current stage of BDFM development, the rotor design cannot

[1] This experimental data was obtained by Xiaoyan Wang.

be considered finalised [109], however it will be argued in chapter 5 that all realistic BDFM rotors will share the same general form of the mutual inductance matrix.

The general type of rotor design, which will be considered, falls within the following assumptions:

1. Each rotor circuit conductor distribution function must contain p_1 and p_2 space-harmonic terms, so that it couples to the stator.

2. Rotors must have (or can be modelled as having) $S = p_1 + p_2$ identical circuits spaced evenly around the circumference. As has generally been assumed so far, the circuits must be constructible from coil groups of the form illustrated in figures 2.2 and 2.3.

3. The rotor may have multiple sets of circuits as described in 2, each set may be different from the other sets, and each set of circuits may be positioned at any angular position around the rotor.

For example if $p_1 = 2$, $p_2 = 4$ then $S = 6$, so the rotor must have 6 identical circuits evenly spaced around the circumference. Further sets of 6 may be added as desired. The nested-loop rotor design, in all its variants, clearly falls into this category as can be seen from figure 2.4, although this class of rotors is considerably broader.

It should be noted that this class of rotor designs does not guarantee that the rotor will cross-couple and allow the machine to operate in synchronous mode. Chapter 5 presents results for a rotor design (rotor 3) within this rotor class which does not cross couple.

Essentially the reason for this is that cross-coupling requires not only that the conductor distribution function contains the correct space harmonic terms, but also that the spatial distribution of rotor coils must be such that harmonic field components of the right frequency are produced. This issue is discussed further in chapter 5.

2.7.1 Rotor-rotor mutual inductance matrices

Firstly we consider a rotor consisting of only the outer loops of each 'nest' (see figure 2.4), that is a rotor with only 6 circuits. Clearly the self-inductance will be the same for every loop, and furthermore the mutual inductance between one loop and all other loops will always be the same, regardless which loop is considered. The self and mutual inductances can be calculated directly from (2.27), for appropriate parameter choices. If instead we consider a slightly more general rotor structure where there can be overlap between adjacent nests, then the mutual inductances will differ. The most general case possible for $S = p_1 + p_2$ circuits will have $Q = \text{floor}(S/2)$ different mutual inductance parameters, where 'floor' denotes round down. Without loss of generality it will be assumed that adjacent elements in the mutual inductance matrix correspond to parameters for adjacent nests. In

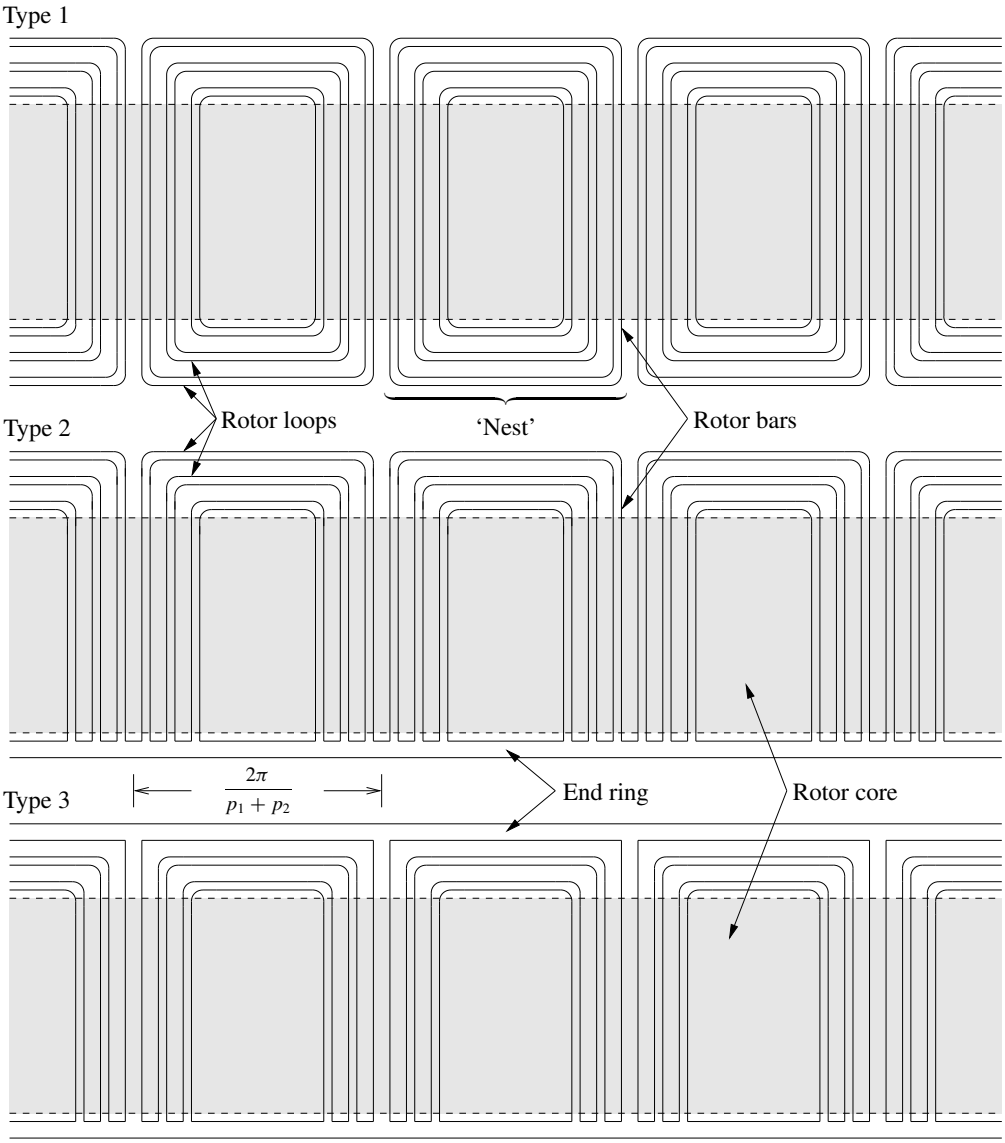

Figure 2.4: Three variant nested loop rotor designs, the difference between the designs is essentially one of ease of fabrication [33, 115]

this case the rotor-rotor mutual inductance matrix for M_{rr} circuit is:

$$M_r = \begin{bmatrix} L_r & M_{r_1} & M_{r_2} & \cdots & M_{r_{Q-1}} & M_{r_Q} & M_{r_{Q-1}} & \cdots & M_{r_2} & M_{r_1} \\ M_{r_1} & L_r & M_{r_1} & M_{r_2} & \cdots & M_{r_{Q-1}} & M_{r_Q} & M_{r_{Q-1}} & \cdots & M_{r_2} \\ M_{r_2} & M_{r_1} & L_r & M_{r_1} & M_{r_2} & \cdots & M_{r_{Q-1}} & M_{r_Q} & M_{r_{Q-1}} & \cdots \\ \cdots & M_{r_2} & M_{r_1} & L_r & M_{r_1} & M_{r_2} & \cdots & M_{r_{Q-1}} & M_{r_Q} & M_{r_{Q-1}} \\ \ddots & \ddots & \ddots & \ddots & \ddots & \ddots & \ddots & \ddots & \ddots & \ddots \\ M_{r_Q} & M_{r_{Q-1}} & \cdots & M_{r_2} & M_{r_1} & L_r & M_{r_1} & M_{r_2} & \cdots & M_{r_{Q-1}} \\ M_{r_{Q-1}} & M_{r_Q} & M_{r_{Q-1}} & \cdots & M_{r_2} & M_{r_1} & L_r & M_{r_1} & M_{r_2} & \cdots \\ \cdots & M_{r_{Q-1}} & M_{r_Q} & M_{r_{Q-1}} & \cdots & M_{r_2} & M_{r_1} & L_r & M_{r_1} & M_{r_2} \\ M_{r_2} & \cdots & M_{r_{Q-1}} & M_{r_Q} & M_{r_{Q-1}} & \cdots & M_{r_2} & M_{r_1} & L_r & M_{r_1} \\ M_{r_1} & M_{r_2} & \cdots & M_{r_{Q-1}} & M_{r_Q} & M_{r_{Q-1}} & \cdots & M_{r_2} & M_{r_1} & L_r \end{bmatrix} \tag{2.51}$$

and mutual inductance matrix of the outer loops of the rotor of figure 2.4, is a special case of M_{rr} where all the mutual terms are equal.

If the rotor in question has N sets of S circuits, such as the rotor shown in figure 2.4, which has 3 sets, then the total mutual inductance matrix can always be written as:

$$M_{rr} = \begin{bmatrix} M_{rr_1} & M_{rr_{12}} & \cdots & M_{rr_{1N}} \\ {M_{rr_{12}}}^{\mathrm{T}} & M_{rr_2} & M_{rr_{23}} & \cdots \\ \vdots & \vdots & \vdots & \vdots \\ {M_{rr_{1N}}}^{\mathrm{T}} & \cdots & {M_{rr_{(N-1)N}}}^{\mathrm{T}} & M_{rr_N} \end{bmatrix} \tag{2.52}$$

where $M_{rr_i} \in \mathbb{R}^{S\times S}$ is the rotor-rotor mutual inductance matrix for the i^{th} set of S circuits, and $M_{rr_{ij}} \in \mathbb{R}S \times S$ is the mutual inductance between the i^{th} and j^{th} sets. It should be noted that from definition A.1 (2.51) is a symmetric circulant matrix. An example of a rotor-rotor mutual inductance matrix is given in equation (B.12), which is the inductance matrix for the prototype 'nested-loop' rotor described in section 5.2.1.

2.7.2 Rotor-Stator mutual inductance matrix

Firstly we consider the mutual inductance between a single stator phase and single rotor circuit. A phase of the stator winding will have a magnetic flux density of the form of (2.39). As the rotor circuit will be formed out of a series connection of coil groups, the conductor distribution function will be the summation of individual coil conductor distribution functions given by (2.26). The resulting mutual inductance can be calculated from the derived expression for mutual inductance, equation (2.4.2).

From the Lemma 2.4, we know that the mutual inductance between a single phase and a single rotor circuit can only contain harmonics common to both stator and rotor coils. Therefore assuming the stator winding is a single or double layer winding, as previously described, then we know that the mutual inductance can contain no more harmonic terms than are present in the expression for the stator magnetic field (2.39), that is odd multiples of stator pole-pairs.

Hence the mutual inductance between one phase of a p_1 pole-pair stator and a single rotor circuit, regardless of the particulars of the circuit itself, can be written $M_{sr} = \sum_{n\in Q} M(n)\cos((\theta_r - \beta_1)n)$, where M is the coefficient for the n^{th} harmonic, θ_r is the rotor position, β_1 is an offset angle, and $Q = p_1(2k-1), k = \{1, 2, 3, \cdots\}$. As discussed in the previous section each rotor circuit is offset from the next by $2\pi/S$ radians, where $S = p_1 + p_2$. Furthermore each stator phase is, of course, offset from the previous by $\frac{2\pi}{3p_1}$ radians for stator 1 and $\frac{2\pi}{3p_2}$ for stator 2. Hence we may write down the rotor-stator mutual inductance matrix:

$$M_{sr} = \begin{bmatrix} \sum_{n\in Q_1} M_1(n)\cos((\theta_r - \beta_1)n) & \sum_{n\in Q_1} M_1(n)\cos((\theta_r - \frac{2\pi}{S} - \beta_1)n) & \cdots \\ \sum_{n\in Q_1} M_1(n)\cos((\theta_r - \frac{2\pi}{3p_1} - \beta_1)n) & \sum_{n\in Q_1} M_1(n)\cos((\theta_r - \frac{2\pi}{S} - \frac{2\pi}{3p_1} - \beta_1)n) & \cdots \\ \sum_{n\in Q_1} M_1(n)\cos((\theta_r - \frac{4\pi}{3p_1} - \beta_1)n) & \sum_{n\in Q_1} M_1(n)\cos((\theta_r - \frac{2\pi}{S} - \frac{4\pi}{3p_1} - \beta_1)n) & \cdots \\ \sum_{n\in Q_2} M_2(n)\cos((\theta_r - \beta_2)n) & \sum_{n\in Q_2} M_2(n)\cos((\theta_r - \frac{2\pi}{S} - \beta_2)n) & \cdots \\ \sum_{n\in Q_2} M_2(n)\cos((\theta_r - \frac{2\pi}{3p_2} - \beta_2)n) & \sum_{n\in Q_2} M_2(n)\cos((\theta_r - \frac{2\pi}{S} - \frac{2\pi}{3p_2} - \beta_2)n) & \cdots \\ \sum_{n\in Q_2} M_2(n)\cos((\theta_r - \frac{4\pi}{3p_2} - \beta_2)n) & \sum_{n\in Q_2} M_2(n)\cos((\theta_r - \frac{2\pi}{S} - \frac{4\pi}{3p_2} - \beta_2)n) & \cdots \end{bmatrix}$$

$$\begin{bmatrix} \sum_{n\in Q_1} M_1(n)\cos((\theta_r - \frac{(S-1)2\pi}{S} - \beta_1)n) \\ \sum_{n\in Q_1} M_1(n)\cos((\theta_r - \frac{(S-1)2\pi}{S} - \frac{2\pi}{3p_1} - \beta_1)n) \\ \sum_{n\in Q_1} M_1(n)\cos((\theta_r - \frac{(S-1)2\pi}{S} - \frac{4\pi}{3p_1} - \beta_1)n) \\ \sum_{n\in Q_2} M_2(n)\cos((\theta_r - \frac{(S-1)2\pi}{S} - \beta_2)n) \\ \sum_{n\in Q_2} M_2(n)\cos((\theta_r - \frac{(S-1)2\pi}{S} - \frac{2\pi}{3p_2} - \beta_2)n) \\ \sum_{n\in Q_2} M_2(n)\cos((\theta_r - \frac{(S-1)2\pi}{S} - \frac{4\pi}{3p_2} - \beta_2)n) \end{bmatrix} \tag{2.53}$$

where $Q_1 = p_1(2k-1),\ Q_2 = p_2(2k-1), k = \{1, 2, 3, \cdots\},\ S = p_1 + p_2,\ p_1, p_2 \in \mathbb{N}$ are the number stator winding 1 and 2 pole pairs, $M_1(n), M_2(n) \in \mathbb{R}$ are the coefficients for the n^{th} absolute harmonic of mutual inductance, and $\beta_1, \beta_2 \in \mathbb{R}$ are offset angles between the first rotor coil and the first phase of stator winding 1 and 2 respectively.

As with the rotor-rotor mutual inductance the rotor may contain additional sets of S identical, equally spaced, rotor circuits. In the case that the stator-rotor mutual inductance matrix has N such sets it becomes:

$$M_{sr} = \begin{bmatrix} M_{sr_1} & M_{sr_2} & \cdots & M_{sr_N} \end{bmatrix} \tag{2.54}$$

where M_{sr_i} is the mutual inductance of the i^{th} set of S equally spaced circuits on the rotor and is given by (2.53) for a suitable choice of parameters.

2.8 Effect of Slotting on Mutual inductance terms

Hitherto all magnetic flux density and mutual inductance calculations have been derived assuming that the stator and rotor are smooth cylinders, i.e. without any slots. The BDFM will generally have a slotted stator and rotor to reduce leakage inductance.

The effect of slotting is to change the profile of the air gap from a uniform ring of constant width, to one where the width varies depending on whether or not the stator and rotor teeth align or not. It is expected, therefore, that the air gap magnetic flux density will change as a result of slotting. Under the stated assumptions the flux density was shown to be inversely proportional to the air gap width, so if the air gap width varies, then it is reasonable to expect the flux density to vary accordingly with a ripple pattern related to position of the slots.

A detailed analysis of slotting effects is beyond the scope of this work, [43, chap. 6] includes a detailed discussion. However a significant effect of slotting which cannot be ignored is that the effective width of the air gap is increased, on average. This will then scale the mutual inductance terms.

The fractional increase in effective air gap width can be approximated by *Carter's Factor*. Henceforth it will be assumed that the air gap width used is the effective air gap width. Appendix C.2 gives details of the calculation method with references.

As noted in [43, sect. 6.11] a significant effect of slotting, which has been ignored, is its effect on higher harmonic components of mutual inductance (*differential leakage* in the vocabulary of the reference).

2.9 BDFM Coupled-Circuit Model

The BDFM coupled circuit model was first presented in [110] and [63]. The model will be presented here, using previously defined notation.

In the BDFM it is convenient to partition v and i into stator 1, stator 2 and rotor quantities, noting that the rotor voltage will always be zero. Note that the subscripted elements are still, themselves, vectors:

$$v \triangleq \begin{bmatrix} v_{s1} \\ v_{s2} \\ v_r \end{bmatrix} = \begin{bmatrix} v_{s1} \\ v_{s2} \\ 0 \end{bmatrix}, \qquad i \triangleq \begin{bmatrix} i_{s1} \\ i_{s2} \\ i_r \end{bmatrix} \tag{2.55}$$

it should be noted that to practically deliver supply voltages of v_{s1} and v_{s2} will, in general, require 4 wire (3 phases plus neutral) connections in each case.

In partitioning the voltage and current it has been shown that for any well-designed BDFM:

1. The mutual inductance between stator 1 and stator 2 is zero by design, see section 2.6.2 for details.

2. The mutual inductance matrices, $M_{12} = {M_{21}}^{\mathrm{T}}$, are functions of the rotor angle, as described in section 2.5.1.

3. The mutual inductance matrices M_{s1}, M_{s2}, M_r are all constant as they link circuits which are not moving relative to one another, see section 2.5.1 for further details.

Therefore substituting (2.55) into (2.6):

$$\begin{bmatrix} v_{s1} \\ v_{s2} \\ 0 \end{bmatrix} = \left(\begin{bmatrix} R_{s1} & 0 & 0 \\ 0 & R_{s2} & 0 \\ 0 & 0 & R_r \end{bmatrix} + \omega_r \begin{bmatrix} 0 & 0 & \frac{dM_{s1r}}{d\theta_r} \\ 0 & 0 & \frac{dM_{s2r}}{d\theta_r} \\ \frac{dM_{s1r}^T}{d\theta_r} & \frac{dM_{s2r}^T}{d\theta_r} & 0 \end{bmatrix} \right) \begin{bmatrix} i_{s1} \\ i_{s2} \\ i_r \end{bmatrix} + \begin{bmatrix} M_{s1} & 0 & M_{s1r} \\ 0 & M_{s2} & M_{s2r} \\ M_{s1r}^T & M_{s2r}^T & M_r \end{bmatrix} \frac{di}{dt} \tag{2.56}$$

The torque equation, from (2.12) and (2.56):

$$\begin{aligned} T_e &= \frac{1}{2} \begin{bmatrix} i_{s1}^T & i_{s2}^T & i_r^T \end{bmatrix} \begin{bmatrix} 0 & 0 & \frac{dM_{s1r}}{d\theta_r} \\ 0 & 0 & \frac{dM_{s2r}}{d\theta_r} \\ \frac{dM_{s1r}^T}{d\theta_r} & \frac{dM_{s2r}^T}{d\theta_r} & 0 \end{bmatrix} \begin{bmatrix} i_{s1} \\ i_{s2} \\ i_r \end{bmatrix} \\ &= \frac{1}{2} \begin{bmatrix} i_r^T \frac{dM_{s1r}^T}{d\theta_r} & i_r^T \frac{dM_{s2r}^T}{d\theta_r} & i_{s1}^T \frac{dM_{s1r}}{d\theta_r} + i_{s2}^T \frac{dM_{s2r}}{d\theta_r} \end{bmatrix} \begin{bmatrix} i_{s1} \\ i_{s2} \\ i_r \end{bmatrix} \\ &= \frac{1}{2} \left(i_r^T \frac{dM_{s1r}^T}{d\theta_r} i_{s1} + i_r^T \frac{dM_{s2r}^T}{d\theta_r} i_{s2} + i_{s1}^T \frac{dM_{s1r}}{d\theta_r} i_r + i_{s2}^T \frac{dM_{s2r}}{d\theta_r} i_r \right) \\ &= i_{s1}^T \frac{dM_{s1r}}{d\theta_r} i_r + i_{s2}^T \frac{dM_{s2r}}{d\theta_r} i_r \\ &= \begin{bmatrix} i_{s1}^T & i_{s2}^T \end{bmatrix} \begin{bmatrix} \frac{dM_{s1r}}{d\theta_r} \\ \frac{dM_{s2r}}{d\theta_r} \end{bmatrix} \begin{bmatrix} i_r \end{bmatrix} \end{aligned} \tag{2.57}$$

At this stage it is convenient to note the mechanical differential equation:

$$J \frac{d\omega_r}{dt} = T_e - T_l \tag{2.58}$$

where J is the combined moment of inertia of the BDFM and load, and T_l is load torque exerted on the BDFM. Frictional forces are neglected.

Stacking equations (2.58), (2.5) and (2.56) gives a complete state-space representation of the dynamics of the BDFM, with the currents in each individual circuit, the position and speed forming the state vector:

$$\frac{d}{dt}\begin{bmatrix} i_{s1} \\ i_{s2} \\ i_r \\ \theta_r \\ \omega_r \end{bmatrix} =$$

$$\begin{bmatrix} \begin{bmatrix} M_{s1} & 0 & M_{s1r} \\ 0 & M_{s2} & M_{s2r} \\ M_{s1r}^T & M_{s2r}^T & M_r \end{bmatrix}^{-1} \left(\left\{ - \begin{bmatrix} R_{s1} & 0 & 0 \\ 0 & R_{s2} & 0 \\ 0 & 0 & R_r \end{bmatrix} - \omega_r \begin{bmatrix} 0 & 0 & \frac{dM_{s1r}}{d\theta_r} \\ 0 & 0 & \frac{dM_{s2r}}{d\theta_r} \\ \frac{dM_{s1r}^T}{d\theta_r} & \frac{dM_{s2r}^T}{d\theta_r} & 0 \end{bmatrix} \right\} \begin{bmatrix} i_{s1} \\ i_{s2} \\ i_r \end{bmatrix} + \begin{bmatrix} v_{s1} \\ v_{s2} \\ 0 \end{bmatrix} \right) \\ \omega_r \\ \frac{1}{J} \left(\begin{bmatrix} i_{s1}^T & i_{s2}^T \end{bmatrix} \begin{bmatrix} \frac{dM_{s1r}}{d\theta_r} \\ \frac{dM_{s2r}}{d\theta_r} \end{bmatrix} \begin{bmatrix} i_r \end{bmatrix} - T_l \right) \end{bmatrix} \tag{2.59}$$

note that the inverse is guaranteed to exist from Lemma 2.3.

It is significant to note that the BDFM is a non-linear parameter-varying system: while the electrical equations are linear in i, they depend on the parameters ω_r and θ_r, which are themselves states of the full system. The dependence on θ_r is particularly problematic to the control engineer because normal machine operation necessitates a non-zero rotor speed, and therefore θ_r varies rapidly. The torque equation is quadratic in i.

Using equation (2.59), with parameters calculated as described earlier in the chapter a dynamic model was implemented in *Simulink*. Simulink is an environment for modelling systems of differential equations, solved by a variable time-stepping procedure, in this particular case a variable step version of the 4$^{\text{th}}$ order Runge-Kutta method was used, for details see [108]. For ease of implementation, and to maximise running speed, the position dependent parameters M_{s1r}, M_{s2r} and their derivatives were computed off-line at 1° intervals and then values interpolated online.

Figure 2.5 shows the implementation of the coupled circuit BDFM model of equation (2.59) implemented in *Simulink*. The block described at 'Mutual inductance matrix calculation' contains a subsystem which implements the required interpolation of the rotor-stator mutual inductance terms, and their derivatives. The same implementation was used for all the BDFM designs considered in this dissertation, with different designs simply requiring different parameter values. As an example of the simulation speed, the simulation of a BDFM with a 'nested-loop' design rotor (described in chapter 5 and appendix B as rotor 1) for 6s took 8.1s of CPU time on a 2.8GHz Pentium 4. The system had 26 states: 6 stator currents, 18 rotor currents and two mechanical states.

The model derived, although relatively simple to implement in simulation, provides little insight into the behaviour of the machine, and there is therefore a strong motivation to transform the system into a simpler form. This work forms the basis of the next chapter.

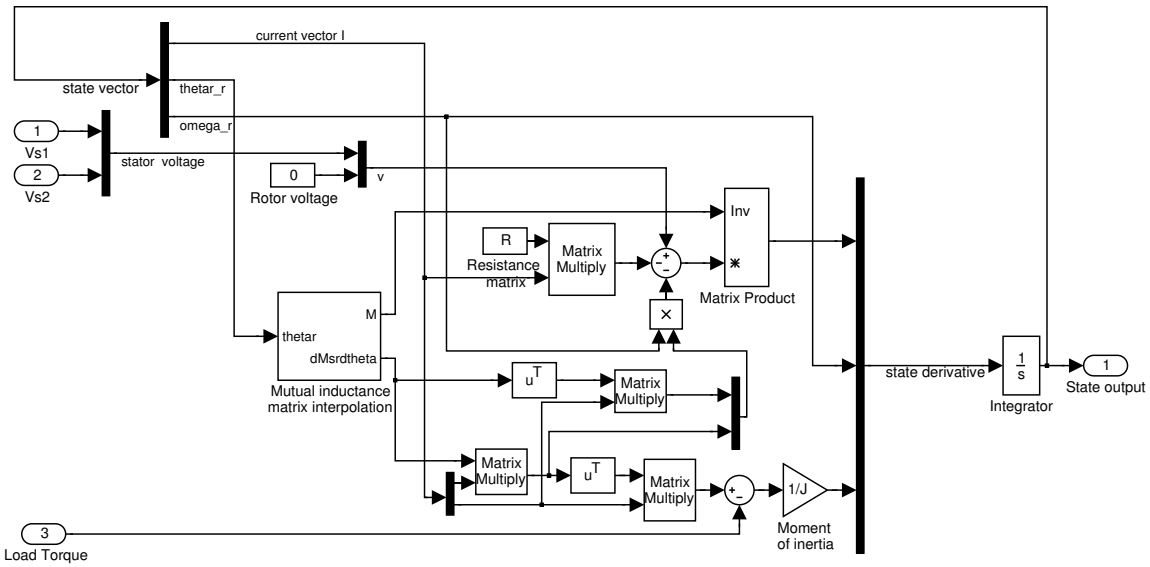

Figure 2.5: Block diagram showing the implementation of the coupled circuit BDFM model, equation (2.59), in *Simulink*

2.10 Conclusions

In this chapter a method of calculating machine inductance parameters which is sufficiently general to cover any rotor or stator winding configuration, comprising of series connected groups of coils, has been presented. The method calculates the self and mutual inductance for each coil group, and then by choice of *combination* matrix, each series connected set of coils is combined into a machine parameter. Furthermore, Carter's factor was used to approximate the effect of slotting on the mutual inductance parameters, and leakage inductances were estimated using standard methods applied on a coil by coil basis.

The proposed method is straightforward to implement on a computer, and allows a general interface for different machine windings or rotor designs.

It was argued that, because the assumptions made in the application of this modelling method are common-place, and have substantial experimental backing in different modelling approaches, the method proposed in this chapter is reliable and will give similar performance to other modelling techniques based on the same assumptions.

Precise conditions were derived for the non-coupling of all harmonics of two stator windings, and a proof given for conditions to avoid unbalanced magnetic pull. It was shown by counter example, that it cannot be assumed that a winding with non-series connections of coil groups will meet the non-coupling requirements for BDFM operation.

A broad class of BDFM rotors was defined, and the mutual inductance for the rotor-rotor and rotor-stator determined using the method previously described.

Using the derived parameters, a coupled-circuit model specific to the BDFM was derived from the general electrical machine equations. This model can accurately model the transient (and steady-state) performance of any BDFM. The model includes the effect of all space-harmonic components of inductance parameters, however no attempt is made to take any saturation effects into account.

Chapter 3

d-q Transformed Model

3.1 Introduction

In chapter 2 a model was derived for the BDFM, and a method of calculating the values of the mutual inductance parameters was presented. The derived coupled-circuit model has position varying parameters, which means that it is not possible to solve the equations analytically for any condition other than with the rotor at standstill.

However, it will be shown that if the model is transformed into the rotor reference frame, that is a reference frame which rotates in synchronism with the rotor, then the position dependency vanishes. Such a transformation will be shown to be achievable by an invertible state transformation of the model equation (2.59).

The transformation adopted is the so-called d-q-0, *direct-quadrature*-zero transformation. It will be shown that the zero sequence part of the transformation is of less interest, and thus the transformation is often referred to as simply d-q transformation.

Li et. al [64, 63] first showed that a d-q transformation could be applied to a BDFM. Their work was generalised to any pole pair configuration BDFM in Boger et. al. [11, 12]. However nowhere in the literature has there been a rigorous proof of why the transformation is effective. In fact, in both papers non-invertible state transformations are used without explanation (the use of a non-invertible state transformation implies a change to the model dynamics). It will be shown that this is of particular consequence when modelling nested-loop rotors. Kemp et al. presented a variation of the model found in [64, 63] for their prototype 6/2 configuration 'nested-loop' design rotor BDFM which does, in fact, retain all observable dynamics [53]. We prove this fact as the model due to Kemp is a special case of that described in this chapter.

Furthermore the generalised transformation given in [11, 12], starts from an idealised machine, rather than explicitly transforming a more general model, where the implicit assumptions become more explicit. In addition, all the d-q-0 BDFM models in the literature are derived for nested-loop rotor BDFMs.

In this chapter a new derivation, with full proofs, for the d-q-0 transformation is presented. The approach adopted is to transform the general coupled-circuit model derived in chapter 2, with all space-harmonic components retained in the stator-stator and rotor-rotor parameters. This approach allows a large class of BDFM configurations to be incorporated in this model. The issue of how to accurately model a nested-loop rotor will be addressed, using a reduced order model.

All the assumptions described in chapter 2 are maintained, including the assumption of 2 double or single layer balanced three phase windings of appropriate pole numbers, as described in section 2.6, and a rotor as described in section 2.7.

In order to improve readability, the majority of the Lemmas used to prove the results are to be found in appendix A, and referenced as appropriate from within the text. While some results in appendix A are standard results collected for convenience; others, particularly Lemmas A.14, A.15, A.16, A.17, A.18 and A.19 are believed to be original.

3.2 The d-q-0 state transformation matrix

We start by giving a physical interpretation of the d-q axis transformation. Figure 3.1, shows an idealised stator winding where the red, yellow and blue coils represent the three phases, each offset from the other by 120°. Two additional coils are shown in figure 3.1, representing fictitious coils on the d and q axes respectively. We now consider how the d and q axis coils relate to stator phases.

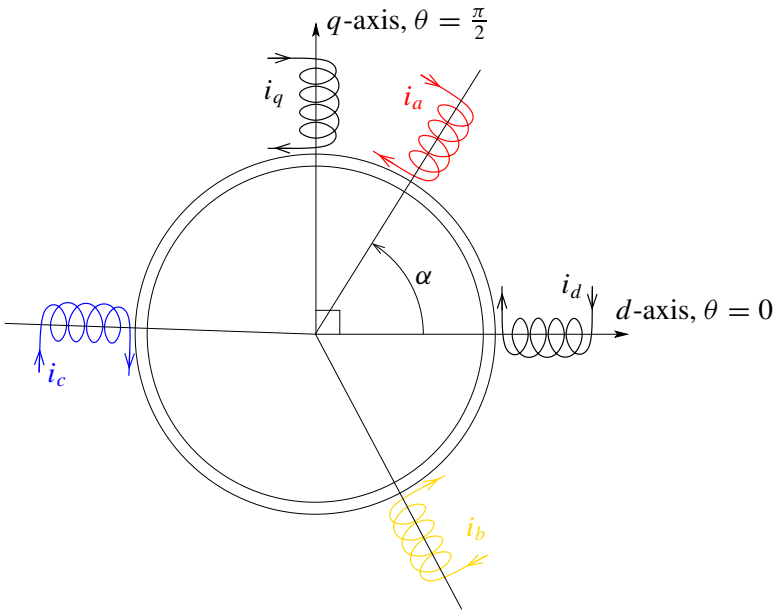

Figure 3.1: A pictorial representation of the d-q transformation, showing three coils representing the phases of a stator winding, and two fictitious coils on the d and q axes by which the stator coils will be represented. The d and q axes have been aligned (arbitrarily) to $\theta = 0$ and $\theta = \frac{\pi}{2}$ respectively.

As we have assumed that the machine windings are balanced, the coils representing the three

phases must be physically identical to one another, but positioned differently within the machine. To facilitate the explanation we assume that each stator coil produces a perfect 2-pole field in the air gap (this assumption does not apply to the BDFM analysis following). Therefore if instantaneous currents, i_a, i_b and i_c flow in the stator coils, then the magnetic flux density distributions due to each of the coils are $B_a(\theta) = i_a k\cos(\theta)$, $B_b(\theta) = i_b k\cos(\theta + \frac{2\pi}{3})$, $B_c(\theta) = i_c k\cos(\theta + \frac{4\pi}{3})$, where θ is the angular position around the air gap.

We firstly consider the flux due to the red phase coil. We want to find a way of producing the same flux density using coils aligned to the d and q axes, as shown in figure 3.1. It turns out that if the d and q axis coils are physically the same as the individual phase coils (but differently aligned), then the same flux density, $B_a(\theta)$, can be achieved by exciting the d and q axis coils with currents $\cos(\alpha)i_a$ and $\sin(\alpha)i_a$ respectively. To show this we consider the magnetic flux density in the air gap due to the d and q coils:

$$B_d(\theta) = i_d k\cos(\theta + \alpha)$$
$$B_q(\theta) = i_q k\cos(\theta - \pi + \alpha) = i_q k\sin(\theta + \alpha)$$

Now if $i_d = \cos(\alpha)i_a$ and $i_q = \sin(\alpha)i_a$, then $B_d(\theta)+B_q(\theta) = \cos(\alpha)i_a k\cos(\theta+\alpha)+\sin(\alpha)i_a k\sin(\theta+\alpha)$, which may be combined using a cosine trigonometric identity to give $B_d(\theta)+B_q(\theta) = i_a k\cos(\theta)$.

Therefore the air gap flux density produced by current i_a in the red phase, i_b in the yellow, and i_c in the blue may be achieved by a d axis current of $i_d = i_a\cos(\alpha)+i_b\cos(\alpha-\frac{2\pi}{3})+i_c\cos(\alpha-\frac{4\pi}{3})$ and q axis current of $i_d = i_a\sin(\alpha)+i_b\sin(\alpha-\frac{2\pi}{3})+i_c\sin(\alpha-\frac{4\pi}{3})$. Therefore the d and q axis currents can be calculated by 'resolving' the phase currents onto the d and q axes. This is the physical basis of the d-q transformation.

α, the angle of the d axis relative to the individual phase, is entirely arbitrary, and can be any differentiable function. It is this freedom to rotate the d-q axis reference frame to any angle that has the useful property that the position-varying mutual inductance terms found in electrical machines may be represented as constant inductance terms by suitable choice of reference frame (i.e. the value of α). Typically aligning the reference frame so that it rotates in synchronism with the rotor achieves the desired effect [56, ch. 3]

However the transformation as is stands is not a 1 to 1 mapping. That is, there is an extra degree of freedom in the 3 phase currents, which does not affect the d and q axis currents. This is the *zero* sequence current. The *zero* (0) sequence current has the interpretation of resolving the currents which produce magnetic fields which do not move parallel to the air gap, that is non-rotating fields. See Krause [56, ch. 3] for further details. It can be shown that the *zero* sequence current is proportional to the sum of the instantaneous three phase currents.

The full transformation from phase currents to d axis, q axis and 0 sequence currents may be expressed as an invertible 3×3 matrix [56, ch. 3]. In the sequel this transformation will be referred to as the d-q-0 transformation.

The d-q-0 transformation has been interpreted as an equivalent representation of the air gap magnetic flux density. However the same transformation may also be applied to the phase voltages, to give equivalent d and q axis and 0 sequence voltages.

Additionally the d-q-0 transformation may be chosen so that it is orthogonal. This has the physical advantage that it becomes a power conserving transformation [52], in other words, the product $v^{\mathrm{T}}i$ is the same whether v and i are expressed as d-q-0 or actual phase quantities.

The d-q-0 transformation may be used to transform the system into a reference frame which rotates in synchronism with the rotor by aligning the d and q axes so that they track the rotor position. It is important to note that while the physical explanation of the d-q-0 transformation assumed coils giving a harmonic-free air gap field, no such assumption is required to use the d-q-0 transformation. Harmonic effects will simply lead to different values of the d-q-0 currents. For a stator winding with p_1 pole pairs [56] gives the d-q-0 transformation as:

$$C_{s1} = \sqrt{\frac{2}{3}} \begin{bmatrix} \cos(p_1\theta_r) & \cos(p_1(\theta_r - \frac{2\pi}{3p_1})) & \cos(p_1(\theta_r - \frac{4\pi}{3p_1})) \\ \sin(p_1\theta_r) & \sin(p_1(\theta_r - \frac{2\pi}{3p_1})) & \sin(p_1(\theta_r - \frac{4\pi}{3p_1})) \\ \frac{1}{\sqrt{2}} & \frac{1}{\sqrt{2}} & \frac{1}{\sqrt{2}} \end{bmatrix} \tag{3.1}$$

for the second stator winding with p_2 pole pairs, the transformation is:

$$C_{s2} = \sqrt{\frac{2}{3}} \begin{bmatrix} \cos(p_2\theta_r) & \cos(p_2(\theta_r - \frac{2\pi}{3p_2})) & \cos(p_2(\theta_r - \frac{4\pi}{3p_2})) \\ \sin(p_2\theta_r) & \sin(p_2(\theta_r - \frac{2\pi}{3p_2})) & \sin(p_2(\theta_r - \frac{4\pi}{3p_2})) \\ \frac{1}{\sqrt{2}} & \frac{1}{\sqrt{2}} & \frac{1}{\sqrt{2}} \end{bmatrix} \tag{3.2}$$

It is noted at this point that some references (e.g. [12]) include a phase offset angle in the second stator transformation matrix. This is because the orientation of the d-axis can be aligned with the stator field without loss of generality (changing the zero position simply changes the physical position of $\theta_r = 0$). However the second stator field cannot, in general, be assumed to be physically aligned with the stator 1 field (as this would place a constraint on where the two windings are physically placed in the stator slots).

In this work it has been chosen not to modify the transformation matrices. This means that some mutual inductance parameters will contain a phase offset term.

In order to transform the rotor into d and q axis components a different transformation matrix is needed. Boger et. al. [11] give the p_1 pole pair rotor transformation matrix for a 'nested-loop' design rotor with a single set of loops as:

$$C_{r1} = \sqrt{\frac{2}{p_1 + p_2}} \begin{bmatrix} \cos(0) & \cos(\frac{2\pi p_1}{p_1+p_2}) & \cos(\frac{2\pi 2p_1}{p_1+p_2}) & \cdots & \cos(\frac{2\pi(p_1+p_2-1)p_1}{p_1+p_2}) \\ \sin(0) & \sin(\frac{2\pi p_1}{p_1+p_2}) & \sin(\frac{2\pi 2p_1}{p_1+p_2}) & \cdots & \sin(\frac{2\pi(p_1+p_2-1)p_1}{p_1+p_2}) \\ \frac{1}{\sqrt{2}} & \frac{1}{\sqrt{2}} & \frac{1}{\sqrt{2}} & \cdots & \frac{1}{\sqrt{2}} \end{bmatrix} \tag{3.3}$$

they also give a similar transformation for p_2 pole pairs, however we will show that it is not necessary to use this transformation. In fact either the transformation for p_1 or p_2 pole pairs can be used.

The transformation proposed by Boger, is a reasonable generalisation of the transformation matrix for the stator phases. The transformation matrix 'resolves' each rotor loop into d and q axis components, and the bottom row is a zero sequence component.

However unlike the stator transformation, the rotor transformation matrix is not square. This means that the transformation does not simply constitute a change of variables, rather it reduces the order of the model, and therefore will result in model which is a (possibly poor) simplification of the original model.

In order to ensure that the model dynamics are unchanged, the transformation must be a *similarity* transformation, that is one which is invertible (and therefore square, and full rank) [131, p. 53]. We will therefore define such a transformation for the rotor.

From Lemma A.10 $C_{r1}{C_{r1}}^{\mathrm{T}} = I$. From Lemma A.12 a matrix whose rows are orthonormal and span the orthogonal complement to the row space of C_{r1} exists. We denote this matrix $C_{r1}^{\perp}$.

Using $C_{r1}^{\perp}$ we may augment original transformation matrix (3.3), to one which is invertible. The rotor transformation matrix for a single set of loops is therefore:

$$C_r = \begin{bmatrix} C_{r1} \\ C_{r1}^{\perp} \end{bmatrix} \tag{3.4}$$

note that not only is C_r full rank (and hence invertible), but is also orthogonal (as the rows of both C_{r1} and $C_{r1}^{\perp}$ are orthonormal). As for the stator transformation matrix orthogonality implies that the transformation is power conserving.

When the rotor has N sets of $S = p_1 + p_2$ circuits, such as is the case with the 'nested-loop' design rotor, then the full rotor d-q-0 transformation becomes (assuming rotor state order in accordance with section 2.7.1):

$$C_r = \begin{bmatrix} \begin{bmatrix} C_{r1} \\ C_{r1}^{\perp} \end{bmatrix} & 0 & 0 \\ 0 & \ddots & 0 \\ 0 & 0 & \begin{bmatrix} C_{rN} \\ C_{rN}^{\perp} \end{bmatrix} \end{bmatrix} \tag{3.5}$$

where each matrix on the diagonal is the same, the differing subscripts are simply to facilitate bookkeeping, that is $C_{r1} = C_{r2} = \cdots = C_{rN}$. Note that because (3.4) is orthogonal so is (3.5).

At this point we also define $C_{r1_{dq}} \in \mathbb{R}^{2\times S}$, $C_{r1_0} \in \mathbb{R}^{1\times S}$, $C_{r_{dq}} \in \mathbb{R}^{2N\times NS}$, which will be useful later on, as follows:

$$\begin{bmatrix} C_{r1_{dq}} \\ C_{r1_0} \end{bmatrix} = C_{r1} \tag{3.6}$$

$$C_{r_{dq}} = \begin{bmatrix} C_{r1_{dq}} & 0 & 0 \\ 0 & \ddots & 0 \\ 0 & 0 & C_{r1_{dq}} \end{bmatrix} \tag{3.7}$$

3.3 Transformation to d-q-0 axes

We will use the transformation described in the previous section to transform the coupled-circuit model derived in chapter 2, with stator windings fulfilling the requirements of section 2.6 and rotor design compliant with the assumptions outlined in section 2.7.

One additional assumption will be required in the derivation: the stator-rotor (and rotor-stator) mutual inductance matrix, given by equation (2.54) can be adequately approximated by the first non-zero term of the series of harmonic inductances. As the rotor must fall within the assumptions of section 2.7 we need the p_1^{th} and p_2^{th} absolute harmonic for the stator 1-rotor and stator 2-rotor coupling respectively. It is significant that, in contrast to [11], we do not place any further constraint on the rotor-rotor and stator-stator mutual inductance terms. In [11] the stator-stator, and rotor-rotor mutual inductance are the fundamental (relative) harmonic terms from the Fourier series representation only.

From section 2.9 and particularly equation (2.56), the BDFM electrical equations can be written as:

$$\begin{bmatrix} v_{s1} \\ v_{s2} \\ 0 \end{bmatrix} = \begin{bmatrix} R_{s1} & 0 & 0 \\ 0 & R_{s2} & 0 \\ 0 & 0 & R_r \end{bmatrix} \begin{bmatrix} i_{s1} \\ i_{s2} \\ i_r \end{bmatrix} + \frac{d}{dt} \left(\begin{bmatrix} M_{s1} & 0 & M_{s1r} \\ 0 & M_{s2} & M_{s2r} \\ M_{s1r}^T & M_{s2r}^T & M_r \end{bmatrix} \begin{bmatrix} i_{s1} \\ i_{s2} \\ i_r \end{bmatrix} \right) \tag{3.8}$$

where the terms are defined in section 2.9.

From (3.1), (3.2), and (3.5) we may define the overall d-q-0 transformation for the BDFM:

$$C = \begin{bmatrix} C_{s1} & 0 & 0 \\ 0 & C_{s2} & 0 \\ 0 & 0 & C_r \end{bmatrix} \tag{3.9}$$

note that as C_{s1}, C_{s2}, C_r are all orthogonal, C is also orthogonal, and hence invertible.

We also define a non-square transformation, $C_{ns} \in \mathbb{R}^{6+2N \times 6+NS}$. From (3.7):

$$C_{ns} = \begin{bmatrix} C_{s1} & 0 & 0 \\ 0 & C_{s2} & 0 \\ 0 & 0 & C_{r_{dq}} \end{bmatrix} \tag{3.10}$$

where N is the number of sets of $S = p_1 + p_2$ rotor circuits.

Using (3.9) we may now define the d-q-0 transformed currents, through an invertible state transformation of the currents in machine variables. The transformed stator currents are denoted $i_{dq0_{s1}}$, $i_{dq0_{s2}}$. The transformed rotor currents we denote by i_{tr_r}, and we will later show that i_{tr_r} can be partitioned into d-q-0 components and other components:

$$\begin{bmatrix} i_{dq0_{s1}} \\ i_{dq0_{s2}} \\ i_{tr_r} \end{bmatrix} \triangleq \begin{bmatrix} C_{s1} & 0 & 0 \\ 0 & C_{s2} & 0 \\ 0 & 0 & C_r \end{bmatrix} \begin{bmatrix} i_{s1} \\ i_{s2} \\ i_r \end{bmatrix} \tag{3.11}$$

$$\Leftrightarrow \begin{bmatrix} i_{s1} \\ i_{s2} \\ i_r \end{bmatrix} = \begin{bmatrix} C_{s1} & 0 & 0 \\ 0 & C_{s2} & 0 \\ 0 & 0 & C_r \end{bmatrix}^{\mathrm{T}} \begin{bmatrix} i_{dq0_{s1}} \\ i_{dq0_{s2}} \\ i_{tr_r} \end{bmatrix} \tag{3.12}$$

Substituting (3.12) into (3.8) and pre-multiplying by C gives:

$$\begin{bmatrix} C_{s1} & 0 & 0 \\ 0 & C_{s2} & 0 \\ 0 & 0 & C_r \end{bmatrix} \begin{bmatrix} v_{s1} \\ v_{s2} \\ 0 \end{bmatrix} = \begin{bmatrix} C_{s1} & 0 & 0 \\ 0 & C_{s2} & 0 \\ 0 & 0 & C_r \end{bmatrix} \begin{bmatrix} R_{s1} & 0 & 0 \\ 0 & R_{s2} & 0 \\ 0 & 0 & R_r \end{bmatrix} \begin{bmatrix} C_{s1} & 0 & 0 \\ 0 & C_{s2} & 0 \\ 0 & 0 & C_r \end{bmatrix}^{\mathrm{T}} \begin{bmatrix} i_{dq0_{s1}} \\ i_{dq0_{s2}} \\ i_{tr_r} \end{bmatrix} + \begin{bmatrix} C_{s1} & 0 & 0 \\ 0 & C_{s2} & 0 \\ 0 & 0 & C_r \end{bmatrix} \frac{d}{dt} \left(\begin{bmatrix} M_{s1} & 0 & M_{s1r} \\ 0 & M_{s2} & M_{s2r} \\ M_{s1r}^T & M_{s2r}^T & M_r \end{bmatrix} \begin{bmatrix} C_{s1} & 0 & 0 \\ 0 & C_{s2} & 0 \\ 0 & 0 & C_r \end{bmatrix}^{\mathrm{T}} \begin{bmatrix} i_{dq0_{s1}} \\ i_{dq0_{s2}} \\ i_{tr_r} \end{bmatrix} \right) \tag{3.13}$$

Defining the d-q-0 transformed voltages in a similar manner gives:

$$\begin{bmatrix} v_{dq0_{s1}} \\ v_{dq0_{s2}} \\ v_{tr_r} \end{bmatrix} \triangleq \begin{bmatrix} C_{s1} & 0 & 0 \\ 0 & C_{s2} & 0 \\ 0 & 0 & C_r \end{bmatrix} \begin{bmatrix} v_{s1} \\ v_{s2} \\ v_r \end{bmatrix} \tag{3.14}$$

Substituting (3.14) into (3.13) and simplifying gives:

$$\begin{bmatrix} v_{dq0_{s1}} \\ v_{dq0_{s2}} \\ v_{tr_r} \end{bmatrix} = \begin{bmatrix} C_{s1} R_{s1} {C_{s1}}^{\mathrm{T}} & 0 & 0 \\ 0 & C_{s2} R_{s2} {C_{s2}}^{\mathrm{T}} & 0 \\ 0 & 0 & C_r R_r {C_r}^{\mathrm{T}} \end{bmatrix} \begin{bmatrix} i_{dq0_{s1}} \\ i_{dq0_{s2}} \\ i_{tr_r} \end{bmatrix} + \begin{bmatrix} C_{s1} & 0 & 0 \\ 0 & C_{s2} & 0 \\ 0 & 0 & C_r \end{bmatrix} \frac{d}{dt} \left(\begin{bmatrix} M_{s1} {C_{s1}}^{\mathrm{T}} & 0 & M_{s1r} {C_r}^{\mathrm{T}} \\ 0 & M_{s2} {C_{s2}}^{\mathrm{T}} & M_{s2r} {C_r}^{\mathrm{T}} \\ M_{s1r}^T {C_{s1}}^{\mathrm{T}} & M_{s2r}^T {C_{s2}}^{\mathrm{T}} & M_r {C_r}^{\mathrm{T}} \end{bmatrix} \begin{bmatrix} i_{dq0_{s1}} \\ i_{dq0_{s2}} \\ i_{tr_r} \end{bmatrix} \right) \tag{3.15}$$

Further simplification and use of the chain rule gives, noting that C_r, M_{s1}, M_{s2}, M_r are all constant:

$$\begin{bmatrix} v_{dq0_{s1}} \\ v_{dq0_{s2}} \\ v_{tr_r} \end{bmatrix} = \begin{bmatrix} C_{s1}R_{s1}{C_{s1}}^{\mathrm{T}} & 0 & 0 \\ 0 & C_{s2}R_{s2}{C_{s2}}^{\mathrm{T}} & 0 \\ 0 & 0 & C_rR_r{C_r}^{\mathrm{T}} \end{bmatrix} \begin{bmatrix} i_{dq0_{s1}} \\ i_{dq0_{s2}} \\ i_{tr_r} \end{bmatrix} +$$
$$\omega_r \begin{bmatrix} C_{s1}M_{s1}\frac{d}{d\theta_r}({C_{s1}}^{\mathrm{T}}) & 0 & C_{s1}\frac{d}{d\theta_r}(M_{s1r}){C_r}^{\mathrm{T}} \\ 0 & C_{s2}M_{s2}\frac{d}{d\theta_r}({C_{s2}}^{\mathrm{T}}) & C_{s2}\frac{d}{d\theta_r}(M_{s2r}){C_r}^{\mathrm{T}} \\ C_r\frac{d}{d\theta_r}(M_{s1r}^T{C_{s1}}^{\mathrm{T}}) & C_r\frac{d}{d\theta_r}(M_{s2r}^T{C_{s2}}^{\mathrm{T}}) & 0 \end{bmatrix} \begin{bmatrix} i_{dq0_{s1}} \\ i_{dq0_{s2}} \\ i_{tr_r} \end{bmatrix} +$$
$$\begin{bmatrix} C_{s1}M_{s1}{C_{s1}}^{\mathrm{T}} & 0 & C_{s1}M_{s1r}{C_r}^{\mathrm{T}} \\ 0 & C_{s2}M_{s2}{C_{s2}}^{\mathrm{T}} & C_{s2}M_{s2r}{C_r}^{\mathrm{T}} \\ C_rM_{s1r}^T{C_{s1}}^{\mathrm{T}} & C_rM_{s2r}^T{C_{s2}}^{\mathrm{T}} & C_rM_r{C_r}^{\mathrm{T}} \end{bmatrix} \frac{d}{dt} \begin{bmatrix} i_{dq0_{s1}} \\ i_{dq0_{s2}} \\ i_{tr_r} \end{bmatrix} \quad (3.16)$$

We have already established that M_{s1}, M_{s2} are symmetric circulant matrices (see remark 2.11). Therefore from Lemmas A.15 and A.16:

$$C_{s1}M_{s1}\frac{d}{d\theta_r}({C_{s1}}^{\mathrm{T}}) = \begin{bmatrix} 0 & p_1(L_1-M_1) & 0 \\ -p_1(L_1-M_1) & 0 & 0 \\ 0 & 0 & 0 \end{bmatrix} = Q_{dq0_{s1}} \quad (3.17)$$

$$C_{s2}M_{s2}\frac{d}{d\theta_r}({C_{s2}}^{\mathrm{T}}) = \begin{bmatrix} 0 & p_2(L_2-M_2) & 0 \\ -p_2(L_2-M_2) & 0 & 0 \\ 0 & 0 & 0 \end{bmatrix} = Q_{dq0_{s2}} \quad (3.18)$$

$$C_{s1}M_{s1}{C_{s1}}^{\mathrm{T}} = \begin{bmatrix} L_1-M_1 & 0 & 0 \\ 0 & L_1-M_1 & 0 \\ 0 & 0 & L_1+2M_1 \end{bmatrix} = M_{dq0_{s1}} \quad (3.19)$$

$$C_{s2}M_{s2}{C_{s2}}^{\mathrm{T}} = \begin{bmatrix} L_2-M_2 & 0 & 0 \\ 0 & L_2-M_2 & 0 \\ 0 & 0 & L_2+2M_2 \end{bmatrix} = M_{dq0_{s2}} \quad (3.20)$$

where M_1, L_1, M_2, L_2 are the mutual and self inductance parameters of the first and second stator winding respectively as in remark 2.11.

As discussed in section 2.7, the class of rotors considered here have N sets of $S = p_1 + p_2$ individual circuits. S is fixed for a particular pole pair choice, but N may be chosen by the designer. Consequently, from section 2.7, the rotor-rotor and stator-rotor mutual inductances can be written as:

$$\begin{bmatrix} M_{s1r} \\ M_{s2r} \end{bmatrix} = \begin{bmatrix} M_{s1r_1} & M_{s1r_2} & \cdots & M_{s1r_N} \\ M_{s2r_1} & M_{s2r_2} & \cdots & M_{s2r_N} \end{bmatrix} \quad (3.21)$$

$$M_r = \begin{bmatrix} M_{r_1} & M_{r_{12}} & \cdots & M_{r_{1N}} \\ {M_{r_{12}}}^{\mathrm{T}} & M_{r_2} & \cdots & \vdots \\ \vdots & \vdots & \ddots & \vdots \\ {M_{r_{1N}}}^{\mathrm{T}} & \cdots & \cdots & M_{r_N} \end{bmatrix} \quad (3.22)$$

where $M_{s1r_j}, M_{s2r_j} \in \mathbb{R}^{3\times S}$, $M_{r_{ji}} \in \mathbb{R}^{S\times S}$.

Now, it is immediate from the choice of rotor class that the diagonal block matrices of (3.22) are symmetric circulant, as explained in section 2.7.1. However, after some consideration it can be seen that this implies that the off-diagonal block matrices (e.g. $M_{r_{12}}$) are non-symmetric circulant. This fact is most easily seen by considering the mutual inductance between a single rotor circuit of one set of S circuits and another entire set of S circuits. The geometry of each circuit within a set of S circuits is the same, the only difference being the position around the circumference of each. Therefore it is reasonably straight forward to see that the mutual inductance between two different sets of S circuits is itself circulant.

Considering, first $C_r M_r {C_r}^{\mathrm{T}}$, from (3.5) and (3.22):

$$C_r M_r {C_r}^{\mathrm{T}} = \begin{bmatrix} \begin{bmatrix} C_{r1} \\ C_{r1}^{\perp} \end{bmatrix} M_{r_1} \begin{bmatrix} C_{r1} \\ C_{r1}^{\perp} \end{bmatrix}^{\mathrm{T}} & \cdots & \ddots \\ \vdots & \ddots & \vdots \\ \ddots & \cdots & \begin{bmatrix} C_{rN} \\ C_{rN}^{\perp} \end{bmatrix} M_{r_N} \begin{bmatrix} C_{rN} \\ C_{rN}^{\perp} \end{bmatrix}^{\mathrm{T}} \end{bmatrix} \tag{3.23}$$

As all block matrices of (3.22) are circulant, with the diagonal blocks symmetric in addition, then with the chosen form of the transformation matrix, applying Lemma A.16 to (3.23) gives:

$$C_r M_r {C_r}^{\mathrm{T}} = \begin{bmatrix} \begin{bmatrix} L_{dq_{r1}} & 0 & 0 & 0 \\ 0 & L_{dq_{r1}} & 0 & 0 \\ 0 & 0 & L_{0_{r1}} & 0 \\ 0 & 0 & 0 & *_{11} \end{bmatrix} & \begin{bmatrix} M_{12_a} & M_{12_b} & 0 & 0 \\ -M_{12_b} & M_{12_a} & 0 & 0 \\ 0 & 0 & M_{0_{12}} & 0 \\ 0 & 0 & 0 & *_{12} \end{bmatrix} & & \cdots \\ \begin{bmatrix} M_{12_a} & -M_{12_b} & 0 & 0 \\ M_{12_b} & M_{12_a} & 0 & 0 \\ 0 & 0 & M_{0_{12}} & 0 \\ 0 & 0 & 0 & *_{12}{}^{\mathrm{T}} \end{bmatrix} & & \ddots & \vdots \\ & \vdots & \cdots & \begin{bmatrix} L_{dq_{rN}} & 0 & 0 & 0 \\ 0 & L_{dq_{rN}} & 0 & 0 \\ 0 & 0 & L_{0_{rN}} & 0 \\ 0 & 0 & 0 & *_{NN} \end{bmatrix} \end{bmatrix} \tag{3.24}$$

where $L_{dq_{rj}}, L_{0_{rj}} \in \mathbb{R}$, $*_{ij} \in \mathbb{R}^{p_1+p_2-3\times p_1+p_2-3}$ are the d and q axis rotor self-inductance, the '0' sequence rotor self-inductance, and a matrix of other inductance terms for the j^{th} set of rotor circuits. $M_{ij_k}, M_{0_{ij}}$ are the mutual inductance terms between different sets of S circuits, for d-q axes and zero sequence respectively. Explicit expressions for $L_{dq_{rj}}, L_{0_{rj}}, M_{ij_k}$, and $M_{0_{ij}}$ can be found in the proof

of Lemma A.16. We use $*$ to denote terms for which the exact value is not relevant, but that are not (typically) zero.

We now consider the stator-rotor mutual inductance terms. As an example, consider $C_{s1}M_{s1r}{C_r}^{\mathrm{T}}$. From (3.21) and (3.5):

$$C_{s1}M_{s1r}{C_r}^{\mathrm{T}} = \begin{bmatrix} C_{s1}M_{s1r_1}\begin{bmatrix} C_{r1} \\ C_{r1}^{\perp} \end{bmatrix}^{\mathrm{T}} & C_{s1}M_{s1r_2}\begin{bmatrix} C_{r1} \\ C_{r1}^{\perp} \end{bmatrix}^{\mathrm{T}} & \cdots & C_{s1}M_{s1r_N}\begin{bmatrix} C_{r1} \\ C_{r1}^{\perp} \end{bmatrix}^{\mathrm{T}} \end{bmatrix} \tag{3.25}$$

the incrementing subscript on the transformation matrix has been dropped as it no longer serves any purpose.

The general term, M_{s1r_j}, corresponding to the stator-rotor mutual inductance between stator 1 and the j^{th} set of rotor circuits, and is of the form of (2.53). The same is true for the M_{s2r_j} terms.

To proceed further we must invoke the additional assumption mentioned: we will assume that M_{s1r_j} and M_{s2r_j} may be well approximated by the first non-zero term of their Fourier series representations. This is a physically reasonable assumption because the mutual inductance terms for a particular term of the Fourier series are derived from the product of the stator magnetic flux density and rotor conductor distribution function (or vice-versa). As the stator winding is specifically (and quite effectively) designed to produce one pole number field only, the harmonic content will be small. Therefore the higher terms in the Fourier series for the stator-rotor mutual inductance will typically be small, and thus the error in neglecting them slight. Nevertheless the omission of these harmonic terms will idealise the machine, in that it becomes impossible for any frequency other than the supply frequencies to appear in the current waveforms in the steady state, which is at odds with physical reality where the stator currents will contain harmonic components.

With this assumption, the terms in (3.25) can be simplified by application of Lemma A.17. Furthermore similar terms in (3.15) may be simplified for the same reasons by Lemmas A.17 and A.18:

$$C_{s1}M_{s1r}{C_r}^{\mathrm{T}} = \left[\begin{bmatrix} M_{1_1}\cos(\phi_{1_1}) & -M_{1_1}\sin(\phi_{1_1}) & 0 \\ M_{1_1}\sin(\phi_{1_1}) & M_{1_1}\cos(\phi_{1_1}) & 0 \\ 0 & 0 & 0 \end{bmatrix} \quad 0^{3\times D} \quad \cdots \right.$$
$$\left. \begin{bmatrix} M_{1_N}\cos(\phi_{1_N}) & -M_{1_N}\sin(\phi_{1_N}) & 0 \\ M_{1_N}\sin(\phi_{1_N}) & M_{1_N}\cos(\phi_{1_N}) & 0 \\ 0 & 0 & 0 \end{bmatrix} \quad 0^{3\times D} \right] \tag{3.26}$$

$$C_{s2}M_{s2r}{C_r}^{\mathrm{T}} = \left[\begin{bmatrix} M_{2_1}\cos(\phi_{2_1}) & M_{2_1}\sin(\phi_{2_1}) & 0 \\ M_{2_1}\sin(\phi_{2_1}) & -M_{2_1}\cos(\phi_{2_1}) & 0 \\ 0 & 0 & 0 \end{bmatrix} \quad 0^{3\times D} \quad \cdots \right.$$
$$\left. \begin{bmatrix} M_{2_N}\cos(\phi_{2_N}) & M_{2_N}\sin(\phi_{2_N}) & 0 \\ M_{2_N}\sin(\phi_{2_N}) & -M_{2_N}\cos(\phi_{2_N}) & 0 \\ 0 & 0 & 0 \end{bmatrix} \quad 0^{3\times D} \right] \tag{3.27}$$

$$C_{s1}\frac{d}{d\theta}(M_{s1r}){C_r}^{\mathrm{T}} = \left[\begin{bmatrix} M_{1_1}p_1\sin(\phi_{1_1}) & M_{1_1}p_1\cos(\phi_{1_1}) & 0 \\ -M_{1_1}p_1\cos(\phi_{1_1}) & M_{1_1}p_1\sin(\phi_{1_1}) & 0 \\ 0 & 0 & 0 \end{bmatrix} \quad 0^{3\times D} \quad \cdots \right.$$
$$\left. \begin{bmatrix} M_{1_N}p_1\sin(\phi_{1_N}) & M_{1_N}p_1\cos(\phi_{1_N}) & 0 \\ -M_{1_N}p_1\cos(\phi_{1_N}) & M_{1_N}p_1\sin(\phi_{1_N}) & 0 \\ 0 & 0 & 0 \end{bmatrix} \quad 0^{3\times D} \right] \tag{3.28}$$

$$C_{s2}\frac{d}{d\theta}(M_{s2r}){C_r}^{\mathrm{T}} = \left[\begin{bmatrix} M_{2_1}p_2\sin(\phi_{2_1}) & -M_{2_1}p_2\cos(\phi_{2_1}) & 0 \\ -M_{2_1}p_2\cos(\phi_{2_1}) & -M_{2_1}p_2\sin(\phi_{2_1}) & 0 \\ 0 & 0 & 0 \end{bmatrix} \quad 0^{3\times D} \quad \cdots \right.$$
$$\left. \begin{bmatrix} M_{2_N}p_2\sin(\phi_{2_N}) & -M_{2_N}p_2\cos(\phi_{2_N}) & 0 \\ -M_{2_N}p_2\cos(\phi_{2_N}) & -M_{2_N}p_2\sin(\phi_{2_N}) & 0 \\ 0 & 0 & 0 \end{bmatrix} \quad 0^{3\times D} \right] \tag{3.29}$$

where M_{1_j}, M_{2_j} are the mutual inductance between stator 1, stator 2 and the j^{th} set of rotor circuits, and ϕ_{1_j}, ϕ_{2_j} are the electrical phase offsets between stator 1, stator 2 and the j^{th} set of rotor circuits. For a precise definition see Lemma A.17. $D = S - 3$, where $S = p_1 + p_2$.

The terms $C_r{M_{s1r}}^{\mathrm{T}}{C_{s_1}}^{\mathrm{T}}$, $C_r{M_{s2r}}^{\mathrm{T}}{C_{s_2}}^{\mathrm{T}}$ may be induced by symmetry, and from Lemma A.17, $C_{s1}M_{s1r}$ and $C_{s2}M_{s2r}$ (and hence ${M_{s1r}}^{\mathrm{T}}{C_{s1}}^{\mathrm{T}}$ and ${M_{s2r}}^{\mathrm{T}}{C_{s2}}^{\mathrm{T}}$) are constant with θ_r, therefore $\frac{d}{d\theta_r}{M_{s1r}}^{\mathrm{T}}{C_{s1}}^{\mathrm{T}} = \frac{d}{d\theta_r}{M_{s2r}}^{\mathrm{T}}{C_{s2}}^{\mathrm{T}} = 0$.

So far the resistance matrices have not been considered. The resistance matrices, R_{s1}, R_{s2}, R_r will be diagonal, as long as the current path of each 'circuit' is independent. For the stator terms this

will always be the case under the present assumptions, however for the rotor terms it may not be the case. If the rotor were a squirrel cage then when modelling, it is more natural to take each 'circuit' as a loop around two adjacent bars and the appropriate parts of the end ring. In this case neighbouring 'circuits' will share common bars. It can be shown that this has the effect of introducing off-diagonal elements in the resistance matrix (see section B.7). However in any case the resistance matrix must be symmetric and *circulant* from definition A.1.

For the present we will assume that all the resistance matrices are circulant, thus allowing for the possibility of modelling cage rotor designs. As all the resistance matrices are circulant, from Lemma A.16 it can be seen that the resulting transformed resistance matrix will be diagonal.

Using (3.17-3.20), (3.24), (3.26-3.29) in (3.16) gives:

$$\begin{bmatrix} v_{dq0_{s1}} \\ v_{dq0_{s2}} \\ v_{tr_r} \end{bmatrix} = \begin{bmatrix} *^{3\times3} & 0 & 0 \\ 0 & *^{3\times3} & 0 \\ 0 & 0 & R_{r_{dq0}} \end{bmatrix} \begin{bmatrix} i_{dq0_{s1}} \\ i_{dq0_{s2}} \\ i_{tr_r} \end{bmatrix} +$$

$$\omega_r \begin{bmatrix} *^{3\times3} & 0 & \begin{bmatrix} *_1^{2\times2} & 0 \\ 0 & 0 \end{bmatrix} & 0^{3\times D} & \cdots & \begin{bmatrix} *_N^{2\times2} & 0 \\ 0 & 0 \end{bmatrix} & 0^{3\times D} \\ 0 & *^{3\times3} & \begin{bmatrix} *_1^{2\times2} & 0 \\ 0 & 0 \end{bmatrix} & 0^{3\times D} & \cdots & \begin{bmatrix} *_N^{2\times2} & 0 \\ 0 & 0 \end{bmatrix} & 0^{3\times D} \\ 0 & 0 & & 0 & & & \end{bmatrix} \begin{bmatrix} i_{dq0_{s1}} \\ i_{dq0_{s2}} \\ i_{tr_r} \end{bmatrix} +$$

$$\begin{bmatrix} *^{3\times3} & 0 & \begin{bmatrix} *_1^{2\times2} & 0 \\ 0 & 0 \end{bmatrix} & 0^{3\times D} & \cdots & \begin{bmatrix} *_N^{2\times2} & 0 \\ 0 & 0 \end{bmatrix} & 0^{3\times D} \\ 0 & *^{3\times3} & \begin{bmatrix} *_1^{2\times2} & 0 \\ 0 & 0 \end{bmatrix} & 0^{3\times D} & \cdots & \begin{bmatrix} *_N^{2\times2} & 0 \\ 0 & 0 \end{bmatrix} & 0^{3\times D} \\ \begin{bmatrix} *_1^{2\times2} & 0 \\ 0 & 0 \\ 0^{D\times3} \end{bmatrix} & \begin{bmatrix} *_1^{2\times2} & 0 \\ 0 & 0 \\ 0^{D\times3} \end{bmatrix} & \begin{bmatrix} *^{2\times2} & 0 \\ 0 & * \\ & 0 \end{bmatrix} & 0^{3\times D} & \cdots & \begin{bmatrix} *^{2\times2} & 0 \\ 0 & * \\ & 0 \end{bmatrix} & 0^{3\times D} \\ \vdots & \vdots & & *^{D\times D} & \cdots & & 0 \\ \begin{bmatrix} *_N^{2\times2} & 0 \\ 0 & 0 \\ 0^{D\times3} \end{bmatrix} & \begin{bmatrix} *_N^{2\times2} & 0 \\ 0 & 0 \\ 0^{D\times3} \end{bmatrix} & & & \ddots & & \\ & & \begin{bmatrix} *^{2\times2} & 0 \\ 0 & * \\ & 0 \end{bmatrix} & 0^{3\times D} & \cdots & \begin{bmatrix} *^{2\times2} & 0 \\ 0 & * \\ & 0 \end{bmatrix} & 0^{3\times D} \\ & & & & & & \\ & & & & & & \\ & & \begin{bmatrix} *^{2\times2} & 0 \\ 0 & * \\ & 0 \end{bmatrix} & 0 & \cdots & \begin{bmatrix} *^{2\times2} & 0 \\ 0 & * \\ & 0 \end{bmatrix} & *^{D\times D} \end{bmatrix} \frac{d}{dt} \begin{bmatrix} i_{dq0_{s1}} \\ i_{dq0_{s2}} \\ i_{tr_r} \end{bmatrix} \tag{3.30}$$

where $*$ denotes a constant (typically) non-zero element, $D = S-3$. Where dimensions are not given for a particular element it is either scalar or the dimension can be deduced.

If we now reorder i_{tr_r} to give i'_{tr_r} so the zero portion of that $C_{s1_r} M_{s1r} {C_r}^{\mathrm{T}}$ and similar elements are collected together. We define the modified rotor resistance $R'_{r_{tr}}$, significantly as $R_{r_{tr}}$ was diagonal, $R'_{r_{tr}}$ must also be diagonal. Hence:

$$\begin{bmatrix} v_{dq0_{s1}} \\ v_{dq0_{s2}} \\ v'_{tr_r} \end{bmatrix} = \begin{bmatrix} *^{3\times3} & 0 & 0 \\ 0 & *^{3\times3} & 0 \\ 0 & 0 & R'_{r_{tr}} \end{bmatrix} \begin{bmatrix} i_{dq0_{s1}} \\ i_{dq0_{s2}} \\ i'_{tr_r} \end{bmatrix} + \omega_r \begin{bmatrix} *^{3\times'3} & 0 & \begin{bmatrix} *_1^{2\times2} & \cdots & *_N^{2\times2} & 0^{2\times ND} \\ 0 & \cdots & 0 & 0 \end{bmatrix} \\ 0 & *^{3\times3} & \begin{bmatrix} *_1^{2\times2} & \cdots & *_N^{2\times2} & 0^{2\times ND} \\ 0 & \cdots & 0 & 0 \end{bmatrix} \\ 0 & 0 & 0 \end{bmatrix} \begin{bmatrix} i_{dq0_{s1}} \\ i_{dq0_{s2}} \\ i'_{tr_r} \end{bmatrix} + \begin{bmatrix} *^{3\times3} & 0 & \begin{bmatrix} *_1^{2\times2} & \cdots & *_N^{2\times2} & 0^{2\times ND} \\ 0 & \cdots & 0 & 0 \end{bmatrix} \\ 0 & *^{3\times3} & \begin{bmatrix} *_1^{2\times2} & \cdots & *_N^{2\times2} & 0^{2\times ND} \\ 0 & \cdots & 0 & 0 \end{bmatrix} \\ \begin{bmatrix} *_1^{2\times2} & 0 \\ \vdots & \vdots \\ *_N^{2\times2} & 0 \\ 0^{ND\times2} & 0 \end{bmatrix} & \begin{bmatrix} *_1^{2\times2} & 0 \\ \vdots & \vdots \\ *_N^{2\times2} & 0 \\ 0^{ND\times2} & 0 \end{bmatrix} & \begin{bmatrix} *_1^{2\times2} & \cdots & *^{2\times2} & 0^{2\times ND} \\ & \ddots & & \\ *^{2\times2} & \cdots & *_N^{2\times2} & 0^{2\times ND} \\ 0^{2\times2} & \cdots & 0^{2\times2} & *^{ND\times ND} \end{bmatrix} \end{bmatrix} \frac{d}{dt} \begin{bmatrix} i_{dq0_{s1}} \\ i_{dq0_{s2}} \\ i'_{tr_r} \end{bmatrix} \tag{3.31}$$

where $D = S - 2$.

By following through rotor terms it can be seen that we can now partition i'_{tr_r} into $\begin{bmatrix} i_{dq_r}{}^{\mathrm{T}} & \bar{i}_{dq_r}^{\mathrm{T}} \end{bmatrix}^{\mathrm{T}}$. Where $i_{dq_r} = \begin{bmatrix} i_{dq_r1}{}^{\mathrm{T}} & \cdots & i_{dq_rN}{}^{\mathrm{T}} \end{bmatrix}$, with each i_{dq_rj} corresponding to the d and q axis currents from the j^{th} set of rotor circuits. Note that the zero sequence circuit in each case has been included in $\bar{i}_{dq_r}$ along with terms corresponding to the orthogonal complement of the d-q transformation, $C_r^{\perp}$ (3.4). Therefore with $\bar{R}_{dq_r}, \bar{M}_{dq_r} \in \mathbb{R}^{ND\times ND}$ (3.31) may be written as:

$$\begin{bmatrix}\begin{bmatrix} v_{dq0_{s1}} \\ v_{dq0_{s2}} \\ v_{dq_r} \end{bmatrix} \\ \bar{v}_{dq_r}\end{bmatrix} = \left(\begin{bmatrix} R_{dq} & 0 \\ 0 & \bar{R}_{dq_r}\end{bmatrix} + \omega_r \begin{bmatrix} Q_{dq} & 0 \\ 0 & 0\end{bmatrix}\right) \begin{bmatrix}\begin{bmatrix} i_{dq0_{s1}} \\ i_{dq0_{s2}} \\ i_{dq_r} \end{bmatrix} \\ \bar{i}_{dq_r}\end{bmatrix} + \begin{bmatrix} M_{dq} & 0 \\ 0 & \bar{M}_{dq_r}\end{bmatrix} \frac{d}{dt} \begin{bmatrix}\begin{bmatrix} i_{dq0_{s1}} \\ i_{dq0_{s2}} \\ i_{dq_r} \end{bmatrix} \\ \bar{i}_{dq_r}\end{bmatrix} \tag{3.32}$$

$$\Leftrightarrow \frac{d}{dt}\begin{bmatrix}\begin{bmatrix} i_{dq0_{s1}} \\ i_{dq0_{s2}} \\ i_{dq_r} \end{bmatrix} \\ \bar{i}_{dq_r}\end{bmatrix} = \begin{bmatrix} M_{dq} & 0 \\ 0 & \bar{M}_{dq_r}\end{bmatrix}^{-1} \left(- \begin{bmatrix} R_{dq} + \omega_r Q_{dq} & 0 \\ 0 & \bar{R}_{dq_r}\end{bmatrix} \begin{bmatrix}\begin{bmatrix} i_{dq0_{s1}} \\ i_{dq0_{s2}} \\ i_{dq_r} \end{bmatrix} \\ \bar{i}_{dq_r}\end{bmatrix} + \begin{bmatrix}\begin{bmatrix} v_{dq0_{s1}} \\ v_{dq0_{s2}} \\ v_{dq_r} \end{bmatrix} \\ \bar{v}_{dq_r}\end{bmatrix}\right) \tag{3.33}$$

$$Q_{dq} = \begin{bmatrix} Q_{dq0_{s1}} & 0 & Q_{dq_{sr1}} \\ 0 & Q_{dq0_{s1}} & Q_{dq_{sr2}} \\ 0 & 0 & 0 \end{bmatrix}, \; M_{dq} = \begin{bmatrix} M_{dq0_{s1}} & 0 & M_{dq_{sr1}} \\ 0 & M_{dq0_{s2}} & M_{dq_{sr2}} \\ {M_{dq0_{sr1}}}^{\mathrm{T}} & {M_{dq_{sr2}}}^{\mathrm{T}} & M_{dq_r} \end{bmatrix} \tag{3.34}$$

As the inductance matrix is block diagonal, its inverse will also be block diagonal from Lemma A.5, therefore it is clear from (3.33) that $\bar{i}_{dq_r}$ is independent of the other currents. And therefore if we can only measure the other currents, it is quite impossible to determine the value of $\bar{i}_{dq_r}$. $\bar{i}_{dq_r}$ is said to be *unobservable* from the output.

Furthermore as there is no voltage supply to the rotor, the rotor voltage will always be zero. It is therefore not possible to affect, in any way, the value of $\bar{i}_{dq_r}$ by changing the supply voltage. $\bar{i}_{dq_r}$ is said to be *uncontrollable* from the input (the supply voltage).

It is well-known to control engineers that removing states from a system which are uncontrollable and unobservable, but unstable will inevitably lead to unsatisfactory performance. Fortunately, with the BDFM, this is not the case. If we consider the rotor-rotor mutual inductance, M_r of (3.8), then from Lemma 2.3 we know it to be positive definite, and furthermore we know it to be symmetric (some definitions of positive definite do not require symmetry), thus all the eigenvalues of M_r must be greater than zero. As the only transformation applied to M_r is a constant, invertible state transformation its eigenvalues will remain unchanged. The same holds true for R_r, the rotor resistance. As M_r and R_r $C_{r1}^{\perp}$ can be chosen so that $\bar{R}_{dq_r}$ and $\bar{M}_{dq_r}$ are diagonal, hence $-\bar{M}_{dq_r}^{-1}\bar{R}_{dq_r}$ is negative definite, thus all eigenvalues are negative. Hence the uncontrollable and unobservable states highlighted are stable and can safely be removed.

Therefore the full d-q transformed BDFM model can be written as:

$$
\begin{aligned}
\begin{bmatrix} v_{dq0_{s1}} \\ v_{dq0_{s2}} \\ 0 \end{bmatrix} &= \left(R_{dq} + \omega_r Q_{dq}\right) \begin{bmatrix} i_{dq0_{s1}} \\ i_{dq0_{s2}} \\ i_{dq_r} \end{bmatrix} + M_{dq} \frac{d}{dt} \begin{bmatrix} i_{dq0_{s1}} \\ i_{dq0_{s2}} \\ i_{dq_r} \end{bmatrix} \\
\Leftrightarrow \frac{d}{dt} \begin{bmatrix} i_{dq0_{s1}} \\ i_{dq0_{s2}} \\ i_{dq_r} \end{bmatrix} &= M_{dq}^{-1} \left(-R_{dq} - \omega_r Q_{dq}\right) \begin{bmatrix} i_{dq0_{s1}} \\ i_{dq0_{s2}} \\ i_{dq_r} \end{bmatrix} + M_{dq}^{-1} \begin{bmatrix} v_{dq0_{s1}} \\ v_{dq0_{s2}} \\ 0 \end{bmatrix} \\
Q_{dq} &= \begin{bmatrix} Q_{dq0_{s1}} & 0 & Q_{dq_{sr1}} \\ 0 & Q_{dq0_{s2}} & Q_{dq_{sr2}} \\ 0 & 0 & 0 \end{bmatrix}, \; M_{dq} = \begin{bmatrix} M_{dq0_{s1}} & 0 & M_{dq_{sr1}} \\ 0 & M_{dq0_{s2}} & M_{dq_{sr2}} \\ {M_{dq_{sr1}}}^{\mathrm{T}} & {M_{dq_{sr2}}}^{\mathrm{T}} & M_{dq_r} \end{bmatrix} \\
R_{dq} &= \begin{bmatrix} R_{dq0_{s1}} & 0 & 0 \\ 0 & R_{dq0_{s2}} & 0 \\ 0 & 0 & R_{dq_r} \end{bmatrix}
\end{aligned}
\tag{3.35}
$$

where $M_{dq0_{s1}}$ is given by (3.19), $M_{dq0_{s2}}$ by (3.20), $Q_{dq0_{s1}}$ by (3.17), $Q_{dq0_{s2}}$ by (3.18). $M_{dq_{sr1}}$ is given by (3.26) with the appropriate elements removed, $M_{dq_{sr2}}$ by (3.27), $Q_{dq_{sr1}}$ by (3.28), $Q_{dq_{sr2}}$ by (3.29), and M_{dq_r} by (3.24). The resistance matrix is diagonal as previously discussed.

We now turn our attention to the torque equation. From (2.12):

$$T_e = \frac{1}{2} i^{\mathrm{T}} \frac{dM}{d\theta_r} i \tag{3.36}$$

substituting with (3.11) and simplifying gives:

$$= \frac{1}{2} \begin{bmatrix} i_{dq0_{s1}} \\ i_{dq0_{s2}} \\ i_{tr_r} \end{bmatrix}^{\mathrm{T}} \begin{bmatrix} C_{s1} & 0 & 0 \\ 0 & C_{s2} & 0 \\ 0 & 0 & C_r \end{bmatrix} \frac{dM}{d\theta_r} \begin{bmatrix} C_{s1} & 0 & 0 \\ 0 & C_{s2} & 0 \\ 0 & 0 & C_r \end{bmatrix}^{\mathrm{T}} \begin{bmatrix} i_{dq0_{s1}} \\ i_{dq0_{s2}} \\ i_{tr_r} \end{bmatrix} \tag{3.37}$$

$$= \frac{1}{2} \begin{bmatrix} i_{dq0_{s1}} \\ i_{dq0_{s2}} \\ i_{tr_r} \end{bmatrix}^{\mathrm{T}} \begin{bmatrix} 0 & 0 & C_{s1} \frac{d}{d\theta_r} (M_{s1r}) {C_r}^{\mathrm{T}} \\ 0 & 0 & C_{s2} \frac{d}{d\theta_r} (M_{s2r}) {C_r}^{\mathrm{T}} \\ C_r \frac{d}{d\theta_r} ({M_{s1r}}^{\mathrm{T}}) {C_{s1}}^{\mathrm{T}} & C_r \frac{d}{d\theta_r} ({M_{s2r}}^{\mathrm{T}}) {C_{s2}}^{\mathrm{T}} & 0 \end{bmatrix} \begin{bmatrix} i_{dq0_{s1}} \\ i_{dq0_{s2}} \\ i_{tr_r} \end{bmatrix} \tag{3.38}$$

$$= \begin{bmatrix} i_{dq0_{s1}} \\ i_{dq0_{s2}} \end{bmatrix}^{\mathrm{T}} \begin{bmatrix} C_{s1} \frac{d}{d\theta_r} (M_{s1r}) {C_r}^{\mathrm{T}} \\ C_{s2} \frac{d}{d\theta_r} (M_{s2r}) {C_r}^{\mathrm{T}} \end{bmatrix} i_{tr_r} \tag{3.39}$$

by adopting the same partition of i_{tr_r} used in (3.33):

$$T_e = \begin{bmatrix} i_{dq0_{s1}} \\ i_{dq0_{s2}} \end{bmatrix}^{\mathrm{T}} \begin{bmatrix} Q_{dq_{sr1}} \\ Q_{dq_{sr2}} \end{bmatrix} i_{dq_r} \tag{3.40}$$

We may now make a general statement about d-q axis transformations for this class of machines:

Remark 3.1. For the class of BDFMs with: single or double layer isolated, series connected stator windings, as discussed in section 2.6, with suitable choice of pole pairs p_1, p_2 as given by theorem 2.12, and a rotor which fulfils the requirements of section 2.7; and then if the mutual inductance between stator and rotor can be adequately approximated by the first non-zero term of their Fourier series representation; then the BDFM equations may be transformed using the non square transformation given by (3.10) which is a power-conserving transformation and removes the states corresponding to $\bar{i}_{dq_r}$. Furthermore, the states removed by this transformation are unobservable, uncontrollable and stable, and do not appear in the torque equation. In the special case of a 'nested-loop' design rotor, the transformation derived is identical to one of the transformations of Boger [12, p. 25]. ♡

Remark 3.2. It is significant that the BDFM, with a rotor within the class outlined, can have its rotor modelled using a single d-q pair for each set of S rotor circuits. This is somewhat surprising because the machine has two stator supplies, of different pole numbers, hence it would be expected that two d-q pairs would be required for each set of rotor circuits. Or in systems theory terminology one would expect matrix M, of Lemma A.17 to be of rank 4, when it is actually rank 2. This fact serves to reinforce the necessity for the rotor to have $S = p_1 + p_2$ circuits per set, rather than any other number. ♡

It it worth mentioning that the d-q transformation outlined may be extended for higher order harmonic couplings between stator and rotor. It can be shown that the stator parameters will remain the same for all higher harmonics, however the rotor parameters will change for some harmonic combinations. This is because the special condition which allowed a single d-q pair to represent a single set of S rotor circuits, as noted in remark 3.2 will only be met if $(k_1 p_2 + k_2 p_2)/(p_1 + p2)$ is an integer where k_1, k_2 are the relative harmonic for each winding. This has the effect that the higher harmonics may require 2 d-q pairs for each set of S circuits, rather than 1, and consequently the rotor-rotor portion of M_{dq} will alter. For each harmonic the stator-rotor parameters will change.

3.3.1 Determination of d-q model rotor current from bar currents

The problem of determination of d-q model rotor current from bar currents will briefly be considered. Clearly the d-q axis rotor current can be computed using (3.5), and then truncated to leave the non-zero portion, as discussed in the previous section.

However, as we have shown, for every set of $S = p_1 + p_2$ circuits on the rotor only 1 d-q pair is controllable from the stator voltages. Therefore it is possible to calculate the d-q rotor currents for each set of S rotor circuits by measuring the currents in only two of the S circuits.

For each of the N sets of S rotor circuits the transformation from bar currents to d-q currents is given by C_{rN}, where C_{rN} is of the form of 3.3. From the preceding discussion we know that:

$$i_{dq_{rN}} = C_{rN} i_{rN} \tag{3.41}$$

where $i_{rN} \in \mathbb{R}^S$, $i_{dq_{rN}} \in \mathbb{R}^2$ and $C_{rN} \in \mathbb{R}^{2\times S}$ and it is full rank. We seek a transformation, $\tilde{C}_{rN} \in \mathbb{R}^{2\times 2}$, such that:

$$i_{dq_{rN}} = \tilde{C}_{rN} P i_{rN} \tag{3.42}$$

where $P \in \mathbb{R}^{2\times S}$, and P is a matrix which has a single 1 in each row, with all other elements zero, and is rank 2 (that is the 1s must be in different columns). For example P might be:

$$P = \begin{bmatrix} I_2 & 0 & \cdots \end{bmatrix} \tag{3.43}$$

From 3.41 and 3.42 we may write:

$$\tilde{C}_{rN} P i_{rN} = C_{rN} i_{rN} \tag{3.44}$$

we have shown in the previous section that $i_{rN} = {C_{rN}}^{\mathrm{T}} i_{dq_{rN}}$, therefore:

$$\tilde{C}_{rN} P {C_{rN}}^{\mathrm{T}} i_{dq_{rN}} = C_{rN} {C_{rN}}^{\mathrm{T}} i_{dq_{rN}} \tag{3.45}$$

as $C_{rN} {C_{rN}}^{\mathrm{T}} = I_2$:

$$\tilde{C}_{rN} P {C_{rN}}^{\mathrm{T}} i_{dq_{rN}} = i_{dq_{rN}} \tag{3.46}$$

as $\tilde{C}_{rN} P {C_{rN}}^{\mathrm{T}}$ is full rank:

$$\Leftrightarrow \tilde{C}_{rN} P {C_{rN}}^{\mathrm{T}} = I_2 \tag{3.47}$$

$$\Leftrightarrow \tilde{C}_{rN} = \left(P {C_{rN}}^{\mathrm{T}}\right)^{-1} \tag{3.48}$$

Therefore for each of the N sets of S rotor circuits a 2 by 2 transformation, which determines the d-q rotor currents from any two bar currents, is given by $\tilde{C}_{rN} = \left(P {C_{rN}}^{\mathrm{T}}\right)^{-1}$

3.4 Model order reduction for Nested-loop rotor

The preceding derivation, culminating in remark 3.1, gives a full transformation for any BDFM rotor in a broad class.

However, each of the N sets of S rotor circuits yields an additional d-q pair. Therefore the overall model is of order $6 + 2N$. It is desirable to reduce the order of the model so that a single d-q pair models the rotor, thus reducing the order to 8.

Boger et. al. proposed a 8 order model (which reduces to 6 if the stator zero-sequence states can be removed), [11]. However, their proposal is simply to sum the contributions from the N different sets of circuits. No comment is made as to whether or not this is a good or poor approximation (in fact they do not mention that it constitutes a model reduction at all).

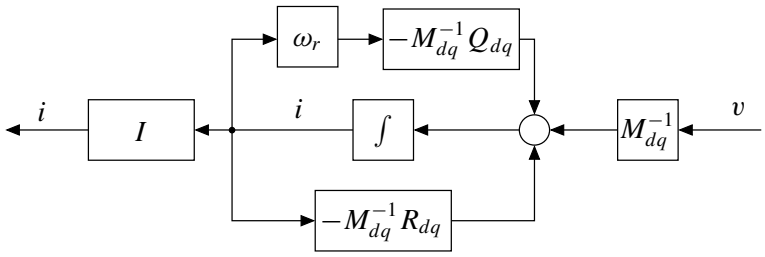

Figure 3.2: Block diagram of d-q transformed BDFM model

We will show that this can lead to a poor approximation, sometimes little better than ignoring inner loops within a nest all together. The physical reason for this is that, in a 'nested-loop' design rotor, the N sets are the different pitch coils within each 'nest'. The difference in pitch means that different currents will be induced into each of the coils, and the mutual coupling between the coils within a 'nest' will lead to circulating currents within each 'nest'. These currents are eliminated if the inductance terms are simply summed, leading to erroneous results. Section B.3 details the mutual inductance matrices for the prototype 'nested-loop' design rotor. Equation (B.13) shows the d-q mutual inductance matrix for this rotor design. Significantly (B.13) confirms the coupling between the sets of rotor circuits by the presence of non-zero off-diagonal elements.

There is, therefore, a need for an improved method of model reduction which reduces the approximation error in some sense.

3.4.1 Model Reduction Techniques

From the preceding analysis it is clear that the *electrical* equations for the BDFM are linear. That is, the currents (and voltages) appear linearly in the equations. Therefore the BDFM equations for the d-q transformed model, (3.35) may be represented by the block diagram in figure 3.2.

It is important that the BDFM may be modelled as a linear system because linear systems are amenable to a rich set of techniques, particularly in terms of model reduction. Model reduction has received considerable attention in the field of linear systems theory.

It will be of use to redraw figure 3.2 separating out the connections between rotor and stator. To simplify the notation we will repartition the state vector, and corresponding matrices into rotor and stator quantities, rather then stator 1, stator 2, and rotor quantities as in equations (3.35):

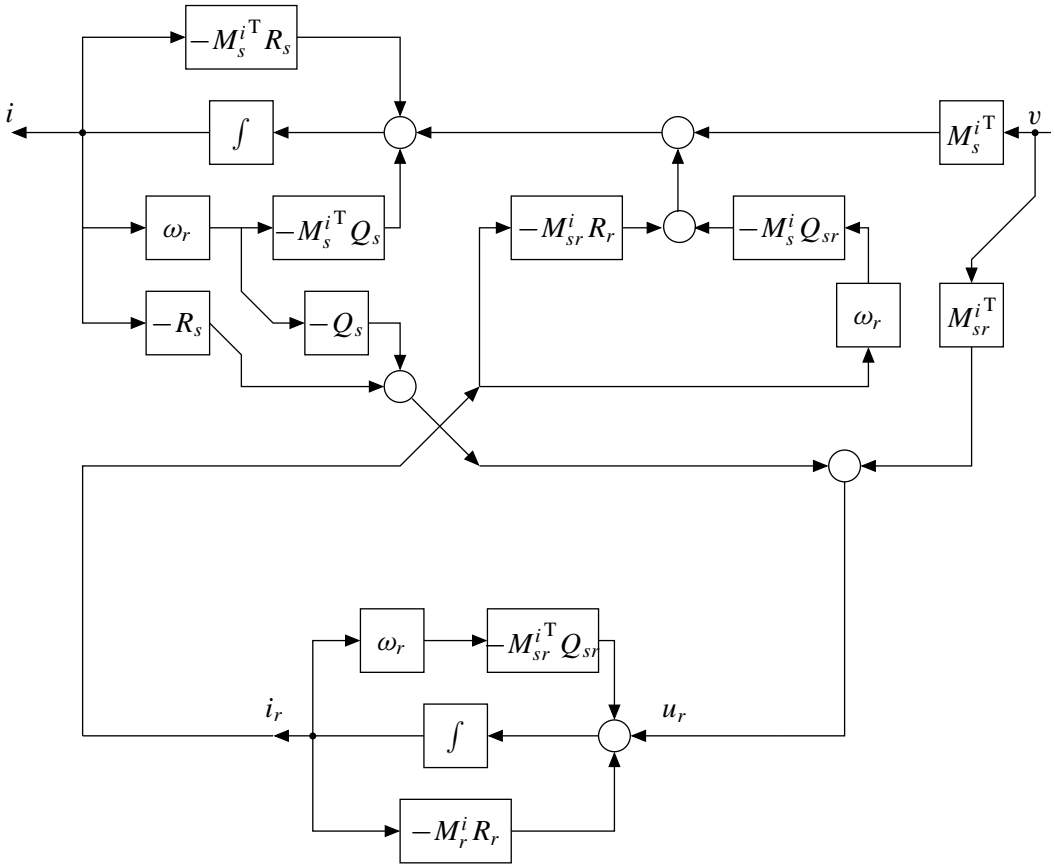

Figure 3.3: Block diagram of d-q transformed BDFM model with rotor and stator separate

$$M_{dq} = \begin{bmatrix} M_s & M_{sr} \\ {M_{sr}}^{\mathrm{T}} & M_r \end{bmatrix} \tag{3.49}$$

$$Q_{dq} = \begin{bmatrix} Q_s & Q_{sr} \\ 0 & 0 \end{bmatrix} \tag{3.50}$$

$$R_{dq} = \begin{bmatrix} R_s & 0 \\ 0 & R_r \end{bmatrix} \tag{3.51}$$

and we partition the inverse of M_{dq} compatibly with M_{dq} as follows, using superscript i to denote that the block matrix belongs to M_{dq}^{-1} rather than M_{dq}. The analytical expression for these elements can be determined from Lemma A.5. Note that $M_s^i \neq M_s^{-1}$ etc.:

$$M_{dq}^{-1} = \begin{bmatrix} M_s^i & M_{sr}^i \\ {M_{sr}^i}^{\mathrm{T}} & M_r^i \end{bmatrix} \tag{3.52}$$

$$\tag{3.53}$$

We start by reviewing some possible model reduction techniques

Linear, Time-invariant Model Reduction Techniques

Linear, time-invariant (LTI) systems have had considerable attention devoted to their analysis, and model reduction is no exception.

Two techniques of LTI model reduction are *balanced truncation* and *optimal Hankel-norm approximation*. Both these techniques offer 'automatic' methods of model reduction for LTI systems, that is, they are mathematical procedures which give results that are guaranteed to be 'good' in some sense.

Before proceeding further is it necessary to introduce some of standard notation of linear systems theory:

Definition 3.1. [131, p. 92] Any function, $x(t) \in \mathbb{R}^n$ may be said to be $\mathcal{L}_2(I)$ space iff:

$$\|x\|_2 \triangleq \left(\int_I |x(t)^{\mathrm{T}} x(t)| dt \right)^{1/2} < \infty$$

where $I \subset \mathbb{R}$ is the interval, which will typically be $[0, \infty)$. Thus a function $x(t)$ is a member of $\mathcal{L}_2(I)$ if $x(t)$ has a bounded 2-norm over the interval I. $\mathcal{L}_2[0, \infty)$ is denoted by the short hand $\mathcal{L}_2^+$.

Definition 3.2. [131, ch. 4] Given a linear system, P, mapping $u \in \mathbb{R}^m$ to $y \in \mathbb{R}^n$ then the *induced 2-norm*, $\|P\|_{i,2}$ is defined as:

$$\|P\|_{i,2} \triangleq \sup_{u(t) \in \mathcal{L}_2^+} \frac{\|y\|_2}{\|u\|_2}$$

where sup stands for supremum, or 'least upper bound'. Hence the induced 2-norm of P is the worst-case gain for any input signal in $\mathcal{L}_2^+$

Both balanced truncation and the optimal Hankel-norm approximation can guarantee that induced 2-norm of the error system will not be more than some upper bound. To explain the precise nature of this upper bound it is necessary to introduce some more systems theory notation:

Definition 3.3. [131, ch. 3] A minimal realization of an LTI system, G, with input $u(t)$ and output $y(t)$ may be written as:

$$\dot{x} = Ax + Bu$$
$$y = Cx + Du$$

or more compactly as: $G = \left[\begin{array}{c|c} A & B \\ \hline C & D \end{array}\right]$. A *minimal realization* is a representation of G for which the dimension of x is minimised.

The *controllability* and *observability* gramians, P and Q respectively are given by the solutions to:

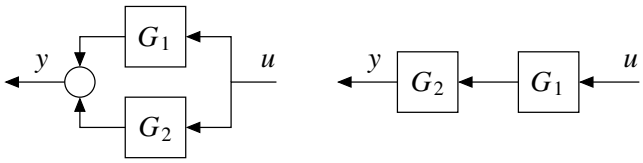

Figure 3.4: Parallel and series connection of systems

$$AP + PA^* + BB^* = 0$$
$$A^*Q + QA + C^*C = 0$$

where $P = P^* \geq 0$, $Q = Q^* \geq 0$, that is P and Q are Hermitian, positive semi-definite.

The *Hankel singular values* of G are $\sqrt{\lambda(PQ)}$, where $\lambda(\cdot)$ denotes the eigenvalues. Furthermore there will always exist an invertible state transformation, T, such that $\tilde{x} = Tx$, and the transformed gramians become $\tilde{P} = TPT^* = (T^{-1})^*QT^{-1} = \tilde{Q} = \Sigma$ where Σ is a diagonal matrix of the Hankel singular values of G in descending order. The realization of G which achieves $\tilde{P} = \tilde{Q} = \Sigma$ is called the *balanced realization*.

Remark 3.3. Series and parallel connection of two systems, G_1, G_2 may be conveniently represented by G_1G_2 and $G_1 + G_2$ respectively. If G_1, G_2 are linear then they can be represented by $G_1 = \left[\begin{array}{c|c} A_1 & B_1 \\ \hline C_1 & D_1 \end{array}\right]$, $G_2 = \left[\begin{array}{c|c} A_2 & B_2 \\ \hline C_2 & D_2 \end{array}\right]$. The parallel connection can be represented by

$$G_1 + G_2 = \left[\begin{array}{cc|c} A_1 & 0 & B_1 \\ 0 & A_2 & B_2 \\ \hline C_1 & C_2 & D_1 + D_2 \end{array}\right]$$

and the series connection by:

$$G_2G_1 = \left[\begin{array}{cc|c} A_1 & 0 & B_1 \\ B_2(C_1 + D_1) & A_2 & 0 \\ \hline D_2C_1 & C_2 & D_2D_1 \end{array}\right]$$

Diagrammatically the connection are illustrated by figure 3.4. ♡

Model reduction by balanced truncation reduces the order of the system by removing the states corresponding to the smaller Hankel singular values. The induced 2-norm of the error system, that is the error between the full-order and reduced order system for any input with unitary 2-norm, will be less than twice the sum of the truncated Hankel singular values [131, ch. 7].

Model reduction by the optimal Hankel norm approximation, seeks to find a reduced order system, $\hat{G}$, such that the Hankel norm of the error system $G - \hat{G}$ is minimised. The Hankel norm of a system

is the maximum Hankel singular value of that system. It turns out that for LTI systems it will always be possible to find $\hat{G}$, and furthermore it will always be possible to find a constant D_0 such that the induced 2-norm of $G - \hat{G} - D_0$ is less than the sum of the truncated Hankel singular values [131, ch. 8],[40].

Both these techniques could be applied to the d-q transformed model of the BDFM previously derived, however the BDFM model, although linear, is not time-invariant. The model is dependent on a parameter, the rotational speed, ω_r thus the techniques can only be applied for a fixed speed. There are, however, generalisations of both balanced truncation and optimal Hankel-norm reduction for linear parameter-varying (LPV) systems, which will now be considered.

Model Reduction Techniques for Linear Parameter Varying Systems

The methods of model reduction for linear parameter varying systems, are rather less established than for the LTI case. Nevertheless methods have appeared in the literature which are applicable. In the BDFM model presented, the parameter variation appears in the 'A' matrix. From figure 3.2 it can be seen that in the BDFM the 'A' matrix becomes $A_1 + \omega_r A_2$. Hence the parameter dependence is *affine* that is, linear with an offset.

Wood et. al. [118] and Wood [119] present generalisations of balanced truncation and Hankel norm approximation for LPV systems. Related work in discrete time, which will not be further discussed here, is presented in Lall and Beck [58], Beck and Doyle [5], Beck and Bendotti [4] and Beck, Doyle and Glover [6].

An LPV system is one where time-dependent parameters enter the state equations through one or more exogenous parameters:

$$\begin{aligned} \dot{x} &= A(\rho)x + B(\rho)u \\ y &= C(\rho)x + D(\rho)u \end{aligned} \tag{3.54}$$

where ρ is the parameter vector which may be time-varying.

In [118] the notions of controllability and observability gramians, balanced realizations, and Hankel singular values is generalised to LPV systems. These are then used to obtain similar bounds for the worst case induced 2-norm error. However, unlike in the LTI case the results do not lead to a unique solution for each system. That is, suppose one wanted to reduce the order of a linear system from 10 to 6: In the LTI case both balanced truncation and the optimal Hankel norm approximation method lead to a unique upper bound on the 2-norm error for that particular system and reduction choice. In the LPV case however, although a bound can be found, there is no guarantee that it is the smallest bound possible. The reason for this will become apparent in the following discussion.

From [118] the generalised gramians are given by any solutions for P and Q to:

$$A(\rho)^{\mathrm{T}}Q + QA(\rho) + C(\rho)^{\mathrm{T}}C(\rho) < 0,\ \ Q = Q^{\mathrm{T}} > 0,\ \ \forall\ \rho(t) \in F_\rho \tag{3.55}$$

$$A(\rho)P + PA(\rho)^{\mathrm{T}} + B(\rho)B(\rho)^{\mathrm{T}} < 0,\ \ P = P^{\mathrm{T}} > 0,\ \ \forall\ \rho(t) \in F_\rho \tag{3.56}$$

where F_ρ is the set of all possible parameter trajectories.

Having found such a P and Q the procedure is then the same as for the LTI case for balanced truncation. Although a Hankel-norm approach is also presented which achieves an analogous bound to the LTI case, the authors note that the additional complexity introduced limits the applicability of the result, and therefore it will not be considered further here.

Note that, from the preceding discussion P and Q are not unique, because (3.55) and (3.56) are inequalities rather than equalities in the LTI case. Because the BDFM d-q transformed equations are affine in their only parameter, ω_r (see figure 3.2), then from Lemma A.7 (3.56,3.55) will be satisfied for all possible ω_r if they are satisfied for the extreme values of ω_r. To be precise, if $\omega_r^{\min} < \omega_r < \omega_r^{\max}$ then (3.56,3.55) are satisfied if:

$$\left.\begin{aligned} &(A_1 + \omega_r^{\max} A_2)^{\mathrm{T}} Q + Q(A_1 + \omega_r^{\max} A_2) + C^{\mathrm{T}} C < 0 \\ &(A_1 + \omega_r^{\min} A_2)^{\mathrm{T}} Q + Q(A_1 + \omega_r^{\min} A_2) + C^{\mathrm{T}} C < 0, \;\; Q = Q^{\mathrm{T}} > 0 \end{aligned}\right\} \tag{3.57}$$

$$\left.\begin{aligned} &(A_1 + \omega_r^{\max} A_2) P + P(A_1 + \omega_r^{\max} A_2)^{\mathrm{T}} + B B^{\mathrm{T}} < 0 \\ &(A_1 + \omega_r^{\min} A_2) P + P(A_1 + \omega_r^{\min} A_2)^{\mathrm{T}} + B B^{\mathrm{T}} < 0, \;\; P = P^{\mathrm{T}} > 0 \end{aligned}\right\} \tag{3.58}$$

The problem of finding a P and Q satisfying (3.57,3.58) (and with any further linear constraint placed on the elements of P and Q) may be efficiently solved. The problem is a *linear matrix inequality* (LMI) which is a convex optimization problem for which efficient algorithms exist [37].

As the upper bound on the error is the sum of the truncated singular values, the smaller the truncated singular values can be made, the tighter the bound that can be achieved. Unfortunately the constraint on P and Q to minimize the square-root of eigenvalues of PQ, or even the eigenvalues themselves, amounts to a non-linear constraint, and therefore the problem becomes non-convex, and hence impractical to solve. In [118] a procedure is proposed that will find a locally optimal solution to the problem, via minimising the trace of a QP pair, which therefore finds the minimum sum of the eigenvalues of the QP pair. Their algorithm is as follows:

1. Find a Q_1 which satisfies (3.57) and minimises $\sum_k \mathrm{trace}(Q_1 P_0(\omega_{r_k}))$ where $P_0(\omega_{r_k})$ is the LTI controllability gramian for $\omega_r = \omega_{r_k}$, and ω_{r_k} is the k^{th} value for ω_r over some grid of range of permissible ω_r values.

2. Solve for a P_1 which satisfies equation (3.58) and minimises trace $P_1 Q_1$.

3. Solve for a Q_2 which satisfies equation (3.57) and minimises trace $Q_2 P_1$.

4. Repeat steps 2 and 3 until the decrease in the cost function satisfies some convergence criterion.

Recall that the trace of a matrix is the sum of the eigenvalues, so this procedure has the effect of trying to find a P and Q for which the sum of the eigenvalues of PQ are small. However the procedure will not necessarily find the global minimum, and furthermore even if it did there may still

be a P and Q which lead to a smaller upper bound on the error between the original and reduced system.

Even if the optimal solution were to be found, one potential shortfall of the previous approach is that the reduction process makes no assumption about the rate of change of the parameter, in our case ω_r. This may lead to further conservatism in the results. Explicit bounds on the rate of variation of the parameter can be included, by making P and Q functions of the parameter, however the existence of a suitable transformation matrix to balance the system becomes potentially, hard to find, see [119] for details. Therefore parameter dependent P and Q will not be considered further.

It is worth mentioning that although the techniques described offer guaranteed bounds on the induced 2-norm of the error, it is possible to easily calculate the induced 2-norm of the error (or indeed of any system) in both the constant system and affine linear parameter varying cases. In the LTI case the induced 2-norm is simply the maximum (technically a supremum) singular value of the frequency response of the system over all frequencies [131, ch. 4]. In the LPV case it is a little more involved.

Theorem 3.4. *[7, Lemma 2.10] & Lemma A.9 Given the LPV system* $G = \left[\begin{array}{c|c} A(\rho) & B(\rho) \\ \hline C(\rho) & D(\rho) \end{array}\right]$ *where* $\rho \in \mathbb{R}^m$ *is a time-varying parameter and* $\gamma \in \mathbb{R} > 0$*. If there exists an* $X = X^{\mathrm{T}} \in \mathbb{R}^{n\times n}$ *such that for all possible parameter trajectories:*

$$\begin{bmatrix} A^{\mathrm{T}}X + XA & XB & C^{\mathrm{T}} \\ B^{\mathrm{T}}X & -I & D^{\mathrm{T}} \\ C & D & -I\gamma^2 \end{bmatrix} < 0$$

then the system G is stable and there exists $\beta < \gamma$ *such that* $||G||_{i,2} \leq \beta$*.*

Using theorem 3.4 an upper bound on the induced 2-norm of a system can be computed by finding the solution X which minimises γ^2. This problem is often known as the $\mathcal{L}_2$ performance problem. Fortunately theorem 3.4 presents this problem as an LMI with linear constraints, which can therefore be directly solved.

However, in general, every parameter value must be checked, which constitutes an infinite number of LMIs to be solved. The parameter space can, however, be gridded and the solution approximated with a finite number of LMIs (see, for example [119] for details). In the case that ρ appears affinely in G then it can be shown that it is only necessary to check the extreme point of the parameter box. As the parameter dependence in the BDFM only appears in 'A', the sufficiency of checking the extreme points can be seen from Lemma A.7 with Lemma A.8. Using Matlab's LMI Control tool box this bound can be computed using the `quadperf` function [37]. The $\mathcal{L}_2$ performance problem may also be represented as an *integral quadratic constraint* (IQC) [74], for which a tool box is available for calculation using Matlab [73].

Stability of the BDFM

The LPV balanced truncation, and the new method of model reduction to be described, require the system to be quadratically stable. We will now prove that the electrical BDFM equations are always quadratically stable.

Theorem 3.5. *Any BDFM satisfying the present assumptions is quadratically stable for any bounded variation in shaft speed.*

Proof. It was established in figure 3.2, that the dq-transformed BDFM equations may be written as:

$$\frac{di}{dt} = A_0 i + \omega_r A_1 i + Bv$$

for suitable choices of A_0, A_1, B as given by figure 3.2. Or equivalently:

$$G = \left[\begin{array}{c|c} A_0 + \omega_r A_1 & B \\ \hline I & 0 \end{array}\right]$$

Quadratic stability can be ensured by finding a single Lyapunov function which holds for all parameter trajectories, that is find a $P = P^{\mathrm{T}} > 0 : A(\rho)^{\mathrm{T}} P + P A(\rho) < 0, \ \forall \rho \in F_\rho$, where F_ρ is the set of permissible parameter trajectories and $A(\rho)$ the system matrix ([7, Def 2.4]).

We first consider the eigenvalues of $R_{dq} \pm Q_{dq}$. Q_{dq} and R_{dq} for the class of machines considered is given in (3.35). As $R_{dq} \pm Q_{dq}$ is block triangular, from Lemma A.6, the eigenvalues of $R_{dq} \pm Q_{dq}$ are the union of the eigenvalues of: $Q_{dq0_{s1}} \pm R_{dq0_{s1}}$, $Q_{dq0_{s2}} \pm R_{dq0_{s2}}$ and R_{dq_r}.

As R_{dq} is diagonal and $R_{dq} > 0$, from the form of $Q_{dq0_{s1}}$ and $Q_{dq0_{s2}}$ then the eigenvalues of $Q_{dq0_{s1}} \pm R_{dq0_{s1}}$ and $Q_{dq0_{s2}} \pm R_{dq0_{s2}}$ have strictly positive real parts.

Furthermore it is easy to show that the eigenvalues of $R_{dq0_{s1}} + Q_{dq0_{s1}}$ are the same as the eigenvalues of $R_{dq0_{s1}} - Q_{dq0_{s1}}$, and similarly the eigenvalues of $R_{dq0_{s2}} + Q_{dq0_{s2}}$ are the same as those of $R_{dq0_{s2}} - Q_{dq0_{s2}}$. Essentially the reason for this is that the upper left 2×2 blocks of $Q_{dq0_{s1}}$ and $Q_{dq0_{s2}}$ are skew-symmetric with real coefficients, and the remainder of the matrices are zero.

Therefore the eigenvalues of $R_{dq} \pm Q_{dq}$ are the same regardless of the sign of Q_{dq} and are strictly in the right half-plane, that is they have positive real parts.

From [32, Th. 3.1] $M_{dq}^{-1}(R_{dq} \pm \omega_r Q_{dq})$ must have all eigenvalues in the left half-plane (i.e. it is Hurwitz), as M_{dq} is positive definite (from Lemma 2.3, and recalling that $M_{dq} = T^{\mathrm{T}} M T$, for some T).

We have established that $M_{dq}^{-1}(R_{dq} \pm \omega_r Q_{dq})$ has the same eigenvalues regardless of the sign of $\omega_r Q_{dq}$. Therefore as the eigenvalues are the same both matrices must, or at least can, have the same Jordan Canonical form (see [131, Theorem 2.4]). Therefore there exists a $T \in \mathbb{C}^{n \times n}$ such that $M_{dq}^{-1}(R_{dq} + \omega_r Q_{dq}) = T M_{dq}^{-1}(R_{dq} - \omega_r Q_{dq}) T^{-1}$, where n is the dimension of M_{dq}. Note that T will, in general, be a function of ω_r.

Now to prove quadratic stability we seek a single Lyapunov function which holds for all $-\omega_{\max} < \omega_r < \omega_{\max}$. Because the BDFM equations are affinely parameter dependent, then from Lemma A.7, if we can find a single P which satisfies the extreme points, i.e. $\omega_{\max}$ and $-\omega_{\max}$ then it will also satisfy the intermediate points.

The systems corresponding to the extreme points may be written as:

$$G_1 = \left[\begin{array}{c|c} A_0 + \omega_{\max} A_1 & B \\ \hline I & 0 \end{array}\right]$$

$$G_2 = \left[\begin{array}{c|c} A_0 - \omega_{\max} A_1 & B \\ \hline I & 0 \end{array}\right]$$

but, from the previous discussion G_2 may also be written as:

$$G_2 = \left[\begin{array}{c|c} A_0 + \omega_{\max} A_1 & TB \\ \hline T^{-1} & 0 \end{array}\right]$$

and therefore both G_1 and G_2 have the same 'A' matrices, thus any P which satisfies $({A_0}^{\mathrm{T}} + \omega_{\max}{A_1}^{\mathrm{T}})P + P(A_0 + \omega_{\max}A_1) < 0$ proves quadratic stability for both G_1 and G_2, and we know that such a P will always exist as $A_0 + \omega_{\max}A_1$ has strictly left half-plane eigenvalues ([47, Th 2.2.1]).

Therefore we know that a P exists for both G_1 and G_2, therefore the BDFM is quadratically stable for any speed variation in the range $-\omega_{\max} < \omega_r < \omega_{\max}$. Then as $\omega_{\max}$ was chosen arbitrarily, quadratic stability is guaranteed for all ω_r □

Discussion of suitable model reduction methods for the BDFM with a nested loop rotor

We return now to our aim, to reduce the order of the d-q transformed BDFM equations so that the rotor is represented by just two states. In other words we wish to find a simplified model of the rotor which is equivalent in complexity to the model that one would derive from the special case when the rotor comprises of only one set of coils. Physically speaking, we are trying to find an single set of rotor coils which reasonably approximate the performance of the true rotor which has multiple sets of coils.

From the previous discussion, it is clear that for dynamic BDFM modelling the machine cannot be considered LTI, but rather LPV, as the rotor shaft speed will not be constant. Now we wish to reduce the order of only the rotor states, leaving the stator states untouched. To apply balanced truncation in this case it is necessary separate the rotor and stator systems, as shown in figure 3.3. If the rotor states are not separated then, although the model reduction techniques can still be used, the helpful physical distinction between rotor and stator states will be lost.

The problem is therefore to approximate the rotor currents, i_r, using only two states. From figure

3.3, it can be seen that the rotor currents are governed by the following differential equation:

$$\frac{di_r}{dt} = -\left(M_r^i R_r + \omega_r {M_{sr}^i}^{\mathrm{T}} Q_{sr}\right) i_r + u \tag{3.59}$$

where u represents the exogenous inputs from the stator currents and input voltage.

The rotor system is balanced by application of the appropriate state transformation, and then states truncated to reduce the order of the rotor to 2. However, there is no simple way to represent the balanced system in terms of mutual inductance, resistance, and Q terms, thus the physical interpretation that the component matrices hold is lost.

The loss of physical meaning of the components doesn't necessarily have any bearing on the efficacy of the method, however it is significant. Although a model is still of use as a 'black box' model, in that its predictive power is unchanged, the designer can no longer easily glean insight from the form of the model.

There is therefore, a need for a method of model reduction which retains some physical interpretation, yet is still an accurate approximation to the original system. We now present such a method.

3.4.2 New BDFM Rotor State Reduction Technique

An alternative approach to the more automatic methods can be found through consideration of the BDFM differential equations. For reasons which will become apparent, it is necessary to diagonalize the rotor mutual inductance matrix, M_r, by means of an orthogonal (invertible) transformation - this will always be possible as M_r is symmetric (as shown in (3.24)). Furthermore the state order will be chosen such as to order the eigenvalues in decreasing order from the top left. This can be achieved with the following state transformation:

$$\begin{bmatrix} i_s \\ \tilde{i}_r \end{bmatrix} = \begin{bmatrix} I & 0 \\ 0 & T \end{bmatrix} \begin{bmatrix} i_s \\ i_r \end{bmatrix} \tag{3.60}$$

where T is a matrix of the eigenvectors of M_r in an appropriate order.

With M_r diagonal we now partition the BDFM equations into three parts, stator, 2 rotor states, remainder of the rotor states. Then the equations may be written as:

$$\begin{bmatrix} v_s \\ 0 \\ 0 \end{bmatrix} = \begin{bmatrix} M_s & \tilde{M}_{sr_1} & \tilde{M}_{sr_2} \\ \tilde{M}_{sr_1}^{\mathrm{T}} & \tilde{M}_{r_1} & 0 \\ \tilde{M}_{sr_2}^{\mathrm{T}} & 0 & \tilde{M}_{r_2} \end{bmatrix} \frac{d}{dt} \begin{bmatrix} i_s \\ \tilde{i}_{r_1} \\ \tilde{i}_{r_2} \end{bmatrix} + \left(\begin{bmatrix} R_s & 0 & 0 \\ 0 & \tilde{R}_{r_1} & \tilde{R}_{r_{12}} \\ 0 & \tilde{R}_{r_{12}}^{\mathrm{T}} & \tilde{R}_{r_2} \end{bmatrix} + \omega_r \begin{bmatrix} Q_s & \tilde{Q}_{sr_1} & \tilde{Q}_{sr_2} \\ 0 & 0 & 0 \\ 0 & 0 & 0 \end{bmatrix} \right) \begin{bmatrix} i_s \\ \tilde{i}_{r_1} \\ \tilde{i}_{r_2} \end{bmatrix} \tag{3.61}$$

note that the off-diagonal resistances will, in general, be non-zero.

Now, notice that if $\tilde{M}_{sr_2}$, $\tilde{R}_{r_{12}}$ and $\tilde{Q}_{sr_2}$ were all zero, then the system would be reducible: $\tilde{i}_{r_2}$ could be removed with no error. It turns out that in the typical BDFM nested-loop rotors which were simulated, these terms were always small, and hence truncating the system by removing $\tilde{i}_{r_2}$ was a good approximation in all the cases tried.

Physically, having a small value of $\tilde{M}_{sr_2}$, (and hence $\tilde{Q}_{sr_2}$) corresponds to having a (relatively) large transformer turns ratio between the stator and that part of the rotor state. This means that smaller voltages are induced, and if the resistances are similar, then the current will be smaller. The effect of diagonalization (and ordering) of M_r has been to prioritise the effect of the stator coupling on the various parts of the rotor, hence by keeping the states corresponding to the most significant M_r singular values (as M_r is symmetric the eigenvalues are the singular values), and removing the other states, the system will be reduced with little error.

The reduction algorithm can be summarised as:

1. Compute T, a matrix of eigenvectors of M_r ordered so that the corresponding eigenvalues decrease from left to right.

2. Partition T into $[\, T_1 \; T_2 \,]$, where T_1 is 2 columns wide.

3. Apply the resulting non-square state 'transformation', $\tilde{i} = \begin{bmatrix} I & 0 \\ 0 & T_1^{\mathrm{T}} \end{bmatrix} i$, which reduces the state order.

Thus application of the above algorithm to (3.61) leads to:

$$\begin{bmatrix} v_s \\ 0 \end{bmatrix} = \begin{bmatrix} M_s & \tilde{M}_{sr_1} \\ \tilde{M}_{sr_1}^{\mathrm{T}} & \tilde{M}_{r_1} \end{bmatrix} \frac{d}{dt} \begin{bmatrix} i_s \\ \tilde{i}_{r_1} \end{bmatrix} + \left(\begin{bmatrix} R_s & 0 \\ 0 & \tilde{R}_{r_1} \end{bmatrix} \begin{bmatrix} Q_s & \tilde{Q}_{sr_1} \\ 0 & 0 \end{bmatrix} \right) \begin{bmatrix} i_s \\ \tilde{i}_{r_1} \end{bmatrix} \tag{3.62}$$

Significantly, the structure of the component mutual inductance, resistance and Q matrices can be shown to be the same as that for a BDFM with a rotor comprising of a single set of coils (i.e. where each rotor 'nest' has only 1 loop in it). This means that the method can be thought of as determining an effective single loop inductance and resistance for each nest. This fact will be used in chapter 5 to compare a 'nested-loop' rotor design to a novel rotor design by comparing terms in the machine equations.

This fact will now be proved. Equation (3.24) gives the general form of the rotor-rotor mutual inductance matrix, however in removing the unobservable and uncontrollable states, the rows and columns containing terms denoted by a $*$ and the zero sequence terms are deleted. In the case of the 'nested loop' design rotor, each of the off-diagonal matrix blocks are themselves diagonal. In other

words, M_{12_b} of (3.24) is zero. Therefore the rotor-rotor inductance matrix has the form:

$$M_{dq_r} = \begin{bmatrix} \begin{bmatrix} L_{dq_{r1}} & 0 \\ 0 & L_{dq_{r1}} \end{bmatrix} & \begin{bmatrix} M_{12_a} & 0 \\ 0 & M_{12_a} \end{bmatrix} & \cdots \\ \begin{bmatrix} M_{12_a} & 0 \\ 0 & M_{12_a} \end{bmatrix} & \ddots & \vdots \\ \vdots & \cdots & \begin{bmatrix} L_{dq_{rN}} & 0 \\ 0 & L_{dq_{rN}} \end{bmatrix} \end{bmatrix} \tag{3.63}$$

Let x be any eigenvector of M_{dq_r} with corresponding eigenvalue, λ_x. We now define, x_a and x_b.

$$x_a = \begin{bmatrix} x_1 & 0 & x_3 & 0 & \cdots & x_{n-1} & 0 \end{bmatrix}^{\mathrm{T}}, \qquad x_b = \begin{bmatrix} 0 & x_2 & 0 & x_4 & 0 & \cdots & 0 & x_n \end{bmatrix}^{\mathrm{T}}$$

where x_i is the i^{th} element of the eigenvector, x. Because of the structure of M_{dq_r} then x_a and x_b are also eigenvectors of M_{dq_r} with the same corresponding eigenvalue, λ_x, as long as $x_a \neq 0$ and $x_b \neq 0$.

From examination of the structure, as $M_{dq_r} x_a = \lambda_x x_a$ and $M_{dq_r} x_b = \lambda_x x_b$ then we can conclude that:

$$x_b = k \begin{bmatrix} 0 & x_1 & 0 & x_3 & 0 & \cdots & 0 & x_{n-1} \end{bmatrix}^{\mathrm{T}}, \quad \text{where } k \in \mathbb{R} \text{ is arbitrary.}$$

If x_b is zero then the corresponding result for x_a applies instead.

Therefore as all the eigenvalues of M_{dq_r} appear in pairs, and the corresponding eigenvectors are of the form of x_a and x_b, then the transformation matrix T_1 will always be of the form:

$$T_1 = \begin{bmatrix} \alpha_1 & 0 \\ 0 & \alpha_1 \\ \alpha_2 & 0 \\ 0 & \alpha_2 \\ \vdots & \vdots \\ \alpha_n & 0 \\ 0 & \alpha_n \end{bmatrix}$$

Therefore, it is immediate that the transformed rotor-rotor mutual inductance, $\tilde{M}_{r_1}$, is of the form kI, that is a scalar multiplied by the identity matrix. It is easy to show that the retained portion of the transformed resistance matrix, $\tilde{R}_{r_1}$, is also of the form kI.

The stator-rotor portions of the mutual inductance and Q matrices may be shown to transform to matrices of the form:

$$\tilde{M}_{sr_1} = \begin{bmatrix} \begin{bmatrix} \tilde{M}_1 \cos(\phi_1) & -\tilde{M}_1 \sin(\phi_1) \\ \tilde{M}_1 \sin(\phi_1) & \tilde{M}_1 \cos(\phi_1) \end{bmatrix} \\ \begin{bmatrix} \tilde{M}_2 \cos(\phi_2) & -\tilde{M}_2 \sin(\phi_2) \\ \tilde{M}_2 \sin(\phi_2) & \tilde{M}_2 \cos(\phi_2) \end{bmatrix} \end{bmatrix}, \qquad \tilde{Q}_{sr_1} = \begin{bmatrix} \begin{bmatrix} \tilde{M}_1 p_1 \sin(\phi_1) & \tilde{M}_1 p_1 \cos(\phi_1) \\ -\tilde{M}_1 p_1 \cos(\phi_1) & \tilde{M}_1 p_1 \sin(\phi_1) \end{bmatrix} \\ \begin{bmatrix} \tilde{M}_2 p_2 \sin(\phi_2) & \tilde{M}_2 p_2 \cos(\phi_2) \\ -\tilde{M}_2 p_2 \cos(\phi_2) & \tilde{M}_2 p_2 \sin(\phi_2) \end{bmatrix} \end{bmatrix}$$

Therefore the new model reduction method reduces the order of the system in such a way that the reduced order model has the same structure as a machine with a rotor comprising of one loop per nest.

3.5 Simulation comparison of different BDFM model reduction techniques

In order to evaluate the new 'nested loop' rotor BDFM model reduction technique, different BDFM configurations were tested. Typical results will be presented, for a range of reduction techniques:

1. The new reduction method, as described in section 3.4.2.

2. 'Biggest loop' method: Model reduction by assuming that the rotor comprises of only the outer loop of each 'nest'. This technique can be easily applied by simply truncating parts of the BDFM system matrices corresponding to the unwanted states.

3. 'Sum loops' method: This is essentially the method proposed in [64, 63, 11, 12]. The model can be reduced by summing the inductance, resistance, etc components for each set of loops into a single lumped parameter set.

4. LPV balanced truncation method: the method described in section 3.4.1, due to [118, 119]. The reduction method is applied only to the rotor, as previously described. Once the balancing transformation has been found, the rotor system can be transformed, and then the component system matrices truncated along with the state. The overall reduced system is given by $G = \left[\begin{array}{cc|c} A_s & A_{sr}\tilde{C}_r & B_s \\ \tilde{B}_r A_{rs} & \tilde{A}_r & \tilde{B}_r B_r \\ \hline I & 0 & 0 \end{array}\right]$.

5. Full dq system: This is the full, untruncated system, as derived in section 3.3.

Figure 3.5 shows the upper bound on the induced 2-norm gain of the error between the full and reduced system in each case. Two lines are plotted for each case, the straight line is for arbitrary speed trajectories within the prescribed range, and is calculated using Theorem 3.4. The non-straight lines are for constant speed, and are calculated from the supremum of the maximum singular value of the frequency response for each speed. Clearly the new method provides significantly better performance (lower error) than the other methods. Note that the summing method and 'biggest loop' method performance are not that different, therefore suggesting that summing contributions is scarcely a better approximation than assuming a simpler rotor structure. The relatively poor performance of the LPV balanced truncation is probably due, partly to the non-convexity of the problem, and hence the solution is only locally optimal, but more significantly, because of the requirement to apply the

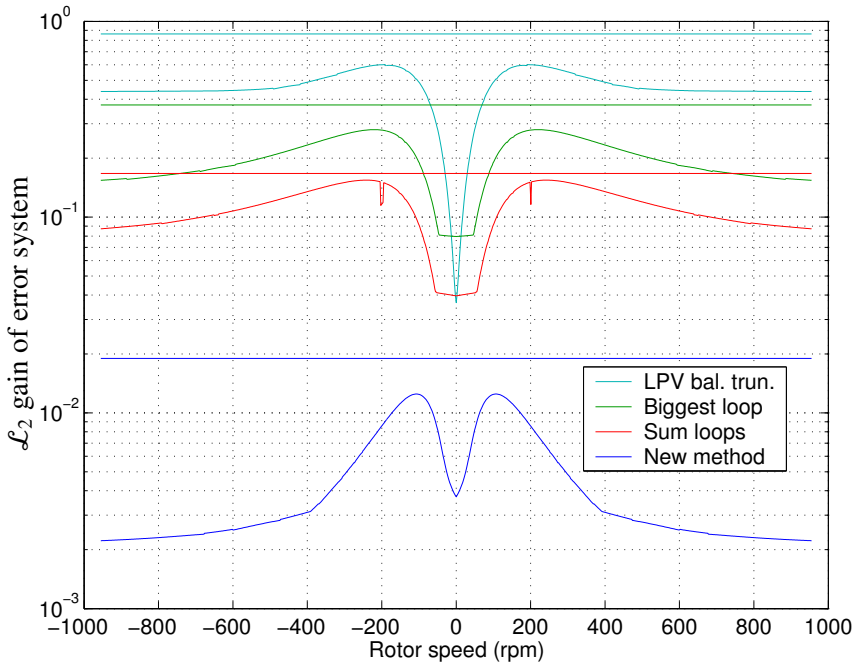

Figure 3.5: Maximum induced 2-norm gain of the error between the full and reduced d-q-0 transformed BDFM 'nested-loop' rotor design models. Straight lines are upper bounds for arbitrary speed variations computed using Theorem 3.4. Curved lines are upper bounds for fixed speeds, calculated from the supremum of the maximum singular value of the frequency response for each speed, the glitches in the red line are due to numerical problems. The upper bound on the induced 2-norm of the full system was 0.7382. The full-order system has 17-states (15 electrical states - of which 5 correspond to zero sequence states, and 2 mechanical states), and the reduced order systems are 8 states (6 electrical and 2 mechanical).

technique only to the rotor states. If this limitation could be removed then the technique would be superior. By way of comparison, the LPV balancing procedure was applied to the entire system, and the results are similar or better than the new reduction method. Notwithstanding these comments, all the methods achieved some amount of effective model reduction. The upper bound on the induced 2-norm of full system was 0.7382, thus if the reduced systems all have similar 2-norm values then the worst case error is 1.4764 (twice 0.7382, from the triangle inequality), so even the LPV balanced truncation method achieved some level of error reduction.

Figures 3.6, 3.7, 3.8, 3.9 and 3.10 show current and rotor shaft speed transients for the BDFM with a 'nested-loop' rotor operating in synchronous mode. The machine was simulated with zero initial current, but with the shaft speed set to synchronous speed (700rpm in this case), the figures show the speed and current transient as the machine attains equilibrium. As expected, the error between the reduced order and full systems is least in the case of the new reduction method. The sum loops method actually appears to be slightly worse than the biggest loop method in the current plot, but

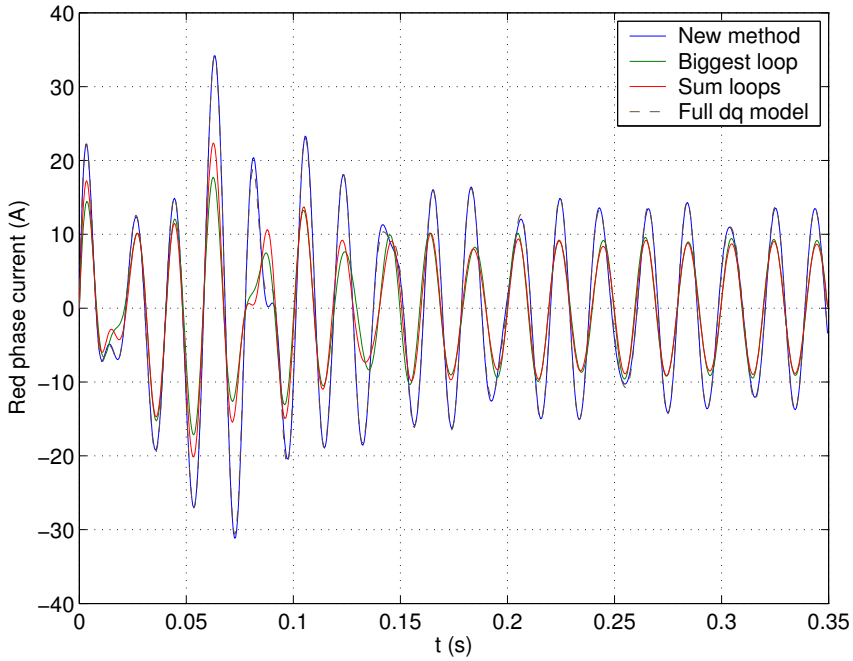

Figure 3.6: Stator 1 phase current transient at startup for a BDFM with a 'nested loop' design rotor in synchronous mode, for different BDFM model reduction methods. Full-order d-q-0 model: 17 states, reduced order models: 8 states

slightly better in the speed plot. The LPV balanced truncation method yielded very poor results in these transient tests, and so has been omitted. Again, these plots serve to illustrate the effectiveness of the new model reduction method. It is significant in figures 3.7, 3.8 and 3.9 , that the new model reduction method achieves good estimation of the rotor bar currents, in contrast to the other method considered. Previously the only available BDFM model which could estimate the rotor currents with some degree of accuracy was the full order d-q model [53].

It is worth adding some confidence to the claim made at the start of the chapter, regarding the additional assumptions made in the d-q-0 transformed BDFM model. It was claimed that the inductive coupling between stator and rotor can be adequately approximated by the first non-zero spatial harmonic of the Fourier series representation of the mutual inductance matrix. The d-q-0 and original coupled circuit model of chapter 2 differ only in this respect.

Figures 3.11 and 3.5 show currents and shaft speed transients at startup for the full order d-q-0 transformed model, and the original coupled-circuit model. The coupled circuit model for this BDFM is 26 states, of which 24 are electrical, and 2 mechanical. The full d-q-0 transformed model has 17 states, 15 electrical and 2 mechanical, however 5 of the electrical states correspond to zero-sequence states, and as the supply in this case was balanced 3-phase, then the zero sequence states will remain at zero.

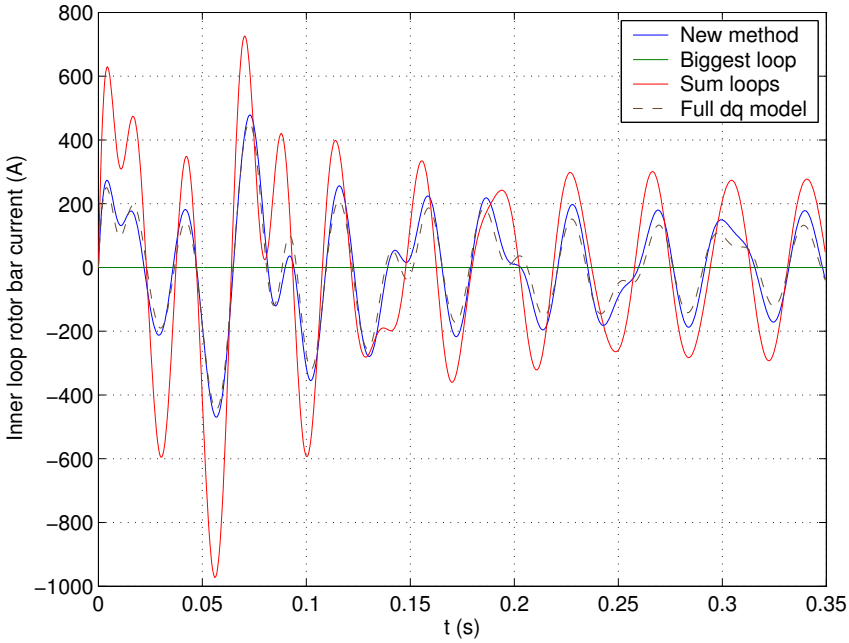

Figure 3.7: Inner loop rotor bar current transient at startup for a BDFM with a 'nested loop' design rotor in synchronous mode, for different BDFM model reduction methods. Full-order d-q-0 model: 17 states, reduced order models: 8 states

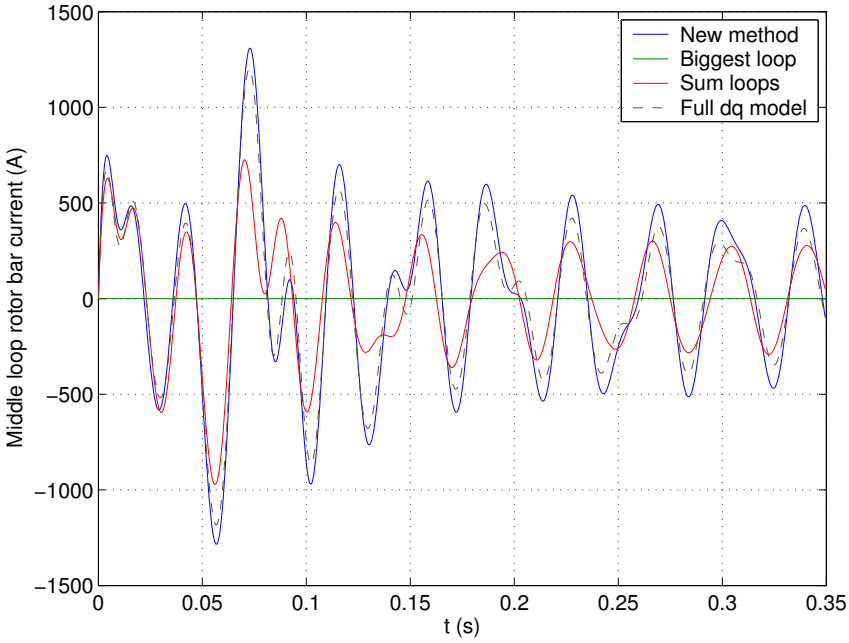

Figure 3.8: Middle loop rotor bar current transient at startup for a BDFM with a 'nested loop' design rotor in synchronous mode, for different BDFM model reduction methods. Full-order d-q-0 model: 17 states, reduced order models: 8 states

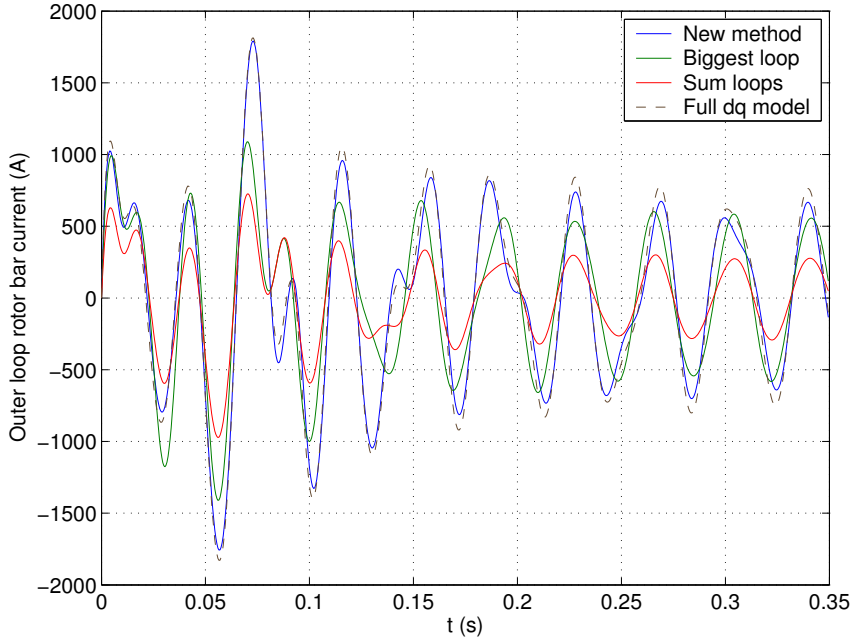

Figure 3.9: Outer loop rotor bar current transient at startup for a BDFM with a 'nested loop' design rotor in synchronous mode, for different BDFM model reduction methods. Full-order d-q-0 model: 17 states, reduced order models: 8 states

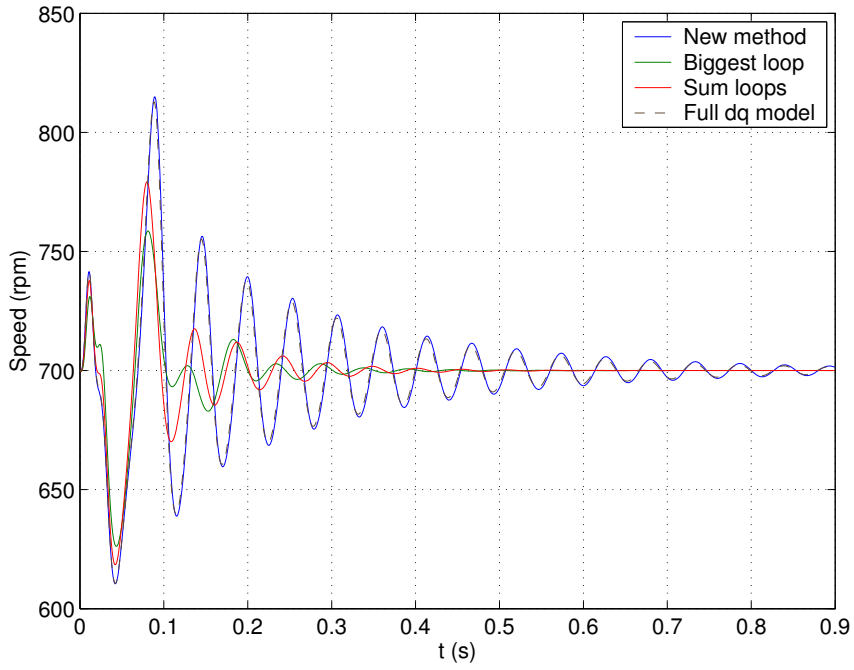

Figure 3.10: Rotor shaft speed transient at startup for a BDFM with a 'nested loop' design rotor in synchronous mode, for different BDFM model reduction methods. Full-order d-q-0 model: 17 states, reduced order models: 8 states. The initial current was zero, the initial shaft speed was the synchronous speed, 700rpm.

The agreement between the two models for the conditions tested is very good, thus giving confidence to the assumption made to derive the d-q-0 model. These results are typical of many operating points, and BDFM models tried.

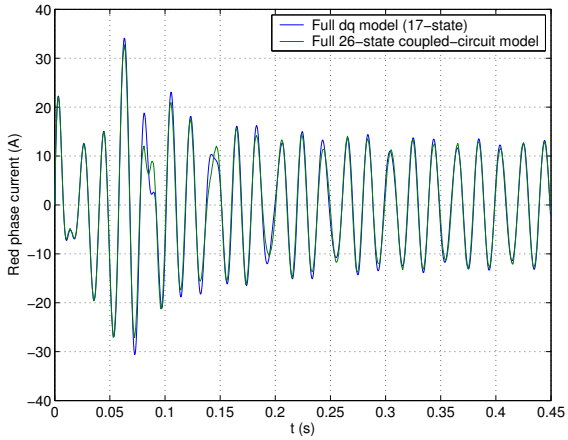

(a) Stator 1 phase current

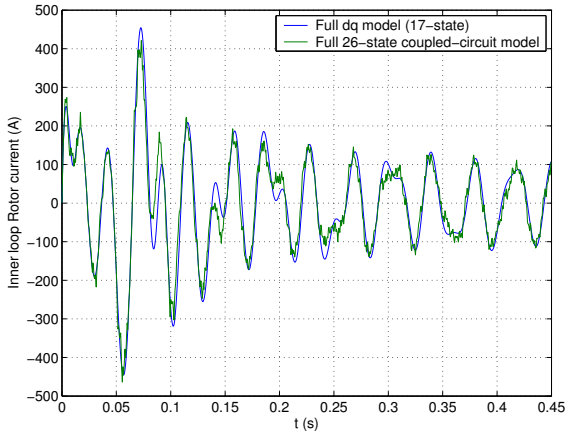

(b) Rotor inner loop bar current

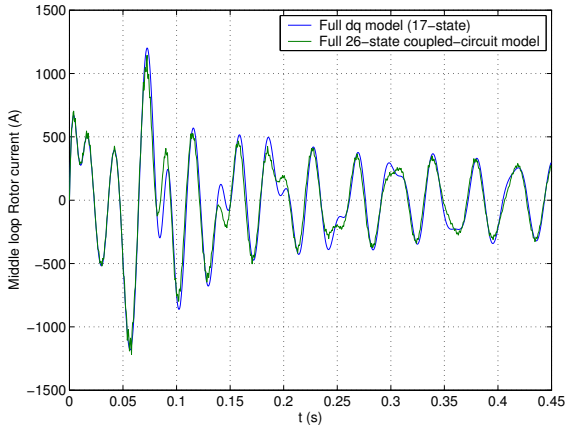

(c) Rotor middle loop bar current

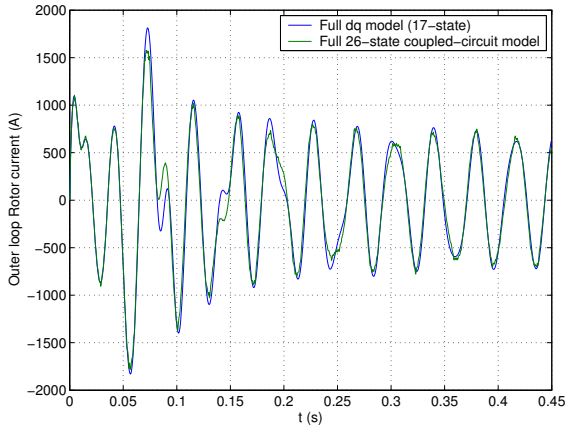

(d) Rotor outer loop bar current

Figure 3.11: Current transients at startup for a BDFM with a 'nested-loop' design rotor in synchronous mode for the original coupled-circuit BDFM model of chapter 2 and the full order d-q-0 transformed BDFM model of this chapter. Full-order d-q-0 model: 17 states (15 electrical, 2 mechanical), coupled-circuit model: 26 states (24 electrical, 2 mechanical)

3.6 Conclusion

In this chapter we present a rigorous derivation of the d-q transformed model for a wide class of BDFMs, including, but not limited to, the nested-loop rotor of Broadway and Burbridge [17]. The model was derived directly from the coupled circuit model presented in chapter 2. The derivation is

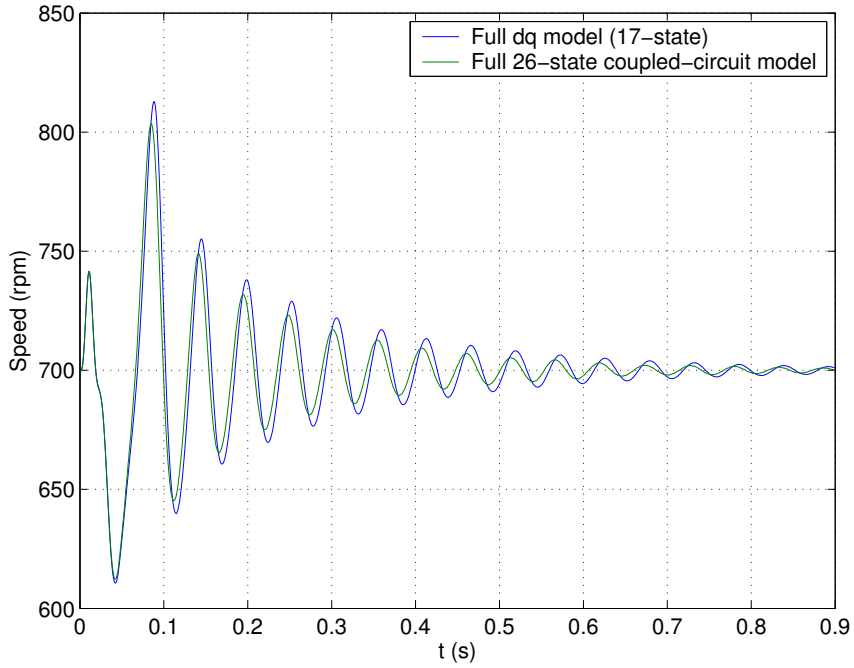

Figure 3.12: Rotor shaft speed transient at startup for a BDFM with a 'nested-loop' design rotor in synchronous mode for the original coupled-circuit BDFM model of chapter 2 and the full order d-q-0 transformed BDFM model of this chapter. Full-order d-q-0 model: 17 states (15 electrical, 2 mechanical), coupled-circuit model: 26 states (24 electrical, 2 mechanical). The initial current was zero, the initial shaft speed was the synchronous speed, 700rpm.

consistent with that presented in [12], although the method is more general.

Furthermore we show that the states removed from the d-q transformed model are unobservable and uncontrollable, but stable. In addition it was proved that all BDFMs in the analysed class are quadratically stable for all shaft speed trajectories.

It has also been shown that the d-q transformation proposed in Boger et. al. [11] is a simplification, and can lead to significant errors, both in dynamic and steady-state performance.

We have derived a new method of reducing the order of the derived d-q model for 'nested-loop' rotor design BDFMs. The new method yields a model of the same order model as that found in [11], but with greatly improved accuracy, in both transient performance and worst case $\mathcal{L}_2$ gain.

Chapter 4

Equivalent Circuit Model and its Implication for BDFM Performance

4.1 Introduction

In chapter 3 the coupled circuit model derived for the BDFM was transformed into d-q axes. In this chapter we show how the d-q transformed model may be further transformed into complex symmetrical components. We then show how, in the steady state, this form of the BDFM model may be written succinctly as an equivalent circuit where the meaning of the parameters has a clear physical interpretation. The performance of the BDFM is then investigated using the equivalent circuit, and some measures of 'goodness' of the BDFM are proposed, in terms of calculable machine parameters. While the development of the equivalent circuit in this dissertation is achieved by way of transformations applied to the d-q model, the author has also shown that it is possible to derive the equivalent circuit by considering the BDFM as two interconnected induction machines [86].

Li et al. used the d-q model for the 6/2 machine of [64], to derive an equivalent circuit representation, which was then used to investigate power flows within the machine [60]. A similar approach was adopted by Gorti et al. [41]. Other references propose equivalent circuits without derivation, [65, 59]. Yet in the literature the equivalent circuits presented are either for an idealised machine, or for a specific machine configuration. There is, therefore, a need for a generalised derivation of the equivalent circuit for a wide class of BDFM machines.

Williamson et. al. analysed the synchronous mode of operation of all nested-loop rotor BDFMs [115] via harmonic analysis. However, the model is not developed into an equivalent circuit form, nor is it used to identify design parameters. Broadway and Burbridge [17], Hunt [48, 49], and Creedy [27] make qualitative comments regarding rotor design, however, nowhere in the current literature has any method been proposed to quantitatively evaluate the performance of BDFM machines with different rotor designs. In this chapter we consider quantitative methods of BDFM evaluation.

Furthermore we briefly consider the issue of magnetic loading for the BDFM, which is not

straightforward because there are two different pole number fields in the air gap during normal operation.

During this chapter the modelling assumptions are exactly the same as for the d-q model, as described in chapter 3.

4.2 Conversion to Symmetrical Components

From [51, sect. 3.7], d-q-0 components may be transformed into positive, negative and zero sequence components using the following unitary (invertible) transformation matrix:

$$\begin{bmatrix} i^+ \\ i^- \\ i_0 \end{bmatrix} = \begin{bmatrix} C & 0 \\ 0 & 1 \end{bmatrix} \begin{bmatrix} i_d \\ i_q \\ i_0 \end{bmatrix} \tag{4.1}$$

where:

$$C = \frac{1}{\sqrt{2}} \begin{bmatrix} 1 & j \\ 1 & -j \end{bmatrix} \tag{4.2}$$

the voltage sequence components are similarly defined.

For brevity the zero sequence components will not be included, however they can be deduced from the d-q model, as the zero sequence are unaffected by the transformation (as the '0' of the d-q-0 components *is* the zero-sequence).

The full transformation matrix will consist of $N+2$ copies of C along the diagonal for a full-order model, or 3 copies of C along the diagonal for a reduced order model. N is the number of sets of $S = p_1 + p_2$ circuits present on the rotor. For the full-order model the whole transformation matrix is:

$$C_{\text{full}} = \begin{bmatrix} C_1 & 0 & \cdots & 0 \\ 0 & C_2 & \ddots & \vdots \\ \vdots & \ddots & \ddots & 0 \\ 0 & \cdots & 0 & C_{N+2} \end{bmatrix} \tag{4.3}$$

where all C_i are equal, the subscripts are simply for book-keeping purposes.

This transformation shall now be applied to the full-order BDFM d-q model of equation (3.35), with the zero-sequence states removed. Equation (3.35) is multiplied by (4.3) from the left and from

the right by the complex conjugate transpose of (4.3) which gives:

$$\begin{bmatrix} v_{c_{s1}} \\ v_{c_{s2}} \\ 0 \end{bmatrix} = (R_c + \omega_r Q_c) \begin{bmatrix} i_{c_{s1}} \\ i_{c_{s2}} \\ i_{c_r} \end{bmatrix} + M_c \frac{d}{dt} \begin{bmatrix} i_{c_{s1}} \\ i_{c_{s2}} \\ i_{c_r} \end{bmatrix} \tag{4.4}$$

$$Q_c = C Q_{dq} C^* = \begin{bmatrix} Q_{c_{s1}} & 0 & Q_{c_{sr1}} \\ 0 & Q_{c_{s1}} & Q_{c_{sr2}} \\ 0 & 0 & 0 \end{bmatrix}, \; M_c = C M_{dq} C^* = \begin{bmatrix} M_{c_{s1}} & 0 & M_{c_{sr1}} \\ 0 & M_{c_{s2}} & M_{c_{sr2}} \\ {M_{c_{sr1}}}^{\mathrm{T}} & {M_{c_{sr2}}}^{\mathrm{T}} & M_{c_r} \end{bmatrix}$$

$$R_c = C R_{dq} C^* = \begin{bmatrix} R_{c_{s1}} & 0 & 0 \\ 0 & R_{c_{s2}} & 0 \\ 0 & 0 & R_{c_r} \end{bmatrix}$$

where Q_c, M_c, $R_c \in \mathbb{C}^{2(N+2)\times 2(N+2)}$, and the elements of which can easily be shown to be:

$$R_c = \left[\begin{array}{cccc|ccccc} R_{dq_1} & 0 & 0 & 0 & 0 & 0 & 0 & \cdots & 0 \\ 0 & R_{dq_1} & 0 & 0 & 0 & 0 & 0 & \cdots & 0 \\ 0 & 0 & R_{dq_2} & 0 & 0 & 0 & 0 & \cdots & 0 \\ 0 & 0 & 0 & R_{dq_2} & 0 & 0 & 0 & \cdots & 0 \\ \hline 0 & 0 & 0 & 0 & R_{dq_{r1}} & 0 & 0 & \cdots & 0 \\ 0 & 0 & 0 & 0 & 0 & R_{dq_{r1}} & 0 & \cdots & 0 \\ \vdots & \vdots & \vdots & \vdots & \vdots & \ddots & \ddots & \ddots & \vdots \\ 0 & 0 & 0 & 0 & 0 & \cdots & 0 & R_{dq_{rN}} & 0 \\ 0 & 0 & 0 & 0 & 0 & \cdots & 0 & 0 & R_{dq_{rN}} \end{array}\right] \tag{4.5}$$

The vertical and horizontal lines demark rotor and stator portions of the matrix. Q_c and M_c are given by:

$$
M_c = \left[\begin{array}{cccc|cccccc}
(L_1 - M_1) & 0 & 0 & 0 & M_{1_1}\exp(j\phi_{1_1}) & 0 & \cdots & \cdots & \cdots & M_{1_N}\exp(j\phi_{1_N}) & 0 \\
0 & (L_1 - M_1) & 0 & 0 & 0 & M_{1_1}\exp(-j\phi_{1_1}) & \cdots & \cdots & \cdots & 0 & M_{1_N}\exp(-j\phi_{1_N}) \\
0 & 0 & (L_2 - M_2) & 0 & 0 & M_{2_1}\exp(j\phi_{2_1}) & \cdots & \cdots & \cdots & 0 & M_{2_N}\exp(j\phi_{2_N}) \\
0 & 0 & 0 & (L_2 - M_2) & M_{2_1}\exp(-j\phi_{2_1}) & 0 & \cdots & \cdots & \cdots & M_{2_N}\exp(-j\phi_{2_N}) & 0 \\
\hline
M_{1_1}\exp(-j\phi_{1_1}) & 0 & 0 & M_{2_1}\exp(j\phi_{2_1}) & L_{dq_{r1}} & 0 & M_{12_r}\exp(-j\phi_{12_r}) & 0 & \cdots & M_{1N_r}\exp(-j\phi_{1N_r}) & 0 \\
0 & M_{1_1}\exp(j\phi_{1_1}) & M_{2_1}\exp(-j\phi_{2_1}) & 0 & 0 & L_{dq_{r1}} & 0 & M_{12_r}\exp(j\phi_{12_r}) & \cdots & 0 & M_{1N_r}\exp(j\phi_{1N_r}) \\
\vdots & \vdots & \vdots & \vdots & M_{12_r}\exp(j\phi_{12_r}) & 0 & L_{dq_{r2}} & 0 & \cdots & M_{2N_r}\exp(-j\phi_{2N_r}) & 0 \\
\vdots & \vdots & \vdots & \vdots & 0 & M_{12_r}\exp(-j\phi_{12_r}) & 0 & L_{dq_{r2}} & \cdots & 0 & M_{2N_r}\exp(j\phi_{2N_r}) \\
\vdots & \vdots & \vdots & \vdots & \vdots & \vdots & \vdots & \vdots & \ddots & \vdots & \vdots \\
M_{1_N}\exp(-j\phi_{1_N}) & 0 & 0 & M_{2_N}\exp(j\phi_{2_N}) & M_{1N_r}\exp(j\phi_{1N_r}) & 0 & M_{2N_r}\exp(j\phi_{2N_r}) & 0 & \cdots & L_{dq_{rN}} & 0 \\
0 & M_{1_N}\exp(j\phi_{1_N}) & M_{2_N}\exp(-j\phi_{2_N}) & 0 & 0 & M_{1N_r}\exp(-j\phi_{1N_r}) & 0 & M_{2N_r}\exp(-j\phi_{2N_r}) & \cdots & 0 & L_{dq_{rN}}
\end{array}\right]
$$

$$
Q_c = \left[\begin{array}{cccc|cccccc}
-jp_1(L_1 - M_1) & 0 & 0 & 0 & -jp_1M_{1_1}\exp(j\phi_{1_1}) & 0 & \cdots & \cdots & -jp_1M_{1_N}\exp(j\phi_{1_N}) & 0 \\
0 & jp_1(L_1 - M_1) & 0 & 0 & 0 & jp_1M_{1_1}\exp(-j\phi_{1_1}) & \cdots & \cdots & 0 & jp_1M_{1_N}\exp(-j\phi_{1_N}) \\
0 & 0 & -jp_2(L_2 - M_2) & 0 & 0 & -jp_2M_{2_1}\exp(j\phi_{2_1}) & \cdots & \cdots & 0 & -jp_2M_{2_N}\exp(j\phi_{2_N}) \\
0 & 0 & 0 & jp_2(L_2 - M_2) & jp_2M_{2_1}\exp(-j\phi_{2_1}) & 0 & \cdots & \cdots & jp_2M_{2_N}\exp(-j\phi_{2_N}) & 0 \\
\hline
0 & 0 & 0 & 0 & 0 & 0 & \cdots & \cdots & 0 & 0 \\
0 & 0 & 0 & 0 & 0 & 0 & \cdots & \cdots & 0 & 0 \\
\vdots & \vdots & \vdots & \vdots & \vdots & \vdots & \cdots & \cdots & \vdots & \vdots \\
\vdots & \vdots & \vdots & \vdots & \vdots & \vdots & \cdots & \cdots & \vdots & \vdots \\
\vdots & \vdots & \vdots & \vdots & \vdots & \vdots & \cdots & \cdots & \vdots & \vdots \\
0 & 0 & 0 & 0 & 0 & 0 & \cdots & \cdots & 0 & 0 \\
0 & 0 & 0 & 0 & 0 & 0 & \cdots & \cdots & 0 & 0
\end{array}\right]
$$

(4.6)

where the symbols used in M_c and Q_c are the same as those used in (3.17-3.20), (3.24) and (3.26-3.29), and $M_{1i_r} = \sqrt{M_{1i_a}^2 + M_{1i_b}^2}$, $\phi_{1i_r} = \arctan\left(M_{1i_b}/M_{1i_a}\right)$.

The torque equation was given by (3.38) for the d-q model. Repartitioning the currents into stator and rotor quantities, and noting that as all components in (3.38) are real, the transpose may be replaced by complex conjugate transpose. (3.38) may therefore be written as:

$$T_e = \frac{1}{2}\begin{bmatrix} i_{dq_s} \\ i_{dq_r} \end{bmatrix}^* \begin{bmatrix} 0 & Q_{dq_{sr}} \\ Q^*_{dq_{sr}} & 0 \end{bmatrix} \begin{bmatrix} i_{dq_s} \\ i_{dq_r} \end{bmatrix} \tag{4.7}$$

Applying the complex transformation to the currents in this equation gives:

$$T_e = \frac{1}{2}\begin{bmatrix} i_{c_s} \\ i_{c_r} \end{bmatrix}^* \begin{bmatrix} 0 & Q_{c_{sr}} \\ Q^*_{c_{sr}} & 0 \end{bmatrix} \begin{bmatrix} i_{c_s} \\ i_{c_r} \end{bmatrix} \tag{4.8}$$

where $i_{c_{s1}}, i_{c_{s2}}, i_{c_r}$ are the symmetrical components of the stator 1, stator 2 and rotor currents. $Q_{c_{sr}}$ denotes the stator-rotor portion of Q_c as defined in (4.6). $Q_{c_{sr}}$ is therefore given by:

$$Q_{c_{sr}} = \begin{bmatrix} -jp_1M_{1_1}\exp(j\phi_{1_1}) & 0 & \cdots & -jp_1M_{1_N}\exp(j\phi_{1_N}) & 0 \\ 0 & jp_1M_{1_1}\exp(-j\phi_{1_1}) & \cdots & 0 & jp_1M_{1_N}\exp(-j\phi_{1_N}) \\ 0 & -jp_2M_{2_1}\exp(j\phi_{2_1}) & \cdots & 0 & -jp_2M_{2_N}\exp(j\phi_{2_N}) \\ jp_2M_{2_1}\exp(-j\phi_{2_1}) & 0 & \cdots & jp_2M_{2_N}\exp(-j\phi_{2_N}) & 0 \end{bmatrix} \tag{4.9}$$

If we now consider a re-ordering of the states of (4.4) using a permutation matrix (hence orthogonal). Particularly we re-order the states so that the new order becomes: $i^+_{s1}, i^-_{s2}, i^+_{r1}, \cdots, i^+_{rN}, i^-_{s1}, i^+_{s2}, i^-_{r1}, \cdots, i^-_{rN}$. This can be achieved with the permutation matrix, P:

$$P = \begin{bmatrix} 1 & \cdot & \cdot & \cdot & \cdot & \cdot & \cdot & \cdot & \cdots & \cdot & \cdot \\ \cdot & \cdot & \cdot & 1 & \cdot & \cdot & \cdot & \cdot & \cdots & \cdot & \cdot \\ \cdot & \cdot & \cdot & \cdot & 1 & \cdot & \cdot & \cdot & \cdots & \cdot & \cdot \\ \cdot & \cdot & \cdot & \cdot & \cdot & \cdot & 1 & \cdot & \cdots & \cdot & \cdot \\ \vdots & \vdots & \vdots & \vdots & \vdots & \vdots & \vdots & \vdots & \cdots & \vdots & \vdots \\ \cdot & \cdot & \cdot & \cdot & \cdot & \cdot & \cdot & \cdot & \cdots & 1 & \cdot \\ \cdot & 1 & \cdot & \cdot & \cdot & \cdot & \cdot & \cdot & \cdots & \cdot & \cdot \\ \cdot & \cdot & 1 & \cdot & \cdot & \cdot & \cdot & \cdot & \cdots & \cdot & \cdot \\ \cdot & \cdot & \cdot & \cdot & \cdot & 1 & \cdot & \cdot & \cdots & \cdot & \cdot \\ \vdots & \vdots & \vdots & \vdots & \vdots & \vdots & \vdots & \vdots & \cdots & \vdots & \vdots \\ \cdot & \cdot & \cdot & \cdot & \cdot & \cdot & \cdot & \cdot & \cdots & \cdot & 1 \end{bmatrix} \tag{4.10}$$

where a single $\cdot$ denotes a zero.

If (4.4) is multiplied from the left by P and the substitution $i_c = P^{\mathrm{T}} i_{c_p}$ made, then it is easy to see that the transformed matrices, PM_cP^{T}, PR_cP^{T}, PQ_cP^{T} are block diagonal. Therefore it is immediate that, as expected [81], the different sequence components are orthogonal, that is a positive sequence does not affect negative sequence components and vice-versa:

$$\begin{bmatrix} v_{c_{p1}} \\ v_{c_{p2}} \end{bmatrix} = \left(PR_cP^{\mathrm{T}} + \omega_r PQ_cP^{\mathrm{T}}\right) \begin{bmatrix} i_{c_{p1}} \\ i_{c_{p2}} \end{bmatrix} + PM_cP^{\mathrm{T}} \frac{d}{dt} \begin{bmatrix} i_{c_{p1}} \\ i_{c_{p2}} \end{bmatrix} \tag{4.11}$$

$$PM_cP^{\mathrm{T}} = \begin{bmatrix} M_c^+ & 0 \\ 0 & \bar{M}_c^+ \end{bmatrix} \tag{4.12}$$

$$PQ_cP^{\mathrm{T}} = \begin{bmatrix} Q_c^+ & 0 \\ 0 & \bar{Q}_c^+ \end{bmatrix} \tag{4.13}$$

$$PR_cP^{\mathrm{T}} = \begin{bmatrix} R_c^+ & 0 \\ 0 & \bar{R}_c^+ \end{bmatrix} \tag{4.14}$$

where $i_{c_{p1}}, i_{c_{p2}}$ are upper and lower partitions of i_c, and similarly for $v_{c_{p1}}, v_{c_{p2}}$. Also:

$$M_c^+ = \left[\begin{array}{cc|ccccc} (L_1 - M_1) & 0 & M_{1_1}\exp(j\phi_{1_1}) & \cdots & \cdots & M_{1_N}\exp(j\phi_{1_N}) \\ 0 & (L_2 - M_2) & M_{2_1}\exp(-j\phi_{2_1}) & \cdots & \cdots & M_{2_N}\exp(-j\phi_{2_N}) \\ \hline M_{1_1}\exp(-j\phi_{1_1}) & M_{2_1}\exp(j\phi_{2_1}) & L_{dq_{r1}} & M_{12_r}\exp(-j\phi_{12_r}) & \cdots & M_{1N_r}\exp(-j\phi_{1N_r}) \\ \vdots & \vdots & M_{12_r}\exp(j\phi_{12_r}) & L_{dq_{r2}} & \cdots & M_{2N_r}\exp(-j\phi_{2N_r}) \\ \vdots & \vdots & \vdots & \vdots & \ddots & \vdots \\ M_{1_N}\exp(-j\phi_{1_N}) & M_{2_N}\exp(j\phi_{2_N}) & M_{1N_r}\exp(j\phi_{1N_r}) & M_{2N_r}\exp(j\phi_{2N_r}) & \cdots & L_{dq_{rN}} \end{array}\right] \tag{4.15}$$

$$Q_c^+ = \left[\begin{array}{cc|ccccc} -jp_1(L_1 - M_1) & 0 & -jp_1M_{1_1}\exp(j\phi_{1_1}) & \cdots & \cdots & -jp_1M_{1_N}\exp(j\phi_{1_N}) \\ 0 & jp_2(L_2 - M_2) & jp_2M_{2_1}\exp(-j\phi_{2_1}) & \cdots & \cdots & jp_2M_{2_N}\exp(-j\phi_{2_N}) \\ \hline 0 & 0 & 0 & \cdots & \cdots & 0 \\ \vdots & \vdots & \vdots & \cdots & \cdots & \vdots \\ \vdots & \vdots & \vdots & \cdots & \cdots & \vdots \\ 0 & 0 & 0 & \cdots & \cdots & 0 \end{array}\right] \tag{4.16}$$

$$R_c^+ = \left[\begin{array}{cc|ccccc} R_{dq_1} & 0 & 0 & 0 & \cdots & 0 \\ 0 & R_{dq_2} & 0 & 0 & \cdots & 0 \\ \hline 0 & 0 & R_{dq_{r1}} & 0 & \cdots & 0 \\ \vdots & \vdots & 0 & \ddots & \ddots & \vdots \\ \vdots & \vdots & \vdots & \ddots & \ddots & 0 \\ 0 & 0 & 0 & \cdots & 0 & R_{dq_{rN}} \end{array}\right] = \left[\begin{array}{cc|c} R_{dq_1} & 0 & 0 \\ 0 & R_{dq_2} & 0 \\ \hline 0 & 0 & R_{dq_r} \end{array}\right] \tag{4.17}$$

$$\text{where:} \qquad R_{dq_r} = \begin{bmatrix} R_{dq_{r1}} & 0 & \cdots & 0 \\ 0 & \ddots & \ddots & \vdots \\ \vdots & \ddots & \ddots & 0 \\ 0 & \cdots & 0 & R_{dq_{rN}} \end{bmatrix}$$

In the BDFM, however, the special rotor design cross-couples positive and negative sequence components from the different stator fields. Recall that in chapter 3 it was argued that rotor states could be transformed into d-q axes using the stator 1 pole number transformation matrix, rather then using two transformation matrices and then recombining. The effect of doing this is to, in effect, reverse the phase sequence of stator 2. If we had used the stator 2 pole number transformation matrix then the stator 1 phase sequence would have been reversed. This is not solely a mathematical phenomenon, it corresponds to the physical reality that if the phase sequences of the stator supplies are the same, then the frequencies of the stator fields viewed in the rotor reference frame are in opposite directions, as shown in section 1.2.

Considering now, the torque equation. After transformation by P, the torque equation becomes:

$$T_e = \frac{1}{2}\begin{bmatrix} i_{c_{p1}} \\ i_{c_{p2}} \end{bmatrix}^* \begin{bmatrix} \begin{bmatrix} 0 & Q^+_{c_{sr}} \\ Q^{+\,*}_{c_{sr}} & 0 \end{bmatrix} & 0 \\ 0 & \begin{bmatrix} 0 & \bar{Q}^+_{c_{sr}} \\ \bar{Q}^{+\,*}_{c_{sr}} & 0 \end{bmatrix} \end{bmatrix} \begin{bmatrix} i_{c_{p1}} \\ i_{c_{p2}} \end{bmatrix} \tag{4.18}$$

where:

$$Q^+_{c_{sr}} = \begin{bmatrix} -jp_1 M_{1_1} \exp(j\phi_{1_1}) & \cdots & \cdots & \cdots & -jp_1 M_{1_N} \exp(j\phi_{1_N}) \\ jp_2 M_{2_1} \exp(-j\phi_{2_1}) & \cdots & \cdots & \cdots & jp_2 M_{2_N} \exp(-j\phi_{2_N}) \end{bmatrix} \tag{4.19}$$

and $i_{c_{p1}}$ and $i_{c_{p2}}$ are the top and bottom partition of the symmetrical component current vector, i_c under the transformation P.

We now consider the supply voltage in the transformed state. Recall that the voltage must be first transformed into d-q-0 axes, then into symmetrical components, removing the zero sequence state, and finally re-ordered by P. The supply voltage is assumed to be a balanced three phase set, which

can be represented by:

$$v_s = \begin{bmatrix} V\cos\left(\phi(t)\right) \\ V\cos\left(\phi(t) - \frac{2\pi}{3}\right) \\ V\cos\left(\phi(t) - \frac{4\pi}{3}\right) \end{bmatrix} \tag{4.20}$$

where $\phi(t)$ is some arbitrary function of time, in steady state it will generally be ωt, and note that V may also be a function of time. This may be transformed to d-q-0 axes using (3.1) or (3.2) if this is the stator 2 supply. For this example we use (3.1):

$$v_{dq_s} = \sqrt{\frac{3}{2}} \begin{bmatrix} V\cos\left(p_1\theta_r - \phi(t)\right) \\ V\sin\left(p_1\theta_r - \phi(t)\right) \\ 0 \end{bmatrix} \tag{4.21}$$

now remove the zero sequence voltage, and converting to sequence components using (4.2) gives:

$$v_{c_s} = \begin{bmatrix} v_s^+ \\ v_s^- \end{bmatrix} = \frac{\sqrt{3}}{2} \begin{bmatrix} V\exp\left(j\left(p_1\theta_r - \phi(t)\right)\right) \\ V\exp\left(-j\left(p_1\theta_r - \phi(t)\right)\right) \end{bmatrix} \tag{4.22}$$

Therefore it is clear that $v_s^+ = \bar{v}_s^-$. It is significant that the equation (4.12), shows that the BDFM is composed of two separate, yet similar, equations, one supplied with $v_{c_{p1}}$ the other supplied by $v_{c_{p2}} = \bar{v}_{c_{p1}}$. Therefore from (4.12) it is clear that $i_{c_{p2}} = \bar{i}_{c_{p1}}$. Hence the torque can be written as:

$$\begin{aligned} T_e &= \frac{1}{2}\begin{bmatrix} i_{c_{p1}} \\ i_{c_{p2}} \end{bmatrix}^* \begin{bmatrix} \begin{bmatrix} 0 & Q_{c_{sr}}^+ \\ Q_{c_{sr}}^{+\,*} & 0 \end{bmatrix} i_{c_{p1}} \\ \begin{bmatrix} 0 & \bar{Q}_{c_{sr}}^+ \\ \bar{Q}_{c_{sr}}^{+\,*} & 0 \end{bmatrix} i_{c_{p2}} \end{bmatrix} = \frac{1}{2} i_{c_{p1}}^* \begin{bmatrix} 0 & Q_{c_{sr}}^+ \\ Q_{c_{sr}}^{+\,*} & 0 \end{bmatrix} i_{c_{p1}} + \frac{1}{2} i_{c_{p2}}^* \begin{bmatrix} 0 & \bar{Q}_{c_{sr}}^+ \\ \bar{Q}_{c_{sr}}^{+\,*} & 0 \end{bmatrix} i_{c_{p2}} \\ &= \frac{1}{2} i_{c_{p1}}^* \begin{bmatrix} 0 & Q_{c_{sr}}^+ \\ Q_{c_{sr}}^{+\,*} & 0 \end{bmatrix} i_{c_{p1}} + \frac{1}{2} \bar{i}_{c_{p1}}^* \begin{bmatrix} 0 & \bar{Q}_{c_{sr}}^+ \\ \bar{Q}_{c_{sr}}^{+\,*} & 0 \end{bmatrix} \bar{i}_{c_{p1}} = \Re\left\{ i_{c_{p1}}^* \begin{bmatrix} 0 & Q_{c_{sr}}^+ \\ Q_{c_{sr}}^{+\,*} & 0 \end{bmatrix} i_{c_{p1}} \right\} \\ &= \Re\left\{ i_{c_{sp1}}^* Q_{c_{sr}}^+ i_{c_{rp1}} + i_{c_{rp1}}^* Q_{c_{sr}}^{+\,*} i_{c_{sp1}} \right\} = \Re\left\{ i_{c_{sp1}}^* Q_{c_{sr}}^+ i_{c_{rp1}} + \bar{i}_{c_{sp1}}^* \bar{Q}_{c_{sr}}^+ \bar{i}_{c_{rp1}} \right\} = 2\Re\left\{ i_{c_{sp1}}^* Q_{c_{sr}}^+ i_{c_{rp1}} \right\} \end{aligned} \tag{4.23}$$

Hence the BDFM may be fully described, in balanced three phase conditions, using:

$$v_{c_{p1}} = (R_c^+ + \omega_r Q_c^+) i_{c_{p1}} + M_c^+ \frac{d i_{c_{p1}}}{dt} \tag{4.24}$$

with the torque given by (4.23).

Note that this is a full dynamic model, which is mathematically equivalent to the full d-q model under balanced conditions.

4.3 Steady-state Equivalent Circuit Representation

We will now show that under steady-state conditions the equations lead to a symmetric impedance matrix, which means that a simple equivalent circuit comprised of passive components exists.

Table 4.1 compares the rms values and frequencies of the voltages under the various modelling stages presented. An immediate consequence of table 4.1 is that if the positive sequence stator 1 current is to be equal in frequency to that of the negative sequence stator 2 current, then $p_1\omega_r - \omega_1 = -p_2\omega_r + \omega_2$, which implies the familiar condition on the rotor speed for BDFM synchronous operation:

$$\omega_r = \frac{\omega_1 + \omega_2}{p_1 + p_2} \tag{4.25}$$

Phase quantity		d/q quantity		Sequence quantity	
rms	freq. (rad/s)	rms	freq. (rad/s)	rms	freq. (rad/s)
Stator 1					
V_1	ω_1	$\sqrt{3}V_1$	$p_1\omega_r - \omega_1$	$\sqrt{\frac{3}{2}}V_1$	$p_1\omega_r - \omega_1$
Stator 2					
V_2	ω_2	$\sqrt{3}V_2$	$p_2\omega_r - \omega_2$	$\sqrt{\frac{3}{2}}V_2$	$p_2\omega_r - \omega_2$

Table 4.1: Comparison of rms values and frequencies for the different models presented under a 3 phase balanced supply in steady-state: coupled-circuit model, d-q axis model, complex sequence components model, the latter two models being in the rotor reference frame

Therefore from (4.24), when (4.25) holds all the non-zero voltage sources are at a frequency of $\omega_1 - p_1\omega_r$. Therefore the currents, $i_{c_{p1}}$ must also be at the same frequency, this can be most easily seen by splitting (4.24) into real and imaginary components and taking the frequency response (Fourier transform). This, of course, makes physical sense, as the d-q (and hence symmetrical components) reference frame chosen is in synchronism with the rotor. The frequency of the currents in the rotor reference frame under steady state conditions we denote by ω_s:

$$\omega_s = p_1\omega_r - \omega_1 = -p_2\omega_r + \omega_2 \tag{4.26}$$

In steady-state conditions, with (4.25) in effect, (4.24) becomes:

$$\sqrt{\frac{3}{2}}V_c = (R_c^+ + \omega_r Q_c^+ + j\omega_s M_c^+)\sqrt{\frac{3}{2}}I_c \tag{4.27}$$

where $\sqrt{\frac{3}{2}}V_c$ and $\sqrt{\frac{3}{2}}I_c$ (V_c, $I_c \in \mathbb{C}^{N+2}$) are vectors of appropriate steady-state sequence components of current and voltage. N is number of sets of $S = p_1 + p_2$ rotor coils in the particular machine. We

now define:

$$M_{c_{s1r}} = \begin{bmatrix} M_{1_1}\exp(j\phi_{1_1}) & \cdots & \cdots & M_{1_N}\exp(j\phi_{1_N}) \end{bmatrix} \tag{4.28}$$

$$M_{c_{s2r}} = \begin{bmatrix} M_{2_1}\exp(-j\phi_{2_1}) & \cdots & \cdots & M_{2_N}\exp(-j\phi_{2_N}) \end{bmatrix} \tag{4.29}$$

$$M_{c_r} = \begin{bmatrix} L_{dq_{r1}} & M_{12_r}\exp(-j\phi_{12_r}) & \cdots & M_{1N_r}\exp(-j\phi_{1N_r}) \\ M_{12_r}\exp(j\phi_{12_r}) & L_{dq_{r2}} & \cdots & M_{2N_r}\exp(-j\phi_{2N_r}) \\ \vdots & \vdots & \ddots & \vdots \\ M_{1N_r}\exp(j\phi_{1N_r}) & M_{2N_r}\exp(j\phi_{2N_r}) & \cdots & L_{dq_{rN}} \end{bmatrix} \tag{4.30}$$

and note that from (4.15) and (4.16) $\omega_r Q_c^+ + j\omega_s M_c^+$ is given by:

$$\omega_r Q_c^+ + j\omega_s M_c^+ = \left[\begin{array}{cc|c} j(L_1 - M_1)(\omega_s - \omega_r p_1) & 0 & j(\omega_s - \omega_r p_1)M_{c_{s1r}} \\ 0 & j(L_2 - M_2)(\omega_s + \omega_r p_2) & j(\omega_s + \omega_r p_2)M_{c_{s2r}} \\ \hline j\omega_s M^*_{c_{s1r}} & j\omega_s M^*_{c_{s2r}} & j\omega_s M_{c_r} \end{array}\right] \tag{4.31}$$

We now define the *slip* between stator 1 and the rotor, and stator 2 and the rotor as follows:

$$s_1 \triangleq \frac{\omega_1/p_1 - \omega_r}{\omega_1/p_1} = \frac{\omega_1 - p_1\omega_r}{\omega_1} = -\frac{\omega_s}{\omega_1} \tag{4.32}$$

$$s_2 \triangleq \frac{\omega_2/p_2 - \omega_r}{\omega_2/p_2} = \frac{\omega_2 - p_2\omega_r}{\omega_2} = \frac{\omega_s}{\omega_2} \tag{4.33}$$

$$\Rightarrow \omega_2 s_2 = -s_1\omega_1 \tag{4.34}$$

The notion of slip will be familiar for readers with a machines background. Slip is so-named because it is the ratio of the difference in rotational speed between the stator magnetic field and the physical rotor speed, normalised by the rotational speed of the stator magnetic field. Therefore the slip is zero when the machine rotates at the stator field speed, and unity at standstill.

Substituting (4.32), (4.33) and (4.31) into (4.27) gives (subject to $\omega_1 \neq 0$ and $\omega_s \neq 0$) :

$$\begin{bmatrix} V_1 \\ V_2 \\ 0 \end{bmatrix} = \left(-j\omega_1 \begin{bmatrix} (L_1 - M_1) & 0 & M_{c_{s1r}} \\ 0 & \frac{s_1}{s_2}(L_2 - M_2) & \frac{s_1}{s_2}M_{c_{s2r}} \\ s_1 M^*_{c_{s1r}} & s_1 M^*_{c_{s2r}} & s_1 M_{c_r} \end{bmatrix} + \begin{bmatrix} R_{dq_1} & 0 & 0 \\ 0 & R_{dq_2} & 0 \\ 0 & 0 & R_{dq_r} \end{bmatrix} \right) \begin{bmatrix} I_1 \\ I_2 \\ I_r \end{bmatrix} \tag{4.35}$$

$$\Rightarrow \begin{bmatrix} V_1 \\ \frac{s_2}{s_1}V_2 \\ 0 \end{bmatrix} = \left(-j\omega_1 \begin{bmatrix} (L_1 - M_1) & 0 & M_{c_{s1r}} \\ 0 & (L_2 - M_2) & M_{c_{s2r}} \\ M^*_{c_{s1r}} & M^*_{c_{s2r}} & M_{c_r} \end{bmatrix} + \begin{bmatrix} R_{dq_1} & 0 & 0 \\ 0 & \frac{s_2}{s_1}R_{dq_2} & 0 \\ 0 & 0 & R_{dq_r}/s_1 \end{bmatrix} \right) \begin{bmatrix} I_1 \\ I_2 \\ I_r \end{bmatrix} \tag{4.36}$$

where $\begin{bmatrix} V_1 \\ V_2 \\ 0 \end{bmatrix} = V_c\exp(-j\omega_s)$, and similarly for I_1, I_2, I_r, that is V_1, V_2 are the complex phasors.

Adopting a change of notation (4.36) becomes:

$$\begin{bmatrix} V_1 \\ \frac{s_2}{s_1}V_2 \\ 0 \end{bmatrix} = \left(-j\omega_1 \begin{bmatrix} L_{c_{s1}} & 0 & M_{c_{s1r}} \\ 0 & L_{c_{s2}} & M_{c_{s2r}} \\ M^*_{c_{s1r}} & M^*_{c_{s2r}} & M_{c_r} \end{bmatrix} + \begin{bmatrix} R_{c_1} & 0 & 0 \\ 0 & \frac{s_2}{s_1}R_{c_2} & 0 \\ 0 & 0 & R_{c_r}/s_1 \end{bmatrix} \right) \begin{bmatrix} I_1 \\ I_2 \\ I_r \end{bmatrix} \tag{4.37}$$

In this new notation from (4.23) the torque equation becomes:

$$\begin{aligned} T_e &= 2\Re\left\{-\exp(-j\omega_s)I_1^* jp_1 M_{c_{s1r}} I_r \exp(j\omega_s) + \exp(-j\omega_s)I_2^* jp_2 M_{c_{s2r}} I_r \exp(j\omega_s)\right\} \\ &= 2\Re\left\{-jI_1^* p_1 M_{c_{s1r}} I_r + jI_2^* p_2 M_{c_{s2r}} I_r\right\} \\ &= 2\Im\left\{I_1^* p_1 M_{c_{s1r}} I_r - I_2^* p_2 M_{c_{s2r}} I_r\right\} \end{aligned} \tag{4.38}$$

Now (4.37) is in a form which admits an equivalent circuit representation. Figure 4.1 shows an equivalent circuit representation. The terms $M_{c_{s1r1}}, M_{c_{s1r2}}, \cdots, M_{c_{s1rN}}$ are the elements of $M_{c_{s1r}}$. $M_{c_{s2r1}}, M_{c_{s2r2}}, \cdots, M_{c_{s2rN}}$ are the elements of $M_{c_{s2r}}$. $M_{c_{sr11}}, M_{c_{sr12}}, \cdots, M_{c_{srNN}}$ are the elements of M_{c_r}. And $R_{c_{r1}}, R_{c_{r2}}, \cdots, R_{c_{rN}}$

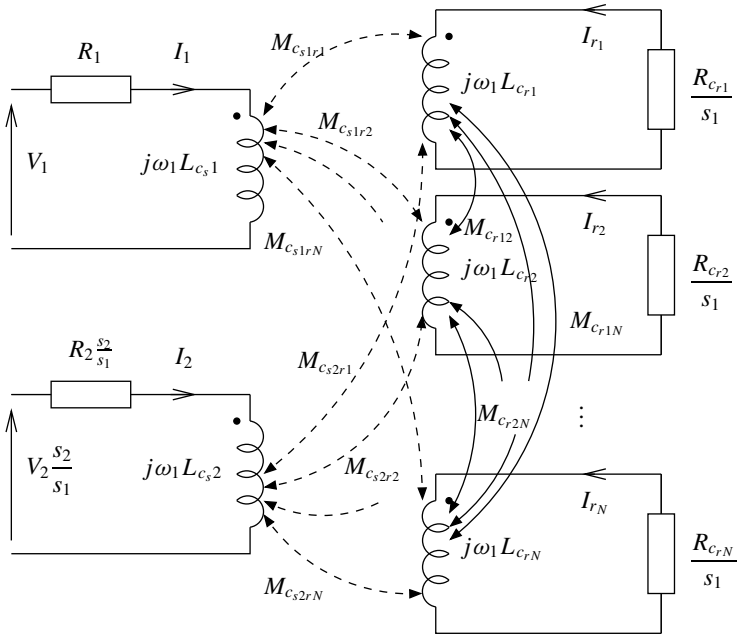

Figure 4.1: Coupled coils Equivalent Circuit for BDFM model with N sets of rotor circuits

Note that as there will, in general, be phase offsets between stator and rotor, and between the different rotor circuits, the mutual inductance terms are complex, rather than real. This means that the equivalent circuit is unusual in that there will be a phase offset at the voltage terminals. This is made explicit in figure 4.2, following the dot convention for the polarity of the mutual inductance terms (see e.g. [30] for details) between currents forming the input and output of each coupled coil. Physically this corresponds to the physical phase offset between coil sets in the machine. It is worth noting that in the case of a 'nested-loop' design rotor, the matrix M_{c_r} is purely real, as the off-diagonal $S \times S$

sub-matrices in the coupled circuit rotor-rotor mutual inductance matrix will be symmetric circulant matrices, rather than just circulant matrices.

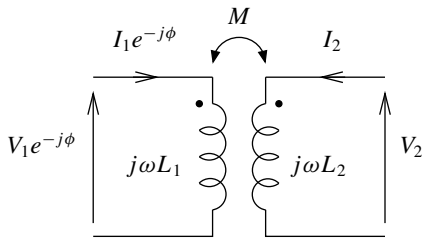

$$V_1e^{-j\phi} = j\omega L_1 I_1 e^{-j\phi} + j\omega M I_2$$
$$V_2 = j\omega L_2 I_2 + j\omega M e^{-j\phi} I_1$$
$$\begin{bmatrix} V_1 \\ V_2 \end{bmatrix} = j\omega \begin{bmatrix} L_1 & Me^{j\phi} \\ Me^{-j\phi} & L_2 \end{bmatrix} \begin{bmatrix} I_1 \\ I_2 \end{bmatrix}$$

Figure 4.2: Circuit equivalent of coupled coils with complex mutual inductance terms

4.4 Equivalent circuit for the BDFM with a single set of rotor coils

We now turn our attention to a sub-class of BDFMs having either a single set of rotor coils, or equivalently a 'nested-loop' design rotor to which the model reduction method described in section 3.4.2 has been applied. While equivalent circuits have been presented for BDFMs with a single set of rotor coils, they have been for specific machines. Both Li et al. [60] and Gorti et al [41] give an equivalent circuit for a 6/2 configuration nested loop machine, however it is not clear how the model order has been reduced. It is most likely that the method of summing the contributions from each loop given in [64, 63] was used (see section 3.5 for details).

We will show that the circuit derived for a specific BDFM configuration in [60, 41] is in fact the correct form for any BDFM of this sub-class, that is with a single set of rotor circuits. Furthermore we will synthesize the equivalent circuit in such as way as to preserve the physical meaning of components, as far as possible.

A BDFM with a single set of rotor circuits is a special case of the general case previously presented in section 2.7. In this case the rotor-rotor coupling term, M_{c_r} is a real scalar.

From figure 4.2 and (4.37) the steady-state equations may be written as:

$$\begin{bmatrix} V_1e^{-j\angle M_{c_{s1r}}} \\ \frac{s_2}{s_1}V_2e^{-j\angle M_{c_{s2r}}} \\ 0 \end{bmatrix} = \left(-j\omega_1 \begin{bmatrix} L_{c_{s1}} & 0 & |M_{c_{s1r}}| \\ 0 & L_{c_{s2}} & |M_{c_{s2r}}| \\ |M_{c_{s1r}}| & |M_{c_{s2r}}| & M_{c_r} \end{bmatrix} + \begin{bmatrix} R_{c_1} & 0 & 0 \\ 0 & \frac{s_2}{s_1}R_{c_2} & 0 \\ 0 & 0 & R_{c_r}/s_1 \end{bmatrix} \right) \begin{bmatrix} I_1e^{-j\angle M_{c_{s1r}}} \\ I_2e^{-j\angle M_{c_{s2r}}} \\ I_r \end{bmatrix}$$

taking the complex conjugate of each side (recalling that now the mutual inductance and resistance terms are real) gives:

$$\begin{bmatrix} \bar{V}_1 e^{j\angle M_{cs1r}} \\ \frac{s_2}{s_1}\bar{V}_2 e^{j\angle M_{cs2r}} \\ 0 \end{bmatrix} = \left(j\omega_1 \begin{bmatrix} L_{cs1} & 0 & |M_{cs1r}| \\ 0 & L_{cs2} & |M_{cs2r}| \\ |M_{cs1r}| & |M_{cs2r}| & M_{cr} \end{bmatrix} + \begin{bmatrix} R_{c1} & 0 & 0 \\ 0 & \frac{s_2}{s_1}R_{c2} & 0 \\ 0 & 0 & R_{cr}/s_1 \end{bmatrix} \right) \begin{bmatrix} \bar{I}_1 e^{j\angle M_{cs1r}} \\ \bar{I}_2 e^{j\angle M_{cs2r}} \\ \bar{I}_r \end{bmatrix} \tag{4.39}$$

It will now be convenient to change notation into a more concise form, defining:

$$\begin{aligned} \tilde{V}_1 &\triangleq \bar{V}_1 e^{j\angle M_{cs1r}} \\ \tilde{V}_2 &\triangleq \bar{V}_2 e^{j\angle M_{cs2r}} \\ \tilde{I}_1 &\triangleq \bar{I}_1 e^{j\angle M_{cs1r}} \\ \tilde{I}_2 &\triangleq \bar{I}_2 e^{j\angle M_{cs2r}} \\ \tilde{I}_r &\triangleq \bar{I}_r \end{aligned} \tag{4.40}$$

Hitherto the steady-state BDFM equations presented have been functions of sequence phasors. From table 4.1 it is clear that the only difference in magnitude between a per-phase quantity and a sequence quantity is a scalar multiple. Furthermore, as the steady-state equations are in terms of phasors, the equations hold regardless of the reference frame chosen. A change of reference frame simply requires a different phase on V and I. Therefore the electrical equations may be considered per-phase equations without modification. Each current in the torque equation, however, must be multiplied by the factor $\sqrt{\frac{3}{2}}$ as given in table 4.1, if per-phase quantities are used.

Using the simplified notation the per-phase steady-state BDFM equations become:

$$\begin{bmatrix} \tilde{V}_1 \\ \frac{s_2}{s_1}\tilde{V}_2 \\ 0 \end{bmatrix} = \left(j\omega_1 \begin{bmatrix} L_{cs1} & 0 & |M_{cs1r}| \\ 0 & L_{cs2} & |M_{cs2r}| \\ |M_{cs1r}| & |M_{cs2r}| & M_{cr} \end{bmatrix} + \begin{bmatrix} R_{c1} & 0 & 0 \\ 0 & \frac{s_2}{s_1}R_{c2} & 0 \\ 0 & 0 & R_{cr}/s_1 \end{bmatrix} \right) \begin{bmatrix} \tilde{I}_1 \\ \tilde{I}_2 \\ \tilde{I}_r \end{bmatrix} \tag{4.41}$$

and multiplying the current phasors in (4.38) by $\sqrt{\frac{3}{2}}$ the torque equation corresponding to the per-phase equivalent circuit is (noting that for $a, b \in \mathbb{C}$, $\Im\{ab\} = \Im\left\{-\bar{a}\bar{b}\right\}$):

$$T_e = 3\Im\left\{-\tilde{I}_1^* p_1 |M_{cs1r}| I_r + \tilde{I}_2^* p_2 |M_{cs2r}| I_r\right\} \tag{4.42}$$

It it worth noting that equation (4.42) is identical to eq. (7) of [41], subject to the factor of 3 as (4.42) a per-phase representation.

Some useful alternative forms of (4.42) may now be derived. From the the first row of (4.41):

$$\tilde{V}_1 \tilde{I}_1^* = j\omega_1 L_{cs1} \tilde{I}_1 \tilde{I}_1^* + j\omega_1 \tilde{I}_1^* |M_{cs1r}| \tilde{I}_r + R_{c1} \tilde{I}_1^* \tilde{I}_1 \tag{4.43}$$

$$\Rightarrow \Re\left\{\tilde{V}_1 \tilde{I}_1^*\right\} - R_{c1}|\tilde{I}_1|^2 = \Re\left\{j\omega_1 \tilde{I}_1^* |M_{cs1r}| \tilde{I}_r\right\} \tag{4.44}$$

and from the second row of (4.42):

$$\frac{s_2}{s_1}\tilde{V}_2\tilde{I}_2^* = j\omega_1 L_{cs2}\tilde{I}_2\tilde{I}_2^* + j\omega_1\tilde{I}_2^*|M_{cs2r}|\tilde{I}_r + \frac{s_2}{s_1}R_{c2}\tilde{I}_2^*\tilde{I}_2 \tag{4.45}$$

$$\Rightarrow \frac{s_2}{s_1}\left(\Re\left\{\tilde{V}_2\tilde{I}_2^*\right\} - R_{c2}|\tilde{I}_2|^2\right) = \Re\left\{j\omega_1\tilde{I}_2^*|M_{cs2r}|\tilde{I}_r\right\} \tag{4.46}$$

noting that (4.42) can be written:

$$T_e = 3\Re\left\{j\tilde{I}_1^* p_1|M_{cs1r}|I_r - j\tilde{I}_2^* p_2|M_{cs2r}|I_r\right\} \tag{4.47}$$

hence, substituting (4.43) and (4.46) in (4.47):

$$T_e = \frac{3p_1}{\omega_1}\left(\Re\left\{\tilde{V}_1\tilde{I}_1^*\right\} - R_{c1}|\tilde{I}_1|^2\right) - \frac{3p_2 s_2}{\omega_1 s_1}\left(\Re\left\{\tilde{V}_2\tilde{I}_2^*\right\} - R_{c2}|\tilde{I}_2|^2\right) \tag{4.48}$$

We may write the per-phase BDFM equations (4.41) as an equivalent circuit as shown in figure 4.3. This form of the equivalent circuit is the same as that found in [60, 41].

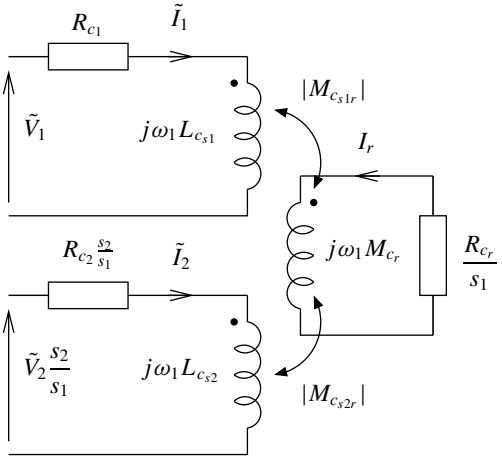

Figure 4.3: Coupled Coils Per-Phase Equivalent Circuit for Single Rotor Circuit BDFM

4.4.1 Physical interpretation of parameters in the per-phase equivalent circuit model

The parameters used in (4.41) are calculated, in the first instance, from the coupled-circuit method described in section 2.5.1, using in particular equation (2.22). These parameter values then undergo transformation to d-q axes, model reduction (if appropriate) and then conversion to symmetrical components as described in sections 3.3, 3.4.2, and 4.2.

However, as noted in section 2.4.3, it is also possible to calculate machine parameters from the Fourier series representation of mutual inductance using (2.27) instead of (2.22). For each harmonic a separate inductance matrix will be given, and an infinite sum of the harmonic terms will, of course, give the same result as the direct calculation method. As the transformation to d-q axes, model

reduction and transformation to symmetrical components are linear operations, the transformations may be directly applied to each harmonic component. Note that the matrix used in model reduction will be the one derived for the full system, and this model reduction technique then applied to each harmonic in turn.

Furthermore the leakage inductance terms, as described in section 2.5.2 may be retained separately and converted to symmetrical components via the same procedure.

We may therefore split the inductance terms into their constituent parts:

$$\begin{aligned} M_{c_r} &= L_{r_1} + L_{r_2} + L_{r_l} + L_{r_h} \\ L_{c_{s1}} &= L_{1_f} + L_{1_h} + L_{1_l} \\ L_{c_{s2}} &= L_{2_f} + L_{2_h} + L_{2_l} \end{aligned} \tag{4.49}$$

These terms correspond to inductance due to leakage, and inductances due to particular space harmonic components. Inductance due to leakage is self-inductance arising from flux which does not cross the air gap, the leakage terms are L_{r_l}, L_{1_l}, L_{2_l}. Of the other terms, we know from section 2.6 that for the class of BDFMs considered, the first non-zero component of the harmonic Fourier series of the inductance matrices will be p_1 for stator 1 and p_2 for stator 2. These harmonic terms, when suitably transformed, become L_{1_f} and L_{2_f} respective, the fundamental space harmonics for the two stator windings.

On the rotor, in general there will be a rich set of harmonics. From Lemma 2.9 we know that the rotor-rotor mutual inductance term can only comprise of harmonics of p_1 and p_2, the fundamental stator field, as the rotor is not directly energised, however in general the magnitude of these harmonic terms is significant. L_{r_1} and L_{r_2} are the p_1, p_2 pole number harmonic components of the rotor self-inductance, that is, the harmonics which link to the stator 1 and 2 respectively. The L_{r_h}, L_{1_h}, and L_{2_h} terms are higher order space harmonic self-inductance terms, which are not included elsewhere, as given by (4.49).

Using the relationships in (4.49), figure 4.3 may be re-written as figure 4.4.

Using standard results, figure 4.4 may be transformed into a 'T' equivalent form using the relationships shown in figures 4.5 and 4.6 (see, for example [20]). Note that in a network sense, the choice of N is entirely arbitrary. However we will choose the turns ratio in each case so that it is the *effective turns ratio* for each coupling. The effective turns ratio, is the square root of the ratio of the fundamental space harmonic self-inductance terms for the rotor and the stator. Equivalently, it is the ratio of the amplitudes of the fundamental air gap mmf waveforms produced by unit current in the stator and rotor [100, p. 381]. Therefore the effective turns ratio for stator 1 - rotor is:

$$N_1 = \sqrt{\frac{L_{1_f}}{L_{r_1}}} \tag{4.50}$$

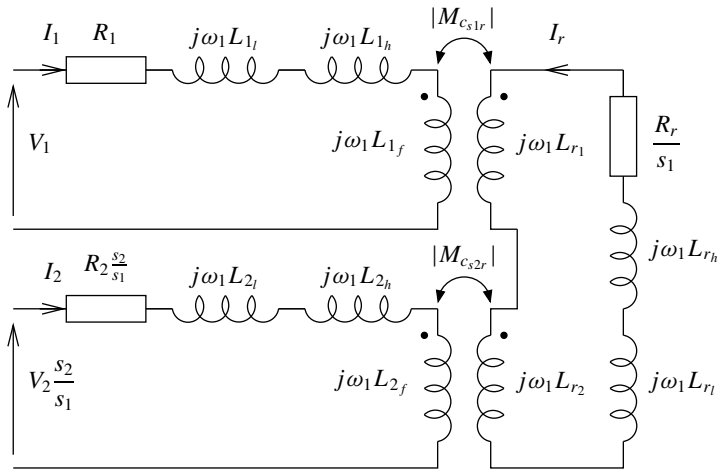

Figure 4.4: Coupled coils Equivalent Circuit Separating M_{c_r}, $L_{c_{s1}}$, $L_{c_{s2}}$

and for stator 2 - rotor:

$$N_2 = \sqrt{\frac{L_{2_f}}{L_{r_2}}} \tag{4.51}$$

Because L_{1_f}, L_{r_1} and L_{2_f}, L_{r_2} represent couplings between same pole number fields with no parasitic effects, the coupling in each case is perfect, therefore:

$$|M_{c_{s1r}}| = \sqrt{L_{1_f} L_{r_1}} \tag{4.52}$$

and

$$|M_{c_{s2r}}| = \sqrt{L_{2_f} L_{r_2}} \tag{4.53}$$

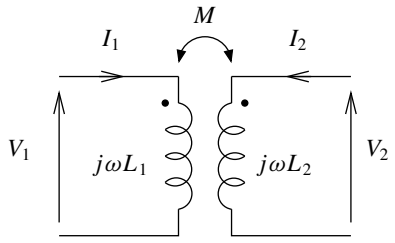

Figure 4.5: Coupled coils

Therefore converting the coupled coils arrangements of figure 4.4 using figure 4.6 gives the equivalent circuit as shown in figure 4.7. Note that from (4.52) and (4.53) the series terms in figure 4.6 are zero.

It is helpful, for physical insight, to note that figure 4.7 is equivalent to figure 4.8. This can be seen by noting that from (4.32) and (4.33) $\omega_s = -s_1\omega_1$. Then as the sign of E_1 and E_{r1} can be

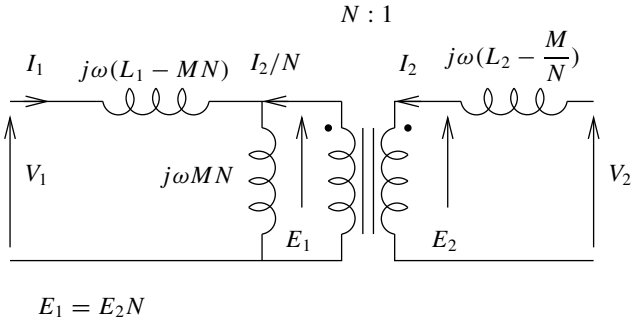

Figure 4.6: Transformer equivalent of coupled coils

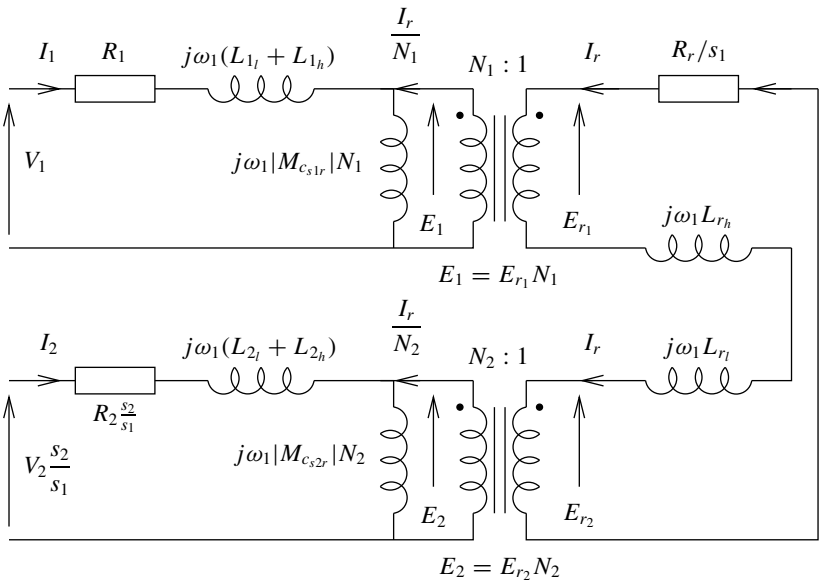

Figure 4.7: BDFM Equivalent circuit with separate inductance components

arbitrarily assigned, figure 4.8 becomes equivalent to figure 4.7 if the direction of positive V_1, I_1 is reversed. Figure 4.8 may be recognised as two normal induction machine equivalent circuits with rotors connected together, which is conceptually how the BDFM operates.

Figure 4.7 may be referred to stator 1 or stator 2, as is customary for the standard induction machine. We will refer all quantities to stator 1, although they could easily be referred to stator 2. The use of the modifier " $'$ " denotes that the quantity is referred. The relationships between the

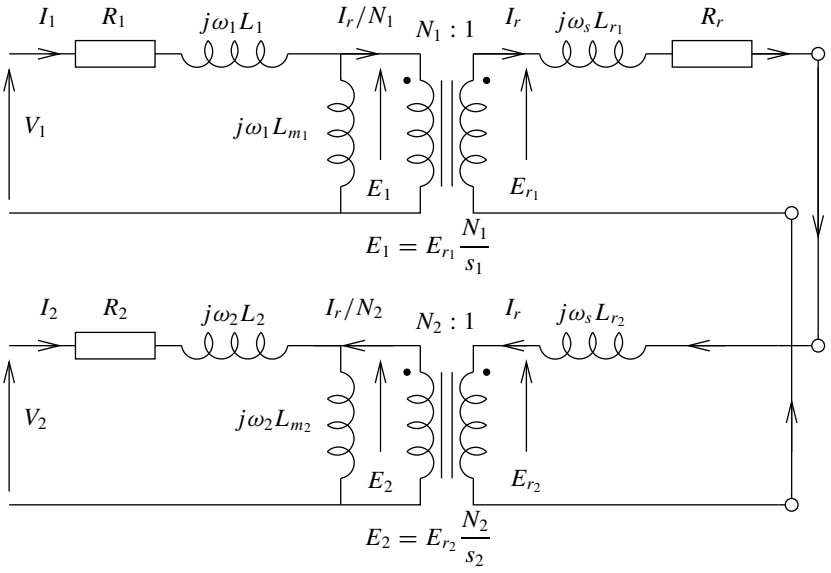

Figure 4.8: BDFM Equivalent represented as two induction machine connected together. Equivalent with figure 4.7 is achieved with $L_{m_1} = |M_{c_{s1r}}|N_1$, $L_{m_2} = |M_{c_{s2r}}|N_2$, $L_1 = (L_{1_l} + L_{1_h})$, $L_2 = (L_{2_l} + L_{2_h})$, $L_{r_1} + L_{r_2} = L_{r_h} + L_{r_l}$

parameter of figure 4.7 and figure 4.9 are:

$$
\begin{aligned}
L_1 &= (L_{1_l} + L_{1_h}) \\
L_2'' &= (L_{2_l} + L_{2_h})\frac{N_1^2}{N_2^2} \\
L_r' &= (L_{r_l} + L_{r_h})N_1^2 \\
R_2'' &= R_2\frac{N_1^2}{N_2^2} \\
R_r' &= R_2 N_1^2 \\
L_{m_1} &= |M_{c_{s1r}}|N_1 = L_{1_f} \qquad \text{from (4.50) and (4.52)} \\
L_{m_2}'' &= (|M_{c_{s2r}}|N_1)\frac{N_1^2}{N_2^2} = L_{2_f}\frac{N_1^2}{N_2^2} \qquad \text{from (4.51) and (4.53)} \\
V_2'' &= \frac{N_1}{N_2}V_2 \\
I_2'' &= \frac{N_2}{N_1}I_2
\end{aligned}
\tag{4.54}
$$

4.4.2 Development of Torque Equations from the Equivalent Circuit

It is interesting to now consider how the conversion of electrical to mechanical energy is represented in the equivalent circuit. This leads to development of expressions for the electrical torque produced by the machine. Such expressions will be developed in terms of supply currents, voltage, and a combination of the two. During these derivations two voltages, V_{r_1} and V_{r_2} are introduced, and are defined

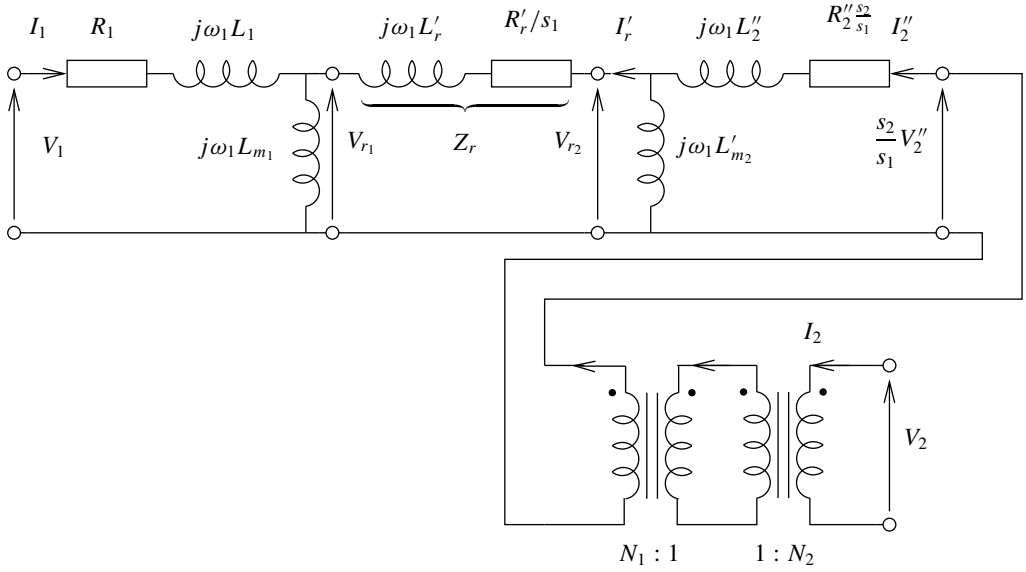

Figure 4.9: BDFM Referred Per-Phase Equivalent Circuit

in figure 4.9. Working in terms of these voltages leads to considerable algebraic simplifications, yet prevents the needs for any simplification to the overall model, as analysis can be performed using these intermediate variables, and then the terminal quantities 'backed-out'. V_{r_1} and V_{r_2} are physically meaningful in that they represent the voltages across the magnetizing inductances of the two windings. Thus a limit on the magnetization of the laminations may be written in terms of a limit on V_{r_1} and V_{r_2}. This point will be discussed further in section 4.7.

By applying the principle of power conservation to figure 4.9 we get:

$$3\Re\{V_1 I_1^*\} + 3\frac{s_2}{s_1}\Re\{V''_2 I''^*_2\} = 3|I_1^2|R_1 + 3|I'^2_r|\frac{R'_r}{s_1} + 3|I''^2_2|R''_2\frac{s_2}{s_1} \tag{4.55}$$

$$3\Re\{V_1 I_1^*\} + 3\Re\{V''_2 I''^*_2\} = 3|I_1^2|R_1 + 3|I'^2_r|R'_r + 3|I''^2_2|R''_2 + \omega_r T \tag{4.56}$$

where T is the torque generated by the machine, with positive values for motoring, and the '3's arise because figure 4.9 is a per-phase equivalent circuit.

From figure 4.9 we may define P_{r_1}, P_{r_2}, the power delivered at the rotor terminals from stator 1 and 2 respectively:

$$P_{r_1} \triangleq 3\Re\{V_{r_1} I_1^*\} = 3\Re\{V_1 I_1^*\} - 3|I_1^2|R_1 \tag{4.57}$$

$$P_{r_2} \triangleq 3\frac{s_1}{s_2}\Re\{V_{r_2} I''^*_2\} = 3\Re\{V''_2 I''^*_2\} - 3|I''^2_2|R''_2 \tag{4.58}$$

Subtracting (4.55) from (4.56) gives the fraction of power not dissipated in the rotor and stator resistances, i.e. the power which is converted to mechanical power:

$$3\Re\{V''_2 I''^*_2\}\left(1 - \frac{s_2}{s_1}\right) = 3|I'^2_r|R'_r\left(1 - \frac{1}{s_1}\right) + 3|I''^2_2|R'_2\left(1 - \frac{s_2}{s_1}\right) + \omega_r T \tag{4.59}$$

Rearranging, and substituting (4.58) for the I_2'' terms gives the torque as:

$$T = \frac{P_{r_2}}{\omega_r}\left(1 - \frac{s_2}{s_1}\right) - \frac{3}{\omega_r}|I_r'^2|R_r'\left(1 - \frac{1}{s_1}\right) \tag{4.60}$$

Alternatively, substituting (4.57) and (4.58) into (4.55) and (4.56) gives:

$$P_{r_1} + \frac{s_2}{s_1}P_{r_2} = 3|I_r'^2|\frac{R_r'}{s_1} \tag{4.61}$$

$$P_{r_1} + P_{r_2} = 3|I_r'^2|R_r' + \omega_r T \tag{4.62}$$

Combining (4.61) and (4.62) and with (4.32), (4.33), (4.25), (1.2) gives the following expression for the torque:

$$T = \frac{p_1}{\omega_1}P_{r_1} - \frac{p_2 s_2}{\omega_1 s_1}P_{r_2} \tag{4.63}$$

which, using (4.57) and (4.58) and some sustained manipulation may be written as:

$$T = \frac{3p_1}{\omega_1}\left(\Re\left\{V_1 I_1^*\right\} - R_1|I_1|^2\right) + \frac{3p_2 s_2}{\omega_1 s_1}\left(-\Re\left\{V_2 I_2^*\right\} + R_2|I_2|^2\right) \tag{4.64}$$

$$= \frac{3p_1}{\omega_1}\left(\Re\left\{V_{r_1} I_1^*\right\}\right) + \frac{3p_2 s_2}{\omega_1 s_1}\left(-V_{r_2} I_2^* \frac{s_1}{s_2}\right) \tag{4.65}$$

$$= 3\frac{R_r}{\omega_1 s_1}p_1|I_r|^2 + \frac{3(p_1+p_2)s_2}{\omega_1 s_1}\left(R_2|I_2|^2 - \Re\left\{V_2 I_2^*\right\}\right) \tag{4.66}$$

$$= 3\frac{R_r}{\omega_1 s_1}p_1|I_r|^2 + \frac{3(p_1+p_2)}{\omega_1 s_c}\left(R_2|I_2|^2 - \Re\left\{V_2 I_2^*\right\}\right) \tag{4.67}$$

$$= 3\frac{(p_1+p_2)}{\omega_1}\left(\Re\left\{V_1 I_1^*\right\} - R_1|I_1|^2\right) - 3\frac{R_r}{s_1\omega_1}p_2|I_r|^2 \tag{4.68}$$

where:

$$s_c = \frac{s_1}{s_2} = -\frac{\omega_2}{\omega_1} = \frac{\omega_1 - (p_1+p_2)\omega_r}{\omega_1} \tag{4.69}$$

Note that (4.64) is the same as (4.48), the torque equation derived from the coupled circuit model, as expected.

It is convenient as this stage to recall the *natural speed*, ω_n for the BDFM, given in (1.2).

$$\omega_n = \frac{\omega_1}{p_1 + p_2}$$

Referring back to the definition of BDFM synchronous speed (4.25), and slips (4.32), (4.33), it is straightforward to see that the rotor speed, ω_r can be written in terms of a deviation from natural speed:

$$\begin{aligned}\omega_r &= \left(1 - \frac{s_1}{s_2}\right)\omega_n \\ &= \frac{s_1}{s_2}\left(\frac{s_2}{s_1} - 1\right)\omega_n\end{aligned} \tag{4.70}$$

Using (4.70), (4.32) and (4.58) the expression for the torque, (4.60), may be written as:

$$T = -\frac{3\Re\{V_{r_2} I_2''^*\}}{\omega_n} + 3|I_r'^2|R_r'\frac{p_1}{\omega_1 s_1} \tag{4.71}$$

or more generally because $\Re\left\{V_{r_1} I_1^*\right\} = -\Re\left\{V_{r_1} I_r'^*\right\}$ and $\Re\left\{V_{r_2} I_2''^*\right\} = \Re\left\{V_{r_2} I_r'^*\right\}$, from (4.65):

$$T = \frac{3p_1}{\omega_1}\left(-\Re\left\{V_{r_1} I_r'^*\right\}\right) + \frac{3p_2}{\omega_1}\left(-\Re\left\{V_{r_2} I_r'^*\right\}\right) \tag{4.72}$$

writing I_r' in terms of V_{r_1} and V_{r_2}:

$$\begin{aligned}
&= \frac{3p_1}{\omega_1}\Re\left\{-V_{r_1}\left(\frac{V_{r_2}^* - V_{r_1}^*}{Z_r^*}\right)\right\} + \frac{3p_2}{\omega_1}\Re\left\{-V_{r_2}\left(\frac{V_{r_2}^* - V_{r_1}^*}{Z_r^*}\right)\right\} \\
&= \frac{3p_1}{\omega_1}\Re\left\{-\frac{V_{r_1}V_{r_2}^*}{Z_r^*} + \frac{|V_{r_1}|^2}{Z_r^*}\right\} + \frac{3p_2}{\omega_1}\Re\left\{-\frac{|V_{r_2}|^2}{Z_r^*} + \frac{V_{r_2}V_{r_1}^*}{Z_r^*}\right\} && (4.73) \\
&= \frac{3p_1}{\omega_1}\left(-\frac{|V_{r_1}V_{r_2}|}{|Z_r|}\cos(\psi+\delta) + \frac{|V_{r_1}|^2}{|Z_r|}\cos(\psi)\right) + \frac{3p_2}{\omega_1}\left(-\frac{|V_{r_2}|^2}{|Z_r|}\cos(\psi) + \frac{|V_{r_1}V_{r_2}|}{|Z_r|}\cos(\psi-\delta)\right) && (4.74) \\
&= \frac{3}{\omega_1}\frac{|V_{r_1}V_{r_2}|}{|Z_r|}\sqrt{p_1^2 + p_2^2 - 2p_1p_2\cos 2\psi}\,\sin\left(\delta - \arctan\left(\frac{(p_1-p_2)\cos\psi}{(p_1+p_2)\sin\psi}\right)\right) + \\
&\qquad \frac{3}{\omega_1}\left(\frac{p_1|V_{r_1}|^2}{|Z_r|} - \frac{p_2|V_{r_2}|^2}{|Z_r|}\right)\cos(\psi) && (4.75)
\end{aligned}$$

where $\psi = \angle Z_r$ and $\delta = \angle V_{r_1} - \angle V_{r_2}$, the phase angle between V_{r_1} and V_{r_2}.

Hence the maximum (and minimum) torques occurs when $(p_2 - p_1)\tan\delta = (p_1 + p_2)\tan\psi$. Furthermore note that from (4.75) for any given torque, there are either 0, 1, or 2 values of δ, for a given set of $|V_{r_1}|$, $|V_{r_2}|$, ω_1, Z_r, p_1 and p_2. There will be zero solutions when the torque is outside the maximum and minimum torque envelopes, one solution when the torque is precisely on these torque envelopes, and two solutions in all other cases. The two solutions will be δ_0 and $\pi - \delta_0$. Physically, if one these values of δ corresponds to a stable operating point, the other typically corresponds to an unstable operating point. This fact is explored further in chapter 7.

A further variant of the torque expression is obtained by re-writing the first term of equation (4.71) in terms of V_{r_1} and V_{r_2}. As no real power is dissipated in L_{m_2}, from figure 4.9 it is straightforward to see that $\Re\left\{V_{r_2} I_2''^*\right\} = \Re\left\{V_{r_2} I_r'^*\right\}$. From figure 4.9 I_r' may be written as $\dfrac{V_{r_2} - V_{r_1}}{Z_r}$ therefore, from 4.71:

$$\begin{aligned}
T &= -\frac{3}{\omega_n}\Re\left\{\frac{V_{r_2}V_{r_2}^* - V_{r_2}V_{r_1}^*}{Z_r^*}\right\} + 3|I_r'^2|R_r'\frac{p_1}{\omega_1 s_1} \\
&= \frac{3}{\omega_n}\left(\frac{|V_{r_1}V_{r_2}|}{|Z_r|}\cos(\psi-\delta) - \frac{|V_{r_2}|^2}{|Z_r|}\cos(\psi)\right) + 3|I_r'^2|R_r'\frac{p_1}{\omega_1 s_1} && (4.76)
\end{aligned}$$

where δ is the angle between V_{r_1} and V_{r_2} and $\psi = \angle Z_r$, as before.

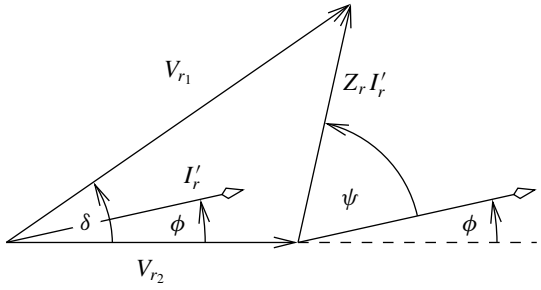

Figure 4.10: BDFM Rotor Circuit Phasor Diagram

4.4.3 Phasor diagram for rotor branch circuit

Figure 4.10 shows the phasor diagram for the rotor branch of the circuit shown in figure 4.9.

Figure 4.10 can be used to determine the power and VAR flow in and out of the rotor terminals on figure 4.9. We therefore define:

$$Q_{r_1} \triangleq -3\Im\left\{V_{r_1} I_r'^*\right\} = 3\Im\left\{V_1 I_1^*\right\} - 3|I_1|^2 L_1\omega_1 - 3\frac{|V_{r_1}|^2}{L_{m_1}\omega_1} \tag{4.77}$$

$$Q_{r_2} \triangleq 3\Im\left\{V_{r_2} I_r'^*\right\}\frac{s_1}{s_2} = 3\Im\left\{V_2 I_2^*\right\} + 3|I_2''|^2 L_2\omega_1\frac{s_1}{s_2} + 3\frac{|V_{r_2}|^2}{L_{m_2}\omega_1}\frac{s_1}{s_2} \tag{4.78}$$

Hence if V_{r_2}, V_{r_1}, and I'_r are known then the VARs produced/consumed at the machine terminals can be calculated. For example if Q_{r_1} and Q_{r_2} are minimised for a given $|I'_r|$, $|V_{r_1}|$ and $|V_{r_2}|$, then the terminal VARs will also be minimised. Therefore specifications on the power factor at the terminals can be translated into specifications at the rotor branch, which is completely described by the phasor diagram in figure 4.10.

4.5 Equivalent Circuit Numerical Simulation

Figures 4.11, 4.12 and 4.13 show the maximum torque envelope for the prototype BDFM previously described with the nested loop rotor. The machine is excited with a constant 240V, at 50Hz on the power (4 pole) winding, and the 8 pole winding excitation is chosen such that: $|V_{r_2}|$ is held constant, and $\angle(V_{r_2})$ is chosen such that the torque is maximum or minimum respectively. The base value chosen is such that at 0rpm $|V_2| = 240V$, and from (4.25), $\omega_2 = 2\pi \times 50$. Maintaining a constant $|V_{r_2}|$ corresponds to maintaining constant flux on the 8 pole winding. However, as the s_1 decreases the impedance of Z'_r increases and therefore $|V_{r_1}|$ changes, thus the 4 pole flux changes. This explains the slight change in torque envelope. Because V_1 is constant it is not possible to compensate for this change directly, rather is must be achieved indirectly by modifying V_2. Section 4.7 discusses the issues surrounding maintaining a constant magnetic loading for different relative amplitudes of 4 and 8 pole fields.

Figure 4.12 shows how the envelope changes with a 10% decrease in L_{r_h}, the rotor excess inductance due to spatial harmonics. The 4 pole flux (i.e. $|V_{r_2}|$) was kept the same in both cases. Note that in changing the value of L_{r_h} this will have changed the 8 pole flux as $|V_{r_1}|$ will have changed. In fact the change is a small (3%) decrease for positive torque and a 1% decrease for negative torque, thus an even greater change in torque envelope would have resulted if the flux level had been maintained.

Figure 4.13, is similar to figure 4.12 except it shows the effect of a voltage limit on the inverter of 240V. It has been assumed that $|V_2|$ is constant and $\angle(V_{r_2})$ is chosen so that the torque is maximized (from (4.75). This gives a unique value V_{r_2}, however it will not necessarily put a bound on $|V_{r_2}|$, which would be required to ensure that the magnetic loading is not exceeded.

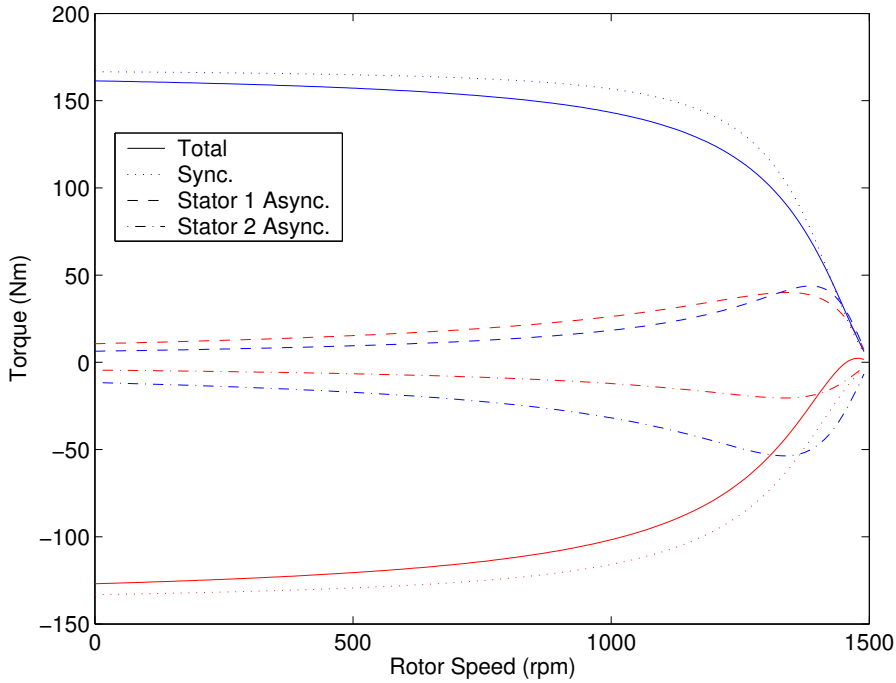

Figure 4.11: The synchronous and asynchronous components of torque on the maximum torque envelope, for constant $|V_{r_2}|$ and $|V_1|$

4.6 Equivalent Circuit Analysis

The preceding analysis leads to a number of general points regarding BDFM operation.

1. The presented equivalent circuit holds for all BDFM operating modes where the shaft speed is constrained by equation (4.25). If this condition does not hold then the machine may be modelled as the sum of two equivalent circuits at different frequencies, one supplied from stator 1, the other from stator 2, and with the unsupplied stator short-circuited. This mode of operation is known as *double cascade induction* mode:

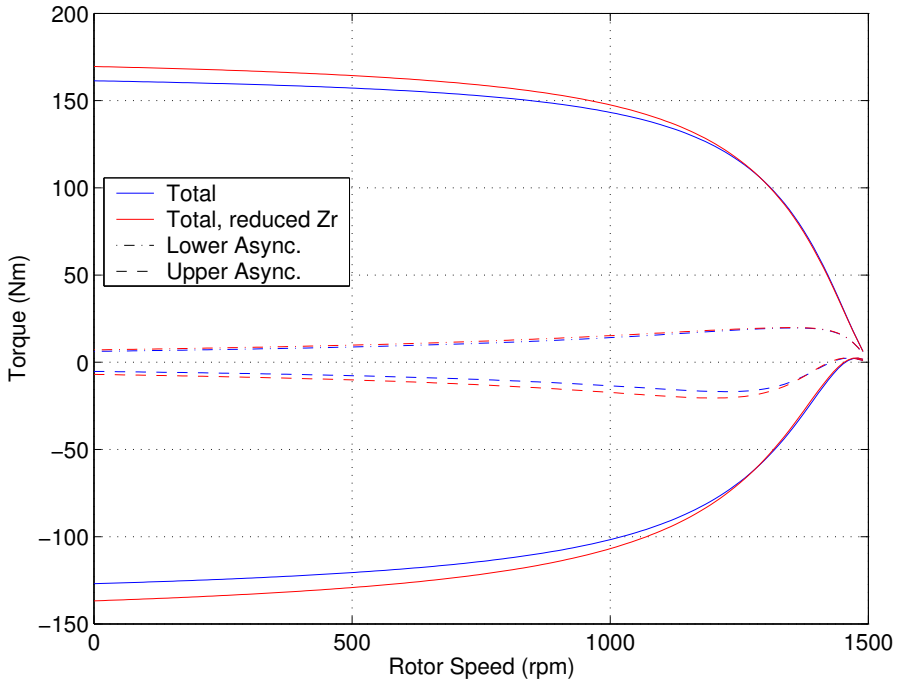

Figure 4.12: Torque envelope (blue) showing the effect of a 10% decrease in L_{r_h} (red)

The preceding derivation requires (4.25) to hold. However, if this is not the case then by the superposition theorem, the machine may be modelled as a machine with stator 1 supplied and stator 2 short-circuited, and a machine with stator 2 supplied and stator 1 short-circuited. The true current in each branch is the sum of the contribution from each circuit. The average torque may be calculated using any of the per-phase torque equations derived, and the contribution from each circuit added. However the true torque will have a significant ripple component, which cannot be calculated using the steady-state equivalent circuit. In this case the torque should be calculated from the full complex currents of the two frequencies concerned, rather than just phasors.

2. The BDFM may operate either as a p_1 or p_2 pole pair induction machine when only stator 1 or stator 2 is supplied and the unsupplied stator is open-circuit. This mode of operation is known as *simple induction* mode:

   It is immediate from figure 4.9 that if $I_2 = 0$, then the machine reduces to a standard induction motor equivalent circuit, but with the rotor 'leakage' inductance equal to $L'_r + L'_{m_2}$, in the case of supply from stator 1. Clearly analogous results hold when supplied from stator 2. The torque reduces to the well-know expression for a standard induction machine (4.66). It is also noteworthy that a good BDFM design will inevitably lead to poor simple induction mode torque. This is because the second stator magnetizing inductance appears in series with the rotor leakage inductance, and typically in a well-designed machine the magnetizing inductance

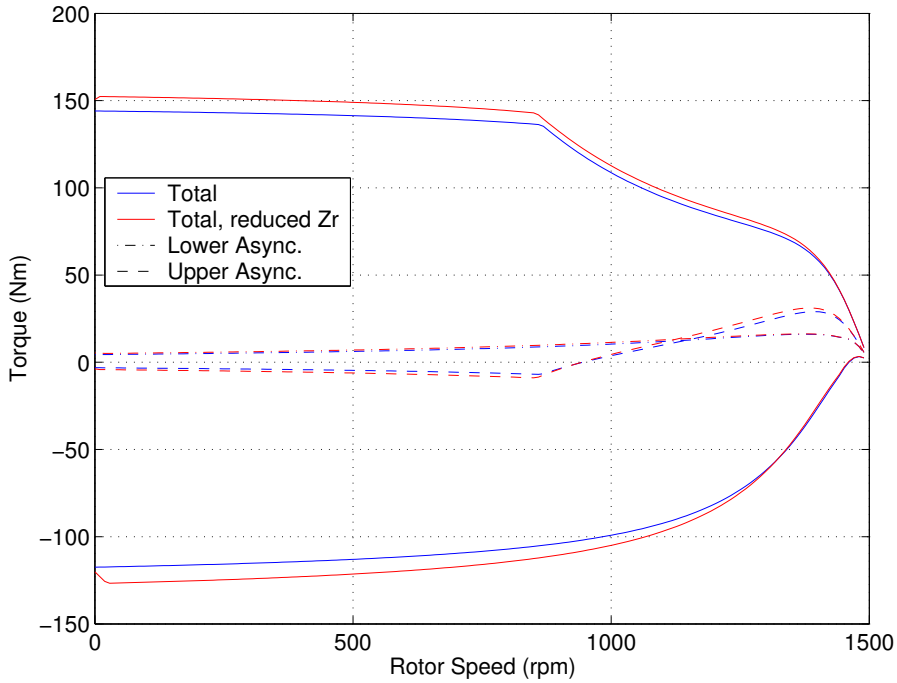

Figure 4.13: Torque envelope (blue) showing the effect of a 10% decrease in L_{r_h} (red) with inverter voltage limit

will be large in comparison to the leakage inductance.

3. The BDFM, when operating according to (4.25), is comprised of synchronous torques and induction machine-like asynchronous torques.

   This can be seen most clearly from equation (4.75). The last two terms are fixed for a given operating speed, and rotor voltage magnitudes, as Z_r is fixed. These terms are induction machine like torque terms, in that they are fixed for a given operating speed, regardless of the phase of the supply voltage. In contrast, the first term is dependent on the sine of δ, the angle between the two rotor supply voltages. This term is reminiscent of the torque of a standard synchronous machine.

4. The asynchronous torques in the BDFM will always be of opposite signs and sum to zero if either, $\psi = \pi/2$, which means the rotor is purely inductive, or $p_1|V_{r_1}| = p_2|V_{r_2}|$:

   These points come directly from equation (4.75).

5. Unlike the conventional induction machine, the BDFM would produce torque if the rotor resistance were zero.

   From (4.75), if $R_r = 0 \Rightarrow \cos(\psi) = 0$, therefore the only non-zero term in the torque expression is the first term. It can be shown that, as $\psi = \frac{\pi}{2}$, the term reduces to the first term of (4.76).

6. All torque in the BDFM falls to zero at the synchronous speed of stator 1:

   From figure 4.8, when s_1 and s_2 are both zero, then I_r is zero; hence from (4.47) the torque will be zero. From (4.32) s_1 is zero at stator 1 synchronous speed, and therefore, from (4.26), ω_s (the frequency of the rotor currents), must be zero. As stator 2 is supplied in such a way that the frequencies of the rotor currents induced match those induced by stator 1, then s_2 must also be zero. This can be seen from (4.32). A corollary to this point is that for a given BDFM with stator 1 and stator 2 (of course of different pole numbers) a wider speed envelope for BDFM operation is obtained if the lower pole number field is connected as stator 1.

7. When stator 2 is short-circuited the BDFM operates in *cascade induction* mode, which is a special case of BDFM synchronous mode (that is, the stator 2 currents are at frequency ω_2, given by (4.25)) similar to that observed when two induction machines are connected in cascade [49]:

   Equation (4.26) gives the frequencies of the rotor currents for the BDFM. As the rotor current frequency in the BDFM is the same for currents induced from both stator supplies, then even if the second stator is short-circuited, the stator 2 current frequency will be at ω_2. Therefore cascade induction mode is a special case of BDFM synchronous mode, where the voltage V_{r_2} of equation (4.76) although non-zero is not an independent variable as it is in synchronous mode.

   Equation (4.67) shows that, when $V_2 = 0$ there are two terms in the torque equation, one is the stator 1 induction mode torque characteristic, the other may be thought of as the induction mode characteristic of the cascade combination of the (effectively) two machines. (4.67) introduces the notion of cascade slip, s_c which has a similar interpretation to standard slip, and for which the 'synchronous' speed is ω_n, (1.2), the natural speed, corresponding to the case that $\omega_2 = 0$.

8. The cascade torque of a BDFM is inherent, and will be present on all functional real-world BDFMs. The absence of a cascade torque implies no BDFM synchronous torque, or that R_2, the second stator resistance is zero.

   Point 7 illustrates the close relationship between cascade torque and synchronous torque, and therefore that its absence implies that there is no synchronous torque. Equation (4.67) shows that if R_2 is zero then there can be no cascade torque. In practice R_2 cannot be zero, so the absence of cascade torque will generally imply that there will be zero synchronous torque.

9. The size of the available BDFM synchronous torque envelope for a machine in practical use is inversely proportional to the rotor impedance, $|Z_r|$ which comprises of leakage reactance, excess harmonic reactance and resistance terms.

   Figure 4.11 shows the three components of torque arising from the three terms of equations (4.75). Notice that the two asynchronous torque terms (marked as 'Stator 2 Async.' and 'Stator 1 Async.' on the diagram) are (and in general will always be) opposite in signs (immediate from

(4.75)), and furthermore will generally be small in comparison with the maximum synchronous torque for relatively large values of s_1. From figure 4.12 the total asynchronous torque is less than 10% of the maximum synchronous torque for $s_1 > \frac{1}{3}$. We assume that we operate the machine with $s_1 > \frac{1}{3}$, which is likely as it is desirable to operate the machine around natural speed, as natural speed will correspond to $s_1 = \frac{p_2}{p_1+p_2}$. Under this condition the maximum torque available is dominated by the first term of equation (4.75) which reduces to the first term of (4.76):

$$T_{\max} \approx \frac{3}{\omega_n} \frac{|V_{r_1} V_{r_2}|}{|Z_r|} \tag{4.79}$$

Now, significantly, the voltages $|V_{r_1}|$ and $|V_{r_2}|$ are the voltages across the magnetizing reactances for the machine (see figure 4.9). Therefore for any given values of $|V_{r_1}|$ and $|V_{r_2}|$ the flux densities of p_1 and p_2 pole number fields will be fixed. It is not immediately obvious what 'rated' flux density should be with two different pole number fields sharing the same iron laminations, however certainly there will be some upper limit, determined by what is considered a 'reasonable' degree of saturation. This point will be discussed further in section 4.7. Therefore the maximum torque available from a machine is inversely proportional to $|Z_r|$.

We may therefore conclude that the maximum rotor impedance for a given maximum output torque is:

$$|Z_{r_{\max}}| = \frac{3}{\omega_n} \frac{|V_{r_1} V_{r_2}|}{T_{\max}} \tag{4.80}$$

Now if we assume that, for any reasonable machine design, in normal operation V_{r_1} and V_{r_2} are close to the supply voltages (i.e. stator drops are small), then equation (4.80) can be used as a design guide. It should be noted, that because of the direction of power flow, the estimate will be an overestimate in some regions, and an underestimate in others, due to the stator drops.

Figures 4.12 and 4.13 serve to illustrate the effect of the series rotor impedance, (Z_r of figure 4.9).

10. The power factor of the stator 1 winding can be controlled by the magnitude of V_{r_2} in synchronous operation, and can always be made to lead, however for a given $|Z_r|$, the more resistive the rotor, the greater the current required:

    From figure 4.10, it is immediate that the phase of I_r' can be controlled by varying the magnitude of V_{r_2} for a given δ. Furthermore, as $0 < \psi < \frac{\pi}{2}$, for speeds less than the stator 1 synchronous speed, it will always be possible to make ϕ negative. If ϕ is negative then for a sufficiently large current it will be possible to make the power factor of stator 1 leading. It is clear that the closer ψ is to 0, the larger the current required for a unity or leading power factor ($\psi = 0$ implies the rotor is purely resistive).

11. If the machine is to operate at a fixed power factor on stator 1, then the smaller $|Z_r|$, the larger the available torque, for a well-designed machine.

    From figure 4.10 a fixed stator 1 power factor will imply a fixed value of ϕ, if it can be assumed that the stator 1 series impedance is relatively small, which is likely to be the case in a well designed machine. If ϕ is fixed then for any operating speed, the phasor diagram is fully described, as Z_r is constant. Therefore from equation (4.75), as $|Z_r|$ decreases, the synchronous torque envelope increases, as the rate of decrease of $|Z_r|$ must always be greater than the corresponding rate of increase of $|V_{r_2}|$. Therefore the available torque increases, as we assume that the induction torques are small because ψ is close to 90°.

12. In the 'nested-loop' design BDFM rotor the components of rotor inductance L_{r_h} and L_{r_l} are both significant, and therefore directly impact the torque envelope:

    Recall that L_{r_h} is the additional inductance which is due to unwanted space harmonic components in the rotor. L_{r_l} is the additional inductance due to leakage effects - that is flux that does not cross the air gap as discussed in appendix C.1. Table 4.2 lists the calculated components of Z_r for the prototype 'nested-loop' design rotor.

X_{r_h} ($\mu\Omega$)	X_{r_l} ($\mu\Omega$)	R_r ($\mu\Omega$)
Nested-loop design rotor		
307	332	74

Table 4.2: Components of Z_r for the prototype 'nested-loop' design rotor at 50Hz

    From table 4.2 when the slip, s_1, is less than 0.11 then $|Z_r|$ is less than 1.41 times its value at $s_1 = 1$. Therefore for the majority of the available operating regime $|Z_r|$ is determined by the inductive components. Indeed, both L_{r_h} and L_{r_l} are significant in determining $|Z_r|$.

4.7 Magnetic Loading for the BDFM

As previously noted, to address the question of what 'rated' magnetic flux density is for a BDFM is not a straightforward question because the iron circuit carries two different frequency magnetic flux density waves. So the question that arises is what, if any, combination of amplitudes of the two flux density waveforms constitute a constant magnetic loading? A conservative answer to this question would be the sum of the amplitudes of the flux density waveforms, as inevitably this peak value will be attained. However intuition suggests that this may lead to conservative results, as the peak value occurs relatively infrequently.

The issue of magnetic loading for the BDFM has received little attention. It is believed that the only significant contribution in this area is due to Broadway [16], however Broadway only discussed the issue for a specific example, rather than presenting any general conclusions.

In conventional induction machines designers use a *specific magnetic loading*, dependent on the electrical steel chosen, which achieves the right balance between under use of the iron (and therefore a reduced output torque from the machine), and causing excess magnetizing current and therefore a poor power factor by driving the iron into saturation, see, for example, [92] for details.

In the conventional induction machine, the specific magnetic loading is traditionally defined as the mean absolute flux per pole in the air gap of a machine. In a BDFM this definition becomes unworkable because of the double feed. We therefore propose the following generalisation of the definition:

$$\bar{B} = \lim_{T\to\infty} \frac{1}{T} \int_0^T \frac{1}{2\pi} \int_0^{2\pi} |B(\theta)| d\theta dt \tag{4.81}$$

where $B(\theta)$ is the flux density in the air gap (assumed uniform along the axis of the machine).

It is clear that this definition is consistent with the concept of 'mean flux per pole', and the well-known result of $\bar{B} = \frac{2\sqrt{2}}{\pi} B_{\text{rms}}$ may be verified.

From similar reasoning to [115] ignoring harmonic fields, the magnetic fields in the air gap of the BDFM may be written as:

$$B(\theta) = B_1 \cos(\omega_1 t - p_1\theta) + B_2 \cos(\omega_2 t - p_2\theta + \gamma) \tag{4.82}$$

These fields may be referred to the rotor reference frame as follows:

$$\theta = \omega_r t + \phi \tag{4.83}$$

from (4.26) we may write:

$$B_r(\phi) = B_1 \cos(\omega_s t + p_1\phi) + B_2 \cos(\omega_s t + p_2\phi + \gamma) \tag{4.84}$$

Therefore, from (4.81) the specific magnetic load for the BDFM is:

$$\bar{B} = \lim_{T\to\infty} \frac{1}{T} \int_0^T \frac{1}{2\pi} \int_0^{2\pi} |B_1 \cos(\omega_s t + p_1\phi) + B_2 \cos(\omega_s t + p_2\phi + \gamma)| d\phi dt \tag{4.85}$$

$$= \frac{\omega_s}{2\pi} \int_0^{\frac{2\pi}{\omega_s}} \frac{1}{2\pi} \int_0^{2\pi} |B_1 \cos(\omega_s t + p_1\phi) + B_2 \cos(\omega_s t + p_2\phi + \gamma)| d\phi dt \tag{4.86}$$

This integral may be evaluated either analytically or numerically. It is useful to note the standard deviation of the time-varying spatial mean signal, as it gives an indication of the degree of ripple to be expected in the specific magnetic loading in a BDFM. It may easily be shown that when $B_2 = 0$ then $\bar{B} = \frac{2}{\pi} B_1$ and when $B_2 = B_1$ then $\bar{B} = 2\left(\frac{2}{\pi}\right)^2 B_1$, regardless of the value of p_1, p_2, ω_s, γ.

Figure 4.14 shows how (4.86) varies with B_2, for unity B_1. Although a simple proof has not been forthcoming, the same relationship (the green line) was found regardless of the pole number

combinations or offset angle chosen. 70 pole number combinations were tried under the standard restrictions on BDFM pole numbers, $p_1 \neq p_2$ and $|p_1 - p_2| > 1$. The dashed green lines show the one standard deviation away from the mean for the case of $p_1 = 2$, $p_2 = 4$. Note that the standard deviation is strongly dependent on the pole number combination chosen, thus suggesting that specific magnetic loading for the BDFM may not be the best measure to determine the magnetic loading for all pole number combinations. Figure 4.14 also includes a plot of the magnetic loading if it is assumed that the total magnetic loading is the sum of loading for each individual field, that is $\bar{B} = \bar{B}_1 + \bar{B}_2$ and, for comparison, an alternative definition of the combined magnetic loading as $\bar{B} = \sqrt{\bar{B}_1^2 + \bar{B}_2^2}$. This alternative can be thought of as the root-mean-square of the rms values of the air gap flux density waves, scaled by $\frac{2\sqrt{2}}{\pi}$.

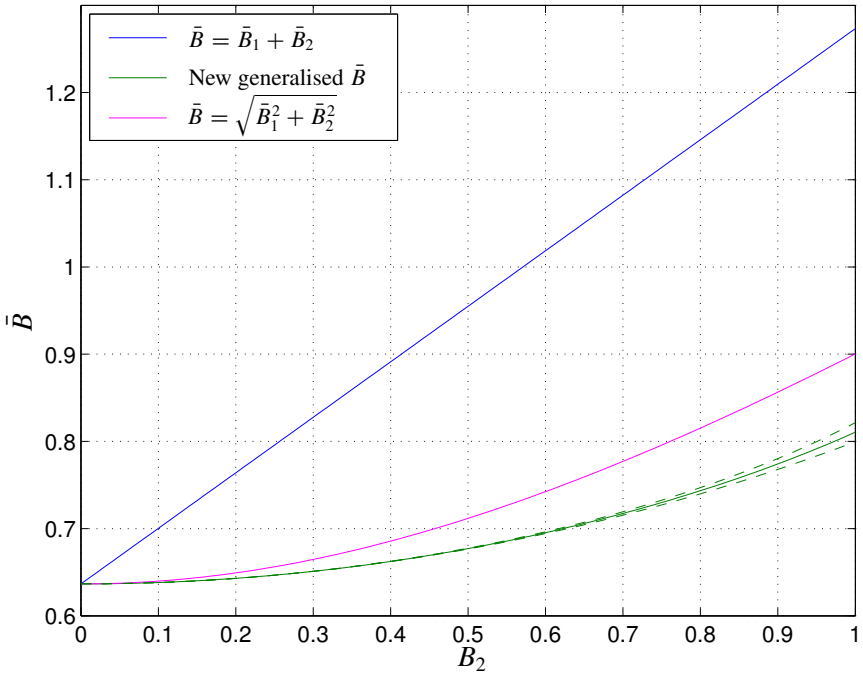

Figure 4.14: $\bar{B}$, the specific magnetic loading a 4/8 BDFM for $B_1 = 1$ (hence $\bar{B}_1 = \frac{2}{\pi}$) as B_2 varies between 0 and 1 (hence $\bar{B}_2$ varies from 0 to $\frac{2}{\pi}$) . Three variations in the definition are shown, the summation of the $\bar{B}$ for each field, the new generalised and averaged $\bar{B}$ and $\bar{B} = \sqrt{\bar{B}_1^2 + \bar{B}_2^2}$, as an analytical alternative

From figure 4.14 it is clear that the generalised magnetic loading is considerably less conservative than assuming that the magnetic loadings for each individual field should be summed. Furthermore it is significant that the variance of the generalised magnetic loading about its mean was small for certain pole number combinations, thus indicating that the average field is well distributed around the circumference of the machine under normal operating conditions. This serves to increase confidence that the generalised magnetic loading is a good measure of iron utilisation. However the alternative

definition, $\bar{B} = \sqrt{\bar{B}_1^2 + \bar{B}_2^2}$ is close in value to the newly proposed generalisation, but has the advantage that it has a simple closed-form representation, which lends itself to analytical calculations. The convenience of this alternative representation is that a specification on the magnetic loading can be translated into a specification in terms of V_{r_1} and V_{r_2}.

It should be noted, however, that to use the new generalised magnetic loading, or indeed the analytical alternative, as a 'drop-in' replacement for its counterpart in the conventional induction machine may lead to higher iron losses and poorer power factor as the peak fields present are higher than in a conventional machine. Nevertheless to assume that the true magnetic loading is the sum of each contribution will inevitably lead to a conservative design.

4.8 Conclusion

In this chapter we have transformed the d-q equations of chapter 3 into a complex dynamic model using sequence components using a similarity transformation. It was shown that the complex form of the BDFM equations can be further reduced, without error, to a system containing $2 + N$ complex states, where N is the number of set of rotor coils.

This complex form of the equivalent circuit was shown to admit an equivalent circuit representation. Various implementations of the equivalent circuit were derived for a BDFM with a single set of rotor coils. Particular care was taken to maintain the physical meaning of the inductance terms, especially the rotor leakage inductance.

The intermediate variables V_{r_1} and V_{r_2} were used to derive expressions for the torque, and investigate the effect that stator 2 can exert on the power factor of stator 1. Bounds on the values that $|V_{r_1}|$ and $|V_{r_2}|$ can take were considered via their relation to the magnetic flux density of each field, where a generalisation of the notion of specific magnetic loading was proposed.

The derived equivalent circuit was then used to explore operating modes and expected behaviour of BDFM machines. This led to the observation that the absence of significant cascade induction mode torque typically implies poor BDFM synchronous torque.

Furthermore it was shown in points 8 and 12 that the available torque envelope in BDFM synchronous mode is inversely proportional to $|Z_r|$, the rotor impedance, or similarly, that if the machine is to operate at a particular power factor, then a larger operating torque is achieved for a smaller $|Z_r|$. It was shown that in an example nested loop rotor design, a significant part of $|Z_r|$ comprises of the impedance due to L_{r_h}, the spatial harmonic inductance term. Therefore the component L_{r_h} is a crucial parameter for a BDFM. This makes physical sense as the rotor must cross-couple between two different pole number fields and therefore it is likely that there will be some harmonic penalty. We propose, therefore, that the ratio of L_{r_h} to the total rotor self inductance $(L_{r_h} + L_{r_l} + L_{r_1} + L_{r_2})$ is a figure of merit for a BDFM rotor in terms of its ability to cross couple between the two pole number fields. This has a direct impact on the available torque envelope for a particular machine.

In the next chapter we will investigate the proposed figure of merit for a range of BDFM rotor designs.

Chapter 5

Possible Rotor Designs and Evaluation

5.1 Introduction

In chapter 4 an equivalent circuit model was derived for the class of BDFM machines considered, as described in chapter 2. This equivalent circuit model was used to investigate the characteristics and performance of the BDFM, and it was proposed in section 4.6 that $|Z_r|$, the rotor impedance is a key parameter in determining the maximum torque envelope for the BDFM. The composition of Z_r was discussed, and three potentially significant components were identified: L_{r_h}, the excess harmonic series rotor inductance, L_{r_l}, the rotor leakage inductance, and R_r, the rotor resistance. Furthermore, it was proposed that the absence of cascade induction torque in a potential BDFM was an indicator that the machine will not generate synchronous torque due to the absence of cross-coupling.

In this chapter these claims will be investigated by considering different possible BDFM rotor configurations. In total, seven different rotor designs will be considered. In order to verify the efficacy of measuring the cascade torque as an indicator of potential BDFM performance, 5 different rotors are considered: 3 potential BDFM rotors, and 2 rotors which do not cross-couple. Then, to illustrate the how Z_r can vary with different rotor designs, 4 different rotor designs are considered and the different components of Z_r are discussed.

The chapter starts with a description of the rotor designs, and motivation for the choice of each design. All rotors considered are tested for the same stator configuration, a D180 frame size machine, originally a 22 kW (143 N m at 1463 rpm) Marelli Motori induction machine configured with 4 and 8 pole stator windings for operation as a BDFM (see appendix B). The 7 designs considered are as follows:

1. 'nested-loop' design rotor: originally proposed and investigated by Broadway and Burbridge [17]. The design of the 'nested-loop' rotor was considered in Wallace et al. [109], in which the effect of the span of loops within each nest was investigated. It was found that loops within the centre of a nest which subtended a small angle contributed little to the torque. However there does not appear to be any other papers in the literature which address the design of the rotor in

any detail. A prototype 'nested-loop' rotor was available for experimental testing.

2. A new design of BDFM rotor requiring two layers comprising of single set of $p_1 + p_2$ circuits, with the coil pitch chosen in such a way as to couple effectively with both pole number fields. The design is developed from comments made in Broadway and Burbridge [17], although there is no evidence that either author ever designed or built such a rotor as they sought a single layer design. A rotor of this design was manufactured and experimental tests from it are presented.

3. A rotor design consisting of 18 isolated loops, each pitched over $7/36$ of the circumference of the rotor, and each loop offset from the next by an equal amount ($1/18$ of the circumference). This rotor will be used to illustrate that linking both p_1 and p_2 (in this case 2 and 4) pole pair fields is not sufficient to ensure cross-coupling. A rotor of this design was manufactured and experimental tests from it are presented.

4. A rotor identical to rotor 3, but with every third coil removed. This rotor illustrates that by enforcing a $p_1 + p_2$ order of rotational symmetry on the design (as opposed to 18 order in the case of rotor 3) cross coupling is achieved. The prototype of rotor 3 was modified to provide an experimental rotor of this design.

5. A cage rotor with only $p_1 + p_2$ bars. This rotor design was the conceptual start for the 'nested-loop' design of rotor, however it was dismissed as it was perceived to have a "...very high referred rotor slot-leakage" [17]. This rotor design is considered by simulation.

6. A wound rotor consisting of two double layer windings (therefore 4 layers in total), one of p_1 pole pairs, the other of p_2 pole pairs. The two windings phases are connected together and the star points are connected together. This rotor design is essentially the same as that used by Lydall [97] (although Lydall did not hard-wire a connection between the two windings), which was dismissed by Hunt as being wasteful of copper [48]. The rotor design is included because, it is likely to have low harmonic content. This rotor design is considered by simulation.

7. A standard squirrel cage induction machine rotor with 40 bars. This rotor is considered in order to illustrate the lack of cross-coupling present in a standard squirrel cage machine. The rotor is the standard rotor supplied with the induction machine which was converted into a BDFM.

For each rotor design appendix B gives details of the mutual inductance matrices, including leakage inductances. Section C.1 gives the slot geometries used in each rotor and the formulae used to estimate leakage inductance in each case

5.2 Rotor Designs

5.2.1 Rotor 1 - the ‘nested-loop’ design rotor

The prototype ‘nested-loop’ rotor is of ‘type 2’ design - see figure 2.4 - that is, the rotor comprises of nested loop terminated with a common end ring at one end only. Figure 5.1 shows the non-end ring end of the prototype rotor. As noted in [115] the difference between types 1, 2 and 3 is essentially one of ease of fabrication.

The rotor consists of 36 slots, and as the prototype machine has $p_1 = 2$ and $p_2 = 4$, the rotor has $N = p_1 + p_2 = 6$ nests. Each nest is allocated 6 slots. Therefore three loops can be housed within each nest sub-tending $5/36$, $3/36$, and $1/36$ of the circumference respectively. Figure B.3 displays this information diagrammatically.

It can be seen from figure 5.1 that the bars are insulated from the laminations. It was chosen to insulated the bars as it was established that BDFM performance is significantly degraded unless there is significant bar-to-lamination impedance [117]. The insulation used was a high temperature paper, such that it would not be damaged by the brazing process needed to join the bars.

Section B.3 gives full details of the design.

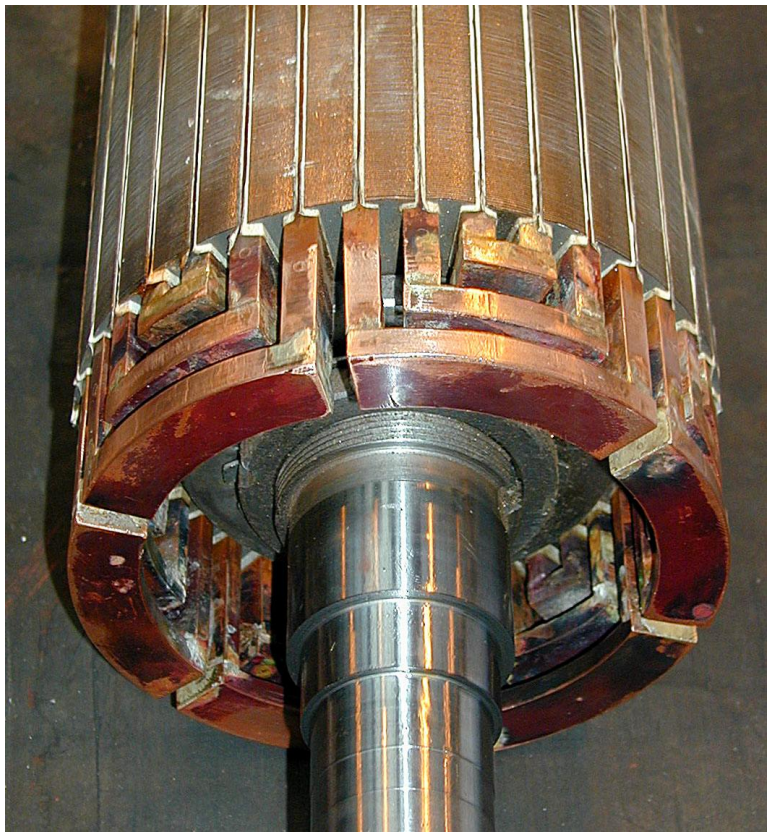

Figure 5.1: Prototype ‘nested-loop’ design rotor, rotor 1

5.2.2 Rotor 2 - the new double layer design rotor

The design of rotors for the BDFM, when undertaken by Broadway and Burbridge, had the objective in mind of designing a rotor which was similar to a cage rotor - that is single layer and manufacturable by conventional casting methods [17]. This approach led to the 'nested-loop' design of rotor. However whether or not the 'nested-loop' rotor is the best design possible, in some sense, has never been established either mathematically or empirically. It is therefore worth investigating whether or not improved performance can be obtained with a different design of rotor.

It is clear from simulations of 'nested-loop' design rotors, and noted in [109] and [53], that loops within a nest, which only subtend a small fraction of the pitch between nests, will have relatively small currents flowing in them, and therefore make little contribution to the output torque of the machine.

The reason for the relatively small currents can be seen from considering the flux linked by a coil of pitch γ, recalling that the flux linked is proportional to the induced voltage as the magnetic flux density waveforms from the two pole number fields are moving at the same speed in the rotor reference frame at BDFM synchronous speed.

Consider an n pole-pair winding. The peak flux linked by a single turn of pitch γ in sinusoidal magnetic flux density of amplitude $\hat{B}$ is:

$$\phi_{\max} \propto \int_{-\gamma/2}^{\gamma/2} \hat{B}\cos(n\theta)d\theta = 2\hat{B}\frac{\sin(n\gamma/2)}{n}$$

In the BDFM there are two fields of p_1 and p_2 pole pairs respectively, having peak flux densities of $\hat{B}_1$ and $\hat{B}_2$. Therefore the peak flux linked is:

$$\phi_{\max} \propto 2\hat{B}_1\frac{\sin(p_1\gamma/2)}{p_1} + 2\hat{B}_2\frac{\sin(p_2\gamma/2)}{p_2} \tag{5.1}$$

which is the peak linkage from each of the two flux density waves. The peak value may be obtained as the phase between the flux density waves can be varied.

Equation (5.1) may be maximised by γ such that $\frac{\partial\phi_{\max}}{\partial\gamma} = 0$:

$$\frac{\partial\phi_{\max}}{\partial\gamma} \propto \frac{1}{2}[\hat{B}_1\cos(p_1\gamma/2) + \hat{B}_2\cos(p_2\gamma/2)] \tag{5.2}$$

hence the maximum is achieved when $\hat{B}_1\cos(p_1\gamma/2) = -\hat{B}_2\cos(p_2\gamma/2)$.

Thus the pitch which can give the maximum flux linkage is dependent on the relative magnitudes of the two pole number fields. However in the case that $\hat{B}_1 = \hat{B}_2$ this is achieved when:

$$\gamma = \frac{2\pi}{p_1 + p_2} \tag{5.3}$$

In the prototype machine the windings were wound to give nominally equal flux densities. Therefore if the coil pitch is chosen such that (5.3) holds then, for $p_1 = 2,\ p_2 = 4$, the pitch is 60°.

It should be noted that the preceding discussion it not a complete picture, as no explicit consideration has been made of the requirement to link both pole number fields, so in practice it is an approximation.

The design problem then is how to maintain a suitable coil pitch to ensure good coupling to both pole number fields, whilst still achieving cross coupling. During the development of the 'nested-loop' design rotor it was noted that cross coupling occurs when the rotor contains $p_1 + p_2$ equally spaced 'phases' [17]. This fact was implicitly proved in chapter 3 by the particular choice of the class of rotors analysed.

This design of rotor will be adopted, however it is necessary to choose both the pitch of the coils making up each phase, and the number of progressive coils in each phase. Figure 5.2 shows calculations, performed using the models techniques developed in chapters 2, 3 and 4, for the harmonic leakage and rotor 8 pole self-inductance. The values are expressed as percentages, of the total rotor self-inductance in the case of the harmonic leakage, and as a percentage of the 4 pole plus 8 pole harmonic inductance components for the 8 pole self-inductance. The values are calculated for 3 different coil pitches, and between 3 and 6 such coils connected in series each one rotor slot advanced on the previous. The rotor has 36 slots.

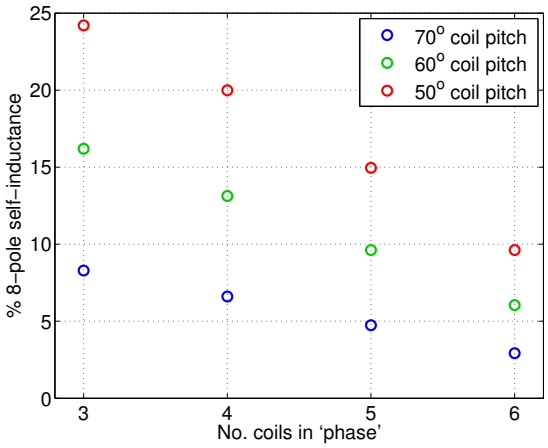

(a) Rotor 8 pole self-inductance as a percentage of 8 pole + 4 pole terms

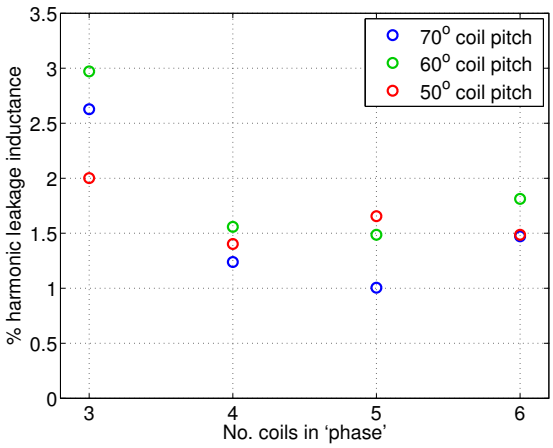

(b) Rotor harmonic leakage inductance as a percentage of total rotor self-inductance

Figure 5.2: Simulated rotor inductance parameter variations for different possible design for Rotor 2. The pitch of the coils making up each 'phase' were varied (different colours on plots), and the number of progressive loops in each 'phase' were varied (horizontal axis)

Figure 5.2(b) shows that having 4 or 5 coils in each phase generally yields a minimum value for the harmonic leakage inductance percentage. However figure 5.2(a), shows that as the number of coils in each 'phase' increases, the 8 pole self-inductance percentage decreases. This is undesirable as it implies that the effective turns ratio from the 8 pole stator to the rotor will be significantly higher than that from the 4 pole stator to the rotor. Therefore the referred rotor impedance to the 8 pole side will be high, thus limiting the current that can be induced in the rotor from the 8 pole stator. This point was first made in Broadway and Burbridge, where it is noted that as the angle between 'phases' will

always exceed half a spatial period of the higher pole number field, the effectiveness of the 'phase' decreases [17, sect. 4.2].

Therefore 4 coils will be used per 'phase' and it only remains to choose the coil pitch. There is little to choose between the options considered in terms of the harmonic leakage, however from figure 5.2(a) decreasing the coil pitch improves the proportion of 8 pole self-inductance. A 60° coil pitch was chosen as it gives a higher overall current than the 50° pitched coils, because the prototype machine stator produces equal amplitude 4 and 8 pole fields. However, if the stator were rewound, the 50° pitched coil would likely to be preferable as the 8 pole coupling is increased, albeit at the expense of the 4 pole coupling.

Figure 5.3 shows a single 'phase' of the new rotor design, with the chosen 60° coil pitch. Figure 5.4 shows a photograph of this rotor design after manufacture. Section B.4 has further details of the rotor including a full winding diagram.

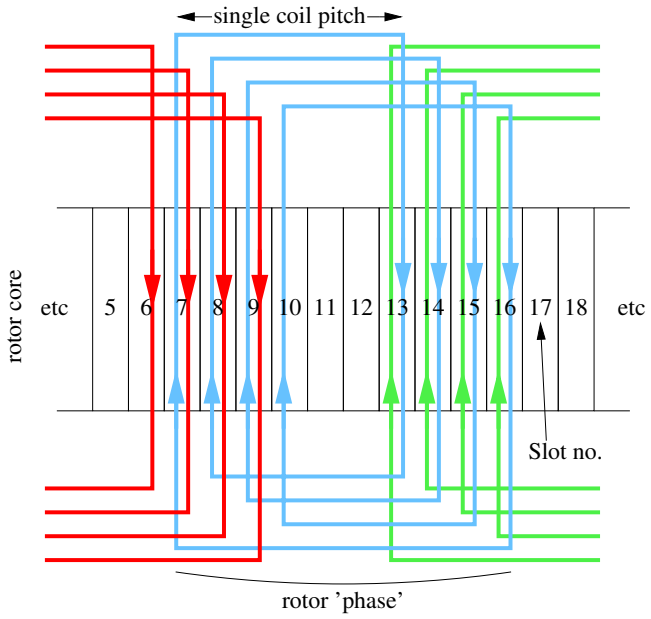

Figure 5.3: Prototype new double-layer design rotor, rotor 2

5.2.3 Rotor 3 - isolated loop rotor

In the discussion of the design of rotor 2, section 5.2.2, the pitch of the coils was discussed. However it was noted that the pitch of the coils is not the only important factor to consider in the design of a rotor for a BDFM which is required to cross-couple.

The isolated loop rotor design consists of 18 coils pitched over 70°, and each coil offset from the next by 20°. Thus the loop pitch is such that it will couple with both the 4 and 8 pole fields. However, if the current distribution due to each field is considered then it can be seen, that the 4 pole field induces a current distribution which is predominantly 4 pole, and is certainly without an 8 pole

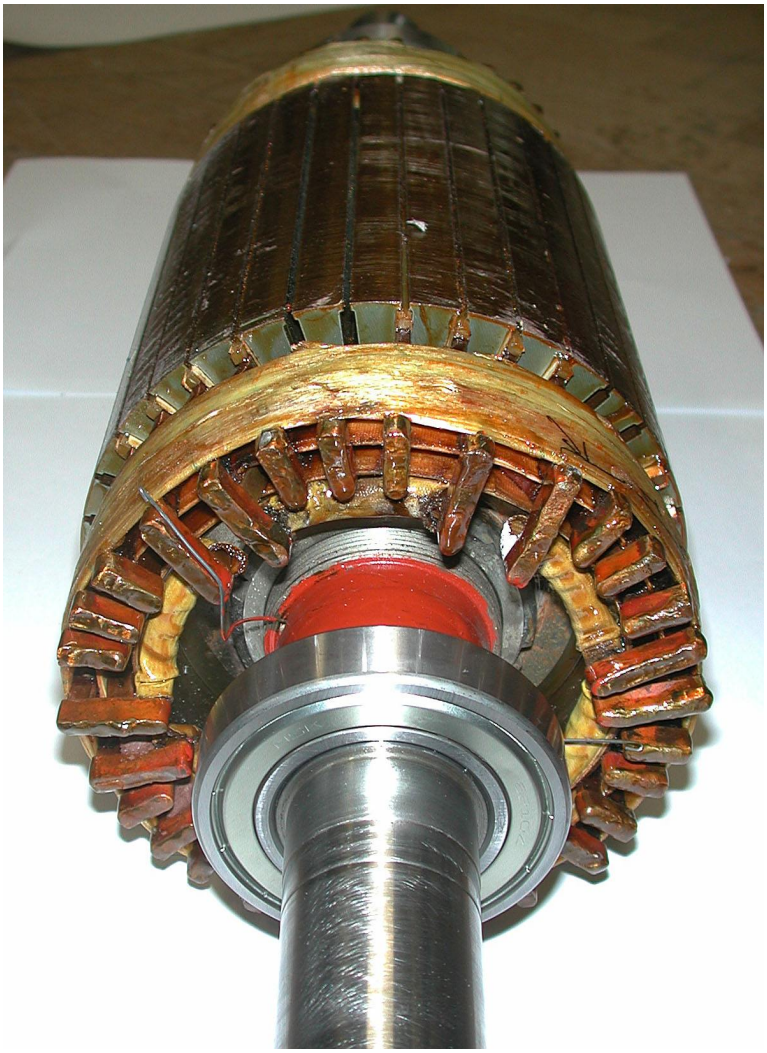

Figure 5.4: Prototype new double-layer design rotor, rotor 2

component; and similarly the 8 pole field induces a predominantly 8 pole current distribution without any 4 pole component. Therefore cross-coupling between the fields cannot take place.

Section B.5 details the design of the rotor, and notes that the rotor is in fact a member of the class of rotors considered in chapter 3. Included in this section is a winding diagram for the machine, and the mutual inductance matrices. The lack of cross-coupling is evident from the rotor-rotor diagonalised machine mutual inductance matrix after the d-q transformation, equation (B.27). From equation (B.27) it is immediate that the dynamics associated with different stator supplies are entirely decoupled. This is consistent with a lack of cross-coupling, which by definition requires coupling between the two stator supplies.

Figure 5.5 shows a photograph of the manufactured prototype rotor.

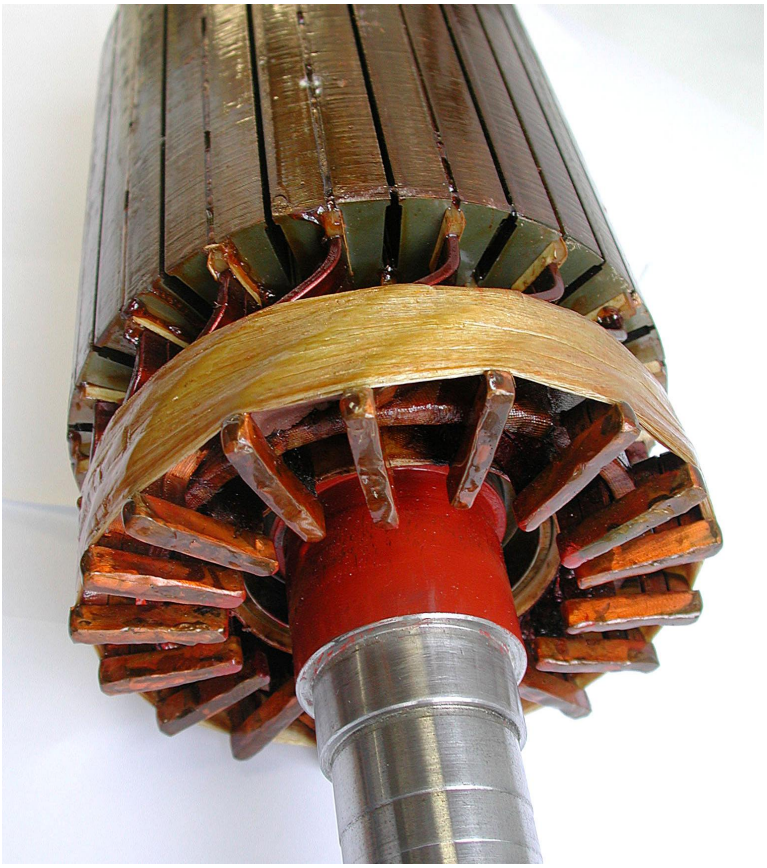

Figure 5.5: Prototype isolated loop design rotor, rotor 3

5.2.4 Rotor 4 - isolated loop rotor with coils removed

As described in the introduction rotor 4 is identical to rotor 3 but with every third loop removed, leaving a total of 12 isolated loops, in 6 groups of 2, where each group is spaced by 40° and each coil within each group spaced by 20° as before.

The removal of one in every three loops is to enforce an order of rotational symmetry of $p_1 + p_2 = 6$. In doing so the rotor is made to cross-couple. This may be understood by considering a cage rotor with $p_1 + p_2$ bars. It is well known that such a rotor will cross-couple between p_1 and p_2 pole pair fields [17, sect. 4.1], and although rotor 4 is not a cage rotor, a similar argument holds.

Full details of the rotor design are given in section B.6. Included in this section are the mutual inductance matrices. The effect of the removal of one in three loops from rotor 3 becomes apparent from the rotor-rotor diagonalised machine mutual inductance matrix after the d-q transformation. Equation (B.27) shows the original rotor with all 18 loops intact. Equation (B.28) shows the mutual inductance matrix for rotor 4. Equation (B.28) clearly shows cross-coupling between the stator supplies, albeit rather weakly in comparison to the direct coupling.

The prototype rotor 4 was made by cutting one in every three bars of rotor 3 with a hacksaw. The

unmodified rotor is shown in figure 5.5.

5.2.5 Rotor 5 - 6 bar squirrel cage rotor design

Rotor 5 is a standard 6 bar squirrel cage rotor. It well known that such a rotor will function as a BDFM rotor, and was the conceptual starting point for Broadway and Burbridge when developing the 'nested-loop' design of rotor [17].

The rotor uses 6 bars of cross-sectional area 4 times that of the bars used in the 'nested-loop' design rotor. Unconventionally, the rotor is assumed to have open slots, of trapezoidal geometry.

It is shown in section B.7 that for the purposes of mutual inductance calculation a cage rotor may be considered to be the same as a set of independent loops spanning the bar pitches. The resistance and leakage inductance matrices do alter and become non-diagonal, although they are still symmetric circulant. Therefore the inductance parameters for rotor 5 may be calculated using the method described in chapter 2 as the rotor is a member of the class of rotors considered.

5.2.6 Rotor 6 - wound rotor design

Rotor 6 consists of identical windings to those on the stator, but short-circuited together with the neutral points connected. As mentioned in the introduction, this rotor is included to illustrate its low harmonic content, but poor copper utilisation, as noted by Hunt [48].

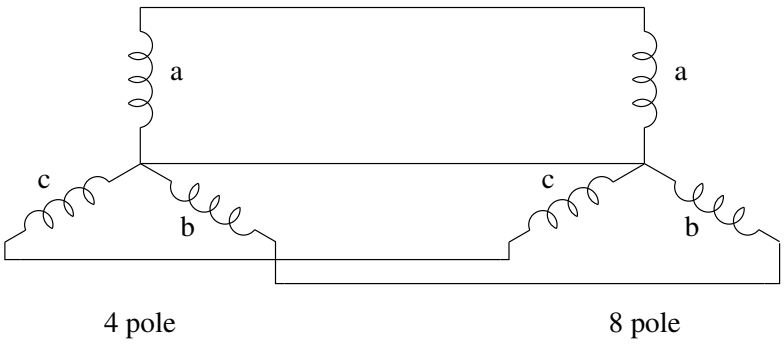

Figure 5.6: Connection diagram for Rotor 6

The rotor does not form part of the class of rotors considered in this dissertation, however it is a simple case to analyse. Figure 5.6 shows the connection of the two 3 phase windings, therefore it is easy to verify that this connection may be represented by the combination matrix (B.35). This combination matrix may be used with the method described in section 2.5.1. It is easily shown that the rotor-rotor mutual inductance and resistance are given by the sum of the individual components and the stator-rotor mutual inductance is the difference between the mutual inductance matrices of the individual rotor windings. Hence it is immediate that rotor 6 will cross-couple both stator fields.

Section B.8 contains full details of the rotor-rotor and stator-rotor inductance terms including the leakage inductance calculation.

5.2.7 Rotor 7 - standard squirrel cage rotor

Rotor 7 is the standard cage rotor used in the induction machine frame used for the prototype BDFM. The rotor is made of cast aluminium, has 40 bars with Boucherot type slots (to give a higher starting resistance due to the skin effect). The rotor slots are closed as can be seen in figure 5.7. The closed nature of the slots complicates the estimation of the leakage inductance, as discussed in section C.1.

This rotor will couple both stator fields, however there will be no cross-coupling for similar reasons to those discussed for rotor 3.

Section B.9 has complete details of the mutual inductance matrices, and the d-q transformation used. The geometry of the rotor does not fall into the class of rotors analysed therefore special treatment is required. It can be shown that the d-q transformation used only removes unobservable/uncontrollable rotor states. Therefore the resulting mutual inductance parameters are a complete description of the machine.

The d-q mutual inductance matrix, (B.45), clearly shows the lack of cross-coupling, as the dynamics due to the stator 1 supply are not coupled to the dynamics from the stator 2 supply.

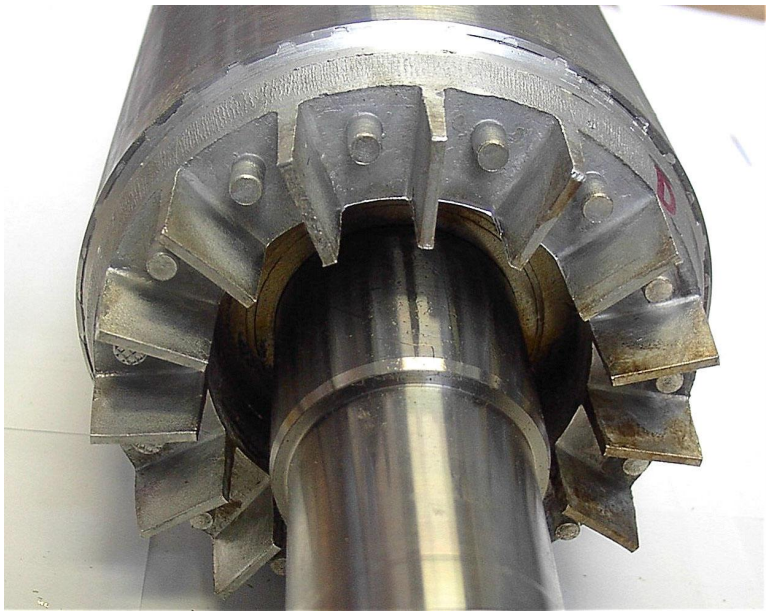

Figure 5.7: Standard squirrel cage rotor 7

5.3 Experimental and Calculated Torque-Speed Curve Results

Of the 5 rotor designs that were manufactured, rotors 1, 2, 3, 4 and 7 were tested using the experimental rig described in appendix E.

As discussed in section 4.6, it is to be expected that simple induction mode and cascade induction mode give a good indication of possible BDFM performance. High torques in simple induction mode suggest poor BDFM performance. The absence of cascade mode torques imply poor BDFM performance. Therefore by determining the simple induction mode and cascade induction mode the rotors may be qualitatively evaluated for BDFM performance, that is presence of significant BDFM synchronous mode torque.

The experiments were done at nominally $90\mathrm{V_{rms}}$ (phase). This voltage was supplied from a 25A 'Variac' variable transformer, and was therefore at nominally 50 Hz. The supply, therefore, has some impedance, although the current was generally low enough so that the supply dip was less than 1%. The operating point was set in each case by driving the DC load motor on the rig to the required speed, and then measuring the torque.

The experimental data is overlaid with the same test done in simulation calculated using the equivalent circuit 4.3, with the parameter values calculated as described. In each case the resistance parameters were increased by 40% from their measured DC values (and calculated values in the case of the rotor) to allow for heating effects.

Figures 5.8 and 5.9 show 4 and 8 pole simple induction mode (second stator open circuit) torque-speed curves respectively. Figures 5.10 and 5.11 show 4 and 8 pole cascade induction mode (second stator short-circuited) torque-speed curves.

5.4 Calculated Rotor Parameters

Using the tools developed in chapters 2, 3, and 4 the parameters for the machines which showed good BDFM performance were calculated. The parameter values correspond to figure 4.3. The intermediate states in the transformations are shown in appendix B. Table 5.1 shows the calculated values.

Table 5.2 compares the parameter values of table 5.1 in a number of ways. As discussed in section 4.6 the parasitic rotor impedance terms, X_{r_h}, X_{r_l}, R_r/s_1 directly affect the available synchronous torque envelope for a BDFM. We therefore define the following dimensionless measures of BDFM performance:

$$\frac{|X_{r_h}|}{|X_{r_1}+X_{r_2}|}, \qquad \frac{|X_{r_l}|}{|X_{r_1}+X_{r_2}|}, \qquad \frac{|R_r/s_1|}{|X_{r_1}+X_{r_2}|} \tag{5.4}$$

It is chosen to normalise the measures by $|X_{r_1}+X_{r_2}|$ as this term represents the total non-parasitic term of the rotor impedance. It is this term which couples, without leakage, to the stator, and the changes in value of this term simply reflect different effective turns ratios between rotor and stator.

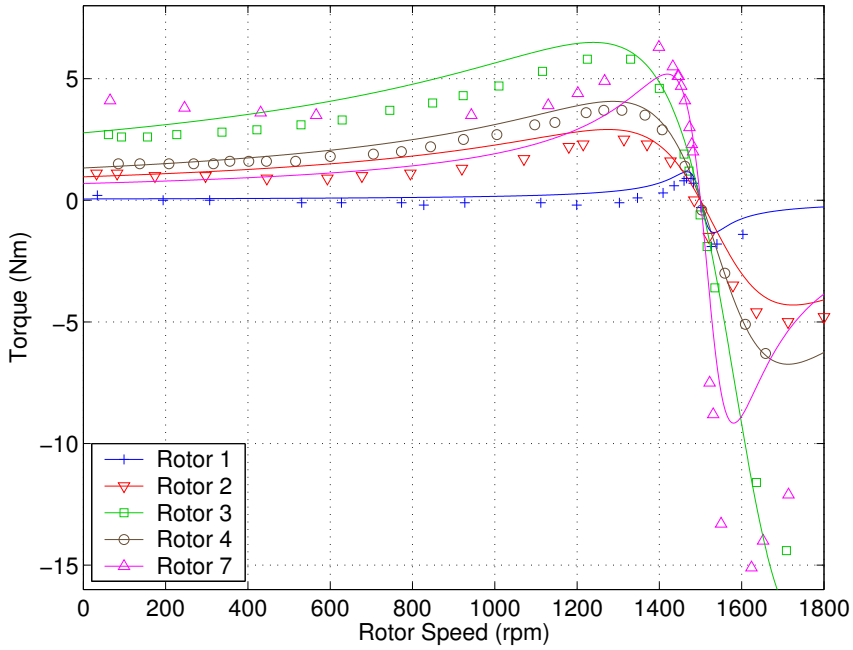

Figure 5.8: Torque-Speed plot in simple induction mode with nominally 90V_{rms} phase supply voltage to 4 pole winding, 8 pole winding open circuit, rotors as described in section 5.1. Experimental results with calculated results superimposed.

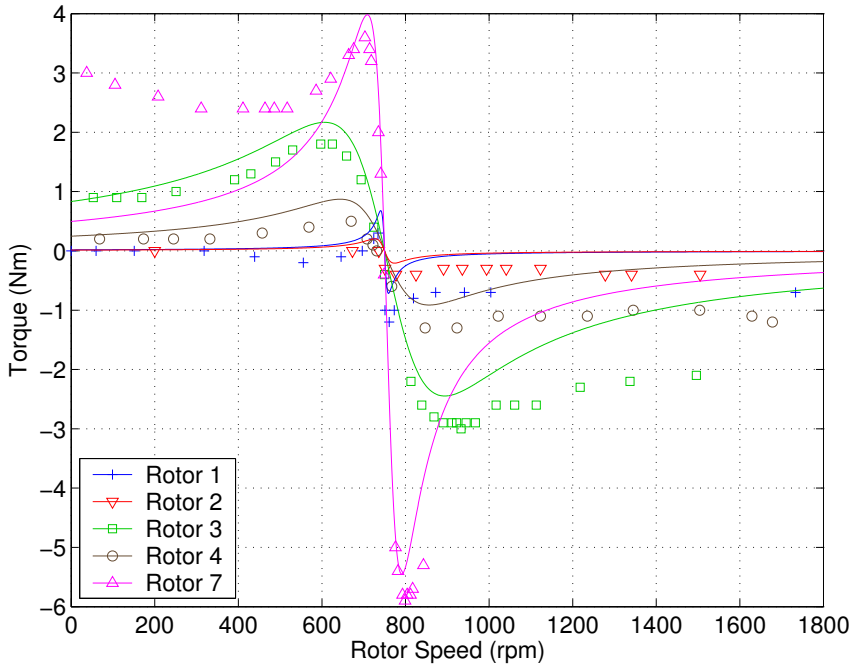

Figure 5.9: Torque-Speed plot in simple induction mode with nominally 90V_{rms} phase supply voltage to 8 pole winding, 4 pole winding open circuit, rotors as described in section 5.1. Experimental results with calculated results superimposed.

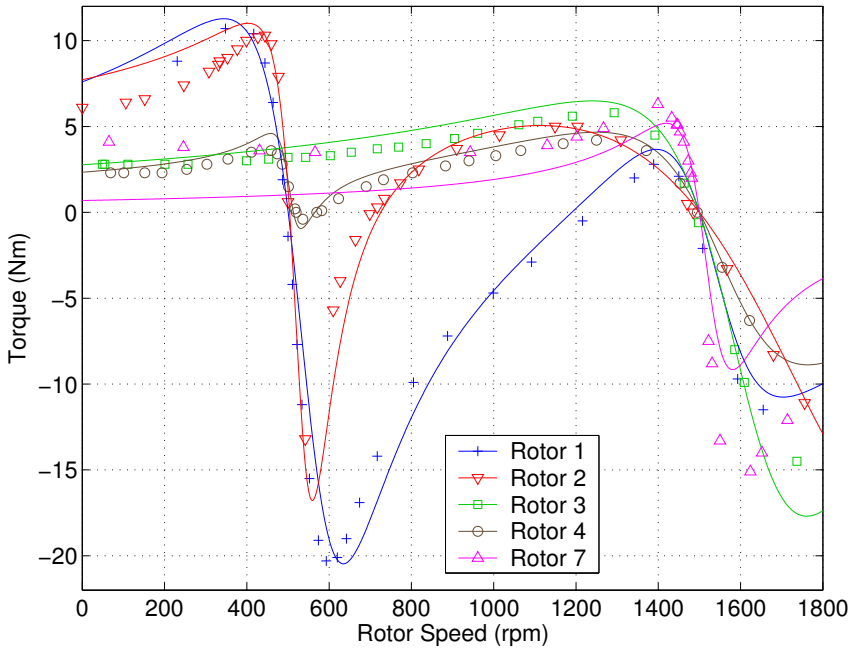

Figure 5.10: Torque-Speed plot in cascade induction mode with nominally 90V_{rms} phase supply voltage to 4 pole winding, 8 pole winding in short circuit, rotors as described in section 5.1. Experimental results with calculated results superimposed.

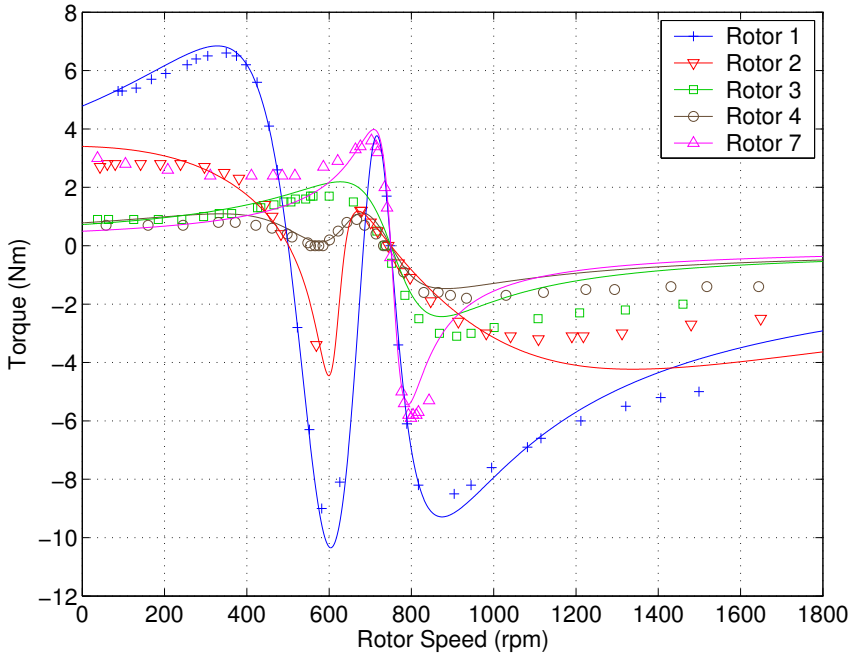

Figure 5.11: Torque-Speed plot in cascade induction mode with nominally 90V_{rms} phase supply voltage to 8 pole winding, 4 pole winding in short circuit, rotors as described in section 5.1. Experimental results with calculated results superimposed.

R_1 (Ω)	L_{1_l} (mH)	L_{1_f} (mH)	$\lvert M_{c_{s1r}}\rvert$ (mH)	L_{r_1} (μH)	L_{r_h} (μH)	L_{r_l} (μH)	R_r (mΩ)	L_{r_2} (μH)	$\lvert M_{c_{s2r}}\rvert$ (mH)	L_{2_f} (mH)	L_{2_l} (mH)	R_2 (Ω)
Rotor 1: nested-loop design												
2.7	3.54	307	2.7	24.1	0.98	1.06	0.074	13	2	314	8	4.4
Rotor 2: new double-layer rotor design												
2.7	3.63	313	9.6	293	5.3	8.82	1.9	44	3.7	321	8.4	4.4
Rotor 5: 6 bar squirrel cage rotor design												
2.7	3.08	339	2.8	23	3.5	0.888	0.028	5.7	1.4	347	6.2	4.4
Rotor 6: Wound rotor design												
2.7	3.32	287	2.9	28.6	0.46	1.02	35	29	2.9	294	7.1	4.4

Table 5.1: Calculated parameter values for different BDFM rotor using coupled circuit approach described in chapters 2, 3, and 4, corresponding to figure 4.4

The final column of table 5.2 shows the total cross-section conductor area in the machine stack (therefore end windings are not included). For example, Rotor 1 has 133mm^2 bar area and 36 bars in total hence the total cross-sectional area of copper is 4774mm^2

5.5 Discussion of Results

5.5.1 Experimental Torque-Speed Curves

- The simulated torque-speed curves give generally good agreement with those found by experiment.

  In figure 5.8 rotors 1-4 show good agreement. In figure 5.9 rotors 1-4 show reasonable agreement. The errors, although proportionally large, are less than 1 N m in all except rotor 3. This is well within the measurement error of the torque transducer, which drifts by around 0.5 N m over the course of an experiment, and the frictional forces on the BDFM, which are up to 0.8 N m. Figures 5.10 and 5.11 also show good agreement for rotors 1-4. The exceptions being rotor 2 at low speeds in 4 pole cascade mode, and 8 pole cascade mode at higher speeds; and rotor 3 at higher speeds in 8 pole cascade. The most probable cause for these errors are inaccurate resistance values.

  Rotor 7 gave consistently less good agreement, particularly in 8 pole mode. The poor agreement at large slips (positive and negative) is due to the Boucherot slots, which are deep slots which rely on the skin effect to increase the effective resistance at large slips where the frequencies of the currents in the rotor are higher. It is therefore expected that the simulated results give

$\lvert X_{r_1}+X_{r_2}\rvert$ (mΩ)	$\lvert X_{r_1}\rvert$ (%)	$\lvert X_{r_2}\rvert$ (%)	$\lvert X_{r_l}\rvert$ (%)	$\lvert X_{r_h}\rvert$ (%)	$\lvert X_{r_l}+X_{r_h}\rvert$ (%)	$\lvert R_r/s_1\rvert$ (%)	$\lvert Z_{r_p}\rvert$ (%)	A_{Cu} (mm^2)
Rotor 1: nested-loop design								
11.6	65.5	34.5	2.9	2.7	5.5	1.9	5.9	4774
Rotor 2: new double-layer rotor design								
106	86.9	13.1	2.6	1.6	4.2	5.4	6.8	1235
Rotor 5: 6 bar squirrel cage rotor design								
9.03	80.1	19.9	3.1	12	15	0.92	15	3182
Rotor 6: Wound rotor design								
18.1	49.6	50.4	1.8	0.8	2.6	585	585	6514

Table 5.2: A comparison of calculated parameter values of table 5.1 expressed as a percentage of $|X_{r_1}+X_{r_2}|$, the rotor fundamental reactances at 50 Hz. The slip, s_1, is assumed to be 0.33, which corresponds to 1000rpm when stator 1 (4 pole) is grid-connected. $|Z_{r_p}| = \frac{\sqrt{(R_r/s_1)^2+(X_{r_l}+X_{r_h})^2}}{|X_{r_1}+X_{r_2}|}$

lower (closer to zero) torques at large slips. However the 4 pole results at small slips are still fairly inconsistent. This is due to the crude estimate of rotor leakage inductance used. The simulated results could be made to coincide much more closely by adjusting the value of leakage inductance used.

- Simple induction mode:
  - All the rotors exhibited some simple induction mode torque, in both 4 and 8 pole modes.
  - For 4 pole simple induction torque: Rotors 7 and 3 gave the largest peak values, rotor 4 a little less, rotor 2 even less and rotor 1 the least. This is to be expected, as rotors 7 and 3 fail to cross-couple but both couple 4 pole fields strongly. Rotor 4 gives somewhat less torque than rotor 3 which is consistent with it producing weak cross-coupling due to the removal of one set of windings. Rotors 1 and 2 exhibit strong cross coupling hence the smaller torques.
  - For 8 pole simple induction torque: Rotors 7 and 3 gave the largest peak values, rotor 4 a little less, rotor 1 even less and rotor 2 the least. For similar reasons to the 4 pole test the results for rotors 7, 3 and 4 are as expected. The very small torque produced by rotor 2 is a reflection of its relatively poor 8 pole coupling combined with its relatively strong cross-coupling. In contrast, the performance of rotor 1 is similar in both 4 pole and 8 pole simple induction mode.

  - The differing magnitudes of the 4 and 8 pole simple mode results for rotor 7 reflect the differing stator impedances for the two supply windings.

- Cascade induction mode:

  - Rotors 3 and 7 showed no noticeable cascade torque. The torque-speed curves are essentially the same as those obtained in simple induction mode. This confirms the absence of cross coupling in these rotor designs.
  - Rotors 1 and 2 showed strong cascade torque and rotor 4 showed weak cascade torque. Rotors 1 and 2 both exhibit significant cross-coupling, therefore it is expected that the cascade mode torque is relatively large. Rotor 4 only produced weak cascade action because its cross-coupling is also weak.
  - As discussed in section 4.6 the cascade torque-speed curve consists of an induction machine-like torque-speed characteristic at 500rpm (cascade synchronous speed for $p_1 = 2,\ p_2 = 4$ at 50 Hz) superimposed on top of the standard machine torque-speed curve.
  - The amplitude of the cascade mode torque-speed characteristic is similar in magnitude to the standard torque-speed characteristic at the machine synchronous speed. This is to be expected as cascade mode in effect lowers the impedance of the rotor as the second stator resistance and leakage inductance appear in parallel with the second stator magnetizing inductance, see figure 4.9.

5.5.2 Calculated machine parameters from tables 5.1 and 5.2

- In consideration of the rotor resistance term, it is desirable to minimise this term as far as possible as it directly impacts the efficiency of the machine. It is immediately apparent that rotor 6 suffers from its large relative rotor resistance, which is particularly bad as this rotor has the largest amount of copper of all the rotor designs. This confirms the point made by Hunt that having a rotor design comprising of two three phase windings is wasteful of copper [48]. Rotor 2 has a relatively large resistance, however it suffers from having a relatively low amount of copper in the design, as compared to 1. This was simply a consequence of manufacturing a prototype rotor with a standard slot shape, and could therefore easily be overcome. If rotor 2 had the same cross-sectional area of copper as that of rotor 1, then the resistance would drop to 1.4%. Rotor 5 has the least resistance percentage, and rotor 1 somewhat higher, but still quite acceptable.

- The values of percentage leakage reactance on the four rotors are similar. The slightly lower value for Rotor 6 is not significant.

- In contrast to the leakage reactance, the values of excessive rotor harmonic reactance differs greatly between the 4 rotor designs. Rotor 6 has the least percentage value of excess harmonic reactance of the four rotors. This is expected as this rotor has the lowest realistic value for any machine of this frame size, as the rotor is comprised to two double layer windings which therefore have a low harmonic content. Rotor 5 has 12% excess harmonic reactance which is over 4 times the next highest value of 2.7% in rotor 1. This relatively high value of excess harmonic reactance confirms the prediction in Broadway and Burbridge that a 6 bar cage rotor suffers from excessive harmonic inductance [17, sect. 4.1]. Rotor 2 achieves a significantly lower value than rotor 1, demonstrating that the better choice of coil pitch has achieved the desired effect of reducing the harmonic content. It is desirable to minimise the value of the excess leakage reactance percentage, not only to increase the available torque but also because it represents some of the generated harmonic magnetic flux densities in the air gap.

5.6 Conclusion

In this chapter seven rotor designs have been considered including a new potential BDFM rotor design. Five of these rotor designs were manufactured and torque-speed curves were measured for 4 different operating modes. From these tests it is clear which rotors will cross-couple and, therefore, are potential BDFM rotors, as predicted from analysis of the equivalent circuit in section 4.6. The use of simple and cascade mode tests to qualitatively test potential BDFM rotors is therefore confirmed.

The experiments were complemented by simulation results obtained using the equivalent circuit model and method of parameter calculation previously derived. The agreement between measured and predicted results was within expected experimental errors and the limitations of the model. Therefore it is possible to have confidence in the modelling and parameter calculation methods described in chapter 2, 3, and 4.

The four rotors which show strong cross-coupling, rotors 1, 2, 5 and 6 were analysed by calculation of their equivalent circuit parameters.

Rotors 1 and 2 are both plausible BDFM rotors if the cross-sectional area of copper in each slot is increased in rotor 2. Rotor 2 should lead to a rotor with a larger torque envelope, and greater efficiency than rotor 1 which has twice the percentage excess harmonic reactance.

Rotor 5 might possibly be considered as a BDFM rotor as it will have low copper losses, however its excessive harmonic reactance is very high, as expected, and this will not only limit the available torque but also introduce unwanted magnetic flux density harmonics. Rotor 6 will not make a good BDFM rotor due to its excessive resistance.

The rotors were evaluated by three measures. Of these measures, the ones providing the most differentiation between rotors were $\frac{|X_{r_h}|}{|X_{r_1}+X_{r_2}|}$ and $\frac{|R_r/s_1|}{|X_{r_1}+X_{r_2}|}$, taking into consideration the area of copper in each rotor. In terms of their effect on $|Z_{r_p}|$ the excess harmonic reactance percentage is the more

significant, as in a typical good rotor design (e.g. rotor 1) $|Z_{r_p}|$ is dominated by the reactive parts. Therefore both the excess harmonic reactance and leakage reactance are crucial parameters in the design of BDFM rotors. The slot shape is the main controlling factor for the leakage reactance, so this should be designed to ensure minimum leakage. The design of the rotor geometry (which determines the rotor harmonic content) may, therefore, be evaluated using the percentage excess harmonic reactance. However the reduction of the excess harmonic reactance must be weighed up against any penalty in terms of rotor resistance. Rotor 6 illustrates the lowest realistic percentage harmonic leakage reactance, however the penalty of increased rotor resistance is too great to make the design viable. Rotor 2 achieves a significant reduction in percentage harmonic leakage reactance (over rotor 1), with no such resistance penalty.

Therefore, as rotor designs other than the nested-loop design achieve an improved BDFM performance, the issue of rotor design is worth further investigation. The measures proposed may be used by the designer to evaluate proposed rotor designs.

There are, however, limitations to the proposed methods of rotor evaluation. The most significant are restrictions imposed by the design of the iron circuit in the machine. Designs aimed at the reduction of leakage reactance may not be feasible as they will lead to either excess iron loss, poor power factor or both. Furthermore the skin effect has been entirely neglected in this analysis. The skin effect will increase the rotor resistance. This will not only have a direct effect on the efficiency of the machine, but will also impact the value of $|Z_{r_p}|$.

Chapter 6

BDFM Parameter Identification

6.1 Introduction

In chapter 2 a method of calculating machine parameters was presented. In chapters 2, 3, and 4 different models were developed for the BDFM, and the transformations between these models derived, thus allowing parameter values for these models to be computed using the method described in chapter 2. These models included different equivalent circuit representations for the BDFM. Chapter 5 showed experimental torque-speed curves for five rotor designs using calculated parameter values. Although the agreement was reasonable, and well within the limitations of the instrumentation and the parameter calculation methods, there is a need for a method of experimentally determining parameters for the machine which leads to models giving closer agreement with experimental data.

Only two previous works are known which consider the problem of parameter estimation for the BDFM, [80, 79]. These works use a frequency domain method to find d-q parameters for a prototype nested-loop design machine. The methods are presented in some detail in simulation, and some (but not all) parameters are estimated from a prototype machine in [79].

Although the method proposed in [80, 79] appears to generalise to a wider class of BDFM machines, a significant amount of equipment is needed to implement such a scheme: 10 kHz multi-channel isolated A/D, closed-loop external speed control for the test rig, variable frequency current source supply for the BDFM [79].

A simple method of parameter estimation is therefore proposed. The method is based on curve fitting torque-speed curves from both simple and cascade induction mode tests. This is a natural generalisation of the standard no-load and locked rotor tests commonly used to estimate parameters in standard induction machines.

The standard no-load test can be used to determine the stator resistance and magnetizing reactance, and if the series stator resistance is measured with DC, then the core loss resistance term can be estimated. The standard locked-rotor can estimate the rotor impedance; it works by assuming that the magnetizing reactance is very much larger than the referred series rotor impedance, which appears

in parallel with the magnetizing reactance (and the core loss resistance). As discussed in section 4.6, the BDFM can operate as a normal induction machine, in simple induction mode, and the no-load test can be applied to get information for both stator supplies. However, as discussed in section 4.6, and confirmed in section 5.5, good BDFM designs will generally have very high referred rotor impedance in simple induction mode, therefore the locked rotor test will not be directly applicable. Although it would be possible to perform the locked rotor test, taking into account the magnetizing reactance, the actual rotor leakage reactances would be prone to large errors as they appear in series with the second stator magnetizing reactance.

Even with the normal induction machine, the standard locked-rotor and no load tests are known to give parameters which lead to models which have significant errors away from the operating points at which the parameters were determined [111]. This problem motivated a number of papers where output error minimization methods were successfully used [29, 66, 78]. As the BDFM is similar to the standard induction machine, approaches of this nature should lead to acceptable results. It should be noted that all the methods considered are off-line methods, which require a special experiment to be performed on the machine in order to determine the parameter values. This is somewhat distinct from on-line methods where no explicit experiment is performed, and parameters are estimated during normal machine operation. There have been efforts to address this (rather more difficult) problem for the induction machine, a recent example is [23].

We begin by describing a new optimization method.

6.2 Parameter Extraction Optimization Method

6.2.1 General Optimization Problem

The optimisation problem to be solved is a non-linear least squares problem, and can be stated as:

Given $Y_i \in \mathbb{R}^k$, $P \in \mathbb{R}^n$, $U \in \mathbb{R}^{k\times m}$, $F_i : P, U \mapsto \mathbb{R}^k$, $i \leq l$

$$\text{Find} \quad P : \min_{P \in W\mathbb{B}+P_0} \sum_{i=1}^{l} S_i \|Y_i - F_i(P,U)\|_2 \tag{6.1}$$

where F_i is a function which estimates the i^{th} measured output for a particular parameter vector, P. U is a matrix of input data points where each row is an individual data point. Y_i is a vector of the measured i^{th} output data due to U. There are k input/output data pairs and m different measured inputs (i.e. U has k rows and m columns). S_i is a scalar weight applied to the i^{th} output error. So there are n parameters, m inputs, k data points for each input, and l outputs. Furthermore, F_i is defined as:

$$F_i(P,U) = \begin{bmatrix} f_i(P,u_1) \\ \vdots \\ f_i(P,u_k) \end{bmatrix}, \qquad U = \begin{bmatrix} u_1 \\ \vdots \\ u_k \end{bmatrix} \tag{6.2}$$

where $f_i : P, u_j \mapsto \mathbb{R}^1$.

$W\mathbb{B} + P_0$ represents the set of possible parameter values chosen from a rectangular set (as $\mathbb{B}$ is a hypercube), centred on P_0 with corners at $P_0 \pm \text{diag}(W)$. Clearly the value of P that gives the minimum cost function value will, in general, not be unique. As stated this is a non-convex optimization problem, and therefore difficult to solve [123].

In order to solve this optimisation problem we use a simple (or crude) random search (also known as a 'Monte Carlo' method). For practical and theoretical details of the algorithm see, for example, [123]. The principal advantage of a simple random search, for our purposes, is its strong resilience to measurement noise and modelling error while guaranteeing convergence to the global minimum. Furthermore, because it requires no gradient information, there is no need for any a priori information about the particular cost function. It can be shown that without any such information, a simple random search is as efficient as any other method, in reaching the global minimum [44]. The simplicity of the algorithm means that implementation is straightforward and, because the method does not depend on the cost function chosen, the algorithm can be applied to different cost functions without modification.

The search is performed across $W\mathbb{B} + P_0$ to find $Q = \{q_1, \cdots, q_N\}$ where $Q : \sum_{i=1}^{m} S_i \|Y_i - F_i(q, U)\|_2 \leq \gamma$, where $\gamma > 0$ is an acceptable value for the cost function to take. We generate guesses for candidate q_ks using the Mersenne Twister [71], a fast uniform random number generator with a long repetition period. Having found Q we then find the, q_k corresponding to the minimum cost, $K_{\min}$. This q_k, called q_{opt} henceforth is an estimate of the global minimizer and $K_{\min}$ an estimation of the global minimum. Furthermore the standard deviation of Q gives an indication of how much confidence one should have in taking q_{opt} as the global minimum.

Although the efficiency could be increased by using a multi-start, (see [123] for details) or probabilistic branch and bound algorithm (such as [106]), the additional complexity of the algorithm, and requirements to have some appreciation of the modelling error and noise, make these algorithms less appealing than they might first appear. Furthermore there is a tradeoff between increased complexity in the algorithm versus the decreased number of iterations required.

6.2.2 Application to BDFM

Notice that thus far it has not been necessary to specify *what* the measured outputs Y are, or either what the estimation functions F are.

We desire to choose the inputs and output such that they are easy to measure 'terminal' quantities. Therefore we are restricted to the stator voltages, currents, the torque and the rotor speed. Furthermore due to the substantial difficulty of trying to measure the phase difference between stator 1 and stator 2 quantities we restrict ourselves to magnitude measurements of stator 2 quantities.

Having decided what quantities to measure, it is necessary to consider what parameters are sought, and determine whether or not finding the parameters uniquely is feasible. The problem of whether or nor the parameters may be determined uniquely from any set of experiments is known as 'identifia-

bility'.

Recognising that the equivalent circuit can predict the behaviour of the machine in both simple induction and cascade modes, we propose then an approach based on the extraction of parameters from measured torque-speed characteristics of the kind shown in figures 5.8-5.11. This approach has the advantage that a single frequency supply may be used to perform the tests. This is in contrast to the only previously published works on BDFM parameter extraction, [80, 79], where a method requiring operation at a range of different supply frequencies is proposed.

Nevertheless, not all the inductance terms in the equivalent circuit shown in figure 4.9 can be unambiguously determined from external measurements. Figure 6.1 shows equivalent forms of the 'T' and 'Γ' networks, details can be derived using, for example, [20].

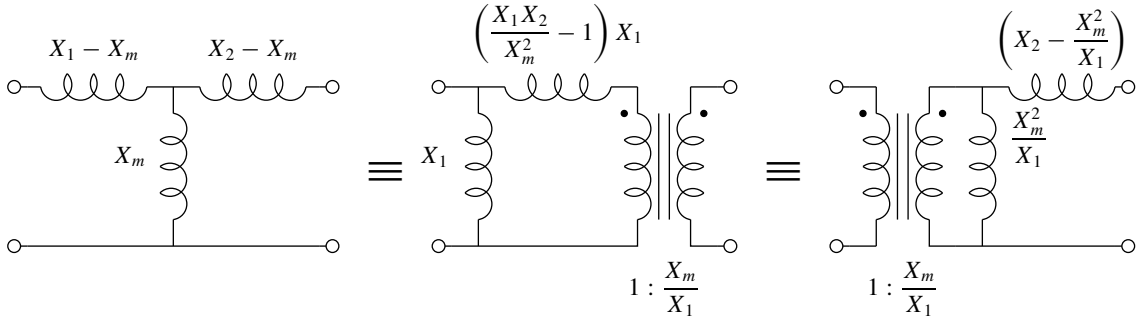

Figure 6.1: Equivalent forms of 'T' and 'Γ' networks

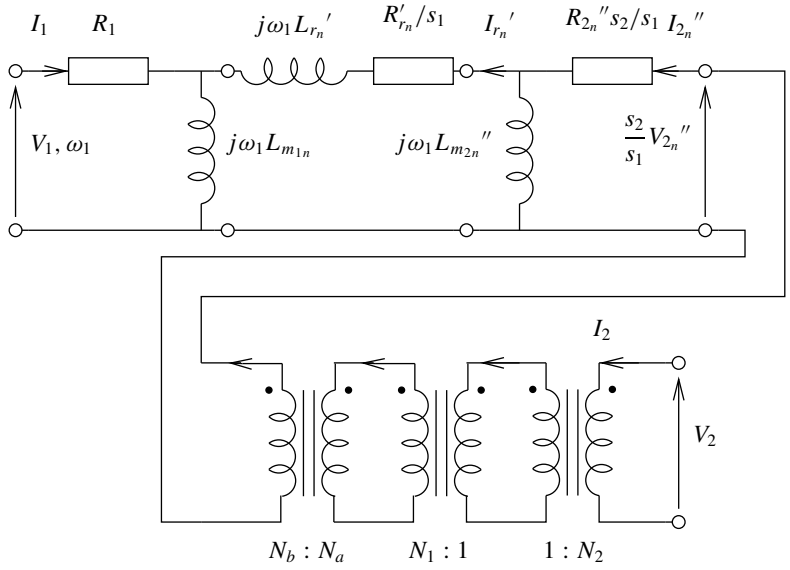

Figure 6.2: Simplified Referred Per-Phase Equivalent Circuit

Using figure 6.1, figure 4.9 may be transformed into an alternative form of the equivalent circuit as shown in fig. 6.2 for which all component values can be determined from the estimation procedure, as the number parameter has reduced. A similar modification was proposed by Slemon in the case

of parameter determination for the equivalent circuit for the standard induction motor [98]. For the circuit to be electrically equivalent to that of fig. 4.9 the parameters, and turns ratios, will assume slightly different values:

$$\begin{aligned} N_a &= \frac{L_{m_1}}{L_1 + L_{m_1}} & N_b &= \frac{L''_{m_2}}{L''_2 + L''_{m_2}} \\ R'_{r_n} &= \frac{R'_r}{N_a^2} & L_{m_{1_n}} &= L_{m_1} + L_1 \\ L''_{m_{2_n}} &= L''_{m_2}\frac{N_b}{N_a^2} & R''_{2_n} &= R''_2\frac{N_b^2}{N_a^2} \\ L'_{r_n} &= \frac{L'_r + L_{m_1}}{N_a^2} - L_{m_{1_n}} + \frac{L''_{m_2}}{N_a^2} - L''_{m_{2_n}} \end{aligned} \tag{6.3}$$

However, in a BDFM the referred series rotor inductance is likely to be larger than the series stator inductance so differences in inductance values between the two circuits will be small. Direct measurements of rotor bar currents, for example using techniques described in [1, 83], would enable all parameters in fig. 4.9 to be determined.

In simple induction mode operation there are 2 inputs, 3 measured outputs, 4 parameters, and N_s data points. The subscript simple/1 is used to indicate simple induction mode referred to stator 1. Y is chosen as follows:

$$Y_{\text{simple/1}_1} = \begin{bmatrix} T_1 \\ \vdots \\ T_k \end{bmatrix}, \qquad Y_{\text{simple/1}_2} = \begin{bmatrix} \Re\{I_{11}\} \\ \vdots \\ \Re\{I_{1k}\} \end{bmatrix} \tag{6.4}$$

$$Y_{\text{simple/1}_3} = \begin{bmatrix} \Im\{I_{11}\} \\ \vdots \\ \Im\{I_{1k}\} \end{bmatrix}, \qquad U_{\text{simple/1}} = \begin{bmatrix} \omega_{r1} & V_{11} \\ \vdots & \vdots \\ \omega_{rk} & V_{1k} \end{bmatrix} \tag{6.5}$$

$$P_{\text{simple/1}} = \begin{bmatrix} R_1 \\ R'_r \\ L'_r + L''_{m_2} \\ L_{m_1} \end{bmatrix} \tag{6.6}$$

$F_{\text{simple/1}_i}$ can be derived from the referred equivalent circuit, figure 6.2, taking $I''_2 = 0$:

$$T = f_{\text{simple/1}_1}(P_{\text{simple/1}}, u_{\text{simple/1}}) \tag{6.7}$$

$$\Re\{I_1\} = f_{\text{simple/1}_2}(P_{\text{simple/1}}, u_{\text{simple/1}}) \tag{6.8}$$

$$\Im\{I_1\} = f_{\text{simple/1}_3}(P_{\text{simple/1}}, u_{\text{simple/1}}) \tag{6.9}$$

If $U_{\text{simple/1}_1}$ is chosen so that the BDFM is exercised over a range of speeds such that the slip (4.32) varies substantially, say from 1 to -0.5, it can be shown from the equivalent circuit that each $f_{\text{simple/1}_i}$ depends strongly on each element of $P_{\text{simple/1}}$, which suggests that there is a unique $P_{\text{simple/1}}$ which solves the optimization problem. However due to the presence of measurement noise and modelling error this will not necessarily be the case. Solving this optimization problem as outlined in section 6.2.1 gives the parameters indicated in (6.6).

However we have not used $|V_2|$ as one of the measurable outputs. It can be seen from figure 6.2, with $V_2'' = V_2 \frac{N_1}{N_2}$ (from figure 4.9):

$$|V_2|\frac{N_1}{N_2} = |I_r'\omega_1|L_{m_2} \tag{6.10}$$

and the ratio of the turns ratios, $\frac{N_1}{N_2}$ is unknown. Therefore all that can be achieved is the determination of $\frac{N_2}{N_1}L_{m_2}$. It is proposed therefore that, having determined the optimal parameter set, linear least-squares is used to determine $\frac{N_2}{N_1}L_{m_2}$:

$$\frac{N_2}{N_1}L_{m_2} = (A^TA)^{-1}A^T\begin{bmatrix}|V_{21}|\\ \vdots \\ |V_{2k}|\end{bmatrix}, \quad A = \begin{bmatrix}|I_{r1}'\omega_{11}|\\ \vdots \\ |I_{rk}'\omega_{1k}|\end{bmatrix}$$

and $|I_{rj}'|$ are calculated from figure 6.2 using the optimal parameter set.

In *cascade induction* mode operation there are 2 inputs, 4 measured outputs, 6 parameters, and N_c data points. The subscript cascade/1 is used to indicate simple induction mode referred to stator 1. Y is chosen as follows:

$$Y_{\text{cascade/1}_1} = \begin{bmatrix}T_1\\ \vdots \\ T_k\end{bmatrix}, \qquad Y_{\text{cascade/1}_2} = \begin{bmatrix}\Re\{I_{11}\}\\ \vdots \\ \Re\{I_{1k}\}\end{bmatrix} \tag{6.11}$$

$$Y_{\text{cascade/1}_3} = \begin{bmatrix}\Im\{I_{11}\}\\ \vdots \\ \Im\{I_{1k}\}\end{bmatrix}, \qquad Y_{\text{cascade/1}_4} = \begin{bmatrix}|I_{21}|\\ \vdots \\ |I_{2k}|\end{bmatrix} \tag{6.12}$$

$$U_{\text{cascade/1}} = \begin{bmatrix}\omega_{r1} & V_{11}\\ \vdots & \vdots \\ \omega_{rk} & V_{1k}\end{bmatrix}, \qquad P_{\text{cascade/1}} = \begin{bmatrix}R_1\\ R_r'\\ L_r'\\ L_{m_1}'\\ R_2''\\ \frac{N_1}{N_2}\end{bmatrix} \tag{6.13}$$

$F_{\text{simple/1}_i}$ can be derived from the referred equivalent circuit, figure 6.2, taking $V_2'' = 0$:

$$T = f_{\text{simple/1}_1}(P_{\text{simple/1}}, u_{\text{simple/1}}) \tag{6.14}$$

$$\Re\{I_1\} = f_{\text{simple/1}_2}(P_{\text{simple/1}}, u_{\text{simple/1}}) \tag{6.15}$$

$$\Im\{I_1\} = f_{\text{simple/1}_3}(P_{\text{simple/1}}, u_{\text{simple/1}}) \tag{6.16}$$

$$|I_2| = f_{\text{simple/1}_4}(P_{\text{simple/1}}, u_{\text{simple/1}}) \tag{6.17}$$

As for the simple mode $U_{\text{cascade/1}_1}$ is chosen so that the BDFM is exercised over a range of speeds such that the slip (4.32) varies substantially. It can be shown from the equivalent circuit that each $f_{\text{cascade/1}_i}$ depends strongly on each element of $P_{\text{cascade/1}}$. However $f_{\text{cascade/1}_i}$ also depends on L_2, and it is not possible to determine this from the measured outputs. Therefore the value extracted from the simple/2 is used, and is explicitly included in $f_{\text{cascade/1}_i}$. In these circumstances there is a unique $P_{\text{cascade/1}}$ which solves the optimization problem, with the same caveat regarding noise and measurement error as in the simple mode procedure. Again the optimization problem is solved as outlined in section 6.2.1 giving the parameters indicated in (6.13).

Although the original problem contained S_i, a weight, it is set to unity without exception for the applications described. The choice of weight can improve the algorithm by compensating for different scaling of the measured outputs, for example if $|V_2|$ had been included as a measured output then it would have been appropriate to scale down the effect of the error on this measurement as it is typically 2 orders of magnitude larger than the other measured outputs.

6.3 Parameter Estimation Results

The method was applied to data similar to that shown in figures 5.8-5.11. Each data set had between 10 and 20 data points. When solving the optimization problem, in order to minimise the execution time of each random test point the mathematical functions governing the behaviour of the machine were simplified as far as possible using the symbolic maths package Maple, and then hard coded in a C function along with the random number generation code. This function was then called from Matlab. With this implementation it was possible to achieve 4×10^5 tests per second on a 2.8GHz Pentium 4 in cascade mode, and slightly more in simple mode.

As an indication of the time taken to solve the optimization to satisfactory accuracy, it took approximately 9×10^8 tests, taking around 40 minutes, to generate 10 candidate solutions of suitable accuracy for rotor 1. Tables 6.1, 6.2 show data from simple induction mode and tables 6.3 and 6.4 from cascade induction mode. The tables show the results of the optimization, along with the standard deviation taken over the best 20 results. The standard deviations are generally considerably smaller than the estimated parameter values, which indicates that the noise level in the measurements is sufficiently low to have confidence in the results, and that the parameters can be uniquely determined. As

	R_1 (Ω)	R'_{r_n} (Ω)	$L'_{r_n} + L''_{m2_n}$ (mH)	L_{m1_n} (mH)	$L''_{m2_n}\frac{N_2}{N_1}$ (mH)
Rotor 1: nested-loop rotor design					
Opt:	4.02	1.2	120	240	137
Std. Dev.:	0.0243	0.00769	0.204	0.0507	0.00879
Rotor 2: new double-layer rotor design					
Opt:	3.52	3.1	65.5	260	105
Std. Dev.:	0.0384	0.0306	0.246	4.44	0.547
Rotor 3: isolated loop rotor design					
Opt:	3.28	1.36	26.1	252	5.46
Std. Dev.:	0.0548	0.00627	0.199	5.19	0.00855
Rotor 4: isolated loop rotor design with removed loops					
Opt:	3.75	2.12	48.2	240	41.1
Std. Dev.:	0.112	0.0553	0.509	11.9	0.276
Rotor 7: standard cage rotor design					
Opt:	3.54	0.486	22.8	253	0
Std. Dev.:	0.049	0.00705	0.202	17.7	0

Table 6.1: Parameter Extraction in simple induction mode with 4 pole supply

an additional measure of effectiveness, the algorithm returns the value of the minimised error which, if suitably normalised, gives a measure of fit 'quality'. This value could be normalised against the experimental data if required.

6.3.1 Comparison of data obtained using estimated parameter values with experimental data

In order to verify the machine parameter values estimated by the technique described, the parameter values tabulated in tables 6.1 to 6.4 were used in the BDFM equivalent circuit model given in figure 6.2 to generate torque-speed data.

The generated torque-speed data was produced at a constant $90V_{rms}$ (phase) stator 1 supply, with stator 2 short and open circuit, to give simple and cascade induction modes. The data was calculated for the 4 pole winding being stator 1 and then for the 8 pole winding as stator 1.

Figure 6.4 shows the same experimental data used in figures 5.8 to 5.11 overlayed with the calcu-

	R_1 (Ω)	R'_{r_n} (Ω)	$L'_{r_n} + L''_{m_{2n}}$ (mH)	$L_{m_{1n}}$ (mH)	$L''_{m_{2n}} \frac{N_2}{N_1}$ (mH)
Rotor 1: nested-loop rotor design					
Opt:	5.58	2.52	507	267	300
Std. Dev.:	0.089	0.0273	1.92	0.692	11.4
Rotor 2: new double-layer rotor design					
Opt:	6.21	30.8	1460	246	491
Std. Dev.:	0.0502	0.314	7.42	0.27	2.53
Rotor 3: isolated loop rotor design					
Opt:	5.46	14	203	272	6.6
Std. Dev.:	0.0419	0.0624	0.464	0.625	0.082
Rotor 4: isolated loop rotor design with removed loops					
Opt:	5.99	32.4	501	268	91.4
Std. Dev.:	0.0847	0.411	3.46	0.81	0.313
Rotor 7: standard cage rotor design					
Opt:	5.08	2.42	78.9	266	0
Std. Dev.:	0.0895	0.0306	0.374	5.06	0

Table 6.2: Parameter Extraction in simple induction mode with 8 pole supply

	R_1 (Ω)	R'_{r_n} (Ω)	L'_{r_n} (mH)	$L_{m_{1n}}$ (mH)	R''_{2_n} (Ω)	$L''_{m_{2n}}$ (mH)	$\frac{N_1}{N_2}$
Rotor 1: nested-loop rotor design							
Opt:	3.63	1.26	35.1	277	2.46	101	0.685
Std. Dev.:	0.106	0.038	0.379	27.1	0.0628	3.83	0.0131
Rotor 2: new double-layer rotor design							
Opt:	3.6	2.92	27.4	299	0.716	40.8	0.408
Std. Dev.:	0.125	0.0673	0.386	32.8	0.0197	1.55	0.00788
Rotor 4: isolated loop rotor design with loops removed							
Opt:	3.61	2	39.8	266	0.188	7.6	0.169
Std. Dev.:	0.176	0.0699	0.986	26.1	0.0223	0.681	0.00718

Table 6.3: Parameter Extraction in cascade induction mode with 4 pole supply

	R_1 (Ω)	R'_{r_n} (Ω)	L'_{r_n} (mH)	$L_{m_{1n}}$ (mH)	R''_{2_n} (Ω)	$L''_{m_{2n}}$ (mH)	$\frac{N_1}{N_2}$
Rotor 1: nested-loop rotor design							
Opt:	5.79	2.82	72.9	288	7.25	391	1.41
Std. Dev.:	0.213	0.0951	0.919	19.5	0.28	25.5	0.0447
Rotor 2: new double-layer rotor design							
Opt:	5.39	23.5	189	281	22.9	1640	2.51
Std. Dev.:	0.391	0.377	1.27	5.52	0.487	39.4	0.0301
Rotor 4: isolated loop rotor design with loops removed							
Opt:	7.61	23.1	337	264	16.7	607	1.59
Std. Dev.:	0.297	1.02	5.77	3.15	0.815	30.1	0.0385

Table 6.4: Parameter Extraction in cascade induction mode with 8 pole supply

lated torque-speed data.

The figures show a generally good agreement between predicted and measured data, and show that the use of parameter values determined by the estimation technique, yield more accurate results than those derived by calculations in some cases. This is, of course, to be expected.

To illustrate the applicability of the parameter extraction method beyond the prediction of solely simple and cascade induction mode torques, the parameters estimated from 4 pole cascade mode, given in table 6.3, were used to predict the maximum and minimum torque envelope for the prototype machine with rotor 1. The parameters were used in the equivalent circuit model, and the model solved to find the peak torque values for given supply voltages, over a range of shaft speeds. The stator 2 phase voltage magnitude was set as $\max\{220\left|\frac{f_2}{f_1}\right|, 20.7\}$, that is linearly proportional to the supply frequency with a 'boost' at lower frequencies. The stator 1 supply phase voltage was fixed at $220\mathrm{V}_{\mathrm{rms}}$, and 50 Hz. It was chosen to measure the maximum and minimum values of the torque, thus each data point was well defined for given supply voltages and frequencies. Each data point was measured by increasing the load torque (or generating torque) until pullout occurred and recording the final torque value immediately prior to pullout. For some operating points the machine dynamics were very lightly damped, or unstable, therefore it was necessary to use the feedback control scheme proposed in section 7.7 to restore stability. The process was repeated for a range of shaft speeds. The experimental apparatus used is described in appendix E.

Figure 6.3 shows the experimental results (blue crosses), with the simulation results overlaid in red. The agreement between the experimental and simulated results is very good. The experimental torque values are less than those predicted from calculation, however this is to be expected as the peak torque value is practically unattainable (although one should be able to get arbitrarily close). The structure in the plot at around natural speed (500rpm) could have been eliminated by making the voltage boost suitably asymmetric about natural speed.

A comparison of calculated and estimated parameter values will now be made.

6.3.2 Comparison of estimated to calculated parameter values

Table 6.5 shows calculated parameter values for the prototype machine with rotors 1, 2, 3 and 7 in the form of the equivalent circuit shown in figure 6.2. These parameter values were calculated using the conversion formulae, (6.3), from the parameters presented in table 5.1 and, in addition, parameter values are given for rotors 3 and 7, which were calculated in the same way.

However, as discussed in chapter 5, rotors 3 and 7 do not cross-couple, therefore parameter values are only given for simple induction mode.

Rotors 1, 2 and 4 cascade induction mode parameters will be compared, as the cascade mode parameters are a superset of the simple mode parameters. Simple mode parameters will be compared for rotors 3 and 7.

We first consider the self-consistency of the estimated parameters. If the machine considered is

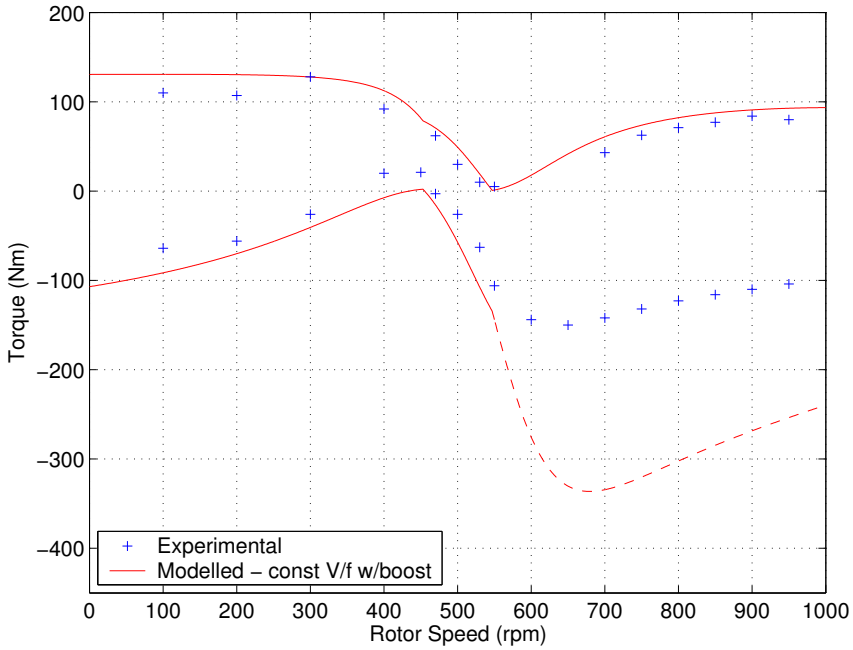

Figure 6.3: Experimental verification of the parameter extraction procedure: maximum synchronous torque envelope with varying rotor speed for rotor 1 ('nested-loop' design) with the 4 pole winding supplied with nominally 220V (phase), the 8 pole is supplied with a const. V/f law with boost, i.e.: $V_8 = \max\{220\left|\frac{f_2}{f_1}\right|, 20.7\}$ (solid lines, with experimental points marked). The parameters values used are those of table 6.3. Where the red line is dashed, it was not possible to experimentally determine the pull-out torque due to insufficient dissipative power in the experimental test rig.

precisely modelled by the equivalent circuit form given in 6.2, then parameter values estimated for the machine supplied from stator 1 or stator 2 should give identical results. Furthermore, these results are related by the square of the turns ratio, $N_1/N2$. The results of parameter estimation when the 4 pole winding was supplied should be equal to the results when the 8 pole winding was supplied divided by the square of the turns ratio.

For rotor 1 the errors ranged from 0.5% to 45% across the different parameters, for rotor 2 the errors ranged from 0.6% to 20% and for rotor 4 the errors went up to 1500%. These results are expected as rotor 2 has only one set of 6 rotor coils and should therefore be precisely modelled. Rotor 1 has 3 sets of 6 rotor coils, the inner, middle and outer loops of each 'nest' and although it was shown in chapter 3 that using the proposed model order reduction technique leads to relative small modelling errors, errors are nonetheless present, and these are reflected in the inconsistency within the parameter values. Rotor 4, has 2 sets of 6 rotor coils, however the coils are not arranged in a manner which leads to good BDFM behaviour, as can be seen from the cascade mode torque-speed curves. It is therefore unsurprising that the machine with this rotor is not well modelled by the circuit of figure 6.2.

We now compare the cascade induction mode estimated parameters for rotors 1 and 2 with those found by calculation.

- The magnetizing inductance, $L_{m_{1n}}$, is between 5% and 10% higher in the calculated parameter values, this is most likely due to the effective air gap being larger than that estimated.
- The ratio N_1/N_2 is in close agreement for both rotors 1 and 2, with the error ranging from 1% to 8%.
- The estimated leakage inductance terms, L'_{r_n}, are within 20% of their calculated values for rotor 2, and within 8% for rotor 1.
- In both rotors 1 and 2, the value of $L''_{m_{2n}}$ is subject to the greatest percentage error, suggesting that the parameter estimation method is relatively insensitive to changes in this parameter value.
- The resistance values are universally higher for the estimated parameter values, which is expected as the calculated resistance values were calculated at room temperature. The estimated values are consistent with an approximately 80 °C rise in temperature, which is plausible.

From the simple induction mode estimated parameter values we may note the following:

- The estimated magnetizing inductance, $L_{m_{1n}}$ is generally lower in simple mode than cascade mode. This suggests that in simple induction mode, the cost function chosen is relatively less sensitive to the value of $L_{m_{1n}}$. The error is particularly noticeable for rotor 7, the standard squirrel cage rotor, which suggests that the effective air gap for the cage rotor may be significantly greater than estimated. This could be the result of localised saturation in the rotor slot bridges.
- The leakage inductance, L'_{r_n}, and rotor resistance estimates for rotors 4 and 7 are up to 100% in error. For rotor 7 the Boucherot slots will inevitably lead to increased error as the resistance changes substantially (by design) with shaft speed. However, the errors for rotor 4 are likely to be due to poor quality data, as the results from rotors 1 and 2 are somewhat better in simple induction mode.

6.3.3 Comparison of estimated parameter values to manufacturer's parameter values

In the case of rotor 7, the standard squirrel cage rotor, it was possible to compare estimated parameter values against those given by the manufacturer. The details of this comparison can be found in [87], where the conclusion was that there was a close agreement, thus corroborating the parameter estimation method.

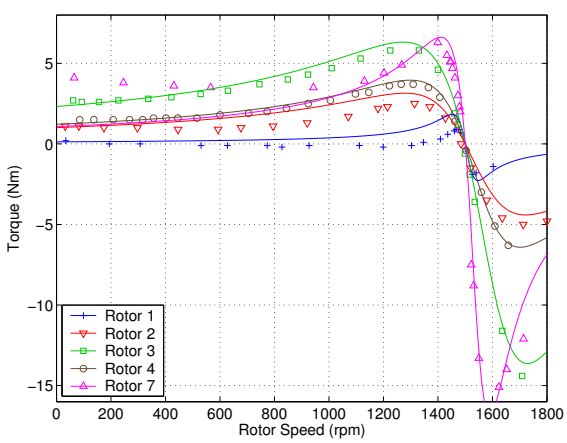

(a) Simple induction mode, 4 pole winding supplied

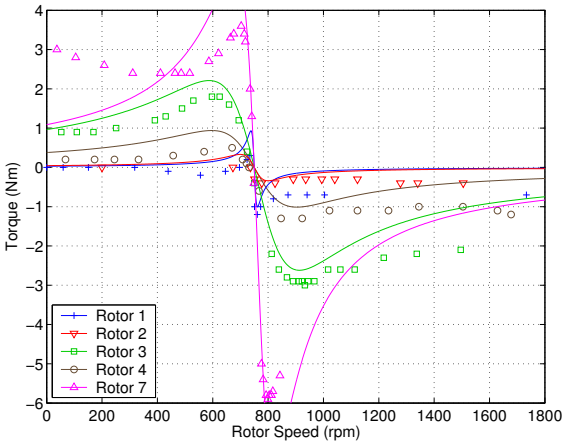

(b) Simple induction mode, 8 pole winding supplied

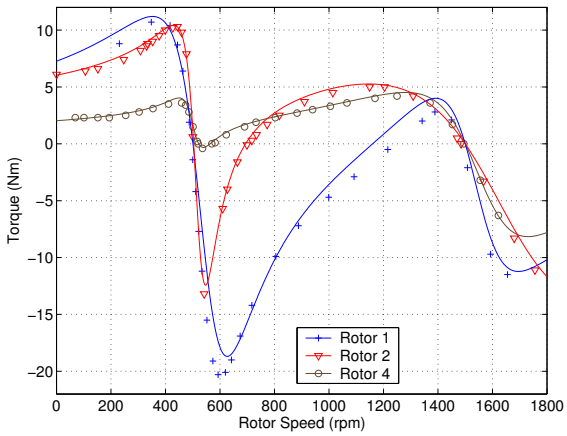

(c) Cascade induction mode, 4 pole winding supplied

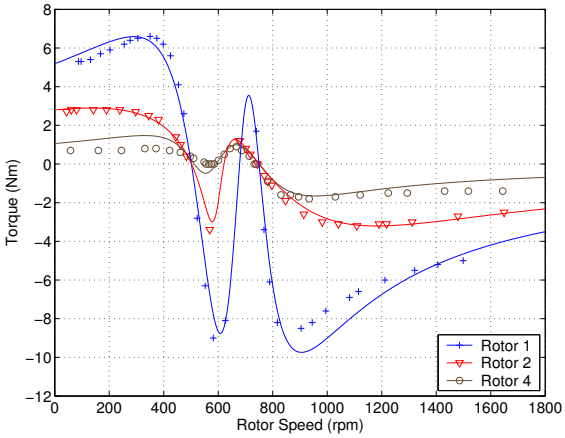

(d) Cascade induction mode, 8 pole winding supplied

Figure 6.4: Torque-Speed plot in simple induction mode with nominally $90V_{rms}$ phase supply voltage. Rotors as described in section 5.1. Experimental results with calculated results using estimated parameter values superimposed.

	R_1 (Ω)	R'_{r_n} (Ω)	L'_{r_n} (mH)	$L_{m_{1n}}$ (mH)	R''_{2_n} (Ω)	$L''_{m_{2n}}$ (mH)	$\frac{N_1}{N_2}$
Rotor 1: Referred to 4 pole side	2.7	0.969	37.3	310	2.16	159	0.703
Rotor 1: Referred to 8 pole side	4.37	1.96	75.4	322	5.45	627	1.42
Rotor 2: Referred to 4 pole side	2.7	2.08	22	317	0.62	46.8	0.377
Rotor 2: Referred to 8 pole side	4.37	14.7	155	329	19	2230	2.65
Rotor 3: Referred to 4 pole side	2.7	1.01	22.5	315	-	-	-
Rotor 3: Referred to 8 pole side	4.37	9.2	213	328	-	-	-
Rotor 7: Referred to 4 pole side	2.7	0.522	35.4	364	-	-	-
Rotor 7: Referred to 8 pole side	4.37	1.54	105	377	-	-	-

Table 6.5: Calculated parameters for the equivalent circuit representation given in figure 6.2

6.4 Relationship of extracted parameters to the d-q axis model

Before concluding this chapter, it will be useful to relate the estimated parameters back to those used in the d-q model. The first stage in this process is to convert the equivalent circuit of figure 6.2 to the coupled coil equivalent circuit representation of figure 4.3.

The left hand side of figure 6.2 may be transformed into a coupled coils representation, using the 'T' equivalent form, but with the left hand inductance zero. The 'T' equivalent form is given by figure 4.6 with $N = 1$ and $L_1 = M$. This transformation, and un-referring R_{2_n} gives the representation shown in figure 6.5.

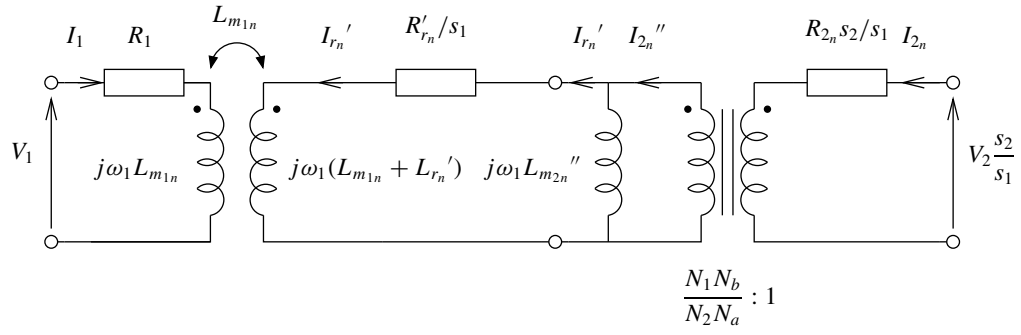

Figure 6.5: An equivalent form of figure 6.2

The right hand side of figure 6.5 may be transformed to coupled coils form again using figure 4.6. We temporarily define $\hat{I}_{2_a} = -I_{2_a}$, $\hat{V}_2 = -V_2$, convert transformer and inductor of figure 6.5 into coupled coil form, using $MN = L_{m_{2_n}}{}''$, $L_2 = M/N = L_{m_{2_n}}{}'' \left(\frac{N_2N_a}{N_1N_b}\right)^2$ and $L_1 = MN$. To

reinstate V_2 and I_{2_a}, we redefine them to be equal to $\hat{V}_2$ and $\hat{I}_{2_a}$ respectively. Alternatively the original sign convention could be maintained by changing the sign of M, this can be deduced from figure 4.5. These manipulations lead to figure 6.6.

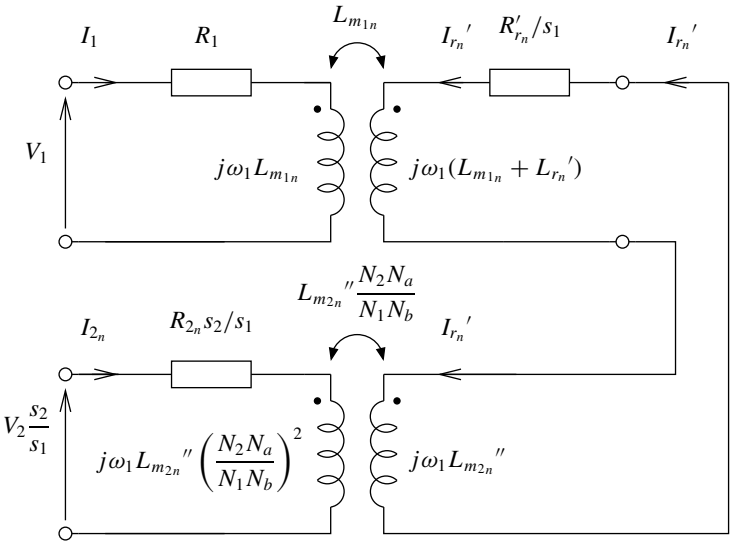

Figure 6.6: A further equivalent form of figure 6.2

Figure 6.6 may be represented as the following matrix equation:

$$\begin{bmatrix} V_1 \\ V_2 \\ 0 \end{bmatrix} = \left(j\omega_1 \begin{bmatrix} L_{m_{1n}} & 0 & L_{m_{1n}} \\ 0 & \frac{s_1}{s_2} L_{m_{2_n}}{}'' \left(\frac{N_2 N_a}{N_1 N_b}\right)^2 & \frac{s_1}{s_2} L_{m_{2_n}}{}'' \frac{N_2 N_a}{N_1 N_b} \\ s_1 L_{m_{1n}} & s_1 L_{m_{2_n}}{}'' \frac{N_2 N_a}{N_1 N_b} & s_1 (L_{m_{1n}} + L'_{r_n} + L_{m_{2_n}}{}'') \end{bmatrix} + \begin{bmatrix} R_1 & 0 & 0 \\ 0 & R_{2_n} & 0 \\ 0 & 0 & R'_{r_n} \end{bmatrix} \right) \begin{bmatrix} I_1 \\ I_{2_n} \\ I'_{r_n} \end{bmatrix} \tag{6.18}$$

Equation (6.18) is in the same form as equation (4.36), if the complex conjugate is taken of each side and the voltage and current symbols redefined.

Tracing back through the derivation of section 4.3, in particular from equation (4.31), with equations (4.15), (4.16) and (4.17) we may disaggregate the mutual inductance, 'Q', and resistance matrices. Therefore equation (6.18) may be re-written as:

$$\begin{bmatrix} V_1 \\ V_2 \\ 0 \end{bmatrix} = \left(R^+ + \omega_r Q^+ + j\omega_s M^+\right) \begin{bmatrix} I_1 \\ I_{2_n} \\ I'_{r_n} \end{bmatrix} \tag{6.19}$$

where:

$$R^+ = \begin{bmatrix} R_1 & 0 & 0 \\ 0 & R_{2_n} & 0 \\ 0 & 0 & R'_{r_n} \end{bmatrix} \qquad Q^+ = \begin{bmatrix} -p_1 L_{m_{1n}} & 0 & -jp_1 L_{m_{1n}} \\ 0 & jp_2 L_{m_{2n}}{}'' \left(\frac{N_2 N_a}{N_1 N_b}\right)^2 & jp_2 L_{m_{2n}}{}'' \frac{N_2 N_a}{N_1 N_b} \\ 0 & 0 & 0 \end{bmatrix}$$

$$M^+ = \begin{bmatrix} L_{m_{1n}} & 0 & L_{m_{1n}} \\ 0 & L_{m_{2n}}{}'' \left(\frac{N_2 N_a}{N_1 N_b}\right)^2 & L_{m_{2n}}{}'' \frac{N_2 N_a}{N_1 N_b} \\ L_{m_{1n}} & L_{m_{2n}}{}'' \frac{N_2 N_a}{N_1 N_b} & (L_{m_{1n}} + L'_{r_n} + L_{m_{2n}}{}'') \end{bmatrix}$$

Following back the derivation in section 4.2, which leads to the d-q axis version of the BDFM model in section 3.3, we may deduce the rotor reference frame d-q axis model:

$$\begin{bmatrix} v_{dq_{s1}} \\ v_{dq_{s2}} \\ 0 \end{bmatrix} = \begin{bmatrix} L_{m_{1n}} & 0 & 0 & 0 & L_{m_{1n}} & 0 \\ 0 & L_{m_{1n}} & 0 & 0 & 0 & L_{m_{1n}} \\ 0 & 0 & L_{m_{2n}}{}'' \left(\frac{N_2 N_a}{N_1 N_b}\right)^2 & 0 & L_{m_{2n}}{}'' \frac{N_2 N_a}{N_1 N_b} & 0 \\ 0 & 0 & 0 & L_{m_{2n}}{}'' \left(\frac{N_2 N_a}{N_1 N_b}\right)^2 & 0 & -L_{m_{2n}}{}'' \frac{N_2 N_a}{N_1 N_b} \\ L_{m_{1n}} & 0 & L_{m_{2n}}{}'' \frac{N_2 N_a}{N_1 N_b} & 0 & (L_{m_{1n}} + L'_{r_n} + L_{m_{2n}}{}'') & 0 \\ 0 & L_{m_{1n}} & 0 & -L_{m_{2n}}{}'' \frac{N_2 N_a}{N_1 N_b} & 0 & (L_{m_{1n}} + L'_{r_n} + L_{m_{2n}}{}'') \end{bmatrix} \frac{d}{dt} \begin{bmatrix} i_{dq_{s1}} \\ i_{dq_{s2}} \\ i_{dq_r} \end{bmatrix} +$$

$$\omega_r \begin{bmatrix} 0 & p_1 L_{m_{1n}} & 0 & 0 & 0 & p_1 L_{m_{1n}} \\ -p_1 L_{m_{1n}} & 0 & 0 & 0 & -p_1 L_{m_{1n}} & 0 \\ 0 & 0 & 0 & p_2 L_{m_{2n}}{}'' \left(\frac{N_2 N_a}{N_1 N_b}\right)^2 & 0 & -p_2 L_{m_{2n}}{}'' \frac{N_2 N_a}{N_1 N_b} \\ 0 & 0 & -p_2 L_{m_{2n}}{}'' \left(\frac{N_2 N_a}{N_1 N_b}\right)^2 & 0 & -p_2 L_{m_{2n}}{}'' \frac{N_2 N_a}{N_1 N_b} & 0 \\ 0 & 0 & 0 & 0 & 0 & 0 \\ 0 & 0 & 0 & 0 & 0 & 0 \end{bmatrix} \begin{bmatrix} i_{dq_{s1}} \\ i_{dq_{s2}} \\ i_{dq_r} \end{bmatrix} +$$

$$\begin{bmatrix} R_1 & 0 & 0 & 0 & 0 & 0 \\ 0 & R_1 & 0 & 0 & 0 & 0 \\ 0 & 0 & R_{2_n} & 0 & 0 & 0 \\ 0 & 0 & 0 & R_{2_n} & 0 & 0 \\ 0 & 0 & 0 & 0 & R'_{r_n} & 0 \\ 0 & 0 & 0 & 0 & 0 & R'_{r_n} \end{bmatrix} \begin{bmatrix} i_{dq_{s1}} \\ i_{dq_{s2}} \\ i_{dq_r} \end{bmatrix} \tag{6.20}$$

6.5 Conclusion

In this chapter a new method of estimating parameters for the BDFM, and indeed standard induction machines has been presented. The method is capable of producing all parameters needed for the referred equivalent circuit, and care has been taken to ensure that the precise meaning, and relationship to other forms of the equivalent circuit, has been maintained.

The parameter estimation method has been demonstrated on five of the seven rotor designs considered in chapter 5, as the remaining two rotor designs were not manufactured. The parameter estimation method has been shown to yield parameter values which lead to a model, the outputs of

which were verified by independent experiments at different operating conditions, and shown to be in reasonable agreement. Furthermore, where possible, the parameter values were compared with those provided by the manufacturer, and found to be in reasonable agreement.

The estimated parameter values were compared with those calculated using the method described in chapters 2, 3 and 4. The parameter values were shown to be in good agreement generally, particularly so when estimated from cascade induction mode tests. The parameter values were demonstrated to give accurate predictions of the maximum and minimum torque envelope. The agreement of the parameter values increases confidence in the accuracy of the parameter calculation method, including the calculation of excess harmonic inductance, which it was argued is a significant parameter in BDFM design.

The chosen solution method to the optimization problem posed by parameter estimation was found to be acceptable. However, particularly when solving the problem of finding cascade induction mode parameter values the crude random search algorithm was found to be relatively slow, as the parameter space is much larger. A significant decrease in computational time was achieved by stopping the random search prematurely and then using a gradient-based algorithm. The gradient-based algorithm was started at the best 1000 points found by the crude random search. The disadvantage of this approach was that the information gained by the standard deviation was largely lost.

Chapter 7

Modelling for Control of the BDFM

7.1 Introduction

In the chapters 2, 3 and 4 dynamic and steady-state models have been developed for the BDFM. In chapter 4 the BDFM was analysed in steady-state and then from that steady-state analysis new rotor designs were considered in chapter 5. We now turn our attention to dynamic analysis of the BDFM, and use this to assist in the design of controllers.

In order to progress the BDFM towards commercial service, not only must the machine be designed to give best possible performance in terms of high efficiency, high output power, and other steady-state measures. However as a prerequisite, the machine must be fully controllable so that it can always maintain these desired operating conditions. Typically these two demands tend to be at odds with one another. For example, as the resistance of the machine windings decreases, the efficiency will increase. However it will be shown in this chapter that as the resistance decreases the system dynamics become more lightly damped.

For example, as a wind turbine generator, the machine must operate at a specific shaft speed to gain the maximum power output from the turbine, while also maintaining a desirable power factor [8]. Similar requirements apply for variable-speed drive applications, such as pump drives [10].

There is therefore a need for robust control algorithms which can regulate the desired quantities. Unfortunately, as noted in chapter 2, the BDFM dynamic equations are non-linear and time-varying, from equation (2.59). Although the transformation to a d-q reference frame synchronous with the rotor in chapter 3 removed the position-varying parameters, the model remains non-linear (the torque equations) and parameter-varying (dependence on shaft speed), as shown in equations (3.35) and (3.40).

Although there are some systematic design procedures for designing non-linear control laws, they generally apply to a tiny subset of non-linear systems encountered, and vary significantly in their performance. This is in contrast to linear systems theory which has a rich set of design methods.

The array of advanced linear design tools motivates the derivation of a linearized model, even

if this model will have significant limitations. Although it is possible to linearize any sufficiently smooth system, the resulting linearized system may be time varying, even if the original system were not explicitly so [26, p. 18]. However, it will be shown that by careful choice of reference frame it is possible to derive a linearized system where the coefficients are constant under certain conditions, and furthermore these equilibrium conditions consist of constant valued inputs. This is in contrast to the only other presented linearized model for the BDFM (which incidentally only applies to a subset of the class of BDFMs analysed here) where the inputs required to keep the shaft speed in equilibrium are sinusoidally varying quantities, thus rendering the linearized system time varying [61]. We will show that in the special case that the machine being analysed has only a single set of rotor circuits, then the linearized model is in a similar form to that derived for the single frame cascade induction machine, [24, 25].

The derivation of a model where constant-valued system inputs are required to hold an operating point was first proposed in [130]. Such a model is known as a synchronous reference frame model as the chosen reference frame is in synchronism with the currents. However in [130] only a current-fed model is presented, and it only applies to a subset of the class of BDFMs considered in this dissertation. In this chapter we derive a synchronous reference frame model for the entire class of BDFMs analysed in chapter 3. We also describe a direct, systematic method for determining equilibrium conditions that, in contrast to [60] does not require gradient-based optimization, and gives all possible solutions.

We then show how the linearised model can be used to design linear control laws for the BDFM. The approach adopted assumes that the objective is speed regulation which should be robust to changes in load torque. This objective covers a wide range of applications.

A simple linear controller was proposed for the BDFM in [127]. However no analysis was presented, and the performance of the controller is significantly worse than that obtained here. We also demonstrate the efficacy of the linearized BDFM model, comparing it against the models of chapters 2 and 3 and against experimental results obtained for the prototype BDFM with rotor 2.

7.2 Synchronous reference frame model

We now derive a synchronous reference frame model for the class of BDFMs analysed in chapter 3. The approach used, although related, is somewhat different to that used in [130], specifically because we present a general transformation for voltage source models, where in [130] it was necessary to separate rotor current components into those induced from stator 1 and 2 respectively, in order to derive the synchronous reference frame model.

The d-q model derived in chapter 3 was aligned to the rotor angular position, which, we showed, removed the dependence on rotor position from the mutual inductance terms. Nevertheless, when the machine is running in equilibrium, that is at a fixed shaft speed in the synchronous mode of

operation, the currents are not constant values. However, during the derivation of the steady-state equivalent circuit representation, it was shown in section 4.3 that under BDFM synchronous operation, the frequencies of currents in the two stators, and in the rotor, are the same in the d-q rotor reference frame.

This fact suggests that if the reference frame is rotated so that it is in synchronism with these currents, then the equilibrium value of the currents will become constant values. It was derived in section 4.3 that when the BDFM is running in synchronous mode, that is, the shaft speed is related to the supply frequencies by:

$$\omega_r = \frac{\omega_1 + \omega_2}{p_1 + p_2} \tag{7.1}$$

then the frequencies of the currents in both stator windings and the rotor, in the rotor reference frame are given by:

$$\omega_s = p_1\omega_r - \omega_1 = -p_2\omega_r + \omega_2 \tag{7.2}$$

Hence we expect that if the reference frame is rotated by $\int \omega_s dt$, then the currents will be constant value in equilibrium. In order to rotate the reference frame we define a transformation matrix for each d-q pair which is a rotation matrix that rotates the signals by $\int_0^t \omega_s dt$.

However, from (7.2), ω_s may be expressed in terms either of ω_1, the stator 1 supply frequency, or ω_2, the stator 2 supply frequency. It makes most conceptual sense to define the transformation matrix, and therefore the synchronous reference frame, in terms of the stator 1 supply, which it is (initially) assumed is of fixed frequency as it is grid connected.

The transformation matrix for the stator 1 supply may now be defined:

$$T_{\text{sync}}(\gamma) = \begin{bmatrix} \cos(p_1\theta_r - \omega_1 t + \gamma) & \sin(p_1\theta_r - \omega_1 t + \gamma) & 0 \\ -\sin(p_1\theta_r - \omega_1 t + \gamma) & \cos(p_1\theta_r - \omega_1 t + \gamma) & 0 \\ 0 & 0 & 1 \end{bmatrix} \tag{7.3}$$

where γ is some constant angular offset.

It is straight forward to show that equation (7.3) transforms stator 1 rotor reference frame voltages to constant values. The results of the transformation are given in table 7.1.

In order to transform the stator 2 voltages and currents, the same form of the transformation matrix is used, however the direction of rotation of the transformation matrix must be reversed. This is because the stator 2 voltages and current rotate around the machine circumference in the opposite sense to the stator 1 voltages and currents in the rotor reference frame. This point was discussed in more detail in section 4.3. As (7.3) is a rotation matrix, the inverse (or equivalently the transpose) of the matrix represents a rotation in the opposite sense.

In order to transform the rotor currents, the same transformation as used on stator 1 is applied. This is because when the rotor currents were transformed from their real values into the rotor reference

frame d-q model, in section 3.3, the transformation matrix used, equation (3.5), was defined using the pole-pairs corresponding to stator 1. Had equation (3.5) been defined using stator 2 pole-pairs, then the direction of the rotation of the rotor currents in the rotor reference frame would have been reversed and consequently the required rotation direction to transform the current into the synchronous reference frame would also have been reversed.

We will refer to this new reference frame where the currents and voltages assume constant values in equilibrium, as the *synchronous reference frame* in the sequel.

There is one additional degree of freedom in the transformation into the synchronous reference frame which has not yet been discussed. That is the constant angular offset, γ. γ can be used to align the stator 1 and stator 2 d and q axes within the synchronous reference frame. We may exploit this fact to simplify the synchronous reference frame model equations by rendering some (or possibly all) the stator-rotor mutual inductance terms diagonal. For the rotor transformations we choose $\gamma = 0$ exclusively.

Table 7.1 (found at the end of the chapter) summarises the stator transformation matrices and the corresponding voltage waveforms in the synchronous reference frame. For convenience the transformations from terminal quantities to the d-q rotor reference frame, equations (3.1) and (3.2), are repeated too.

7.2.1 Transformation from the rotor reference frame to the synchronous reference frame

In section 3.3 the d-q axis model in the rotor reference frame was derived. The final form of the model was given in equation (3.35). In order to transform the rotor reference frame d-q model into the synchronous reference frame we need to define the complete transformation matrix, which will comprise of $N+2$ copies of (7.3) along the diagonal, where N is the number of sets of rotor circuits, as discussed in section 3.3. As discussed in the preceding section the phase offset, γ is set to zero for the rotor circuits, and to values which diagonalize the stator-rotor mutual inductance matrices in the case of the stator transformations. The full transformation matrix is:

$$\mathcal{T}_{\text{sync}} = \begin{bmatrix} T_{\text{sync}}(\phi_{1_1}) & 0 & 0 & 0 & \cdots & 0 \\ 0 & T_{\text{sync}}(\phi_{2_1})^{-1} & 0 & 0 & \cdots & 0 \\ 0 & 0 & T_{\text{sync}}(0) & 0 & \cdots & 0 \\ \vdots & \ddots & \ddots & \ddots & \ddots & \vdots \\ 0 & \cdots & 0 & 0 & T_{\text{sync}}(0) & 0 \\ 0 & \cdots & 0 & 0 & 0 & T_{\text{sync}}(0) \end{bmatrix} \tag{7.4}$$

where ϕ_{1_1} and ϕ_{2_1} are the angles of the first stator-rotor mutual inductance for stator 1 and 2 respectively as used in equations (3.26) and (3.27). The use of the inverse transformation for stator 1 reflects the opposing direction of the currents

The d-q model in the synchronous reference frame may now be derived. From (3.35):

$$\begin{bmatrix} v^s_{dq0_{s1}} \\ v^s_{dq0_{s2}} \\ 0 \end{bmatrix} = \left(\mathcal{T}_{\text{sync}} R_{dq} \mathcal{T}^{-1}_{\text{sync}} + \omega_r \mathcal{T}_{\text{sync}} Q_{dq} \mathcal{T}^{-1}_{\text{sync}} + \mathcal{T}_{\text{sync}} M_{dq} \frac{d}{dt} \mathcal{T}^{-1}_{\text{sync}} \right) \begin{bmatrix} i^s_{dq0_{s1}} \\ i^s_{dq0_{s2}} \\ i^s_{dq_r} \end{bmatrix} + \mathcal{T}_{\text{sync}} M_{dq} \mathcal{T}^{-1}_{\text{sync}} \frac{d}{dt} \begin{bmatrix} i^s_{dq0_{s1}} \\ i^s_{dq0_{s2}} \\ i^s_{dq_r} \end{bmatrix} \quad (7.5)$$

where M_{dq}, Q_{dq}, R_{dq} are given in equation (3.35), and $v^s_{dq0_{s1}}$ denotes the stator 1 supply voltage vector in the synchronous reference frame, as given in table 7.1. Similar notation is used for the other voltages and currents.

The torque equation in the rotor reference frame is given in equation (3.38). Transforming into the synchronous reference frame gives:

$$T_e = \frac{1}{2} \begin{bmatrix} i^s_{dq0_{s1}} \\ i^s_{dq0_{s2}} \\ i^s_{dq_r} \end{bmatrix}^{\text{T}} \mathcal{T}_{\text{sync}} \begin{bmatrix} 0 & 0 & Q_{dq_{sr1}} \\ 0 & 0 & Q_{dq_{sr2}} \\ {Q_{dq_{sr1}}}^{\text{T}} & {Q_{dq_{sr2}}}^{\text{T}} & 0 \end{bmatrix} \mathcal{T}^{-1}_{\text{sync}} \begin{bmatrix} i^s_{dq0_{s1}} \\ i^s_{dq0_{s2}} \\ i^s_{dq_r} \end{bmatrix} \quad (7.6)$$

We therefore define:

$$R_{\text{sync}} \triangleq \mathcal{T}_{\text{sync}} R_{dq} \mathcal{T}^{-1}_{\text{sync}} \quad (7.7)$$

$$Q_{\text{sync}}(\omega_1, \omega_r) \triangleq \omega_r \mathcal{T}_{\text{sync}} Q_{dq} \mathcal{T}^{-1}_{\text{sync}} + \mathcal{T}_{\text{sync}} M_{dq} \frac{d}{dt} \mathcal{T}^{-1}_{\text{sync}} \quad (7.8)$$

$$M_{\text{sync}} \triangleq \mathcal{T}_{\text{sync}} M_{dq} \mathcal{T}^{-1}_{\text{sync}} \quad (7.9)$$

$$S_{\text{sync}} \triangleq \mathcal{T}_{\text{sync}} \begin{bmatrix} 0 & 0 & Q_{dq_{sr1}} \\ 0 & 0 & Q_{dq_{sr2}} \\ {Q_{dq_{sr1}}}^{\text{T}} & {Q_{dq_{sr2}}}^{\text{T}} & 0 \end{bmatrix} \mathcal{T}^{-1}_{\text{sync}} \quad (7.10)$$

In terms of the new variable the equations are:

$$\begin{bmatrix} v^s_{dq0_{s1}} \\ v^s_{dq0_{s2}} \\ 0 \end{bmatrix} = \left(R_{\text{sync}} + Q_{\text{sync}} \right) \begin{bmatrix} i^s_{dq0_{s1}} \\ i^s_{dq0_{s2}} \\ i^s_{dq_r} \end{bmatrix} + M_{\text{sync}} \frac{d}{dt} \begin{bmatrix} i^s_{dq0_{s1}} \\ i^s_{dq0_{s2}} \\ i^s_{dq_r} \end{bmatrix}$$

$$T_e = \frac{1}{2} \begin{bmatrix} i^s_{dq0_{s1}} \\ i^s_{dq0_{s2}} \\ i^s_{dq_r} \end{bmatrix}^{\text{T}} S_{\text{sync}} \begin{bmatrix} i^s_{dq0_{s1}} \\ i^s_{dq0_{s2}} \\ i^s_{dq_r} \end{bmatrix} \quad (7.11)$$

Hence the full dynamic equations in state-space form become:

$$\frac{d}{dt}\begin{bmatrix} i^s_{dq0_{s1}} \\ i^s_{dq0_{s2}} \\ i^s_{dq_r} \\ \theta_r \\ \\ \omega_r \\ \\ \end{bmatrix} = \begin{bmatrix} M^{-1}_{\text{sync}} \left((-R_{\text{sync}} - Q_{\text{sync}}) \begin{bmatrix} i^s_{dq0_{s1}} \\ i^s_{dq0_{s2}} \\ i^s_{dq_r} \end{bmatrix} + \begin{bmatrix} v^s_{dq0_{s1}} \\ v^s_{dq0_{s2}} \\ 0 \end{bmatrix} \right) \\ \omega_r \\ \frac{1}{2J} \begin{bmatrix} i^s_{dq0_{s1}} \\ i^s_{dq0_{s2}} \\ i^s_{dq_r} \end{bmatrix}^{\text{T}} S_{\text{sync}} \begin{bmatrix} i^s_{dq0_{s1}} \\ i^s_{dq0_{s2}} \\ i^s_{dq_r} \end{bmatrix} - \frac{T_l}{J} \end{bmatrix} \tag{7.12}$$

where J is the moment of inertia of the machine, and T_l is the load torque.

We now consider the result of the transformation to the synchronous reference frame, particularly we show that R_{sync}, S_{sync} and M_{sync} are constant-valued, and Q_{sync} is linearly dependent on ω_1 and ω_r only.

7.2.2 Evaluation of component matrices in the synchronous reference frame

As R_{dq} is diagonal and the resistance values appear in pairs it is easy to show that:

$$R_{\text{sync}} = \mathcal{T}_{\text{sync}} R_{dq} \mathcal{T}^{-1}_{\text{sync}} = R_{dq}$$

because each resistance pair may be represented at the identity multiplied by a scalar which therefore commutes with the transformation matrix.

Similarly the stator-stator portions of M_{dq} must remain unchanged under the transformation as they too have the same structure. From consideration of the rotor-rotor terms, as given in equation (3.24), it can be seen that the rotor-rotor terms remain unchanged, as all the rotor transformation matrices have been chosen to be the same. The stator-rotor portions of M_{dq} which comprise of a scaled rotation matrix of angle ϕ_{1_1} for stator 1 and ϕ_{2_1} for stator 2 will be diagonalised, and the remaining terms will be rotated by $-\phi_{1_1}$ or $-\phi_{2_1}$ respectively. Hence M_{sync} comprises of constant terms only.

As Q_{dq} is closely related to M_{dq} similar comments apply. However it is convenient to observe that, from the definitions of Q_{dq}, equations (3.17), (3.18), (3.28) and (3.29), the following relationship holds between Q_{dq} and M_{dq}:

$$p_1\omega_r \begin{bmatrix} M_{dq0_{s1}} & 0 & M_{dq_{sr1}} \end{bmatrix} \begin{bmatrix} \begin{bmatrix} 0 & 1 & 0 \\ -1 & 0 & 0 \\ 0 & 0 & 0 \end{bmatrix} & & \\ & \ddots & \\ & & \begin{bmatrix} 0 & 1 & 0 \\ -1 & 0 & 0 \\ 0 & 0 & 0 \end{bmatrix} \end{bmatrix} = \begin{bmatrix} Q_{dq0_{s1}} & 0 & Q_{dq_{sr1}} \end{bmatrix} \tag{7.13}$$

where $M_{dq0_{s1}}$, $Q_{dq0_{s1}}$ are the stator 1-stator 1 components and $M_{dq_{sr1}}$, $Q_{dq_{sr1}}$ the stator 1-rotor of M_{dq} and Q_{dq} respectively as given in (3.35). A similar relationship holds for the stator 2 components.

The remaining term, $Q_{\text{sync}}(\omega_r, \omega_1) = \omega_r \mathcal{T}_{\text{sync}} Q_{dq} \mathcal{T}_{\text{sync}}^{-1} + \mathcal{T}_{\text{sync}} M_{dq} \frac{d}{dt} \mathcal{T}_{\text{sync}}^{-1}$ will now be analysed. From (7.3):

$$\begin{aligned}\frac{d}{dt} T_{\text{sync}}^{-1} &= (p_1\omega_r - \omega_1) \begin{bmatrix} -\sin(p_1\theta_r - \omega_1 t + \gamma) & -\cos(p_1\theta_r - \omega_1 t + \gamma) & 0 \\ \cos(p_1\theta_r - \omega_1 t + \gamma) & -\sin(p_1\theta_r - \omega_1 t + \gamma) & 0 \\ 0 & 0 & 0 \end{bmatrix} \\ &= (-p_1\omega_r + \omega_1) \begin{bmatrix} 0 & 1 & 0 \\ -1 & 0 & 0 \\ 0 & 0 & 0 \end{bmatrix} T_{\text{sync}}^{-1}\end{aligned}$$

Therefore we may write:

$$\begin{aligned} Q_{\text{sync}}(\omega_r, \omega_1) = \mathcal{T}_{\text{sync}} \Bigg(& \begin{bmatrix} p_1\omega_r \begin{bmatrix} 0 & 1 & 0 \\ -1 & 0 & 0 \\ 0 & 0 & 0 \end{bmatrix} & & & \\ & p_2\omega_r \begin{bmatrix} 0 & 1 & 0 \\ -1 & 0 & 0 \\ 0 & 0 & 0 \end{bmatrix} & & \\ & & \begin{bmatrix} 0 & 0 & 0 \\ 0 & 0 & 0 \\ 0 & 0 & 0 \end{bmatrix} & \\ & & & \ddots \end{bmatrix} M_{dq} + \\ & (-p_1\omega_r + \omega_1) M_{dq} \begin{bmatrix} \begin{bmatrix} 0 & 1 & 0 \\ -1 & 0 & 0 \\ 0 & 0 & 0 \end{bmatrix} & & & \\ & \begin{bmatrix} 0 & -1 & 0 \\ 1 & 0 & 0 \\ 0 & 0 & 0 \end{bmatrix} & & \\ & & \begin{bmatrix} 0 & 1 & 0 \\ -1 & 0 & 0 \\ 0 & 0 & 0 \end{bmatrix} & \\ & & & \ddots \end{bmatrix} \Bigg) \mathcal{T}_{\text{sync}}^{-1} \end{aligned} \tag{7.14}$$

It is easy to verify from (7.4) that $\mathcal{T}_{\text{sync}}$ and $\mathcal{T}_{\text{sync}}^{-1}$ commute with their neighbouring matrices in (7.14), therefore:

$$\begin{aligned} Q_{\text{sync}}(\omega_r, \omega_1) = & \begin{bmatrix} p_1\omega_r \begin{bmatrix} 0 & 1 & 0 \\ -1 & 0 & 0 \\ 0 & 0 & 0 \end{bmatrix} & & & \\ & p_2\omega_r \begin{bmatrix} 0 & 1 & 0 \\ -1 & 0 & 0 \\ 0 & 0 & 0 \end{bmatrix} & & \\ & & \begin{bmatrix} 0 & 0 & 0 \\ 0 & 0 & 0 \\ 0 & 0 & 0 \end{bmatrix} & \\ & & & \ddots \end{bmatrix} \mathcal{T}_{\text{sync}} M_{dq} \mathcal{T}_{\text{sync}}^{-1} + \\ & (-p_1\omega_r + \omega_1) \mathcal{T}_{\text{sync}} M_{dq} \mathcal{T}_{\text{sync}}^{-1} \begin{bmatrix} \begin{bmatrix} 0 & 1 & 0 \\ -1 & 0 & 0 \\ 0 & 0 & 0 \end{bmatrix} & & & \\ & \begin{bmatrix} 0 & -1 & 0 \\ 1 & 0 & 0 \\ 0 & 0 & 0 \end{bmatrix} & & \\ & & \begin{bmatrix} 0 & 1 & 0 \\ -1 & 0 & 0 \\ 0 & 0 & 0 \end{bmatrix} & \\ & & & \ddots \end{bmatrix} \end{aligned} \tag{7.15}$$

Therefore as M_{sync} is constant, $Q_{\text{sync}}(\omega_r, \omega_1)$ is linearly dependent on ω_1 and ω_r.

Furthermore it can be noted that equation (7.14) shows that the first three rows, that is the rows corresponding to stator 1, of $Q_{\text{sync}}(\omega_r, \omega_1)$ are independent of ω_r. This can be seen by noting that

due to the structure of M_{dq} the 3×3 blocks of M_{dq} commute with matrices of the form: $\begin{bmatrix} 0 & 1 & 0 \\ 0 & -1 & 0 \\ 0 & 0 & 0 \end{bmatrix}$, therefore as there is no direct coupling between stator 1 and stator 2 it can be seen that the terms in ω_r cancel out.

Similarly it is easy to show that S_{sync} can be written as:

$$S_{\text{sync}} = \mathcal{T}_{\text{sync}} \left(\begin{bmatrix} p_1 \begin{bmatrix} 0 & 1 & 0 \\ -1 & 0 & 0 \\ 0 & 0 & 0 \end{bmatrix} & & & \\ & p_2 \begin{bmatrix} 0 & 1 & 0 \\ -1 & 0 & 0 \\ 0 & 0 & 0 \end{bmatrix} & & \\ & & \begin{bmatrix} 0 & 0 & 0 \\ 0 & 0 & 0 \\ 0 & 0 & 0 \end{bmatrix} & \\ & & & \ddots \end{bmatrix} M_{dq} + M_{dq} \begin{bmatrix} p_1 \begin{bmatrix} 0 & -1 & 0 \\ 1 & 0 & 0 \\ 0 & 0 & 0 \end{bmatrix} & & & \\ & p_2 \begin{bmatrix} 0 & -1 & 0 \\ 1 & 0 & 0 \\ 0 & 0 & 0 \end{bmatrix} & & \\ & & \begin{bmatrix} 0 & 0 & 0 \\ 0 & 0 & 0 \\ 0 & 0 & 0 \end{bmatrix} & \\ & & & \ddots \end{bmatrix} \right) \mathcal{T}_{\text{sync}}^{-1} \quad (7.16)$$

which can be written as:

$$S_{\text{sync}} = \begin{bmatrix} p_1 \begin{bmatrix} 0 & 1 & 0 \\ -1 & 0 & 0 \\ 0 & 0 & 0 \end{bmatrix} & & & \\ & p_2 \begin{bmatrix} 0 & 1 & 0 \\ -1 & 0 & 0 \\ 0 & 0 & 0 \end{bmatrix} & & \\ & & \begin{bmatrix} 0 & 0 & 0 \\ 0 & 0 & 0 \\ 0 & 0 & 0 \end{bmatrix} & \\ & & & \ddots \end{bmatrix} \mathcal{T}_{\text{sync}} M_{dq} \mathcal{T}_{\text{sync}}^{-1} + \mathcal{T}_{\text{sync}} M_{dq} \mathcal{T}_{\text{sync}}^{-1} \begin{bmatrix} p_1 \begin{bmatrix} 0 & -1 & 0 \\ 1 & 0 & 0 \\ 0 & 0 & 0 \end{bmatrix} & & & \\ & p_2 \begin{bmatrix} 0 & -1 & 0 \\ 1 & 0 & 0 \\ 0 & 0 & 0 \end{bmatrix} & & \\ & & \begin{bmatrix} 0 & 0 & 0 \\ 0 & 0 & 0 \\ 0 & 0 & 0 \end{bmatrix} & \\ & & & \ddots \end{bmatrix} \quad (7.17)$$

Hence as M_{sync} is constant, then so is S_{sync}.

It is interesting to note that Youla and Bongiorno proved that a reference frame transformation will exist for any electrical machine, with linear electrical dynamics, which transforms the differential equations into an LTI system under the condition of constant rotor angular velocity [121]. It is not, therefore, surprising that such a transformation can be found for the BDFM.

By way of an example consider a rotor with a single set of rotor circuits (or equivalently one to which the model reduction technique of chapter 3 has been applied), with zero sequence states removed:

$$\begin{bmatrix} v^s_{dq_{s1}} \\ v^s_{dq_{s2}} \\ 0 \end{bmatrix} = \begin{bmatrix} R_{dq_1} & 0 & 0 & 0 & 0 & 0 \\ 0 & R_{dq_1} & 0 & 0 & 0 & 0 \\ 0 & 0 & R_{dq_2} & 0 & 0 & 0 \\ 0 & 0 & 0 & R_{dq_2} & 0 & 0 \\ 0 & 0 & 0 & 0 & R_{dq_r} & 0 \\ 0 & 0 & 0 & 0 & 0 & R_{dq_r} \end{bmatrix} \begin{bmatrix} i^s_{dq_{s1}} \\ i^s_{dq_{s2}} \\ i^s_{dq_r} \end{bmatrix} +$$

$$\begin{bmatrix} L_{dq_1} & 0 & 0 & 0 & M_{1_1} & 0 \\ 0 & L_{dq_1} & 0 & 0 & 0 & M_{1_1} \\ 0 & 0 & L_{dq_2} & 0 & M_{2_1} & 0 \\ 0 & 0 & 0 & L_{dq_2} & 0 & -M_{2_1} \\ M_{1_1} & 0 & M_{2_1} & 0 & L_{dq_r} & 0 \\ 0 & M_{1_1} & 0 & -M_{2_1} & 0 & L_{dq_r} \end{bmatrix} \frac{d}{dt} \begin{bmatrix} i^s_{dq_{s1}} \\ i^s_{dq_{s2}} \\ i^s_{dq_r} \end{bmatrix} +$$

$$\begin{bmatrix} 0 & \omega_1 L_{dq_1} & 0 & 0 \\ -\omega_1 L_{dq_1} & 0 & 0 & 0 \\ 0 & 0 & 0 & ((p_1+p_2)\omega_r - \omega_1)L_{dq_2} \\ 0 & 0 & -((p_1+p_2)\omega_r - \omega_1)L_{dq_2} & 0 \\ 0 & (\omega_1 - p_1\omega_r)M_{1_1} & 0 & (-\omega_1 + p_1\omega_r)M_{2_1} \\ (p_1\omega_r - \omega_1)M_{1_1} & 0 & (p_1\omega_r - \omega_1)M_{2_1} & 0 \end{bmatrix}$$

$$\begin{bmatrix} 0 & \omega_1 M_{1_1} \\ -\omega_1 M_{1_1} & 0 \\ 0 & -((p_2+p_1)\omega_r - \omega_1)M_{2_1} \\ -((p_2+p_1)\omega_r - \omega_1)M_{2_2} & 0 \\ 0 & (\omega_1 - p_1\omega_r)L_{dq_r} \\ (p_1\omega_r - \omega_1)L_{dq_r} & 0 \end{bmatrix} \begin{bmatrix} i^s_{dq_{s1}} \\ i^s_{dq_{s2}} \\ i^s_{dq_r} \end{bmatrix} \tag{7.18}$$

The torque equation is given by:

$$T_e = \frac{1}{2} \begin{bmatrix} i^s_{dq_{s1}} \\ i^s_{dq_{s2}} \\ i^s_{dq_r} \end{bmatrix}^{\mathrm{T}} \begin{bmatrix} 0 & 0 & 0 & 0 & 0 & p_1 M_{1_1} \\ 0 & 0 & 0 & 0 & -p_1 M_{1_1} & 0 \\ 0 & 0 & 0 & 0 & 0 & -p_2 M_{2_1} \\ 0 & 0 & 0 & 0 & -p_2 M_{2_1} & 0 \\ 0 & -p_1 M_{1_1} & 0 & -p_2 M_{2_1} & 0 & 0 \\ p_1 M_{1_1} & 0 & -p_2 M_{2_1} & 0 & 0 & 0 \end{bmatrix} \begin{bmatrix} i^s_{dq_{s1}} \\ i^s_{dq_{s2}} \\ i^s_{dq_r} \end{bmatrix} \tag{7.19}$$

7.3 Synchronous Reference Frame Model Equilibrium Conditions

As it is assumed that stator 1 is connected to the grid, then (from table 7.1) α_1, ω_1, ϕ_{1_1} and V_1 are constant, for a given machine and grid. α_1 has the physical interpretation of a constant phase 'offset' between the machine and the supply grid. As the instantaneous phase of the supply grid is, in a sense, arbitrary, α_1 may be set freely. Therefore without loss of generality we set $\alpha_1 = -\phi_{1_1}$.

From table 7.1 the phase of the stator 2 voltage in the synchronous reference frame is given by $(-p_1 - p_2)\theta_r + \int \omega_2 dt + \omega_1 t + \alpha_2 + \phi_{2_1}$. It is immediate that when (7.1) holds, this phase must be a constant value. Therefore in equilibrium ω_2 must be given by:

$$\omega_2^e = (p_1 + p_2)\omega_r - \omega_1 \tag{7.20}$$

The equilibrium currents may be found for any supply voltage by solving the synchronous reference frame dynamic equations, (7.11), for steady-state conditions, that is $\frac{d}{dt}\begin{bmatrix} i^s_{dq0_{s1}} \\ i^s_{dq0_{s2}} \\ i^s_{dq_r} \end{bmatrix} = 0$.

It is assumed that it is desired to specify a value of the stator 2 voltage magnitude, and solve to find the equilibrium currents, and stator 2 voltage phase offset in the synchronous reference frame. Once this phase offset has been determined, the value of α_2, which constitutes the stator 2 voltage phase offset may be calculated from table 7.1.

Under steady-state conditions, from (7.11), the voltage and current equations are related as follows:

$$\begin{bmatrix} v^s_{dq0_{s1}} \\ v^s_{dq0_{s2}} \\ 0 \end{bmatrix} = \left(R_{\text{sync}} + Q_{\text{sync}}\right) \begin{bmatrix} i^s_{dq0_{s1}} \\ i^s_{dq0_{s2}} \\ i^s_{dq_r} \end{bmatrix} \tag{7.21}$$

Using (7.21), the torque can be expressed in terms of the voltage (noting that $R_{\text{sync}} + Q_{\text{sync}}$ will always be invertible as long as the resistances are non-zero). We omit the zero sequence components as they do not produce torque:

$$T_e = \frac{1}{2}\begin{bmatrix} v^s_{dq_{s1}} \\ v^s_{dq_{s2}} \\ 0 \end{bmatrix}^{\mathrm{T}} (R_{\text{sync}} + Q_{\text{sync}})^{-1^{\mathrm{T}}} S_{\text{sync}} (R_{\text{sync}} + Q_{\text{sync}})^{-1} \begin{bmatrix} v^s_{dq_{s1}} \\ v^s_{dq_{s2}} \\ 0 \end{bmatrix} \tag{7.22}$$

partitioning $(R_{\text{sync}} + Q_{\text{sync}})^{-1^{\mathrm{T}}} S_{\text{sync}} (R_{\text{sync}} + Q_{\text{sync}})^{-1}$ into stator 1, stator 2 and rotor portions, and noting that it must be symmetric as S_{sync} is symmetric, the torque may be written as:

$$T_e = \frac{1}{2}\begin{bmatrix} v^s_{dq_{s1}} \\ v^s_{dq_{s2}} \\ 0 \end{bmatrix}^{\mathrm{T}} \begin{bmatrix} A_{11} & A_{12} & \star \\ A_{12}{}^{\mathrm{T}} & A_{22} & \star \\ \star & \star & \star \end{bmatrix} \begin{bmatrix} v^s_{dq_{s1}} \\ v^s_{dq_{s2}} \\ 0 \end{bmatrix} \tag{7.23}$$

where A_{xy} denotes the partition of $A = (R_{\text{sync}} + Q_{\text{sync}})^{-1^{\mathrm{T}}} S_{\text{sync}} (R_{\text{sync}} + Q_{\text{sync}})^{-1}$ and $\star$ is used to denote portions of A which do not contribute to the torque.

Multiplying out (7.23), and combining terms, gives:

$$T_e = \frac{1}{2} v^s_{dq_{s1}}{}^{\mathrm{T}} A_{11} v^s_{dq_{s1}} + v^s_{dq_{s1}}{}^{\mathrm{T}} A_{12} v^s_{dq_{s2}} + \frac{1}{2} v^s_{dq_{s2}}{}^{\mathrm{T}} A_{22} v^s_{dq_{s2}} \tag{7.24}$$

As A_{22} will be of the form of a scalar multiplied by a rotation matrix, then the final term only depends on the magnitude of $v^s_{dq_{s2}}$, (that is $\sqrt{v^s_{dq_{s2}}{}^{\mathrm{T}} v^s_{dq_{s2}}}$) rather than its phase. Therefore the equilibrium conditions may be calculated from the following procedure:

1. Compute $A = (R_{\text{sync}} + Q_{\text{sync}})^{-1\text{T}} S_{\text{sync}} (R_{\text{sync}} + Q_{\text{sync}})^{-1}$.

2. Choose a magnitude for the stator 2 voltage, hence compute $\frac{1}{2} {v^s_{dq_{s2}}}^{\text{T}} A_{22} v^s_{dq_{s2}}$ (as ${v^s_{dq_{s2}}}^{\text{T}} A_{22} v^s_{dq_{s2}}$ is independent of the phase of $v^s_{dq_{s2}}$).

3. Write the stator 2 voltage in terms of a magnitude, $\sqrt{3}V_2$, and phase angle, ζ:

$$v^s_{dq_{s2}} = \sqrt{3} V_2 \begin{bmatrix} \cos(\zeta) \\ \sin(\zeta) \end{bmatrix} \tag{7.25}$$

4. Determine the maximum and minimum possible values for the electrical torque, given this stator 2 voltage magnitude. From (7.24) the maximum and minimum torques are give by:

$$T_e^{\max} = \frac{1}{2} {v^s_{dq_{s1}}}^{\text{T}} A_{11} v^s_{dq_{s1}} + \sqrt{{v^s_{dq_{s1}}}^{\text{T}} A_{12} A_{12}^{\text{T}} v^s_{dq_{s1}}} \sqrt{3} V_2 + \frac{1}{2} {v^s_{dq_{s2}}}^{\text{T}} A_{22} v^s_{dq_{s2}} \tag{7.26}$$

$$T_e^{\min} = \frac{1}{2} {v^s_{dq_{s1}}}^{\text{T}} A_{11} v^s_{dq_{s1}} - \sqrt{{v^s_{dq_{s1}}}^{\text{T}} A_{12} A_{12}^{\text{T}} v^s_{dq_{s1}}} \sqrt{3} V_2 + \frac{1}{2} {v^s_{dq_{s2}}}^{\text{T}} A_{22} v^s_{dq_{s2}} \tag{7.27}$$

5. For equilibrium the desired electrical torque, T_e will be equal to the load torque, T_l. Clearly an equilibrium will only be possible if $T_e^{\min} \leq T_l \leq T_e^{\max}$. Note that in the equality conditions there is only one solution for the phase of the stator 2 voltage, however at all other conditions there are two unique solutions. From (7.24), the solutions may be found by solving for the angle, ζ:

$${v^s_{dq_{s1}}}^{\text{T}} A_{12} \begin{bmatrix} \cos(\zeta) \\ \sin(\zeta) \end{bmatrix} = \frac{1}{\sqrt{3} V_2} \left(T_l - \frac{1}{2} {v^s_{dq_{s1}}}^{\text{T}} A_{11} v^s_{dq_{s1}} - \frac{1}{2} {v^s_{dq_{s2}}}^{\text{T}} A_{22} v^s_{dq_{s2}} \right) = K \tag{7.28}$$

Therefore the solutions are given by:

$$\zeta = \arcsin(K/\sqrt{a^2 + b^2}) - \text{arctan2}(a, b) \tag{7.29}$$

$$\zeta = \pi - \arcsin(K/\sqrt{a^2 + b^2}) - \text{arctan2}(a, b) \tag{7.30}$$

where arctan2 denotes the 4 quadrant inverse tangent function of a/b (see [107, sect. 2-115]) and:

$$\begin{bmatrix} a & b \end{bmatrix} = {v^s_{dq_{s1}}}^{\text{T}} A_{12} \tag{7.31}$$

6. Having now determined $v^s_{dq_{s2}}$ completely, the equilibrium currents may now be found from equation (7.21), as $v^s_{dq_{s1}}$ is already known.

7. If desired, the terminal voltages and currents may be calculated by using the inverse of the transformations given in table 7.1

7.4 Linearization of the Model

The model, given in equations (7.11), may now be linearized. The model is linearized by determining the first term of the Taylor series expansion evaluated about the chosen equilibrium conditions (see for example [26, p. 18], or [54]).

We seek a model of the form:

$$\frac{d}{dt}(\Delta x) = A\Delta x + B\Delta u \tag{7.32}$$

where $x \in \mathbb{R}^n$ represents the state vector, and $u \in \mathbb{R}^m$ the input vector, and the original nonlinear system can be represented as $\dot{x} = f(x, u, t)$.

Following [26, p. 18] $A = \nabla_x f(x_e, u_e, t)$, $B = \nabla_u f(x_e, u_e, t)$, where $\nabla_x f$ denotes:

$$\nabla_x f = \begin{bmatrix} \frac{\partial f_1}{\partial x_1} & \frac{\partial f_1}{\partial x_2} & \cdots \\ \frac{\partial f_2}{\partial x_1} & \frac{\partial f_2}{\partial x_2} & \cdots \\ \vdots & \vdots & \ddots \end{bmatrix}$$

As the stator 1 supply is constant, as discussed, it may simply be regarded as parameter which affects equilibrium conditions.

We seek a model of the form:

$$\frac{d}{dt}\begin{bmatrix} \Delta i^s_{dq0_{s1}} \\ \Delta i^s_{dq0_{s2}} \\ \Delta i^s_{dq_r} \\ \Delta\theta_r \\ \Delta\omega_r \end{bmatrix} = A\begin{bmatrix} \Delta i^s_{dq0_{s1}} \\ \Delta i^s_{dq0_{s2}} \\ \Delta i^s_{dq_r} \\ \Delta\theta_r \\ \Delta\omega_r \end{bmatrix} + B\begin{bmatrix} \Delta V_2 \\ \Delta\alpha_2 \\ \Delta T_l \end{bmatrix} \tag{7.33}$$

where A and B constant matrices which depend on the particular equilibrium condition, and Δ is used to denote 'small changes' in the variables from their equilibrium values. The other symbol retain their meanings from the previous sections.

The linearized model is then:

$$\frac{d}{dt}\begin{bmatrix} \Delta i^s_{dq0_{s1}} \\ \Delta i^s_{dq0_{s2}} \\ \Delta i^s_{dq_r} \\ \Delta\theta_r \\ \Delta\omega_r \end{bmatrix} = \begin{bmatrix} M^{-1}_{\text{sync}}\left(-R_{\text{sync}} - Q_{\text{sync}}(\omega_1, \omega^e_r)\right) & M^{-1}_{\text{sync}}\begin{bmatrix} 0 \\ \left.\frac{\partial v^s_{dq0_{s2}}}{\partial\theta_r}\right|_{\text{eqm.}} \\ 0 \end{bmatrix} & -M^{-1}_{\text{sync}}\frac{\partial Q_{\text{sync}}}{\partial\omega_r}(\omega_1) \begin{bmatrix} i^{se}_{dq0_{s1}} \\ i^{se}_{dq0_{s2}} \\ i^{se}_{dq_r} \end{bmatrix} \\ \begin{bmatrix} 0 & 0 & 0 \end{bmatrix} & 0 & 1 \\ \frac{1}{J}\begin{bmatrix} i^{se}_{dq0_{s1}}{}^{\text{T}} & i^{se}_{dq0_{s2}}{}^{\text{T}} & i^{se}_{dq_r}{}^{\text{T}} \end{bmatrix} S_{\text{sync}} & 0 & 0 \end{bmatrix} \begin{bmatrix} \Delta i^s_{dq0_{s1}} \\ \Delta i^s_{dq0_{s2}} \\ \Delta i^s_{dq_r} \\ \Delta\theta_r \\ \Delta\omega_r \end{bmatrix} + \begin{bmatrix} M^{-1}_{\text{sync}}\begin{bmatrix} 0 \\ \frac{1}{V_2} v^{se}_{dq0_{s2}} \\ 0 \end{bmatrix} & M^{-1}_{\text{sync}}\begin{bmatrix} 0 \\ \left.\frac{\partial v^s_{dq0_{s2}}}{\partial\alpha_2}\right|_{\text{eqm.}} \\ 0 \end{bmatrix} & 0 \\ 0 & 0 & 0 \\ 0 & 0 & -\frac{1}{J} \end{bmatrix} \begin{bmatrix} \Delta V_2 \\ \Delta\alpha_2 \\ \Delta T_l \end{bmatrix} \tag{7.34}$$

where the superscript e indicates an equilibrium value (e.g. $i^{se}_{dq0_{s1}}$). $\frac{\partial Q_{\text{sync}}}{\partial\omega_r}(\omega_1)$ denotes the partial derivative of Q_{sync} with respect to ω_r, as Q_{sync} was shown to be linearly dependent on ω_r then the derivative will be a constant, that is only a function of the constant ω_1. $\left.\frac{\partial v^s_{dq0_{s2}}}{\partial\alpha_2}\right|_{\text{eqm.}}$ denotes a partial derivative of the stator 2 supply voltage, which is subsequently evaluated at the equilibrium conditions; this will be discussed in the sequel. $\frac{1}{V_2}v^{se}_{dq0_{s2}}$ is the partial derivative of the stator 2 voltage with respect to the voltage magnitude, V_2, and then evaluated at the equilibrium conditions.

The presence of partial derivatives of the stator voltages in (7.34) deserves some clarification. From table 7.1 the stator 1 winding voltages are constant in the synchronous reference frame, that is they are independent of the input and state variables of (7.34). However the stator 2 winding voltage is a function of θ_r, which is one of the states of (7.34) as well as the control inputs V_2 and α_2. Therefore the linearised system must contain a term by which $\Delta\theta_r$ affects the machine currents, $\left.\frac{\partial v^s_{dq0_{s2}}}{\partial\theta_r}\right|_{\text{eqm.}}$. Also the '$B$' contains similar terms which derive from the partial derivatives of the stator 2 voltages. It is significant, however, that these terms are constant valued when evaluated at their steady-state

operating conditions. From table 7.1:

$$\left.\frac{\partial v^s_{dq0_{s2}}}{\partial \theta_r}\right|_{\text{eqm.}} = (-p_1 - p_2)\begin{bmatrix} -\sqrt{3}V_2^e \sin(\zeta^e) \\ -\sqrt{3}V_2^e \cos(\zeta^e) \\ 0 \end{bmatrix} \tag{7.35}$$

$$\left.\frac{\partial v^s_{dq0_{s2}}}{\partial V_2}\right|_{\text{eqm.}} = \begin{bmatrix} \sqrt{3}\cos(\zeta^e) \\ -\sqrt{3}\sin(\zeta^e) \\ 0 \end{bmatrix} = \frac{1}{V_2} v^{se}_{dq0_{s2}} \tag{7.36}$$

$$\left.\frac{\partial v^s_{dq0_{s2}}}{\partial \alpha_2}\right|_{\text{eqm.}} = \begin{bmatrix} -\sqrt{3}V_2^e \sin(\zeta^e) \\ -\sqrt{3}V_2^e \cos(\zeta^e) \\ 0 \end{bmatrix} \tag{7.37}$$

7.4.1 Conclusions for the Linearized Model

From the derivation of the linearized model a number of conclusions can be drawn about BDFM behaviour in the synchronous mode of operation which corroborate well-known results:

- The BDFM has a synchronous mode of operation much a like a synchronous machine, that is changes in load torque do not affect the steady-state shaft speed. This can be seen as a consequence of the natural 'integral action', which is present in (7.34): because part of the state vector contains $\Delta\theta_r$, then the only possible equilibrium conditions are when $\Delta\omega_r = 0$, as all others much imply $\frac{d\Delta\theta_r}{dt} \neq 0$. Therefore any changes in load torque imply a change in $\Delta\theta_r$ and the current, but not $\Delta\omega_r$. This change in physical angle was observed using a strobe on the prototype machine, a phenomenon also noted by other authors (e.g. [115, 125]).

- Changes in both magnitude (of sufficiently small amount) and phase (by any amount) of the stator 2 supply voltage do not affect the steady-state shaft speed. From similar reasoning to that applied to the load torque, changes to V_2 cannot affect $\Delta\omega_r$, or else the equilibrium cannot be maintained. From table 7.1, it can be seen that any change in the phase of V_2, α_2, may be matched by a change in θ_r and the value of the stator 2 supply voltage in the synchronous reference frame remain constant.

7.4.2 Simplification of Linearized Model

It is possible to simplify the linearized model derived if it is assumed that the electrical dynamics are sufficiently fast such that they can be considered to be constant. It must be emphasised that this assumption is not true, and may not even be a good approximation. Even if it were a good approximation, it is entirely possible that the simplified model may not be stable when a full linearized model (and hence the BDFM) is, and vice-versa. Nevertheless the simplicity of the model, makes the simplification worth consideration, although its application may be very limited.

From (7.34), if the electrical dynamics can be considered constant, then the linearized system may be written in terms of only the mechanical states:

$$\frac{d}{dt}\begin{bmatrix}\Delta\theta_r\\ \Delta\omega_r\end{bmatrix} = \begin{bmatrix} 0 & 1 \\ K_{\text{sync}}\begin{bmatrix}0\\ \left.\frac{\partial v^s_{dq0_{s2}}}{\partial\theta_r}\right|_{\text{eqm.}}\\ 0\end{bmatrix} & -K_{\text{sync}}\frac{\partial Q_{\text{sync}}}{\partial\omega_r}(\omega_1)\begin{bmatrix} i^{se}_{dq0_{s1}}\\ i^{se}_{dq0_{s2}}\\ i^{se}_{dq_r}\end{bmatrix}\end{bmatrix}\begin{bmatrix}\Delta\theta_r\\ \Delta\omega_r\end{bmatrix} + \begin{bmatrix} 0 & 0 & 0 \\ K_{\text{sync}}\begin{bmatrix}0\\ \frac{1}{V_2}v^{se}_{dq0_{s2}}\\ 0\end{bmatrix} & K_{\text{sync}}\begin{bmatrix}0\\ \left.\frac{\partial v^s_{dq0_{s2}}}{\partial\alpha_2}\right|_{\text{eqm.}}\\ 0\end{bmatrix} & -\frac{1}{J}\end{bmatrix}\begin{bmatrix}\Delta V_2\\ \Delta\alpha_2\\ \Delta T_l\end{bmatrix} \tag{7.38}$$

where:

$$K_{\text{sync}} = \frac{1}{J}\begin{bmatrix} i^{se}_{dq0_{s1}}{}^{\text{T}} & i^{se}_{dq0_{s2}}{}^{\text{T}} & i^{se}_{dq_r}{}^{\text{T}}\end{bmatrix} S_{\text{sync}}\left(R_{\text{sync}} + Q_{\text{sync}}(\omega_1, \omega^e_r)\right)^{-1} \tag{7.39}$$

which, from (7.23) can be written as:

$$= \frac{1}{J}\begin{bmatrix} v^{se}_{dq_{s1}}\\ v^{se}_{dq_{s2}}\\ 0\end{bmatrix}^{\text{T}}\begin{bmatrix} A_{11} & A_{12} & A_{13}\\ A_{12}{}^{\text{T}} & A_{22} & A_{23}\\ A_{13}{}^{\text{T}} & A_{23}{}^{\text{T}} & A_{33}\end{bmatrix} \tag{7.40}$$

7.4.3 Linearization Example

By way of an example we consider the linearization applied to a BDFM with a single set of rotor coils, with equations given by (7.18) and (7.19).

$$
\left[\begin{bmatrix}
L_{dq_1} & 0 & 0 & 0 & M_{1_1} & 0 \\
0 & L_{dq_1} & 0 & 0 & 0 & M_{1_1} \\
0 & 0 & L_{dq_2} & 0 & M_{2_1} & 0 \\
0 & 0 & 0 & L_{dq_2} & 0 & -M_{2_1} \\
M_{1_1} & 0 & M_{2_1} & 0 & L_{dq_r} & 0 \\
0 & M_{1_1} & 0 & -M_{2_1} & 0 & L_{dq_r}
\end{bmatrix} \begin{matrix} 0 & 0 \\ & \\ & \\ & \\ & \\ & \end{matrix}
\right.
$$

$$
\left.\begin{matrix}
0 & & & & 1 & 0 \\
0 & & & & 0 & J
\end{matrix}\right]
\frac{d}{dt}
\begin{bmatrix}
\Delta i^s_{dq0_{s1}} \\
\Delta i^s_{dq0_{s2}} \\
\Delta i^s_{dq_r} \\
\Delta\theta_r \\
\Delta\omega_r
\end{bmatrix} =
$$

$$
\begin{bmatrix}
R_{dq_1} & \omega_1 L_{dq_1} & 0 & 0 & 0 \\
-\omega_1 L_{dq_1} & R_{dq_1} & 0 & 0 & -\omega_1 M_{1_1} \\
0 & 0 & R_{dq_2} & ((p_1+p_2)\omega_r^e - \omega_1)L_{dq_2} & 0 \\
0 & 0 & -((p_1+p_2)\omega_r^e - \omega_1)L_{dq_2} & R_{dq_2} & -((p_2+p_1)\omega_r^e - \omega_1)M_{2_2} \\
0 & (\omega_1 - p_1\omega_r^e)M_{1_1} & 0 & (-\omega_1 + p_1\omega_r^e)M_{2_1} & R_{dq_r} \\
(p_1\omega_r^e - \omega_1)M_{1_1} & 0 & (p_1\omega_r^e - \omega_1)M_{2_1} & 0 & (p_1\omega_r^e - \omega_1)L_{dq_r} \\
0 & 0 & 0 & 0 & 0 \\
i^{se}_{qr} p_1 M_{1_1} & -i^{se}_{dr} p_1 M_{1_1} & -i^{se}_{qr} p_2 M_{2_1} & -i^{se}_{dr} p_2 M_{2_1} & -i^{se}_{qs1} p_1 M_{1_1} - i^{se}_{qs2} p_2 M_{2_1}
\end{bmatrix}
$$

$$
\begin{bmatrix}
\omega_1 M_{1_1} & 0 & 0 \\
0 & 0 & 0 \\
-((p_2+p_1)\omega_r^e - \omega_1)M_{2_1} & (p_1+p_2)\sqrt{3}V_2^e \sin(\zeta^e) & (p_1+p_2)L_{dq_2} i^{se}_{qs2} - (p_2+p_1)M_{2_1} i^{se}_{qr} \\
0 & (p_1+p_2)\sqrt{3}V_2^e \cos(\zeta^e) & -(p_1+p_2)L_{dq_2} i^{se}_{ds2} - (p_2+p_1)M_{2_2} i^{se}_{dr} \\
(\omega_1 - p_1\omega_r^e)L_{dq_r} & 0 & -p_1 M_{1_1} i^{se}_{qs1} + p_1 M_{2_1} i^{se}_{qs2} - p_1 L_{dq_r} i^{se}_{qr} \\
R_{dq_r} & 0 & p_1 M_{1_1} i^{se}_{ds1} + p_1 M_{2_1} i^{se}_{ds2} + p_1 L_{dq_r} i^{se}_{dr} \\
0 & 0 & 1 \\
i^{se}_{ds1} p_1 M_{1_1} - i^{se}_{ds2} p_2 M_{2_1} & 0 & 0
\end{bmatrix}
\begin{bmatrix}
\Delta i^s_{dq0_{s1}} \\
\Delta i^s_{dq0_{s2}} \\
\Delta i^s_{dq_r} \\
\Delta\theta_r \\
\Delta\omega_r
\end{bmatrix} +
$$

$$
\begin{bmatrix}
0 & 0 & 0 \\
0 & 0 & 0 \\
\sqrt{3}\cos(\zeta^e) & -\sqrt{3}V_2^e \sin(\zeta^e) & 0 \\
-\sqrt{3}\sin(\zeta^e) & -\sqrt{3}V_2^e \cos(\zeta^e) & 0 \\
0 & 0 & 0 \\
0 & 0 & 0 \\
0 & 0 & 0 \\
0 & 0 & -1
\end{bmatrix}
\begin{bmatrix}
\Delta V_2 \\
\Delta\alpha_2 \\
\Delta T_l
\end{bmatrix} \tag{7.41}
$$

It is interesting to note that (7.41) is similar in form to the linearized model of the doubly-fed cascade induction machine analysed by Cook and Smith [24]. This similarity is not unexpected as the form of the BDFM equations in the synchronous reference frame, are similar to those derived in [24].

The simplified linearised model becomes:

$$\frac{d}{dt}\begin{bmatrix}\Delta\theta_r\\ \Delta\omega_r\end{bmatrix} = \begin{bmatrix} 0 & 1 \\ \begin{matrix}K_{\text{sync}_3}(p_1+p_2)\omega_r^e\sqrt{3}V_2^e\sin(\zeta^e) - \\ K_{\text{sync}_4}(p_1+p_2)\omega_r^e\sqrt{3}V_2^e\cos(\zeta^e)\end{matrix} & \begin{matrix}K_{\text{sync}_3}((p_1+p_2)L_{dq_2}i_{qs2}^{se} - (p_2+p_1)M_{2_1}i_{qr}^{se}) + \\ K_{\text{sync}_4}(-(p_1+p_2)L_{dq_2}i_{ds2}^{se} - (p_2+p_1)M_{2_2}i_{dr}^{se}) + \\ K_{\text{sync}_5}(-p_1M_{1_1}i_{qs1}^{se} + p_1M_{2_1}i_{qs2}^{se} - p_1L_{dq_r}i_{qr}^{se}) + \\ K_{\text{sync}_6}(p_1M_{1_1}i_{ds1}^{se} + p_1M_{2_1}i_{ds2}^{se} + p_1L_{dq_r}i_{dr}^{se})\end{matrix}\end{bmatrix}\begin{bmatrix}\Delta\theta_r\\ \Delta\omega_r\end{bmatrix} + \begin{bmatrix} 0 & 0 & 0 \\ K_{\text{sync}_3}\sqrt{3}\cos(\zeta^e) - K_{\text{sync}_4}\sqrt{3}\sin(\zeta^e) & -K_{\text{sync}_3}\sqrt{3}V_2^e\sin(\zeta^e) - K_{\text{sync}_4}\sqrt{3}V_2^e\cos(\zeta^e) & -\frac{1}{J}\end{bmatrix}\begin{bmatrix}\Delta V_2\\ \Delta\alpha_2\\ \Delta T_l\end{bmatrix} \quad (7.42)$$

where K_{sync_n} denotes the n^{th} element of the row vector K_{sync}, defined in (7.40).

7.5 Simulated Results

The synchronous reference frame model and linearised model was implemented using the Matlab/Simulink computer modelling environment. The nested-loop design rotor, rotor number 1 was simulated being subject to a step increase in instantaneous phase on the the stator 2 voltage supply. That is, α_2 of table 7.1, was subject to a step increase at $t = 0$. The machine was configured to run at an equilibrium point, which was determined by the method described in section 7.3. It is expected that if the machine is in a stable operating point the operating point will recover after the increase in phase. This phenomenon can be understood from the stator 2 voltage in the synchronous reference frame, given in table 7.1: as α_2 changes θ_r changes in such a way to cancel out the change. Five different model variants were compared:

1. Full 26 state coupled-circuit model of chapter 2, 6 states for the stator currents, 18 states for rotor currents and two mechanical states.

2. Full order d-q transformed model (with zero sequence states removed), as described in chapter 3. The prototype nested-loop rotor BDFM has 3 sets of 6 loops, therefore the model has 4 stator states, 6 rotor states and 2 mechanical states, giving a total of 12 states.

3. Reduced order d-q transformed model, using the new method described in section, 3.4.2. The rotor is reduced to 2 states, hence there are 8 states in total.

4. Linearized version of the full d-q model with 12 states.

5. Linearized version of the reduced order d-q model with 8 states.

As discussed in chapter 3 the reduced order d-q model appears to be a very good approximation of the full order system. This proposition was corroborated during this series of tests, to the extent

that at the scale of the graphs there was no visible difference between the two. For this reason the reduced order d-q model, and linearised version have been omitted from all but figure 7.2(b), to aide clarity.

The responses of the shaft speed and d-axis stator 1 current in the synchronous reference frame have been compared at different operating points. These measurements were chosen as they illustrate the performance of the different models, the other current measurements had a similar accuracy.

Figures 7.1(a) and 7.1(b) show the speed response to a small phase change at two different operating points, one stable, the other unstable. Figures 7.1(c) and 7.1(d) show the d-axis synchronous reference frame current under the same conditions. In each case the response of the 26 state full coupled circuit model, the full d-q model and the linearized d-q model were included.

Figures 7.2(a) and 7.2(b) show the the speed response at the same stable operating point used in figure 7.1, but with a much larger phase change. Figure 7.2(a) may be compared with figure 7.1(a), where the phase changes were 6° and 60° respectively. Figures 7.2(a) and 7.2(b) compare the full-order linearized d-q model and reduced order linearized d-q model.

Figures 7.2(c) and 7.2(d) show the real part of the eigenvalues of the linearized full order system at the stable and unstable operating points. The figures show the change in eigenvalues as the operating point changes, brought on by a change in load torque. No values are given outside certain bounds, as this bound corresponds to the maximum torque available from the machine at those voltage magnitudes. Two sets of eigenvalues are plotted in each case, one set in blue and the other in red. The two sets of eigenvalues corresponding to the same load torque and voltage magnitude, but differing voltage phase, as described in section 7.3.

Figure 7.3 shows the real parts of the eigenvalues of the full order linearised model and the reduced order linearised model.

From figures 7.1, 7.2 and 7.3 we may draw the following conclusions:

- The full-order and reduced order d-q model are accurate representations of the full coupled circuit model in this case.
- The full-order linearized model is an excellent approximation of the full system, however as the system is perturbed away from the operating point the accuracy decreases, as expected.
- The reduced order linearised model is also an excellent approximations of the full system, this fact is corroborated by the eigenvalue plots, which are almost co-incident with those of the full order model, except for the extra eigenvalues, which are stable
- The stability of an operating point was predicted by the linearized model, as expected.
- The stability of the simulated prototype BDFM with a nested loop rotor varied significantly with both load torque, stator voltage magnitudes and shaft speed. Certain regions were naturally unstable.

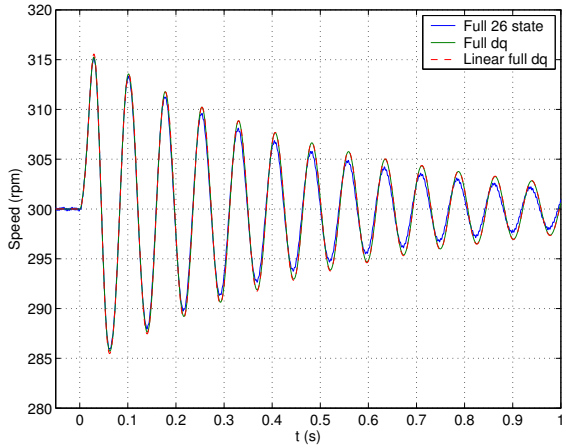

(a) Speed response to 6° phase change at a stable operating point

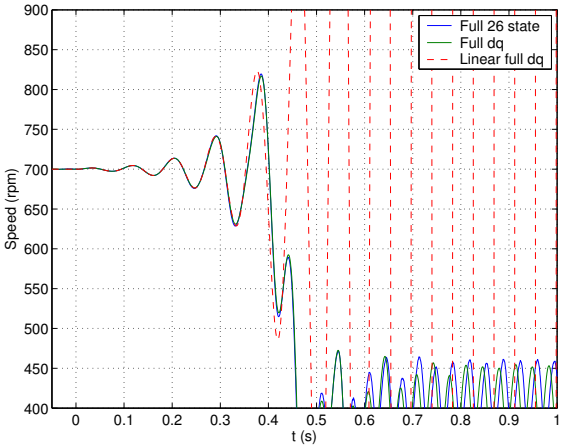

(b) Speed response response to 6° phase change at an unstable operating point

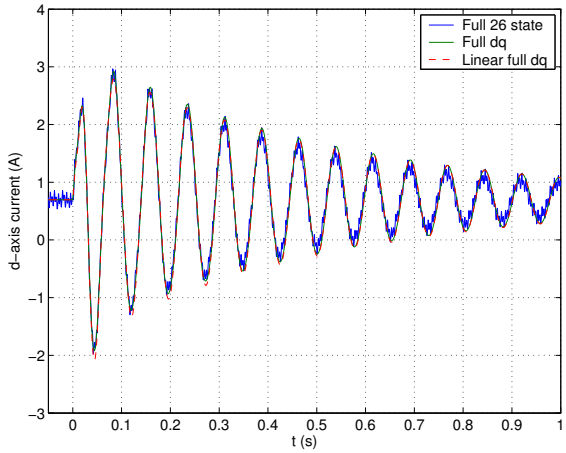

(c) d-axis stator 1 current response to 6° phase change in sync. ref. frame at a stable operating point

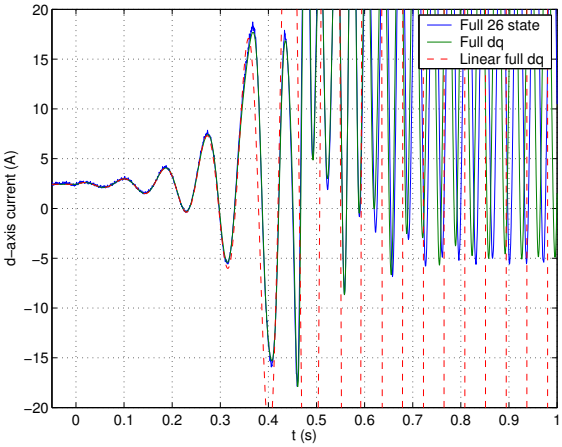

(d) d-axis stator 1 current in sync. ref. frame at an unstable operating point

Figure 7.1: Nested-loop design rotor response to a step change in stator 2 voltage phase. The stable operating point was, 300 rpm, 240V_{rms} stator 1 phase voltage, 216V_{rms} stator 2 phase voltage, 5 N m load torque, and the phase change was 6° as indicated. The unstable operating point was 700 rpm, 240V_{rms} stator 1 phase voltage, 96V_{rms} stator 2 phase voltage, 5 N m load torque, and the phase change was 0.5°.

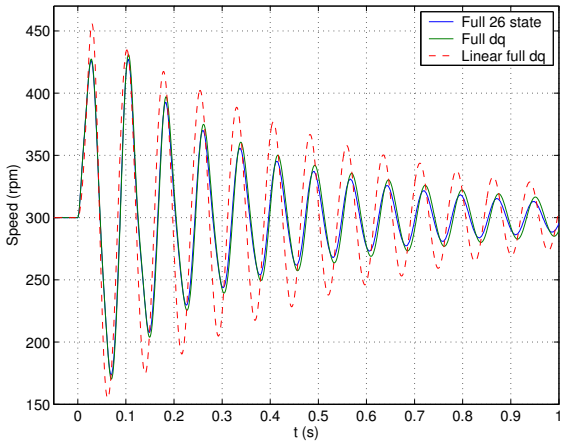

(a) Speed response to 60° phase change at a stable operating point

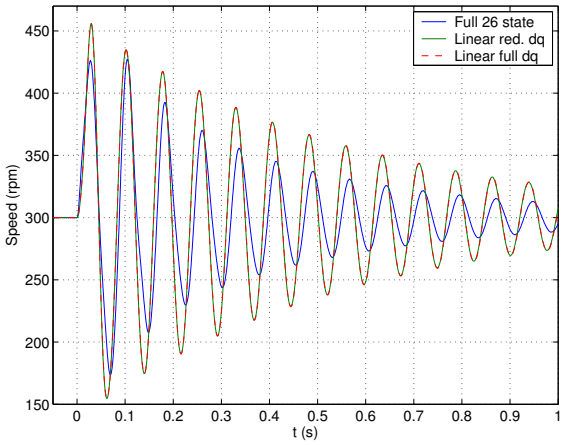

(b) Speed response to 60° phase change at a stable operating point showing reduced order linearized model

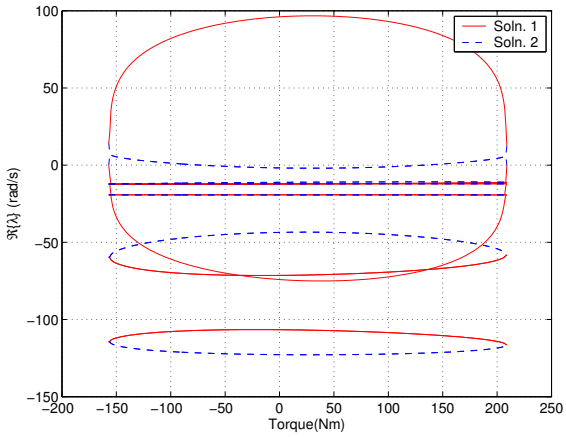

(c) real part of the eigenvalues of linearized model at a stable operating point

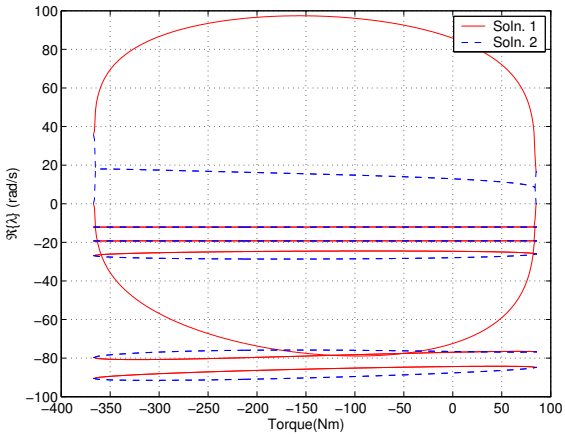

(d) real part of the eigenvalues of linearized model at a unstable operating point

Figure 7.2: The response of the prototype nested loop rotor to a 60° phase change, and the real part of the eigenvalues of the linearized model at the two operating points (shown in blue). Additionally the real part of the eigenvalues of the other solution to another operating point having the same voltage magnitudes, load torque but differing voltage phase (shown in red). The operating points are described in figure 7.1

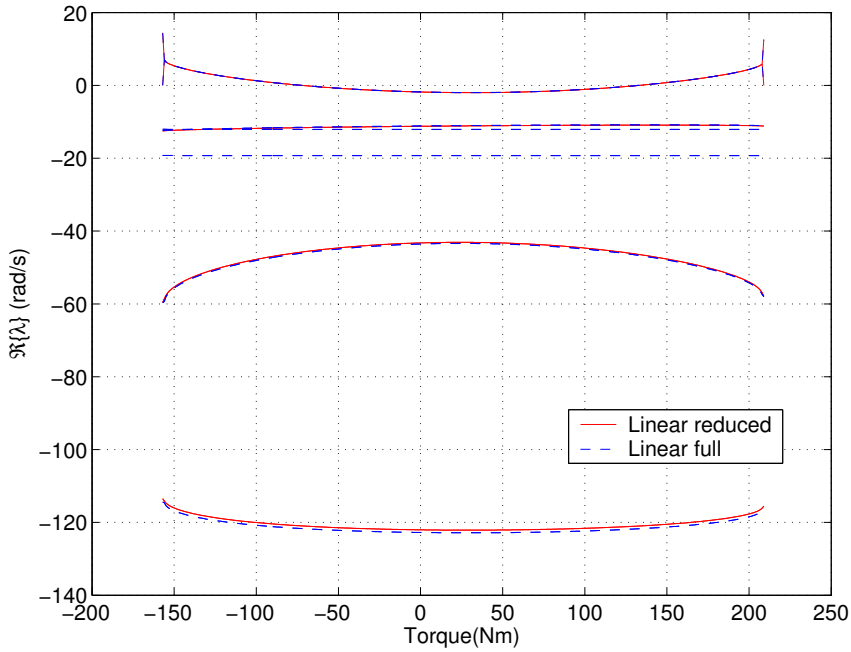

Figure 7.3: The real parts of the eigenvalues of the full order linearized model, and reduced order linearised model at the stable operating point described in figure 7.1

7.6 Open-loop Experimental Results

Rotor 2 was tested open-loop, in the prototype machine. Full details of the experimental apparatus are given in appendix E. As with the simulated results a step change in phase was applied to the stator 2 voltage source, and the response of the shaft speed logged. The experimental data was compared with simulated data generated using the parameter values found in section 6, and a calculated value for the moment of inertia of the drive train. However as the dimensions of the rotor of the DC load motor can only be estimated, this value could be significantly in error, the value was therefore adjusted to $J = 0.59\text{kgm}^2$, which was still within estimation error range of the calculated value, but gave a natural frequency closer to that found in practice. The resistance values were increased to $R_1 = 4\Omega$ and $R_2 = 5.5\Omega$ (from the estimated values of $R_1 = 3.6\Omega$ and $R_2 = 4.3\Omega$) to compensate for additional supply impedances present. This increase in impedance was necessary for the simulated results to be stable at the second operating point.

Figure 7.4 shows the response at an unstable operating point, and figure 7.5 at a stable operating point. It is significant to note that the two operating points differ only in their supply voltage, yet one is stable and the other unstable (as the oscillations in figure 7.4 are divergent and whereas those in figure 7.5 are convergent). Figure 7.6 shows the maximum real part of the linearized system eigenvalues over a range of torques at the two operating conditions. Although the same general 'shape' is obtained in both conditions, the centre point moves, which made one operating point unstable at no-load. Figure 7.6 suggests that stability would be achieved if the load torque was increased, which is precisely what

was found in practice.

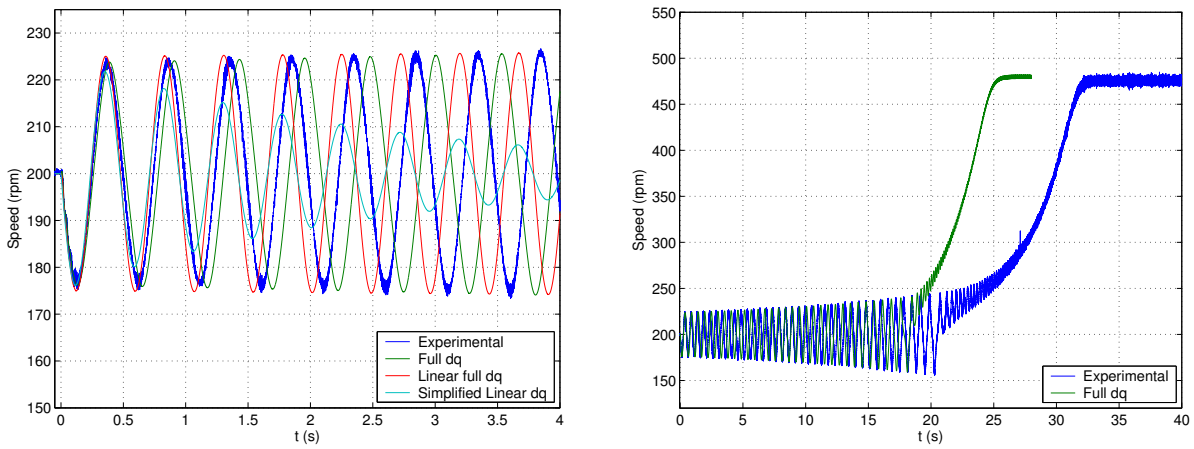

(a) (b)

Figure 7.4: Speed response to a $-67.5°$ phase change applied to the stator 2 voltage supply. $V_1 = 90\text{V}_{\text{rms}}$, $V_2 = 81.5\text{V}_{\text{rms}}$, 0 N m load torque. Both sub-figures show the same event at different time scales

Figures 7.4 and 7.6 show that the full d-q model and its linearization are in reasonable agreement with reality. The simplified linearized d-q model (as described in section 7.4.2) is also included for comparison, however although the natural frequency is approximately right, the damping is in significant error in both figures.

However the damping of the full d-q model and its linearization is still at odds with that found in experiment. It is likely that effects, such as supply impedance and frictional forces are partly the cause, combined with the inevitable errors in the parameter values in the simulation model.

Figure 7.4 shows that the natural frequency of the full d-q model and its linearized counterpart are somewhat in error. However the amount of error is comparable with that found in figure 7.2(a) between the non-linear and linearized models, allowing for the differing time scales.

In conclusion, the results found by experiment on the prototype machine are in good agreement with those obtained from simulation. However, the machine dynamics themselves are very lightly damped, or unstable at the operating conditions investigated. Even the stable operating condition is hardly usable as a commercial drive, furthermore it was found that if the stator resistances were halved in value in simulation tests, then neither operating point was stable for any load torque with any stator 2 supply voltage. Therefore the use of feedback to stabilize the operating point will now be considered.

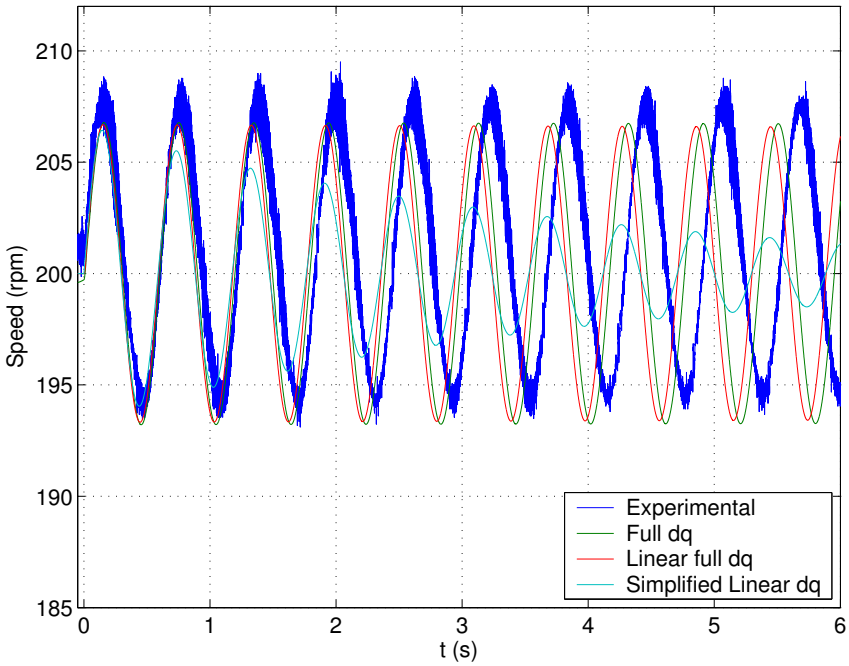

Figure 7.5: Speed response to a 22.5° phase change applied to the stator 2 voltage supply. $V_1 = 68\mathrm{V_{rms}}$, $V_2 = 70\mathrm{V_{rms}}$, 0 N m load torque.

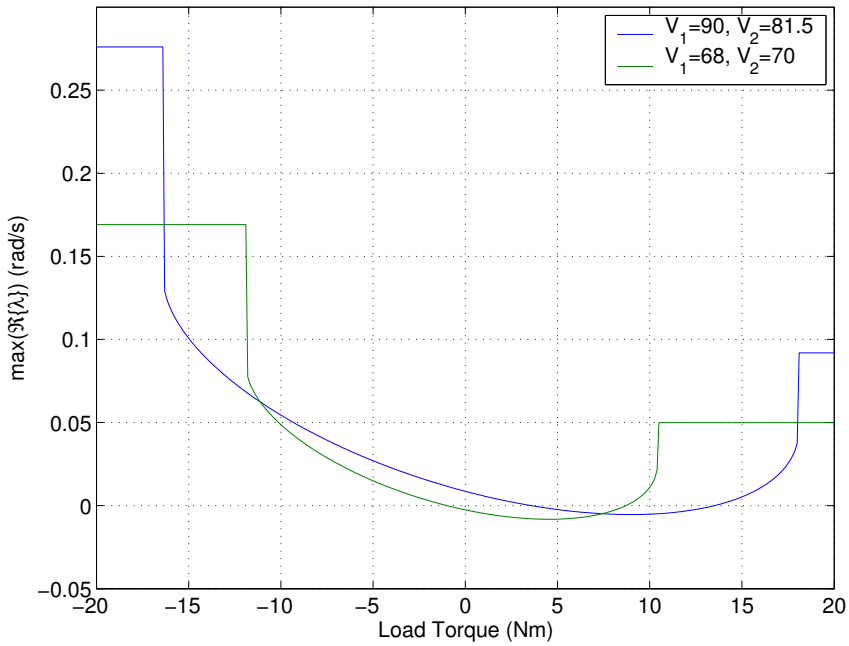

Figure 7.6: Comparison of the maximum real part of the eigenvalues of the linearized system at two different supply voltage corresponding to the operating condition of figures 7.4 and 7.5, against load torque. The horizontal lines do not correspond to valid operating conditions as the particular combinations of supply voltages cannot deliver the torque.

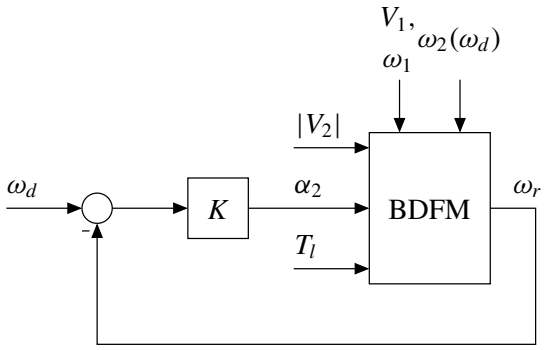

Figure 7.7: Stator 2 phase angle control concept

7.7 Closed-loop 'stator 2 phase angle control'

In section 7.6 it was found that there are operating points within the machine operation envelope which are very lightly damped or unstable. Such regions have been found by other groups (e.g [61]). In [84] the author described two control strategies which can be used to stabilize the BDFM. The first of these, 'stator 2 phase angle control' will now be described.

The essential idea is to feed back the speed error as the value of α_2, the phase input to the stator 2 supply, as shown in figure 7.7. V_1 and V_2 represent the stator 1 and 2 voltages, which will be of the form given in table 7.1, and T_l is the load torque. Together these parameters set the operating point.

The designer must choose K to stabilise the closed loop. The idea is to choose K so it robustly stabilizes the system, such that the load torque and stator 2 supply voltage magnitude can be set within some range (that is the operating point can be changed slightly) without loosing stability. However, although the linearised model is accurate in some neighbourhood of the operating point, as soon as the operating point changes, the model will no longer be correct. Furthermore the system is not (or may not) be accurately represented by the linearized model in transition between operating points. Typically if the transition is sufficiently slow, then the linearized model will be accurate. This complicates the design of K.

A full discussion on the design of K is beyond the scope of this dissertation, however some practical methods are proposed, and then some possible extensions are discussed in section 7.9.

If K is restricted to controllers without integral action, then the operating point cannot be changed if the system is stable. This is because α_2 can never be a ramp in the steady-state, and therefore the steady-state shaft speed must remain unchanged. Although this might appear restrictive, the operating point may still be changed by modifying ω_2, and it is actually advantageous because it means that there will be no steady-state error.

Furthermore if K does contain integral action, any error introduced will be constant in the steady-state. The error will be proportional to the fixed errors in the measured and demanded value of ω_1, ω_2 and ω_r. However, as these errors can easily be made of the order 1 part in 2^{16} (by the use of 16 bit precision electronics), then such steady state errors are small enough to make the use of integral

action in the controller possible. The addition of integral action to the controller was found to improve the ability of the controller to stabilize large deviations from an operating point.

Regardless of how K is chosen, the steady-state operating point may be set by choice of V_1, ω_1, V_2, ω_2, and then stabilized by K. The designer therefore has freedom to optimize for steady-state performance, without concern for stability which can be ensured by the design of K.

In practice it was found that proportional or proportional-integral controllers could be tuned to give reasonable damping in experiments on the prototype BDFM. Furthermore, these controllers were found stabilize the system over a significant range of operating points. During these experiments the value of ω_2 was set open-loop by the value of ω_d from equation 7.1 as shown in figure 7.7. $|V_2|$ was chosen as a function of ω_d: $|V_2| = k \max\{\frac{|\omega_d - \omega_n|}{\omega_n}, 0.2\}$, that is, $|V_2|$ was proportional to the deviation from natural speed with a boost at low values.

7.7.1 Experimental Results

The control algorithm was implemented in simulation and on the experimental test rig described in appendix E. Although the analysis in this section requires the synchronous reference frame model, the implementation of the control law simply requires the creation of 3 phase balanced voltages for the stator 2 supply. This is achieved by the inverter, the input of which was designed to accept three parameters, ω_2, V_2 and α_2. Thus ω_2 and V_2 are fixed for the operating point and $\alpha_2 = K_p(\omega_d - \omega_r) + \int K_i(\omega_d - \omega_r)dt$.

Figure 7.8 shows the same operating point as figure 7.5 stabilized with a PI controller, $K_p = 1$, $K_i = 3$, with all measurements in radians (and radians per second).

We now consider the robustness of the controller by changing the operating point. This is achieved by varying the load torque and shaft speed: figures 7.9(c) and 7.9(d) show the response to a step change in load torque, which is now well damped.

Figure 7.9 shows 50 rpm step responses up and down for the BDFM stabilized with the same PI controller. Note that moving operating speed changes the operating point and so the system dynamics are no longer the same. Furthermore, as discussed, the dynamics in transit between operating points are likely to be poorly predicted by a linear model. The stator 2 voltage magnitude, $|V_2|$ was scaled linearly with the demanded shaft speed: $|V_2| = |V_2^o| \left|\frac{\omega_d - \omega_n}{\omega_n}\right|$ where ω_d is the demanded speed, ω_n is the natural speed as given by (1.2), and $|V_2^o|$ is a constant reference voltage.

The oscillations in the rising edge of figure 7.8(a) do not appear in the linearized model, and furthermore the linearized model suffers from a steady-state offset when the shaft speed is changed. This is to be expected from the form of the linearized model, equation (7.34).

The results show that even simple PI control can achieve stability which is robust to modest changes in operating conditions, furthermore the linear model is shown to accurately predict the closed loop system even under changes in load torque, which constitute a change in operating point. However it was found that if a step change in equilibrium speed greater than about 60 rpm was de-

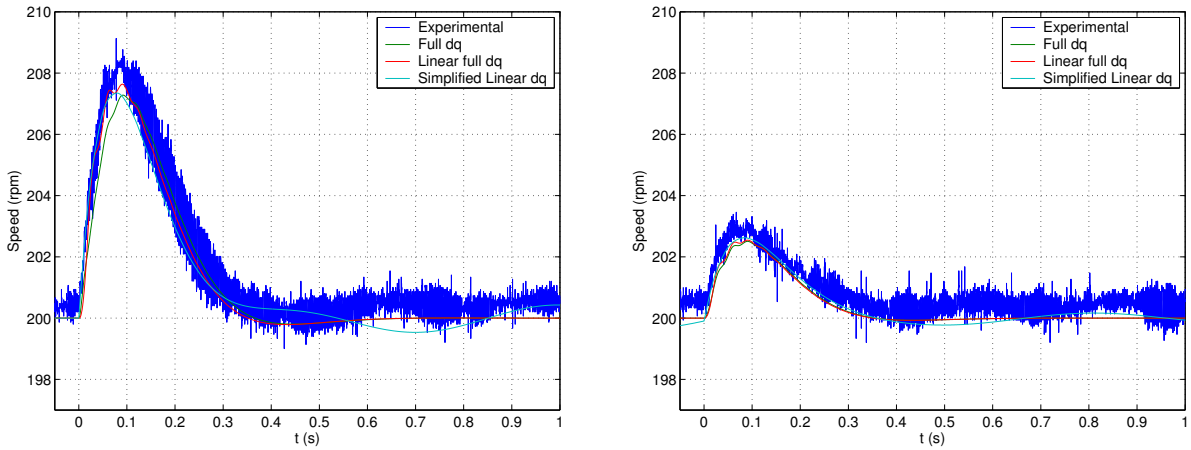

(a) 67.5° step change in stator 2 voltage phase

(b) 22.5° step change in stator 2 voltage phase

Figure 7.8: Closed-loop speed response under 'stator 2 voltage phase angle control' to a 67.5° and 22.5° step phase change applied to the stator 2 voltage supply. The step phase change was introduced by augmenting α_2 of figure 7.7 by injecting a disturbance d, where d represents the step change. $V_1 = 68\text{V}_{\text{rms}}$, $V_2 = 70\text{V}_{\text{rms}}$, 0 N m load torque, the same operating condition as figure 7.5

manded then the system lost stability.

7.8 Control when $\int \omega_2 dt = (p_1 + p_2)\theta_r - \int \omega_1 dt$

The concept of 'stator 2 phase angle' control was to stabilize a open-loop operating point of the machine, however no attempt was made to stabilize transitions from one operating shaft speed to another.

It can be seen from (7.34) that if $\int \omega_2 dt = (p_1 + p_2)\theta_r - \int \omega_1 dt$, then $\frac{\partial v^s_{dq0_{s2}}}{\partial \theta_r} = 0$ as $v^s_{dq0_{s2}}$ is no longer a function of θ_r. This has the effect of removing $\Delta\theta_r$ as a state from the linearized model. Therefore the linearized model can now have many different equilibrium speeds. This implies a loss of the natural integral action maintaining the synchronous speed, and the machine now behaves more like an asynchronous machine where its steady-state operating point is not robust to torque perturbations.

However the integral action can be restored though the design of a suitable controller, K. The configuration of the feedback loop is the same as that for stator 2 phase angle control, as shown in figure 7.7. It was found that reasonable performance could be achieved with $K_p = 0.3$ and $K_i = 0.6$.

Figure 7.10 shows experimental and simulated results from this control strategy. The first thing to note is that figures 7.10(c) and 7.10(d) show that the system was stable for 100 rpm demanded step changes in ω_r. Furthermore it was found that the same controller gains permitted 100 rpm step changes within the speed range from 0 to 600 rpm. Beyond that range the robustness was found to

deteriorate, and different gains were required for adequate performance

However figures 7.10(a) and 7.10(b) show a degraded torque disturbance rejection over that shown in figure 7.9. Furthermore there is a steady-state error introduced, as was also the case in the speed step responses.

The steady-state error was due to the implementation of $\int \omega_2 dt = (p_1 + p_2)\theta_r - \int \omega_1 dt$. Instead of using θ_r measurement directly, $\int \omega_r dt$ was used which therefore led to errors being introduced. It was found by simulation that a 0.1% error in the value of ω_r was sufficient to produce the steady-state error observed in the experiment. This order of the error is consistent with the limitations of the speed transducer (see appendix E). A steady-state error persisted despite integral action in the controller as the errors in ω_r led to constant errors in angular *speed* error, which is therefore a *ramp* error in phase; hence single integral action cannot drive the steady-state error to zero.

The steady-state error can, however, be reduced by as much as is desired by reducing the error in implementing $\int \omega_2 dt = (p_1 + p_2)\theta_r - \int \omega_1 dt$. Practically speaking this was achieved by using the measured position, θ_r (rather than integrating ω_r), and by generating $\int \omega_1 dt$ using a phase-locked loop locked onto the stator 1 voltage. The input to the inverter was then the instantaneous phase of the desired stator 2 voltage, rather than the angular frequency. This alternative design was implemented in software using the experimental test rig, and was found to substantially remove the speed offset. However this was achieved at the expense of requiring the measurement of the instantaneous stator 1 voltage at a high sample rate.

7.9 Future work on linear model based control

Two linear control strategies have been presented in this chapter. Both strategies are scalar strategies and therefore assume that the magnitude of the stator 2 will be set open loop (or in a very slow closed loop). This is a reasonable assumption for general motor drive and generator applications where the bandwidth requirements of speed tracking are considerably more stringent than any other consideration.

The speed step response rise-time of both strategies compared favourably to previously published results. For a 50 rpm step the rise time for stator 2 phase angle control was 750 ms and the fall time 350 ms. For the second strategy the rise time was approximately 1500 ms and the fall time 2000 ms. Previously published rise times are 15000 ms for so-called scalar control [127, 126], and between 300 ms and 1200 ms for various field-orientated control schemes [126, 124].

It must be emphasised that the design of controllers for these strategies has not been thoroughly considered, so the presented results are likely to be worse than those that could be expected in the future. We will now briefly consider methods of improving controller performance.

Although there are fundamental limitations in linear design methods when applied to non-linear plants, a significant improvement in performance is typically obtained by designing a series of lin-

ear controllers for different operating points and then scheduling between these controllers for the implementation. This technique, known as gain scheduling, seeks to find a controller which is parameterised in some way on operating points. Traditionally such methods were ad-hoc methods where a plant was linearized at a number of operating points, and controllers designed for each. There are two problems with these methods, firstly that while each controller will stabilize its own operating point, and possibly neighbouring operating points, it may not stabilise the transition between the two. Secondly switching between two (or more) controllers which stabilize an operating point can actually introduce instability.

Recent advances on the formulation of gain scheduling problems as LMIs has led to solutions to both these difficulties in some circumstances. Rugh and Shamma give an thorough summary of research to date, with a good list of references, [89], and Apkarian and Adams is recommended for controller synthesis [3].

Rugh and Shamma describe two different methods of achieving gain scheduling. The more recent of these methods, 'quasi-LPV' control, uses LMIs to find parameter dependent controllers which guarantee stability and some performance measures [89, sect. 5]. Unfortunately the method requires that the scheduling variable (possibly a vector) is measurable in real time. This presents a significant problem for application of these methods to the BDFM. The BDFM operating points depend on the load torque, shaft speed, voltages and currents, and the rotor current is very unlikely to be available for measurement in real time.

Rugh and Shamma also give a summary of developments in the traditional gain-scheduling approach where a set of linear controllers are designed for a set of equilibria and then interpolated in some way to produce parameter dependent controllers [89, sect. 4]. In the BDFM the steady-state operating points of the BDFM depend only the supply voltages, shaft speed, and load torque (as the current can be computed in the steady-state). It is likely that the load torque dependence can be replaced by a dependence on the stator currents. Therefore the linear controllers would only depend on these measurable parameters. Under certain conditions, which include bounding the rate of variation of the parameters, stability can be guaranteed.

Whether or not it is possible to obtain a stability guarantee gain scheduled controllers are likely to be applicable. One appealing aspect of the approach is that one might choose to specify the only one scheduling parameter, say the shaft speed, if all the other parameters can be expressed as a function of the shaft speed. In an application where the BDFM is connected to a device for which the load torque is a known function of speed (for example if the BDFM was operating as a pump), and the voltages were specified open loop, then a gain scheduled controller would only need to be parameterised on the shaft speed. In [84] the author presented results from a gain-scheduled version of stator 2 phase angle control, where the BDFM was stabilized over a wide speed range, which illustrates that such an approach is possible.

There is also scope for including uncertainty explicitly in the model, and designing control laws

which achieve guaranteed stability, and possibly guaranteed performance in the face of this uncertainty. Apkarian and Adams (and others) have shown that it can be achieved for unstructured time-varying uncertainty in the case of quasi-LPV methods [3]. However at the time of writing no results have appeared for the inclusion of structured uncertainty, which is likely to limit the application to the BDFM. The linearization gain scheduling methods can incorporate uncertainty in the design of linear controllers for each operating point. However this does not imply any guarantees for the global properties of the closed loop system. However if a controller has been designed using the linearization gain scheduling methods (or indeed by the quasi-LPV methods) its stability can be investigated using LPV analysis techniques [120]. The practical implementation of the necessary LMIs is similar to that described in [3] for the LPV synthesis problem.

7.10 Conclusions

In this chapter we have presented a synchronous reference frame model for the full class of BDFM machines considered in chapter 2. The synchronous reference frame was shown to be simply an invertible state transformation of the rotor reference frame dq model of chapter 3

The synchronous reference was used to determine all equilibrium points, and it was noted that in general there are either 2, 1 or 0 possible equilibrium points for a given stator 1 voltage, load torque and stator 2 voltage magnitude.

The synchronous reference frame model was then linearized about its equilibrium points. Simulation results were presented for the 'nested-loop' design rotor, comparing the full range of models, from the coupled circuit model of chapter 2, through the full d-q and then reduced order d-q models of chapter 3, to the linearized versions of these models.

Excellent agreement was found for all operating conditions investigated. The linearized models predicted the stability and damping accurately. The exception to this was the simplified linearized model, which did not correctly predict the damping.

Experimental results were presented for the double-layer rotor design, rotor 2 in open-loop conditions, and the linearized model, using parameters estimated in chapter 6, gave good predictions of stability and dynamic performance.

Two linear control strategies were presented, stator 2 phase angle control and control when $\int \omega_2 dt = (p_1 + p_2)\theta_r - \int \omega_1 dt$. It was shown that both strategies could stabilize previously unstable operating points, and the performance of these controllers compared favourably to previously published results.

It was concluded that the use of gain-scheduled controllers for these control strategies would be likely to further improve performance.

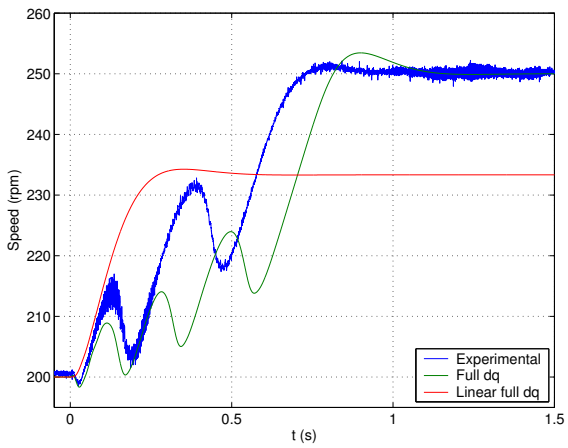

(a) Speed step response from 200 rpm to 250 rpm

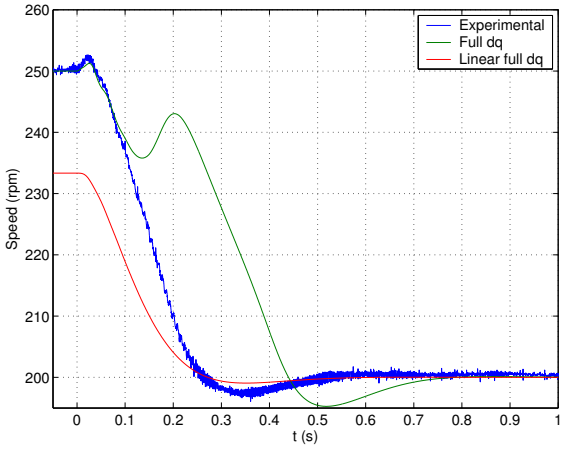

(b) Speed step response from 250 rpm to 200 rpm

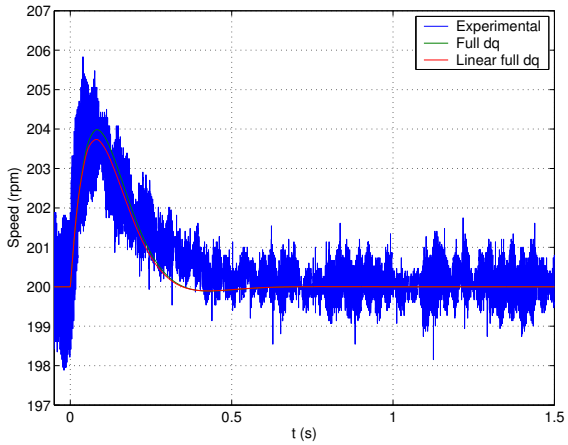

(c) Response to load torque step from 7 N m to 0 N m

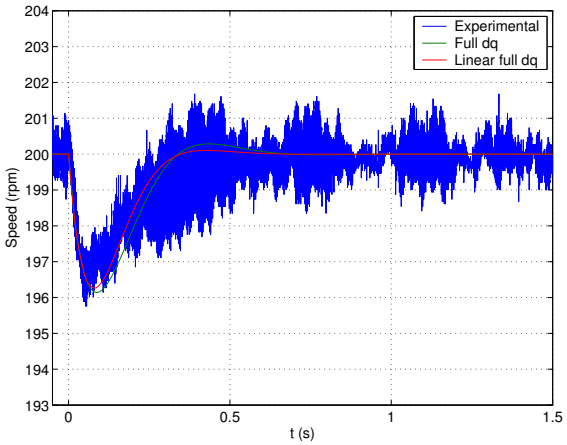

(d) Response to load torque step from 0 N m to 7 N m

Figure 7.9: Closed-loop speed response under 'stator 2 voltage phase angle control' to demanded step speed change from 200 rpm to 250 rpm and back down, and step change in load torque from 0 N m to 7 N m and back down. $V_1 = 68\text{V}_{\text{rms}}$, $V_2 = 70\text{V}_{\text{rms}}$, 0 N m load torque for speed steps, the same operating condition as figure 7.5

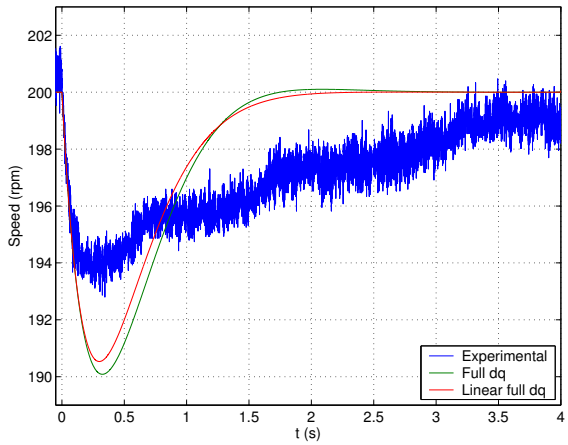

(a) Response to 5 N m step increase in torque

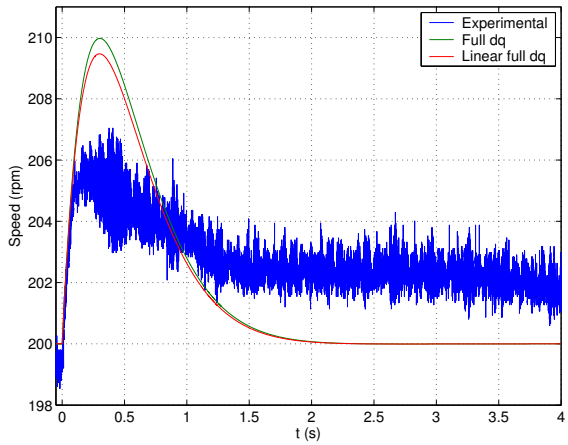

(b) Response to 5 N m step decrease in torque

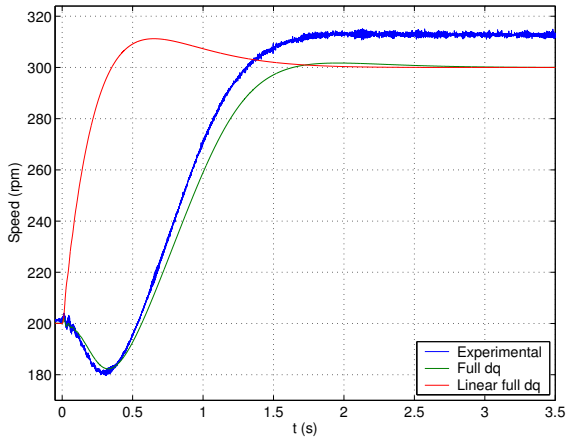

(c) Step response from 200 rpm to 300 rpm

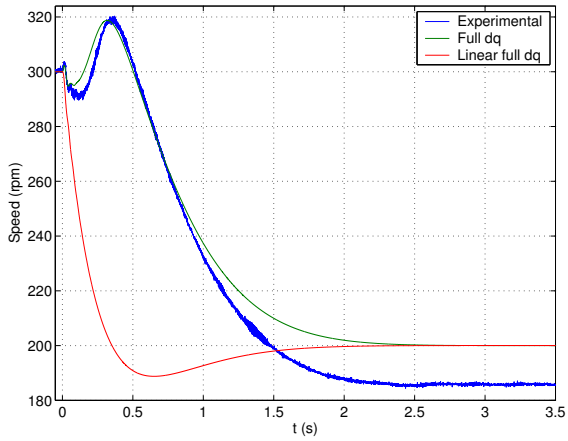

(d) Step response from 300 rpm to 200 rpm

Figure 7.10: Closed-loop speed step response when $\int \omega_2 dt = (p_1 + p_2)\theta_r - \int \omega_1 dt$ to demanded step speed change from 200 rpm to 300 rpm and back down, and step change in load torque from 0 N m to 5 N m and back down. $V_1 = 68\mathrm{V_{rms}}$, $V_2 = 70\mathrm{V_{rms}}$, 0 N m load torque for speed steps, the same operating condition as figure 7.5

	Terminal Phase Voltage	Rotor ref. frame d-q quantity	Sync. ref. frame. d-q quantity
Stator 1			
Voltage:	$\begin{bmatrix} \sqrt{2}V_1\cos(\omega_1 t+\alpha_1) \\ \sqrt{2}V_1\cos(\omega_1 t+\alpha_1-\frac{2\pi}{3}) \\ \sqrt{2}V_1\cos(\omega_1 t+\alpha_1+\frac{2\pi}{3}) \end{bmatrix}$	$\begin{bmatrix} \sqrt{3}V_1\cos(p_1\theta_r-\omega_1 t-\alpha_1) \\ \sqrt{3}V_1\sin(p_1\theta_r-\omega_1 t-\alpha_1) \\ 0 \end{bmatrix}$	$\begin{bmatrix} \sqrt{3}V_1\cos(\alpha_1+\phi_{1_1}) \\ -\sqrt{3}V_1\sin(\alpha_1+\phi_{1_1}) \\ 0 \end{bmatrix}$
Transformation:		$\sqrt{\frac{2}{3}}\begin{bmatrix} \cos(p_1\theta_r) & \cos(p_1(\theta_r-\frac{2\pi}{3p_1})) & \cos(p_1(\theta_r-\frac{4\pi}{3p_1})) \\ \sin(p_1\theta_r) & \sin(p_1(\theta_r-\frac{2\pi}{3p_1})) & \sin(p_1(\theta_r-\frac{4\pi}{3p_1})) \\ \frac{1}{\sqrt{2}} & \frac{1}{\sqrt{2}} & \frac{1}{\sqrt{2}} \end{bmatrix}$	$\begin{bmatrix} \cos(p_1\theta_r-\omega_1 t+\phi_{1_1}) & \sin(p_1\theta_r-\omega_1 t+\phi_{1_1}) & 0 \\ -\sin(p_1\theta_r-\omega_1 t+\phi_{1_1}) & \cos(p_1\theta_r-\omega_1 t+\phi_{1_1}) & 0 \\ 0 & 0 & 1 \end{bmatrix}$
Stator 2			
Voltage:	$\begin{bmatrix} \sqrt{2}V_2\cos(\int\omega_2 dt+\alpha_2) \\ \sqrt{2}V_2\cos(\int\omega_2 dt+\alpha_2-\frac{2\pi}{3}) \\ \sqrt{2}V_2\cos(\int\omega_2 dt+\alpha_2+\frac{2\pi}{3}) \end{bmatrix}$	$\begin{bmatrix} \sqrt{3}V_2\cos(p_2\theta_r-\int\omega_2 dt-\alpha_2) \\ \sqrt{3}V_2\sin(p_2\theta_r-\int\omega_2 dt-\alpha_2) \\ 0 \end{bmatrix}$	$\begin{bmatrix} \sqrt{3}V_2\cos((-p_1-p_2)\theta_r+(\int\omega_2 dt+\omega_1 t)+\alpha_2+\phi_{2_1}) \\ -\sqrt{3}V_2\sin((-p_1-p_2)\theta_r+(\int\omega_2 dt+\omega_1 t)+\alpha_2+\phi_{2_1}) \\ 0 \end{bmatrix}$
Transformation:		$\sqrt{\frac{2}{3}}\begin{bmatrix} \cos(p_2\theta_r) & \cos(p_2(\theta_r-\frac{2\pi}{3p_2})) & \cos(p_2(\theta_r-\frac{4\pi}{3p_2})) \\ \sin(p_2\theta_r) & \sin(p_2(\theta_r-\frac{2\pi}{3p_2})) & \sin(p_2(\theta_r-\frac{4\pi}{3p_2})) \\ \frac{1}{\sqrt{2}} & \frac{1}{\sqrt{2}} & \frac{1}{\sqrt{2}} \end{bmatrix}$	$\begin{bmatrix} \cos(p_1\theta_r-\omega_1 t+\phi_{2_1}) & -\sin(p_1\theta_r-\omega_1 t+\phi_{2_1}) & 0 \\ \sin(p_1\theta_r-\omega_1 t+\phi_{2_1}) & \cos(p_1\theta_r-\omega_1 t+\phi_{2_1}) & 0 \\ 0 & 0 & 1 \end{bmatrix}$

Table 7.1: Comparison of stator voltages in different reference frames

Chapter 8

Feedback Linearization for the BDFM

In chapter 7 a synchronous reference frame model for the considered class of BDFM machines was derived, the model linearized, and two control strategies proposed based on the linearized model.

The shortcoming of this approach is that linear controller designs for large deviations from an equilibrium point cannot be systematically approached. This is because the linearized model is only accurate for small deviations from the equilibrium point and, although the non-linear model can be used to predict the performance further away from the equilibrium point, it does not aid the design of controllers.

There is, therefore, a need for a systematic method of controller design for large deviations from an equilibrium point. As discussed in section 1.1, a 'direct torque control' method was proposed for the BDFM, although never implemented [13, 14, 128], and a number of variations of a field orientated control scheme were proposed and some of these were implemented [125, 129, 130, 126, 124]. The field-orientated control schemes all require a current source inverter.

We therefore develop non linear control schemes for the BDFM which may be implemented using voltage source inverters.

Feedback linearization (FBL) was first applied to the BDFM by the author in [82, 84]. FBL was applied to the coupled circuit model for a 'nested-loop' design rotor BDFM. However this led to a high order model for which the majority of the states (the rotor currents) could not easily be measured. An equivalent approach is used in this chapter in the d-q synchronous reference frame. It has the advantage of reduced state dimension, and constant current and voltage values in the steady-state.

We give two applications of FBL to the BDFM, one regulating speed only and one regulating both speed and flux. We discuss the choice of observer to estimate unmeasurable states, and investigate the entire controller implementation in simulation. We conclude the chapter with some initial experimental results from an implementation of the FBL control schemes on the prototype machine.

8.1 Feedback Linearization

We start with some definitions and then give a concise introduction to FBL. The results presented here are taken from Isidori and Slotine and Li [50, 101], to which the reader is referred for full details.

8.1.1 Preliminaries

Definition 8.1. [101, Def. 6.1]Lie Derivative: Given a scalar function $h(x)$, $h \in \mathbb{R}$ and a vector function $f(x) \in \mathbb{R}^n$, where $x \in \mathbb{R}^n$, then the Lie derivative of h with respect of f is written as $L_f h$ and is given by,

$$L_f h(x) = \nabla_x(h) f(x)$$

$L_f h(x)$ is scalar since $\nabla_x h$ is a row vector, and $f(x)$ a column vector. The following notation is also used:

$$\begin{aligned} L_g L_f h(x) &= \nabla_x(L_f h(x)) g(x) \\ L_f^2 h(x) &= L_f L_f h(x) = \nabla_x(L_f h(x)) f(x) \\ L_f^k &= L_f L_f^{k-1} h(x) = \nabla_x(L_f^{k-1} h(x)) f(x) \\ L_f^0 h(x) &= h(x) \end{aligned}$$

where $g \in \mathbb{R}^n$ is also a vector function.

Definition 8.2. [50, p. 137] Relative degree: Given a SISO nonlinear system, within input $u \in \mathbb{R}$, output $y \in \mathbb{R}$, and state $x \in \mathbb{R}^n$:

$$\begin{aligned} \dot{x} &= f(x) + g(x)u \\ y &= h(x) \end{aligned}$$

where f, g, and h are sufficiently smooth functions, the system is said to have relative degree r at point x^o if,

1. $L_g L_f^k h(x) = 0$, for all x in a neighbourhood of x^o and all $k < r - 1$,
2. $L_g L_f^{r-1} h(x^o) \neq 0$

Furthermore the system has relative degree r in the region $D_o \subset D$ if the above conditions hold for all $x \in D_o$.

It may therefore be shown that for a SISO system the relative degree is exactly equal to the number of times that one has to differentiate the output, y until the input u explicitly appears in the expression [101, p. 247]. It is possible for a system *not* to have an well defined relative degree, this can occur

if, for example, the function multiplying the input is not generally zero, but happens to be zero at precisely x^o [50, p. 137].

The idea of FBL is to construct a nonlinear state transformation which renders the system linear, or at least the states which are observable at the output must be linear. In order for such a state transformation to exist, the Jacobian of the transformation must be invertible [101, p. 250].

A state transformation satisfying this requirement is the so-called *normal form* [50, Prop. 4.1.3]. If a system has a (well-defined) relative degree, r at x^o, (hence $r \leq n$), then:

$$\begin{aligned}
\phi_1(x) &= h(x) \\
\phi_2(x) &= L_f h(x) \\
&\vdots \\
\phi_r(x) &= L_f^{r-1} h(h)
\end{aligned}$$

If r is strictly less than n, it is always possible to find $n - r$ more functions $\phi_{r+1}(x), \cdots, \phi_n(x)$ such that the mapping

$$\Phi(x) = \begin{pmatrix} \phi_1(x) \\ \vdots \\ \phi_n(x) \end{pmatrix}$$

has a Jacobian matrix that is nonsingular at x^o and therefore qualifies as a local state transformation in a neighbourhood of x^o. Furthermore it is possible to choose the value of these additional functions at x^o arbitrarily, and it can be shown that they may be chosen in such a way that they are not a function of the input u.

The benefit of applying this transformation is shown when the original system is written in the new coordinates $z_i = \phi_i(x)$, $1 \leq i \leq n$, hence $\dot{z}_i = \nabla_x \phi_i \dot{x}_i$. Therefore the system in transformed coordinates can be shown to be ([50, p. 143]):

$$\begin{aligned}
\dot{z}_1 &= z_2 \\
\dot{z}_2 &= z_3 \\
&\vdots \\
\dot{z}_{r-1} &= z_r \\
\dot{z}_r &= b(z) + a(z)u = L_g L_f^{r-1} h(\Phi^{-1}(z))u + L_f^r h(\Phi^{-1}(z)) \\
\dot{z}_{r+1} &= q_{r+1}(z) + p_{r+1}(z)u \\
&\vdots \\
\dot{z}_n &= q_n(z) + p_n(z)u \\
y &= h(x) = z_1
\end{aligned}$$

where $z \in \mathbb{R}^n$ is the new state variable, and z_k is the k^{th} element of z. $q_k \in \mathbb{R}$ and $p_k \in \mathbb{R}$ are some functions of z (see [50, Remark 4.1.3]).

It is immediate that if u is chosen so that $u = \frac{1}{a(z)}(-b(z) - \eta)$, then the r^{th} state becomes $\dot{z}_r = \eta$, which renders the system from η to y linear. When $r = n$ the entire system becomes linear, and in this case the system is exactly linearised which is also described as 'input-state' linearization. If $r < n$, then the input-output system is linear and the transformation is known as an 'input-output' linearization.

When the system is MIMO similar results apply. The system considered has m outputs, n states and l inputs and is of the form:

$$\begin{aligned} \dot{x} &= f(x) + \textstyle\sum_{j=1}^{l} g_j(x)u_j \\ y_1 &= h_1(x) \\ &\vdots \\ y_m &= h_m(x) \end{aligned}$$

where $f \in \mathbb{R}^n$, $g_j\mathbb{R}^n$, $h_i \in \mathbb{R}$, n is the state dimension. For each output, y_i the relative degree, r_i is taken as the smallest integer such that for at least one g_j $L_{g_j}L_f^{r_i-1}h_i(x^o) \neq 0$. Therefore r_i is exactly the number of times one has to differentiate the i^{th} output y_i in order to have at least one component of the input vector u explicitly appearing [50, p.220]. Differentiating the system r_i times gives:

$$\begin{bmatrix} y_1^{r_1} \\ \vdots \\ y_m^{r_m} \end{bmatrix} = \begin{bmatrix} L_f^{r_i}h_1(x) \\ \vdots \\ L_f^{r_m}h_m(x) \end{bmatrix} + \begin{bmatrix} L_{g_1}L_f^{r_1-1}h_1(x) & L_{g_2}L_f^{r_1-1}h_1(x) & \cdots & L_{g_l}L_f^{r_1-1}h_1(x) \\ L_{g_1}L_f^{r_2-1}h_2(x) & L_{g_2}L_f^{r_2-1}h_2(x) & \cdots & L_{g_l}L_f^{r_2-1}h_2(x) \\ \cdots & \cdots & \cdots & \cdots \\ L_{g_1}L_f^{r_m-1}h_m(x) & L_{g_2}L_f^{r_m-1}h_m(x) & \cdots & L_{g_l}L_f^{r_m-1}h_m(x) \end{bmatrix} \begin{bmatrix} u_1 \\ \vdots \\ u_l \end{bmatrix} \tag{8.1}$$

$$= B(x) + A(x) \begin{bmatrix} u_1 \\ \vdots \\ u_l \end{bmatrix} \tag{8.2}$$

For the relative degree to be well-defined, in addition to the condition for SISO systems, is it also necessary that $A(x)$ in (8.2) be at least rank m at x^o, where m is the dimension of the output [50, Rem. 5.1.3, Prop. 5.1.2]. In this case it can be shown that the system is exactly (input-state) linearizable iff $\sum_{i=1}^{m} r_i = n$, or if $\sum_{i=1}^{m} r_i < n$ then the system is input-output linearizable ([50, Lemma 5.2.1& Sect. 5.3]. In order to linearize the system input, u is chosen so that:

$$B(x) + A(x) \begin{bmatrix} u_1 \\ \vdots \\ u_l \end{bmatrix} - \begin{bmatrix} \eta_1 \\ \vdots \\ \eta_m \end{bmatrix} = 0 \tag{8.3}$$

where $v \in \mathbb{R}^m$ is the new input to the linearized system. Note that if $l > m$ then there will not be a unique solution for u, however as long as (8.3) is satisfied the linearization will still hold. In this case

the linearized system transfer function can be shown to be:

$$\begin{bmatrix} y_1 \\ \vdots \\ y_m \end{bmatrix} = \begin{bmatrix} \frac{1}{s^{r_1}} & 0 & \cdots & 0 \\ 0 & \frac{1}{s^{r_2}} & \cdots & 0 \\ \vdots & \ddots & \ddots & \vdots \\ 0 & 0 & \cdots & \frac{1}{s^{r_m}} \end{bmatrix} \begin{bmatrix} \eta_1 \\ \vdots \\ \eta_m \end{bmatrix} \tag{8.4}$$

As (8.4) comprises of m independent linear systems, m SISO controllers can be designed to stabilize the system. The robustness of the linearized system is dependent on robust design of these 'outer-loop' controllers.

As FBL can be viewed as a state transformation, it is clear that unless the sum of the relative degrees of all the outputs are exactly equal to the number of states in the system, then the linearized system is not a complete description of the original system. Specifically there are $n - \sum_{i=1}^{m} r_i$ states which are unobservable at the output and uncontrollable from the new system input, η. These states give rise to the *zero dynamics* of the linearized system [50, sect. 4.3].

Hence although it is straightforward to design linear controllers to stabilize the observable states, for which the transfer functions are simply of the form $1/s^r$, such a controller will not affect the zero dynamics of the system. Therefore if the zero dynamics happen to be unstable, then the system does not have internal stability, and therefore the controller cannot work satisfactorily in practice.

8.2 Application to the BDFM

8.2.1 BDFM model in terms of flux linkages

The models derived for the BDFM in previous chapters may be represented wholly, or in part, in terms of circuit flux linkages, rather than circuit currents. From definition 2.7, the flux linkage of a circuit is $\lambda = Mi$ where M is the mutual inductance and i the current, thus flux and current are related by a linear transformation, which, from Lemma 2.3, must be invertible.

In the case that the BDFM has only one d-q pair representing the rotor states, then (ignoring zero sequence states) the machine has only 6 states. In this case the machine can be fully described by stator 1 and 2 currents, and either the stator 1, stator 2 or rotor fluxes. The most useful choice is the stator 2 flux, as the stator 2 flux is strongly dependent on the stator 2 voltage, which is the control input. The rotor flux could be used, however it is considerably more difficult to measure the rotor flux than the stator flux.

Therefore in the synchronous reference frame the currents are transformed:

$$\begin{bmatrix} i^s_{dq_{s1}} \\ i^s_{dq_{s2}} \\ \lambda^s_{dq_{s2}} \end{bmatrix} = \begin{bmatrix} I & 0 & 0 \\ 0 & I & 0 \\ 0 & M_{\text{sync}_{22}} & M_{\text{sync}_{rr}} \end{bmatrix} \begin{bmatrix} i^s_{dq_{s1}} \\ i^s_{dq_{s2}} \\ i^s_{dq_r} \end{bmatrix} \tag{8.5}$$

$$= \mathcal{T}_\lambda \begin{bmatrix} i^s_{dq_{s1}} \\ i^s_{dq_{s2}} \\ i^s_{dq_r} \end{bmatrix} \tag{8.6}$$

where $M_{\text{sync}_{rr}}$ and $M_{\text{sync}_{22}}$ are the stator 2-rotor and rotor-rotor portions of $M_{\text{sync}_{rr}}$ (the stator 1-stator 2 portion is always zero by design). Note that as $M_{\text{sync}_{rr}}$ is rank 2 then the transformation is always invertible.

It may be shown that the 2-norm of stator flux linkages is approximately proportional to the rms flux density in the air gap of the corresponding pole number field. This can be shown by considering the flux linkage in the coupled circuit model in chapter 2, from where the air gap flux density can be related to the mutual inductance terms. It is significant that the stator flux linkage is related to the rms air gap flux density because the allowable air gap flux density for a machine is limited by the iron laminations, as discussed in section 4.7.

Therefore, from (7.12), the full dynamic model in terms of stator 2 flux becomes:

$$\frac{d}{dt}\begin{bmatrix} i^s_{dq_{s1}} \\ i^s_{dq_{s2}} \\ \lambda^s_{dq_{s2}} \\ \theta_r \\ \\ \omega_r \end{bmatrix} = \begin{bmatrix} \mathcal{T}_\lambda M^{-1}_{\text{sync}} \mathcal{T}^{-1}_\lambda \left((-\mathcal{T}_\lambda R_{\text{sync}} \mathcal{T}^{-1}_\lambda - \mathcal{T}_\lambda Q_{\text{sync}} \mathcal{T}^{-1}_\lambda) \begin{bmatrix} i^s_{dq_{s1}} \\ i^s_{dq_{s2}} \\ \lambda^s_{dq_{s2}} \end{bmatrix} + \mathcal{T}_\lambda \begin{bmatrix} v^s_{dq_{s1}} \\ v^s_{dq_{s2}} \\ 0 \end{bmatrix} \right) \\ \\ \omega_r \\ \\ \frac{1}{2J} \begin{bmatrix} i^s_{dq_{s1}} \\ i^s_{dq_{s2}} \\ \lambda^s_{dq_{s2}} \end{bmatrix}^{\text{T}} \mathcal{T}_\lambda S_{\text{sync}} \mathcal{T}^{-1}_\lambda \begin{bmatrix} i^s_{dq_{s1}} \\ i^s_{dq_{s2}} \\ \lambda^s_{dq_{s2}} \end{bmatrix} - \frac{T_l}{J} \end{bmatrix} \tag{8.7}$$

We now consider the speed regulation problem for the BDFM using FBL. We assume that the torque is an unmeasured disturbance, and propose two methods, one where only the speed is regulated, and a second where both the speed and the flux are regulated.

8.2.2 Control strategy 1: Speed Only Regulation

We have two control inputs, the d and q axis components of $v^s_{dq_{s2}}$. We have one output, ω_r. From section 8.1.1 we differentiate the output, ω_r until the input appears:

$$y_1 = \omega_r \tag{8.8}$$

$$\frac{dy_1}{dt} = \frac{d\omega_r}{dt} = \frac{1}{2J}\begin{bmatrix} i^s_{dq_{s1}} \\ i^s_{dq_{s2}} \\ \lambda^s_{dq_{s2}} \end{bmatrix}^{\mathrm{T}} \mathcal{T}_\lambda S_{\mathrm{sync}} \mathcal{T}_\lambda^{-1} \begin{bmatrix} i^s_{dq_{s1}} \\ i^s_{dq_{s2}} \\ \lambda^s_{dq_{s2}} \end{bmatrix} - \frac{T_l}{J} \tag{8.9}$$

$$\frac{d^2y_1}{dt^2} = \frac{d\dot{\omega}_r}{dt} = \frac{1}{J}\begin{bmatrix} i^s_{dq_{s1}} \\ i^s_{dq_{s2}} \\ \lambda^s_{dq_{s2}} \end{bmatrix}^{\mathrm{T}} \mathcal{T}_\lambda S_{\mathrm{sync}} \mathcal{T}_\lambda^{-1} \frac{d}{dt} \begin{bmatrix} i^s_{dq_{s1}} \\ i^s_{dq_{s2}} \\ \lambda^s_{dq_{s2}} \end{bmatrix} - \frac{1}{J}\frac{dT_l}{dt} \tag{8.10}$$

$$= \frac{d\dot{\omega}_r}{dt} = \frac{1}{J}\begin{bmatrix} i^s_{dq_{s1}} \\ i^s_{dq_{s2}} \\ \lambda^s_{dq_{s2}} \end{bmatrix}^{\mathrm{T}} \mathcal{T}_\lambda S_{\mathrm{sync}} M^{-1}_{\mathrm{sync}} \left((-R_{\mathrm{sync}}\mathcal{T}_\lambda^{-1} - Q_{\mathrm{sync}}\mathcal{T}_\lambda^{-1}) \begin{bmatrix} i^s_{dq_{s1}} \\ i^s_{dq_{s2}} \\ \lambda^s_{dq_{s2}} \end{bmatrix} + \begin{bmatrix} v^s_{dq_{s1}} \\ v^s_{dq_{s2}} \\ 0 \end{bmatrix} \right) - \frac{1}{J}\frac{dT_l}{dt} \tag{8.11}$$

Therefore the relative degree is 2 as long as the state vector is non-zero, and the system may be input-output linearized by choosing $v^s_{dq_{s2}}$ such that:

$$P_1(R_{\mathrm{sync}}\mathcal{T}_\lambda^{-1} + Q_{\mathrm{sync}}\mathcal{T}_\lambda^{-1}) \begin{bmatrix} i^s_{dq_{s1}} \\ i^s_{dq_{s2}} \\ \lambda^s_{dq_{s2}} \end{bmatrix} + \frac{dT_l}{dt} + \frac{\eta}{J} = P_1 \begin{bmatrix} I \\ 0 \\ 0 \end{bmatrix} v^s_{dq_{s1}} + P_1 \begin{bmatrix} 0 \\ I \\ 0 \end{bmatrix} v^s_{dq_{s2}} \tag{8.12}$$

where:

$$P_1 = \begin{bmatrix} i^s_{dq_{s1}} \\ i^s_{dq_{s2}} \\ \lambda^s_{dq_{s2}} \end{bmatrix}^{\mathrm{T}} \mathcal{T}_\lambda S_{\mathrm{sync}} M^{-1}_{\mathrm{sync}} \tag{8.13}$$

where η is the new dummy input to the system, and therefore the system transfer function becomes: $\omega_r(s) = \dfrac{\eta}{s^2}$.

However it is clear that (8.12) is an under determined set of equations, that is for any chosen η there are an infinite number of valid solutions. We therefore propose choosing the solution giving the minimum value of $\|v^s_{dq_{s2}}\|_2$, and which may be computed by:

$$v^s_{dq_{s2}} = (A^{\mathrm{T}}A)^{-1}A^{\mathrm{T}} \left(P_1(R_{\mathrm{sync}}\mathcal{T}_\lambda^{-1} + Q_{\mathrm{sync}}\mathcal{T}_\lambda^{-1}) \begin{bmatrix} i^s_{dq_{s1}} \\ i^s_{dq_{s2}} \\ \lambda^s_{dq_{s2}} \end{bmatrix} + \frac{dT_l}{dt} + \frac{\eta}{J} - P_1 \begin{bmatrix} I \\ 0 \\ 0 \end{bmatrix} v^s_{dq_{s1}} \right) \tag{8.14}$$

where:

$$A = P_1 \begin{bmatrix} 0 \\ I \\ 0 \end{bmatrix}$$

As the linear dynamics comprise of a double integrator, they may be stabilized through the use of a phase lead compensator,

$$K_1 = \frac{\omega_x^2 \sqrt{\alpha} s + \omega_x^3}{s + \omega_x \sqrt{\alpha}} \tag{8.15}$$

where ω_x is the desired loop cross-over point (in radians per second), and α is the desired 'spread' of the pole and zero, which controls the amount of phase lead (and hence the damping and robustness). In this dissertation $\omega_x = 100$ and $\alpha = 200$, which gives a phase margin of 82°.

We now consider the case of speed and flux regulation.

8.2.3 Control Strategy 2: Speed and Flux Regulation

The system now has two outputs, ω_r and $\|\lambda^s_{dq_{s2}}\|_2$. The relative degree for the ω_r output is known to be 2 from section 8.2.2. To determine the relative degree for the $\|\lambda^s_{dq_{s2}}\|_2$ output we differentiate it repeatedly:

$$y_2 = \|\lambda^s_{dq_{s2}}\|_2 = \sqrt{{\lambda^s_{dq_{s2}}}^{\mathrm{T}} \lambda^s_{dq_{s2}}} = \sqrt{\begin{bmatrix} i^s_{dq_{s1}} \\ i^s_{dq_{s2}} \\ \lambda^s_{dq_{s2}} \end{bmatrix}^{\mathrm{T}} \begin{bmatrix} 0 & 0 & 0 \\ 0 & 0 & 0 \\ 0 & 0 & I \end{bmatrix} \begin{bmatrix} i^s_{dq_{s1}} \\ i^s_{dq_{s2}} \\ \lambda^s_{dq_{s2}} \end{bmatrix}} \tag{8.16}$$

$$\frac{dy_2}{dt} = \frac{d\|\lambda^s_{dq_{s2}}\|_2}{dt} = \frac{{\lambda^s_{dq_{s2}}}^{\mathrm{T}} \dot{\lambda}^s_{dq_{s2}}}{\sqrt{{\lambda^s_{dq_{s2}}}^{\mathrm{T}} \lambda^s_{dq_{s2}}}} = \frac{1}{\sqrt{{\lambda^s_{dq_{s2}}}^{\mathrm{T}} \lambda^s_{dq_{s2}}}} \begin{bmatrix} i^s_{dq_{s1}} \\ i^s_{dq_{s2}} \\ \lambda^s_{dq_{s2}} \end{bmatrix}^{\mathrm{T}} \begin{bmatrix} 0 & 0 & 0 \\ 0 & 0 & 0 \\ 0 & 0 & I \end{bmatrix} \frac{d}{dt} \begin{bmatrix} i^s_{dq_{s1}} \\ i^s_{dq_{s2}} \\ \lambda^s_{dq_{s2}} \end{bmatrix} \tag{8.17}$$

$$= \frac{1}{\sqrt{{\lambda^s_{dq_{s2}}}^{\mathrm{T}} \lambda^s_{dq_{s2}}}} \begin{bmatrix} i^s_{dq_{s1}} \\ i^s_{dq_{s2}} \\ \lambda^s_{dq_{s2}} \end{bmatrix}^{\mathrm{T}} \begin{bmatrix} 0 & 0 & 0 \\ 0 & 0 & 0 \\ 0 & 0 & I \end{bmatrix} \mathcal{T}_\lambda M_{\mathrm{sync}}^{-1} \left((-R_{\mathrm{sync}} \mathcal{T}_\lambda^{-1} - Q_{\mathrm{sync}} \mathcal{T}_\lambda^{-1}) \begin{bmatrix} i^s_{dq_{s1}} \\ i^s_{dq_{s2}} \\ \lambda^s_{dq_{s2}} \end{bmatrix} + \begin{bmatrix} v^s_{dq_{s1}} \\ v^s_{dq_{s2}} \\ 0 \end{bmatrix} \right) \tag{8.18}$$

Therefore the relative degree for the $\|\lambda^s_{dq_{s2}}\|_2$ output is 1, as long as $\lambda^s_{dq_{s2}} \neq 0$.

Therefore $v^s_{dq_{s2}}$ should be chosen such that:

$$\begin{bmatrix} \eta_1 \\ \eta_2 \end{bmatrix} = \begin{bmatrix} \frac{1}{J} P_1 (-R_{\mathrm{sync}} \mathcal{T}_\lambda^{-1} - Q_{\mathrm{sync}} \mathcal{T}_\lambda^{-1}) \begin{bmatrix} i^s_{dq_{s1}} \\ i^s_{dq_{s2}} \\ \lambda^s_{dq_{s2}} \end{bmatrix} + \frac{P_1}{J} \begin{bmatrix} v^s_{dq_{s1}} \\ v^s_{dq_{s2}} \\ 0 \end{bmatrix} - \frac{1}{J} \frac{dT_l}{dt} \\ P_2 (-R_{\mathrm{sync}} \mathcal{T}_\lambda^{-1} - Q_{\mathrm{sync}} \mathcal{T}_\lambda^{-1}) \begin{bmatrix} i^s_{dq_{s1}} \\ i^s_{dq_{s2}} \\ \lambda^s_{dq_{s2}} \end{bmatrix} + P_2 \begin{bmatrix} v^s_{dq_{s1}} \\ v^s_{dq_{s2}} \\ 0 \end{bmatrix} \end{bmatrix} \tag{8.19}$$

where P_1 is given in (8.13) and:

$$P_2 = \frac{1}{\sqrt{\lambda^s_{dq_{s2}}{}^{\mathrm{T}} \lambda^s_{dq_{s2}}}} \begin{bmatrix} i^s_{dq_{s1}} \\ i^s_{dq_{s2}} \\ \lambda^s_{dq_{s2}} \end{bmatrix}^{\mathrm{T}} \begin{bmatrix} 0 & 0 & 0 \\ 0 & 0 & 0 \\ 0 & 0 & I \end{bmatrix} \mathcal{T}_\lambda M^{-1}_{\mathrm{sync}} \tag{8.20}$$

Rearranging (8.19) gives:

$$\begin{bmatrix} \\ \eta_1 \\ \\ \\ \eta_2 \\ \\ \end{bmatrix} = \begin{bmatrix} \frac{1}{J} P_1 (-R_{\mathrm{sync}} \mathcal{T}_\lambda^{-1} - Q_{\mathrm{sync}} \mathcal{T}_\lambda^{-1}) \begin{bmatrix} i^s_{dq_{s1}} \\ i^s_{dq_{s2}} \\ \lambda^s_{dq_{s2}} \end{bmatrix} + \frac{P_1}{J} \begin{bmatrix} I \\ 0 \\ 0 \end{bmatrix} v^s_{dq_{s1}} - \frac{1}{J} \frac{dT_l}{dt} \\ \\ P_2 (-R_{\mathrm{sync}} \mathcal{T}_\lambda^{-1} - Q_{\mathrm{sync}} \mathcal{T}_\lambda^{-1}) \begin{bmatrix} i^s_{dq_{s1}} \\ i^s_{dq_{s2}} \\ \lambda^s_{dq_{s2}} \end{bmatrix} + P_2 \begin{bmatrix} I \\ 0 \\ 0 \end{bmatrix} v^s_{dq_{s1}} \end{bmatrix} + P_3 v^s_{dq_{s2}} \tag{8.21}$$

where:

$$P_3 = \begin{bmatrix} \frac{P_1}{J} \begin{bmatrix} 0 \\ I \\ 0 \end{bmatrix} \\ \\ P_2 \begin{bmatrix} 0 \\ I \\ 0 \end{bmatrix} \end{bmatrix} \tag{8.22}$$

It may be verified that P_3 is full rank if $i^s_{dq_{s1}} \neq 0$ and $i^s_{dq_{s2}} \neq 0$ and $\lambda^s_{dq_{s2}} \neq 0$. Therefore equation (8.21) may be uniquely solved to give $v^s_{dq_{s2}}$ and the linearization is valid in all practical situations.

The FBL system may be stabilized by two linear controllers: K_1 (as given in (8.15)) for the speed term, and $K_2 = \omega_x$ for the flux term, where ω_x is the desired loop bandwidth. K_2 need only be a constant gain as the flux output has relative degree 1. In this dissertation we choose:

$$K_2 = 100 \tag{8.23}$$

It is noteworthy that equation (8.21) is similar to equation (15) of [14], as indeed were the methods used to reach it. However the authors do not appear to have realised that this constitutes FBL, and furthermore their derivation is not in the synchronous reference frame.

8.3 Towards A Practical Implementation

We now discuss issues related to the practical implementation the FBL control laws described. The first point which is immediate is that the solution of (8.21) or (8.12) requires the derivative of the load torque to be known. This is very unlikely to be available as a measurement, however normally

the load torque will be constant, and therefore the derivative is zero. During torque transients, if the derivative term is assumed to be zero, then any change in torque appears as a disturbance at the input, which will be attenuated by the linear outer loop controller. Therefore we will assume that the torque derivative is zero for controller implementation. The second point which is immediate is that the full state must be measured in order to implement the controller. The stator currents can be measured, but it will not be desirable to measure the stator 2 flux. This is because it would require the addition of instrumentation to the inside of the machine, which would necessitate the controller manufacturer (who will probably not manufacture the machine) modifying the machine. Therefore it will be assumed that it is necessary to estimate at least the stator 2 flux.

8.3.1 Zero Dynamics and Idealized FBL Stability

As discussed in section 8.1.1, when the total relative degree of a system is less than the state dimension, then there are unobservable states, known as zero dynamics. These states must be stable if the system is to be internally stable, as they are not controllable. If the system is not internally stable then the controller is likely to be unusable. The analytical analysis of the zero dynamics is beyond the scope of this dissertation, however the *local* stability of equilibria can be investigated numerically by performing a standard linearization and then eigenvalue analysis.

Calculation of Equilibrium Points

The equilibrium points for both FBL methods were determined numerically by using a constrained optimization technique. For both methods the equilibria may be found by setting the derivative term zero in (8.7) and solving the resulting equation, omitting the ω_r state. As the input, $v^s_{dq_{s2}}$ only appears in the uppermost equations, the lower equation may be considered a non-linear constraint on the state vector. The equilibria are found by substituting (8.14) or (8.21) for $v^s_{dq_{s2}}$, and then minimizing the 2-norm of the derivative vector subject to the aforementioned constraint. This was achieved using the Matlab function `fmincon`. However to reduce the chance of missing possible solutions the optimization was started from 100 randomly generated starting points, and all results with 2-norms suitably close to zero retained. In both cases multiple equilibria were found for a given load torque, shaft speed and stator 1 supply voltage.

Local Stability Analysis of Idealized FBL

Figure 8.1 illustrates the effect of stable and unstable zero dynamics for the first FBL scheme. Figure 8.1(b) shows the maximum real part of all the eigenvalues of the system when linearized an a range of of operating points. It is clear that there are a substantial range of speeds where the zero dynamics are unstable for the load torques considered. We now show the transient response at two equilibria at 200 rpm, the first with $T_l = 0\,\mathrm{N\,m}$ with stable zero dynamics, and the second with $T_l = 5\,\mathrm{N\,m}$ with

unstable zero dynamics.

Figure 8.1(a), shows the resulting speed transient at startup. The 'noise' on the signal for the unstable equilibrium is due to imperfections in implementation of FBL. As these imperfections are tiny (due only to errors in the ODE solver), it serves to illustrate why internal stability is necessary - in practice there will be much larger imperfections in the implementation of FBL and consequently greater output errors. Figures 8.1(c) and 8.1(d) show the current and flux at the stable and unstable equilibriums.

Therefore we conclude that, even in the case of (nominally) perfect implementation of FBL, if the zero dynamics are not stable, then the controller will not be practically usable, as expected. The same conclusion can be drawn from a similar analysis of the second FBL scheme.

8.3.2 Practical Implementation

As previously discussed, the implementation of FBL requires an observer to estimate the stator 2 flux, or rotor currents. As the BDFM electrical equations are linear parameter varying, parameterised on the speed, standard observer design techniques are not applicable. Four observer designs were considered. The first three use the measurable stator currents along with the stator voltages, however the fourth only uses the stator voltages.

1. Time varying Kalman filter: as the Kalman filter equations have been solved for linear time varying systems the filter may be applied. However the computational burden is significant as the state covariance estimate must be computed in real time [105, sect. 4.5].

2. LPV observer design using LMIs, adapted from an observer for a conventional induction machine in [77], designed to give minimum induced 2-norm error.

3. Novel time varying observer design where stability can always be guaranteed using appropriate gain choices: presented by the author in [85].

4. Open-loop 'observer' comprising of the electrical system equations. Such an 'observer' is stable for any variation in shaft speed from Theorem 3.5.

Of the four designs it was found, through simulation studies, that the robustness of FBL using an observer was actually *worse* with the three observers which use current feedback. This is because the use of feedback tends to worsen the estimate of the *phase* of a signal, but generally gives an improved estimate of the magnitude. However, AC electrical machines are generally much more sensitive to changes in phase than changes in magnitude [67]. Therefore the open-loop observer, which simply consists of the first row of (8.7), was used.

In the implementation of the FBL controller it is necessary to convert the measured signals into the synchronous reference frame, and the demanded output voltage from the synchronous reference frame and back into terminal quantities. From a series of simulation tests it became apparent that

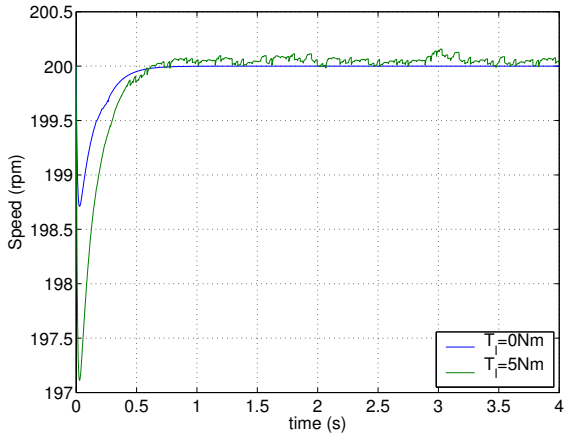

(a) [Speed transient

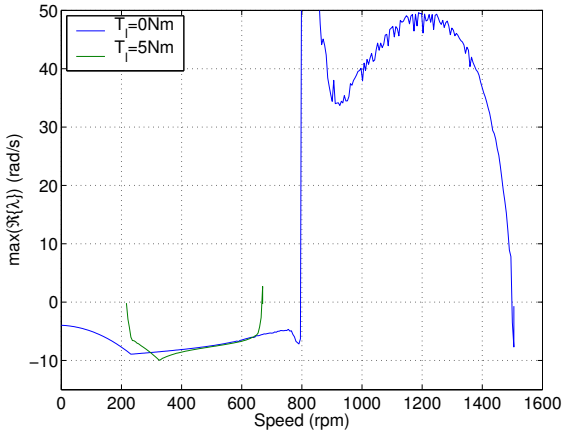

(b) Maximum real part of linearized system eigenvalues

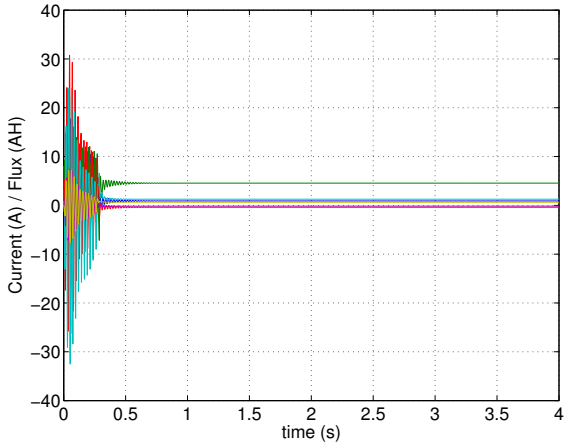

(c) Current and flux transients at $T_l = 0\,\mathrm{N\,m}$

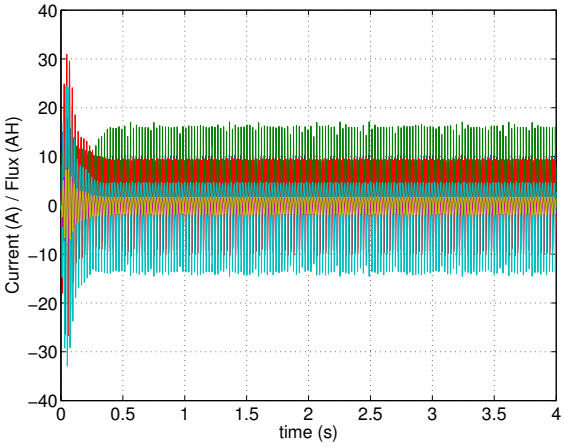

(d) Current and flux transients at $T_l = 5\,\mathrm{N\,m}$

Figure 8.1: Local stability analysis, of FBL method 1 with $V_1 = 67.6\mathrm{V_{rms}}$, showing maximum real part of the linearized system eigenvalues, and the speed and current transients at an equilibrium point. At 5 N m the operating point is unstable, and at 0 N m it is stable, as can be seen from the the maximum real part of the eigenvalues.

the FBL controllers were very sensitive to any angular errors during this conversion. Such errors, although generally constant, were found in the experimental apparatus. Therefore a simple adaption law was derived to null out any offset prior to engaging the FBL controller. The adaption controller was:

$$K_{\text{adap}} = \int_0^t \left(\frac{{i^s_{dq_{s2}}}^{\mathrm{T}} \begin{bmatrix} 0 & -1 \\ 1 & 0 \end{bmatrix} \hat{i}^s_{dq_{s2}}}{\|i^s_{dq_{s2}}\|_2 \|\hat{i}^s_{dq_{s2}}\|_2} \right) dt \tag{8.24}$$

K_{adap} is the integral of the sine of the angular difference between the measured stator 2 current, $i^s_{dq_{s2}}$, and that estimated by the observer $\hat{i}^s_{dq_{s2}}$. Therefore the adaption law drives any angular error between $\hat{i}^s_{dq_{s2}}$ and $i^s_{dq_{s2}}$ to zero by adjusting the angular offset of the d-q transformation. Once the angular error has been nulled the adaption law was disengaged. The reference frame transformation is given in table 7.1, however a software phase-locked loop was used to force $\phi_{1_i} + \alpha_1 = 0$ and then ϕ_{2_i}, which is unknown, was set to $\phi_{2_i} = \theta_T$ where θ_T is the angular offset found using the adaption law. The value of $\int \omega_1 dt$ was determined from the phase-locked loop.

Figure 8.2 shows the block diagram of the implementation of the FBL controllers. Figure 8.3 shows simulated responses of the two FBL controllers, using this implementation, where a deliberate mis-match has been introduced between the parameters used in the simulated machine and those used in the simulated observer and controller. The machine model used is the full coupled circuit model developed in chapter 2, using calculated parameter values. The controller and observer used the estimated parameter values given in table 6.3. The model moment of inertia was also deliberately mis-matched by a factor of 2. The figures show that despite this modelling mis-match the controller performance was good, and the system stabilized, and furthermore that there is some decoupling between flux and speed in the second FBL scheme even with flux estimation. However the linearized system transfer functions are clearly not $1/s^2$ and $1/s$ for speed and flux respectively because the transient response is around an order of magnitude slower than predicted. This suggests that the model mis-match has introduced some attenuation into the loop. Figure 8.4 shows that when V_1 is increased the linearized system transfer function more closely approximates the ideal double integrator, as the damping factor is approximately correct, and the rise time was around 50 ms whereas under perfect linearization it would have been 30 ms. This is in contrast to figure 8.3 where the rise time is approximately 500 ms, and the damping factor is significantly different.

Figure 8.5 shows results from experimental implementation of the speed only regulation FBL controller. The steady-state offset is due to errors in the linearization. It was found that improved performance was achieved with a controller with a very high proportional gain, therefore $K_1 = 2000$. Nevertheless, the step down transient response is very good, and at 190 ms is faster than any previously published controller results for the BDFM. Figure 8.6 shows speed and flux step changes for the second FBL scheme implemented on the prototype machine. The cross coupling between speed and flux and the steady-state errors are due to shortcoming of the linearization. Again it was found that (relatively) large proportional gains gave better performance than the designed speed controller,

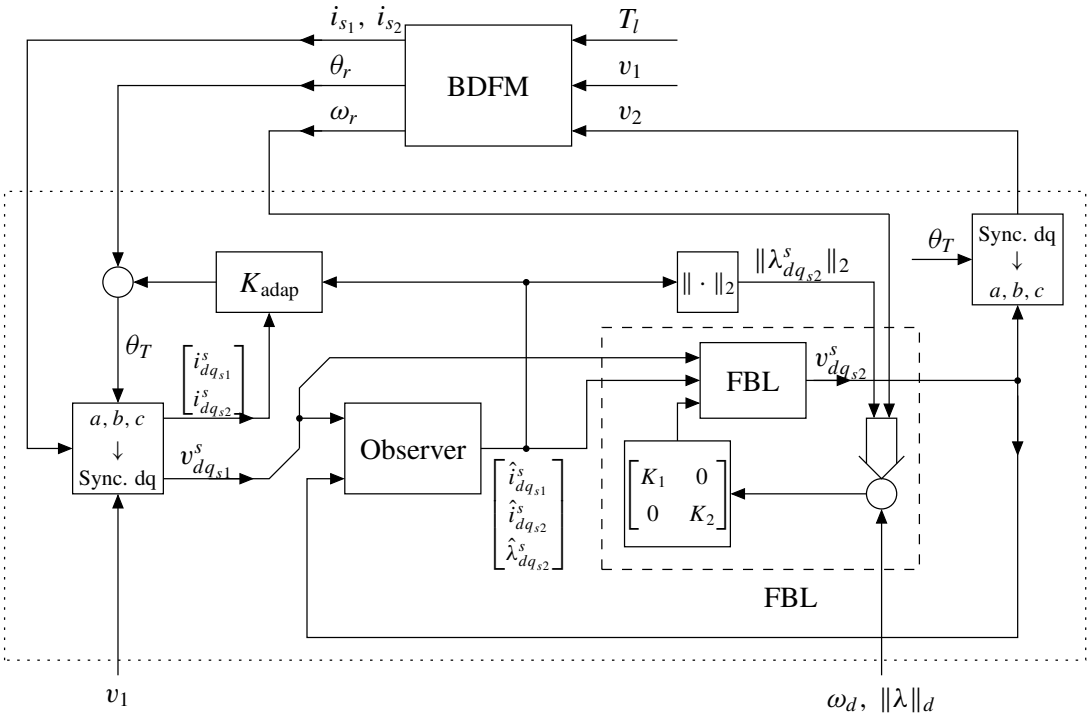

Figure 8.2: Block diagram of FBL controller implementation

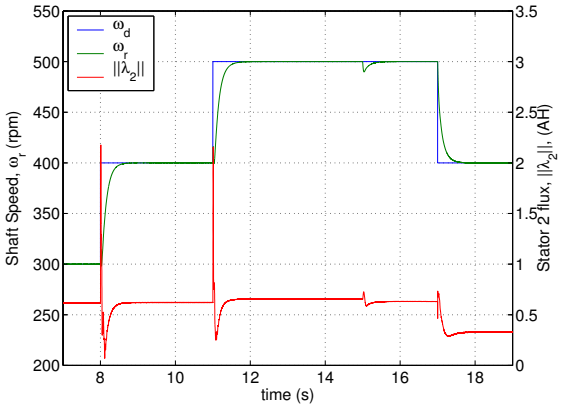

(a) Speed regulation only FBL

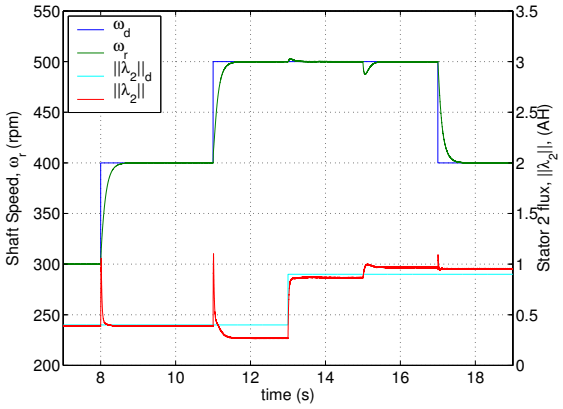

(b) Speed and Flux regulation FBL

Figure 8.3: Transient response of simulated FBL speed and flux controller, using open-loop observer and adaptive angle offset tuning with $V_1 = 67.6\text{V}_{\text{rms}}$. Deliberate model mis-match introduced between machine model and controller model. Step change in load torque at $t = 15\,\text{s}$ from $0\,\text{N m}$ to $10\,\text{N m}$, and step changes in speed and flux as shown. The actual, rather than estimated flux is shown.

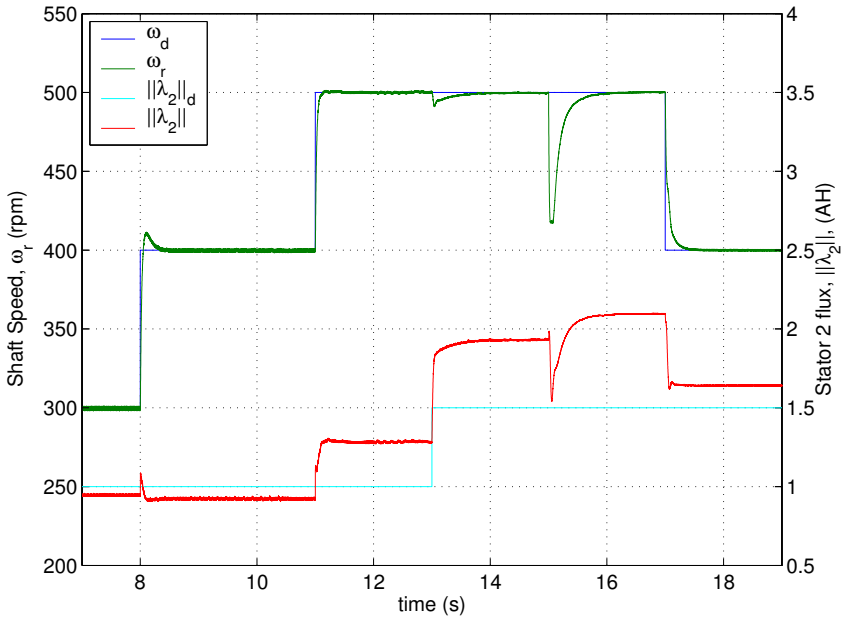

Figure 8.4: Transient response of simulated FBL controllers, using open-loop observer and adaptive angle offset tuning with $V_1 = 240\mathrm{V_{rms}}$. With a higher value of V_1 the linearization error appears to decrease. Step change in load torque at $t = 15\,\mathrm{s}$ from $5\,\mathrm{N\,m}$ to $105\,\mathrm{N\,m}$, and step changes in speed and flux as shown. The actual, rather than estimated flux is shown.

equation (8.15). It was found that K_2 could not be increased beyond $K_2 = 10$ without loosing regulation. The need for high gains to minimize the steady-state error is an indication that that feedback linearization has not been effective at low frequencies, and therefore the ideal of infinite gain has not been attained. The implementation bandwidth was 3.33 kHz for both controllers, in each period the cpu time was busy for 240 µs in each case.

8.4 Conclusion

In this chapter controllers using feedback linearization have been developed for the BDFM, one controlling speed only, and the other controlling flux and speed.

The controllers were presented using a transformed version of the synchronous reference frame model where the stator 2 flux replaced the rotor current state. If the rotor has more than 2 states then the derivation is similar, however some of the rotor currents will still appear in the state vector.

The control strategies were shown to give promising performance in simulation, even with introduced model mis-match.

Initial attempts were made to implement the FBL strategies on the prototype machine, and met with some success. The FBL controller held an equilibrium, and could be made to control the machine. However there was a significant departure from the ideal feedback linearized system transfer

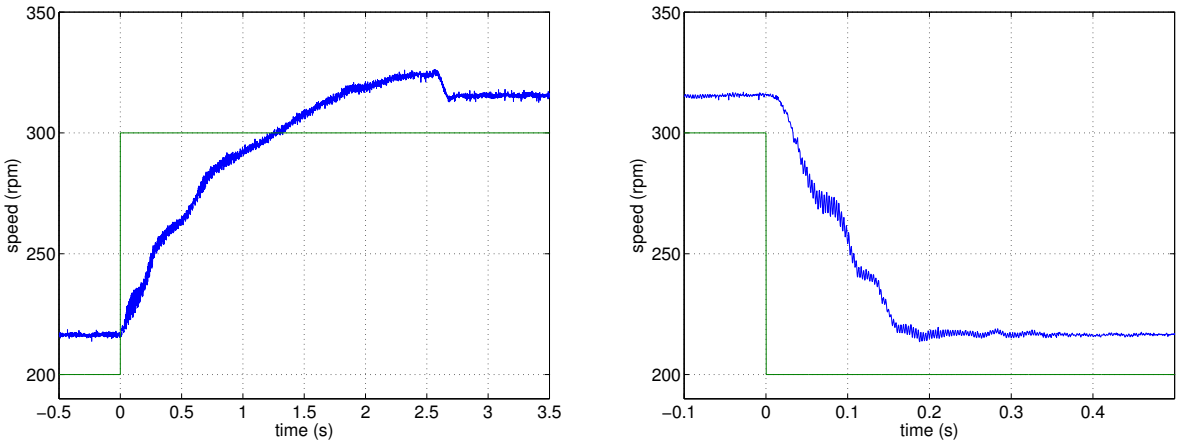

Figure 8.5: Experimental step up and step down speed transients for the speed only FBL implementation. The error in the linearization is apparent though the steady-state offset. $V_1 = 67.6\text{V}_{\text{rms}}$, the load torque was nominally zero. The speed controller was $K_1 = 2000$.

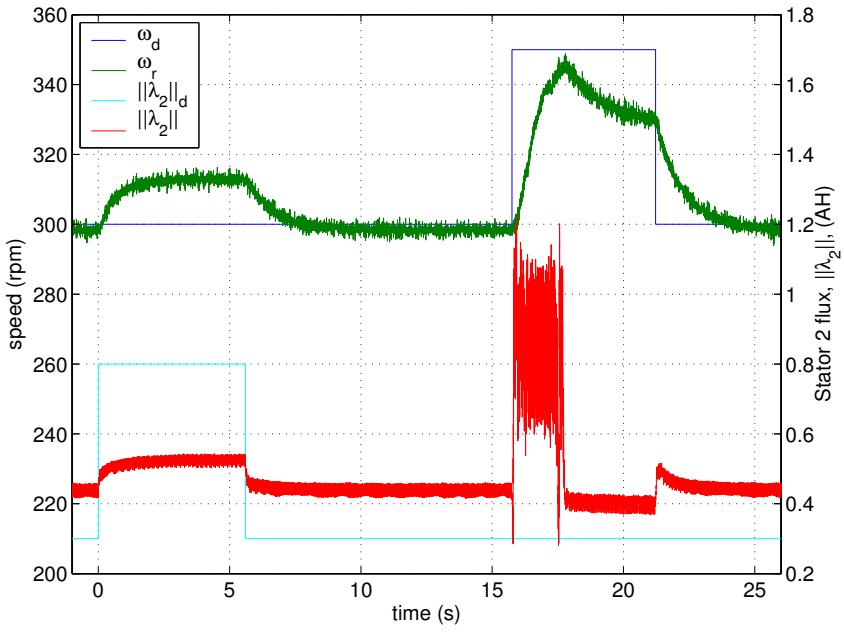

Figure 8.6: Experimental results for the speed and flux regulation FBL controller at nominally no load. The cross coupling between speed and flux is due to errors in the linearization. Note that as the flux has not been measured, the red line shows flux estimated by the observer. $V_1 = 67.6\text{V}_{\text{rms}}$, the load torque was nominally zero. The controllers for speed and flux were $K_1 = 1000$, $K_2 = 10$.

function in each case, most notably the absence of high gains at lower frequencies. Therefore further investigation into the cause of this error is required. However, despite the difficulties the application of FBL to the BDFM deserves further attention.

Chapter 9

Conclusions and Future Work

9.1 Conclusions

The objectives of this dissertation have been: to derive generalised models for a broad class of BDFMs, and to use these models to analyse the steady-state and dynamic performance; to propose a new rotor design and new methods of speed control for the machine. The specific contributions of this dissertation will now be summarised.

1. A generalised framework was developed for the coherent derivation of models for a wide class of BDFMs, of which a machine with any 'nested-loop' design rotor is a subset. The coherence between the different models allowed parameters calculated for the generalised coupled circuit to be transformed to provide parameter values for the other models:

   (a) A method of computing mutual inductance parameters where the user specifies the geometry and connection of the individual coils for each circuit was developed. Two calculation methods were proposed, one giving the total inductance, and the other decomposing the inductance into Fourier series terms. The method assumed finite width, but zero depth conductors. The estimation of leakage inductance was included in the method using standard techniques. The methods allowed parameter calculation for any electrical machine (Chapter 2).

   (b) A generalised coupled circuit model was derived and implemented in software using calculated parameter values which can model any electrical machine (Chapter 2).

   (c) The generalised coupled-circuit model was transformed into a d-q axis model in the rotor reference frame for a wide class of BDFMs by means of invertible matrix transformations, unlike all previously published models. The only additional assumption required was the lack of harmonic terms other than the fundamental in the stator-rotor mutual inductance matrices, this assumption was shown to be reasonable for all the examples considered. The invertibility of the transformation matrices showed that the transformed model was

precisely equivalent. It was shown that the position dependence of the model was removed. The proof made use of the circulant nature of the mutual inductance matrices for the class of machine considered (Chapter 3).

(d) The rotor reference frame d-q axis model was shown to reduce to a model with $6 + 2N$ states (including stator zero sequence states), where N is the number of sets of rotor circuits for the entire class of BDFMs considered and without any observable error. It was shown that the remaining states are stable, and uncontrollable/unobservable, the proof again made use of the circulant properties of the inductance matrices (Chapter 3).

(e) The dynamic rotor reference frame d-q axis model was transformed into complex sequence components for the entire class of BDFMs considered. It was shown that the dynamic sequence component model for the entire class of BDFMs considered could comprise of $2 + N$ complex states (excluding stator zero sequence states) (Chapter 4).

(f) The dynamic rotor reference frame d-q axis model was transformed into a synchronous reference frame d-q axis model for the entire class of BDFMs considered. The transformation was achieved by invertible matrix transformation, therefore the full dynamic nature of the model was preserved, however the steady-state values became constant quantities (Chapter 7).

(g) The complex sequence model was solved for steady-state conditions, and used to synthesize an equivalent circuit model for the full class of BDFMs considered. The coherence of the derivation allowed the physical meaning of the component parameters to be retained (Chapter 4).

(h) The synchronous reference frame d-q model was linearized for the full class of BDFMs considered, and a method of calculation of all equilibrium points was given (Chapter 7).

(i) A model reduction technique for the rotor reference frame d-q model was proposed for 'nested-loop' rotor designs. The technique was shown to be a very good approximation of the full order model for all the examples considered. Furthermore the technique was shown to yield a model which is itself a member of the class of BDFMs considered, thus allowing the model to be transformed into the other forms derived (Chapter 3).

2. The equivalent circuit model was used to investigate the effect of rotor impedance parameters on the performance of the machine:

(a) The rotor impedance was shown to limit the maximum torque available from the machine, or equivalently the torque available for a particular stator power factor. In particular the rotor impedance was shown to significantly depend on excess harmonic inductance, L_{r_h} (Chapter 4).

(b) Seven rotor designs were investigated for the BDFM, five rotors were manufactured and two studied in simulation using calculated parameter values (Chapter 5).

(c) The use of cascade induction mode torque-speed measurements were shown to give a qualitative assessment of rotors' ability to cross-couple, and hence their performance as BDFM rotors. Experimental measurements were taken for the five rotors (Chapters 4 and 5).

(d) Dimensionless measures were proposed to evaluate potential BDFM rotors. Each measure quantified different components of rotor impedance in the equivalent circuit (Chapter 5).

(e) The rotors which exhibited cross-coupling were quantitatively assessed by these measures, and both the 'nested-loop' design, rotor 1 and the new double layer design, rotor 2 were found to have good performance (Chapter 5).

(f) The issue of magnetic loading for the BDFM was investigated, and was shown to translate to constraints on equivalent circuit voltages (Chapter 4).

3. A new method of parameter estimation for the BDFM, by experimental means, was proposed for a class of machines having one set of rotor circuits. This class includes machines with a 'nested-loop' rotor when the new model reduction method is applied. The method was applied to the five experimental rotor designs, and the parameter values verified by independent dynamic and steady-state experiments; by comparison against parameters calculated by the coupled circuit method, and, where possible, compared with manufacturers' parameter data. The parameter values were found to be in good agreement, thus verifying both the model and parameter estimation method (Chapter 6 and 7).

4. The stability of the BDFM was investigated:

   (a) Theorem 3.5 proved that the electrical states of any BDFM in the class of machines considered are quadratically stable. That is for any finite 2-norm supply voltage and any finite shaft speed (possibly with an unbounded rated of change), the 2-norm of currents remains bounded (Chapter 3).

   (b) The linearized version of the synchronous reference frame d-q axis model was used to analyse the local open-loop stability of equilibria in the synchronous mode of operation. The analysis was found to be in close agreement to that found by experiment (Chapter 7).

5. Control strategies were proposed to stabilize and improve the damping of speed regulation for the BDFM:

   (a) A linear control scheme, 'stator 2 phase angle control' was proposed to stabilize and improve the damping of these equilibria. The scheme was verified by experiment, and

was found to give dynamic performance similar to alternative non-linear control schemes when operating close to the operating set point (Chapter 7).

(b) A control scheme where the stator 2 instantaneous voltage is phase-locked to the rotor position was proposed and its stability analysed using the linearized model. Experimental results were presented showing an improvement in robustness to changes in operating point (Chapter 7).

(c) Two methods of applying feedback linearization to the BDFM were presented, shown to work in simulation, and an initial attempt made to implement them on the prototype machine (Chapter 8).

6. Possible pole number combinations for BDFMs were characterised for most practical situations:

(a) Theorem 2.15 gave necessary and sufficient conditions for avoiding unbalanced magnetic pull, under the assumption that the air gap flux density contained no harmonic fields.

(b) Theorem 2.12 gave necessary and sufficient conditions for non-coupling of isolated single layer stator winding pole combinations, which are sufficient for double layer windings.

9.2 Future Work

The work of this dissertation suggests a number of possible directions for research:

9.2.1 Analysis of the BDFM

1. The d-q axis model could be extended to include harmonic terms. In the first instance it is likely to be most straight forward to proceed in the rotor reference frame, the results could be checked by experiment and against the coupled-circuit model. This would complement the steady-state harmonic analysis of Williamson et. al. [115].

2. The general analysis framework presented assumed that leakage inductance terms only contributed to the self inductance of each coil. It is likely the analysis will generalise directly to allow mutual leakage inductance parameters.

3. The model reduction method proposed for 'nested-loop' rotor designs, although shown to be accurate, comes with no performance guarantees. Further investigation may yield such guarantees, or at least give more specific guidance as to circumstances when the reduction method is likely to be accurate.

4. It was shown that the d-q model in the rotor reference frame could be reduced to a model with $6 + 2N$ states. It is believed that this is a minimal realisation for the system, i.e. that it is not

possible to reduce the system order further without observing an error. However a proof of this is difficult as the system is parameterised by the shaft speed. There are, however, some results in the literature on necessary and sufficient conditions for the minimality of parameter varying systems which may apply to the BDFM [5].

5. The class of rotors considered was neither necessary nor sufficient as functional BDFM rotor designs. Rotor 6 is a functional BDFM rotor, but is not within the class, and rotor 3 is within the class and is not a functional rotor. A simple necessary condition was given in chapter 2, and it may be possible to tighten this condition so that it becomes necessary and sufficient. One way to proceed would be to attempt to characterise the class of rotors encompassed by the necessary condition, although this is likely to be a challenging problem.

6. The new model order reduction method was used to reduce the order of 'nested-loop' design rotors to a rotor which had a single effective set of loops. The reduction technique diagonalized the rotor-rotor self-inductance matrix, and then truncated the system. However the model could be left un-truncated (and therefore free from error) and then transformed into an equivalent circuit representation. This will, in general, lead to off-diagonal resistance terms, but these can be synthesised by a cage structure, as is the case with the squirrel cage rotor. This would lead to a full equivalent circuit representation for nested-loop rotor designs.

7. The analysis in this dissertation has exclusively been for BDFM machines where the synchronous speed is $\frac{\omega_1+\omega_2}{p_1+p_2}$. However it was first noted by Hunt that reversing the phase sequence of the second stator would lead to a machine with a natural speed given by $\omega_r = \frac{\omega_1}{p_1-p_2}$. For Hunt's purposes this mode of operation was not "...of much commercial value." [49, p. 407]. This fact was first noted by Field in comments on Hunt's original paper [48, p. 669]. It is believed that the next mention of this 'differential' mode of operation did not appear until 1997 in Williamson et. al. [115]. Williamson et. al. comment that the subtractive mode would require a rotor with an "unfeasibly small numbers of rotor bars". This comment stems from the assumption that the rotor will be of 'nested loop' design, and in differential mode the rotor must have a number of 'nests' equal to $p_1 - p_2$, rather than $p_1 + p_2$. The problem with this is that it will lead to a relatively high value of rotor leakage inductance due to excess harmonic inductance: L_{r_h} in the notation of chapter 4. However, as has been illustrated in this dissertation it is possible to reduce L_{r_h} by judicious rotor design, therefore the differential BDFM mode should be considered. It is anticipated that analysis in the differential mode will be similar to the additive mode, and it is likely that many of the results will carry over, including the analysis using circulant matrices. The differential mode offers a higher natural speed, and therefore the possibility to run the machine at a higher speed, which will deliver more power from the same frame size machine.

8. Although the modelling techniques presented have been shown to yield good agreement with experimental results, all the tests, with the exception of that shown in figure 6.3 were performed at relatively low flux densities. As the modelling techniques assume infinite iron permeability the accuracy will deteriorate as the flux density increases. Initial attempts to derive saturation factors to compensate led to the conclusion that such factors would, in general, be time and load varying [34]. Therefore further work is required to investigate how allowances can be made for saturation.

9.2.2 BDFM Machine Design

1. Although the magnetic loading for the BDFM was addressed, the treatment requires experimental verification, and the approach may not turn out to be the right compromise. The verification may take the form of loss measurements under different loading conditions, possibly through the use of calorimetric measurement, or through the use of finite elements analysis.

2. This dissertation presented a quantitative method of evaluating BDFM rotors by the evaluation of easily calculable machine parameter values. This suggests the possibility of searching for an optimum rotor design. The search will require the parameterisation of a class of rotor designs over which to search, and the search may be performed numerically or possibly analytically.

3. The experimental procedure to estimate machine parameter values was used without the measurement of rotor bar currents. As described in chapter 6, if these measurements are taken, possibly using Bluetooth technology [83], then the stator-rotor turns ratio can be determined and it is likely that all parameter values will be determined with greater accuracy.

4. This dissertation has principally been concerned with the analysis of the BDFM, albeit with emphasis on its implication for machine design. However nowhere in the current literature are there any design guidelines for the BDFM. Such guidelines could be developed from the equivalent circuit, which retains accuracy whilst being elegant in its simplicity. Issues to consider include how the machine parameter values affect the rating of the machine, its efficiency and power factor, and whether the stator 1-rotor-stator 2 turns ratios affect the performance. The proposed performance measures contribute in this direction, however they do not provide a complete picture.

9.2.3 Stability analysis and control, including parameter estimation

1. As discussed in chapter 7, the use of gain scheduling on the two control strategies proposed is likely to lead to a controller with improved performance over a wider range. Unfortunately recent developments in gain scheduling, offering guaranteed stability and performance are not immediately applicable as they require measurement of all the machine currents, including the

rotor currents. Nevertheless it is likely that gain scheduling will lead to satisfactory performance.

2. Prempain et. al. recently presented a LPV based control algorithm for the standard induction machine [77]. A similar scheme will apply to the BDFM, and offers a systematic method of non-linear controller design for the BDFM, however the stability of the overall system, and in particular the zero dynamics will need careful consideration.

3. Hopfensperger et. al. presented two control schemes for the cascaded doubly-fed machine [46, 45]. These schemes should be investigated, in particular their claimed validity to the BDFM.

4. Although a number of practical control schemes have been presented for the BDFM [125, 129, 130, 126, 124], the stability and performance of these schemes has not been investigated. Using the generalised transformation to the synchronous reference frame presented in this dissertation, the stability of such schemes may be analysed, possibly leading to directions to guarantee stability or even performance.

5. Recent developments in model predictive control have lead to the possibility of considering the problem of controlling an electrical machine as a search for an optimal inverter switching pattern. For the induction machine it has been shown, albeit only in simulation at present, that such a strategy can lead to reduced losses without any performance degradation [76]. A similar approach could be investigated for the BDFM.

6. A off-line parameter estimation method was proposed in this dissertation for the BDFM. However, as discussed above, model-based control algorithms often require accurate machine parameters, some of which change significantly during machine operation (such that the resistance parameters). Therefore on-line parameter estimation techniques could be investigated. One possibility is to design an adaptive observer, such as the extended Kalman filter (although this has no convergence guarantees), alternatively approaches such as that proposed by Castaldi et. al. for the induction machine may be applicable to the BDFM [23].

7. The initial attempts to implement feedback linearization met with limited success. Future work should investigate the stability of the proposed feedback linearization controllers, and seek to address the reasons for the partial experimental success. It is also possible to use feedback linearization to control different outputs other than the speed and flux, for example the speed and stator 1 power factor could be controlled. This can be achieved by appropriate choice of output function.

Appendix A

Mathematics

A.1 Trigonometric Results

Lemma A.1. *Given* $w = \exp(\frac{2\pi j}{n})$ *then* $\sum_{k=0}^{n-1} w^{kp} \exp(j\phi) = 0$ *where* $p \in \mathbb{Z} \neq tn$ *where* $t \in \mathbb{Z}$, *and* $\phi \in \mathbb{R}$. *Hence* $\sum_{k=0}^{n-1} \cos(\frac{2\pi kp}{n} + \phi) + j \sin(\frac{2\pi kp}{n} + \phi) = 0$ *and therefore* $\sum_{k=0}^{n-1} \cos(\frac{2\pi kp}{n} + \phi) = \sum_{k=0}^{n-1} \sin(\frac{2\pi kp}{n} + \phi) = 0$

Proof.

$$\sum_{k=0}^{n-1} w^{kp} \exp(j\phi) = \exp(j\phi) \sum_{k=0}^{n-1} w^{kp+\phi}$$
$$= \exp(j\phi) \left(\exp(0) + \exp(\frac{2\pi pj}{n}) + \exp(\frac{2\pi 2pj}{n}) + \cdots + \exp(\frac{2\pi (n-1)p}{n}) \right)$$

Noting that $\exp(\frac{2\pi pj}{n}) \neq 1$ due to the restrictions on p, and that $\exp(\phi j) \neq 0$:

$$\Rightarrow \exp(j\phi) \sum_{k=0}^{n-1} w^{kp} \left(1 - \exp(\frac{2\pi pj}{n}) \right) = \exp(j\phi) \left(\exp(0) + \exp(\frac{2\pi pj}{n}) + \exp(\frac{2\pi 2pj}{n}) + \cdots \right.$$
$$\left. + \exp(\frac{2\pi (n-1)p}{n}) \right) \left(1 - \exp(\frac{2\pi pj}{n}) \right)$$
$$= \exp(j\phi)\big(1 - \exp(2\pi pj)\big) = 0$$

□

A.2 Linear Algebra

Theorem A.2. *[38, p. 270, vol. 1] A matrix* $A \in \mathbb{R}^{n \times n}$, *such that* $A = A^{\mathrm{T}}$ *(A is symmetric) has a orthonormal basis of eigenvectors for* $\mathbb{R}^n$.

Theorem A.3. *A symmetric matrix,* $A = A^{\mathrm{T}} \in \mathbb{R}^{n \times n}$, *can be written as:*

$$A = T \Lambda T^{\mathrm{T}}$$

where Λ is a diagonal matrix of the eigenvalues of A, and T is a matrix of corresponding eigenvectors of A.

Proof. From Theorem A.2 the eigenvectors of A form a basis for $\mathbb{R}^n$. Let $x_1, x_2, \cdots, x_n$ represent the eigenvectors of A, and $\lambda_1, \lambda_2, \cdots, \lambda_n$ the corresponding eigenvalues. Furthermore let:

$$T = \begin{bmatrix} x_1 & x_2 & \cdots & x_n \end{bmatrix}$$

as the eigenvectors for a basis for $\mathbb{R}^n$ then T is rank n (full rank) and thus T^{-1} exists. Furthermore as the basis is orthonormal hence T is orthogonal, that is $TT^{\mathrm{T}} = I$ hence $T^{-1} = T^{\mathrm{T}}$. Therefore:

$$AT = A\begin{bmatrix} x_1 & x_2 & \cdots & x_n \end{bmatrix} = \begin{bmatrix} Ax_1 & Ax_2 & \cdots & Ax_n \end{bmatrix} = \begin{bmatrix} \lambda_1 x_1 & \lambda_2 x_2 & \cdots & \lambda_n x_n \end{bmatrix} = T\Lambda$$
$$\Rightarrow A = T\Lambda T^{\mathrm{T}}$$

□

Lemma A.4. *A real symmetric matrix has real eigenvalues.*

Proof. Let $x \in \mathbb{R}^n$ be an eigenvector of $A = A^{\mathrm{T}} \in \mathbb{R}^{n\times n}$, and λ the corresponding eigenvalue. Note that we know x to be real from Theorem A.2. From the definition of eigenvectors:

$$Ax = \lambda x$$

and as both A and x are real Ax is real, hence λ is real. □

Lemma A.5. *[131, sect. 2.3] Let A be a square matrix partitioned as follows:*

$$A \triangleq \begin{bmatrix} A_{11}A_{12} \\ A_{21}A_{22} \end{bmatrix}$$

where A_{11} and A_{22} are also square matrices.

If A and A_{11} are non-singular then:

$$\begin{bmatrix} A_{11}A_{12} \\ A_{21}A_{22} \end{bmatrix}^{-1} = \begin{bmatrix} A_{11}^{-1} + A_{11}^{-1}A_{12}\Delta^{-1}A_{21}A_{11}^{-1} & -A_{11}^{-1}A_{12}\Delta^{-1} \\ -\Delta^{-1}A_{21}A_{11}^{-1} & \Delta^{-1} \end{bmatrix}$$

where $\Delta \triangleq A_{22} - A_{21}A_{11}^{-1}A_{12}$ and furthermore it can be shown that A is non-singular if and only if Δ is non-singular.

If A and A_{22} are non-singular then:

$$\begin{bmatrix} A_{11}A_{12} \\ A_{21}A_{22} \end{bmatrix}^{-1} = \begin{bmatrix} \hat{\Delta}^{-1} & -\hat{\Delta}^{-1}A_{12}A_{22}^{-1} \\ -A_{22}^{-1}A_{21}\hat{\Delta}^{-1} & A_{22}^{-1} + A_{22}^{-1}A_{21}\hat{\Delta}^{-1}A_{12}A_{22}^{-1} \end{bmatrix}$$

where $\hat{\Delta} \triangleq A_{11} - A_{12}A_{22}^{-1}A_{21}$ and furthermore it can be shown that A is non-singular if and only if $\hat{\Delta}$ is non-singular.

Lemma A.6. *The eigenvalues of a square upper or lower (block) triangular matrix, $T \in \mathbb{C}^{n\times n}$, are the union of the eigenvalues of the (block) matrices on the diagonal.*

Proof. Without loss of generality we assume T to be upper block triangular:

$$T = \begin{bmatrix} A & B \\ 0 & D \end{bmatrix}$$

where $A \in \mathbb{C}^{m\times m}$,$D \in \mathbb{C}^{n-m\times m-n}$, and B is compatibly partitioned. Let $x_d \in \mathbb{C}^{n-m}$ be an eigenvector of D, with corresponding eigenvalue $\lambda_d \in \mathbb{C}$. Therefore it is immediate that:

$$\begin{bmatrix} A & B \\ 0 & D \end{bmatrix} \begin{bmatrix} 0 \\ x_d \end{bmatrix} = \lambda_d \begin{bmatrix} 0 \\ x_d \end{bmatrix}$$

hence we conclude that λ_d also an eigenvalue of T, and indeed by induction that all eigenvalue of D are eigenvalues of T.

Similarly, let $x_a \in \mathbb{C}^m$ be an eigenvector of A, with corresponding eigenvalue $\lambda_a \in \mathbb{C}$. Again it is immediate that:

$$\begin{bmatrix} A & B \\ 0 & D \end{bmatrix} \begin{bmatrix} x_a \\ 0 \end{bmatrix} = \lambda_a \begin{bmatrix} x_a \\ 0 \end{bmatrix}$$

and hence we conclude that the eigenvalues of A are also eigenvalues of T. The proof for a lower triangular T follows the same lines. □

Lemma A.7. *Given: $A = A_0 + \rho_1 A_1 + \cdots + \rho_n A_n \in \mathbb{R}^{k\times k}$, $C \in \mathbb{R}^{j\times k}$ and $Q = Q^{\mathrm{T}} > 0$, $Q \in \mathbb{R}^{k\times k}$ with $\rho_n^{min} \rho_n < \rho_n^{max} \in \mathbb{R}$ then:*

$$A^{\mathrm{T}}Q + QA + C^{\mathrm{T}}C < 0$$
$$\Leftrightarrow {A^i}^{\mathrm{T}}Q + QA^i + C^{\mathrm{T}}C < 0 \; \forall A^i$$

where A^i denotes the i^{th} extreme point of A. The extreme points are the points corresponding to the 'corners' of the parameter box containing A. There are 2^n such corners.

Proof. We will prove the result for a single parameter, the result for n parameters follows by induction. Hence without loss of generality let $A = A_0 + \rho_1 A_1$ and $\rho_1^{\min} < \rho_1 < \rho_1^{\max}$.

Note that A can be written as $A = A_0 + (\rho_1^{\min}(1-\alpha) + \rho_1^{\max}\alpha)A_1,\ 0 < \alpha < 1$. By definition We have:

$$(A_0 + A_1\rho_1^{\min})^{\mathrm{T}}Q + Q(A_0 + A_1\rho_1^{\min}) + C^{\mathrm{T}}C < 0$$
$$(A_0 + A_1\rho_1^{\max})^{\mathrm{T}}Q + Q(A_0 + A_1\rho_1^{\max}) + C^{\mathrm{T}}C < 0$$

hence from definition 2.10, as $\alpha > 0$ and $1 - \alpha > 0$:

$$(A_0 + A_1(\alpha\rho_1^{\max} + (1-\alpha)\rho_1^{\min}))^{\mathrm{T}}Q + Q(A_0 + A_1(\alpha\rho_1^{\max} + (1-\alpha)\rho_1^{\min})) + C^{\mathrm{T}}C < 0$$

and this is exactly equivalent to $A^{\mathrm{T}}Q + QA + C^{\mathrm{T}}C < 0$, as all possible values of ρ_1 are covered. □

Lemma A.8. *[36, Lemma 3.2] & [93, Prop. 1.34] (Shur Complement):*
Given $P = P^* \in \mathbb{C}^{n\times n}$, $R = R^* \in \mathbb{C}^{m\times m}$ and $S \in \mathbb{C}^{n\times m}$ then:

$$\begin{bmatrix} P & S \\ S^* & R \end{bmatrix} < 0 \Leftrightarrow \begin{cases} R & < 0 \\ P - SR^{-1}S^* & < 0 \end{cases} \Leftrightarrow \begin{cases} P & < 0 \\ R - S^*P^{-1}S & < 0 \end{cases}$$

Lemma A.9. *The following LMIs are equivalent:*

$$\begin{bmatrix} A^{\mathrm{T}}X + XA & XB & \gamma^{-1}C^{\mathrm{T}} \\ B^{\mathrm{T}}X & -I & \gamma^{-1}D^{\mathrm{T}} \\ \gamma^{-1}C & \gamma^{-1}D & -I \end{bmatrix} < 0$$

$$\begin{bmatrix} A^{\mathrm{T}}X\gamma + \gamma XA & \gamma XB & C^{\mathrm{T}} \\ B^{\mathrm{T}}X\gamma & -I\gamma & D^{\mathrm{T}} \\ C & D & -I\gamma \end{bmatrix} < 0$$

$$\begin{bmatrix} A^{\mathrm{T}}X + XA & XB & C^{\mathrm{T}} \\ B^{\mathrm{T}}X & -I & D^{\mathrm{T}} \\ C & D & -I\gamma^2 \end{bmatrix} < 0$$

where $\gamma \in \mathbb{R} > 0$ and $X \in \mathbb{R}^{n\times n} = X^{\mathrm{T}}$.

Proof. Applying Lemma A.8 to the first LMI yields the following equivalent condition:

$$\begin{bmatrix} A^{\mathrm{T}}X + XA & XB \\ B^{\mathrm{T}}X & -I \end{bmatrix} - \begin{bmatrix} \gamma^{-1}C^{\mathrm{T}} \\ \gamma^{-1}D^{\mathrm{T}} \end{bmatrix} (-I)^{-1} \begin{bmatrix} \gamma^{-1}C & \gamma^{-1}D \end{bmatrix} < 0, \quad -I < 0$$

which, as $\gamma > 0$, is equivalent to:

$$\begin{bmatrix} A^{\mathrm{T}}X + XA & XB \\ B^{\mathrm{T}}X & -I \end{bmatrix} - \begin{bmatrix} C^{\mathrm{T}} \\ D^{\mathrm{T}} \end{bmatrix} (-I\gamma^2)^{-1} \begin{bmatrix} C & D \end{bmatrix} < 0, \quad -I\gamma^2 < 0$$

applying the Shur complement again, in reverse, yields the third LMI. The second LMI is obtained by multiplying through by γ. □

Lemma A.10. *The rows of Q are orthonormal to one another, that is: $QQ^{\mathrm{T}} = I$, and furthermore, if Q is square then $Q^{\mathrm{T}}Q = I$, where:*

$$Q = \sqrt{\frac{2}{n}} \begin{bmatrix} \cos(\phi) & \cos(\frac{2\pi p}{n} + \phi) & \cos(\frac{2\pi 2p}{n} + \phi) & \cdots & \cos(\frac{2\pi(n-1)p}{n} + \phi) \\ \sin(\phi) & \sin(\frac{2\pi p}{n} + \phi) & \sin(\frac{2\pi 2p}{n} + \phi) & \cdots & \sin(\frac{2\pi(n-1)p}{n} + \phi) \\ \frac{1}{\sqrt{2}} & \frac{1}{\sqrt{2}} & \frac{1}{\sqrt{2}} & \cdots & \frac{1}{\sqrt{2}} \end{bmatrix}$$

where $\phi \in \mathbb{R}$, $n \in \mathbb{N}, n \geq 3$, $p \in \mathbb{Z} \neq tn, t \in \mathbb{Z}$.

Proof.

$$QQ^{\mathrm{T}} = \frac{2}{n}\begin{bmatrix} \cos(\phi) & \cos(\frac{2\pi p}{n}+\phi) & \cdots & \cos(\frac{2\pi(n-1)p}{n}+\phi) \\ \sin(\phi) & \sin(\frac{2\pi p}{n}+\phi) & \cdots & \sin(\frac{2\pi(n-1)p}{n}+\phi) \\ \frac{1}{\sqrt{2}} & \frac{1}{\sqrt{2}} & \cdots & \frac{1}{\sqrt{2}} \end{bmatrix}\begin{bmatrix} \cos(\phi) & \sin(\phi) & \frac{1}{\sqrt{2}} \\ \cos(\frac{2\pi p}{n}+\phi) & \sin(\frac{2\pi p}{n}+\phi) & \frac{1}{\sqrt{2}} \\ \vdots & \vdots & \vdots \\ \cos(\frac{2\pi(n-1)p}{n}+\phi) & \sin(\frac{2\pi(n-1)p}{n}+\phi) & \frac{1}{\sqrt{2}} \end{bmatrix}$$

From Lemma A.1, it can be seen that terms due to the product of non-trigonometric terms and trigonometric terms will be zero. Hence:

$$= \frac{2}{n}\begin{bmatrix} \cos(\phi)^2 + \cos(\frac{2\pi p}{n}+\phi)^2 + \cdots + \cos(\frac{2\pi(n-1)p}{n}+\phi)^2 \\ \sin(\phi)\cos(\phi) + \sin(\frac{2\pi p}{n}+\phi)\cos(\frac{2\pi p}{n}+\phi) + \cdots + \sin(\frac{2\pi(n-1)p}{n}+\phi)\cos(\frac{2\pi(n-1)p}{n}+\phi) \\ 0 \end{bmatrix}$$

$$\begin{bmatrix} \cos(\phi)\sin(\phi) + \cos(\frac{2\pi p}{n}+\phi)\sin(\frac{2\pi p}{n}+\phi) + \cdots + \cos(\frac{2\pi(n-1)p}{n}+\phi)\sin(\frac{2\pi(n-1)p}{n}+\phi) & 0 \\ \sin(\phi)^2 + \sin(\frac{2\pi p}{n}+\phi)^2 + \cdots + \sin(\frac{2\pi(n-1)p}{n}+\phi)^2 & 0 \\ 0 & \frac{n}{2} \end{bmatrix}$$

Using the trigonometric identities $\cos(A)^2 = \frac{1}{2}+\frac{1}{2}\cos(2A)$, $\sin(A)^2 = \frac{1}{2}-\frac{1}{2}\cos(2A)$, $\sin(A)\cos(A) = \sin(2A)$ with Lemma A.1 gives:

$$= \frac{2}{n}\begin{bmatrix} \frac{n}{2} & 0 & 0 \\ 0 & \frac{n}{2} & 0 \\ 0 & 0 & \frac{n}{2} \end{bmatrix}$$

□

Definition A.1. A matrix, $C \in \mathbb{C}^{n\times n}$ is *circulant* if there exists $c_0, \cdots, c_{n-1}$ such that $C_{ij} = c_{(i-j+n) \mod n}$ where the rows and columns of C are numbered between 0 and $n-1$. $k \mod n$ means the k modulo n i.e. the remainder after dividing k by n.

For $n = 6$ a circulant matrix is:

$$C = \begin{bmatrix} c_0 & c_1 & c_2 & c_3 & c_4 & c_5 \\ c_5 & c_0 & c_1 & c_2 & c_3 & c_4 \\ c_4 & c_5 & c_0 & c_1 & c_2 & c_3 \\ c_3 & c_4 & c_5 & c_0 & c_1 & c_2 \\ c_2 & c_3 & c_4 & c_5 & c_0 & c_1 \\ c_1 & c_2 & c_3 & c_4 & c_5 & c_0 \end{bmatrix}$$

Definition A.2. A matrix $F \in \mathbb{C}^{n\times n}$ is a *Fourier* matrix if $F_{qr} = w^{(q-1)(r-1)}/\sqrt{n}$, where $w = \exp(\frac{j2\pi}{n})$. A Fourier matrix is of the form:

$$F = \frac{1}{\sqrt{n}} \begin{bmatrix} 1 & 1 & 1 & \cdots & 1 \\ 1 & w & w^2 & \cdots & w^{(n-1)} \\ 1 & w^2 & w^4 & \cdots & w^{2(n-1)} \\ \vdots & \vdots & \vdots & \ddots & \vdots \\ 1 & w^{(n-2)} & w^{2(n-2)} & \cdots & w^{(n-2)(n-1)} \\ 1 & w^{(n-1)} & w^{2(n-1)} & \cdots & w^{(n-1)(n-1)} \end{bmatrix}$$

Lemma A.11. *Any Fourier matrix, $F \in \mathbb{C}^{n\times n}$, as detailed in definition A.2 is unitary, i.e $F^{-1} = F^*$, and hence full rank.*

Proof. From the definition F^* may be written:

$$F^* = \frac{1}{\sqrt{n}} \begin{bmatrix} 1 & 1 & 1 & \cdots & 1 \\ 1 & w^{-1} & w^{-2} & \cdots & w^{-(n-1)} \\ 1 & w^{-2} & w^{-4} & \cdots & w^{-2(n-1)} \\ \vdots & \vdots & \vdots & \ddots & \vdots \\ 1 & w^{-(n-2)} & w^{-2(n-2)} & \cdots & w^{-(n-2)(n-1)} \\ 1 & w^{-(n-1)} & w^{-2(n-1)} & \cdots & w^{-(n-1)(n-1)} \end{bmatrix}$$

hence:

$$F^*F = \frac{1}{n} \begin{bmatrix} 1 & 1 & 1 & \cdots & 1 \\ 1 & w^{-1} & w^{-2} & \cdots & w^{-(n-1)} \\ 1 & w^{-2} & w^{-4} & \cdots & w^{-2(n-1)} \\ \vdots & \vdots & \vdots & \ddots & \vdots \\ 1 & w^{-(n-2)} & w^{-2(n-2)} & \cdots & w^{-(n-2)(n-1)} \\ 1 & w^{-(n-1)} & w^{-2(n-1)} & \cdots & w^{-(n-1)(n-1)} \end{bmatrix} \begin{bmatrix} 1 & 1 & 1 & \cdots & 1 \\ 1 & w & w^2 & \cdots & w^{(n-1)} \\ 1 & w^2 & w^4 & \cdots & w^{2(n-1)} \\ \vdots & \vdots & \vdots & \ddots & \vdots \\ 1 & w^{(n-2)} & w^{2(n-2)} & \cdots & w^{(n-2)(n-1)} \\ 1 & w^{(n-1)} & w^{2(n-1)} & \cdots & w^{(n-1)(n-1)} \end{bmatrix}$$

by considering the unit circle it is easy to see that $\sum_0^{n-1} w^{kn} = 0, k \in \mathbb{Z} \neq 0$. Hence:

$$F^*F = I$$

□

Lemma A.12. *[131, p.19] Let $D \in \mathbb{R}^{n\times k}$ $(n > k)$ be such that $D^*D = I$, thus the columns of D are orthonormal. Then there exists a matrix, $D^\perp \in \mathbb{R}^{n\times(n-k)}$ such that $\begin{bmatrix} D & D^\perp \end{bmatrix}$ is a unitary matrix.*

Theorem A.13. *For any circulant matrix $C \in \mathbb{C}^{n\times n}$ the columns of the Fourier matrix, F of compatible dimension are the eigenvectors of C, and that the corresponding eigenvalue is $\lambda = \sum_{j=0}^{n-1} c_j w^{j(i-1)}$, where $1 \leq i \leq n$ denotes the column number of F. Furthermore, if $x \in \mathbb{C}^n$ is an eigenvector of C then $\bar{x}$ is also an eigenvector, and if $C \in \mathbb{R}^{n\times n}$ and the corresponding eigenvalue for x is λ then the eigenvalue of $\bar{x}$ is $\bar{\lambda}$. Finally, from Lemma A.11, C is diagonalisable, that is the eigenvectors of C are distinct.*

Proof. We shall show that for each column of F, $\exists\lambda_i : CF_i = \lambda_i F_i$, where F_i denotes the i^{th} column of F. CF may be written:

$$CF = \frac{1}{\sqrt{n}} \begin{bmatrix} c_0 & c_1 & c_2 & c_3 & \cdots & c_{n-1} \\ c_{n-1} & c_0 & c_1 & c_2 & \cdots & c_{n-2} \\ c_{n-2} & c_{n-1} & c_0 & c_1 & \cdots & c_{n-3} \\ \vdots & \vdots & \vdots & \ddots & \ddots & \vdots \\ c_2 & c_3 & \cdots & c_{n-1} & c_0 & c_1 \\ c_1 & c_2 & c_3 & \cdots & c_{n-1} & c_0 \end{bmatrix} \begin{bmatrix} 1 & 1 & 1 & \cdots & 1 \\ 1 & w & w^2 & \cdots & w^{(n-1)} \\ 1 & w^2 & w^4 & \cdots & w^{2(n-1)} \\ \vdots & \vdots & \vdots & \ddots & \vdots \\ 1 & w^{(n-2)} & w^{2(n-2)} & \cdots & w^{(n-2)(n-1)} \\ 1 & w^{(n-1)} & w^{2(n-1)} & \cdots & w^{(n-1)(n-1)} \end{bmatrix}$$

hence:

$$CF_1 = \frac{1}{\sqrt{n}} \begin{bmatrix} c_0 & c_1 & c_2 & c_3 & \cdots & c_{n-1} \\ c_{n-1} & c_0 & c_1 & c_2 & \cdots & c_{n-2} \\ c_{n-2} & c_{n-1} & c_0 & c_1 & \cdots & c_{n-3} \\ \vdots & \vdots & \vdots & \ddots & \ddots & \vdots \\ c_2 & c_3 & \cdots & c_{n-1} & c_0 & c_1 \\ c_1 & c_2 & c_3 & \cdots & c_{n-1} & c_0 \end{bmatrix} \begin{bmatrix} 1 \\ 1 \\ 1 \\ \vdots \\ 1 \\ 1 \end{bmatrix} = \frac{1}{\sqrt{n}} \begin{bmatrix} \sum_{i=0}^{n-1} c_i \\ \sum_{i=0}^{n-1} c_i \\ \sum_{i=0}^{n-1} c_i \\ \vdots \\ \sum_{i=0}^{n-1} c_i \\ \sum_{i=0}^{n-1} c_i \end{bmatrix} = \lambda_1 F_1$$

noting that $w^n = 1$ (from definition A.2):

$$CF_2 = \frac{1}{\sqrt{n}} \begin{bmatrix} c_0 & c_1 & c_2 & c_3 & \cdots & c_{n-1} \\ c_{n-1} & c_0 & c_1 & c_2 & \cdots & c_{n-2} \\ c_{n-2} & c_{n-1} & c_0 & c_1 & \cdots & c_{n-3} \\ \vdots & \vdots & \vdots & \ddots & \ddots & \vdots \\ c_2 & c_3 & \cdots & c_{n-1} & c_0 & c_1 \\ c_1 & c_2 & c_3 & \cdots & c_{n-1} & c_0 \end{bmatrix} \begin{bmatrix} 1 \\ w \\ w^2 \\ \vdots \\ w^{(n-2)} \\ w^{(n-1)} \end{bmatrix}$$

$$= \frac{1}{\sqrt{n}} \begin{bmatrix} c_0 + wc_1 + w^2c_2 + \cdots + w^{(n-1)}c_{n-1} \\ w[c_0 + wc_1 + w^2c_2 + \cdots + w^{(n-1)}c_{n-1}] \\ w^2[c_0 + wc_1 + w^2c_2 + \cdots + w^{(n-1)}c_{n-1}] \\ \vdots \\ w^{(n-2)}[c_0 + wc_1 + w^2c_2 + \cdots + w^{(n-1)}c_{n-1}] \\ w^{(n-1)}[c_0 + wc_1 + w^2c_2 + \cdots + w^{(n-1)}c_{n-1}] \end{bmatrix} = \lambda_2 F_2$$

by induction we conclude $CF_i = \lambda_i F_i$. By inspection the i^{th} eigenvalue, $\lambda_i = \sum_{j=0}^{n-1} c_j w^{j(i-1)}$.

If x denotes any column of F, then there will always exist a column of F which is equal to $\bar{x}$, as $w^{kn} = 1 \forall k \in \mathbb{Z}$ and $\bar{w} = w^{-1}$, so multiplication of each element of $\bar{x}$ by an appropriate representation of 1 gives a column of F.

Therefore if x if an eigenvector of C, then $\bar{x}$ is also an eigenvector, the and if λ is the eigenvalue corresponding to x then, as $\lambda_i = \sum_{j=0}^{n-1} c_j w^{j(i-1)}$, it is clear that the eigenvalue of $\bar{x}$ is $\bar{\lambda}$ if C is real. □

Lemma A.14. *Given a circulant (not necessarily symmetric) matrix, $C \in \mathbb{R}^{n\times n}$, $n \in \mathbb{N} \geq 3$, then:*

$$QCQ^{\mathrm{T}} = \begin{bmatrix} |\lambda| \begin{bmatrix} \cos(\angle\lambda) & \sin(\angle\lambda) \\ -\sin(\angle\lambda) & \cos(\angle\lambda) \end{bmatrix} & 0 \\ 0 & \lambda_0 \end{bmatrix}$$

where $\lambda \in \mathbb{C}$, $\lambda_0 \in \mathbb{R}$ are eigenvalues of C,and the third column of Q^{T} is the corresponding eigenvector to λ_0. Furthermore, if C is symmetric then the first and second columns of Q^{T} are eigenvectors of C corresponding to eigenvalue λ, and of course, from Theorem A.4 λ must be real. Where:

$$Q = \sqrt{\frac{2}{n}} \begin{bmatrix} \cos(\phi) & \cos(\frac{2\pi p}{n} + \phi) & \cos(\frac{2\pi 2p}{n} + \phi) & \cdots & \cos(\frac{2\pi(n-1)p}{n} + \phi) \\ \sin(\phi) & \sin(\frac{2\pi p}{n} + \phi) & \sin(\frac{2\pi 2p}{n} + \phi) & \cdots & \sin(\frac{2\pi(n-1)p}{n} + \phi) \\ \frac{1}{\sqrt{2}} & \frac{1}{\sqrt{2}} & \frac{1}{\sqrt{2}} & \cdots & \frac{1}{\sqrt{2}} \end{bmatrix}$$

$$\lambda = \sum_{i=0}^{n-1} c_i w^i$$

$$\lambda_0 = \sum_{i=0}^{n-1} c_i$$

where $p \in \mathbb{N}$, $p \neq nt, t \in \mathbb{N}$. c_i is the element on the i^{th} column of row 1 of C, and $w = \exp(\frac{j2\pi}{n})$.

Proof. Firstly, we know that the third column is an eigenvector from Theorem A.13. We now assume, without loss of generality, that $p < n$, as for all $p > n \exists p_1 > 0 : p = p_1 + nk, k, p_1 \in \mathbb{N}$ and $\exp(\frac{2\pi nk}{n}) = 1$.

$$C \begin{bmatrix} \exp(j\phi) \\ \exp(\frac{2\pi pj}{n} + j\phi) \\ \exp(\frac{2\pi 2pj}{n} + j\phi) \\ \vdots \\ \exp(\frac{2\pi(n-1)pj}{n} + j\phi) \end{bmatrix} = \exp(j\phi) C \begin{bmatrix} \exp(0) \\ \exp(\frac{2\pi pj}{n}) \\ \exp(\frac{2\pi 2pj}{n}) \\ \vdots \\ \exp(\frac{2\pi(n-1)pj}{n}) \end{bmatrix} = \exp(j\phi) C \begin{bmatrix} \cos(0) + j\sin(0) \\ \cos(\frac{2\pi p}{n}) + j\sin(\frac{2\pi p}{n}) \\ \cos(\frac{2\pi 2p}{n}) + j\sin(\frac{2\pi 2p}{n}) \\ \vdots \\ \cos(\frac{2\pi(n-1)p}{n}) + j\sin(\frac{2\pi(n-1)p}{n}) \end{bmatrix}$$

and from Theorem A.13, for some $\lambda \in \mathbb{C}$:

$$= \exp(j\phi)\lambda \begin{bmatrix} \cos(0) + j\sin(0) \\ \cos(\frac{2\pi p}{n}) + j\sin(\frac{2\pi p}{n}) \\ \cos(\frac{2\pi 2p}{n}) + j\sin(\frac{2\pi 2p}{n}) \\ \vdots \\ \cos(\frac{2\pi(n-1)p}{n}) + j\sin(\frac{2\pi(n-1)p}{n}) \end{bmatrix} = |\lambda| \begin{bmatrix} \cos(\phi + \angle\lambda) + j\sin(\phi + \angle\lambda) \\ \cos(\frac{2\pi p}{n} + \phi + \angle\lambda) + j\sin(\frac{2\pi p}{n} + \phi + \angle\lambda) \\ \cos(\frac{2\pi 2p}{n} + \phi + \angle\lambda) + j\sin(\frac{2\pi 2p}{n} + \phi + \angle\lambda) \\ \vdots \\ \cos(\frac{2\pi(n-1)p}{n} + \phi + \angle\lambda) + j\sin(\frac{2\pi(n-1)p}{n} + \phi + \angle\lambda) \end{bmatrix}$$

recalling that C is real, taking real and imaginary parts gives:

$$C \begin{bmatrix} \sin(\phi) \\ \sin(\frac{2\pi p}{n} + \phi) \\ \sin(\frac{2\pi 2p}{n} + \phi) \\ \vdots \\ \sin(\frac{2\pi(n-1)p}{n} + \phi) \end{bmatrix} = \lambda \begin{bmatrix} \sin(\phi + \angle\lambda) \\ \sin(\frac{2\pi p}{n} + \phi + \angle\lambda) \\ \sin(\frac{2\pi 2p}{n} + \phi + \angle\lambda) \\ \vdots \\ \sin(\frac{2\pi(n-1)p}{n} + \phi + \angle\lambda) \end{bmatrix}$$

$$C \begin{bmatrix} \cos(\phi) \\ \cos(\frac{2\pi p}{n} + \phi) \\ \cos(\frac{2\pi 2p}{n} + \phi) \\ \vdots \\ \cos(\frac{2\pi(n-1)p}{n} + \phi) \end{bmatrix} = \lambda \begin{bmatrix} \cos(\phi + \angle\lambda)) \\ \cos(\frac{2\pi p}{n} + \phi + \angle\lambda)) \\ \cos(\frac{2\pi 2p}{n} + \phi + \angle\lambda)) \\ \vdots \\ \cos(\frac{2\pi(n-1)p}{n} + \phi + \angle\lambda)) \end{bmatrix}$$

hence if C is symmetric then $\angle\lambda = 0$, and we can conclude that the rows of Q are all eigenvectors of C:

$$CQ^{\mathrm{T}} = Q^{\mathrm{T}} \begin{bmatrix} \lambda & 0 & 0 \\ 0 & \lambda & 0 \\ 0 & 0 & \lambda_0 \end{bmatrix}$$

The eigenvalue results come directly from Theorem A.13.

If C is not necessarily symmetric the we proceed as follows. Defining:

$$x = \begin{bmatrix} \exp(j\phi) \\ \exp(\frac{2\pi pj}{n} + j\phi) \\ \exp(\frac{2\pi 2pj}{n} + j\phi) \\ \vdots \\ \exp(\frac{2\pi(n-1)pj}{n} + j\phi) \end{bmatrix}$$

then with the previous discussion and from Lemma A.13:

$$C \begin{bmatrix} x & \bar{x} \end{bmatrix} = \begin{bmatrix} x & \bar{x} \end{bmatrix} \begin{bmatrix} \lambda & 0 \\ 0 & \bar{\lambda} \end{bmatrix}$$

now notice:

$$C\begin{bmatrix} x & \bar{x}\end{bmatrix}\begin{bmatrix}\frac{1}{2} & -\frac{j}{2}\\ \frac{1}{2} & \frac{j}{2}\end{bmatrix} = \begin{bmatrix} x & \bar{x}\end{bmatrix}\begin{bmatrix}\lambda & 0\\ 0 & \bar{\lambda}\end{bmatrix}\begin{bmatrix}\frac{1}{2} & -\frac{j}{2}\\ \frac{1}{2} & \frac{j}{2}\end{bmatrix}$$
$$= \begin{bmatrix} x & \bar{x}\end{bmatrix}\begin{bmatrix}\frac{1}{2} & -\frac{j}{2}\\ \frac{1}{2} & \frac{j}{2}\end{bmatrix}\begin{bmatrix}1 & 1\\ j & -j\end{bmatrix}\begin{bmatrix}\lambda & 0\\ 0 & \bar{\lambda}\end{bmatrix}\begin{bmatrix}\frac{1}{2} & -\frac{j}{2}\\ \frac{1}{2} & \frac{j}{2}\end{bmatrix}$$
$$= \begin{bmatrix} x & \bar{x}\end{bmatrix}\begin{bmatrix}\frac{1}{2} & -\frac{j}{2}\\ \frac{1}{2} & \frac{j}{2}\end{bmatrix}\begin{bmatrix}\Re\lambda & \Im\lambda\\ -\Im\lambda & \Re\lambda\end{bmatrix}$$

Now notice that $\begin{bmatrix} x & \bar{x}\end{bmatrix}\begin{bmatrix}\frac{1}{2} & -\frac{j}{2}\\ \frac{1}{2} & \frac{j}{2}\end{bmatrix}$ is proportional to the first two columns of Q^{T}, hence recalling that the third column of Q^{T} is an eigenvector of C then we may write:

$$CQ^{\mathrm{T}} = Q^{\mathrm{T}}\begin{bmatrix}|\lambda|\begin{bmatrix}\cos(\angle\lambda) & \sin(\angle\lambda)\\ -\sin(\angle\lambda) & \cos(\angle\lambda)\end{bmatrix} & 0\\ 0 & \lambda_0\end{bmatrix}$$

□

Lemma A.15. *Given a symmetric circulant matrix, $C \in \mathbb{R}^{n\times n}$, $n \in \mathbb{N} \geq 3$, that is, a circulant matrix such that $C = C^{\mathrm{T}}$, then:*

$$QC\frac{d}{dt}(Q^{\mathrm{T}}) = \frac{d\phi}{dt}\begin{bmatrix}0 & \lambda & 0\\ -\lambda & 0 & 0\\ 0 & 0 & 0\end{bmatrix}$$

where $\lambda = \sum_{i=0}^{n-1} c_i w^i$ and:

$$Q = \sqrt{\frac{2}{n}}\begin{bmatrix}\cos(\phi) & \cos(\frac{2\pi p}{n}+\phi) & \cos(\frac{2\pi 2p}{n}+\phi) & \cdots & \cos(\frac{2\pi(n-1)p}{n}+\phi)\\ \sin(\phi) & \sin(\frac{2\pi p}{n}+\phi) & \sin(\frac{2\pi 2p}{n}+\phi) & \cdots & \sin(\frac{2\pi(n-1)p}{n}+\phi)\\ \frac{1}{\sqrt{2}} & \frac{1}{\sqrt{2}} & \frac{1}{\sqrt{2}} & \cdots & \frac{1}{\sqrt{2}}\end{bmatrix}$$

where $p \in \mathbb{N}$, $p \neq nt, t \in \mathbb{N}$. c_i is the element on the i^{th} column of row 1 of C, and $w = \exp(\frac{j2\pi}{n})$.

Proof. From Lemma A.14 we may write:

$$QC = \begin{bmatrix}\lambda & 0 & 0\\ 0 & \lambda & 0\\ 0 & 0 & \lambda_0\end{bmatrix}Q$$

post multiplying by $\frac{d}{d\phi}(Q^{\mathrm{T}})$:

$$QC\frac{d}{d\phi}(Q^{\mathrm{T}}) = \begin{bmatrix}\lambda & 0 & 0\\ 0 & \lambda & 0\\ 0 & 0 & \lambda_0\end{bmatrix}Q\frac{d}{d\phi}(Q^{\mathrm{T}})$$

Differentiating Q gives:

$$\frac{dQ}{d\phi} = \sqrt{\frac{2}{n}} \begin{bmatrix} -\sin(\phi) & -\sin(\frac{2\pi p}{n} + \phi) & -\sin(\frac{2\pi 2p}{n} + \phi) & \cdots & -\sin(\frac{2\pi(n-1)p}{n} + \phi) \\ \cos(\phi) & \cos(\frac{2\pi p}{n} + \phi) & \cos(\frac{2\pi 2p}{n} + \phi) & \cdots & \cos(\frac{2\pi(n-1)p}{n} + \phi) \\ 0 & 0 & 0 & \cdots & 0 \end{bmatrix}$$

Using a similar argument to that found Lemma A.10:

$$QC\frac{d}{d\phi}(Q^{\mathrm{T}}) = \begin{bmatrix} 0 & \lambda & 0 \\ -\lambda & 0 & 0 \\ 0 & 0 & 0 \end{bmatrix}$$

Applying the chain rule then gives the result. □

Lemma A.16. *Given a circulant matrix (not necessarily symmetric), $C \in \mathbb{R}^{n\times n}$, $n \in \mathbb{N} \geq 3$, then:*

$$\begin{bmatrix} Q \\ Q^{\perp} \end{bmatrix} C \begin{bmatrix} Q \\ Q^{\perp} \end{bmatrix}^{\mathrm{T}} = \begin{bmatrix} \lambda & 0 & 0 & 0 \\ 0 & \lambda & 0 & 0 \\ 0 & 0 & \lambda_0 & 0 \\ 0 & 0 & 0 & S \end{bmatrix}$$

if C is symmetric, or otherwise:

$$\begin{bmatrix} Q \\ Q^{\perp} \end{bmatrix} C \begin{bmatrix} Q \\ Q^{\perp} \end{bmatrix}^{\mathrm{T}} = \begin{bmatrix} |\lambda| \begin{bmatrix} \cos(\angle\lambda) & \sin(\angle\lambda) \\ -\sin(\angle\lambda) & \cos(\angle\lambda) \end{bmatrix} & \begin{matrix} 0 & 0 \\ \lambda_0 & 0 \end{matrix} \\ \begin{matrix} 0 & \\ 0 & \end{matrix} & \begin{matrix} 0 & S \end{matrix} \end{bmatrix}$$

where $\lambda, \lambda_0 \in \mathbb{R}^1$ and $S \in \mathbb{R}^{(n-3)\times(n-3)}$ and:

$$Q = \sqrt{\frac{2}{n}} \begin{bmatrix} \cos(\phi) & \cos(\frac{2\pi p}{n} + \phi) & \cos(\frac{2\pi 2p}{n} + \phi) & \cdots & \cos(\frac{2\pi(n-1)p}{n} + \phi) \\ \sin(\phi) & \sin(\frac{2\pi p}{n} + \phi) & \sin(\frac{2\pi 2p}{n} + \phi) & \cdots & \sin(\frac{2\pi(n-1)p}{n} + \phi) \\ \frac{1}{\sqrt{2}} & \frac{1}{\sqrt{2}} & \frac{1}{\sqrt{2}} & \cdots & \frac{1}{\sqrt{2}} \end{bmatrix}$$

where $p \in \mathbb{N}, p \neq nt, t \in \mathbb{N}$, and $Q^{\perp}$ an orthogonal matrix whose rows span the orthogonal complement of the subspace spanned by the rows of Q. Furthermore $\lambda = \sum_{i=0}^{n-1} c_i w^i$ and $\lambda_0 = \sum_{i=0}^{n-1} c_i$, where c_i is the element on the i^{th} column of row 1 of C, and $w = \exp(\frac{j2\pi}{n})$.

Proof. The proof follows the same steps whether or not C is symmetric, therefore without loss of generality we assume C is symmetric. Lemma A.14 proves that each column of Q^{T} is an eigenvector

with corresponding eigenvalues $\lambda, \lambda, \lambda_0$. Therefore we may write:

$$CQ^{\mathrm{T}} = Q^{\mathrm{T}} \begin{bmatrix} \lambda & 0 & 0 \\ 0 & \lambda & 0 \\ 0 & 0 & \lambda_0 \end{bmatrix}$$

$$\Rightarrow QCQ^{\mathrm{T}} = QQ^{\mathrm{T}} \begin{bmatrix} \lambda & 0 & 0 \\ 0 & \lambda & 0 \\ 0 & 0 & \lambda_0 \end{bmatrix}$$

from Lemma A.10:

$$\Rightarrow QCQ^{\mathrm{T}} = \begin{bmatrix} \lambda & 0 & 0 \\ 0 & \lambda & 0 \\ 0 & 0 & \lambda_0 \end{bmatrix}$$

We now consider the entire transformation. Firstly note that an orthogonal $Q^{\perp}$ exists as $QQ^{\mathrm{T}} = I$ (Lemma A.12). Therefore we may write:

$$\begin{bmatrix} Q \\ Q^{\perp} \end{bmatrix} C \begin{bmatrix} Q \\ Q^{\perp} \end{bmatrix}^{\mathrm{T}} = \begin{bmatrix} Q \\ Q^{\perp} \end{bmatrix} \begin{bmatrix} CQ^{\mathrm{T}} & CQ^{\perp\mathrm{T}} \end{bmatrix} = \begin{bmatrix} QCQ^{\mathrm{T}} & QCQ^{\perp\mathrm{T}} \\ Q^{\perp}CQ^{\mathrm{T}} & Q^{\perp}CQ^{\perp\mathrm{T}} \end{bmatrix}$$

Noting that $CQ^{\mathrm{T}} = Q^{\mathrm{T}} \left[\begin{smallmatrix} \lambda & 0 & 0 \\ 0 & \lambda & 0 \\ 0 & 0 & \lambda_0 \end{smallmatrix}\right]$, and because C^{T} is also circulant from Lemma A.14 that $QC = \left[\begin{smallmatrix} \lambda_l & 0 & 0 \\ 0 & \lambda_l & 0 \\ 0 & 0 & \lambda_{0l} \end{smallmatrix}\right] Q$, and that by definition $Q^{\perp}Q^{\mathrm{T}} = 0$:

$$\begin{bmatrix} Q \\ Q^{\perp} \end{bmatrix} C \begin{bmatrix} Q \\ Q^{\perp} \end{bmatrix}^{\mathrm{T}} = \begin{bmatrix} QCQ^{\mathrm{T}} & 0 \\ 0 & Q^{\perp}CQ^{\perp\mathrm{T}} \end{bmatrix} = \begin{bmatrix} \begin{bmatrix} \lambda & 0 & 0 \\ 0 & \lambda & 0 \\ 0 & 0 & \lambda_0 \end{bmatrix} & 0 \\ 0 & Q^{\perp}CQ^{\perp\mathrm{T}} \end{bmatrix}$$

□

Lemma A.17. *Given M as defined below, and Q, $Q^{\perp}$ as defined in Lemma A.16 (with $n = p,\ p = p_1,\ \phi = 0$) then M is rank 2 and:*

$$\begin{bmatrix} Q_{p_1} & 0 \\ 0 & Q_{p_2} \end{bmatrix} M \begin{bmatrix} Q \\ Q^{\perp} \end{bmatrix}^{\mathrm{T}} = 3\sqrt{\frac{2}{3}} \begin{bmatrix} \begin{bmatrix} \frac{M_1}{2}\sqrt{\frac{p_1+p_2}{2}}\cos(\beta_1 p_1) & -\frac{M_1}{2}\sqrt{\frac{p_1+p_2}{2}}\sin(\beta_1 p_1) & 0 \\ \frac{M_1}{2}\sqrt{\frac{p_1+p_2}{2}}\sin(\beta_1 p_1) & \frac{M_1}{2}\sqrt{\frac{p_1+p_2}{2}}\cos(\beta_1 p_1) & 0 \\ 0 & 0 & 0 \end{bmatrix} & 0 \\ \begin{bmatrix} \frac{M_2}{2}\sqrt{\frac{p_1+p_2}{2}}\cos(\beta_2 p_2) & \frac{M_2}{2}\sqrt{\frac{p_1+p_2}{2}}\sin(\beta_2 p_2) & 0 \\ \frac{M_2}{2}\sqrt{\frac{p_1+p_2}{2}}\sin(\beta_2 p_2) & -\frac{M_2}{2}\sqrt{\frac{p_1+p_2}{2}}\cos(\beta_2 p_2) & 0 \\ 0 & 0 & 0 \end{bmatrix} & 0 \end{bmatrix}$$

where:

$$M = \begin{bmatrix} M_1\cos((\theta-\beta_1)p_1) & M_1\cos((\theta-\frac{2\pi}{p}-\beta_1)p_1) & \cdots \\ M_1\cos((\theta-\frac{2\pi}{3p_1}-\beta_1)p_1) & M_1\cos((\theta-\frac{2\pi}{p}-\frac{2\pi}{3p_1}-\beta_1)p_1) & \cdots \\ M_1\cos((\theta-\frac{4\pi}{3p_1}-\beta_1)p_1) & M_1\cos((\theta-\frac{2\pi}{p}-\frac{4\pi}{3p_1}-\beta_1)p_1) & \cdots \\ M_2\cos((\theta-\beta_2)p_2) & M_2\cos((\theta-\frac{2\pi}{p}-\beta_2)p_2) & \cdots \\ M_2\cos((\theta-\frac{2\pi}{3p_2}-\beta_2)p_2) & M_2\cos((\theta-\frac{2\pi}{p}-\frac{2\pi}{3p_2}-\beta_2)p_2) & \cdots \\ M_2\cos((\theta-\frac{4\pi}{3p_2}-\beta_2)p_2) & M_2\cos((\theta-\frac{2\pi}{p}-\frac{4\pi}{3p_2}-\beta_2)p_2) & \cdots \end{bmatrix}$$

$$\begin{bmatrix} M_1\cos((\theta-(p-1)\frac{2\pi}{p}-\beta_1)p_1) \\ M_1\cos((\theta-(p-1)\frac{2\pi}{p}-\frac{2\pi}{3p_1}-\beta_1)p_1) \\ M_1\cos((\theta-(p-1)\frac{2\pi}{p}-\frac{4\pi}{3p_1}-\beta_1)p_1) \\ M_2\cos((\theta-(p-1)\frac{2\pi}{p}-\beta_2)p_2) \\ M_2\cos((\theta-(p-1)\frac{2\pi}{p}-\frac{2\pi}{3p_2}-\beta_2)p_2) \\ M_2\cos((\theta-(p-1)\frac{2\pi}{p}-\frac{4\pi}{3p_2}-\beta_2)p_2) \end{bmatrix}$$

and $p{=}p_1+p_2,\ M_1, M_2 \in \mathbb{R}^1,\ n \in \mathbb{N},\ p_1, p_2 \in \mathbb{N},\ \beta_1, \beta_2, \theta \in \mathbb{R}^1$, *and:*

$$Q_{p_1} = \sqrt{\frac{2}{3}}\begin{bmatrix} \cos(p_1\theta) & \cos(p_1(\theta-\frac{2\pi}{3p_1})) & \cos(p_1(\theta-\frac{4\pi}{3p_1})) \\ \sin(p_1\theta) & \sin(p_1(\theta-\frac{2\pi}{3p_1})) & \sin(p_1(\theta-\frac{4\pi}{3p_1})) \\ \frac{1}{\sqrt{2}} & \frac{1}{\sqrt{2}} & \frac{1}{\sqrt{2}} \end{bmatrix}$$

$$Q_{p_2} = \sqrt{\frac{2}{3}}\begin{bmatrix} \cos(p_2\theta) & \cos(p_2(\theta-\frac{2\pi}{3p_2})) & \cos(p_2(\theta-\frac{2\pi}{3p_2})) \\ \sin(p_2\theta) & \sin(p_2(\theta-\frac{2\pi}{3p_2})) & \sin(p_2(\theta-\frac{4\pi}{3p_2})) \\ \frac{1}{\sqrt{2}} & \frac{1}{\sqrt{2}} & \frac{1}{\sqrt{2}} \end{bmatrix}$$

Proof.

Recalling that $\cos(A)\cos(A-\phi) = \frac{1}{2}\cos(\phi) + \frac{1}{2}\cos(2A-\phi)$, $\sin(A)\cos(A-\phi) = \frac{1}{2}\sin(\phi) + \frac{1}{2}\sin(2A-\phi)$, and using Lemma A.1:

$$\begin{bmatrix} Q_{p_1} & 0 \\ 0 & Q_{p_2} \end{bmatrix} M = 3\sqrt{\frac{2}{3}}\begin{bmatrix} \frac{M_1}{2}\cos(\beta_1 p_1) & \frac{M_1}{2}\cos(\beta_1 p_1+\frac{2\pi p_1}{p}) & \cdots & \frac{M_1}{2}\cos(\beta_1 p_1+\frac{2\pi p_1(p-1)}{p}) \\ \frac{M_1}{2}\sin(\beta_1 p_1) & \frac{M_1}{2}\sin(\beta_1 p_1+\frac{2\pi p_1}{p}) & \cdots & \frac{M_1}{2}\sin(\beta_1 p_1+\frac{2\pi p_1(p-1)}{p}) \\ 0 & 0 & \cdots & 0 \\ \frac{M_2}{2}\cos(\beta_2 p_2) & \frac{M_2}{2}\cos(\beta_2 p_2+\frac{2\pi p_2}{p}) & \cdots & \frac{M_2}{2}\cos(\beta_2 p_2+\frac{2\pi p_2(p-1)}{p}) \\ \frac{M_2}{2}\sin(\beta_2 p_2) & \frac{M_2}{2}\sin(\beta_2 p_2+\frac{2\pi p_2}{p}) & \cdots & \frac{M_2}{2}\sin(\beta_2 p_2+\frac{2\pi p_2(p-1)}{p}) \\ 0 & 0 & \cdots & 0 \end{bmatrix} \tag{A.1}$$

Now from Lemma A.19 (A.1) is rank 2, with the first two rows spanning the entire row space. Furthermore it is clear that the first two rows of Q are in the row space of the first two rows, hence $Q^{\perp}$ is in the null space. As $\cos(\phi) = \cos(\phi + 2\pi)$, and similarly for $\sin(\phi)$, the RHS of the previous expression may be written as:

$$3\sqrt{\frac{2}{3}}\begin{bmatrix} \frac{M_1}{2}\cos(\beta_1 p_1) & \frac{M_1}{2}\cos(\beta_1 p_1 + \frac{2\pi p_1}{p}) & \cdots & \frac{M_1}{2}\cos(\beta_1 p_1 + \frac{2\pi p_1(p-1)}{p}) \\ \frac{M_1}{2}\sin(\beta_1 p_1) & \frac{M_1}{2}\sin(\beta_1 p_1 + \frac{2\pi p_1}{p}) & \cdots & \frac{M_1}{2}\sin(\beta_1 p_1 + \frac{2\pi p_1(p-1)}{p}) \\ 0 & 0 & \cdots & 0 \\ \frac{M_2}{2}\cos(\beta_2 p_2) & \frac{M_2}{2}\cos(\beta_2 p_2 + \frac{2\pi p_2}{p} - \frac{2\pi p}{p}) & \cdots & \frac{M_2}{2}\cos(\beta_2 p_2 + \frac{2\pi p_2(p-1)}{p} - \frac{2\pi p(p-1)}{p})) \\ \frac{M_2}{2}\sin(\beta_2 p_2) & \frac{M_2}{2}\sin(\beta_2 p_2 + \frac{2\pi p_2}{p} - \frac{2\pi p}{p}) & \cdots & \frac{M_2}{2}\sin(\beta_2 p_2 + \frac{2\pi p_2(p-1)}{p} - \frac{2\pi p(p-1)}{p}) \\ 0 & 0 & \cdots & 0 \end{bmatrix}$$

$$= 3\sqrt{\frac{2}{3}}\begin{bmatrix} \frac{M_1}{2}\cos(\beta_1 p_1) & \frac{M_1}{2}\cos(\beta_1 p_1 + \frac{2\pi p_1}{p}) & \cdots & \frac{M_1}{2}\cos(\beta_1 p_1 + \frac{2\pi p_1(p-1)}{p}) \\ \frac{M_1}{2}\sin(\beta_1 p_1) & \frac{M_1}{2}\sin(\beta_1 p_1 + \frac{2\pi p_1}{p}) & \cdots & \frac{M_1}{2}\sin(\beta_1 p_1 + \frac{2\pi p_1(p-1)}{p}) \\ 0 & 0 & \cdots & 0 \\ \frac{M_2}{2}\cos(-\beta_2 p_2) & \frac{M_2}{2}\cos(-\beta_2 p_2 + \frac{2\pi p_1}{p}) & \cdots & \frac{M_2}{2}\cos(-\beta_2 p_2 + \frac{2\pi p_1(p-1)}{p}) \\ -\frac{M_2}{2}\sin(-\beta_2 p_2) & -\frac{M_2}{2}\sin(-\beta_2 p_2 + \frac{2\pi p_1}{p} & \cdots & -\frac{M_2}{2}\sin(-\beta_2 p_2 + \frac{2\pi p_1(p-1)}{p}) \\ 0 & 0 & \cdots & 0 \end{bmatrix}$$

multiplying this by Q^{T}, and then simplifying using $\cos(A+\phi)\cos(A) = \frac{1}{2}\cos(\phi) + \frac{1}{2}\cos(2A+\phi)$, $\sin(A+\phi)\cos(A) = \frac{1}{2}\sin(\phi) + \frac{1}{2}\sin(2A+\phi)$, $\cos(A+\phi)\sin(A) = -\frac{1}{2}\sin(\phi) + \frac{1}{2}\sin(2A+\phi)$, $\cos(A+\phi)\sin(A) = -\frac{1}{2}\sin(\phi) + \frac{1}{2}\sin(2A+\phi)$, $\sin(A+\phi)\sin(A) = \frac{1}{2}\cos(\phi) - \frac{1}{2}\cos(2A+\phi)$ with Lemma A.1 gives:

$$3\sqrt{\frac{2}{3}}\sqrt{\frac{2}{p_1+p_2}}\begin{bmatrix} \frac{M_1}{2}\frac{p_1+p_2}{2}\cos(\beta_1 p_1) & -\frac{M_1}{2}\frac{p_1+p_2}{2}\sin(\beta_1 p_1) & 0 \\ \frac{M_1}{2}\frac{p_1+p_2}{2}\sin(\beta_1 p_1) & \frac{M_1}{2}\frac{p_1+p_2}{2}\cos(\beta_1 p_1) & 0 \\ 0 & 0 & 0 \\ \frac{M_2}{2}\frac{p_1+p_2}{2}\cos(\beta_2 p_2) & \frac{M_2}{2}\frac{p_1+p_2}{2}\sin(\beta_2 p_2) & 0 \\ \frac{M_2}{2}\frac{p_1+p_2}{2}\sin(\beta_2 p_2) & -\frac{M_2}{2}\frac{p_1+p_2}{2}\cos(\beta_2 p_2) & 0 \\ 0 & 0 & 0 \end{bmatrix}$$

hence:

$$\begin{bmatrix} Q_{p_1} & 0 \\ 0 & Q_{p_2} \end{bmatrix} M \begin{bmatrix} Q \\ Q^{\perp} \end{bmatrix}^{\mathrm{T}} = 3\sqrt{\frac{2}{3}}\begin{bmatrix} \begin{bmatrix} \frac{M_1}{2}\sqrt{\frac{p_1+p_2}{2}}\cos(\beta_1 p_1) & -\frac{M_1}{2}\sqrt{\frac{p_1+p_2}{2}}\sin(\beta_1 p_1) & 0 \\ \frac{M_1}{2}\sqrt{\frac{p_1+p_2}{2}}\sin(\beta_1 p_1) & \frac{M_1}{2}\sqrt{\frac{p_1+p_2}{2}}\cos(\beta_1 p_1) & 0 \\ 0 & 0 & 0 \end{bmatrix} & 0 \\ \begin{bmatrix} \frac{M_2}{2}\sqrt{\frac{p_1+p_2}{2}}\cos(\beta_2 p_2) & \frac{M_2}{2}\sqrt{\frac{p_1+p_2}{2}}\sin(\beta_2 p_2) & 0 \\ \frac{M_2}{2}\sqrt{\frac{p_1+p_2}{2}}\sin(\beta_2 p_2) & -\frac{M_2}{2}\sqrt{\frac{p_1+p_2}{2}}\cos(\beta_2 p_2) & 0 \\ 0 & 0 & 0 \end{bmatrix} & 0 \end{bmatrix}$$

□

Lemma A.18. *Given M as defined in Lemma A.17, and Q, $Q^{\perp}$ are defined as in Lemma A.16 (with $n = p,\ p = p_1,\ \phi = 0$) then M is rank 2 and:*

$$\begin{bmatrix} Q_{p_1} & 0 \\ 0 & Q_{p_2} \end{bmatrix} \frac{d}{d\theta}(M) \begin{bmatrix} Q \\ Q^{\perp} \end{bmatrix}^{\mathrm{T}} = 3\sqrt{\frac{2}{3}} \begin{bmatrix} \begin{bmatrix} \frac{M_1}{2}\sqrt{\frac{p_1+p_2}{2}}p_1\sin(\beta_1 p_1) & \frac{M_1}{2}\sqrt{\frac{p_1+p_2}{2}}p_1\cos(\beta_1 p_1) & 0 \\ -\frac{M_1}{2}\sqrt{\frac{p_1+p_2}{2}}p_1\cos(\beta_1 p_1) & \frac{M_1}{2}\sqrt{\frac{p_1+p_2}{2}}p_1\sin(\beta_1 p_1) & 0 \\ 0 & 0 & 0 \end{bmatrix} & 0 \\ \begin{bmatrix} \frac{M_2}{2}\sqrt{\frac{p_1+p_2}{2}}p_2\sin(\beta_2 p_2) & -\frac{M_2}{2}\sqrt{\frac{p_1+p_2}{2}}p_2\cos(\beta_2 p_2) & 0 \\ -\frac{M_2}{2}\sqrt{\frac{p_1+p_2}{2}}p_2\cos(\beta_2 p_2) & -\frac{M_2}{2}\sqrt{\frac{p_1+p_2}{2}}p_2\sin(\beta_2 p_2) & 0 \\ 0 & 0 & 0 \end{bmatrix} & 0 \end{bmatrix}$$

where: $p{=}p_1 + p_2,\ M_1, M_2 \in \mathbb{R}^1,\ n \in \mathbb{N},\ p_1, p_2 \in \mathbb{N},\ \beta_1, \beta_2, \theta \in \mathbb{R}^1$, and Q_{p_1}, Q_{p_2} are defined in Lemma A.17

Proof. Differentiating M by θ changes the cosine terms to negative sine terms, which is equivalent to augmenting the angular offset in each term by $\pi/2$, and multiplying the resultant by p_1, or p_2 respectively. Following this change through the proof in Lemma A.17 gives the desired result. □

Lemma A.19. *The matrix $Q \in \mathbb{R}^{4\times(p_1+p_2)}$ is rank 2, and furthermore the first two rows span the whole of the row space of Q, where Q is defined as:*

$$Q = \begin{bmatrix} A\cos(\phi_1) & A\cos(\phi_1 + \frac{2\pi p_1}{p_1+p_2}) & \cdots & A\cos(\phi_1 + \frac{2\pi p_1(p_1+p_2-1)}{p_1+p_2}) \\ A\sin(\phi_1) & A\sin(\phi_1 + \frac{2\pi p_1}{p_1+p_2}) & \cdots & A\sin(\phi_1 + \frac{2\pi p_1(p_1+p_2-1)}{p_1+p_2}) \\ B\cos(\phi_2) & B\cos(\phi_2 + \frac{2\pi p_2}{p_1+p_2}) & \cdots & B\cos(\phi_2 + \frac{2\pi p_2(p_1+p_2-1)}{p_1+p_2}) \\ B\sin(\phi_2) & B\sin(\phi_2 + \frac{2\pi p_2}{p_1+p_2}) & \cdots & B\sin(\phi_2 + \frac{2\pi p_2(p_1+p_2-1)}{p_1+p_2}) \end{bmatrix}$$

where $\phi_1, \phi_2, A, B \in \mathbb{R}$ and $p_1, p_2 \in \mathbb{N}$.

Proof.

Firstly note that from Lemma A.10, that the first two rows are linearly independent. To proceed with the proof we define $X \in \mathbb{C}^{1\times(p_1+p_2)}$ as follows, noting that X is a linear combination of rows 1 and 2 of Q:

$$X = \begin{bmatrix} A\exp(-j\phi_1) & A\exp(-j\phi_1 - j\frac{2\pi p_1}{p_1+p_2}) & \cdots & A\exp(-j\phi_1 - j\frac{2\pi p_1(p_1+p_2-1)}{p_1+p_2}) \end{bmatrix}$$

rearranging X gives:

$$\begin{aligned} &= \frac{A}{B}\exp(-j\phi_2 - j\phi_1)\begin{bmatrix} B\exp(j\phi_2) & B\exp(j\phi_2 - j\frac{2\pi p_1}{p_1+p_2}) & \cdots & B\exp(j\phi_2 - j\frac{2\pi p_1(p_1+p_2-1)}{p_1+p_2}) \end{bmatrix} \\ &= \frac{A}{B}\exp(-j\phi_2 - j\phi_1)\Big[B\exp(j\phi_2)\exp(0) \quad B\exp(j\phi_2 - \tfrac{2\pi p_1}{p_1+p_2})\exp(j2\pi\tfrac{p_1+p_2}{p_1+p_2}) \quad \cdots \\ &\qquad\qquad B\exp(j\phi_2 - j\tfrac{2\pi p_1(p_1+p_2-1)}{p_1+p_2}))\exp(j2\pi\tfrac{(p_1+p_2)(p_1+p_2-1)}{p_1+p_2})\Big] \\ &= \frac{A}{B}\exp(-j\phi_2 - j\phi_1)\begin{bmatrix} B\exp(j\phi_2) & B\exp(j\phi_2 + j\frac{2\pi p_2}{p_1+p_2}) & \cdots & B\exp(j\phi_2 + j\frac{2\pi p_2(p_1+p_2-1)}{p_1+p_2}) \end{bmatrix} \end{aligned}$$

similarly we may define Y, also a linear combination of the first two rows of Q:

$$Y = \frac{A}{B}\exp(j\phi_2 + j\phi_1)\left[B\exp(-j\phi_2) \quad B\exp(-j\phi_2 - j\tfrac{2\pi p_2}{p_1+p_2}) \quad \cdots \quad B\exp(-j\phi_2 - j\tfrac{2\pi p_2(p_1+p_2-1)}{p_1+p_2})\right]$$

Now taking $\frac{B}{2A}\exp(j\phi_1 + j\phi_2)X + \frac{B}{2A}\exp(-j\phi_1 - j\phi_2)Y$ gives the 3rd row of Q and $-\frac{jB}{2A}\exp(j\phi_1 + j\phi_2)X + \frac{jB}{2A}\exp(-j\phi_1 - j\phi_2)Y$ gives the 4th row of Q. □

Appendix B

Prototype Machine Stator and Rotor Design Details

In this chapter the details of the prototype machine stator and rotor designs, as described in chapter 5, are given. Table B.1 summarises the configuration of the prototype machine stator.

Parameter		**Value**
Frame size		D180
Stator core length		190mm
Stator slots		48
Stator winding 1	Poles	4
	coils per phase	16 (series connected)
	turns per coil	10
	Configuration	star
	wire diameter	1.2mm
	rated current	6.78Arms (with 6A/mm^2)
	Measured† air gap flux density	0.31Trms at 238Vrms
	at 50Hz, at *phase voltage* given	0.12Trms at 95Vrms
Stator winding 2	Poles	8
	coils per phase	16 (series connected)
	turns per coil	20
	Configuration	star
	wire diameter	1.2mm
	rated current	6.78Arms (with 6A/mm^2)
	Measured† air gap flux density	0.30Trms at 238Vrms
	at 50Hz, at *phase voltage* given	0.12Trms at 95Vrms

Table B.1: Prototype machine stator summary specification. † measured at the winding synchronous speed with a single pole pitch search coil.

B.1 Prototype machine frame details

The prototype machine frame was a standard induction machine frame, manufactured by Marelli Motori SpA. The details are given in table B.2.

Parameter	Value
Frame size	180mm
Marelli Part No.	A4C180L4
Rated output power	22kW
Rated Speed	1465rpm
Rated Torque	143Nm
Peak torque	358Nm
Rated efficiency	90.3%
Moment of Inertia	0.11kgm^2
Weight	122kg

Table B.2: Original Marelli Motori SpA. 4 pole induction machine specification used for the Prototype BDFM frame

B.2 Prototype Machine Stator Windings

We now detail the stator windings design and analysis on the prototype machine. We begin by reviewing the standard winding factors used in 3-phase machine.

B.2.1 Machine Winding Factors

Winding factors are commonly used in the design of AC electrical machine windings.

The per-phase magnetizing inductance and air gap magnetic flux density of a balanced three phase winding when excited with a balanced three phase source is given by [43, eqs. (78), (81), p. 40]:

$$L = \frac{3wd\mu_0 N_{\text{ph}}^2}{\pi g} \sum_{n \in Q} \left(\frac{K_n}{n} \right)^2 \tag{B.1}$$

$$B(\theta, t) = \frac{3\mu_0 \hat{I} N_{\text{ph}}}{\pi g} \sum_{n \in Q} \left(\frac{K_n}{n} \right) \cos(n\theta \pm \omega t) \tag{B.2}$$

where w is the machine stack length, g is the effective air gap width (as defined in section C.2), d is the machine diameter, N is the number of turns per phase, n is the pole number (number of pole pairs) of the field being considered, K_n is the combined winding factor for the n pole number field and the current in the winding in one phase is $\hat{I}\cos(\omega t)$.

For a balanced three phase winding only odd harmonics of the fundamental p pole number field appear, with the exception of third harmonics. It can be shown that for a balanced three phase winding:

$$Q = p|6c + 1| \tag{B.3}$$

where $c = \{0, \pm1, \pm2, \pm3, \cdots\}$. For proof see [43, eq. (36b)].

The winding factor for the n^{th} harmonic, K_n comprises of the following terms:

$$K_{d_n} = \frac{\sin(nM_p\alpha_s/2)}{M_p \sin(n\alpha_s/2)} \tag{B.4}$$

$$K_{p_n} = \cos(nM_s\alpha_s/2) \tag{B.5}$$

$$K_{s_n} = \frac{\sin(nw_s/2)}{nw_s/2} \tag{B.6}$$

$$K_n = K_{d_n} K_{p_n} K_{s_n} \tag{B.7}$$

where M_p is the number of slots per phase per pole, α_s, w_s are the slot pitch and slot mouth width in radians as in figure 2.2, M_s is the number of slots that the winding is short-pitched by . Equations (B.4) and (B.5) can be found in [99] as equations (10.130) and (10.131). Equation (B.6) is found in [112], although it is effectively proved by noting that (2.24) contains K_{s_n} as a factor.

B.2.2 Stator Winding details

Table B.3 shows the details of the stator windings. Figures B.1 and B.2 show colour coded winding diagrams for the 8 and 4 pole windings respectively.

Further machine parameters relating to dimensions and the like can be found in tables C.2 and C.1.

Throughout this dissertation unless otherwise stated, the stator state order will be 4 pole states then 8 pole states. The numerical values for the stator mutual inductance given are for the nested-loop design rotor, Rotor 1. The values differ slightly for the different rotors because the effective air gap changes. Mutual inductance (excluding leakage) is inversely proportional to effective air gap width, therefore the stator mutual inductance terms for other rotors can be closely approximated by scaling the terms given as appropriate.

The subscripts are in the order of: coil group number,connection number within a coil. So for example a_{21} means coil number 2, connection number 1, and current in the 'out' direction. A bar ($\bar{a}$) means return path current direction.

No. slots short pitch. M_s	No. slots /phase/pole M_p	No. layers	Turns per coil	No. coils per phase	No. turns per phase N_{ph}	Wire dia. (mm)	Wire area (mm^2)	Fund. dist. fac. K_d	Fund. pitch fac. K_p	Fund. slot w. fac. K_s	Fund. winding fac. K
Stator 4 pole winding											
2	4	2	10	16	160	1.2	1.13	0.9577	0.9659	0.9998	0.9248
Stator 8 pole winding											
1	2	2	20	16	320	1.2	1.13	0.9659	0.9659	0.9991	0.9322

Table B.3: Stator winding details and fundamental winding factors

Slot:	1	2	3	4	5	6	7	8	9	10	11	12
8 pole:	a_{11}	a_{12}	$\bar{c}$	$\bar{c}$	b_{11}	b	$\bar{a}_{21}$	$\bar{a}_{22}$	c_{11}	c	$\bar{b}$	$\bar{b}$
	a_{82}	$\bar{c}$	$\bar{c}$	b	b	$\bar{a}_{11}$	$\bar{a}_{12}$	c	c	$\bar{b}$	$\bar{b}$	a_{21}
4 pole:	A_{11}	A_{12}	A_{13}	A_{14}	$\bar{C}$	$\bar{C}$	$\bar{C}$	$\bar{C}$	B_{11}	B	B	B
	A_{43}	A_{44}	$\bar{C}$	$\bar{C}$	$\bar{C}$	$\bar{C}$	B	B	B	B	$\bar{A}_{11}$	$\bar{A}_{12}$

Slot:	13	14	15	16	17	18	19	20	21	22	23	24
8 pole:	a_{31}	a_{32}	$\bar{c}$	$\bar{c}$	b	b	$\bar{a}_{41}$	$\bar{a}_{42}$	c	c	$\bar{b}$	$\bar{b}$
	a_{22}	$\bar{c}$	$\bar{c}$	b	b	$\bar{a}_{31}$	$\bar{a}_{32}$	c	c	$\bar{b}$	$\bar{b}$	a_{41}
4 pole:	$\bar{A}_{21}$	$\bar{A}_{22}$	$\bar{A}_{23}$	$\bar{A}_{24}$	C_{11}	C	C	C	$\bar{B}$	$\bar{B}$	$\bar{B}$	$\bar{B}$
	$\bar{A}_{13}$	$\bar{A}_{14}$	C	C	C	C	$\bar{B}$	$\bar{B}$	$\bar{B}$	$\bar{B}$	A_{21}	A_{22}

Slot:	25	26	27	28	29	30	31	32	33	34	35	36
8 Pole:	a_{51}	a_{52}	$\bar{c}$	$\bar{c}$	b	b	$\bar{a}_{61}$	$\bar{a}_{62}$	c	c	$\bar{b}$	$\bar{b}$
	a_{42}	$\bar{c}$	$\bar{c}$	b	b	$\bar{a}_{51}$	$\bar{a}_{52}$	c	c	$\bar{b}$	$\bar{b}$	a_{61}
4 pole:	A_{31}	A_{32}	A_{33}	A_{34}	$\bar{C}$	$\bar{C}$	$\bar{C}$	$\bar{C}$	B	B	B	B
	A_{23}	A_{24}	$\bar{C}$	$\bar{C}$	$\bar{C}$	$\bar{C}$	B	B	B	B	$\bar{A}_{31}$	$\bar{A}_{32}$

Slot:	37	38	39	40	41	42	43	44	45	46	47	48
8 pole:	a_{71}	a_{72}	$\bar{c}$	$\bar{c}$	b	b	$\bar{a}_{81}$	$\bar{a}_{82}$	c	c	$\bar{b}$	$\bar{b}$
	a_{62}	$\bar{c}$	$\bar{c}$	b	b	$\bar{a}_{71}$	$\bar{a}_{72}$	c	c	$\bar{b}$	$\bar{b}$	a_{81}
4 pole:	$\bar{A}_{41}$	$\bar{A}_{42}$	$\bar{A}_{43}$	$\bar{A}_{44}$	C	C	C	C	$\bar{B}$	$\bar{B}$	$\bar{B}$	$\bar{B}$
	$\bar{A}_{33}$	$\bar{A}_{34}$	C	C	C	C	$\bar{B}$	$\bar{B}$	$\bar{B}$	$\bar{B}$	A_{41}	A_{42}

Thus for phase a of the power (8 pole) winding the connections are as follows:

$(a_{11}, \bar{a}_{11})$, $(a_{12}, \bar{a}_{12})$, $(a_{21}, \bar{a}_{21})$, $(a_{22}, \bar{a}_{22})$, $(a_{31}, \bar{a}_{31})$, $(a_{32}, \bar{a}_{32})$, $(a_{41}, \bar{a}_{41})$, $(a_{42}, \bar{a}_{42})$,
$(a_{51}, \bar{a}_{51})$, $(a_{52}, \bar{a}_{52})$, $(a_{61}, \bar{a}_{61})$, $(a_{62}, \bar{a}_{62})$, $(a_{71}, \bar{a}_{71})$, $(a_{72}, \bar{a}_{72})$, $(a_{81}, \bar{a}_{81})$, $(a_{82}, \bar{a}_{82})$

Thus phase a starts in slot 1, top and ends in slot 44 top. Phase B starts at slot 5 top, and ends at slot 48 top, phase C starts at slot 9 top, and ends at slot 4, top.

Phase A for the control (4 pole) winding goes as follows:

$(A_{11}, \bar{A}_{11})$, $(A_{12}, \bar{A}_{12})$, $(A_{13}, \bar{A}_{13})$, $(A_{14}, \bar{A}_{14})$, $(A_{21}, \bar{A}_{21})$, $(A_{22}, \bar{A}_{22})$, $(A_{23}, \bar{A}_{23})$, $(A_{24}, \bar{A}_{24})$,
$(A_{31}, \bar{A}_{31})$, $(A_{32}, \bar{A}_{32})$, $(A_{33}, \bar{A}_{33})$, $(A_{34}, \bar{A}_{34})$, $(A_{41}, \bar{A}_{41})$, $(A_{42}, \bar{A}_{42})$, $(A_{43}, \bar{A}_{43})$, $(A_{44}, \bar{A}_{44})$

Thus phase A starts in slot 1, top and ends in slot 40 top. Phase B starts at slot 9, top and finishes in slot 48, top, phase C starts at slot 17, top, and ends at slot 8, top.

Stator combination matrices

With reference to figures B.2 and B.1, the coil group order for the mutual inductance matrices is as follows:

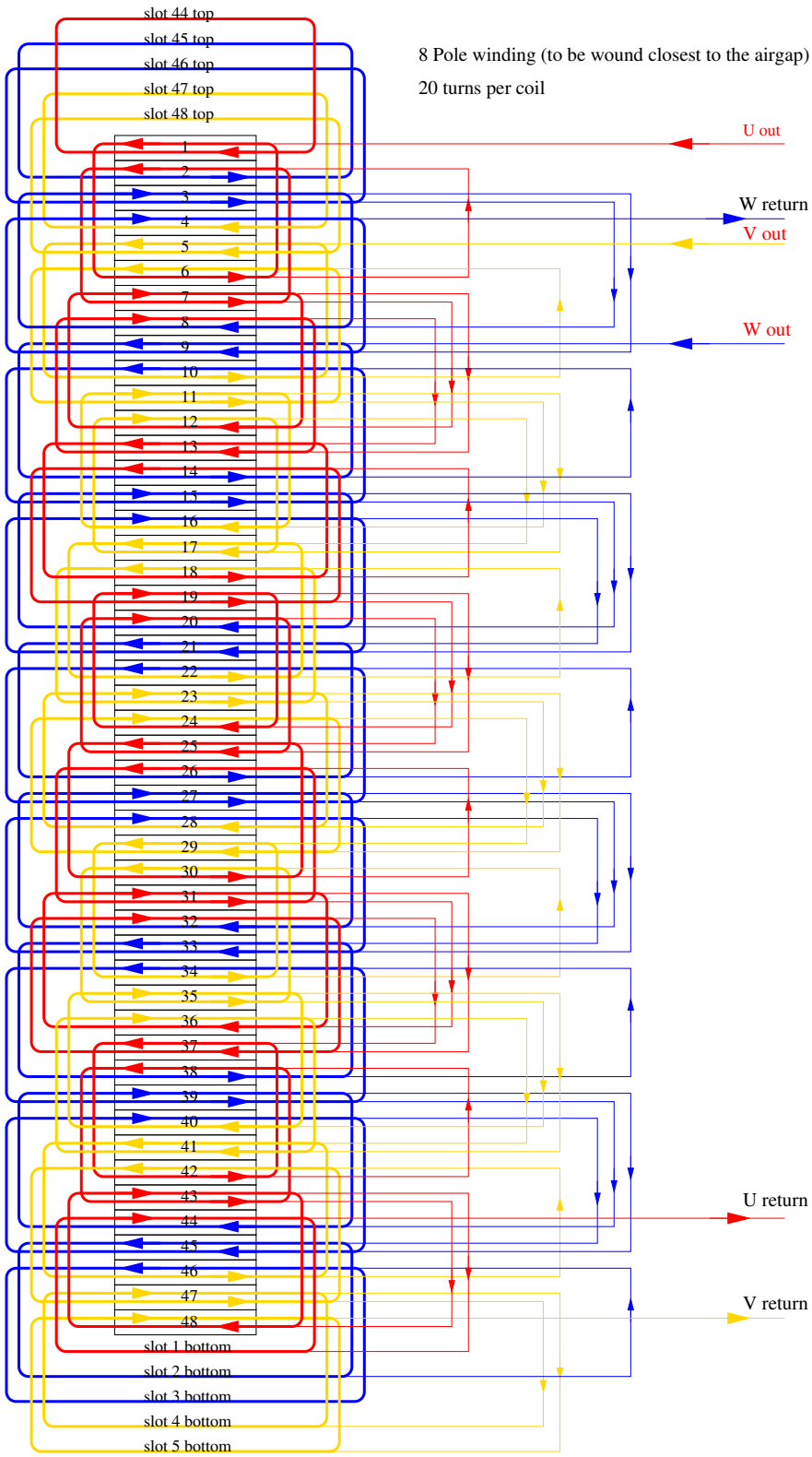

Figure B.1: 8 pole winding diagram

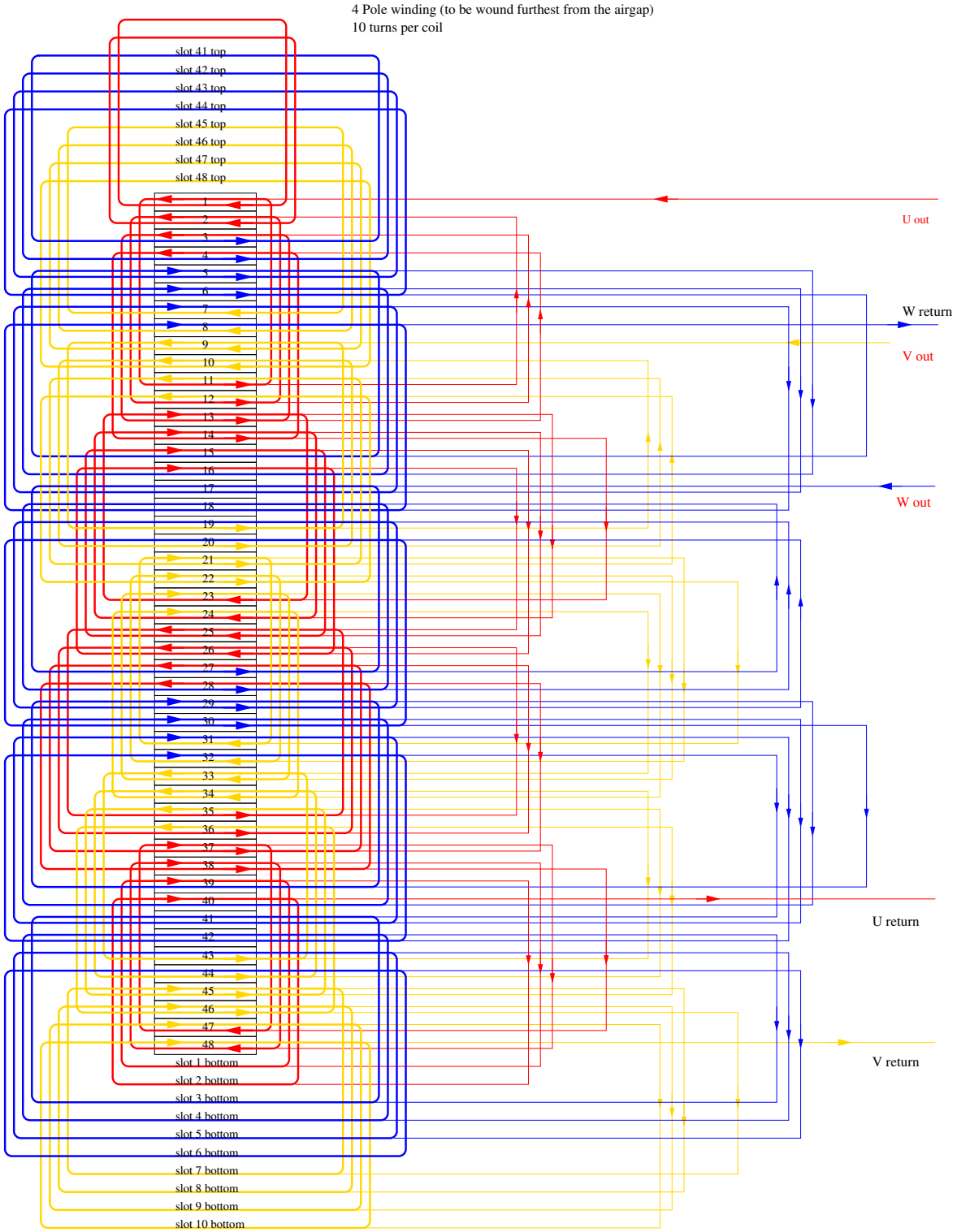

Figure B.2: 4 pole winding diagram

Element	Description
$1 \cdots 16$	4 pole winding red phase
$17 \cdots 32$	4 pole winding yellow phase
$33 \cdots 48$	4 pole winding blue phase
$49 \cdots 64$	8 pole winding red phase
$65 \cdots 80$	8 pole winding yellow phase
$81 \cdots 96$	8 pole winding blue phase

The combination matrix to combine individual coil inductances into winding inductances is given by:

$$T_s = \begin{bmatrix} Q_4 & 0 & 0 & 0 & 0 & 0 \\ 0 & Q_4 & 0 & 0 & 0 & 0 \\ 0 & 0 & Q_4 & 0 & 0 & 0 \\ 0 & 0 & 0 & Q_8 & 0 & 0 \\ 0 & 0 & 0 & 0 & Q_8 & 0 \\ 0 & 0 & 0 & 0 & 0 & Q_8 \end{bmatrix} \tag{B.8}$$

where:

$$Q_4 = \begin{bmatrix} Q_a & -Q_a & Q_a & -Q_a \end{bmatrix}, \qquad Q_a = \begin{bmatrix} 1 & 1 & 1 & 1 \end{bmatrix}$$
$$Q_8 = \begin{bmatrix} Q_b & -Q_b & Q_b & -Q_b & Q_b & -Q_b & Q_b & -Q_b \end{bmatrix}, \qquad Q_b = \begin{bmatrix} 1 & 1 \end{bmatrix}$$

The resulting mutual inductance matrix, leakage inductance matrix as calculated by the methods described in appendix C.1, and excess harmonic inductance is given by:

$$M_{ss} = 10^{-3} \times \begin{bmatrix} 210 & -96.3 & -96.3 & 0 & 0 & 0 \\ -96.3 & 210 & -96.3 & 0 & 0 & 0 \\ -96.3 & -96.3 & 210 & 0 & 0 & 0 \\ 0 & 0 & 0 & 217 & -97.4 & -97.4 \\ 0 & 0 & 0 & -97.4 & 217 & -97.4 \\ 0 & 0 & 0 & -97.4 & -97.4 & 217 \end{bmatrix} \quad M_{ss_l} = 10^{-3} \times \begin{bmatrix} 3.5 & 0 & 0 & 0 & 0 & 0 \\ 0 & 3.5 & 0 & 0 & 0 & 0 \\ 0 & 0 & 3.5 & 0 & 0 & 0 \\ 0 & 0 & 0 & 8.0 & 0 & 0 \\ 0 & 0 & 0 & 0 & 8.0 & 0 \\ 0 & 0 & 0 & 0 & 0 & 8.0 \end{bmatrix} \tag{B.9}$$

$$M_{ss}^{hl} = 10^{-3} \times \begin{bmatrix} 6.6 & 5.6 & 5.6 & 0 & 0 & 0 \\ 5.6 & 6.6 & 5.6 & 0 & 0 & 0 \\ 5.6 & 5.6 & 6.6 & 0 & 0 & 0 \\ 0 & 0 & 0 & 10.0 & 6.1 & 6.1 \\ 0 & 0 & 0 & 6.1 & 10.0 & 6.1 \\ 0 & 0 & 0 & 6.1 & 6.1 & 10.0 \end{bmatrix} \tag{B.10}$$

Transforming these using the d-q transformation matrices, (3.1) and (3.2) (the leakage inductance matrix is unchanged as it is diagonal):

$$M_{dq0_s} = 10^{-3} \times \begin{bmatrix} 307 & 0 & 0 & 0 & 0 & 0 \\ 0 & 307 & 0 & 0 & 0 & 0 \\ 0 & 0 & 17.8 & 0 & 0 & 0 \\ 0 & 0 & 0 & 314 & 0 & 0 \\ 0 & 0 & 0 & 0 & 314 & 0 \\ 0 & 0 & 0 & 0 & 0 & 22.2 \end{bmatrix} \quad M_{dq0_s}^{hl} = 10^{-3} \times \begin{bmatrix} 1.04 & 0 & 0 & 0 & 0 & 0 \\ 0 & 1.04 & 0 & 0 & 0 & 0 \\ 0 & 0 & 17.8 & 0 & 0 & 0 \\ 0 & 0 & 0 & 3.88 & 0 & 0 \\ 0 & 0 & 0 & 0 & 3.88 & 0 \\ 0 & 0 & 0 & 0 & 0 & 22.2 \end{bmatrix} \tag{B.11}$$

Stator winding arrangement for parallel coil groups

With reference to the coil pitch table in section B.2.2:

Thus for phase a of the 8 pole winding the connections are as follows:

A: $(a_{11}, \bar{a}_{11})$, $(a_{12}, \bar{a}_{12})$, $(a_{21}, \bar{a}_{21})$, $(a_{22}, \bar{a}_{22})$

B: $(a_{31}, \bar{a}_{31})$, $(a_{32}, \bar{a}_{32})$, $(a_{41}, \bar{a}_{41})$, $(a_{42}, \bar{a}_{42})$

C: $(a_{51}, \bar{a}_{51})$, $(a_{52}, \bar{a}_{52})$, $(a_{61}, \bar{a}_{61})$, $(a_{62}, \bar{a}_{62})$

D: $(a_{71}, \bar{a}_{71})$, $(a_{72}, \bar{a}_{72})$, $(a_{81}, \bar{a}_{81})$, $(a_{82}, \bar{a}_{82})$

where A,B,C,D are the 4 sets of coil groups to be connected in parallel.

Phase A for the control 4 pole winding goes as follows:

A: $(A_{11}, \bar{A}_{11})$, $(A_{12}, \bar{A}_{12})$, $(A_{13}, \bar{A}_{13})$, $(A_{14}, \bar{A}_{14})$

B: $(A_{21}, \bar{A}_{21})$, $(A_{22}, \bar{A}_{22})$, $(A_{23}, \bar{A}_{23})$, $(A_{24}, \bar{A}_{24})$,

C: $(A_{31}, \bar{A}_{31})$, $(A_{32}, \bar{A}_{32})$, $(A_{33}, \bar{A}_{33})$, $(A_{34}, \bar{A}_{34})$

D:$(A_{41}, \bar{A}_{41})$, $(A_{42}, \bar{A}_{42})$, $(A_{43}, \bar{A}_{43})$, $(A_{44}, \bar{A}_{44})$

where A,B,C,D are the 4 sets of coil groups to be connected in parallel.

B.3 Rotor 1: Nested-loop Rotor Design Details

The state order used for rotor 1 is: 6 inner rotor loops, 6 middle rotor loops, 6 outer rotor loops. This order is preserved when transformed to dq axes.

B.3.1 Rotor-rotor inductance terms

Figure B.3 shows the arrangement of the rotor bars in the prototype nested-loop rotor. This arrangement leads to a rotor-rotor mutual inductance matrix given by (B.12), calculated using the method described in section 2.7.1:

$$M_{rr} = 10^{-8}\times$$

$$\begin{bmatrix}
465 & -14 & -14 & -14 & -14 & -14 & 468 & -43 & -43 & -43 & -43 & -43 & 439 & -71 & -71 & -71 & -71 & -71 \\
-14 & 465 & -14 & -14 & -14 & -14 & -43 & 468 & -43 & -43 & -43 & -43 & -71 & 439 & -71 & -71 & -71 & -71 \\
-14 & -14 & 465 & -14 & -14 & -14 & -43 & -43 & 468 & -43 & -43 & -43 & -71 & -71 & 439 & -71 & -71 & -71 \\
-14 & -14 & -14 & 465 & -14 & -14 & -43 & -43 & -43 & 468 & -43 & -43 & -71 & -71 & -71 & 439 & -71 & -71 \\
-14 & -14 & -14 & -14 & 465 & -14 & -43 & -43 & -43 & -43 & 468 & -43 & -71 & -71 & -71 & -71 & 439 & -71 \\
-14 & -14 & -14 & -14 & -14 & 465 & -43 & -43 & -43 & -43 & -43 & 468 & -71 & -71 & -71 & -71 & -71 & 439 \\
468 & -43 & -43 & -43 & -43 & -43 & 1372 & -128 & -128 & -128 & -128 & -128 & 1318 & -213 & -213 & -213 & -213 & -213 \\
-43 & 468 & -43 & -43 & -43 & -43 & -128 & 1372 & -128 & -128 & -128 & -128 & -213 & 1318 & -213 & -213 & -213 & -213 \\
-43 & -43 & 468 & -43 & -43 & -43 & -128 & -128 & 1372 & -128 & -128 & -128 & -213 & -213 & 1318 & -213 & -213 & -213 \\
-43 & -43 & -43 & 468 & -43 & -43 & -128 & -128 & -128 & 1372 & -128 & -128 & -213 & -213 & -213 & 1318 & -213 & -213 \\
-43 & -43 & -43 & -43 & 468 & -43 & -128 & -128 & -128 & -128 & 1372 & -128 & -213 & -213 & -213 & -213 & 1318 & -213 \\
-43 & -43 & -43 & -43 & -43 & 468 & -128 & -128 & -128 & -128 & -128 & 1372 & -213 & -213 & -213 & -213 & -213 & 1318 \\
439 & -71 & -71 & -71 & -71 & -71 & 1318 & -213 & -213 & -213 & -213 & -213 & 2165 & -354 & -354 & -354 & -354 & -354 \\
-71 & 439 & -71 & -71 & -71 & -71 & -213 & 1318 & -213 & -213 & -213 & -213 & -354 & 2165 & -354 & -354 & -354 & -354 \\
-71 & -71 & 439 & -71 & -71 & -71 & -213 & -213 & 1318 & -213 & -213 & -213 & -354 & -354 & 2165 & -354 & -354 & -354 \\
-71 & -71 & -71 & 439 & -71 & -71 & -213 & -213 & -213 & 1318 & -213 & -213 & -354 & -354 & -354 & 2165 & -354 & -354 \\
-71 & -71 & -71 & -71 & 439 & -71 & -213 & -213 & -213 & -213 & 1318 & -213 & -354 & -354 & -354 & -354 & 2165 & -354 \\
-71 & -71 & -71 & -71 & -71 & 439 & -213 & -213 & -213 & -213 & -213 & 1318 & -354 & -354 & -354 & -354 & -354 & 2165
\end{bmatrix} \tag{B.12}$$

The leakage inductances as calculated using the methods described in appendix C.1 are 9.7753×10^{-7}, 1.0278×10^{-6}, and 1.0781×10^{-6} for the inner, middle and outer loops respectively. As

explained in appendix C.1 it has been assumed that the leakage inductances only affect the self-inductance terms, hence the full M_{rr} matrix has, additionally, the appropriate leakage terms added on the diagonal.

When converted to d-q axes and the observable/uncontrollable parts removed, as discussed in section 3.3, the rotor-rotor mutual inductance matrix becomes:

$$M_{rr_{dq}} = 10^{-8}\times\begin{bmatrix} 479 & 0 & 0 & 510 & 0 & 0 & 510 & 0 & 0\\ 0 & 479 & 0 & 0 & 510 & 0 & 0 & 510 & 0\\ 0 & 0 & 394 & 0 & 0 & 255 & 0 & 0 & 85\\ 510 & 0 & 0 & 1499 & 0 & 0 & 1531 & 0 & 0\\ 0 & 510 & 0 & 0 & 1499 & 0 & 0 & 1531 & 0\\ 0 & 0 & 255 & 0 & 0 & 734 & 0 & 0 & 255\\ 510 & 0 & 0 & 1531 & 0 & 0 & 2520 & 0 & 0\\ 0 & 510 & 0 & 0 & 1531 & 0 & 0 & 2520 & 0\\ 0 & 0 & 85 & 0 & 0 & 255 & 0 & 0 & 394 \end{bmatrix} \quad M^{l}_{rr_{dq}} = 10^{-8}\times\begin{bmatrix} 98 & 0 & 0 & 0 & 0 & 0 & 0 & 0 & 0\\ 0 & 98 & 0 & 0 & 0 & 0 & 0 & 0 & 0\\ 0 & 0 & 98 & 0 & 0 & 0 & 0 & 0 & 0\\ 0 & 0 & 0 & 103 & 0 & 0 & 0 & 0 & 0\\ 0 & 0 & 0 & 0 & 103 & 0 & 0 & 0 & 0\\ 0 & 0 & 0 & 0 & 0 & 103 & 0 & 0 & 0\\ 0 & 0 & 0 & 0 & 0 & 0 & 108 & 0 & 0\\ 0 & 0 & 0 & 0 & 0 & 0 & 0 & 108 & 0\\ 0 & 0 & 0 & 0 & 0 & 0 & 0 & 0 & 108 \end{bmatrix} \tag{B.13}$$

$$M^{h2}_{rr_{dq}} = 10^{-8}\times\begin{bmatrix} 84 & 0 & 0 & 242 & 0 & 0 & 371 & 0 & 0\\ 0 & 84 & 0 & 0 & 242 & 0 & 0 & 371 & 0\\ 0 & 0 & 0 & 0 & 0 & 0 & 0 & 0 & 0\\ 242 & 0 & 0 & 698 & 0 & 0 & 1069 & 0 & 0\\ 0 & 242 & 0 & 0 & 698 & 0 & 0 & 1069 & 0\\ 0 & 0 & 0 & 0 & 0 & 0 & 0 & 0 & 0\\ 371 & 0 & 0 & 1069 & 0 & 0 & 1638 & 0 & 0\\ 0 & 371 & 0 & 0 & 1069 & 0 & 0 & 1638 & 0\\ 0 & 0 & 0 & 0 & 0 & 0 & 0 & 0 & 0 \end{bmatrix} \quad M^{h4}_{rr_{dq}} = 10^{-8}\times\begin{bmatrix} 82 & 0 & 0 & 206 & 0 & 0 & 235 & 0 & 0\\ 0 & 82 & 0 & 0 & 206 & 0 & 0 & 235 & 0\\ 0 & 0 & 0 & 0 & 0 & 0 & 0 & 0 & 0\\ 206 & 0 & 0 & 523 & 0 & 0 & 594 & 0 & 0\\ 0 & 206 & 0 & 0 & 523 & 0 & 0 & 594 & 0\\ 0 & 0 & 0 & 0 & 0 & 0 & 0 & 0 & 0\\ 235 & 0 & 0 & 594 & 0 & 0 & 676 & 0 & 0\\ 0 & 235 & 0 & 0 & 594 & 0 & 0 & 676 & 0\\ 0 & 0 & 0 & 0 & 0 & 0 & 0 & 0 & 0 \end{bmatrix} \tag{B.14}$$

where $M_{rr_{dq}}$ is the full d-q rotor-rotor mutual inductance matrix excluding leakage effects, $M^{l}_{rr_{dq}}$ is the leakage inductance matrix, $M^{h2}_{rr_{dq}}$ and $M^{h4}_{rr_{dq}}$ are the 4 pole and 8 pole harmonic components (the first two non-zero components) of the rotor-rotor mutual inductance matrix.

This d-q model may be reduced in order, after removal of the zero-sequence terms, as described in section 3.4.2. The matrix used to reduce the order of the rotor states for this machine is:

$$T = \begin{bmatrix} 0 & 0.2108 & 0 & 0.5768 & 0 & 0.7892\\ -0.2108 & 0 & -0.5768 & 0 & -0.7892 & 0 \end{bmatrix} \tag{B.15}$$

Applying (B.15) to (B.13), the resulting rotor-rotor mutual inductance terms become:

$$M_{rr_{dq}} = 10^{-8}\times\begin{bmatrix} 3777 & 0\\ 0 & 3777 \end{bmatrix} \qquad M^{l}_{rr_{dq}} = 10^{-8}\times\begin{bmatrix} 106 & 0\\ 0 & 106 \end{bmatrix} \tag{B.16}$$

$$M^{h2}_{rr_{dq}} = 10^{-8}\times\begin{bmatrix} 2411 & 0\\ 0 & 2411 \end{bmatrix} \qquad M^{h4}_{rr_{dq}} = 10^{-8}\times\begin{bmatrix} 1268 & 0\\ 0 & 1268 \end{bmatrix} \tag{B.17}$$

where, $M_{rr_{dq}}$ is the reduced order d-q rotor-rotor mutual inductance matrix, $M^{l}_{rr_{dq}}$ is the reduced order leakage inductance matrix, $M^{h2}_{rr_{dq}}$ and $M^{h4}_{rr_{dq}}$ are the 4 pole and 8 pole harmonic components (the first two non-zero components) of the rotor-rotor mutual inductance matrix.

Subtracting equations (B.17) from $M_{rr_{dq}}$ gives the harmonic leakage (or differential leakage) inductance in the rotor, that is the additional series inductance that appears due to the production of unwanted space harmonics by the rotor:

$$M^{hl}_{rr_{dq}} = 10^{-8}\times\begin{bmatrix} 98 & 0\\ 0 & 98 \end{bmatrix} \tag{B.18}$$

B.3.2 Rotor-Stator inductance details

Figure B.4 shows the rotor-stator mutual inductance for a inner, middle, and outer loop between both 4 and 8 pole stator phases. The data is overlaid with the fundamental component in each case, calculated from the FFT.

Equation (B.19) shows the mutual inductance between stator and rotor for the reduced order dq model.

$$M_{dq_{sr}} = 10^{-6} \times \begin{bmatrix} 2408 & 1253 \\ -1253 & 2408 \\ 345 & 1954 \\ 1954 & -345 \end{bmatrix} \tag{B.19}$$

B.4 Rotor 2: New Double Layer Rotor Design Details

B.4.1 Rotor-rotor inductance terms

Figure B.5 shows the arrangement of the rotor bars in the prototype double-layer winding rotor. This arrangement leads to a rotor-rotor mutual inductance matrix given by (B.20), calculated using the method described in section 2.7.1:

$$M_{rr} = 10^{-6} \times \begin{bmatrix} 312 & -31 & -83 & -83 & -83 & -31 \\ -31 & 312 & -31 & -83 & -83 & -83 \\ -83 & -31 & 312 & -31 & -83 & -83 \\ -83 & -83 & -31 & 312 & -31 & -83 \\ -83 & -83 & -83 & -31 & 312 & -31 \\ -31 & -83 & -83 & -83 & -31 & 312 \end{bmatrix} \tag{B.20}$$

The leakage inductance for each rotor 'phase' as calculated using the methods described in appendix C.1 are 8.8×10^{-6}. As explained in appendix C.1 it has been assumed that the leakage inductances only affect the self-inductance terms, hence the full M_{rr} matrix has, additionally, the appropriate leakage terms added on the diagonal.

When converted to d-q axes, as described in section 3.3, rotor-rotor mutual inductance matrix

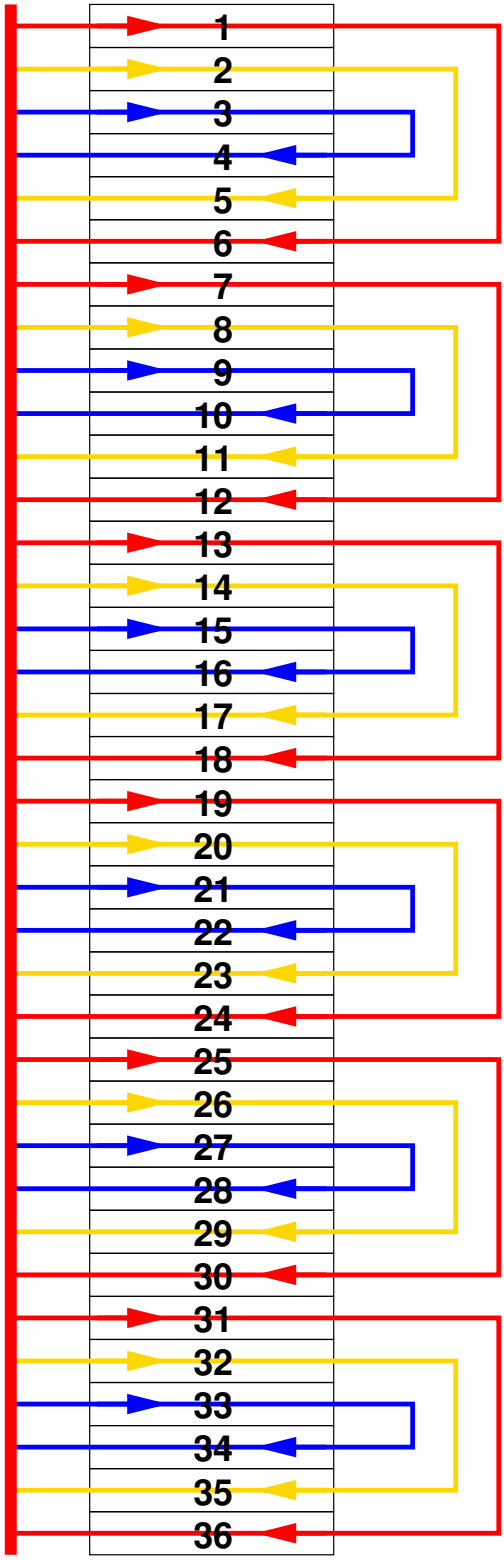

Figure B.3: Rotor 1: Prototype nested-loop design rotor

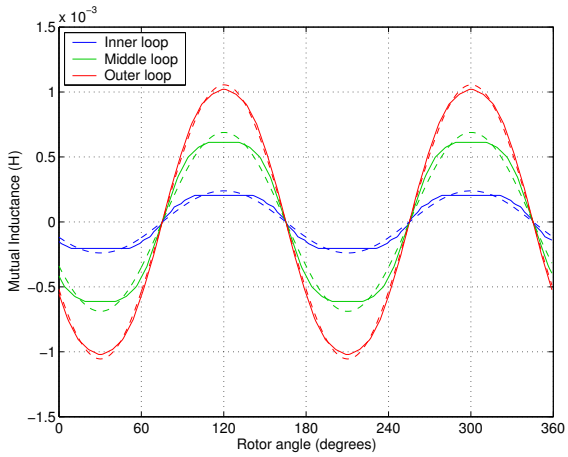

(a) Stator 1 - Rotor Mutual Inductance

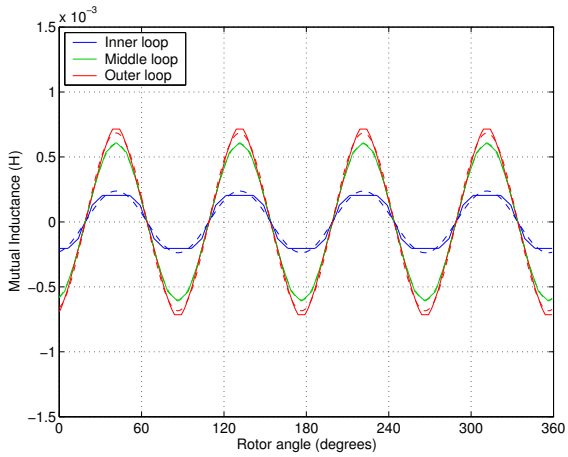

(b) Stator 2 - Rotor Mutual Inductance

Figure B.4: Stator-Rotor mutual inductance for Rotor 1, the prototype nested loop rotor for the individual loops of a particular nest. The dotted lines show the fundamental component of the fields.

becomes:

$$M_{rr_{dq}} = 10^{-6} \times \begin{bmatrix} 342 & 0 & 0 \\ 0 & 342 & 0 \\ 0 & 0 & 0 \end{bmatrix} \qquad M^{l}_{rr_{dq}} = 10^{-6} \times \begin{bmatrix} 9 & 0 & 0 \\ 0 & 9 & 0 \\ 0 & 0 & 9 \end{bmatrix} \tag{B.21}$$

$$M^{h2}_{rr_{dq}} = 10^{-6} \times \begin{bmatrix} 293 & 0 & 0 \\ 0 & 293 & 0 \\ 0 & 0 & 0 \end{bmatrix} \qquad M^{h4}_{rr_{dq}} = 10^{-6} \times \begin{bmatrix} 44 & 0 & 0 \\ 0 & 44 & 0 \\ 0 & 0 & 0 \end{bmatrix} \tag{B.22}$$

where $M_{rr_{dq}}$ is the full d-q rotor-rotor mutual inductance matrix excluding leakage effects, $M^{l}_{rr_{dq}}$ is the leakage inductance matrix, $M^{h2}_{rr_{dq}}$ and $M^{h4}_{rr_{dq}}$ are the 4 pole and 8 pole harmonic components (the first two non-zero components) of the rotor-rotor mutual inductance matrix.

Subtracting equations (B.22) from $M_{rr_{dq}}$ gives the harmonic leakage (or differential leakage) inductance in the rotor, that is the additional series inductance that appears due to the production of unwanted space harmonics by the rotor:

$$M^{hl}_{rr_{dq}} = 10^{-6} \times \begin{bmatrix} 5 & 0 & 0 \\ 0 & 5 & 0 \\ 0 & 0 & 0 \end{bmatrix} \tag{B.23}$$

B.4.2 Rotor-Stator inductance details

Figure B.6 shows the rotor-stator mutual inductance between a rotor phase and a 4 and 8 pole stator phase. The data is overlaid with the fundamental component in each case, calculated from the FFT.

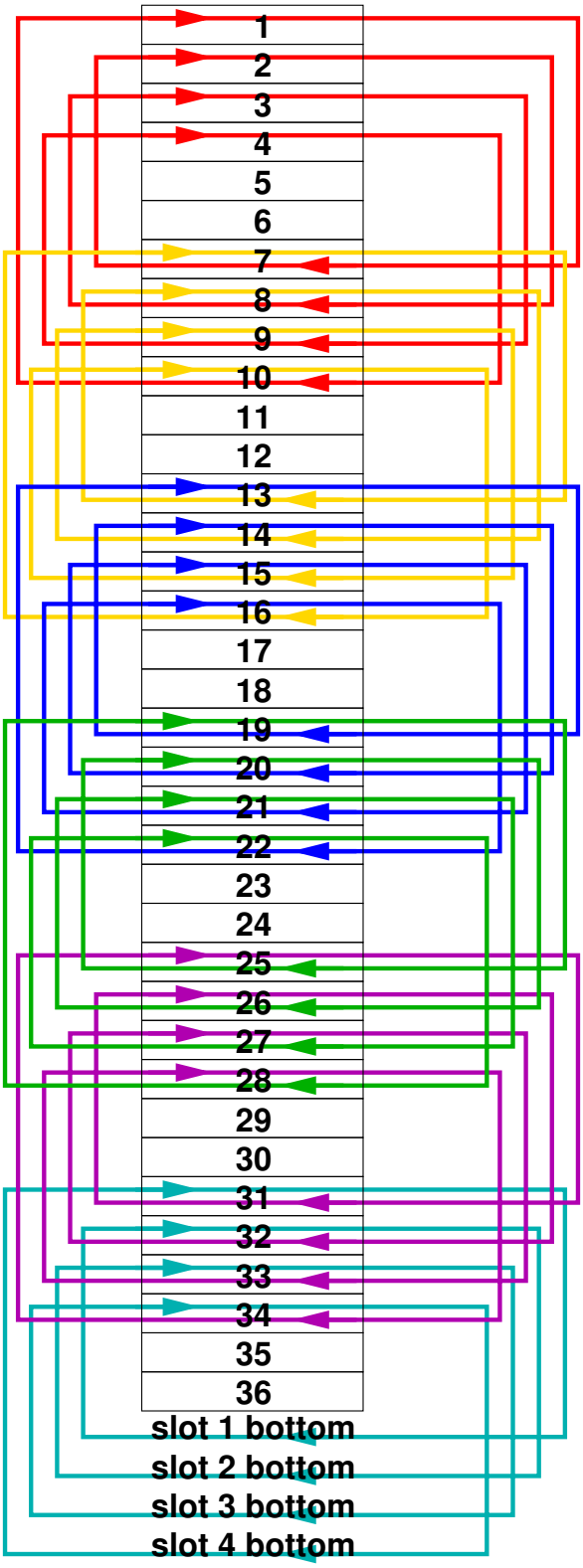

Figure B.5: Prototype rotor 2: double-layer design rotor

Equation (B.24) shows the mutual inductance between stator and rotor for the dq model.

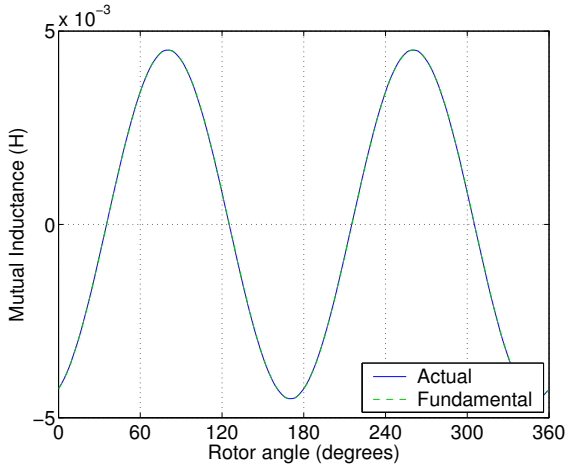

(a) Stator 1 - Rotor Mutual Inductance

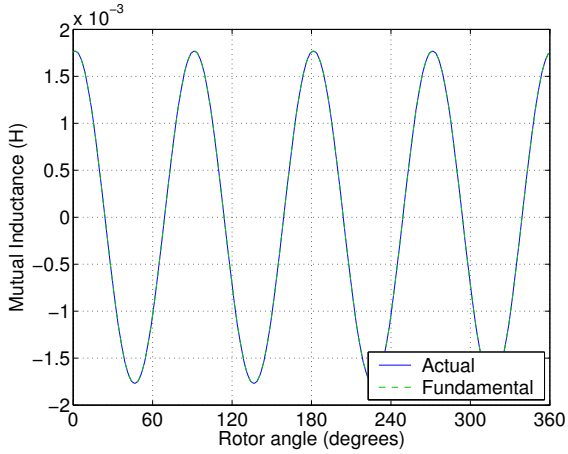

(b) Stator 2 - Rotor Mutual Inductance

Figure B.6: Stator-Rotor mutual inductance for Rotor 2, the prototype double-layer rotor. The dotted lines show the fundamental component of the fields.

$$M_{dq_{sr}} = 10^{-6} \times \begin{bmatrix} -9119 & -2875 & 0 \\ 2875 & -9119 & 0 \\ 0 & 0 & 0 \\ 3690 & 651 & 0 \\ 651 & -3690 & 0 \\ 0 & 0 & 0 \end{bmatrix} \tag{B.24}$$

B.5 Rotor 3: Isolated loop rotor design

The state order used for rotor 3 is: 6 loops spaced by 60°, then another 6 loops again spaced by 60° and offset from the previous set by 20°, then a third set of 6 loops again evenly spaced by 60° and offset from the previous set by 20°. The 3 sets are colour-coded on the winding diagram, figure B.7.

B.5.1 Rotor inductance terms

Figure B.7 shows the arrangement of the rotor bars in the prototype isolated loop rotor. This arrangement leads to a rotor-rotor mutual inductance matrix given by (B.25), calculated using the method

described in section 2.7.1:

$$M_{rr} = 10^{-6}\times \begin{bmatrix}
29 & -2 & -7 & -7 & -7 & -2 & 19 & -7 & -7 & -7 & -7 & 8 & 8 & -7 & -7 & -7 & -7 & 19 \\
-2 & 29 & -2 & -7 & -7 & -7 & 8 & 19 & -7 & -7 & -7 & -7 & 19 & 8 & -7 & -7 & -7 & -7 \\
-7 & -2 & 29 & -2 & -7 & -7 & -7 & 8 & 19 & -7 & -7 & -7 & -7 & 19 & 8 & -7 & -7 & -7 \\
-7 & -7 & -2 & 29 & -2 & -7 & -7 & -7 & 8 & 19 & -7 & -7 & -7 & -7 & 19 & 8 & -7 & -7 \\
-7 & -7 & -7 & -2 & 29 & -2 & -7 & -7 & -7 & 8 & 19 & -7 & -7 & -7 & -7 & 19 & 8 & -7 \\
-2 & -7 & -7 & -7 & -2 & 29 & -7 & -7 & -7 & -7 & 8 & 19 & -7 & -7 & -7 & -7 & 19 & 8 \\
19 & 8 & -7 & -7 & -7 & -7 & 29 & -2 & -7 & -7 & -7 & -2 & 19 & -7 & -7 & -7 & -7 & 8 \\
-7 & 19 & 8 & -7 & -7 & -7 & -2 & 29 & -2 & -7 & -7 & -7 & 8 & 19 & -7 & -7 & -7 & -7 \\
-7 & -7 & 19 & 8 & -7 & -7 & -7 & -2 & 29 & -2 & -7 & -7 & -7 & 8 & 19 & -7 & -7 & -7 \\
-7 & -7 & -7 & 19 & 8 & -7 & -7 & -7 & -2 & 29 & -2 & -7 & -7 & -7 & 8 & 19 & -7 & -7 \\
-7 & -7 & -7 & -7 & 19 & 8 & -7 & -7 & -7 & -2 & 29 & -2 & -7 & -7 & -7 & 8 & 19 & -7 \\
8 & -7 & -7 & -7 & -7 & 19 & -2 & -7 & -7 & -7 & -2 & 29 & -7 & -7 & -7 & -7 & 8 & 19 \\
8 & 19 & -7 & -7 & -7 & -7 & 19 & 8 & -7 & -7 & -7 & -7 & 29 & -2 & -7 & -7 & -7 & -2 \\
-7 & 8 & 19 & -7 & -7 & -7 & -7 & 19 & 8 & -7 & -7 & -7 & -2 & 29 & -2 & -7 & -7 & -7 \\
-7 & -7 & 8 & 19 & -7 & -7 & -7 & -7 & 19 & 8 & -7 & -7 & -7 & -2 & 29 & -2 & -7 & -7 \\
-7 & -7 & -7 & 8 & 19 & -7 & -7 & -7 & -7 & 19 & 8 & -7 & -7 & -7 & -2 & 29 & -2 & -7 \\
-7 & -7 & -7 & -7 & 8 & 19 & -7 & -7 & -7 & -7 & 19 & 8 & -7 & -7 & -7 & -2 & 29 & -2 \\
19 & -7 & -7 & -7 & -7 & 8 & 8 & -7 & -7 & -7 & -7 & 19 & -2 & -7 & -7 & -7 & -2 & 29
\end{bmatrix} \tag{B.25}$$

The rotor loop leakage inductance as calculated using the methods described in appendix C.1 is 3.3055×10^{-6}H. As explained in appendix C.1 it has been assumed that the leakage inductances only affect the self-inductance terms, hence the full M_{rr} matrix has, additionally, the appropriate leakage terms added on the diagonal.

Transformation to d-q axes is achieved by the method described in section 3.3. This rotor design can be considered as three sets of 6 evenly spaced coils, and thus the method of section 3.3. The resulting mutual inductance matrix (with zero-sequence state removed for brevity) is:

$$M_{dq} = 10^{-6} \times \begin{bmatrix}
315\times10^3 & 0 & 0 & 0 & -2784 & 122 & -2211 & -1696 & -603 & -2720 \\
0 & 315\times10^3 & 0 & 0 & -122 & -2784 & 1696 & -2211 & 2720 & -603 \\
0 & 0 & 328\times10^3 & 0 & 617 & 736 & 832 & -480 & -328 & -902 \\
0 & 0 & 0 & 328\times10^3 & 736 & -617 & -480 & -832 & -902 & 328 \\
-2784 & -122 & 617 & 736 & 34 & 0 & 18 & 13 & 3 & 22 \\
122 & -2784 & 736 & -617 & 0 & 34 & -13 & 18 & -22 & 3 \\
-2211 & 1696 & 832 & -480 & 18 & -13 & 34 & 0 & 18 & 13 \\
-1696 & -2211 & -480 & -832 & 13 & 18 & 0 & 34 & -13 & 18 \\
-603 & 2720 & -328 & -902 & 3 & -22 & 18 & -13 & 34 & 0 \\
-2720 & -603 & -902 & 328 & 22 & 3 & 13 & 18 & 0 & 34
\end{bmatrix} \tag{B.26}$$

where the leakage inductance is included, and is unaffected by the dq transformation.

The rotor-rotor portion of the mutual inductance matrix may be diagonalised by an appropriate state transformation, the eigenvectors of the rotor-rotor mutual matrix. Applying this transformation

to the whole mutual inductance matrix (using the identity matrix for the stator potion) gives:

$$M_{dq} = 10^{-6} \times \begin{bmatrix} 315\times10^3 & 0 & 0 & 0 & 211 & 4822 & 0 & 0 & 0 & 0 \\ 0 & 315\times10^3 & 0 & 0 & -4822 & 211 & 0 & 0 & 0 & 0 \\ 0 & 0 & 328\times10^3 & 0 & 0 & 0 & -1212 & -1140 & 0 & 0 \\ 0 & 0 & 0 & 328\times10^3 & 0 & 0 & -1140 & 1212 & 0 & 0 \\ 211 & -4822 & 0 & 0 & 79 & 0 & 0 & 0 & 0 & 0 \\ 4822 & 211 & 0 & 0 & 0 & 79 & 0 & 0 & 0 & 0 \\ 0 & 0 & -1212 & -1140 & 0 & 0 & 14 & 0 & 0 & 0 \\ 0 & 0 & -1140 & 1212 & 0 & 0 & 0 & 14 & 0 & 0 \\ 0 & 0 & 0 & 0 & 0 & 0 & 0 & 0 & 9 & 0 \\ 0 & 0 & 0 & 0 & 0 & 0 & 0 & 0 & 0 & 9 \end{bmatrix} \tag{B.27}$$

As can be seem from (B.27) this rotor decouples the different stator supplies. There is no longer any cross-coupling achieved by the rotor, as is expected.

B.6 Rotor 4: Isolated loop design rotor with one set of loops removed

This rotor is identical rotor 3 but with one set of 6 loops removed. Figure B.7 shows rotor 3. Rotor 4 is the same, but with the loops marked in blue removed.

B.6.1 Rotor inductance terms

As rotor is a subset of rotor 3 so are the mutual inductance terms. The rotor-rotor inductance is given by the upper-left 12×12 partition of equation (B.25). The leakage inductance per coil is the same, at 3.3055×10^{-6}H.

The d-q transformed machine mutual inductance is the upper-left 8×8 partition of (B.26). However when diagonalizing the d-q transformed model the results differ significantly from those obtained for rotor 3:

$$M_{dq} = 10^{-6} \times \begin{bmatrix} 315\times10^3 & 0 & 0 & 0 & 3939 & 55 & -117 & 2 \\ 0 & 315\times10^3 & 0 & 0 & 55 & -3939 & -2 & -117 \\ 0 & 0 & 328\times10^3 & 0 & -706 & -103 & -1143 & 167 \\ 0 & 0 & 0 & 328\times10^3 & 103 & -706 & 167 & 1143 \\ 3939 & 55 & -706 & 103 & 57 & 0 & 0 & 0 \\ 55 & -3939 & -103 & -706 & 0 & 57 & 0 & 0 \\ -117 & -2 & -1143 & 167 & 0 & 0 & 12 & 0 \\ 2 & -117 & 167 & 1143 & 0 & 0 & 0 & 12 \end{bmatrix} \tag{B.28}$$

Thus equation (B.28) demonstrates that unlike rotor 3 where the 4 and 8 pole stator currents were decoupled from each other, there is cross-coupling in the case of rotor 4.

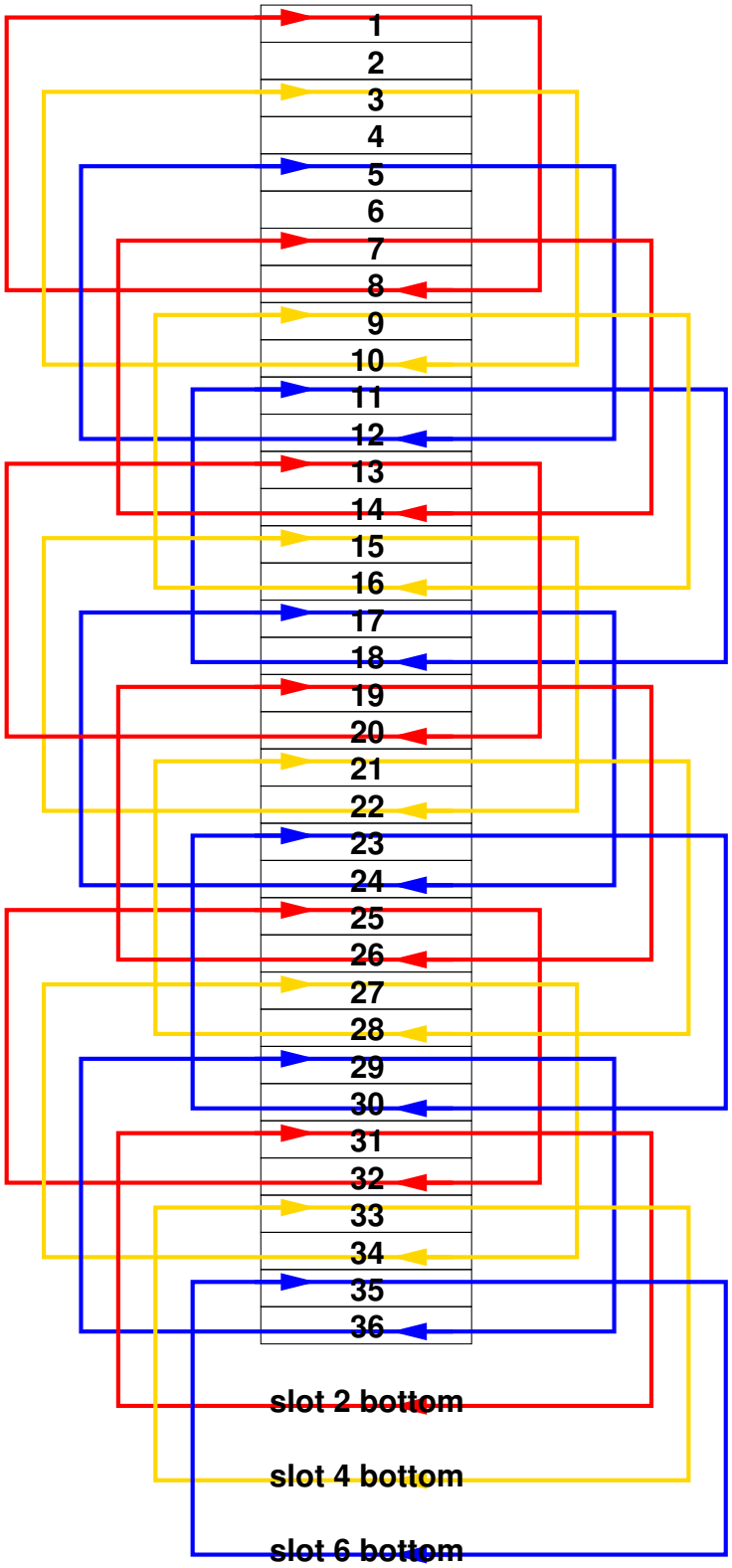

Figure B.7: Prototype rotor 3: Isolated loop rotor design

B.7 Rotor 5: 6 bar cage rotor design

B.7.1 Rotor-rotor inductance terms

A cage rotor may be analysed by mesh loop analysis. As such the for an n bar cage there will be n such loops to fully describe the cage (assuming that no flux is linked though the end ring). Figure B.8 shows an example cage, with two loops illustrated, with currents I_1 and I_2 flowing respectively. Having defined the rotor circuits as such the bar current may be expressed in terms of the loop currents as illustrated in figure B.8.

For the purposes of mutual inductance calculation an n bar cage is therefore identical to n isolated loops replacing the virtual loops forms from the analysis. Therefore the mutual inductance calculation is the same as for the other rotor designs. However the resistance and leakage inductance matrices will be of the following form:

$$R = \begin{bmatrix} 2R_{\text{bar}} + 2R_{\text{end}} & -R_{\text{bar}} & 0 & \cdots & 0 & -R_{\text{bar}} \\ -R_{\text{bar}} & 2R_{\text{bar}} + 2R_{\text{end}} & -R_{\text{bar}} & 0 & \cdots & 0 \\ 0 & \ddots & \ddots & \ddots & \ddots & \vdots \\ \vdots & \ddots & \ddots & \ddots & \ddots & 0 \\ 0 & \cdots & 0 & -R_{\text{bar}} & 2R_{\text{bar}} + 2R_{\text{end}} & -R_{\text{bar}} \\ -R_{\text{bar}} & 0 & \cdots & 0 & -R_{\text{bar}} & 2R_{\text{bar}} + 2R_{\text{end}} \end{bmatrix}$$

where R_{bar} and R_{end} are the resistance (or inductance) due to the bar and end ring respectively.

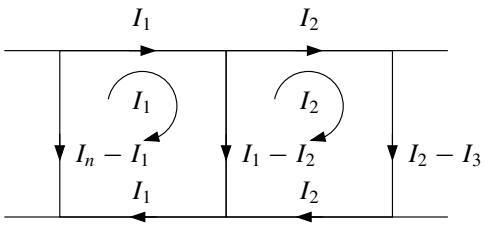

Figure B.8: Mesh loop analysis of cage rotors

The rotor-rotor mutual inductance may therefore be calculated by the method described in section 2.7.1:

$$M_{rr} = 10^{-7} \times \begin{bmatrix} 271 & -51 & -56 & -56 & -56 & -51 \\ -51 & 271 & -51 & -56 & -56 & -56 \\ -56 & -51 & 271 & -51 & -56 & -56 \\ -56 & -56 & -51 & 271 & -51 & -56 \\ -56 & -56 & -56 & -51 & 271 & -51 \\ -51 & -56 & -56 & -56 & -51 & 271 \end{bmatrix} \tag{B.29}$$

The leakage inductance for each bar and end winding was calculated using the methods described in appendix C.1. The bar leakage was found to be $2.40 \times 10^{-7} H$ and the end ring leakage 1.02×10^{-7}H. Therefore the leakage inductance matrix is:

$$M_{rr}^{l} = 10^{-7} \times \begin{bmatrix} 7 & -2 & 0 & 0 & 0 & -2 \\ -2 & 7 & -2 & 0 & 0 & 0 \\ 0 & -2 & 7 & -2 & 0 & 0 \\ 0 & 0 & -2 & 7 & -2 & 0 \\ 0 & 0 & 0 & -2 & 7 & -2 \\ -2 & 0 & 0 & 0 & -2 & 7 \end{bmatrix} \tag{B.30}$$

When transformed to d-q axes using the method described in section 3.3, the rotor-rotor mutual inductance matrix becomes:

$$M_{rr_{dq}}^{l} = 10^{-7} \times \begin{bmatrix} 9 & 0 & 0 \\ 0 & 9 & 0 \\ 0 & 0 & 3 \end{bmatrix} \qquad M_{rr_{dq}} 10^{-7} \times \begin{bmatrix} 322 & 0 & 0 \\ 0 & 322 & 0 \\ 0 & 0 & 0 \end{bmatrix} \tag{B.31}$$

$$M_{rr_{dq}}^{h2} 10^{-7} \times \begin{bmatrix} 230 & 0 & 0 \\ 0 & 230 & 0 \\ 0 & 0 & 0 \end{bmatrix} \qquad M_{rr_{dq}}^{h4} 10^{-7} \times \begin{bmatrix} 57 & 0 & 0 \\ 0 & 57 & 0 \\ 0 & 0 & 0 \end{bmatrix} \tag{B.32}$$

where $M_{rr_{dq}}$ is the full d-q rotor-rotor mutual inductance matrix excluding leakage effects, $M_{rr_{dq}}^{l}$ is the leakage inductance matrix, $M_{rr_{dq}}^{h2}$ and $M_{rr_{dq}}^{h4}$ are the 4 pole and 8 pole harmonic components (the first two non-zero components) of the rotor-rotor mutual inductance matrix.

Subtracting equations (B.32) from $M_{rr_{dq}}$ gives the harmonic leakage (or differential leakage) inductance in the rotor, that is the additional series inductance that appears due to the production of unwanted space harmonics by the rotor:

$$M_{rr_{dq}}^{hl} = 10^{-7} \times \begin{bmatrix} 35 & 0 & 0 \\ 0 & 35 & 0 \\ 0 & 0 & 0 \end{bmatrix} \tag{B.33}$$

B.7.2 Rotor-Stator inductance details

Figure B.9 shows the rotor-stator mutual inductance between a rotor phase and a 4 and 8 pole stator phase. The data is overlaid with the fundamental component in each case, calculated from the FFT. Equation (B.24) shows the mutual inductance between stator and rotor for the dq model.

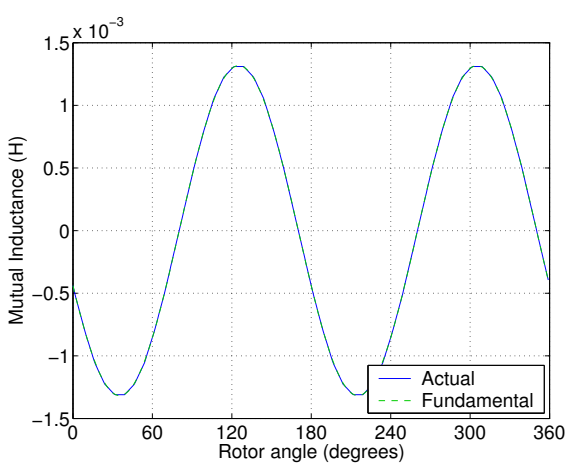

(a) Stator 1 - Rotor Mutual Inductance

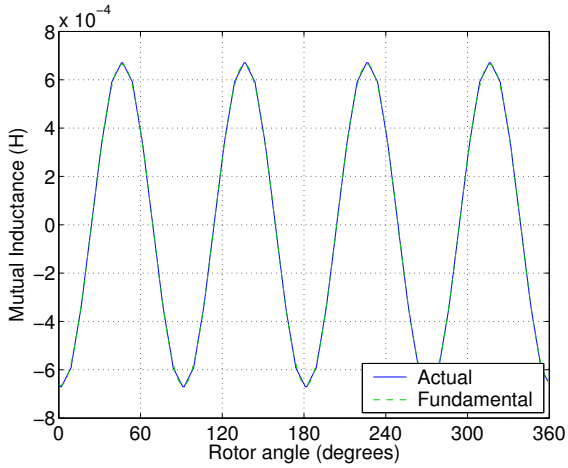

(b) Stator 2 - Rotor Mutual Inductance

Figure B.9: Stator-Rotor mutual inductance for Rotor 5, the prototype double-layer rotor. The dotted lines show the fundamental component of the fields.

$$M_{dq_{sr}} = 10^{-6} \times 10^{-6} \times \begin{bmatrix} -839 & 2660 & 0 \\ -2660 & -839 & 0 \\ 0 & 0 & 0 \\ -1378 & -243 & 0 \\ -243 & 1378 & 0 \\ 0 & 0 & 0 \end{bmatrix} \tag{B.34}$$

B.8 Rotor 6: Wound Rotor Design Details

B.8.1 Rotor-rotor inductance terms

Figures B.1 and B.2 show the winding diagram for the stator winding of the prototype machine. Rotor 6 has the same windings as the stator winding connected together in a star short-circuit including a neutral connection.

The connection is achieved using the following combination matrix:

$$T_c = \begin{bmatrix} 1 & 0 & 0 & 0 & 0 & -1 \\ 0 & 1 & 0 & 0 & -1 & 0 \\ 0 & 0 & 1 & -1 & 0 & 0 \end{bmatrix} \tag{B.35}$$

Therefore the rotor-rotor mutual inductance matrix given by (B.36), calculated using the method

described in section 2.7.1:

$$M_{rr} = 110^{-7} \times \begin{bmatrix} 400 & -181 & -181 \\ -181 & 400 & -181 \\ -181 & -181 & 400 \end{bmatrix} \tag{B.36}$$

The leakage inductance is calculated in exactly the same was as for the stator using the methods described in appendix C.1. The leakage inductance matrix is given by:

$$M^{l}_{rr} = 10^{-7} \times \begin{bmatrix} 10 & 0 & 0 \\ 0 & 10 & 0 \\ 0 & 0 & 10 \end{bmatrix} \tag{B.37}$$

When converted to d-q axes, as described in section 3.3, rotor-rotor mutual inductance matrix becomes:

$$M_{rr_{dq}} = 10^{-7} \times \begin{bmatrix} 10 & 0 & 0 \\ 0 & 10 & 0 \\ 0 & 0 & 10 \end{bmatrix} \qquad M^{l}_{rr_{dq}} = 10^{-7} \times \begin{bmatrix} 581 & 0 & 0 \\ 0 & 581 & 0 \\ 0 & 0 & 37 \end{bmatrix} \tag{B.38}$$

$$M^{h2}_{rr_{dq}} = 10^{-7} \times \begin{bmatrix} 286 & 0 & 0 \\ 0 & 286 & 0 \\ 0 & 0 & 0 \end{bmatrix} \qquad M^{h4}_{rr_{dq}} = 10^{-7} \times \begin{bmatrix} 290 & 0 & 0 \\ 0 & 290 & 0 \\ 0 & 0 & 0 \end{bmatrix} \tag{B.39}$$

where $M_{rr_{dq}}$ is the full d-q rotor-rotor mutual inductance matrix excluding leakage effects, $M^{l}_{rr_{dq}}$ is the leakage inductance matrix, $M^{h2}_{rr_{dq}}$ and $M^{h4}_{rr_{dq}}$ are the 4 pole and 8 pole harmonic components (the first two non-zero components) of the rotor-rotor mutual inductance matrix.

Subtracting equations (B.39) from $M_{rr_{dq}}$ gives the harmonic leakage (or differential leakage) inductance in the rotor, that is the additional series inductance that appears due to the production of unwanted space harmonics by the rotor:

$$M^{hl}_{rr_{dq}} = 10^{-7} \times \begin{bmatrix} 5 & 0 & 0 \\ 0 & 5 & 0 \\ 0 & 0 & 37 \end{bmatrix} \tag{B.40}$$

B.8.2 Rotor-Stator inductance details

Figure B.10 shows the rotor-stator mutual inductance between a rotor phase and a 4 and 8 pole stator phase. The data is overlaid with the fundamental component in each case, calculated from the FFT. Equation (B.41) shows the mutual inductance between stator and rotor for the dq model.

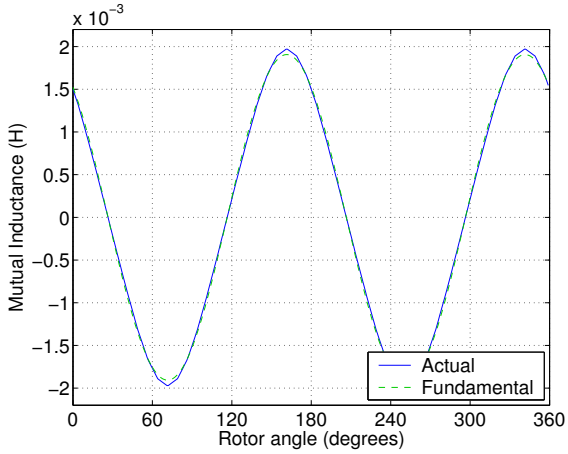

(a) Stator 1 - Rotor Mutual Inductance

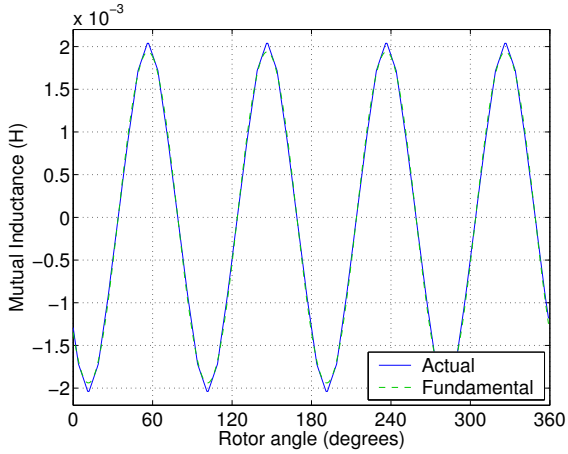

(b) Stator 2 - Rotor Mutual Inductance

Figure B.10: Stator-Rotor mutual inductance for Rotor 6, the prototype double-layer rotor. The dotted lines show the fundamental component of the fields.

$$M_{dq_{sr}} = 10^{-6} \times \begin{bmatrix} 2341 & -1639 & 0 \\ -1639 & -2341 & 0 \\ 0 & 0 & 0 \\ -1866 & 2224 & 0 \\ -2224 & -1866 & 0 \\ 0 & 0 & 0 \end{bmatrix} \tag{B.41}$$

B.9 Rotor 7: Standard Squirrel Cage Rotor Details

B.9.1 Rotor-rotor inductance terms

The rotor is a standard 40 bar squirrel cage rotor with Boucherot slots to give a higher rotor resistance at high slips though the skin effect.

The calculation procedure is identical to that for Rotor 5 described in section B.7. Using this

method the rotor-rotor mutual inductance matrix is:

$$M_{rr} = 10^{-8} \times \begin{bmatrix} 471 & 14 & -13 & -13 & \cdots & -13 & 14 \\ 14 & 471 & 14 & -13 & \cdots & -13 & -13 \\ -13 & 14 & 471 & 14-13 & \cdots & -13 & \\ \ddots & \ddots & \ddots & \ddots & \ddots & \ddots & \vdots \\ -13 & \cdots & -13 & 14 & 471 & 14 & -13 \\ -13 & -13 & \cdots & -13 & 14 & 471 & 14 \\ & & & & & & \\ 14 & -13 & \cdots & -13 & -13 & 14 & 471 \end{bmatrix} \tag{B.42}$$

The rotor bar and end ring leakage inductance is calculated using the methods described in appendix C.1. The bar leakage is 1.25×10^{-6}H and the end ring leakage is 1.34×10^{-6}H. These inductance parameters are added to the rotor-rotor mutual inductance as described in section B.7

Transformation to d-q axes is achieved by the method described in section 3.3. However as the cage rotor has 40 bars it cannot directly be considered to be part of the class of rotor designs. Therefore a different d-q transformation was used:

$$C_{dq} = \begin{bmatrix} C_{dq_{p_1}} & 0 \\ 0 & C_{dq_{p_2}} \end{bmatrix} \tag{B.43}$$

where:

$$C_{dq_p} = \sqrt{\frac{2}{40}} \begin{bmatrix} \cos(0) & \cos(\frac{2p\pi}{40}) & \cos(\frac{4p\pi}{40}) & \cos(\frac{6p\pi}{40}) & \cdots & \cos(\frac{78p\pi}{40}) \\ \sin(0) & \sin(\frac{2p\pi}{40}) & \sin(\frac{4p\pi}{40}) & \sin(\frac{6p\pi}{40}) & \cdots & \sin(\frac{78p\pi}{40}) \\ \frac{1}{\sqrt{2}} & \frac{1}{\sqrt{2}} & \frac{1}{\sqrt{2}} & \frac{1}{\sqrt{2}} & \cdots & \frac{1}{\sqrt{2}} \end{bmatrix} \tag{B.44}$$

and $p_1 = 2,\ p_2 = 4$ for the prototype stator winding.

It can be shown that this non-square transformation matrix truncates only unobservable/uncontrollable states.

The resulting mutual inductance matrix (with zero-sequence state removed for brevity) is:

$$M_{dq} = 10^{-6} \times \begin{bmatrix} 363645 & 0 & 0 & 0 & -574 & 1260 & 0 & 0 \\ 0 & 363645 & 0 & 0 & -1260 & -574 & 0 & 0 \\ 0 & 0 & 377345 & 0 & 0 & 0 & -1374 & -96 \\ 0 & 0 & 0 & 377345 & 0 & 0 & 96 & -1374 \\ -574 & -1260 & 0 & 0 & 6 & 0 & 0 & 0 \\ 1260 & -574 & 0 & 0 & 0 & 6 & 0 & 0 \\ 0 & 0 & -1374 & 96 & 0 & 0 & 6 & 0 \\ 0 & 0 & -96 & -1374 & 0 & 0 & 0 & 6 \end{bmatrix} \tag{B.45}$$

where the leakage inductance is included. The other rotor-rotor inductance parameters in d-q axes are given by:

$$M_{rr_{dq}} = 10^{-7} \times \begin{bmatrix} 54 & 0 & 0 & 0 \\ 0 & 54 & 0 & 0 \\ 0 & 0 & 53 & 0 \\ 0 & 0 & 0 & 53 \end{bmatrix} \qquad M^{l}_{rr_{dq}} = 10^{-7} \times \begin{bmatrix} 4 & 0 & 0 & 0 \\ 0 & 4 & 0 & 0 \\ 0 & 0 & 11 & 0 \\ 0 & 0 & 0 & 11 \end{bmatrix} \tag{B.46}$$

$$M^{h2}_{rr_{dq}} = 10^{-7} \times \begin{bmatrix} 53 & 0 & 0 & 0 \\ 0 & 53 & 0 & 0 \\ 0 & 0 & 0 & 0 \\ 0 & 0 & 0 & 0 \end{bmatrix} \qquad M^{h4}_{rr_{dq}} = 10^{-7} \times \begin{bmatrix} 0 & 0 & 0 & 0 \\ 0 & 0 & 0 & 0 \\ 0 & 0 & 52 & 0 \\ 0 & 0 & 0 & 52 \end{bmatrix} \tag{B.47}$$

where $M_{rr_{dq}}$ is the full d-q rotor-rotor mutual inductance matrix excluding leakage effects, $M^{l}_{rr_{dq}}$ is the leakage inductance matrix, $M^{h2}_{rr_{dq}}$ and $M^{h4}_{rr_{dq}}$ are the 4 pole and 8 pole harmonic components (the first two non-zero components) of the rotor-rotor mutual inductance matrix.

Subtracting equations (B.47) from $M_{rr_{dq}}$ gives the harmonic leakage (or differential leakage) inductance in the rotor, that is the additional series inductance that appears due to the production of unwanted space harmonics by the rotor:

$$M^{hl}_{rr_{dq}} = 10^{-8} \times \begin{bmatrix} 2 & 0 & 0 & 0 \\ 0 & 2 & 0 & 0 \\ 0 & 0 & 9 & 0 \\ 0 & 0 & 0 & 9 \end{bmatrix} \tag{B.48}$$

B.10 Machine slot utilisation

Table B.4 shows the slot utilisation of the machine for different rotors.

Conductor area (mm^2)	Conductor metal	Slot area (mm^2)	Fill factor
Stator			
67.86	Cu	135.47	0.500
Rotor 1: 'Nested-loop' design			
133	Cu	147.23	0.903
Rotor 2: New double layer design*			
51.46	Cu	70	0.74
Rotors 3 and 4*			
51.46	Cu	70	0.74
Rotor 5: 6 bar squirrel cage design (simulation only)			
205.84	Cu	280	0.74
Rotor 6: wound rotor (simulation only)			
135.72	Cu	135.47	1.00
Rotor 7: standard squirrel cage rotor			
116.60	Al	116.60	1.00

Table B.4: Slot utilisation of the stator and rotors for the prototype machine. (* values for slots which contain conductors only)

M530-65A 0.65mm thick 5.3W/kg loss at 1.5T	
B (T)	H (A/m)
0.1	44
0.2	59.5
0.3	69.6
0.4	78.2
0.5	86.6
0.6	95
0.7	104
0.8	113
0.9	125
1.0	138
1.1	159
1.2	196
1.3	270
1.4	454
1.5	1040
1.6	2630
1.7	5620
1.8	10100

Table B.5: Magnetisation data for stator laminations for prototype BDFM

Appendix C

Leakage Inductance and Effective Air Gap

In this chapter the procedure used to estimate the leakage inductance are described, and the notion of effective air gap reviewed and the chosen method of estimation described.

The symbols used in this chapter are similar to those used in figures 2.2 and 2.1, however in this chapter all dimension are in metres unless otherwise specified, whereas in figure 2.2 all measurements other than the air gap width were in radians. In this chapter λ is used to denote permeance, y_s is used to denote slot pitch in metres (hence $y_s \approx \alpha_s \frac{d}{2}$, and $w_o \approx w_s \frac{d}{2}$ where d is the diameter, and α_s and w_s as depicted in figure 2.2).

C.1 Leakage Inductance

The calculation of leakage inductance is greatly simplified by the calculation of *specific permeance*. Permeance is the reciprocal of reluctance.

Specific permeance is defined as the self-inductance per unit length of coil per turns squared. Thus to calculate the self inductance of a coil due to leakage the permeances around the length of the coil should be summed and the the result multiplied by the number of turns squared.

The sources of permeance will now be considered. For full details, and derivation of results see [31], and [18] for trapezoidal slot geometry (and simplifications adopted here).

An estimation of the slot bridge permeance for the cage rotor considered is taken from [9].

C.1.1 Slot and Tooth-top Permeance

Figure C.1 shows a trapezoidal slot. The dotted boxes within the slot represent different conductor positions that will be considered. A square slot, can of course, be considered as a special case of a trapezoidal slot. It will be assumed that slot leakage can be adequately modelled by trapezoidal slot

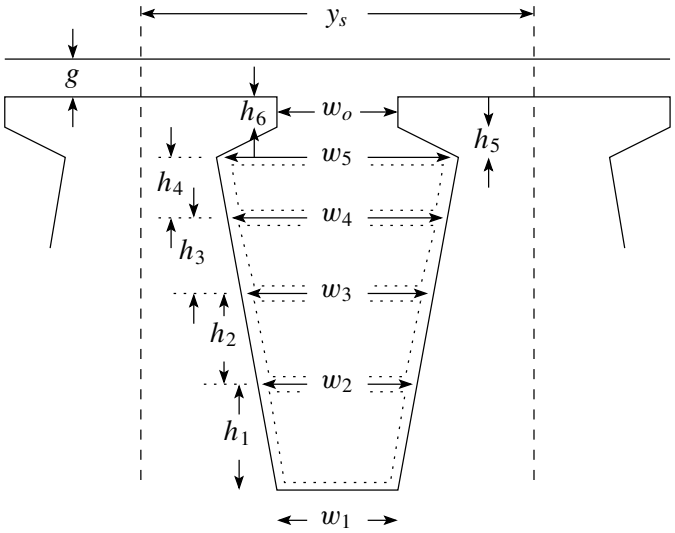

Figure C.1: Slot shape used for permeance calculations

geometry even if the slot it not exactly trapezoidal (such as having a semi-circular end).

For the conductors in the bottom position in figure C.1 the slot permeance is:

$$\lambda_{s_1} = \mu_0 \left[\frac{2h_1}{3(w_1 + w_2)} + \frac{2(h_2 + h_3 + h_4)}{(w_5 + w_2)} + \frac{2h_5}{(w_5 + w_o)} + \frac{h_6}{w_o} + \frac{g}{y_s} \right] \tag{C.1}$$

The first term of C.1 accounts for the permeance inside the conductor being considered, with the average slot width being taken. The second to fourth terms account for the permeance in the region above the conductor and the final term is the 'tooth-top' permeance.

For other conductors the first and second terms are adjusted accordingly:

$$\lambda_{s_2} = \mu_0 \left[\frac{2h_2}{3(w_2 + w_3)} + \frac{2(h_3 + h_4)}{(w_5 + w_3)} + \frac{2h_5}{(w_5 + w_o)} + \frac{h_6}{w_o} + \frac{g}{y_s} \right] \tag{C.2}$$

$$\lambda_{s_3} = \mu_0 \left[\frac{2h_3}{3(w_3 + w_4)} + \frac{2h_4}{(w_5 + w_4)} + \frac{2h_5}{(w_5 + w_o)} + \frac{h_6}{w_o} + \frac{g}{y_s} \right] \tag{C.3}$$

$$\lambda_{s_4} = \mu_0 \left[\frac{2h_4}{3(w_4 + w_5)} + \frac{2h_5}{(w_5 + w_o)} + \frac{h_6}{w_o} + \frac{g}{y_s} \right] \tag{C.4}$$

C.1.2 Overhang Permeance

Overhang permeance accounts for coupling arising from the end windings which overhang the lamination stack. Figure C.2 shows a diagram of an end winding.

Under the assumption that the overhang forms two sides of a square at each end coil (see figure C.2) [31] gives an empirical formula:

$$\lambda_o = \mu_0 \left[0.366 \log_e \left(\frac{2a}{b} \right) + 0.11 \right] \tag{C.5}$$

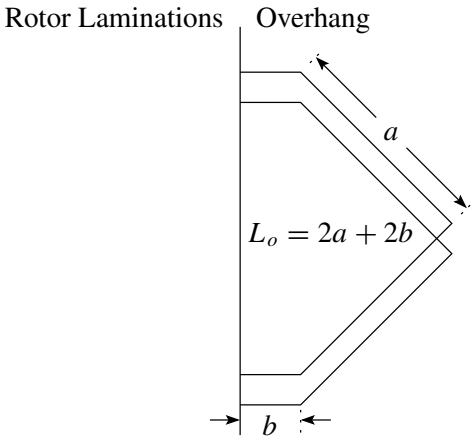

Figure C.2: Assumed end winding configuration for overhang permeance calculations

which for typical values of a and b gives:

$$\approx \mu_0 \tag{C.6}$$

.

It is assumed that there is zero mutual coupling between adjacent coils (if this is not the case [31] gives suitable modifications to (C.6).

C.1.3 Zig-zag Permeance

'Zig-zag' permeance accounts for coupling where the flux density path zig-zags between teeth on opposing sides of the air gap. It is only applicable when both rotor and stator have open slots.

Assuming that the slot pitch can be assumed to be average of the rotor and stator pitch, and that that half the zig-zag flux links the stator and half the rotor, [31] gives the permeance as:

$$\lambda_z = \mu_0 \frac{y_{s_a}}{12g} \left(1 - \frac{w_o + w_{o_r}}{y_{s_a}}\right)^2 \tag{C.7}$$

where figure C.3 explains the symbols.

C.1.4 Leakage flux per coil

The leakage flux per coil can then be calculated from the specific permeances previous stated. The permeances described in sections C.1.1 and C.1.3 both act over the lamination stack length, w_s, whereas the overhang permeance acts over the overhang length, L_o.

A description of the calculation is given for each rotor in described in chapter 5.

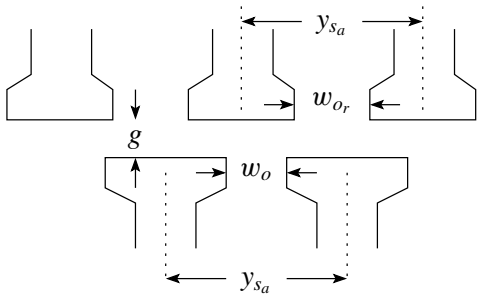

Figure C.3: Assumed slot configuration for calculation of 'zig-zag' permeance

Stator and rotor 6

The machine being considered has two two layer windings on the stator for the power and control winding supplies. Therefore the stator leakage for the winding closest to the air gap (in our case the 8 pole winding) is as follows:

$$L_{\text{coil}_8} = t_8^2(w_s(\lambda_{s_3} + \lambda_{s_4} + 2\lambda_z) + 2L_o\lambda_o) \tag{C.8}$$

For the 4 pole winding:

$$L_{\text{coil}_4} = t_4^2(w_s(\lambda_{s_1} + \lambda_{s_2} + 2\lambda_z) + 2L_o\lambda_o) \tag{C.9}$$

Rotor 6, which is considered in simulation only, is assumed to have the same slot shape and winding arrangement as the stator.

Rotor 1: 'nested-loop' design, and rotor 5: squirrel cage rotor with 6 bars

On both rotors1 and 5 the rotor bars take up the entire slot therefore the slot permeance is:

$$\lambda_{s_n} = \mu_0\left[\frac{2(h_{1_n} + h_{2_n} + h_{3_n} + h_{4_n})}{3(w_{1_n} + w_{5_n})} + \frac{2h_{5_n}}{w_{5_n} + w_{o_n}} + \frac{h_{6_n}}{w_{o_n}} + \frac{g}{y_{s_n}}\right] \tag{C.10}$$

However the zig-zag permeance and overhang permeance expressions are the same.

Therefore the leakage inductance is:

$$L_{\text{nested}} = 2w_s(\lambda_{s_n} + \lambda_z) + L_{o_n}\lambda_o \tag{C.11}$$

ignoring any leakage due to the end ring at one end, and noting that L_{o_n} is dependent on the location of the particular loop within a nest.

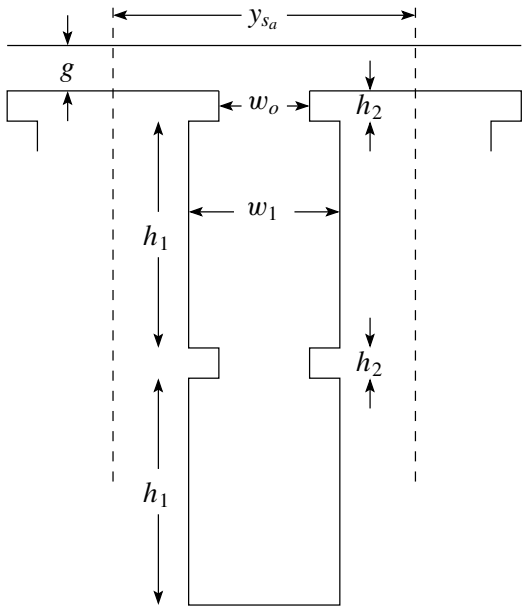

Figure C.4: Rotors 2, 3 and 4 slot detail

Rotor 2: new double layer design

The rotor has a dual layer winding and the slot shape is unusual (and non-ideal), due to economic reasons which would not affect a commercial machine, a diagram of the slot is shown in figure C.4.

Rotor 2 only uses the top slot shown in figure C.4, and each 'phase' consists of 4 loops. Each of the loops comprises of a conductor taking half the area of the top slot; the out and return paths of the loop are in the top and bottom portion of the slot respectively. Therefore:

$$L_{\text{phase}} = 4(w_s(\mu_0\left[2\frac{h_1/2}{3w_1} + \frac{h_1/2}{w_1} + 2\frac{h_2}{w_o} + 2\frac{g}{y_s}\right] + 2\lambda_z) + 2L_o\lambda_o) \tag{C.12}$$

Rotor 3: A rotor design consisting of 18 isolated loops

Rotor 3 has 18 separate loops comprised of copper strip which takes the up the whole slot area of the top then bottom slot of figure C.4 respectively. Rotor 4 is identical in construction to rotor 3, but with fewer loops, hence the inductance per loop is unchanged.

The leakage inductance of a single loop is therefore:

$$L_{\text{loop}} = w_s(\mu_0\left[2\frac{h_1}{3w_1} + \frac{h_1}{w_1} + \frac{h_2}{w_o} + 2\frac{h_2}{w_o} + 2\frac{g}{y_s}\right] + 2\lambda_z) + 2L_o\lambda_o \tag{C.13}$$

Rotor 7: Standard squirrel cage design

Rotor 7 has closed slots, and therefore a different approach is required to calculate the permeance. Birch and Butler give a computational method for estimating the slot permeance as a function of the

rotor m.m.f. (magneto-motive force) [9]. However the slot geometries of the cage rotor considered are close enough to the example given in the paper to take the results straight from figure 3 of [9]. The prototype rotor slot bridge depth on the slot line is 0.85mm, the slot top radius is 2.5mm and the air gap is 0.55mm.

λ	m.m.f. (A-turns)
7.5	100
3.5	200
2.8	300
2.5	400

Thus assuming around 300 A-turns then the specific permeance is 2.8. This permeance must be added to the slot permeance to determine the leakage inductance for a single bar:

$$L_{\text{bar}} = 2.8\mu_0 w_s + w_s(\mu_0 \left[\frac{h_1/2}{3w_1} + \frac{g}{y_s}\right] + \lambda_z)$$

The leakage due to the end ring is approximated using the same method as for an end winding:

$$L_{\text{end}} = L_o \lambda_o$$

Therefore the total leakage inductance matrix will be a symmetric circulant matrix with $2L_{\text{bar}} + 2L_{\text{end}}$ on the diagonal, and $-L_{\text{bar}}$ offset by ± 1 column from the diagonal.

The dimensions for the slot leakage calculations have been assumed to be the same as those for the progressive loop rotor.

Parameter Values for Leakage calculation

Table C.1 shows the slot and overhang dimensions for leakage flux calculation on the stator rotor designs considered. Table C.2 contains physical geometries of the considered rotors and stator, and the effective air gap as calculated using Carter's factor.

C.2 Effective air gap

In 1900 Carter [21] first derived a correction factor for the air gap to allow for the effect of having an open slot. The initial result was expanded and given in a more complete form in [22], equation (8). Broadly the assumption made is that slots are parallel and infinitely deep, slot pitch length is infinite. Furthermore it is assumed that the teeth themselves are made of material of infinite magnetic permeability.

Carter's factor is given by:

$$K = \frac{y_s}{y_s - \gamma g} \tag{C.14}$$

w_o (mm)	w_1 (mm)	w_2 (mm)	w_3 (mm)	w_4 (mm)	w_5 (mm)	g (mm)	h_1 (mm)	h_2 (mm)	h_3 (mm)	h_4 (mm)	h_5 (mm)	h_6 (mm)	y_s (mm)	w (mm)	L_o (mm)	t
Stator (and rotor 6 with $t = 0.1$ and $w = 189.9$) 4 pole (furthest from the air gap)																
3.2	8.111	7.731	7.335	6.471	5.473	-	2.845	2.992	6.532	7.556	0.656	1.13	11.457	195.5	160	10
Stator (and rotor 6 with $t = 0.2$ and $w = 189.9$) 8 pole (closest to the air gap)																
3.2	8.111	7.731	7.335	6.471	5.473	-	2.845	2.992	6.532	7.556	0.656	1.13	11.457	195.5	75	20
Rotor 1: 'Nested-loop' design																
2.8	5.68	-	-	-	9.433	0.547	19.48	0	0	0	1.207	0.65	15.182	189.9	100,60,20	1
Rotor 2: New double layer design																
2.1	3.74	-	-	-	-	0.555	18.71	2.27	-	-	-	-	15.180	190.2	110	1
Rotors 3 and 4: isolated loop designs																
2.1	3.74	-	-	-	-	0.555	18.71	2.27	-	-	-	-	15.180	189.9	140	1
Rotor 5: 6 bar squirrel cage design																
8.4	22.72	-	-	-	37.72	0.547	19.48	0	0	0	1.207	0.65	91.091†	189.9	110	1

Table C.1: Slot and overhang dimensions for calculation of leakage flux for the different rotors, see figures C.4, C.1 and C.2 for details. † the value used in calculation of zig-zag permeance was 15.182mm, to coincide with rotor 1.

diameter	Stack length	rotor-stator stack overlap	No. slots	Carter Factor	Carter Factor (Approx.)	Carter Factor (Ossana Approx.)	air gap	air gap (tol.)	slot mouth width	air gap (eff.)
d	w			K			g		w_o	g_{eff}
(mm)	(mm)	(mm)					(mm)	±(mm)	(mm)	(mm)
Stator (3 values are given for three different air gaps)										
175.065	195.5	-	48	1.179	1.193	1.253	0.547	-	3.2	-
175.065	195.5	-	48	1.178	1.192	1.252	0.555	-	3.2	-
175.065	195.5	-	48	1.186	1.198	1.259	0.510	-	3.2	-
Rotor 1: 'Nested-loop' design										
173.971	189.9	189.9	36	1.104	1.114	1.167	0.547	0.03	2.8	0.712
Rotor 2: New double layer design										
173.955	190.2	189.4	36	1.064	1.138	1.120	0.555	0.03	2.1	0.696
Rotors 3 and 4: isolated loop designs										
173.955	189.9	188.3	36	1.064	1.138	1.120	0.555	0.03	2.1	0.696
Rotor 5: 6 bar squirrel cage design (simulation only)										
173.971	189.9	189.9	6	$K = 1$ by assumption			0.547	0.03	8.4	0.645
Rotor 6: wound rotor (simulation only)										
173.971	189.9	189.9	48	1.181	1.194	1.255	0.547	0.03	3.2	0.762
Rotor 7: standard squirrel cage rotor										
174.046	190.3	189.3	40	closed slots			0.510	0.02	-	0.605

Table C.2: Physical data for the experimental (and simulation) BDFM stator and rotor designs

where

$$\gamma = \frac{4}{\pi}\left[\frac{w_o}{2g}\arctan\left(\frac{w_o}{2g}\right) - \log_e\sqrt{1+\left(\frac{w_o}{2g}\right)}\right] \tag{C.15}$$

and where w_o is the slot mouth width, y_s is the slot pitch (in distance units) and g is the air gap width as per figure C.1.

When both rotor and stator have open slots it is assumed that the resultant Carter factor is the product of the Carter factors for the stator and rotor respectively (see [43, sect. 6.1] and references therein for details and experimental justification).

$$K_{\text{total}} = K_r K_s \tag{C.16}$$

where K_r and K_s are the rotor and stator Carter factors respectively.

As noted in [43] the assumption of infinite slot pitch length is not always reasonable. In [22] and [39, ch. 17], Carter's original calculation is generalised for the case of a regular slotting pattern. [39] claims that Carter's initial assumption i.e. equations (C.14) is quite sufficient for practical application, which is at odds with [43, p. 56]. In practice as long as the ratio $\frac{w_o}{g}$ is sufficiently large (or equivalently the ratio $\frac{w_o}{y_s - w_o}$ sufficiently small, however in normal machines this is rarely the case) then (C.14) is a good approximation. Sometimes these assumptions are not reasonable, and [43, sect. 6.1] gives the following two alternative approximations which have empirical justification:

When $\frac{w_o}{g} < 12$:

$$K \approx \frac{y_s}{y_s + g - \frac{3}{4}w_o} \tag{C.17}$$

Or an alternative approximate formula is given as

$$K \approx \frac{y_s + 8g}{y_s - w_o + 8g} \tag{C.18}$$

Appendix D

Previous BDFMs

Location	Frame name	Frame size (mm)	Air gap (mm)	Air gap dia. (mm)	Stack Length (mm)	Poles	No. Rotor Slots	No. Stator Slots	Original Torque (Nm)	Claimed power kW	Ref.	Year
Broadway/Burbridge												
Bristol, UK	-					6/2	48 (40 used)				[17]	1970
Bristol, UK	-			177.8	69.85	18/12	60	54			[17]	1970
Spée/Wallace												
Oregon	NEMA 254T	158.75	0.6	210	75	6/2	44	36	40		[110, 104, 127, 11]	1989-1995
Brune/Spée/Wallace												
Oregon	NEMA 182T	114.30				6/2			12		[19]	1994
Williamson												
Cambridge	D160	160			273	8/4	36	48	70		[114]	1997
McMahon/Ali Lotia												
Cambridge	D100	100	0.42	91.7	96	6/2	32	36	15	2	[68]	2000
McMahon/FKI												
Cambridge	D180	180	0.55	175	190	8/4	36	48	140			2001
Shoudao et. al.												
China						6/2				30	[96]	2000
Runcos/WEG												
Brazil						12/8				100†	[90]	2004

Table D.1: Prototype nested-loop rotor BDFMs. † This value is hard to believe from the evidence presented.

Appendix E

Experimental Apparatus

The test rig for the prototype BDFM is shown in figure E.3. Details on the prototype machine can be found in appendix B. The test rig was designed and assembled for the purposes of this research. The purpose of the design was to produce a test rig which would allow steady-state and dynamic tests to be performed on the prototype BDFM machine over its full potential operating range. The operating range was considered to be 0-150 N m and 0-2000 rpm. In practice the extremes of this operating envelope were not attainable, due to limitations that will be discussed in the sequel.

The apparatus will now be described.

E.1 Apparatus Description

The apparatus is depicted in figures E.2 and E.3. The apparatus consists broadly of three parts: the prototype BDFM machine and power supplies; the DC load motor and power supplies and control and instrumentation hardware. In addition a Yokogawa 3 phase power meter, part number WT130 was available for confirmatory measurements.

The DC machine armature was supplied from two unregulated 220V, 30A DC supplies which could be connected in series or parallel giving a maximum power of 13.2 kW, this was the maximum power the rig could supply. The DC machine field winding was supplied from a regulated 600V, 4A DC supply.

The BDFM stator 1 winding was supplied from the 3 phase, 50 Hz grid, connected through a 25A per phase Variac, variable from 0 to 245V_{rms} (phase). The stator 2 winding was connected to an inverter through a L-C line filter. The PWM switching frequency was variable, but normally set to 10 kHz.

The control and instrumentation was based around a dedicated slave PC, with an AMD 'Athlon' 1.4 GHz processor. This slave PC ran a real-time operating system, specifically designed to be programmed by, and interface to Simulink/Matlab, called 'xPC Target'. This slave PC will be referred to as the target PC. The target PC contained a number of peripheral boards to perform data acquisi-

tion and output data. The target PC performed data logging, this data was accessible over a TCP/IP network connection for subsequent downloading. The target PC was programmed, and monitored from a host PC running Matlab/Simulink under MS Windows. The host PC simply functioned as an interface to the target PC. Figure E.1 shows a typical screen shot of the the target PC when running. The screen shot shows the basic signal monitoring features of the target computer. The screen shot shows current and voltage wave forms, along with some numerical data.

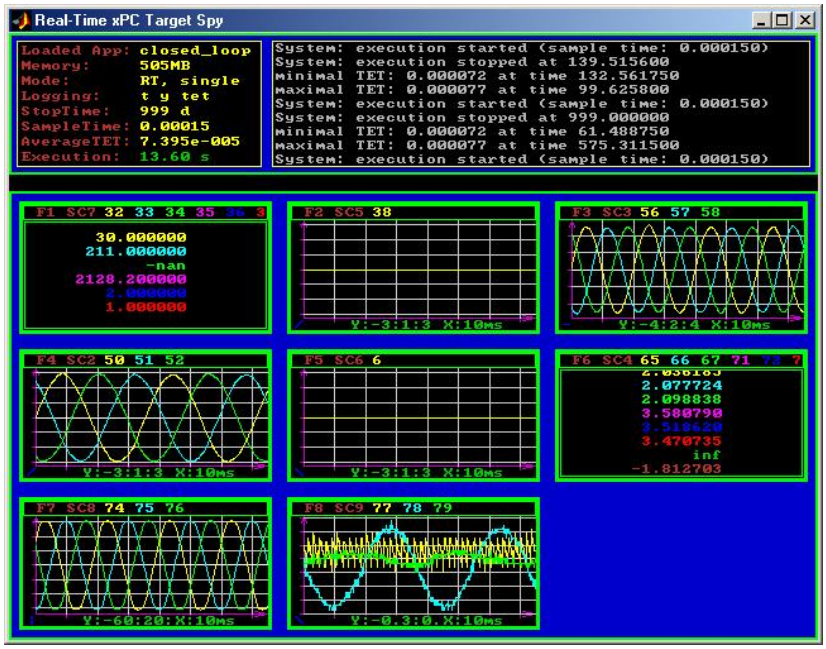

Figure E.1: Typical screen shot of the target PC, showing current and voltage wave forms and numerical data

Due to the extremely high levels of E-M interference generated by the inverter the elimination of noise from measurements was particularly problematic. Where possible signals were isolated using opto-isolators and low impedance earthing was provided throughout. These measures combined with some filtering gave acceptable performance.

E.1.1 xPC Target PC and peripheral boards

Table E.1 gives details of the peripheral boards in the target PC. The FPGA based inverter output board was specified by the author and designed by George Makrides[70].

E.1.2 Torque Transducer

The transducer was manufactured by Hottinger Baldwin Messtecknik (HBN), Germany part number T30FN with display unit and amplifier part numbers DA3417 and MD555. The transducer was rated 0-1000 N m at up to 5 kHz and up to 3000 rpm. In practice, the power supply to the transducer was

Manufacturer/Part No.	Description	Specification	Purpose
Measurement Computing / PCI-DIO96H	96 bit digital I/O	Organised in 8-bit groups, 5V levels, read latency approx. 750 ns, write latency approx 250 ns.	Receiving parallel data from voltage A/D, total read time approx. 9 µs for 6×16 bit inputs.
Measurement Computing / PCI-DIO96H	96 bit digital I/O	Organised in 8-bit groups, 5V levels, read latency approx. 750 ns, write latency approx 250 ns.	Receiving parallel data from speed and position calculations, total read time approx. 4 µs.
Measurement Computing / PCI-DAS1602/16	16 single-ended (or 8 differential) input 16-bit A/D, 2 16-bit D/A, 24 bit digital I/O	A/D 200kSamples/s (one input), hence read latency approx. 5 µs per input.	Measurement of analogue current signals from Hall effect sensors, torque reading from transducer, flux reading from integrating amplifier. Total read time, approx 40 µs.
PLX-9030 and Xilinx Spartan 2e FPGA	Custom designed implementation of space-vector modulation, to generate switching patterns for the inverter. Variable dead-time (0-4 µs), switching frequency (1-50 kHz), modulation frequency (-200 to 200 Hz), av. latency $\frac{1}{2}$ switching period, hence 50 µs at 10 kHz		

Table E.1: xPC Target PC peripheral boards

poorly decoupled resulting in large amounts of noise being picked up from the inverter. Therefore the useful bandwidth was only a few Hz.

E.1.3 DC load motor

The DC load motor specifications are given in table E.2. For further details see [69]. As previously mentioned the maximum power the DC machine could deliver was 13.2 kW, which was the supply limit. The maximum power the machine can dissipate is 13.9 kW which was limited by the load resistors.

Parameter	**Value**
Manufacturer	GEC, UK
Frame size	SD160XLB
Nature	separately excited
Rated power	24 kW
Rated speed	1750 rpm
Armature voltage	460V
Armature current	61A
Field winding voltage	360V
Field winding current	1.83A
Armature resistance	0.428 Ω
Armature inductance	7.5 mH
Field winding resistance	196.7 Ω
Field winding inductance	74 H

Table E.2: DC load motor specification

E.1.4 Inverter Output Filter

The inverter output filter was a 3 phase L-C filter. The filter was manufactured by Schaffner, part number FN 5010-18-99 and was a star connected L-C filter with L=3.5 mH and C=1.5 µF giving the resonant pole at approximately 2.2 kHz. The filter is rated at $18A_{rms}$ per phase, and $400V_{rms}$ line at 40 °C. The manufacturer states that the filter can be used with switching frequencies from 4 kHz to 16 kHz.

E.1.5 Inverter

The inverter comprised of 3 half-bridge IGBT modules. The modules were Semikron 'SKiiP 432 GB 120 - 207 CTV' modules, which contain two N-channel IGBT devices in series and accompanying

gate drive circuitry, including measures to protect the devices from overheating due to desaturation, undervoltage and short circuit protection. The latter ensures that a suitable 'dead-time' between firing high and low side devices is employed.

The devices were rated at 1200V and 400A. The devices were supplied from a 600V DC link derived from a uncontrolled 3 phase rectifier connected directly to the mains.

The devices were mounted in an earthed protective enclosure on a heat sink with forced air cooling. The overall inverter rating was calculated as $200A_{rms}$ per phase with a 600V DC link at 8 kHz switching frequency, or $100A_{rms}$ per phase at a 600V DC link at 25 kHz switching frequency.

The inverter also included a 'brake-chopper', Semikron part number SKAI 100 E, which provided 'bang-bang' regulation of the DC link voltage by switching in the inverter protection resistors when the DC link voltage exceeded around 680V. This facility was necessary when testing the BDFM, as when the machine is in operation as a generator, above natural speed, or as a motor below natural speed, the inverter connected winding regenerates power, which would otherwise cause the DC link voltage to increase.

E.1.6 Position and Speed Measurements

The position and speed measurements were derived from an optical encoder (or 'resolver'), which produced 2500 pulses per revolution. A state-machine was implemented on a fast 8-bit micro controller, a Scenix SX28 running at 50MIPS, to determine the rotor angular position to an accuracy of 0.036°. The data was sent as 15 bit parallel data, with one bit representing the direction of rotation for the last transition. The data was fed into the input of one of the digital I/O cards. Handshaking was achieved by an assertion from the digital I/O card that a read was imminent; during this time the SX28 refrained from modifying its output pins. The latency between position updates was approximately 2 µs.

The speed measurement was achieved with another SX28 micro controller, which used a 50MHz clock to time pulse widths. This data was output as a floating point number with a 5 bit exponent, 12 bit mantissa, and a saturation bit, to one of the digital I/O cards. The speed was computed by the target PC by performing the requisite division. As the optical encoder gave 2500 pulses per revolution the minimum speed measurable before saturation occurred was approximately 0.07 rpm. At 1000 rpm the speed measurement was accurate to better than 1 rpm, at 2000 rpm the accuracy was better than about 4rpm. As with the position measurement, handshaking was achieved by means of an assertion from the I/O board.

The outputs from the optical encoder were isolated using opto-isolators to ensure that no ground loops were present and to protect the equipment.

E.1.7 Analogue to Digital Converters

The stator 1 and stator 2 phase currents were measured using Hall effect current sensors, LEM part number LTA-100P, wound for a maximum current of $25A_{rms}$. The Hall effect sensors provide galvanic isolation, however it was necessary to place the sensors in the return current path, rather than the out current path, to reduce the capacitive coupling between the sensor circuitry and the noisy supply voltage to stator 2 from the inverter. The sensors were read by the DAS1602/16 16 bit A/D card. The sensor bandwidth was approximately 100 kHz, hence the bandwidth was limited by the sample rate.

The voltage measurement was achieved with a custom designed A/D board designed by the author and implemented by Davor Dukic and Iskandar Samad. The board consists of 6 parallel 16 bit A/D converters, AD677, driven by a differential input with a 2 kHz 4 pole Butterworth anti-aliasing filter. The converters were isolated via opto-isolators, and the data conversion controlled by 7 PIC micro controllers. The data was acquired by one of the digital I/O boards, in parallel format. The maximum input voltage was $\pm$1000V peak, and the input impedance was 1 MΩ.

E.1.8 DC Machine load resistors and Inverter dump resistors

The inverter dump resistors were six 24Ω, 10A resistors connected as three in series and the two such sets in parallel, giving a total resistance of 36Ω at 20A, or 10 kW at 600V. Therefore the inverter could withstand 10 kW of regeneration.

The DC machine load resistors comprises of three resistors each configured at 10.5 Ω and rated at 21A. Generally either two or three resistors were connected in parallel giving a minimum resistance of 3.5 Ω at a current of 63A, and total power dissipation of 13.9 kW, which was the maximum power which could be dissipated by the test rig.

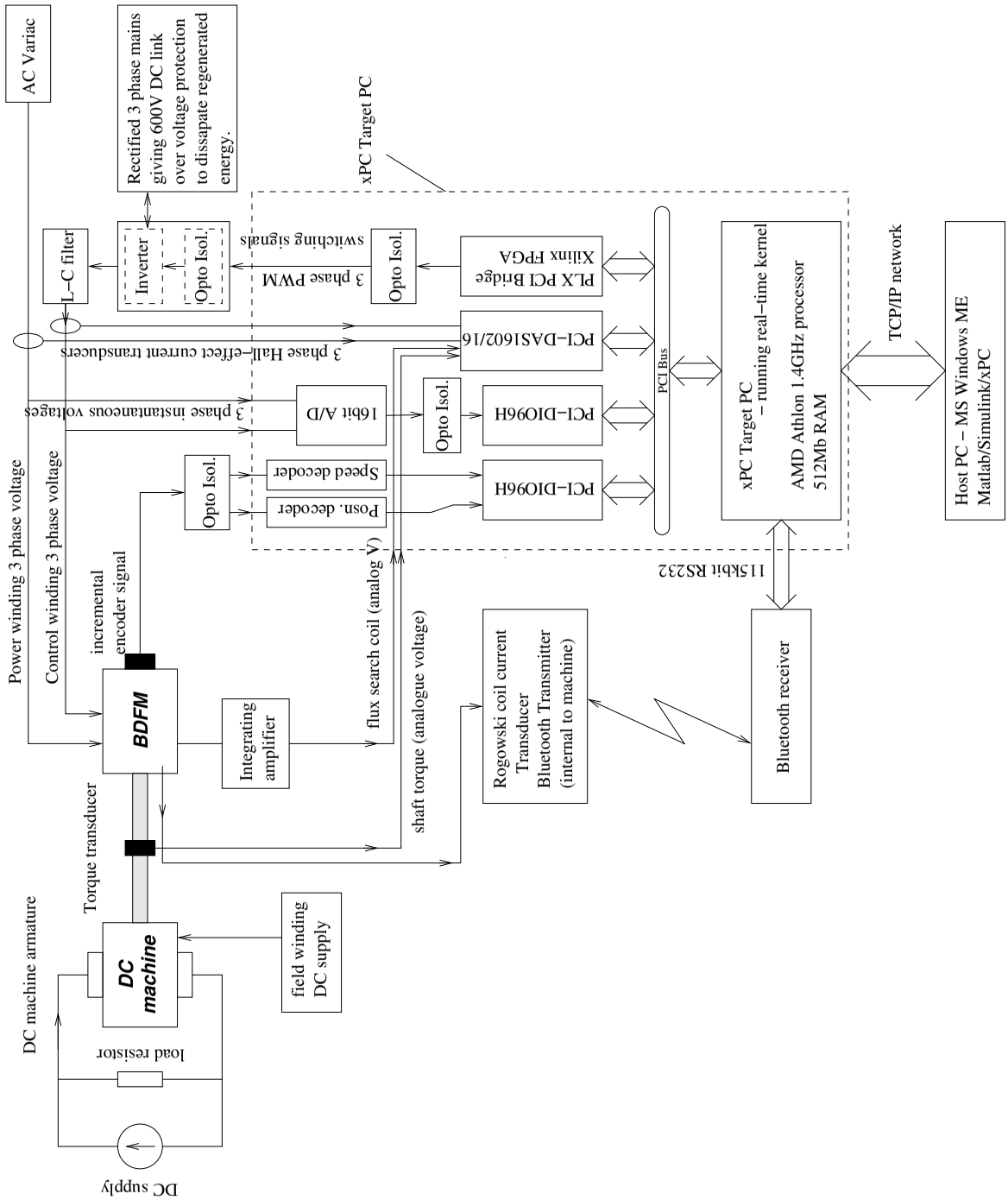

Figure E.2: Test rig functional diagram for the prototype BDFM

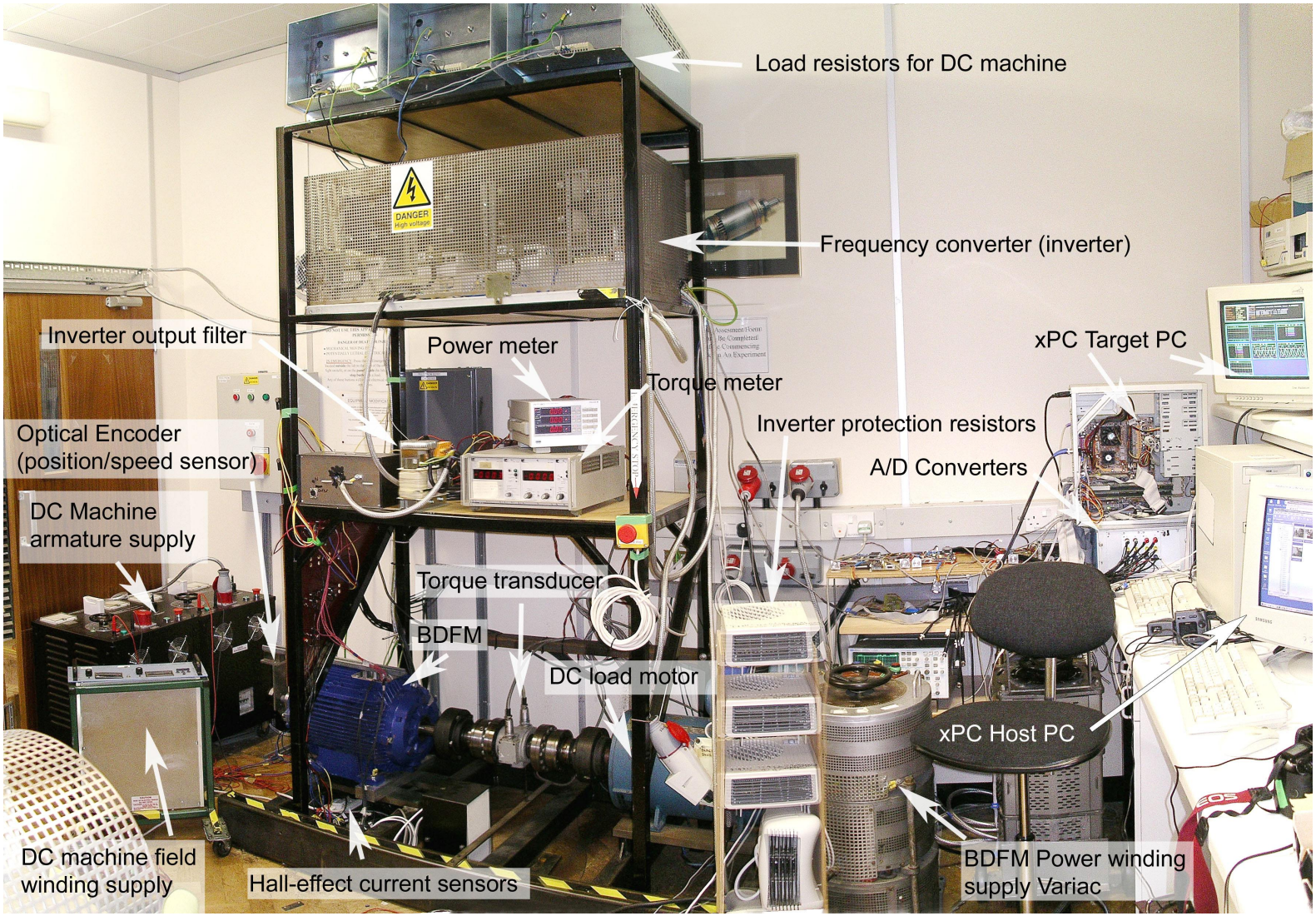

Figure E.3: Test rig for the prototype BDFM

Bibliography

[1] E. Abdi-Jalebi, P. C. Roberts, and R. A. McMahon. Real-time rotor bar current measurement using a rogowski coil transmitted using wireless technology. In *18th Intl. Power Systems Conf. (PSC2003), Iran*, volume 5, pages 1–9, October 2003.

[2] Gerald C. Alexander. Characterization of the brushless, doubly-fed machine by magnetic field analysis. In *Proc. IEEE Industry Applications Society (IAS) Annual Mtg.*, pages 67–74, Seattle,WA, October 7-12 1990. IEEE.

[3] Pierre Apkarian and Richard J. Adams. Advanced gain-scheduling techniques. *IEEE Transactions on Control Systems Technology*, 6(1):21–32, January 1998.

[4] Carolyn Beck and Pascale Bendotti. Model reduction methods for unstable uncertain systems. In *Proc. Conference on Decision and Control*. IEEE CSS, December 1997.

[5] Carolyn Beck and John Doyle. A necessary and sufficient minimality condition for uncertain systems. *IEEE Trans. Automatic Control*, 44(10):1802–1813, October 1999.

[6] Carolyn Beck, John Doyle, and Keith Glover. Model reduction of multidimensional and uncertain systems. *IEEE Trans. Automatic Control*, 41(10):1466–1477, October 1996.

[7] G. Becker and A. Packard. Robust performance of linear parametrically varying systems using parametrically-dependent linear feedback. *Systems and Control Letters*, 23, 1994.

[8] Shibashis Bhowmik, René Spée, and Johan H. R. Enslin. Performance optimization for doubly fed wind power generation systems. *IEEE Trans. Industry Applications*, 35(4):949–958, July/August 1999.

[9] T. S. Birch and O. I. Butler. Permeance of closed-slot bridges and its effect on induction motor current consumption. *Proc. IEE*, 118(1), January 1971.

[10] M. Boger, A. Wallace, and R. Spée. Investigation of appropriate pole number combinations for brushless doubly fed machines as applied to pump drives. *IEEE Transactions on Industry Applications*, 31(5):1022–1028, 1996.

[11] M. Boger, A. Wallace, R. Spée, and R. Li. General pole number model of the brushless doubly-fed machine. *IEEE Transactions on Industry Applications*, 31(5):1022–1028, 1995.

[12] M. S. Boger. *Aspects of Brushless Doubly-Fed Induction Machines*. PhD thesis, University of Cambridge, 1997.

[13] W. R. Brassfield, R. Spée, and T. G. Habetler. Direct torque control for brushless doubly-fed machines. In *Conf. Record of 1992 IEEE Industry Applications Society (IAS) Annual Meeting*, pages 615–622. IEEE, 4-9 October 1992. Houston, TX, USA.

[14] W. R. Brassfield, R. Spée, and T. G. Habetler. Direct torque control for brushless doubly fed machines. *IEEE Transactions on Industry Applications*, 32(5):1098–1103, 1996.

[15] A. R. W. Broadway. Cageless induction machine. *Proc. IEE*, 118(11):1593–1600, November 1971.

[16] A. R. W. Broadway. Brushless cascade alternator. *Proc. IEE*, 1974.

[17] A. R. W. Broadway and L. Burbridge. Self-cascaded machine: a low-speed motor or high frequency brushless alternator. *Proceedings, Institution of Electrical Engineers*, 117:1277–1290, 1970.

[18] G. S. Brosan and J. T. Hayden. *Advanced Electrical Power and Machines*. Sir Isaac Pitman & Sons Ltd., 1966.

[19] Chris S. Brune, René Spée, and Alan K. Wallace. Experimental evaluation of a variable-speed, doubly-fed wind-power generation system. *IEEE Trans. Industry Applications*, 30(3):648–655, May/June 1994.

[20] A. Bruce Carlson. *Circuits: Engineering Concepts and Analysis of Linear Electric Circuits*. John Wiley & Sons Inc., New York, 1996.

[21] F. W. Carter. Note on air-gap and interpolar induction. *Institution of Electrical Engineers Journal*, 29, 1900.

[22] F. W. Carter. The magnetic field of the dynamo-electric machine. *Institution of Electrical Engineers Journal*, 64, 1926.

[23] Paolo Castaldi, Walter Geri, Marcello Montanari, and Andrea Tilli. A new adaptive approach for on-line parameter and state estimation of induction motors. *Control Engineering Practice*, 13(1):81–94, January 2005.

[24] C. D. Cook and B. H. Smith. Stability and stabilisation of doubly-fed single frame cascade induction machines. *IEE Proceedings*, 126(11):1168–1174, 1979.

[25] C. D. Cook and B. H. Smith. Effects of machine parameter values on dynamic response and stability regions of doubly-fed cascade induction machines. *IEE Proceedings - B Electrical Power Applications*, 130(2):137–142, 1983.

[26] Peter A. Cook. *Nonlinear Dynamical Systems*. Prentice Hall, 1994.

[27] F. Creedy. Some developments in multi-speed cascade induction motors. *Institution of Electrical Engineers, Journal*, pages 511–537, 1920.

[28] Henry D'Angelo. *Linear Time-Varying Systems: Analysis and Synthesis*. Series in Electrical Engineering. Allyn and Bacon, 1970.

[29] J. A. de Kock, F. S. van der Merwe, and H. J. Vermeulen. Induction motor parameter estimation through an output error technique. *IEEE Trans. on Energy Conversion*, 9(1):69–75, March 1994.

[30] A. Draper. *Electrical Circuits Including Machines*. Longmans, 1 edition, 1964.

[31] A. Draper. *Electrical Machines*. Longmans, 2 edition, 1967.

[32] Guang-Ren Duan and Ron J. Patton. A note on hurwitz stability of matrices. *Automatica*, 34(4):509–511, 1998.

[33] A. C. Ferreira. *Analysis of the Brushless Doubly-Fed Induction Machine*. PhD thesis, University of Cambridge, 1996.

[34] A. C. Ferreira and S. Williamson. Time-stepping finite-element analysis of brushless doubly fed machine taking iron loss and saturation into account. *IEEE Transactions on Industry Applications*, 35(3):583–588, 1999.

[35] A.E. Fitzgerald, Jr. Charles Kingsley, and Stephen D. Umans. *Electric Machinery*. Electrical Engineering. McGraw-Hill, New York, 4 edition, 1983.

[36] Pascal Gahinet and Pierre Apkarian. A linear matrix inequality approach to $\mathcal{H}_\infty$ control. *Int. J. of Robust and Nonlinear Control*, 4, 1994.

[37] Pascal Gahinet, Arkadi Nemirovski, Alan J. Laub, and Mahmoud Chilali. *LMI Control Toolbox User's Guide*. The Mathworks Inc., 1995. available from `http://www.mathworks.com/access/helpdesk/help/pdf_doc/lmi/lmi.pdf`.

[38] F. R. Gantmacher. *The Theory of Matrices*. Chelsea, New York, 2 edition, 1990. 2 vols.

[39] William. J. Gibbs. *Conformal Transformations in Electrical Engineering*. Chapman & Hall Ltd., London, 1958.

[40] Keith Glover. All optimal hankel-norm approximations of linear multivariable systems and their $\mathcal{L}_\infty$-error bounds. *Int. J. Control*, 39(6):1115–1193, 1984.

[41] B. V. Gorti, G. C. Alexander, and R. Spée. Power balance considerations for brushless doubly-fed machines. *IEEE Transactions on Energy Conversion*, 11(4):687–692, December 1996.

[42] B. V. Gorti, G. C. Alexander, R. Spée, and A. K. Wallace. Characteristics of a brushless doubly-fed machine in current-fed mode of operation. In *Proc. Conference on Industrial Automation & Control (I,A & C)*, pages 143–148. IEEE/IAS, IEEE, 5-7 January 1995. Hyderabad, India.

[43] Bedřich Heller and Václav Hamata. *Harmonic Field Effects in Induction Machines*. Elsevier Scientific Publishing Co., 1977.

[44] Y. C. Ho and D. L. Pepyne. Simple explanation of the no-free-lunch theorem and its implications. *J. of Optimization Theory and Applications*, 115(3):549–570, December 2002.

[45] B. Hopfensperger, D. J. Atkinson, and R. A. Lakin. Stator flux orientated control of a cascaded doubly-fed induction machine. *Proc. IEE B - Electric Power Applications*, 146(6):597–605, November 1999.

[46] B. Hopfensperger, D. J. Atkinson, and R. A. Lakin. Combined magnetising flux orientated control of the cascaded doubly-fed induction machine. *Proc. IEE B - Electric Power Applications*, 148(4):354–362, July 2001.

[47] Roger A. Horn and Charles R. Johnson. *Topics in Matrix Analysis*. Cambridge University Press, 1991.

[48] Louis J. Hunt. A new type of induction motor. *Institution of Electrical Engineers, Journal*, pages 648–677, 1907.

[49] Louis J. Hunt. The 'cascade' induction motor. *Institution of Electrical Engineers, Journal*, pages 406–434, 1914.

[50] A. Isidori. *Nonlinear Control Systems 3rd Edition*. Springer, 1995.

[51] Morris Jevons. *Electrical Machine Theory*. Blackie & Son Limited, London, 1966.

[52] Charles V. Jones. *The Unified Theory of Electrical Machines*. Butterworths,London, 1967.

[53] Alson Kemp, Michael Boger, Ernesto Wiedenbrüg, and Alan Wallace. Investigation of rotor-current distributions in brushless doubly-fed machines. In *Proc. IEEE Industry App. Soc. Annual Mtg.*, pages 638–643. IEEE, 6-10 October 1996. San Diego, CA.

[54] Hassan K. Khalil. *Nonlinear Systems*. Prentice-Hall, Inc., New Jersey, 2 edition, 1996.

[55] Brian Kock, René Spée, and Bryan Clever. A comparison of stack preparation methods for bar insulation in diecast rotors. In *Proc. IEEE Industry Applications Society Annual Meeting*, volume 1, pages 182–187. IEEE IAS, IEEE, New Orleans, October 5-9 1997.

[56] Paul C. Krause, Oleg Wasynczuk, and Scott D. Sudhoff. *Analysis of electric machinery and drive systems*. IEEE Press Wiley, New York, second edition, 2002.

[57] Alexander Kusko and Clement Somuah. Speed control of a single-frame cascade induction motor with slip-power pump back. *IEEE Trans. Industry Applications*, IA-14(2):97–105, 1978.

[58] Sanjay Lall and Carolyn Beck. Error-bounds for balanced model-reduction of linear time-varying systems. *IEEE Trans. Automatic Control*, 48(6):946–956, June 2003.

[59] H. K. Lauw. Brushless doubly-fed motor control system. US Patent No.: 5,239,251, August 1993.

[60] R. Li, R. Spée, A. K. Wallace, and G. C. Alexander. Synchronous drive performance of brushless doubly-fed motors. *IEEE Transactions on Industry Applications*, 30(4):963–970, July/August 1994.

[61] R. Li, A. Wallace, and R. Spée. Determination of converter control algorithms for brushless doubly-fed induction motor drives using Floquet and Lyapunov techniques. *IEEE Transactions on Energy Conversion*, 10(1):78–85, 1995.

[62] Ruqi Li, Alan Wallace, and René Spée. Determination of converter control algorithms for stable brushless doubly-fed drives using floquet and lyapunov techniques. In *Proc. Power Electronics Specialists Conference (PESC)*, pages 571–577. IEEE, 24-27 June 1991. Cambridge, MA.

[63] Ruqi Li, Alan Wallace, and René Spée. Dynamic simulation of brushless doubly-fed machines. *IEEE Transactions on Energy Conversion*, 6(3):445–452, 1991.

[64] Ruqi Li, Alan Wallace, and René Spée. Two-axis model development of cage-rotor brushless doubly-fed machines. *IEEE Transactions on Energy Conversion*, 6(3):453–460, 1991.

[65] Yuefeng Liao. Design of a brushless doubly-fed induction motor for adjustable speed drive applications. In *Proc. IEEE Industry App. Soc. Annual Mtg.*, pages 850–855. IEEE, 6-10 October 1996.

[66] Antonio Marcus Nogueira Lima, Cursino Brandão Jacobina, and Eurico Bezerra de Souza Filho. Nonlinear parameter estimation of steady-state induction machine models. *IEEE Trans. on Industrial Electronics*, 44(3):390–397, June 1997.

[67] R. D. Lorenz. Observers and state filters in drives and power electronics. In *Proc. IEEE IAS OPTIM*, Brasov, Romania, May 16-18 2002. IEEE/IAS. Keynote paper.

[68] Mohammed Ali Lotia. Control strategies for variable speed brushless doubly-fed induction motor drives. Master's thesis, University of Cambridge, 2000.

[69] R.A. Majzoub. *The role of damper windings in suppressing electromechanical oscillations of diesel-driven synchronous generators*. PhD thesis, University of Cambridge, June 2001.

[70] George Makrides. The design and implementation of a hardware platform for driving and controlling brushless doubly-fed machines. Mphil., University of Cambridge, August 2004.

[71] M. Matsumoto and T. Nishimura. Mersenne twister: A 623-dimensionally equidistributed uniform pseudorandom number generator. *ACM Trans. on Modeling and Computer Simulation*, 8(1):3–30, January 1998. `http://www.math.sci.hiroshima-u.ac.jp/~m-mat/eindex.html`.

[72] R. G. Meadows. *Electric Network Analysis*. Penguin Education, 1972.

[73] Alexandre Megretski, Chung-Yao Kao, Ulf Johnsson, and Anders Rantzer. *A Guide to IQCβ: Software for Robustness Analysis*, February 2003. available from `http://www.math.kth.se/~cykao/`.

[74] Alexandre Megretski and Anders Rantzer. System analysis via integral quadratic constraints. *IEEE Trans. Automatic Control*, 42(6):819–830, June 1997.

[75] S. Müller, M. Deicke, and Rik M. de Doncker. Doubly fed induction generator systems for wind turbines. *IEEE Industry Applications Magazine*, pages 26–33, May/June 2002.

[76] Georgios Papafotiou, Tobias Geyer, and Manfred Morari. Optimal direct torque control of three-phase symmetric induction motors. Technical Report AUT03-07, Eidgen ossische Technische Hochschule (ETH), Zürich, Switzerland, April 2003. available from `http://control.ee.ethz.ch/research/publications/publications.msql?id=1614`.

[77] E. Prempain, I. Postlethwaite, and A. Benchaib. A linear parameter variant H_∞ control design for an induction motor. *Control Engineering Practice*, 10(6):633–644, June 2002.

[78] Amuliu Bogdan Proca and Ali Keyhani. Identification of variable frequency induction motor models from operating data. *IEEE Trans. on Energy Conversion*, 17(1):24–31, March 2002.

[79] Ashok Ramchandran and Gerald C. Alexander. Frequency-domain parameter estimations for the brushless doubly-fed machine. In *Conference Record of PCC 1993*, pages 346–351, Power Conversion Conference, Yokohama 1993, 1993. IEEE. 19-21 Apr 1993.

[80] Ashok Ramchandran, Gerald C. Alexander, and Réné Spée. Off-line parameter estimation for the doubly-fed machine. In *Proceedings of Conference on Industrial Electronics, Control, Instrumentation, and Automation, 1992. 'Power Electronics and Motion Control'*, volume 3, pages 1294–1298. IEEE, 1992. 9-13 Nov 1992.

[81] N. S. Risley and Richard S. Burington. A matric theory development of the theory of symmetric components. *London, Edinburgh & Dublin Philosophical Magazine*, 27(184):605–613, May 1939.

[82] P. C. Roberts. Control of a bdfm motor. Master's thesis, University of Cambridge, 2000.

[83] P. C. Roberts, E. Abdi-Jalebi, R. A. McMahon, and T. J. Flack. Real-time rotor bar current measurements using bluetooth technology for a brushless doubly-fed machine (BDFM). In *Int. Conf. Power Electronics, Machines and Drives (PEMD)*, volume 1, pages 120–125. IEE, March 2004.

[84] P. C. Roberts, T. J. Flack, J. M. Maciejowski, and R. A. McMahon. Two stabilising control strategies for the brushless doubly-fed machine (BDFM). In *Int. Conf. Power Electronics, Machines and Drives (PEMD) (Conf. Pub. No. 487)*, pages 341–346. IEE, 4-7 June 2002. Bath, UK.

[85] P. C. Roberts, J. M. Maciejowski, R. A. McMahon, and T. J. Flack. A simple rotor current observer with an arbitrary rate of convergence for the brushless doubly-fed (induction) machine (BDFM). In *Proc. IEEE Joint CCA, ISIC, CACSD*, pages 266–271, Taipai, Taiwan, 2-4 September 2004. paper no. 683.

[86] P. C. Roberts, R. A. McMahon, P. J. Tavner, J. M. Maciejowski, and T. J. Flack. An equivalent circuit for the brushless doubly-fed machine (BDFM) including parameter estimation. *Proc. IEE B - Elec. Power App.*, 2004. accepted for publication, November 2004.

[87] P. C. Roberts, R. A. McMahon, P. J. Tavner, J. M. Maciejowski, T. J. Flack, and X. Wang. Performance of rotors for the brushless doubly-fed (induction) machine (BDFM). In *Proc. 16th Int. Conf. Electrical Machines (ICEM)*, pages 450–455, September 2004. 5th-8th, Cracow, Poland.

[88] P. Rochelle, R. Spée, and A. K. Wallace. The effect of stator winding configuration on the performance of brushless doubly-fed machines in adjustable speed drives. In *Conference record of the IEEE Industry Applications Society Annual Meeting*, pages 331–337, Seattle,WA, October 7-12 1990. IEEE.

[89] Wilson J. Rugh and Jeff S. Shamma. Research on gain scheduling. *Automatica*, 36(10):1401–1425, October 2000.

[90] F. Rüncos, R. Carlson, A. M. Oliveira, P. Kuo-Peng, and N. Sadowski. Performance analysis of a brushless doubly-fed cage induction generator. In *Proc. 2nd Nordic Windpower Conf.*, 2004. 1-2 March.

[91] Mulukutla S. Sarma. *Electric Machines: Steady-state Theory and Dynamic Performance*. West Publishing Company, 1986.

[92] M. G. Say. *The Performance and Design of Alternating Current Machines*. Sir Isaac Pitman & Sons Ltd., 2 edition, 1948.

[93] Carsten Scherer and Siep Weiland. Lecture notes DISC course on linear matrix inequalities in control. Dutch Institute of Systems and Control, Delft, Netherlands, April 1999. available from `http://www.ocp.tudelft.nl/sr/personal/Scherer/lmi.pdf`.

[94] Fukuo Shibata and Toshio Kohrin. A brushless, self-excited polyphase synchronous generator. *IEEE Trans. on Power Apparatus and Systems*, PAS-102(8):2413–2419, August 1983.

[95] Fukuo Shibata and Kouji Taka. Speed control for brushless cascade induction motors in control range of slips $s_1 > 1$ and $s_2 > 1$. *IEEE Trans. on Energy Conversion*, EC-2(2):246–253, June 1987.

[96] Huang Shoudao, Huang Keyuan, Zhou Lawu, and Lai Lieen. A study of the control strategy on rotor field orientation for brushless doubly-fed machine. In *Proc. 3rd Power Electronics and Motion Control Conference (PIEMC) 2000*, volume 1, pages 508–513, Beijing, China, 5-18 August 2000 2000. IEEE.

[97] Siemens Brothers & Co. Ltd. and Francis Lydall. Improvements in polyphase induction motors. British Patent No.: 16839, July 1902.

[98] Gordon R. Slemon. Modelling of induction machines for electric drives. In *Conference record of the IEEE Industry Applications Society Annual Meeting*, volume 1, pages 111–115. IEEE, October 7-12 1989.

[99] Gordon R. Slemon. *Electrical Machines and Drives*. Addison-Wesley, 1992.

[100] G.R. Slemon and A. Straughen. *Electrical Machines*. Addison-Wesley, 1980.

[101] Jean-Jaques E. Slotine and Weiping Li. *Applied Nonlinear Control*. Prentice-Hall, 1991.

[102] B. H. Smith. The theory and performance of a twin stator induction machine. *IEEE Transactions on Power Apparatus and Systems*, 85(2):123–131, February 1966.

[103] B. H. Smith. Synchronous behaviour of doubly-fed twin stator induction machine. *IEEE Transactions on Power Apparatus and Systems*, 86(10):1227–1236, 1967.

[104] R. Spée, A. K. Wallace, and H. K. Lauw. Performance simulation of brushless doubly-fed adjustable speed drives. In *Conference record of the IEEE Industry Applications Society Annual Meeting*, San Diego, CA, 1989. IEEE.

[105] Robert F. Stengel. *Optimal Control and Estimation*. Dover Publications Inc., 1994.

[106] Z. Bo Tang. Adaptive partitioned search to global optimization. *IEEE Transactions on Automatic Control*, 39(11):2235–2244, November 1994.

[107] The Mathworks, editor. *Matlab Function Reference*, volume 1. The Mathworks Inc., 7.0 edition, 2004. `http://www.mathworks.com/access/helpdesk/`.

[108] The Mathworks, editor. *Using Simulink*. The Mathworks Inc., 2004. `http://www.mathworks.com/access/helpdesk/`.

[109] A. K. Wallace, P. Rochelle, and R. Spée. Rotor modelling and development for brushless doubly-fed machines. In *Conference record of the International Conference on Electrical Machines*, volume 1, Cambridge,MA, August 12-15 1990. ICEM.

[110] A. K. Wallace, R. Spée, and H. K. Lauw. Dynamic modelling of brushless doubly-fed machines. In *Conference record of the IEEE Industry Applications Society Annual Meeting*, San Diego, CA, 1989. IEEE.

[111] Samuel S. Waters and Ronald D. Willoughby. Modeling of induction motors for system studies. *IEEE Trans. on Industry Applications*, IA-19(5):875–878, September 1983.

[112] S. Williamson. Field analysis for rotating induction machines and its relationship to the equivalent-circuit method. *IEE Proc. Pt. B - Elec. Power App.*, 127(2):83–90, March 1980.

[113] S. Williamson. Power factor improvement in cage-rotor induction motors. *IEE Proceedings - B Electrical Power Applications*, 130(2):121–129, 1983.

[114] S. Williamson and A. C. Ferreira. Generalised theory of the brushless doubly-fed machine. part 2: Model verification and performance. *IEE Proceedings - Electric Power Applications*, 144(2):123–129, 1997.

[115] S. Williamson, A. C. Ferreira, and A. K. Wallace. Generalised theory of the brushless doubly-fed machine. part 1: Analysis. *IEE Proceedings - Electric Power Applications*, 144(2):111–122, 1997.

[116] S. Williamson and E. R. Laithwaite. Generalised harmonic analysis for the steady-state performance of sinusoidally excited cage induction motors. *IEE Proceedings - B Electric Power Applications*, 132(3):157–163, 1985.

[117] Stephen Williamson and Michael Boger. Impact of inter-bar current on the performance of the brushless doubly fed motor. *IEEE Trans. Industry Applications*, 35(2):453–460, March/April 1999.

[118] G. D. Wood, P. J. Goddard, and K. Glover. Approximation of linear parameter-varying systems. In *Proc. 35th Conference on Decision and Control (CDC)*, pages 406–411, Kobe, Japan, December 1996. IEEE CSS.

[119] Giles David Wood. *Control of Parameter-Dependent Mechanical Systems*. PhD thesis, University of Cambridge, 1995.

[120] Fen Wu, Xin Hua Yang, Andy Packard, and Greg Becker. Induced $\mathcal{L}_2$-norm control for LPV systems with bounded parameter variation rates. *Int. Journal of Robust and Nonlinear Control*, 6(9-10):983–998, November 1996.

[121] Dante C. Youla and Jr. Joseph J. Bongiorno. A floquet theory of the general linear rotating machine. *IEEE Trans. Circuits and Systems*, CAS-27(1):15–19, January 1980.

[122] Hugh D. Young. *University Physics*. Addison Wesley, 8 edition, 1992.

[123] Anatoly A. Zhigljavsky. *Theory of Global Random Search*. Kluwer Academic Publishers, 1991.

[124] D. Zhou and R. Spée. Field orientated control development for brushless doubly-fed machines. In *Conference record of the Industry Applications Society (IAS) Annual Meeting 1996*, volume 1, pages 304–310. IEEE, 6-10 October 1996. Taipai, Taiwan.

[125] D. Zhou, R. Spée, and G. C. Alexander. Experimental evaluation of a rotor flux oriented control algorithm for brushless doubly-fed machines. *IEEE Transactions on Power Electronics*, 12(1):72–78, 1997.

[126] D. Zhou, R. Spée, G. C. Alexander, and A. K. Wallace. A simplified method for dynamic control of brushless doubly-fed machines. In *Conference record of the 22nd Industrial Electronics, Control and Instrumentation Conference (IECON) 1996*, volume 2, pages 946–951. IEEE, 5-10 August 1996. Taipai, Taiwan.

[127] D. Zhou, R. Spée, and A. K. Wallace. Laboratory control implementations for doubly-fed machines. In *Proceedings of the IECON '93*, volume 2, pages 1181–1186, IEEE Conf. on Industrial Electronics, Control, and Instrumentation, 1993. 15-19 Nov 1993.

[128] D. Zhou, R. Spée, and A. K. Wallace. Model reference adaptive speed control for doubly-fed machines. In *Proceedings of International Conference on Industrial Electronics, Control and Instrumentation (IECON)*, volume 2. IEEE, 1993.

[129] Dongsheng Zhou, R. Spée, and G. C. Alexander. Experimental evaluation of a rotor flux orientated control algorithm for brushless doubly-fed machines. In *Conference record of the 27th Power Electronics Specialists Conference (PESC) 1996*, volume 1, pages 913–919. IEEE, 23-27 June 1996. Baveno, Italy.

[130] Dongsheng Zhou and René Spée. Synchronous frame model and decoupled control development for doubly-fed machines. In *Conference record of the 25th Power Electronics Specialists Conference (PESC) 1994*, volume 2, pages 1229–1236. IEEE, 20-23 June 1994. Taipei, Taiwan.

[131] Kemin Zhou, John C. Doyle, and Keith Glover. *Robust and Optimal Control*. Prentice-Hall, 1996.

Author Index